THE UNIVERSITY OF QUEENSLAND

AUSTRALIA

Innovations in Microbial Biodiscovery, Targeting Silent Metabolism and New Chemical Diversity

Zeinab GalalElDeen Mohamed Khalil

Master degree in Microbiology and Immunology, 2008

Bachelor degree with honour in Pharmaceutical Sciences, 2001

A thesis submitted for the degree of Doctor of Philosophy at

The University of Queensland in 2013

Institute for Molecular Bioscience

Abstract

After 100 years of exploring microbial metabolites, there is genetic evidence of a potential silent secondary metabolism that may yield different classes of bioactive secondary metabolites. Secondary metabolite production is often limited by factors that have a great impact on the metabolic turnover such as culture conditions, including temperature, pH, media and salinity as well as strain improvement, optimization of media composition, variation in the culture conditions and exposure to chemical signalling such as in the case of microbial co-culture. As well as low molecular weight signalling molecules can play an important role in the regulation of secondary metabolite production, and in accessing silent genetic potential. We believe that silent genes may remain dormant and do not produce any metabolites until they become activated. They can be activated by chemical stimuli produced by other competing microbes. Such molecular tools could be used to unlock the silent secondary metabolism and more leading to next generation antibiotics. In recent years, microtiter plates have been presented as an alternative technique traditional shake flasks for optimizing cultivation of different microorganisms. For example, Duetz *et al*. developed a cultivation system employing 24 or 96-well square-shape microtiter plates (MTP).

The aims of my research were to focuses on the isolation and structure elucidation of microbial natural products derived from marine or terrestrial microbes. At the same time, it focuses on finding new autoregulators that act as triggers to improve cellular development and activate the production of new secondary metabolites.

Chapter 1 – Introduction: Activation of microbial secondary metabolites

This chapter will outline an overview on the activation of secondary metabolites and the historical impact of microbial biodiscovery and the challenges for the discovery of new metabolites.

Chapter 2 - Developing a micro-bioreactor technique for cultivation of microbes

This chapter will explain and illustrates the new strategy for cultivating microbes in the micro-bioreactor through developing a high-throughput (HTP) microbial biodiscovery methodology based on this system, testing and validating a number of critical hypotheses –efficacy, reproducibility, HTP practicality and HTP versatility.

Chapter 3 - Activation of microbial secondary metabolites

This chapter seeks to address the questions of how to activate silent secondary metabolites by looking for nature chemical cues that stimulate metabolism. This study explored two different

sources of chemical cues; (1) microbial crude extracts, (2) lipopolysaccharide (LPS) from the Gram-negative bacteria (*Escherichia coli*).

Chapter 4 - Beach warefare: An *Aspergillus* stimulates antifungal defences in a *Streptomyces* sp.

The chapter outlines the effect of nitric oxide synthase (NOS) on secondary metabolites production, heronapyrrole production in *Streptomyces* sp. as well as it illustrates for the first instance a co-evolution between a *Streptomyces* sp. and an *Aspergillus* sp. and the discovery and quantification of the potency of two new classes of small molecule bNOS activators.

Chapter 5 – Rare marine-derived fungal alkaloids reveal diketomorpholines as inhibitors of P-glycoprotein mediated multi-drug resistance in cancers, and a promising new scaffold for medicinal chemistry

The chapter illustrates the isolation of new diketomorpholine shornephine A, its methanolysis artifact *seco*-shornephine A, and two known and one new diketopiperazine, 15b-β-hydroxyl-5-*N*-acetyladreemin, 5-*N*-acetyladreemin and 15b-β-methoxy-5-*N*-acetyladreemin respectively in which two of these metabolites were inhibitors of P-glycoprotein, a critical determinant in many multidrug resistant cancers, responsible for efflux of many clinically important chemotherapeutics. The positive results towards P-gp inhibition promoted the synthesis of different diketomorpholines analogues to probe the structure activity relationship.

Chapter 6 – Desotamides: New cyclic hexapeptides with anti-tuberculosis activity

This chapter illustrates the structural elucidation of known desotamide and six new analogues in which all of the desotamides showed antibacterial activity against Gram positive bacteria while only two metabolites showed good activity against *Mycobacterium tuberculosis*.

Chapter 7 – Aranciamycins: New Anthraquinones antibiotics

This chapter illustrates the isolation and structural elucidation of two new and two known aranciamycins metabolites from *Streptomyces* sp. in which they possesses antibacterial activity against Gram positive bacteria.

Chapter 8 – Citrinaline X: Importance of physicochemical characterization

This chapter illustrates the isolation and structural elucidation of new citrinaline B and known citrinin metabolites in which citrinaline B possess moderate metallo-β-lactamase activity supported by molecular modelling studies.

Chapter 9 – Additional microbial chemical diversity

The chapter briefly illustrates the structural elucidation of the known metabolites that have been isolated during PhD study.

Chapter 10 – Microbial community isolation and analysis

The chapter explains the collection of different terrestrial samples from different regions in Australia and outlines the methods used for the isolation of microbes and the preservation techniques. It also outlines the chemical and biological analysis of microbial crude extracts.

Chapter 11 – Publications

This chapter shows the screening process in the biodiscovery paradigm for the discovery of new antibiotics against Gram negative/positive bacteria and fungi.

Declaration by author

This thesis is composed of my original work, and contains no material previously published or written by another person except where due reference has been made in the text. I have clearly stated the contribution by others to jointly-authored works that I have included in my thesis.

I have clearly stated the contribution of others to my thesis as a whole, including statistical assistance, survey design, data analysis, significant technical procedures, professional editorial advice, and any other original research work used or reported in my thesis. The content of my thesis is the result of work I have carried out since the commencement of my research higher degree candidature and does not include a substantial part of work that has been submitted to qualify for the award of any other degree or diploma in any university or other tertiary institution. I have clearly stated which parts of my thesis, if any, have been submitted to qualify for another award.

I acknowledge that an electronic copy of my thesis must be lodged with the University Library and, subject to the General Award Rules of The University of Queensland, immediately made available for research and study in accordance with the *Copyright Act 1968*.

I acknowledge that copyright of all material contained in my thesis resides with the copyright holder(s) of that material. Where appropriate I have obtained copyright permission from the copyright holder to reproduce material in this thesis.

Publications during candidature

Peer-reviewed papers

Salim, A. A.; **Khalil, Z.**; Capon, R. J. Structural and stereochemical investigations into bromotyrosine-derived metabolites from southern Australian marine sponges, *Pseudoceratina* spp. *Tetrahedron* **2012**, 68, 9802-9807.

Zhang, H.; **Khalil, Z.**; Conte, M. M.; Plisson, F; Capon, R. J. A search for kinase inhibitors and antibacterial agents: bromopyrrolo-2-aminoimidazoles from a deep-water Great Australian Bight sponge, *Axinella* sp. *Tetrahedron Letters* **2012**, 53, 3784-3787.

Plisson, F.; Huang, XC.; Zhang, H.; **Khalil, Z.**; Capon, R. J. Lamellarins as Inhibitors of P-Glycoprotein-Mediated Multidrug Resistance in a Human Colon Cancer Cell Line. *Chemistry-An Asian Journal* **2012**, 7, 1616-1623.

Plisson, F.; Conte, M.; **Khalil, Z.**; Huang, XC.; Piggott, A. M.; Capon, R. J. Kinase Inhibitor Scaffolds against Neurodegenerative Diseases from a Southern Australian Ascidian, *Didemnum* sp. *ChemMedChem* **2012**, 7, 983-990.

Raju, R.; Piggott, A. M.; **Khalil, Z.**; Bernhardt, P. V.; Capon, R. J. Heronamycin A: a new benzothiazine ansamycin from an Australian marine-derived *Streptomyces* sp. *Tetrahedron Letters* **2012**, 53, 1063-1065.

Zhang, H.; Xiao, X.; Conte, M.; **Khalil, Z.**; Capon, R. J. Spiralisones A-D: acylphloroglucinol hemiketals from an Australian marine brown alga, *Zonaria spiralis*. *Organic & Biomolecular Chemistry* **2012**, 10, 9671-9676.

Zhang, H.; Conte, M.; **Khalil, Z.**; Huang, XC.; Capon, R. J. New dictyodendrins as BACE inhibitors from a southern Australian marine sponge, *Ianthella* sp. *RSC Advances*, **2012**, 2, 4209-4214.

Zhang, H.; Conte, M.; Huang, XC.; **Khalil, Z** ; Capon, R. J. A search for BACE inhibitors reveals new biosynthetically related pyrrolidones, furanones and pyrroles from a southern Australian marine sponge, *Ianthella* sp. *Organic & Biomolecular Chemistry* **2012**, 10, 2656-2663.

Ajala, O. S.; Piggott, A. M.; Plisson, F.; **Khalil, Z.**; Huang, XC.; Adesegun, S. A.; Coker, H. A. B.; Capon, R. J. Ikirydinium A: a new indole alkaloid from the seeds of *Hunteria umbellata* (K. Schum). *Tetrahedron Letters* **2011**, 52, 7125-7127.

Zhang, H.; **Khalil, Z.**; Capon, R. J. Fascioquinols A-F: bioactive meroterpenes from a deep-water southern Australian marine sponge, *Fasciospongia* sp. *Tetrahedron* **2011**, 67, 2591-2595.

Fremlin, L.; Farrugia, M.; Piggott, A. M.; **Khalil, Z.**; Lacey, E.; Capon, R. J. Reveromycins Revealed: New polyketide spiroketals from Australian marine-derived and terrestrial *Streptomyces* spp. A case of natural products vs. artifacts. *Organic & Biomolecular Chemistry* **2011**, 9, 1201-1211.

Raju, R.; Piggott, A. M.; Diaz, L. X. B. ; **Khalil, Z.**; Capon, R. J. Heronapyrroles A-C: Farnesylated 2-Nitropyrroles from an Australian Marine-Derived *Streptomyces* sp. *Organic Letters* **2010**, 12, 5158-5161.

Peng, C.; Gunaherath, G. M. K. B.; Piggott, A. M.; **Khalil, Z.**; Conte, M.; Capon, R. J. 9-(5'-Deoxy-5'-thio-beta-D-xylofuranosyl)adenine Disulfide from the Southern Australian Marine Sponge *Trachycladus laevispirulifer*: the First Natural Occurrence of a Nucleoside Disulfide. *Australian Journal of Chemistry* **2010**, 63, 873-876.

Salim, A. A.; Rae, J.; Fontaine, F.; Conte, M.; **Khalil, Z.**; Martin, S.; Parton, R. G.; Capon, R. J. Heterofibrins: inhibitors of lipid droplet formation from a deep-water southern Australian marine sponge, *Spongia* (*Heterofibria*) sp. *Organic & Biomolecular Chemistry* **2010**, 8, 3188-3194.

Conferences Abstracts

Poster Presentation "Shornephine A: A Novel diketomorpholine from a marine derived fungus inhibits P-glycoprotein" at the 2nd Division of Chemistry and Structural Biology Symposium – Brisbane, Australia (November 2012).

Oral and Poster Presentation " Exploring the chemical diversity of Microbes" at the 2nd Division of Chemistry and Structural Biology Symposium – Brisbane, Australia (November 2011).

Poster Presentation, "Exploring the chemical diversity of terrestrial and marine microbes" at 27th international symposium of discovery of natural products (ISCNP27/ICOB7) at Southbank, Brisbane, Queensland, Australia (July 2011).

Poster Presentation, "The development of new metallo-beta-lactamase inhibitor leads from natural and synthetic compounds" at 27th international symposium of discovery of natural products (ISCNP27/ICOB7) at Southbank, Brisbane, Queensland, Australia (July 2011).

Oral Presentation, "Strategies for reinvigorating new microbial drug discovery" at Brisbane Biological & Organic Chemistry Symposium (BBOCS) – Brisbane, Australia (November 2011).

Poster presentation, "Microbial biodiscovery" at 11th International Symposium on the Genetics of Industrial Microorganisms (GIM2010) at Melbourne, Australia (July 2010).

Publications included in this thesis

Salim, A. A.; **Khalil, Z.**; Capon, R. J. Structural and stereochemical investigations into bromotyrosine-derived metabolites from southern Australian marine sponges, *Pseudoceratina* spp. *Tetrahedron* **2012**, 68, 9802-9807. Incorporated in Chapter 11

Contributor	Statement of contribution
Salim, A. A.	Designed experiments (80%) Data analysis (80%) Wrote the paper (40%)
Khalil, Z.	Designed experiments (20%) Data analysis (20%) Wrote and edited paper (10%)
Capon, R. J.	Wrote and edited paper (50%)

Zhang, H.; **Khalil, Z.**; Conte, M. M.; Plisson, F; Capon, R. J. A search for kinase inhibitors and antibacterial agents: bromopyrrolo-2-aminoimidazoles from a deep-water Great Australian Bight sponge, *Axinella* sp. *Tetrahedron Letters* **2012**, 53, 3784-3787. Incorporated in Chapter 11.

Contributor	Statement of contribution
Zhang, Hua	Designed experiments (60%) Data analysis (80%) Wrote the paper (30%)
Khalil, Z.	Designed experiments (20%) Data analysis (10%) Wrote and edited paper (10%)
Conte, Melissa	Designed experiments (10%) Data analysis (5%) Wrote and edited paper (5%)
Plisson, Fabien	Designed experiments (10%) Data analysis (5%) Wrote and edited paper (5%)
Capon, Robert J.	Wrote and edited paper (50%)

Plisson, F.; Huang, XC.; Zhang, H.; **Khalil, Z.**; Capon, R. J. Lamellarins as Inhibitors of P-Glycoprotein-Mediated Multidrug Resistance in a Human Colon Cancer Cell Line. *Chemistry-An Asian Journal* **2012**, 7, 1616-1623. Incorporated in Chapter 11

Contributor	Statement of contribution
Plisson, F.	Designed experiments (50%) Data analysis (60%) Wrote the paper (30%)
Hunag, X.	Designed experiments (30%) Data analysis (30%) Wrote and edited paper (10%)
Zhang, H.	Designed experiments (10%)
Khalil, Z.	Designed experiments (10%) Data analysis (10%) Wrote and edited paper (10%)
Capon, R. J.	Wrote and edited paper (50%)

Plisson, F.; Conte, M.; **Khalil, Z.**; Huang, XC.; Piggott, A. M.; Capon, R. J. Kinase Inhibitor Scaffolds against Neurodegenerative Diseases from a Southern Australian Ascidian, *Didemnum* sp. *ChemMedChem* **2012**, 7, 983-990. Incorporated in Chapter 11.

Contributor	Statement of contribution
Plisson, F.	Designed experiments (50%) Data analysis (60%) Wrote the paper (60%)
Conte, M.	Designed experiments (10%)
Khalil, Z.	Designed experiments (10%) Data analysis (15%) Wrote and edited paper (15%)
Huang, X.	Designed experiments (30%)
Piggott, A. M.	Wrote and edited paper (10%)
Capon, R. J.	Wrote and edited paper (30%)

Raju, R.; Piggott, A. M.; **Khalil, Z.**; Bernhardt, P. V.; Capon, R. J. Heronamycin A: a new benzothiazine ansamycin from an Australian marine-derived *Streptomyces* sp. *Tetrahedron Letters* **2012**, 53, 1063-1065. Incorporated in Chapter 11.

Contributor	Statement of contribution
Raju, R.	Designed experiments (60%) Data analysis (60%)
Piggott, A.	Wrote and edited paper (40%)
Khalil, Z.	Designed experiments (20%) Data analysis (20%) Wrote and edited paper (10%)
Bernhardt, P. V.	Designed experiments (20%) Data analysis (20%)
Capon, R. J.	Wrote and edited paper (50%)

Zhang, H.; Xiao, X.; Conte, M.; **Khalil, Z.**; Capon, R. J. Spiralisones A-D: acylphloroglucinol hemiketals from an Australian marine brown alga, *Zonaria spiralis*. *Organic & Biomolecular Chemistry* **2012**, 10, 9671-9676. Incorporated in Chapter 11.

Contributor	Statement of contribution
Zhang, H.	Designed experiments (60%) Data analysis (60%) Wrote the paper (40%)
Xiao, X.	Designed experiments (25%) Data analysis (30%) Wrote the paper (10%)
Conte, M.	Designed experiments (10%)
Khalil, Z.	Designed experiments (5%) Data analysis (10%) Wrote and edited paper (5%)
Capon, R. J.	Wrote and edited paper (50%)

Zhang, H.; Conte, M.; **Khalil, Z.**; Huang, XC.; Capon, R. J. New dictyodendrins as BACE inhibitors from a southern Australian marine sponge, *Ianthella* sp. *RSC Advances*, **2012**, 2, 4209-4214. Incorporated in Chapter 11.

Contributor	Statement of contribution
Zhang, H.	Designed experiments (60%) Data analysis (40%) Wrote the paper (60%)
Conte, M.	Designed experiments (20%) Data analysis (20%)
Khalil, Z.	Designed experiments (10%) Data analysis (20%) Wrote and edited paper (5%)
Huang, XC.	Designed experiments (10%) Data analysis (20%) Wrote and edited paper (5%)
Capon, R. J.	Wrote and edited paper (40%)

Zhang, H.; Conte, M.; Huang, XC.; **Khalil, Z** ; Capon, R. J. A search for BACE inhibitors reveals new biosynthetically related pyrrolidones, furanones and pyrroles from a southern Australian marine sponge, *Ianthella* sp. *Organic & Biomolecular Chemistry* **2012**, 10, 2656-2663. Incorporated in Chapter 11.

Contributor	Statement of contribution
Zhang, H.	Designed experiments (60%) Data analysis (40%) Wrote the paper (60%)
Conte, M.	Designed experiments (20%) Data analysis (20%)
Huang, XC.	Designed experiments (10%) Data analysis (20%) Wrote and edited paper (5%)
Khalil, Z.	Designed experiments (10%) Data analysis (20%) Wrote and edited paper (5%)
Capon, R. J.	Wrote and edited paper (40%)

Fremlin, L.; Farrugia, M.; Piggott, A. M.; **Khalil, Z.**; Lacey, E.; Capon, R. J. Reveromycins Revealed: New polyketide spiroketals from Australian marine-derived and terrestrial *Streptomyces* spp. A case of natural products vs. artifacts. *Organic & Biomolecular Chemistry* **2011**, 9, 1201-1211. Incorporated in Chapter 11.

Contributor	Statement of contribution
Fremlin, L.	Desigened experiments (60%)
Farrugia, M.	Designed experiments (20%)
Piggott, A. M.	Wrote and edited paper (40%)
Khalil, Z.	Designed experiments (10%) Data analysis (10%) Wrote and edited paper (10%)
Lacey, E.	Designed experiments (10%)
Capon, R. J.	Wrote and edited paper (50%)

Ajala, O. S.; Piggott, A. M.; Plisson, F.; **Khalil, Z.**; Huang, XC.; Adesegun, S. A.; Coker, H. A. B.; Capon, R. J. Ikirydinium A: a new indole alkaloid from the seeds of *Hunteria umbellata* (K. Schum). *Tetrahedron Letters* **2011**, 52, 7125-7127. Incorporated in Chapter 11.

Contributor	Statement of contribution
Ajala, O. S.	Designed experiments (60%) Data analysis (40%)
Piggott, A. M.	Data analysis (20%) Wrote and edited paper (20%)
Plisson, F.	Designed experiments (20%) Data analysis (20%) Wrote and edited paper (10%)
Khalil, Z.	Designed experiments (10%) Data analysis (10%) Wrote and edited paper (10%)
Huang, XC.	Designed experiments (10%) Data analysis (10%) Wrote and edited paper (10%)
Capon, R. J.	Wrote and edited paper (50%)

Zhang, H.; **Khalil, Z.**; Capon, R. J. Fascioquinols A-F: bioactive meroterpenes from a deep-water southern Australian marine sponge, *Fasciospongia* sp. *Tetrahedron* **2011**, 67, 2591-2595. Incorporated in Chapter 11.

Contributor	Statement of contribution
Zhang, H.	Designed experiments (80%) Data analysis (75%) Wrote the paper (40%)
Khalil, Z.	Designed experiments (20%) Data analysis (15%) Wrote and edited paper (10%)
Capon, Robert J.	Wrote and edited paper (50%)

Raju, R.; Piggott, A. M.; Diaz, L. X. B. ; **Khalil, Z.**; Capon, R. J. Heronapyrroles A-C: Farnesylated 2-Nitropyrroles from an Australian Marine-Derived *Streptomyces* sp. *Organic Letters* **2010**, 12, 5158-5161. Incorporated in Chapter 11.

Contributor	Statement of contribution
Raju, R.	Designed experiments (60%) Data analysis (60%)
Piggott, A. M.	Wrote and edited paper (40%) Data analysis (30%)
Diaz, L. X. B.	Designed experiments (10%)
Khalil, Z.	Designed experiments (30%) Data analysis (10%) Wrote and edited paper (10%)
Capon, R. J.	Wrote and edited paper (50%)

Peng, C.; Gunaherath, G. M. K. B.; Piggott, A. M.; **Khalil, Z.**; Conte, M.; Capon, R. J. 9-(5'-Deoxy-5'-thio-beta-D-xylofuranosyl)adenine Disulfide from the Southern Australian Marine Sponge *Trachycladus laevispirulifer*: the First Natural Occurrence of a Nucleoside Disulfide. *Australian Journal of Chemistry* **2010**, 63, 873-876. Incorporated in Chapter 11.

Contributor	Statement of contribution
Peng, C.	Designed experiments (70%) Data analysis (50%)
Gunaherath, G.	Wrote and edited paper (10%) Data analysis (10%)
Piggott, A. M.	Wrote and edited paper (40%) Data analysis (30%)
Khalil, Z.	Designed experiments (20%) Data analysis (10%) Wrote and edited paper (10%)
Conte, M.	Designed experiments (10%)
Capon, R. J.	Wrote and edited paper (40%)

Salim, A. A.; Rae, J.; Fontaine, F.; Conte, M.; **Khalil, Z.**; Martin, S.; Parton, R. G.; Capon, R. J. Heterofibrins: inhibitors of lipid droplet formation from a deep-water southern Australian marine sponge, *Spongia* (*Heterofibria*) sp. *Organic & Biomolecular Chemistry* **2010**, 8, 3188-3194. Incorporated in Chapter 11.

Contributor	Statement of contribution
Salim, A. A.	Designed experiments (50%) Data analysis (60%) Wrote the paper (50%)
Rae, J.	Designed experiments (10%)
Fontaine, F.	Designed experiments (20%) Data analysis (20%)
Conte, M.	Designed experiments (10%) Data analysis (10%)
Khalil, Z.	Designed experiments (10%) Data analysis (10%) Wrote and edited paper (5%)
Martin, S.	Designed experiments (20%)
Parton, R. G.	Designed experiments (10%)
Capon, R. J.	Wrote and edited paper (45%)

Contributions by others to the thesis

The multidrug resistance assays in Chapter 5 (cytotoxicity MTT assays, MDR reversal assay and flow cytometry) were optimised and performed *in-house* with support of Dr Xiao-Cong Huang (as part of his PhD studies). Dr Andrew Piggott acquired high-resolution mass spectral (HRESIMS) data and contributed to this thesis for critical analysis. Dr Angela Salim for her help in the structure elucidation of citrinaline X. Dr Antje Blumenthal, Diamantina Institute, The Univeristy of Queensland for screening the desotamides against *Mycobacterium bovis*. Dr Waleed Hussein brought technical advice for use of Molegero software, synthetic procedures. Dr Katheryn Green for technical help and acquiring the electron microscope images. John Griffin for his help and acquiring the Confocol and BD microscope images. Prof. Robert Capon contributed to this thesis for critical analysis and help on practical work and drafting.

Statement of parts of the thesis submitted to qualify for the award of another degree

None.

Acknowledgements

I wish to express my deepest appreciation to my research supervisor, Professor Robert J. Capon for the many years of endless enthusiasm, brilliant guidance and continuous encouragement and support I am forever grateful for him providing me with an opportunity to learn and work under his perfect guidance leading to the successful completion of this thesis.

My appreciation goes out to all the members of Capon research group, especially Dr. Andrew M. Piggott for acquiring and teaching high resolution mass spectra, his assistance with the NMR and in sorting out the technical problems faced with the equipment and Dr Angela Salim for teaching the semi-preparative HPLC and for answering all my questions in the beginning of my PhD and teaching me how to perform structure elucidation. Dr Ernest Lacey (MST) for providing continuous help and support. Thanks also to the following people, Dr. Xiao-cong Huang for *in vitro* screening of the compounds isolated, Melissa Conte for teaching me the cytotoxicity assay and Dr Ian Lane (floor manger) for his help and support.

A special thanks to Dr. Amanda Carozzi for handling all the paperwork and enquiries relating to postgraduate studies and for providing continuous support. I also acknowledge University of Queensland for the provision of a University of Queensland Research Scholarship (UQRS) scholarship and UQ International Research Tuition Awards (UQIRTA). A special thanks for Institute of Molecular Bioscience for the provision of writing scholarship award with additional financial support provided by Prof. Robert J. Capon

Finally, a very special thanks to my dear husband, Dr Waleed Hussein, for his incalculable and unwavering support during my whole study and my two lovely boys, Yassin and Youssef for bearing me during my tough times. My parents, Dr GalalElDeen Khalil and Mrs Aziza Mowafi for their words of encouragement and love. My little brother, Salah who always cheers me up with his jokes. My lovely grandma Salwa whose prayers for me and her words were quite important. My sister in law, Hager and my little nephew Moazz, their smiles made a big difference in my life.

Keywords

microbial natural products, nitric oxide synthase, P-glyoprotein, lipopolysaccharide, microbioreactor.

Australian and New Zealand Standard Research Classifications (ANZSRC)

ANZSRC code: 030502, Natural Products Chemistry, 50%

ANZSRC code: 060503, Microbial Ecology, 15%

ANZSRC code: 030401, Biologically Active Molecules, 35%

Fields of Research (FoR) Classification

FoR code: 0304, Medicinal and Biomolecular Chemistry, 50%

FoR code: 0605, Microbiology, 50%

Table of contents

List of Figures

List of Tables

List of Schemes

List of Abbreviations used in the thesis

Companies/Organizations

IMB	Institute for Molecular Bioscience
MST	Microbial Screening Technologies Pty Ltd

Biology

ATCC	American Type Culture Collection
ED_{50}	Effective Dose affecting 50% of the test subject
IC_{50}	Inhibitory Concentration 50 (concentration at which 50% of organisms are inhibited)
MIC	Minimum Inhibitory Concentration
MTT	3-(4,5-dimethylthiazol-2-yl)-2,5-diphenyltetrazolium bromide
MRSA	methicillin resistant *Staphylococcus aureus*
VREF	vancomycin resistant *Enterococcus faecium*
P-gp	permeability glycoprotein
SW620	colorectal adenocarcinoma ATCC CCL-227
SW620 Ad300	P-gp–overexpressing human colon adenocarcinoma cell line resistant to Adriamycin 300 ng/mL
KB-3-1	P-gp overexpressing human cervical carcinoma cell line
KV-3-1	human cervical cell line
E. coli	*Escherichia coli*
S. aureus	*Staphylococcus aureus*
B. subtilis	*Bacillus subtilis*
Ps. aeruginosa	*Pseudomonaus aeruginosa*

Chemical and Reagents

Ala	alanine
ABA	aminobutyric acid

DMSO	dimethyl sulfoxide
$CDCl_3$	deuterated chloroform
Acetone-d_6	deuterated acetone
MeOH-d_4	deuterated methanol
MeOH	MeOH
MeCN	acetonitrile
CH_2Cl_2	dichloromethane
DEANO	diethylamino nitric oxide
SIN	3-morpholinosydnonimine
SNAP	*S*-nitroso-*N*-acetylpenicillamine
CPTIO	2-(4-carboxyphenyl)-4,4,5,5-tetramethylimidazoline-1-oxyl-3-oxide
FDAA	N_α-(2,4-dinitro-5-fluorophenyl)-D-alaninamide
Leu	leucine
Ile	isoleucine
allo-Ile	*allo*-isoleucine
Asn	aspartic acid
Gly	glycine
Orn	ornithine
Arg	arginine
Lys	lysine
MTPA	α-methoxy-α-trifluoromethylphenylacetic acid
Pro	proline
4-hydroxy-Pro	4-hydroxy-proline
Tyr	tyrosine
Phe	phenylalanine
TFA	trifluoroacetic acid
Trp	tryptophan
AcOH	acetic acid
EtOH	ethanol
AG	aminoguanidine
NAME	nitro-L-arginine-methyl ester
NMMA	N^G-methyl-L-arginine
R-Mosher	(*R*)-3,3,3-trifluoro-2-methoxy-2-phenylpropanoic acid
S-Mosher	(*S*)-3,3,3-trifluoro-2-methoxy-2-phenylpropanoic acid

Phe lactic acid	Phenyl lactic acid
DCC	N,N'-dicyclohexylcarbodiimide
DMAP	4-dimethylaminopyridine
LPS	lipopolysaccharide
2,4-DNP	2,4-dinitrophenol

Chromatography and Spectroscopy

$[\alpha]_D$	optical rotation (room temperature)
DAD	Diode Array Detector
ESIMS	Electrospray Ionization Mass Spectrometry
HRESIMS	High Resolution Electrospray Ionization Mass Spectrometry
HPLC	High Performance Liquid Chromatography
MS	Mass Spectrometry
NMR	Nuclear Magnetic Resonance
UV-vis	Ultraviolet-visible
CD	*Circular dichroism*

Nuclear Magnetic Resonance

COSY	Correlation Spectroscopy
HSQC	Heteronuclear Single Quantum Coherence
HMBC	Heteronuclear Multiple Bond Correlation
J	coupling constant (in Hz)
NOESY	Nuclear Overhauser Effect Spectroscopy
ROESY	Rotational nuclear Overhauser Effect Spectroscopy
br	broad
s	singlet
d	doublet
t	triplet
q	quartet
m	multiplet

Other

Kd	dissociation constant
ACM	Australian Collection of Microbes
rt	room temperature
t_R	retention time
aq	aqueous
ATP	adenosine triphosphate
bNOS	bacterial nitric oxide synthase
iNOS	inducible nitric oxide synthase
eNOS	endothelial nitric oxide synthase
nNOS	neuronal nitric oxide synthase
NADPH	nicotinamide-adenine-dinucleotide phosphate
NO	nitric oxide
H_4B	tetrahydrobiopterin
BSA	bovine serum albumin
Calcein	AM calcein acetomethoxy derivative
GS	gain in sensitivity
FAR	fluorescence arbitrary ratio
CFU	colony-forming unit
CO_2	carbon dioxide
DMEM	Dulbecco/Vogt modified Eagle's minimal essential medium
RPMI	Roswell Park Memorial Institute (RPMI) 1640 medium
EDTA	ethylenediaminetetraacetic acid
ELSD	evaporative light scattering detector
ESI	electrospray ionisation
ESIMS	electrospray ionisation mass spectrum
FBS	foetal bovine serum
HPLC	high performance liquid chromatography
HR	high resolution
HTS	high-throughput screening
LR	low resolution
MDR	multidrug resistance

MS	mass spectrometry
NEAA	non-essential amino acids
NMR	nuclear magnetic resonance
PBS	phosphate buffer serum
PTFE	polytetrafluoroethylene
SAR	Structure-Activities Relationships
RFU	relative fluorescent unit
RPMI	1640 Roswell Park Memorial Institute medium
TLC	thin layer chromatography
UV	ultraviolet
DKP(s)	diketopiperazines(s)
DKM(s)	diketomorpholine(s)
Trp-mandelic	Tryptophan mandelic diketomorpholine
Trp-Phenyl lactic	Tryptophan phenyl lactic acid diketomorpholine
mg	milligram
g	gram
min	minutes
h	hour
sp.	species
approx.	Approximately
HIV	human immunodeficiency
MTP(s)	microtiter plate(s)
MBR(s)	micro-bioreactor plate(s)
CDW	cell density weight
KDO	3-deoxy-D-manno-2-octulosonate
ROS	reactive oxygen species
QS	quorum sensing
d	day

1 Chapter 1. Introduction to Microbial Biodiscovery

1.1 Historical impact of microbial natural products

Natural products continue to play a crucial role in the discovery of new drugs and drug leads.[1] Biodiscovery from microbial resources can be defined as the exploration of microbial metabolic products that provide important benefits to the fields of medicine, agriculture and biotechnology.[2] It has been reported that approximately 50% of approved drugs in the market are derived from microbial origin (Table 1.1).[3] Actinomycetes and fungi are very important groups of microorganisms that are known for their ability to produce secondary metabolites with therapeutic activities.[4] Actinobacteria produce over half of the bioactive compounds that are present in the antibiotic literature.[5] These compounds include well-known antibacterials such as aminoglycosides and tetracyclines, antifungals such as amphotericin B (**1.01**), anticancer agents such as adriamycin (**1.02**), immunosuppressants such as tacrolimus (**1.03**) and anthelmintics such as avermectin (**1.04**), plus numerous other valuable therapeutic drugs. Fungi also play a vital role in the microbial discovery, with the genus *Penicillium* providing several well-known drugs (e.g. penicillins) (Table 1.1).[6] Therefore, the drug discovery process is considered as a very critical issue in the industrial field as it is a very expensive process and it requires multiple steps to produce new drug potentials to target specific disease.[2,7,8]

Table 1.1. Examples of marketed antibiotics originated from microbial origin[3]

Original metabolite	Commercial products	Producing organism
Penicillins	Penicillin G, V, Ampicillin, Methicillin	*Penicillium* spp., *Aspergillus* spp.
Cephalosporins	Mefoxin, Ceclor	*Acremonuim* spp.
Thienamycin	Primaxin, Invanz	*Streptomyces cattleya*
Erythromycin	Erythrocin, Zithromax	*Saccharopolyspora erythraea*
Vancomycin	Vancocin	*Streptomyces orientalis*
Fosfomycin	Monuril	*Streptomyces fradiae*
Daptomycin	Cubicin	*Streptomyces roseosporus*

Despite this great success in the discovery of valuable antibiotics and other pharmaceutical active agents, there has been a dramatic decline in the discovery of new antibiotics in the 21st century. Despite a 2007 review[9] revealing that 70% of hospital-acquired infections in the US are resistant to one or more antibiotics, with the exception of the narrow spectrum antibiotic daptomycin (**1.05**), and linezolid (**1.06**), very few new classes of clinically relevant antibiotics have been approved over

the last 40 years. Tigecycline (**1.07**) is one of a new class of antibiotics derived from the tetracycline nucleus. This broad-spectrum antibiotic was approved for the treatment of complicated skin infections and is also active against MRSA, vancomycin-resistant *Enterococcus faecium* and beta-lactamase-producing bacteria as *Escherichia coli* and *Klebsiella pneumonia*.[10,11]

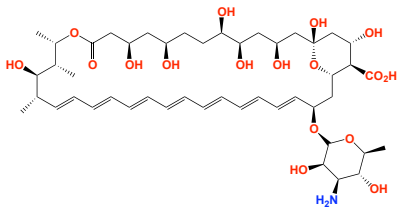

amphotericin B (**1.01**)

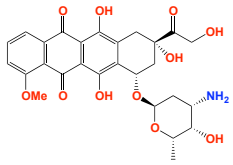

adriamycin (**1.02**)

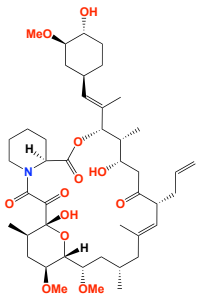

tacrolimus (**1.03**)

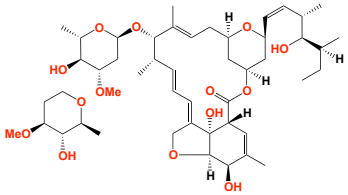

avermectin (**1.04**)

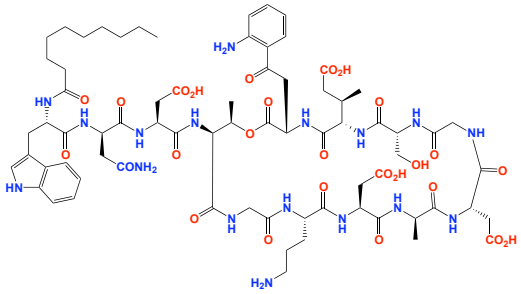

daptomycin (**1.05**)

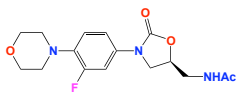

linezolid (**1.06**)

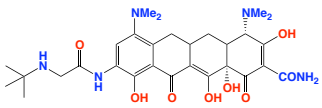

tigecycline (**1.07**)

1.2 Therapeutic fields responsive to natural products

Microbial secondary metabolites are highly potent and selective for the treatment of many diseases. Many of these metabolites can be interpreted to be a signal molecule or defense mechanism against competitors or pathogens, an aid to the survival of the microorganism.

1.2.1 Bacterial pathogens

Natural products are still the main source of promising new antibiotics for the treatment of bacterial diseases. Platensimycin (**1.08**), was first reported in 2006 from *Streptomyces platensis* by Merck researchers,[12] followed by the isolation of platencin (**1.09**).[13-15] In 2008, another platensimycin analogues B_1-B_3 (**1.10** - **1.12**)[16] and platensimycin B_4 (**1.13**)[17]. This class of antibiotics demonstrated a novel mode of action against Gram-positive bacteria through inhibition of cellular lipid biosynthesis. Because of this unique role, it shows no cross resistance to MRSA, VRE or other antibiotic resistant microbes.

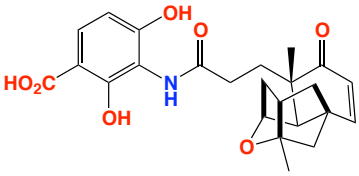

platensimycin (**1.08**)

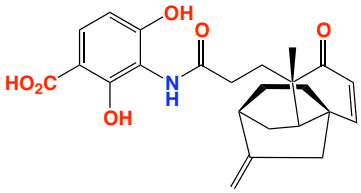

platencin (**1.09**)

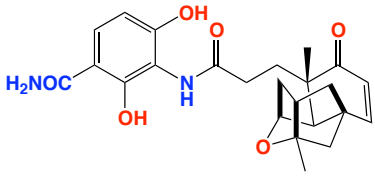

platensimycin B_1 (**1.10**)

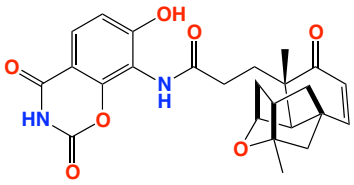

platensimycin B_2 (**1.11**)

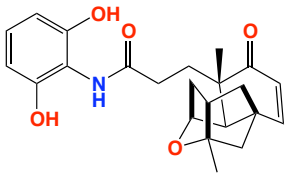

platensimycin B_3 (**1.12**)

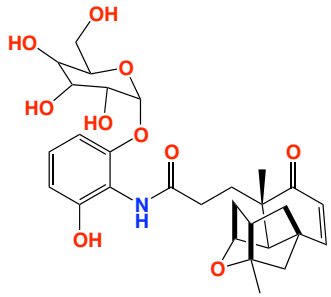

platensimycin B_4 (**1.13**)

1.2.2 Fungal pathogens

The need for the discovery of new antifungal agents continues, as we seek to treat the opportunistic infections in immune-compromised patients and the emerging resistance to existing antifungal agents. Jacob *et al.*[18] recently discussed the whole cell screening techniques targeting natural products and their mode of action including the use of genetically modified fungal strains in which the antifungal drug is targeting the cell wall and cell membrane. Caspofungin (**1.14**), is a promising new antifungal agents derived from pneumocandin, a natural product produced by *Glarea lozoyensis*.[19]

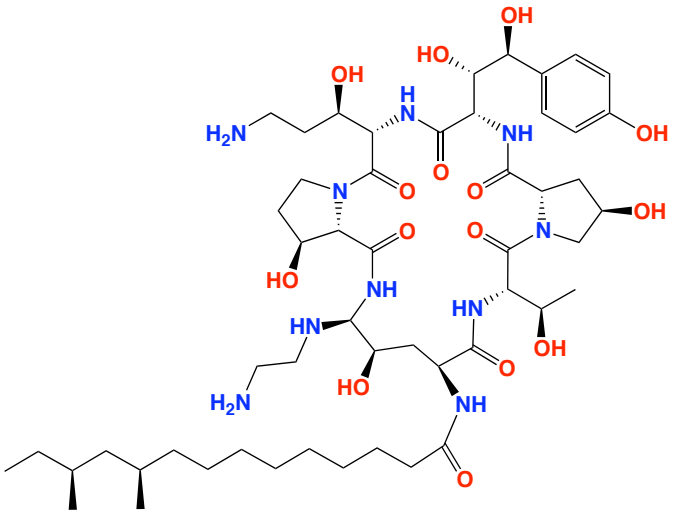

caspofungin (**1.14**)

1.2.3 Viral pathogens

New anti-HIV (human immunodeficiency) drugs are targeting the point of entrance of the virus into the cell such as interferon signaling and cell surface receptors as CCR5-human cytokine receptor and CD4.[20] Many antiviral lectins are from algal origin and they are mainly small proteins that bind to carbohydrates found on the viral envelopes and prevent the transmission of HIV.[21] In addition, viral polymerases are the key for viral replication and are considered as promising targets for anti-viral drugs, with inhibitors for viral polymerase and proteases in clinical use for the treatment of AIDS and chronic hepatitis. All drugs that are in the market for the treatment of HIV are synthetic in origin, although the activities of many natural products have been explored in the recent years.[22] Yu *et al*.[23] discovered a plant-derived modified betulinic acid derivative, DSB (**1.15**) as a first in class HIV maturation inhibitor. This natural product is currently in Phase II clinical trials.[23]

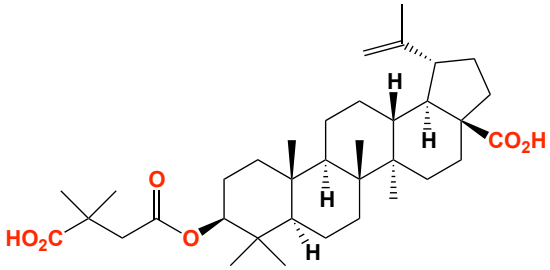

DSB (**1.15**)

1.3 Resistance to microbial natural products

1.3.1 Antibiotics and the resistance in nature

The discovery of antibiotics more than 70 years ago initiated an era of drug innovation in human and animal health. These discoveries were interrupted by the emergence of antibiotic resistance, largely due to the widespread overuse of antibiotics in both medicine and agriculture.[24] Notwithstanding the outstanding list of antibiotics that were discovered from microbial sources, especially soil microbes, resistance to these antibiotics evolved in the environment long before they were developed as commercial antibiotics.[25] The resistance we see in the clinic today is to a great extent similar to the environmental one. Although the resistance in both contexts are similar, clinical resistance tends to increase substantially with time. Therefore there should be a certain mechanism that keeps control of resistance in the environment.[26-28]

1.3.2 Anticancer resistance

Cancer cells become resistant to anticancer drugs by several mechanisms. One way is to pump drugs out of cells by increasing the activity of efflux pumps, such as ATP-dependent transporters. Alternatively, resistance can occur as a result of reduced drug influx - a mechanism reported for agents that interact with intracellular carriers or enter the cell by means of endocytosis. In cases where drug accumulation is unchanged, activation of detoxifying proteins, such as cytochrome P450 mixed-function oxidases, can promote drug resistance. Cells can also activate mechanisms that repair drug-induced DNA damage. Finally, disruptions in apoptotic signalling pathways (e.g. p53 or ceramide) allow cells to become resistant to drug-induced cell death.[29]

In order to overcome these problems, we need to better understand the microbial genomics. In the last 10 years, advances in genomics have revealed new knowledge of a silent microbial secondary metabolism, offering a glimpse of a new source of potentially valuable biomedical agents and tools. To access this genetic resource requires molecular tools capable of activating latent secondary metabolism gene clusters, to build knowledge of microbial systems biology, and facilitate access to new microbial natural products.

1.4 Silent resources

After 100 years of discovering microbes, there is great evidence that microbes are capable of producing different classes of bioactive secondary metabolites. However, strong evidence revealed that we are only scratching the surface of microbial genomes. Microbes share and accumulate multiple secondary metabolite gene clusters, which are capable of producing different bioactive metabolites, with a wide range of biological activities.[30] Some challenges limit our ability to access the microbial genome; for example both the bacteria and fungi harbour massive number of genes in which these genes usually remain dormant and do not produce any metabolites under normal laboratory conditions until they become activated. It is very probable that these genes are activated by chemical stimuli produced by other competing microbes. Such chemical stimuli represent valuable molecular tools that could be used to unlock the silent secondary metabolism, improving prospective for next generation antibiotics.[31]

1.4.1 Detection of silent secondary gene cluster

A 2001 study by Omura *et al*., on the genome of *Streptomyces avermitilis*, the microbial source of anthelmintic drug avermectins, revealed an 8.7 Mbp linear chromosome with 25 recognizable

secondary metabolite gene clusters accounting for 6.4% of the genome. This study concluded that there are many uncharacterized genes involved in the secondary metabolism. Twenty-five secondary metabolite gene clusters were found in the genome of *S. avermitilis.* Four of them are responsible for the production of melanin pigment on solid medium, two are derived from tyrosine and one is an aromatic polyketide. Another melanin is an ochronotic pigment, which is derived from homogentiginic acid and produced, in both solid and liquid media.[32] *S. avermitilis* has the highest number of secondary metabolite gene clusters of all bacterial genomes sequenced. The production of different metabolites can be attributed to the presence of many gene clusters, which can encode for enzymes for the activation of different secondary metabolic pathway. The report concluded that there are *"many other uncharacterized genes involved in secondary metabolism".*

In 2002, Bentley *et al.*[33] reported that the genome of *Streptomyces coelicolor* contained 20 secondary metabolite gene clusters and metabolic enzymes of known or predicated secondary metabolites. Furthermore, the genome contained an unprecedented proportion of regulatory genes that are involved in response to external stimuli and stresses. *S. coelicolor* contains duplicated genes that operate in different phases during colonial development, which if stimulated could lead to new pharmaceutical compounds. The report concluded by noting *"The abundance of previously uncharacterized metabolic enzymes, particularly those likely to be involved in the production of natural products, is a resource of enormous potential values"*. In 2005, McAlpine *et al*.[34] reported the genome analysis of *Streptomyces aizunensis* to detect the presence of hitherto unexpressed natural product in which different media where used to express microbial secondary metabolites. Udwary *et al*.[35] analysed the genome of *Salinospora tropica* to show a large percentage of its genome is dedicated to natural product assembly. In addition, this study identified secondary metabolic biosynthetic gene clusters from the complete genome sequence of *S. tropica* revealing an unrealised secondary metabolism potential and the importance of the understanding and the control for the secondary metabolite pathway.

Therefore, modern genomics has redefined our understanding of microbial secondary metabolism. The computational analysis of microbial metabolism provides the sequencing of thousands of microbial genomes. This knowledge will provide a new pathway to access the microbial molecular diversity and also will help to develop more tools and methodologies to take advantage of this potential. In addition, the previous articles noted a growing appreciation of a global microbial genome that encompasses molecular discovery value than previously appreciated. On the other hand, while learning that microbes possess a secondary metabolism, the challenge is how to activate

and benefit from that the activation of silent secondary gene clusters and produce new pharmaceutical compounds.

1.5 Activating of silent genes

1.5.1 Effect of culturing conditions on secondary metabolite production

The choice of the cultivation parameters is crucial for the production of secondary metabolites by microorganisms. It is well known fact that a change in culture conditions (temperature, pH, oxygen etc.) can affect secondary metabolites production. Any small change in the culture medium may impact not only the level of production of certain compounds, but also the diversity.[36] Paranagama *et al.*[37] studied the effect of tap water and distilled water on the metabolite profiling of two plant associated fungus, the first fungus, *Paraphaeosphaeria quadriseptata*, by the changing the water used in fermentation from tap to distilled resulted in the production of six new compounds, cytosporones F – I (**1.16** – **1.19**), 5′-hydroxymonocillin (**1.20**) and quadriseptin A (**1.21**).

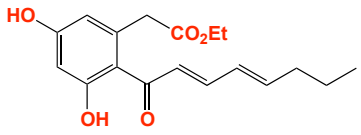

cytosporone F (**1.16**)

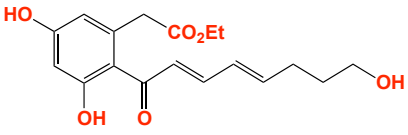

cytosporone G (**1.17**)

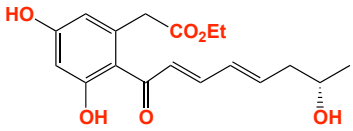

cytosporone H (**1.18**)

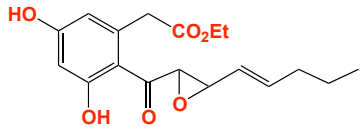

cytosporone I (**1.19**)

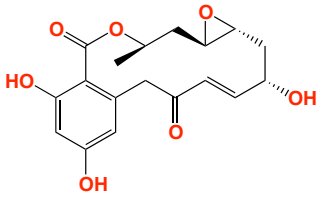

5'-hydroxymonocillin (**1.20**)

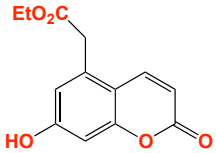

quadriseptin A (**1.21**)

The second fungus, *Chaetomium chiversii,* produced radicicol (**1.22**) on solid phase media, but shifted to chaetochromin (**1.23**) in liquid phase.[37]

In addition to various culture conditions, Ayer *et al.*, have studied the impression of the diverse stress conditions on secondary metabolite production. They were able to isolate jadomycin B (**1.24**), a glycosylated nezoxazolophenanthridine antibiotic from *Streptomyces venezuelae*. The aglycone jadomycin was produced in a galactose-isoleucine medium at 37 °C.[38] Increasing the temperature to 42 °C increased the level of production of jadomycin B (**1.24**). Other parameters were found to increase the production of jadomycin B such as addition of ethanol as well as bacteriophage infection.[39] Also, Overy *et al*. cultivated different strains of necrotrophic *Penicillium* strains in

different macerated host tissue media. This led to the stimulation of production of corymbiferone (**1.25**) and corymbiferan lactones I – IV (**1.26** – **1.28**).[40]

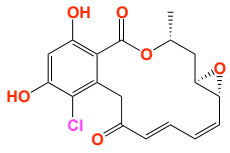

radicicol (**1.22**)

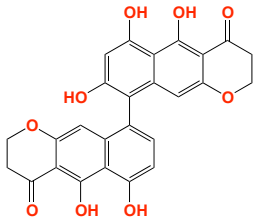

chaetochromin (**1.23**)

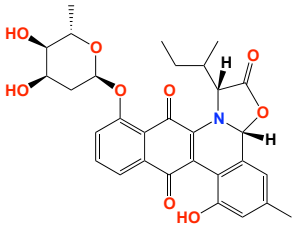

jadomycin B (**1.24**)

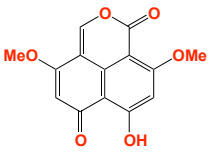

corymbiferone (**1.25**)

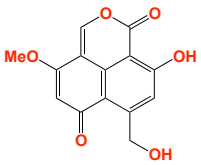

corymbiferan lactone I (**1.26**)

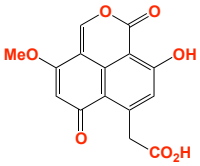

corymbiferan lactone II (**1.27**)

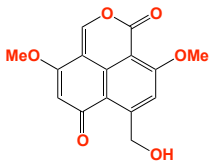

corymbiferan lactone III (**1.28**)

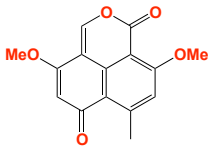

corymbiferan lactone IV (**1.29**)

1.5.2 Novel metabolites in co-cultures

The functional role of natural products in microbes has long been a topic of discussion. It was found that some natural products result from the interaction of the organism with its own environment. Cueto *et al.,* cultured a marine *Pestalotia* sp. with an unidentified antibiotic resistant marine bacterium, resulting in the biosynthesis of pestalone (**1.30**), a new benzophenone. This compound could not be detected when each strain was cultivated independently. Pestalone was found to be active against MRSA and vancomycin-resistant *Enterococcus faecium*.[41] The marine derived fungus *Emericella* sp. was challenged with the actinomycete *Salinispora arenicola*. This co-culture activated the production of two new cyclic depsipeptides, emericellamide A (**1.31**) and emericellamide B (**1.32**).[42] Latifi *et al*. reported another interesting example of the synergistic function of co-culturing in 2006. A co-culture between *Pseudomonas aeruginosa* and *Enterobacter* sp. stimulated *P. aeruginosa* to produce the blue pigment pyocyanin, (**1.33**).[43] To establish whether any other microorganism can induce the production of pyocyanin, *P. aeruginosa* was cultivated with different microorganisms. These results showed that *P. aeruginosa* lost its ability to produce pyocyanin when co-cultured with other microbes.[44] These related examples highlight the role that co-culture can play in the regulation of secondary metabolite production.

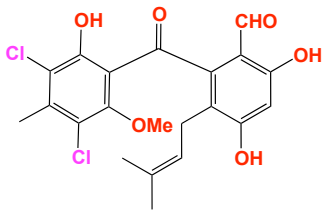

pestalone (**1.30**)

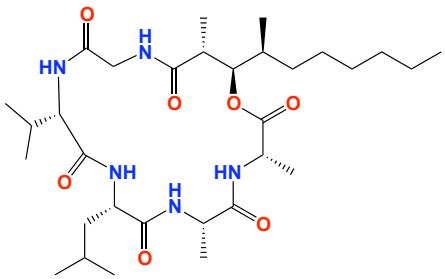

emericellamide A (**1.31**)

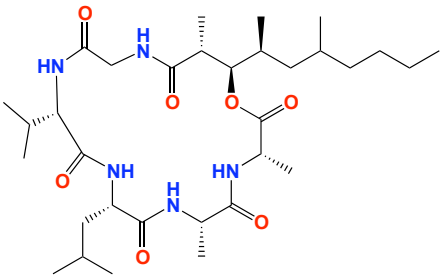

emericellamide B (**1.32**)

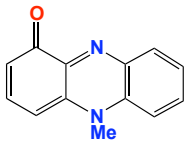

pyocyanin (**1.33**)

Although these strategies have been studied and can lead to promising results, it is nevertheless a time consuming and unpredictable process that while it can express silent metabolites, is not up to the challenge of activating the broad array of silent metabolites hidden within the global microbial genome. In order to access the microbial genome, new approaches informed by the microbial evolution need to be acquired.[45]

1.5.3 Autoregulators

Autoregulators are compounds that act as triggers to improve cellular development and activate silent secondary metabolite genes, leading to the production of secondary metabolites. Knowing that a microbe is genetically far more capable than previously suspected, reveals a potential, but activating that potential is another challenge entirely. Even without detailed knowledge of the microbial genome, early researchers enjoyed some success in stimulating microbial secondary metabolites. For example, it had been recognized that morphological differentiation during the growth of *Streptomyces* sp. was closely associated with the secondary metabolites production. More specifically, the transition from primary to secondary metabolism occurred simultaneously with the formation of the aerial hyphae. In exploring these phenomena a selection of low molecular weight metabolites were found to act as regulators of secondary metabolism.

1.5.3.1 γ-Butyrolactones of actinomycetes

The potential value of autoregulators as tools to regulate antibiotic production was quickly recognized, such that γ-butyrolactones came under intense investigation. An early example, of such

a regulator (called an autoregulator) discovered in 1979 was A-factor (**1.34**), a γ-butyrolactone produced by *Streptomyces griseus*. A-factor induced both aerial mycelium formation in *S. griseus* and production of the antibiotic streptomycin, with A-factor appearing prior to streptomycin production and disappearing before streptomycin reached its maximum level.[46]

In addition to its effect on streptomycin (**1.35**) production,[47] other achievements of A-factor included inducing the production of pristinamycins in a mutant strain of *S. pristinaespiralis*, in which pristinamycins biosynthesis was otherwise blocked, and initiating the production in *S. griseus* (under phosphate depletion) of the parasiticidal metabolites grixazones A and B (**1.36** and **1.37**). Other closely related naturally occurring microbial γ-butyrolactone autoregulators included the virginiae butenolides (**1.38**) (eg. VB-A), which activated the production of virginoamycin that consists of 75% virginamycin M_1 (**1.39**) and 25% virginamycin S_1 (**1.40**), IM-2 (**1.41**), which activated the production of showdomycin (**1.42**) and minimycin (**1.43**), and SCB1 (**1.44**), which activated the production of actinorhodine (**1.45**) and undecylprodigiosin (**1.46**). IM-2 is noteworthy in that it both activates and suppress secondary metabolism. For instance, biosynthesis of the antituberculosis antibiotic D-cycloserine by *S. lavendulae* was completely suppressed in the presence of IM-2. Further investigations into the autoregulation of microbial secondary metabolism revealed that this capability was not limited to γ-butyrolactones.

A limited selection of *Streptomyces* metabolites have been described as promoters of morphogenesis and secondary metabolism, and include the thiazole/oxazole peptide, the polyether pamamycin-607 (**1.47**) and the siderophore desferrioxamine E (**1.48**). Pamamycin-607 (**1.47**) plays an important role in the regulation of aerial mycelium production in 67% of *Streptomyces*.[48] Desferrioxamine E (**1.48**) simulates secondary metabolites production in different strains of actinomycetes such as *Streptomyces coelicolor*.[49] However there are some non-butyrolactone *Streptomyces* metabolites that have been discovered as promoters of secondary metabolites, including thiazole/oxazole peptide goadsporin. Goadsporin (**1.49**) is an oligopeptide consisting of 19 amino acids, which acts on the sporulation pathway and regulates secondary metabolites production for *Streptomyces*.[50]

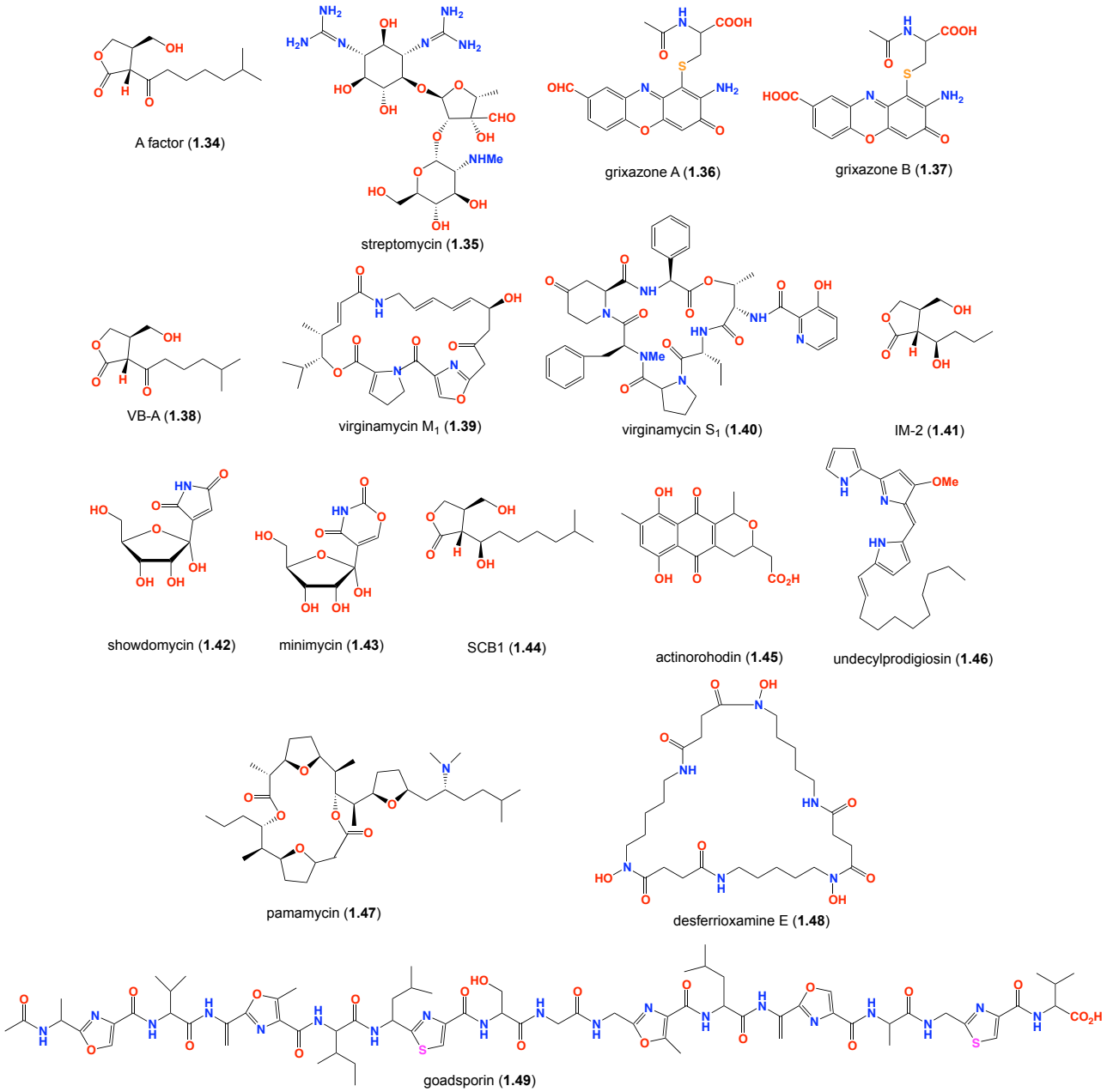

1.5.3.2 Homoserine lactones of Gram-negative bacteria

Acyl homoserine lactones (acyl-HSLs) are important intercellular signalling molecules used by many bacteria to monitor their population density in quorum-sensing control of gene expression.[51] These signals are synthesized by members of the LuxI family of proteins.[51] Homoserine lactones (HSLs) function by "quorum sensing" in which they reach a particular extracellular concentration due to high cell density. They act in bioluminescence, antibiotic biosynthesis, animal pathogenicity, plant pathogenicity and extracellular enzyme synthesis.[52] HSLs are similar in structure to A-factor. They can also induce exoenzymes, which are plant and animal virulence defense against *E. carotovora* and *P. aeruginosa* respectively.[53]

1.6 Genomics-inspired screening for novel natural products

The idea of screening extract libraries on different types of microorganisms has emerged as an important aspect to determine new metabolites. Microbial metabolites (gene activators) may be capable of eliciting the expression of silent secondary metabolism on other microbes. The activation of silent gene clusters will advance the discovery of next generation antibiotics. Zazopoulos *et al.*[54] analysed the genome of different actinomycetes looking for the genes that were responsible for the production "enydiyne" class of antitumor agents. These loci remain inactive until certain chemical or physical signals activate them. After optimizing the growth conditions, Zazopoulos *et al.*[54] were able to induce the expression of the gene cluster and leading to production of "enydiyne". In addition, McAlpine *et al*. scanned the genome of *Streptomyces aizunensis*. The genome scanning identified 11 gene clusters coding for the biosynthesis of wide range of bioactive metabolites. One of these gene clusters was responsible for the production of type I polyketide synthase generating a novel polyketide with characteristic UV absorbance at 300 nm. Varying the culture conditions helped trigger the biosynthesis of compound ECO-02301 (**1.50**).[34] Scanning the genome sequence of *Aspergillus nidulans* revealed the presence of three copies of genes that codes for proteins with high similarity to anthranylate synthases (ASs). These enzymes are responsible for the conversion of chorismate to anthranilic acid, which is important for the synthesis of tryptophan. By altering the cultivation conditions, four new prenylated quinoline alkaloids aspoquinolones I, II and III (**1.51** - **1.54**) were produced.[55]

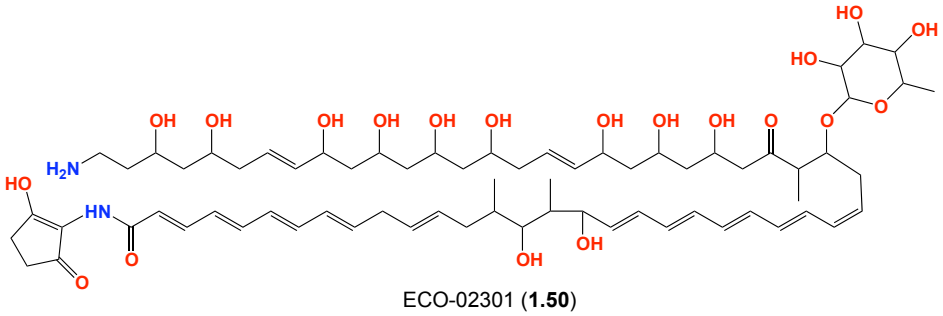

ECO-02301 (**1.50**)

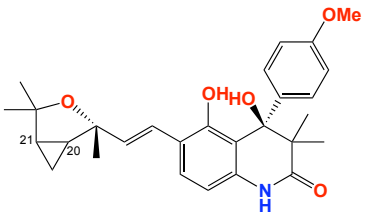

aspoquinolone I (**1.51**) 20 **(*S*)**; 21 **(*R*)**

aspoquinolone II (**1.52**) 20 (*R*); 21 (*S*)

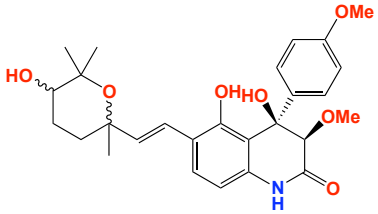

aspoquinolone III (**1.53/54**)

The strategy of epigenetic modifiers (gene activators) was further studied by many researchers. Some of these studies reported that *Aspergillus* sp. contains nuclear transcriptional regulator LaeA, that controls secondary metabolite production, suggesting the existence of different regulatory mechanisms that ensure secondary metabolites production at certain developmental stages or under specific environmental conditions.[56-58] Cichewicz *et al.* treated twelve fungi with several DNA methyltransferase and histone deacetylase inhibitors. Eleven strains were found to respond, with the production of new or enhancement of known natural products. One of these strains, *Cladosporium cladosporioides*, was treated with 5-azacytidine, and led to the production of oxylipins I, II and III (**1.55 - 1.57**).[59]

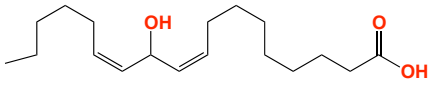

oxylipin I (**1.55**)

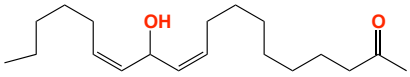

oxylipin II (**1.56**)

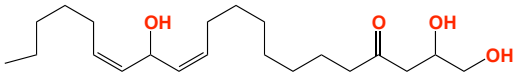

oxylipin III (**1.57**)

All these observations listed above highlight that the microbial genome offers for greater molecular potential that previously imagined, and that molecular tools are required to access this resource.

1.7 Focus of this thesis

This thesis focuses on the discovery of microbial secondary metabolites and the activation of microbial secondary metabolites. Putting this aspect as the main target, we started collecting different soil samples from regions in Australia to construct a terrestrial microbial library. We were able to screen this library together with some microbes from marine microbial library as well as the Australian collection of microbes (ACM) library that contains more than 5,000 different species of *Streptomyces* sp. In the same time, the microbioreactor technique had been used for screening the microbial libraries and constructing the microbial extract library which was subjected for both chemical profiling analysis using our HPLC-DAD-MS and biological profiling using our different biological assays (in house) as antimicrobial, cytotoxic, P-glycoprotein (P-gp), kinase, *Mycobacterium bovis* (BCG) assay (Figure 1.1). The second chapter reports the optimization conditions that have been performed in the microbioreactor to optimize the culture conditions. The third, fourth and fifth illustrates the activation of microbial secondary metabolites and the isolation of novel metabolites that possess biological activity. Chapter 4 illustartes the co-evolution between fungus and bacteria, Chapter 5 illustartes the isolation of new diketomorpholine metabolites and

explains its P-glycoprotein inhibiotor activity. The last chapters (Chapter 6,7 and 8) explain the isolation, structural elucidation and biological activity of the novel metabolites, desotamides, aranciamycins and citrinaline X.

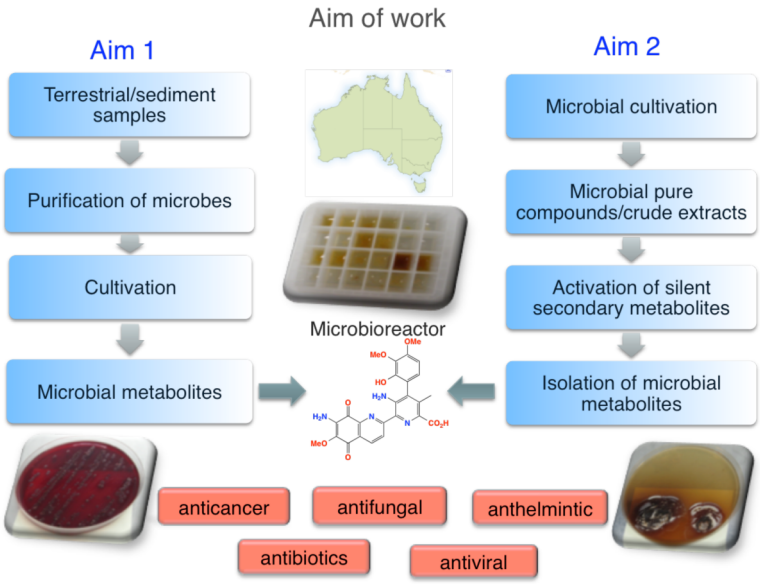

Figure 1.1. General figure for the PhD projects includes isolation of microbes, microbial secondary metabolites and activation of silent secondary metabolites

2 Chapter 2. Developing a Micro-bioreactor technique for Microbial cultivation

2.1 Introduction

Microbial (bacterial and fungal) secondary metabolites remain an important source for molecular diversity that can improve drug discovery. Traditional microbial biodiscovery employs to liquid and solid phase culture approaches. Small-scale cultivation in either liquid or solid phase is considered the preferred means for initial discovery "lead identification" for natural products. Small-scale liquid cultivations are typically performed in shake flasks (10 – 80 mL), which can be time consuming and costly exercise when dealing with hundreds to thousands of isolates. Notwithstanding these limitations, shake flasks have been used for cultivating microbes since 1940, and are still the method of choice for many laboratories.[60] Major limitations of shake flasks are their reliance on surface aeration, which may lead to reduction in the oxygen transfer.[61] Some researchers have experimented the use of flaks with baffles which can increase the oxygen transfer rate at lower shaking frequencies, however, at high speeds this can lead to splashing that can lead to oxygen starvation which in turn slows the cell growth and likely alters secondary metabolite production.[62] There is a clear need for an innovate new approach to facilitate high-throughput small-scale culture of microbes, for the purpose of biodiscovery.

2.1.1 Progression from shake flasks to micro-bioreactors

Microscale culture technology has attracted great interest in recent years. Among some microbiologists, microtiter plates (MTP) have become an alternative technique for optimizing cultivation conditions. The use of small-scale liquid cultivation volumes is viewed as fast and effective. The number of wells contained in MTPs range from 6, 12, 24, 96 to 384, and allow for high-throughput cultivation and screening.[63] Duetz *et al*. developed a cultivation system to make use of 24 or 96-well square-shape micro-bioreactor plates (MBR).[64] Oxygen transfer rate in this system was 38 mmol O_2/L/h in 0.5 mL culture, while 18 mmol O_2/L/h in 1 mL culture volume. For example, this cultivation system allowed *Pseudomonas putida* to grow on glucose minimal medium (18 h) and reach a cell density of 9 g (dry weight)/L. To prevent cross contamination between the cultures during shaking, the MTP was covered with a spongy silicone layer (8 mm thick) perforated with holes (1.5 mm diameter) positioned directly above the centers of the wells. This spongy

silicone layer was covered with a rigid polypropylene layer with 96 holes 6 mm in diameter and the whole system was capped with stainless steel sandwich cover.[65]

2.1.2 Different types of micro-bioreactors

In 2000, Wolfgang *et al.*[64] used the 96-well MTP from Duetz *et al*. to study the growth and production of secondary metabolites on different *Streptomyces* strains in micro-cultures, assessing the growth of mycelium-forming *Streptomyces* strains cultivated in one mL liquid micro-cultures versus large Erlenmeyer flasks. The flasks were filled with the appropriate media required for the growth of *Streptomyces* to 1/5 of the total volume and incubated at 30 °C for 15 days with 300 rpm in an incubator shaker. In the same time, liquid micro-cultures containing one mL broth media were incubated at the same conditions. This study reported that the evaporation rate of the culture volume was minimal (4 to 7.5%) and proved that the cell density weight (CDW) was much better in the micro-cultures than the flask. These authors also performed a time-course study on secondary metabolite production for 5 *Streptomyces* strains, confirming that secondary metabolites production was the same between micro-cultures and flasks, with very small culture to culture deviation.[64] In 2005, Harms *et al*.[66] demonstrated two high quality bioprocessing micro-bioreactors for commercial use, both consist of the 24-well format. The difference between these reactors was that the first lacks a plate seal and requires the use of a laminar flow hood. By comparison, the second system employed a sterilized plate cap, and a motor for agitation control. Both contained optical sensors for monitoring pH and dissolved oxygen. In 2005, Kensy *et al.*[67] developed a new method to measure the dissolved oxygen and pH in standard 24-well MTP using fluorophores at the bottom of the 24-well MTPs. This new technology consists of sensor dish reader for 24-well MTP. The reader consists of controller and 24 optical read out units placed in the center below each well. This new method provided continuous measurements for different parameters in 24-well MTPs during shaking. The drawbacks for this method were fluctuations in the light intensity, scattering of light and auto fluorescence within same culture. All these systems contributed to the evolution of a more robust model system.

2.1.3 Applikon system

Applikon Biotechnology® developed a micro-bioreactor cultivation system (Figure 2.1), which turns microtiter plates into reliable and easy operating cultivation systems for microbes, which reliable, easy to operate, and offers reproducible cultivation results. Applikon micro-bioreactor is available in both 24 and 96 well microtiter plate formats. Both formats provide benefits compared

to shake flasks that include, (1) lower cost, (2) stackable design - lower footprint, (3) comparable performance - cell density, (4) no well-to-well contamination and (5) well-to-well reproducibility.

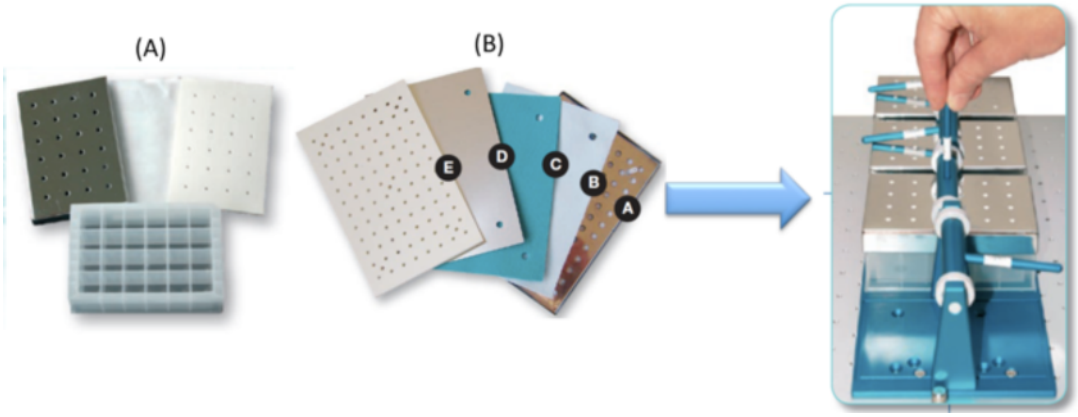

Figure 2.1. Applikon bioreactor system; (A) 24-well microbioreactor plate, (B) stainless steel cover plus sandwich covers

2.1.4 Chapter outlines

While the Applikon micro-bioreactor has been used by a number of microbiology laboratories, to the best of our knowledge this technology has not been employed in a microbial biodiscovery format. To develop high-throughput (HTP) microbial biodiscovery methodology based on this system, we needed to independently test and validate a number of critical hypotheses – that go to the issues of efficacy, reproducibility, HTP practicality and HTP versatility.

Efficacy: Micro-bioreactor technology will generate secondary metabolite yields and diversity comparable to shake flasks.

Reproducibility: Micro-bioreactor technology will return high levels of reproducibility, particularly in secondary metabolites yields and diversity.

HTP practicality: Micro-bioreactor technology produces a practical HTP format that does not suffer from well-well cross contamination.

HTP versatility: Micro-bioreactor technology provides a HTP format suited to multiple culture media.

To test these hypotheses, the bacterial isolates CMB-TB365 and CMB-TB385, obtained during a program of environmental sampling (see Chapter 10) were chosen for these studies. These studies were carried out in duplicate/triplicate in a 24 well micro-bioreactor format, with each well extracted in situ with EtOAc (2 mL), decanted, concentrated under N_2, re-constituted to approximately 1 mg/mL in MeOH, and analyzed by HPLC-DAD-MS.

2.2 Results and discussion

2.2.1 Efficacy

To test the efficacy hypothesis, twenty microbes were chosen from the microbial library (Chapter 10) and cultivated in the micro-bioreactor and shake flask. After the cultivation period, the cell biomass and crude extracts weight were determined.

2.2.1.1 Biomass and crude extract determination in the microbioreactor and flask

From the microbial library, the effect of microbioreactor on the microbial cultivation was tested and the results were compared to the culture conditions in the shake flasks. Therefore, 20 different microbes (15 actinomycetes and 5 fungi) were chosen from the terrestrial library. The microbes were cultivated in both microbioreactor and Erlenmeyer flask (250 mL). In the microbioreactor, broth (1.5 mL) was added to the wells in the presence of microbe, while in the shake flask, broth (80 mL) was added in the presence of the microbe. Both the micro-biorecator and the flasks were incubated at 26 °C, 190 rpm. After the incubation period, the broth in the microbioreactor was extracted by the addition of 2 mL EtOAc and the plate was shaken for another 30 min. In the shake flask, the broth was extracted with EtOAc (80 mL × 3). The crude extract from the microbioreactor was dried under N_2 while the crude extract from shake flask was dried *in vacuo*. At the same time, the colonies from both experiments were centrifuged and dried down in the biological hood for 24 h. This study showed that there is almost no difference between the microbioreactor and the flask, the microbes (actinomycetes or fungi) were cultivated and grew to an optimum concentration in which they were capable to express their secondary metabolites as shown in Figure 2.2 and Figure 2.3.

From the micro-bioreactor, the cell dry weight (CDW) was determined by collecting the broth and biomass attached to the walls. The entire cells were filtered through pre-weighed filter paper and the filter was washed twice with water and left to dry at room temperature. CDW in the shake flask cultivations was determined by withdrawing 5 mL samples from the broth, followed by filtration, washing and drying steps.

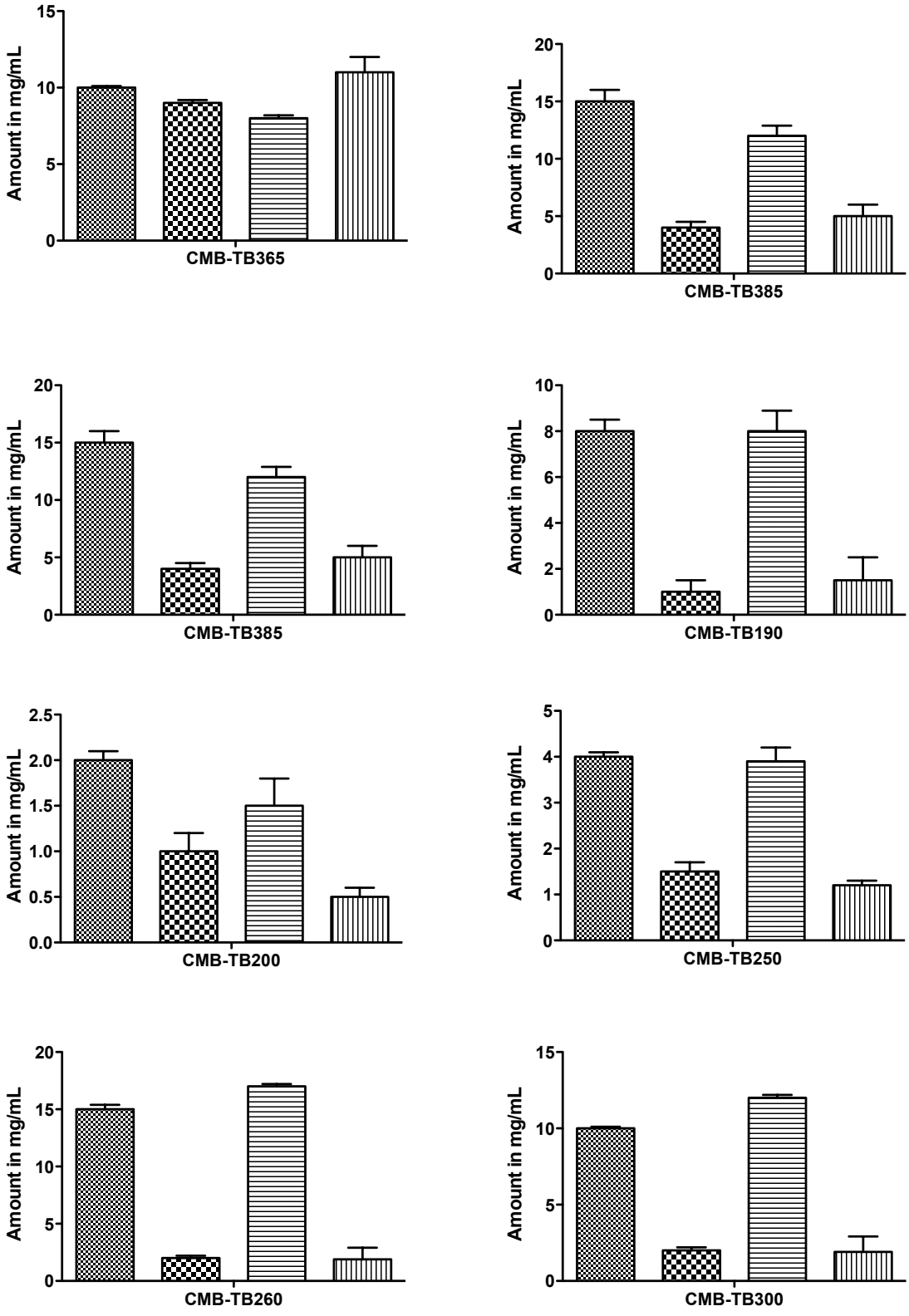

Figure 2.2. Study showing a comparison between the microbioreactor and shake flask, colonies from micro-bioreactor ( ), crude extract from micro-bioreactor ( ), colonies from shake flask ( ) and crude extract from shake flask ( ) for different microbes. CMB-TF = terrestrial fungi, CMB-TB = terrestrial bacteria

Continued Figure 2.2

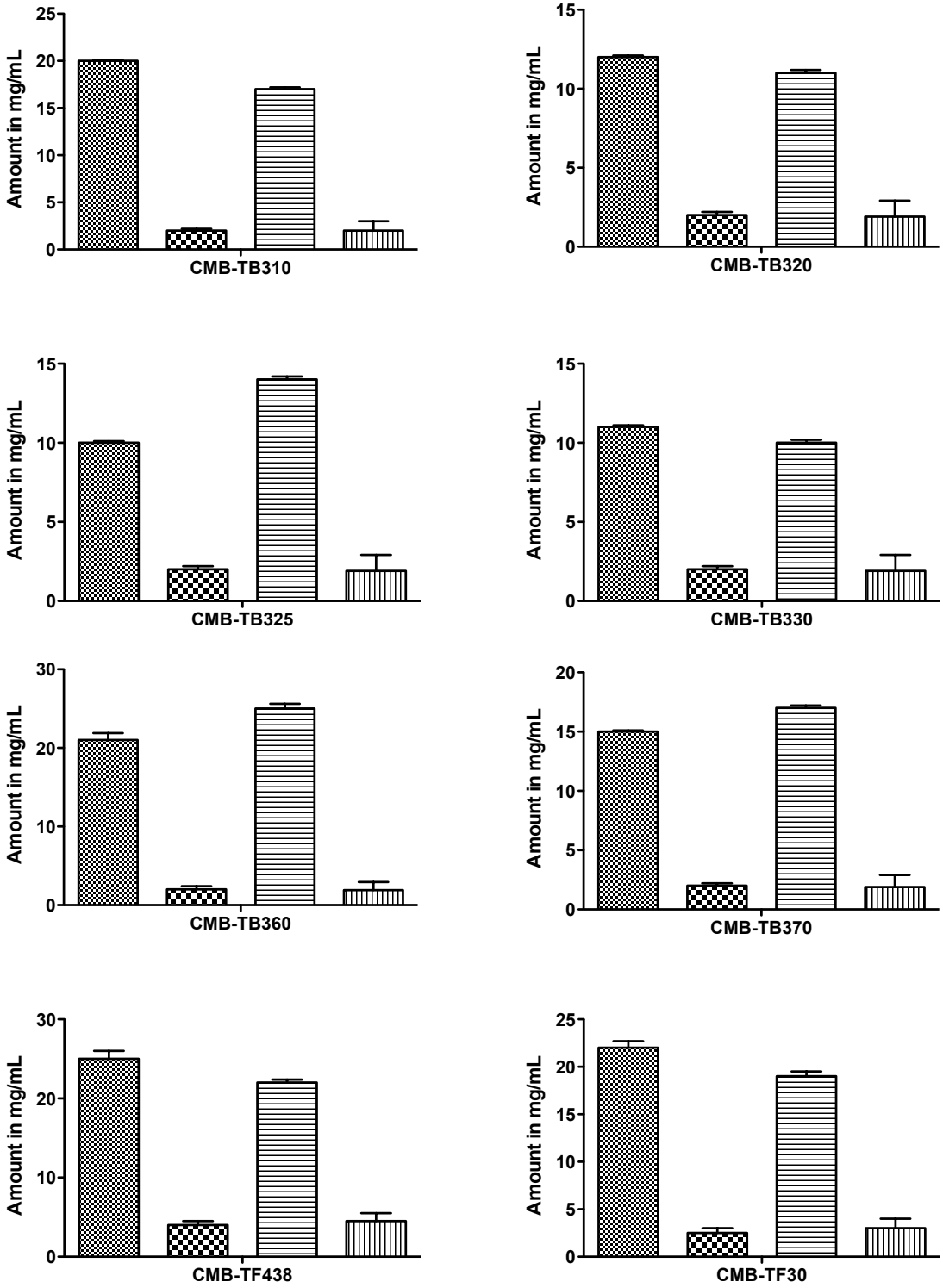

Figure 2.2. Study showing a comparison between the microbioreactor and shake flask, colonies from micro-bioreactor ( ), crude extract from micro-bioreactor ( ), colonies from shake flask ( ) and crude extract from shake flask ( ) for different microbes. CMB-TF = terrestrial fungi, CMB-TB = terrestrial bacteria

Continued Figure 2.2

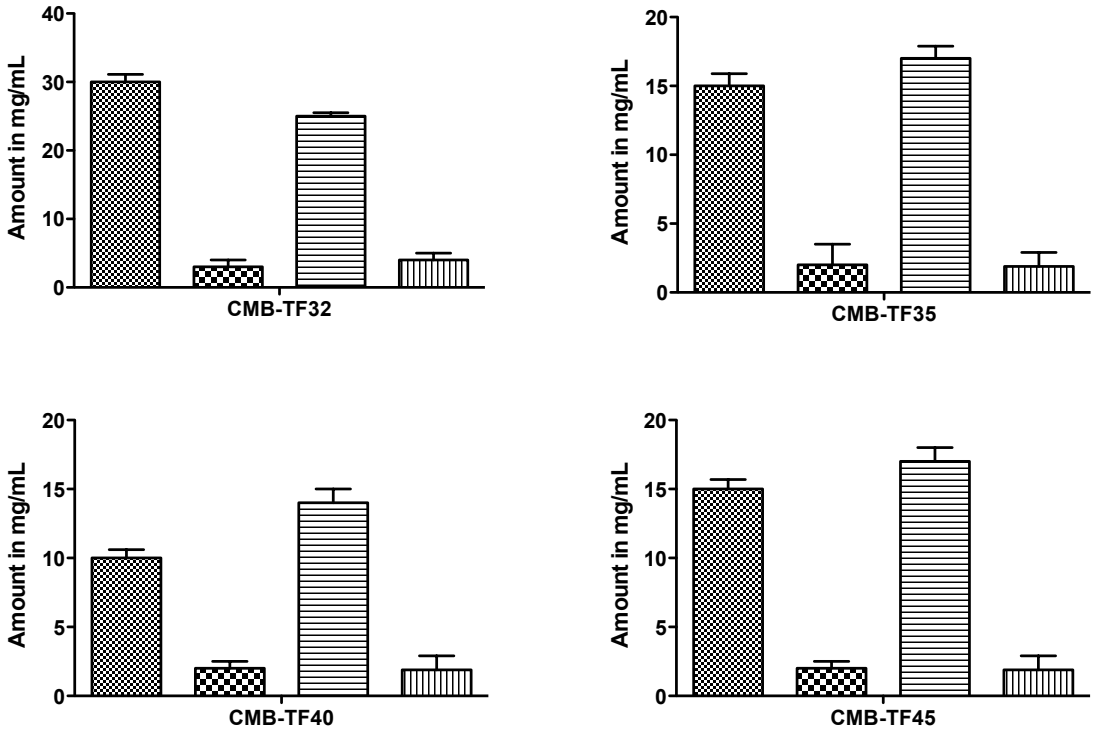

Figure 2.2. Study showing a comparison between the microbioreactor and shake flask, colonies from micro-bioreactor (▨), crude extract from micro-bioreactor (▩), colonies from shake flask (▤) and crude extract from shake flask (▥) for different microbes. CMB-TF = terrestrial fungi, CMB-TB = terrestrial bacteria

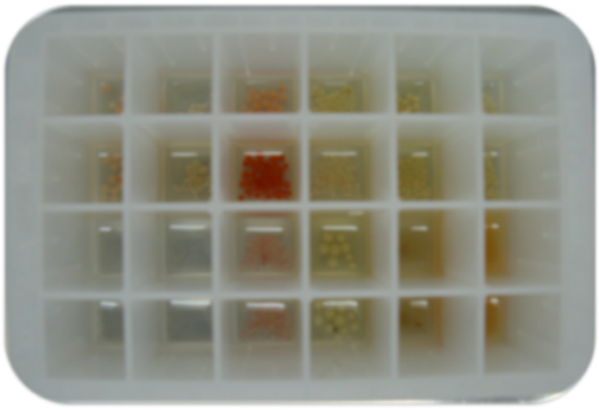

Figure 2.3. Picture for the micro-bioreactor showing the growth of different microbes

All the above experiments were performed in triplicate and therefore we can conclude that the amount of cell mass and crude extracts was efficient compared to the shake flask. In fact in some cases the growth of microbes in the micro-bioreactor was far much better than the shake flask.

2.2.2 Reproducibility

After proving that the microbioreactor is capable of allowing the microbes to grow without affecting the microbial growth and the microbial secondary metabolites expression. We mainly focused on two actinomycetes strains CMB-TB365 and CMB-TB385 due to their capability of producing different metabolites.

2.2.2.1 Case study #1 for CMB-TB365

2.2.2.1.1 Growth phase-dependent production of secondary metabolites for CMB-TB0365

Growth of CMB-TB365 in the micro-bioreactor (1.5 mL) was compared to the growth in the shake flask (80 mL). Twenty wells of 24 wells of micro-bioreactor were each filled with M1 broth (1.5 mL) and spore taken by the loop. The growth stages of actinomycetes CMB-TB0365 in liquid culture in both the micro-bioreactor and the flask were determined by extracting the broth with EtOAc (2 mL) from every well. The crude extracts were dried down under N_2, re-dissolved in MeOH and analysed using HPLC-DAD-MS and measured spectrophotometrically at 400 nm. Samples (50 μL) were withdrawn from each well aseptically and transferred into a flat bottom microtiter plate for spectrophotometric analysis (Figure 2.4). Since the cultivation of CMB-TB365 was conducted over extended period of time, it was important to observe that after 7 days of cultivation the loss of culture volume due to evaporation was minimal. There was almost no difference between the cultivation process on the micro-bioreactor and shake flask (Figure 2.5).

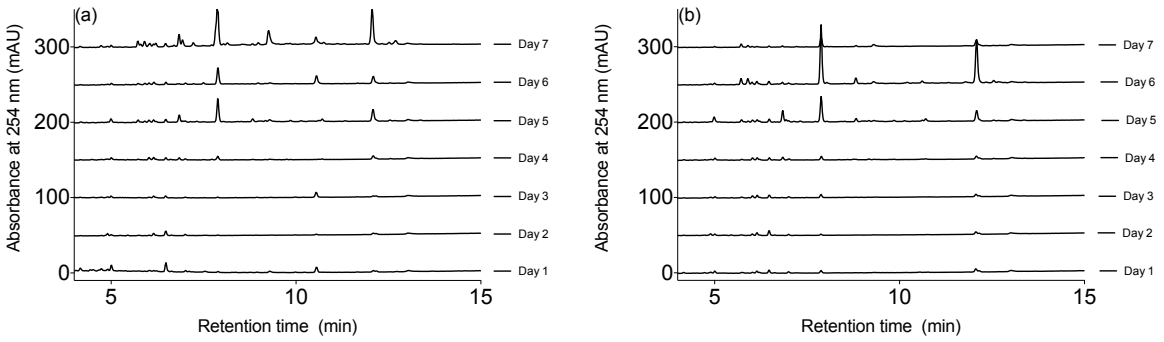

Figure 2.4. HPLC-DAD chromatogram of analytical gradient H_2O/MeCN plus 0.05% HCO_2H, using Zorbax C_8 for the crude extract from strain CMB-TB365 over incubation period from 1 to 7 d in (a) the micro-bioreactor and (b) shake flask

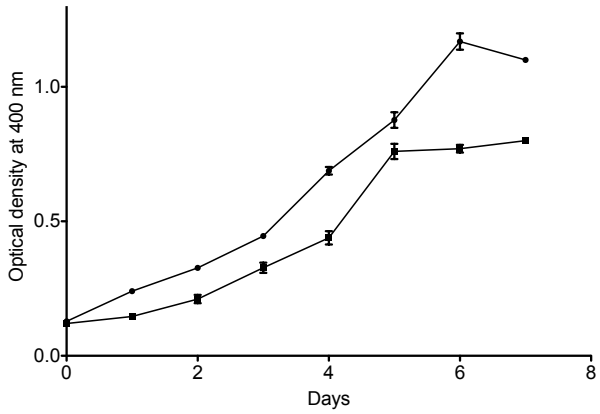

Figure 2.5. Time course of secondary metabolite production for strain CMB-TB365 during 7 d of cultivation in micro-bioreactor (1.5 mL) and shake flask. Filled circles represent the crude from micro-bioreactor while filled squares represent the crude extract from shake flask.

2.2.2.2 Case study #2 for CMB-TB385

2.2.2.2.1 Growth phase-dependent production of secondary metabolites for CMB-TB0385

The same procedure described above was repeated with strain CMB-TB385 (Figure 2.6 and Figure 2.7).

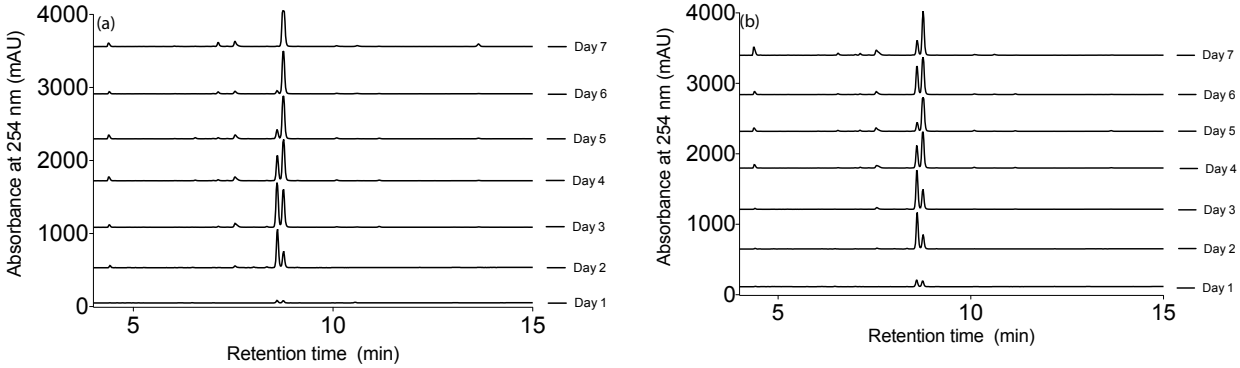

Figure 2.6. HPLC-DAD chromatogram of analytical gradient H_2O/MeCN plus 0.05% HCO_2H, using Zorbax C_8 for the crude extract from strain CMB-TB385 over incubation period from 1 to 7 d in (a) micro-bioreactor and (b) shake flask

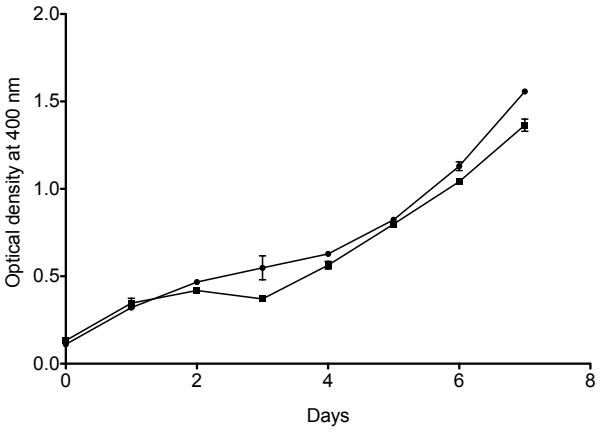

Figure 2.7. Time course of secondary metabolite production of strain CMB-TB385 during 7 d of cultivation in micro-bioreactor (1.5 mL) and shake flask (80 mL). Filled circles represent the crude from micro-bioreactor while filled squares represent the crude extract from shake flask.

The progress of microbial cultivation in the micro-bioreactor was compared with parallel cultivations carried out by the same organism in both micro-bioreactor and shake flask. Both OD and HPLC-DAD-MS monitored growth of microbes and secondary metabolites production in the micro-bioreactor and shake flask. In the micro-bioreactor, the growth of the two strains CMB-TB365 and CMB-TB385 was slightly higher than the shake flask which could be attributed to the small cross sectional dimensions in the micro-bioreactor that gives rapid heat and mass transfer. The crude extract production was monitored and it was observed that the amount of crude extract was not affected by cultivation the microbes in the micro-bioreactor, in fact we proved that the micro-bioreactor can allow the microbe to grow and produce crude extract that is enough to be analysed using HPLC-DAD-MS.

2.2.3 Practicality

To further evaluate the performance of micro-bioreactor, the hypothesis of practicality was tested in order to determine that there is no risk of cultivating both actinomycetes and fungi in the same plate, different microbes were cultivated from the microbial library in the presence of media (1.5 mL). The media in the micro-bioreactor was inoculated with a single colony from a seed culture cultivated on ISP-2 agar plate. After inoculation, the plates were incubated at 26 °C, 190 rpm for 7 days (Figure 2.8).

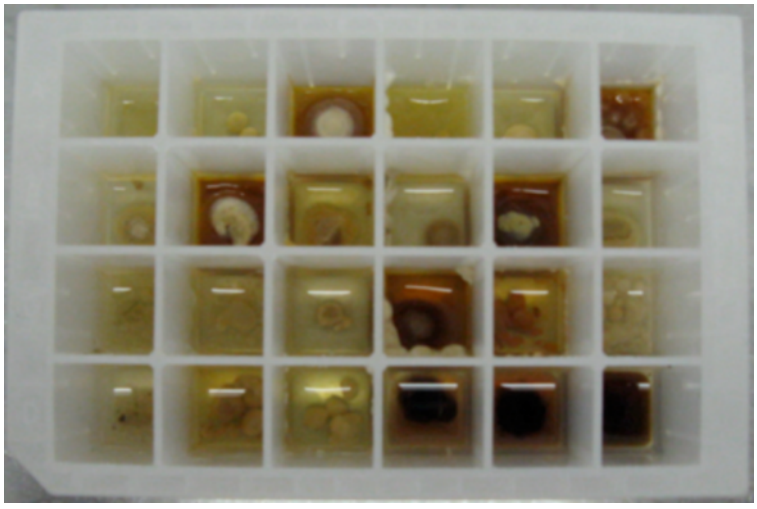

Figure 2.8. Micro-bioreactor showing the growth of different fungi and actinomyetes

2.2.4 Versatility

To test the hypothesis of versatility, two microbes (CMB-TB365 and CMB-TB385) were cultivated in different media.

2.2.4.1 Case study #1 CMB-TB365

The study on the production of secondary metabolites on CMB-TB365 was evaluated on 12 different media. The media was inoculated from the plate containing the spores. An aliquot of each media (1.5 mL) was dispensed into 24 wells of the micro-bioreactor and incubated at 26.5 °C for 7 d, 190 rpm. After the incubation period, the broth was extracted with EtOAc (2 mL) and the organic layer was dried under N_2, re-dissolved in MeOH and analysed using HPLC-DAD-MS. The results show that the maximum growth rates and secondary metabolite production were different for the same strain on different media. However, CMB-TB365 showed the best production on M8 and M1 media. These results were not surprising as we expected that the microbes could behave differently when cultivated on different media but it emphasis the capability of the microbe to grow in the micro-bioreactor (Figure 2.9).

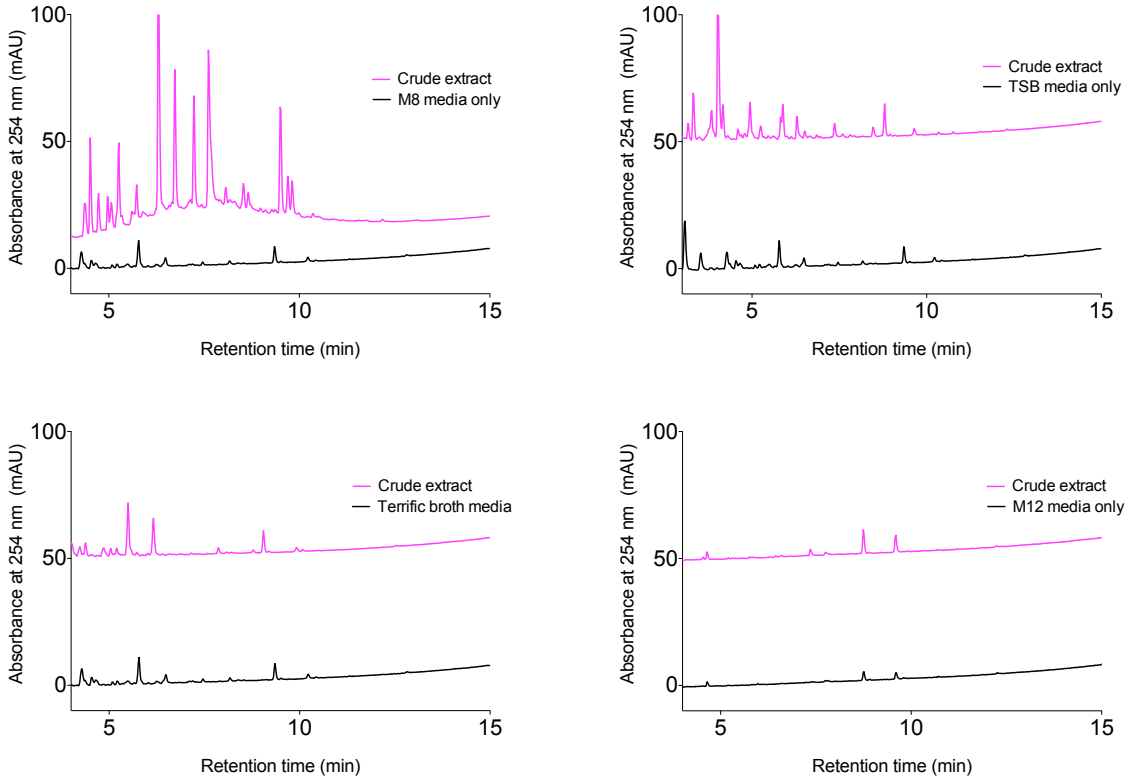

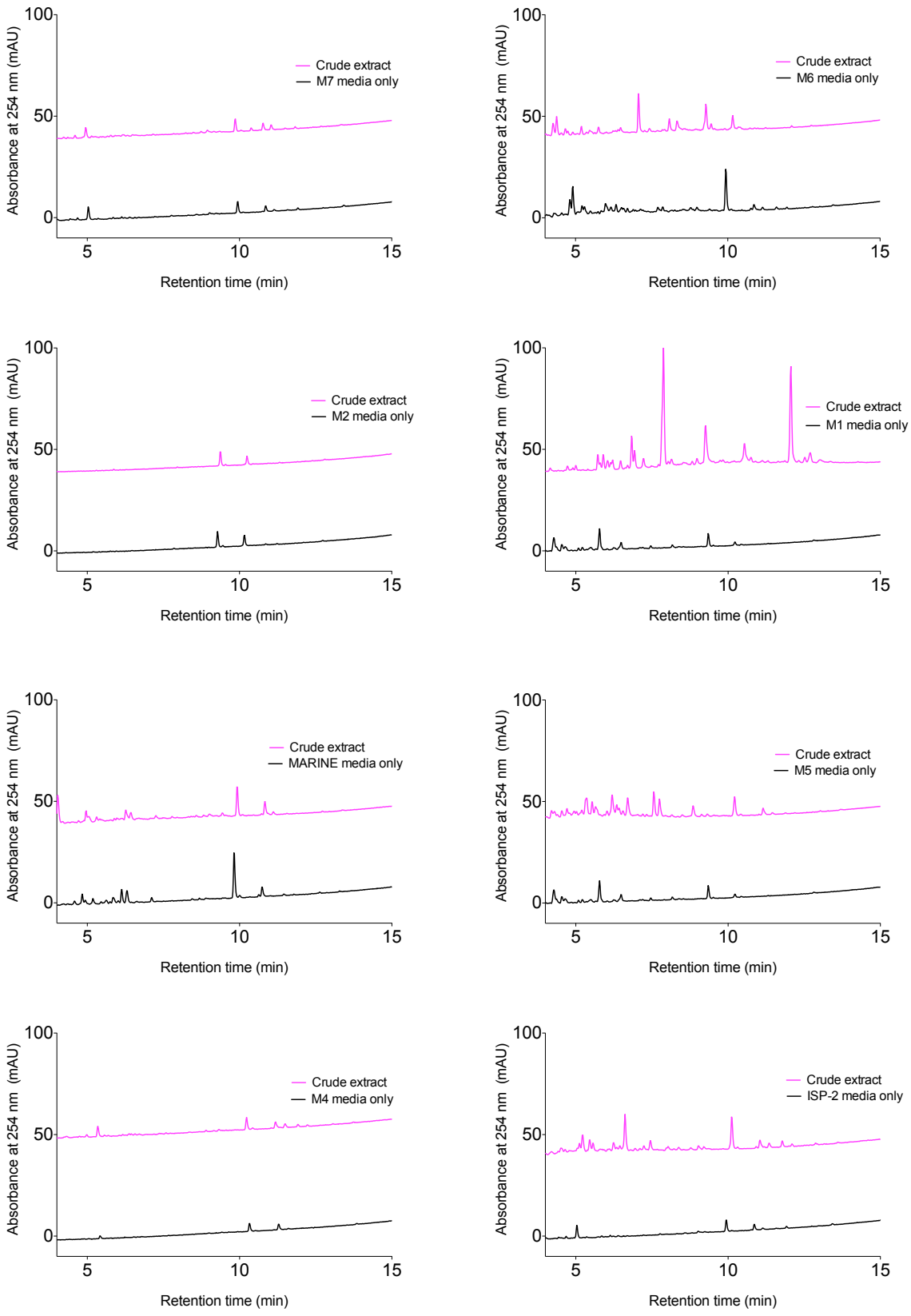

Figure 2.9. HPLC-DAD chromatograms of analytical gradient, H_2O/MeCN plus 0.05% HCO_2H using Zorbax C_8 for the crude extracts from CMB-TB365 cultivated in different media in the micro-bioreactor

2.2.4.2 Case study #2 for CMB-TB385

As discussed earlier with strain CMB-TB365, the same procedure had been repeated with strain CMB-TB385 using the same twelve media (Figure 2.10).

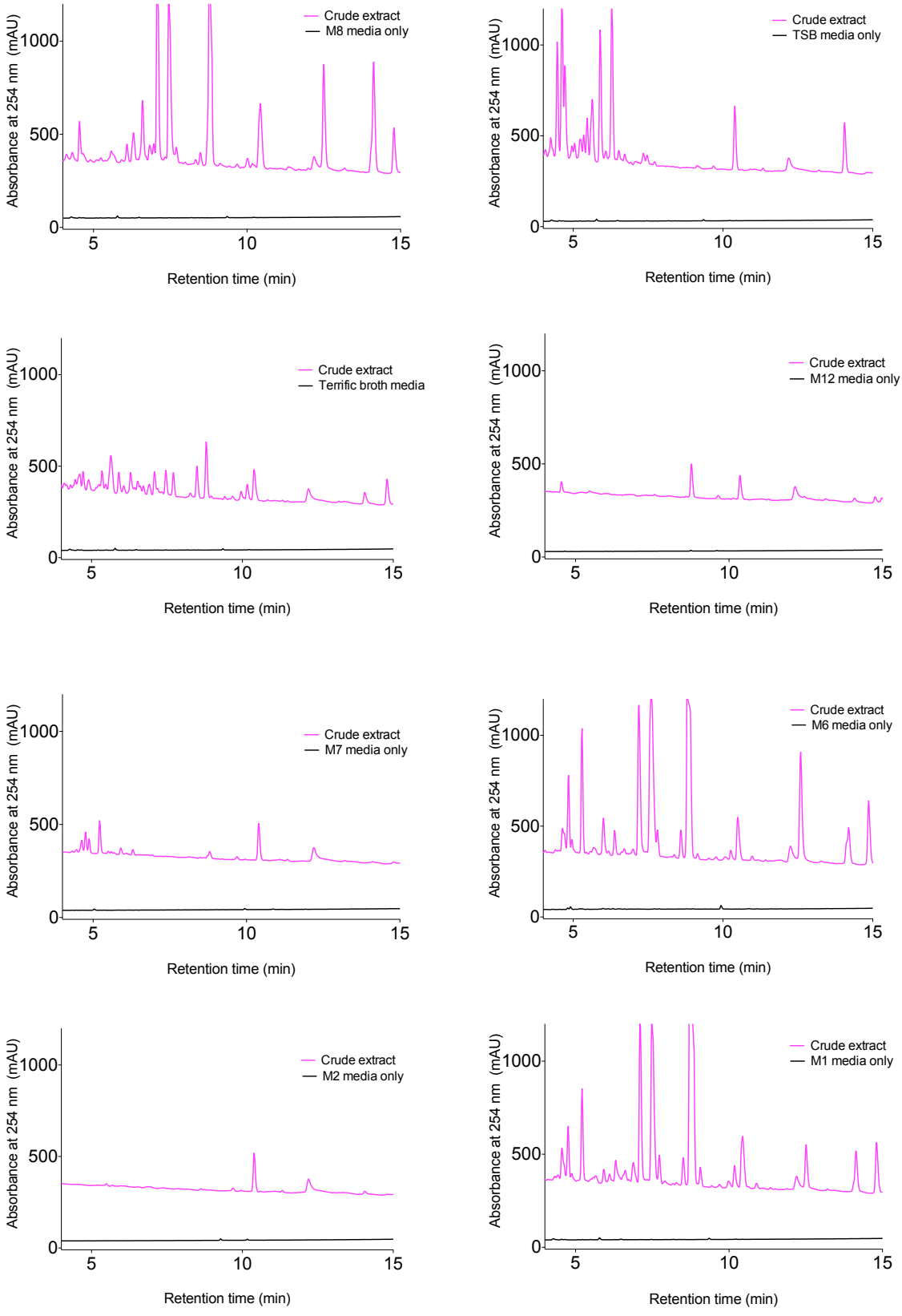

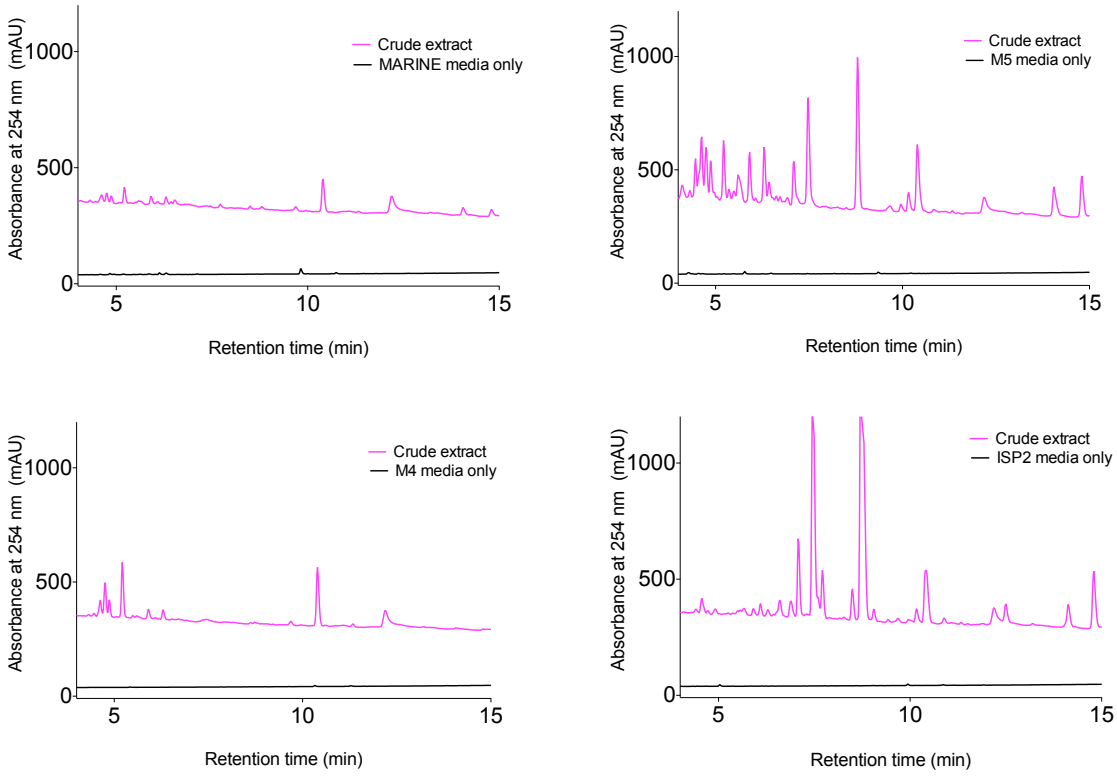

Figure 2.10. HPLC-DAD chromatograms of analytical gradient, H_2O/MeCN plus 0.05% HCO_2H using Zorbax C_8 for the crude extracts from CMB-TB385 cultivated in different media in the micro-bioreactor

These results were similar to the one from CMB-TB365, in which CMB-TB385 was capable to grow and produce its secondary metabolites when cultivated on ISP2, M5, M1 and M6.

2.3 Conclusion

We have demonstrated that the simple and low cost micro-bioreactor can speed up the bioprocessing techniques by using small amount of reagents and very few seed cultures. The results obtained from the micro-bioreactor were parallel to the ones obtained from the shake flask, in fact in some cases the growth of the microbes in the micro-bioreactor was superior to the shake flask. The microbioreactor has the potential of replacing the normal conventional scale process and offers a high-throughput efficient and analytical technique in addressing some of the challenges encountered in bioprocessing starting that includes bacterial growth and secondary metabolites production. In our case studies, we proved that microbes were capable of growing in the micro-bioreactor and the production of microbial secondary metabolites was reproducible and detectable in HPLC-DAD-MS.

In this respect, it was notable to start use this new micro-bioreactor cultivation system and to carry out further studies in the chemical profiling for microbes. In order to perform these tasks, the

system had been optimized in respect of the culture volume, method of extraction, colonies dry weight and secondary metabolites profiling. Around 20 different microbes have been chosen for the study, in which the biomass yields were similar or better than in the shake flask. Secondary metabolites production were further studied on two *Streptomyces* sp. strains with codes (CMB-TB365 and CMB-TB385). Secondary metabolites levels were within the range compared to those determined in the shake flask. Comparison between different media showed the almost the same metabolites production in the shake flask and micro-bioreactor. In the case of fungi the higher surface to volume ratio in the square wells of micro-bioreactor compared to shake flask provided a good substrate for the attachment, growth and morphological differentiation in which the aerial hyphae formulation and sporulation were observed. Also, there was no signs of cross contamination when cultivating both the fungi and actinomycetes in the same plate, which make it a good tool for screening different microbes in the same place. This new technique allows the cultivation of large number of microbes and generation of the microbial crude extract library (220) in which their biological activity were screened against our in house biological assay and continue working on the hits (chapter 3).

In conclusion, this new micro-bioreactor technique facilitates cost- and labour-efficient, massive reproducible cultivations of different microbes including actinomycetes and fungi suitable for screening purposes or activation of microbial secondary metabolites studies.

2.4 Experimental section

2.4.1 Cultivation of strains for chemical profiling

2.4.1.1 Actinomycetes

Strains were chosen from the terrestrial library for chemical investigation depending on their chemical profiling as well as their morphological appearance. A primary culture of the strain was started using the total volume of the preserved frozen stock as a seed culture in 100 mL of media in a shake flask at 190 rpm for 7 – 10 d. After the cultivation period, the whole culture was extracted with EtOAc (100 mL × 3), and the decanted EtOAc extract was concentrated *in vacuo*. Chemical profiling was achieved by HPLC-DAD (Zorbax C_8 analytical column, 150 × 4.6 mm, 5 μm, eluting with 1.0 mL/min 90 – 0% H_2O/MeCN (0.05% HCO_2H modifier) over 15 min, then held for 5 min) and detecting at 210 and 254 nm (DAD). Archived crude extracts were stored at −32 °C in 96 well microtiter plate.

2.4.1.2 Fungi

Fungi colonies were inoculated onto agar petri dish from cryo-preserved stock. After 5 – 10 d, agar subculture samples (approx. 1.5 cm^3) were excised from the plate and used to inoculate broth media (80 mL) in a shake flask. Cultivation conditions and media used were identical to those used for actinomycetes. Archived crude extracts were stored at −32 °C in 96-well microtiter plate for further investigation.

2.4.2 Growth phase studies

2.4.2.1 Growth phase-dependent production of secondary metabolites for both strains CMB-TB0365 and CMB-TB0385

Two strains CMB-TB0365 and CMB-TB0385 were chosen to be cultivated with the crude extract library for the activation of secondary metabolites production. These strains were cultivated for 7 d in M1 and ISP-2 broth media respectively at 190 rpm. Liquid micro-cultures were cultivated in polypropylene deep well plates with 40 mm deep wells and cross section of 17 × 17 mm. The plates were covered by the sandwich covers. The sandwich covers were designed to provide headspace refreshment. They consist of stainless steel lid for rigid support, micro fibre layer, extruded or ePTFE (0.2 μm pores) for sterility and soft silicone layer to seal the mini-reactors. These sandwich

covers also act to secure the oxygen concentration and to limit the evaporation of water. These micro-cultures enclosed 1.5 mL broth and inoculated with spores from the seed culture. Plates were put on cover clamp and then mounted on orbital platform shaker and incubated at 26.5 °C with shaking at 150 rpm. For the micro-bioreactor and the flask, metabolites productions in liquid cultures were determined by withdrawing 50 μL everyday to measure the OD at 400 nm. At the same time, for the micro-bioreactor, 1.5 mL ethyl acetate was added to one well daily. The plate was incubated for 2 h and then the ethyl acetate layer was transferred to 8 mL vial and concentrated to dryness under N_2. For the flasks, 1 mL of the culture broth was withdrawn into 8 mL vial and then 1 mL of EtOAc was added, then the EtOAc layer was concentrated to dryness under N_2. The crude extracts were solubilised in 100 μL MeOH. The extracts were analysed using Zorbax C_8 analytical column, 150 × 4.6 mm, 5 μm, eluting with 1.0 mL/min 90 – 0% H_2O/MeCN (0.05% HCO_2H modifier) over 15 min, then held for 5 min and detecting at 210 and 254 nm (DAD).

2.4.2.2 Effect of different media on the secondary metabolites produced by Strain CMB-TB0365 and CMB-TB0385

The expression of secondary metabolites might depend on the culture conditions especially the media components. Therefore, 12 different media were selected from the literature (Appendix 1) for the cultivation of CMB-TE0385. These twelve media were prepared in duplicate as water and ocean seawater based media.

In this experiment, 1.35 mL from each medium was transferred to a 24 well microtiter plate. Then 15 μL of the seed culture of strain CMB-TB0365 and CMB-TB0385 was transferred to all the wells. The plates were incubated on linear shaker 190 rpm at 26.5 °C for 7 d. After the incubation time, 2 mL of EtOAc was added to all the wells and the plates were further shaken for another 2 h. The organic layer was then transferred to 8 mL vial and dried under N_2. The crude extract was subjected to chemical profiling using the CMB standard gradient, Zorbax C_8 analytical column, 150 × 4.6 mm, 5 μm, eluting with 1.0 mL/min 90 – 0% H_2O/MeCN (0.05% HCO_2H modifier) over 15 min, then held for 5 min and detecting at 210 and 254 nm (DAD).

3 Chapter 3. Activation of Microbial Secondary Metabolites

3.1 General outlines

Chapter 1 raised the importance of activating microbial secondary metabolites noting the need for new tools to access the full microbial genome, while Chapter 2 commented on the construction and operation of a micro-bioreactor, and its validation against multiple strains, plus reproducibility of yields and productivity. Chapter 3 looks more closely as the challenge of activating microbial secondary metabolite production. It is well known that altering culture conditions (i.e media composition, temperature, pH, etc.) can lead to significant changes in the expression of microbial secondary metabolites. Although this technique has been successfully used for over a century, it is nevertheless a somewhat unpredictable process that to date has still failed to activate the full suite of "silent" metabolites. This chapter seeks to address the questions of how to activate silent secondary metabolites by looking for nature chemical cues that stimulate metabolism. This study explored two different sources of chemical cues; (1) microbial crude extracts, (2) lipopolysaccharide (LPS) from the Gram-negative bacterium (*Escherichia coli*).

3.1.1 Microbial crude extracts

It is quite evident that microbial (bacteria or fungi) crude extracts contain several important bioactive compounds and some have already shown their therapeutic activity. Unfortunately, most of the compounds have not properly been evaluated for the exploration of new lead molecule. Moreover, some of the mechanisms of actions of few bioactive compounds have not been identified so far. Hence, extensive research is required to find out the activity of compounds in the microbial crude extracts and to exploit their therapeutic potential to unlock silent secondary metabolites. Therefore, this study aimed to develop a new program through extensive investigation of the bioactivity of crude extracts isolated from different microbes including actinomycetes and fungi. This chapter will explain the construction of microbial crude extracts library using the micro-bioreactor technique and the usage of this library to activate microbial secondary metabolites in microbes.

3.1.2 Lipoplysaccharide

The lipolysaccharide (LPS) is the main component of the cell wall of all the Gram-negative bacteria. The composition of the cell wall of the Gram-negative bacteria is made up of an outer membrane, inner plasma membrane and a peptidoglycan layer in the periplasm. The inner cell wall

is mainly considered of phospholipids while the outer surface of the outer membrane is composed of 90% LPS, plus the addition of some phospholipids and proteins. LPS consists of phospholipids in which the hydrophilic portion contains different polysaccharide made of core and outer portion.[68,69]

LPS is a tripartite molecule comprising a membrane-anchored lipid A moiety, a core oligosaccharide and an O-antigen polysaccharide made up of repeating units. 3-deoxy-D-manno-2-octulosonate (KDO) residues link lipid A to the core oligosaccharide, which can also be decorated with other (often nonstoichiometric) substituents, such as phosphate and phosphoethanolamine. LPS is only found in Gram-negative bacteria.[70]

LPS contributes to the structural integrity of the cell wall, as a barrier that prevents the penetration of toxic substances such as antimicrobial agents. The outer polysaccharide component of LPS is composed of up to 40 repeating units that extend into the extracellular environment. The outer polysaccharide – also referred to as the O-antigen of the bacteria – varies among different Gram-negative bacteria and is the major antigenic determinant involved in interactions with antibodies, porins, LPS-binding protein. The presence or absence of O-antigen determines whether the LPS is rough or smooth. Full-length O-chains would render the LPS smooth, whereas the absence or reduction of O-chains would make the LPS rough.[69]

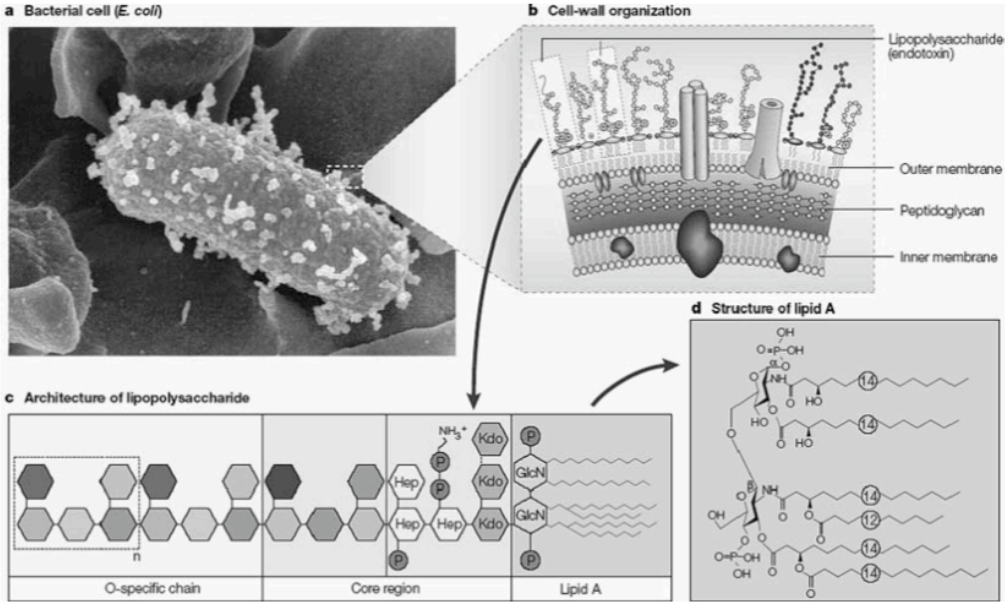

Figure 3.1. A Gram-negative bacterium. Electron micrograph of *Escherichia coli* (a) together with a schematic representation of the location of lipopolysaccharide (LPS; endotoxin) in the bacterial cell wall (b) and the architecture of LPS. (c). Also shown is the primary structure of the toxic center of LPS, the lipid A component (d). GlcN, D-glucosamine; Hep, L-glycero-D-manno-heptose; Kdo, 2-keto-3-deoxy-octulosonic acid; P, phosphate. Figure from Giuliani *et al*.[69]

Bacteria with rough LPS usually have more penetrable cell membranes to hydrophobic antibiotics, since a rough LPS is more hydrophobic. O-antigen is exposed on the very outer surface of the bacterial cell, and, as a consequence, is a target for recognition by host antibodies. The Core domain always contains an oligosaccharide component that attaches directly to lipid A and commonly contains sugars such as heptose and 3-deoxy-D-mannooctulosonic acid (also known as KDO, keto-deoxyoctulosonate). The LPS Cores of many bacteria also contain non-carbohydrate components, such as phosphate, amino acids, and ethanolamine substituents.[68] The hydrophobic, membrane-anchoring region of LPS is called lipid A. This part of the LPS is well conserved among bacterial species, and is considered as the most active moiety of LPS, responsible for many of the pathophysiological effects associated with infection. Lipid A is composed of phosphorylated glucosamine disaccharide decorated with saturated acyl chains linked through amide and ester bonds. When bacterial cells are lysed by the immune system, fragments of membrane containing lipid A are released into the circulation, causing fever, diarrhoea, and even fatal endotoxic shock (also called septic shock)[70] as shown in Figure 3.1. LPS plays a vital role in mediating interaction between Gram-negative bacteria and environment, influencing colonization and immunological responses. Investigators provided different evidences the LPS can play a crucial role beyond our understanding. For example, consider the case study for *Helicobacter pylori* responsible for chronic gastritis, which may develop into ulcers or cancers.[71,72] This kind of microbial invasion is recognized by the host and promotes an inflammatory response, leading to the release of macrophages and neutrophils. For the immunity response to be activated requires the recognition of the microbial chemistry associated with structural units as flagella, lipoproteins, peptidoglycan and LPS.[73]

LPS is considered to be a potentially potent signal driving inflammation.[74] In order to overcome this problem, the *H. pylori* acquired an important adaptation, a modified lipid A region with a much lower endotoxic effect and a low ability to stimulate immune response.[75,76] In addition, *H.pylori* also expresses an O-antigen that decrease Lewis blood group antigens present in the human cells and therefore avoids an immune response[77] and inhibits phagocytosis. The antiphagocytic mechanism is regulated by the bacterial surface structure in which the LPS mediate direct bacteria/phagocyte interaction and inhibits the ingestion by human blood granulocytes.[78] In 2008, Hui *et al.* proved that LPS was capable of inducing a proliferation of B-cells and that this effect was dose dependent manner. They examined the accessory roles of LPS-activated murine splenic B cells in initiating/modulating T-cell in the immune system.[79] There is a great demand on the use of microbes for the environmental remediation purposes. It has been proved that LPS in *Pseudomonas*

aeruginosa is the key factor in the process that controls the ability on reducing metals in the respiratory cycle and uptake of solvated metal ions from the surrounding environment as well as absorb metal ions. There are some experimental evidence that prove that *P. aeruginosa* has the ability to bind to ions such as Cu^{2+}, Fe^{3+}, La^{3+}, Eu^{3+} and UO_2^{2+} in the cell wall which suggests that the binding site for the metal ions is located in the LPS unit.[80-82]

In the environment, which is rich with both pathogenic microbes and eukaryotic organisms, the crucial defence mechanism, which is the innate immunity, becomes the only and the first defence mechanism in plants and eukaryotic organisms.[83-85] Bacterial LPSs from the outer membrane of the Gram-negative bacteria is considered as main elicitors of associated plant innate immunity. LPS has been reported to induce the immune response in plants that includes oxidative brust, NO production, calcium influx mechanism, the induction of pathogenesis related (PR) gene expression and alterations in the cell wall that includes the deposition of callose and phenolics, in which LPS has been added from different sources of bacteria to the cell suspension of leaves.[86-90] All these common effects from different LPS sources suggest that LPS has a common shared molecule determinant which is lipid A and indeed isolated lipid A was also active.[91] The concentrations of LPS that is required to induce of the effects described above are in the range of 5 - 100 mg/mL, which may suggests that plants possess low affinity system/less sensitive to LPSs compared to mammalian cells, which can respond at concentrations in the range of pg/mL to ng/mL.[91]

In mammals, it was observed that LPS is a potent activator of the hypothalamo-pituitary-adrenal axis (HPA)[92] by stimulating CRH secretion and there is strong evidence for CRH-independent effects[93,94] which in turn plays an important role in the stress response and acute infection to maintain homeostasis. It appears that LPS may act on each tissue comprising the HPA axis, because there is evidence for a pituitary-independent effect of LPS on the adrenal gland, which in turn causing the LPS to increase corticosterone secretion in both intact and hypophysectomized rats.[95] More recently, it has been shown that LPS inhibits ACTH-stimulated corticosterone secretion by cultured rat zona glomerulosa cells, although the effect on basal secretion was not determined.[96] It has been shown that LPS from Gram negative bacteria (*Escherichia coli* LPS) has the affinity to bind/act though Toll-like receptors (TLRs), specifically exerting a direct stimulatory effect on the induction of cortisol but not aldosterone secretion by human adrenocortical cells.[97] Based on all these information, LPS from *Escherichia coli* was tested on different microbes including actinomycetes (*Streptomyces* sp.) and fungi. This chapter seeks to test the hypothesis that microbes have many silent gene clusters that remain dormant under normal laboratory conditions, but can be activated in response to the chemical signal.

3.2 Results and discussion

3.2.1 Assembly of an integrated set of microbial diversity libraries

During my PhD, the library of microbes was assembled in which it consists of around 440 microbes including actinomycetes, fungi and unicellular bacteria with the codes CMB-TB (terrestrial bacteria) and CMB-TF (terrestrial fungi). In addition, Capon group has access to the pre-existing library of Australian marine bacteria (CMB-M) and fungi (CMB-MF) plus around 5000 different species including 500 different species of *Streptomyces* from Australian Collection of Microbes (ACM). Having access to this vast number of strains, the micro-bioreactor was used to construct a selected library of microbial crude extracts by subjection a subset of isolates (~ 500) to liquid cultivation using the micro-bioreactor. Solvent extraction and high throughput HPLC-DAD-HRMS and HPLC-DAD-MS analysis provided qualitative and quantitative data defining a structurally diverse set of metabolites (Scheme 3.1).

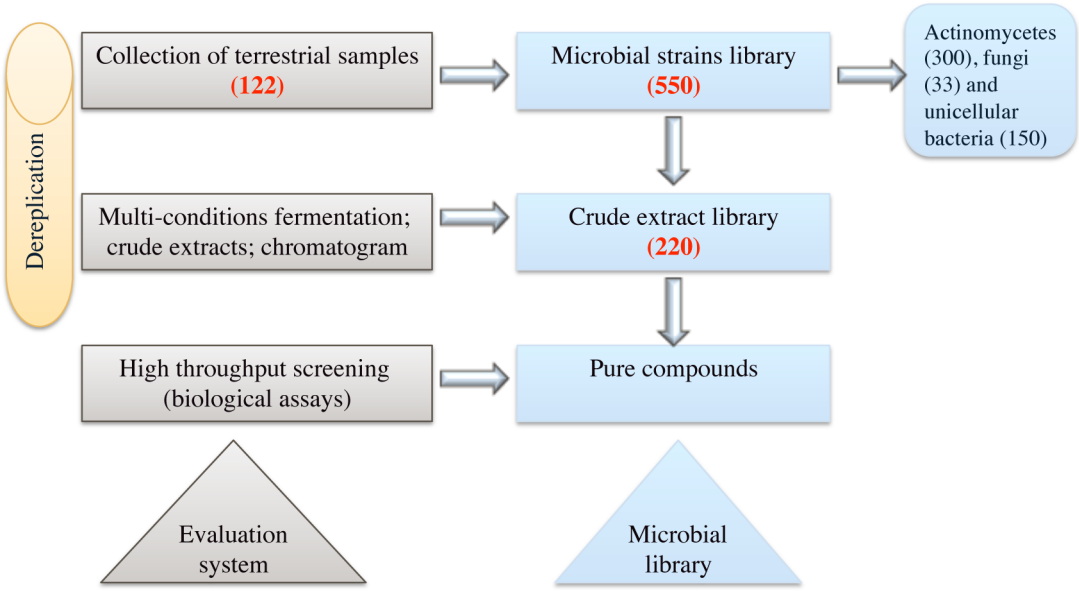

Scheme 3.1. Flow chart for the construction of microbial library and crude extract

3.2.2 Activation of silent microbial secondary metabolites

In an innovative combinatorial assay, the microbial biodiversity library was incubated in the presence of the metabolite rich extract library and pure compound library to generate a library of activated microbial crude extract (**Scheme 3.2**).

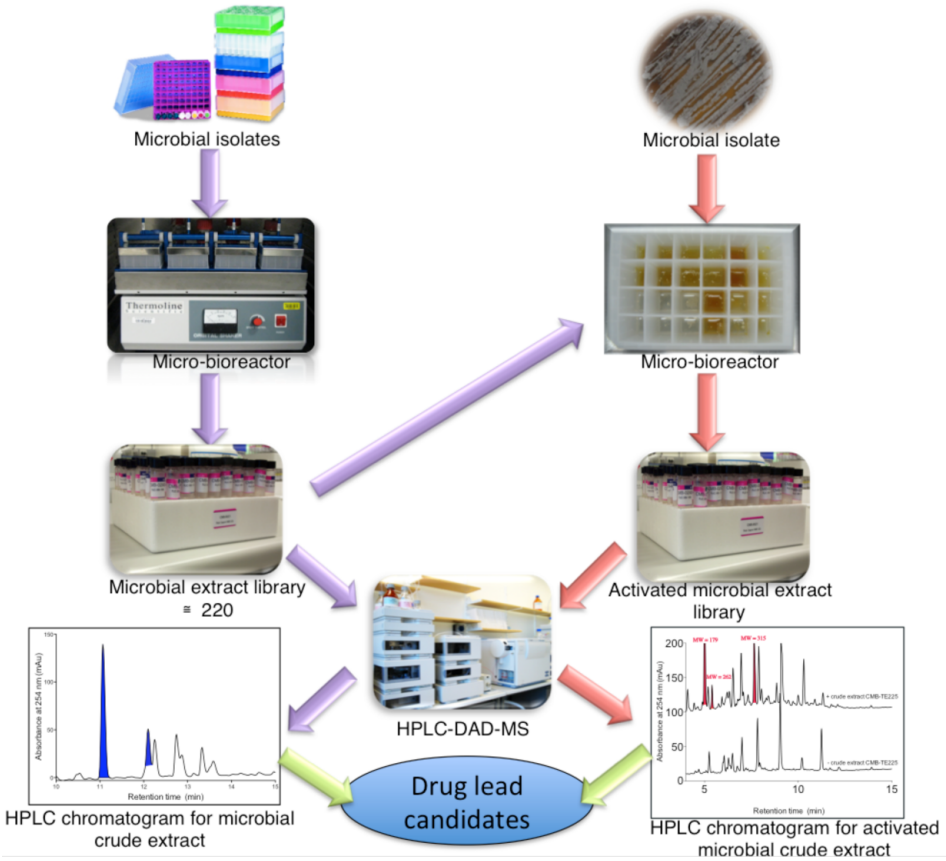

Scheme 3.2. Scheme of the high-throughput activation of microbial secondary metabolites using crude extracts/pure compounds

3.2.3 Activation of silent metabolites using microbial crude extracts

A terrestrial actinomycete (CMB-TB365) was chosen for this study to be cultivated in the presence of the microbial extract library. Strain CMB-TB0365 was cultivated on M1 media in the microbioreactor (1.45 mL) in the presence of 0.1 mg of the microbial crude extract (1% DMSO). CMB-TB365 was challenged with around 200 crude extracts. The plates were incubated at 26.5 °C for 7 – 10 days at 190 rpm. The cultures were treated *in situ* with EtOAc (2 mL), shaken for 1 h and the decanted organic layer was dried under N_2, re-dissolved in MeOH (100 μL) prior to analysis by HPLC-DAD-MS. Therefore, 200 experiments revealed two hits, in which the crude extracts from microbial isolates CMB-TB225 and CMB-TB464 were able to activate silent microbial metabolites in strain CMB-TB365 (Figure 3.2 and Figure 3.3). This study supported our original hypothesis that the organic extracts from microbial cultures possess chemical cues capable of activating otherwise silent secondary metabolites. Future studies should employ a larger combination of extracts and microbial cultures and should concentrate on isolating both the "activated" metabolites, and the chemical cues responsible for "activation".

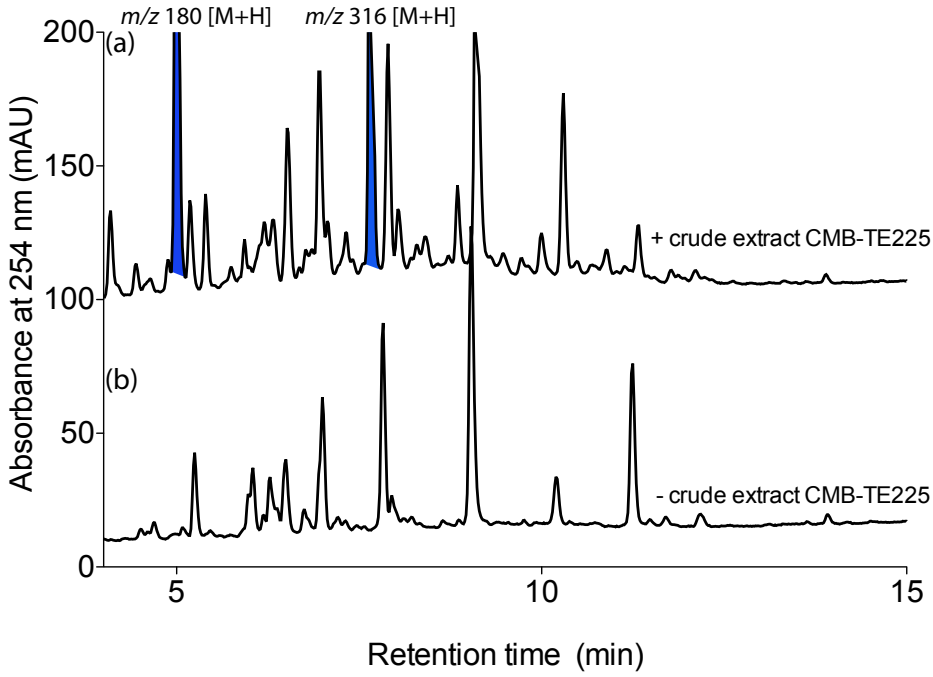

Figure 3.2. HPLC-DAD chromatogram, analytical gradient H_2O/MeCN, 0.05% HCO_2H using Zorbax C_8 of the activation of microbial secondary metabolites for strain CM-TB365 in the presence of (a) crude extract from CMB-TE225 and (b) absence of crude extract CMB0TE225

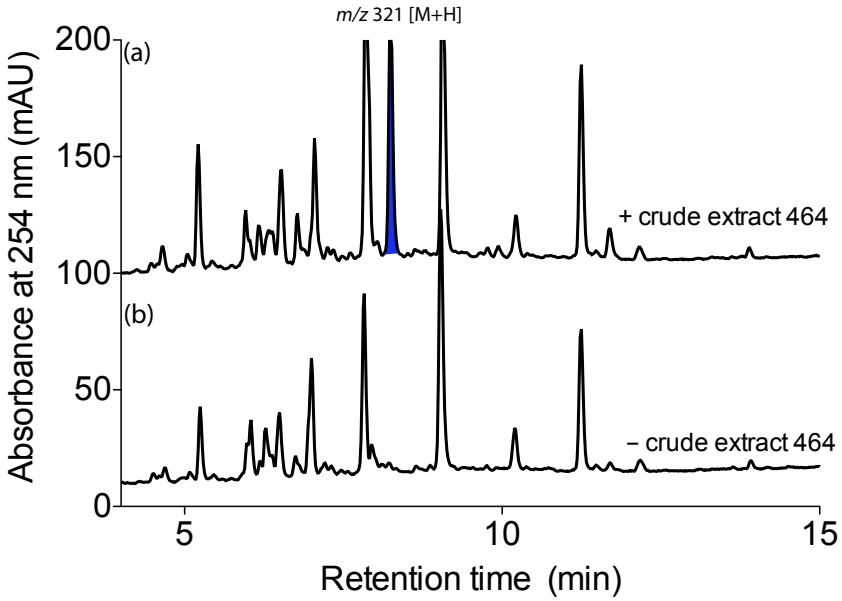

Figure 3.3. HPLC-DAD chromatogram, analytical gradient H_2O/MeCN, 0.05% HCO_2H using Zorbax C_8 of the activation of microbial secondary metabolites of strain CMB-TB365 in the presence of (a) crude extract from CMB-TE464 and (b) absence of crude extract CMB-TE464

3.2.4 Activation of silent metabolites using LPS

In this section, we will describe the activation of microbial secondary metabolites upon the addition of lipopolysaccharide (LPS) isolated from *Escherichia coli* purchased from Sigma-Aldrich and the effect on different actinomycetes and fungi. Extracts from different actinomycetes and fungi that showed secondary metabolites activation with LPS were screened against antibacterial assay. All the hits were tested against antimicrobial assay and they showed Gram-negative inhibition. The hits that showed antimicrobial effect where further more subjected to large-scale cultivation and the isolation of the microbial metabolites. Antibacterial extracts conformed to the criteria of the project and were considered 'lead' extracts for further investigation. 'Leads' were found in three actinomycetes and two fungi. Bioassay-guided fractionation of the microbial extract led to the identification of 5 known compounds and one new metabolite. This chapter will show the isolation, purification and structural elucidation of ten different microbial compounds including 1 new compound.

LPS was added to different culture media of 40 different actinomycetes and 30 different fungi. The LPS is soluble in water and was added at a final concentration 1 ng/mL to all the culture media of the microbes. The microbes were incubated for a period of 7 – 10 days at 27 °C. After the incubation period the whole broth/agar was extracted with EtOAc and the organic layer of concentrated *in vacuo*. The organic was re-dissolved in MeOH (100 µL) and analyzed by HPLC-DAD-MS. The crude extracts that showed activation/enhancement of microbial secondary metabolites were subjected to further analysis by scaling up the cultivation process and isolation of the activated/enhancement secondary metabolites.

Therefore, a study has been done by testing around 40 different actinomycetes/fungi from the Australian collection of microbes (ACM); with and without the presence of LPS. This study confirmed that LPS added at low concentration could activate secondary metabolites in both bacteria and fungi. The activated crude extracts have been tested against their antibacterial activity against different Gram-negative and Gram-positive bacteria. This chapter will outline the chemical analysis of the promising activating events (Scheme 3.3, Figure 3.5, Figure 3.6 and Figure 3.7).

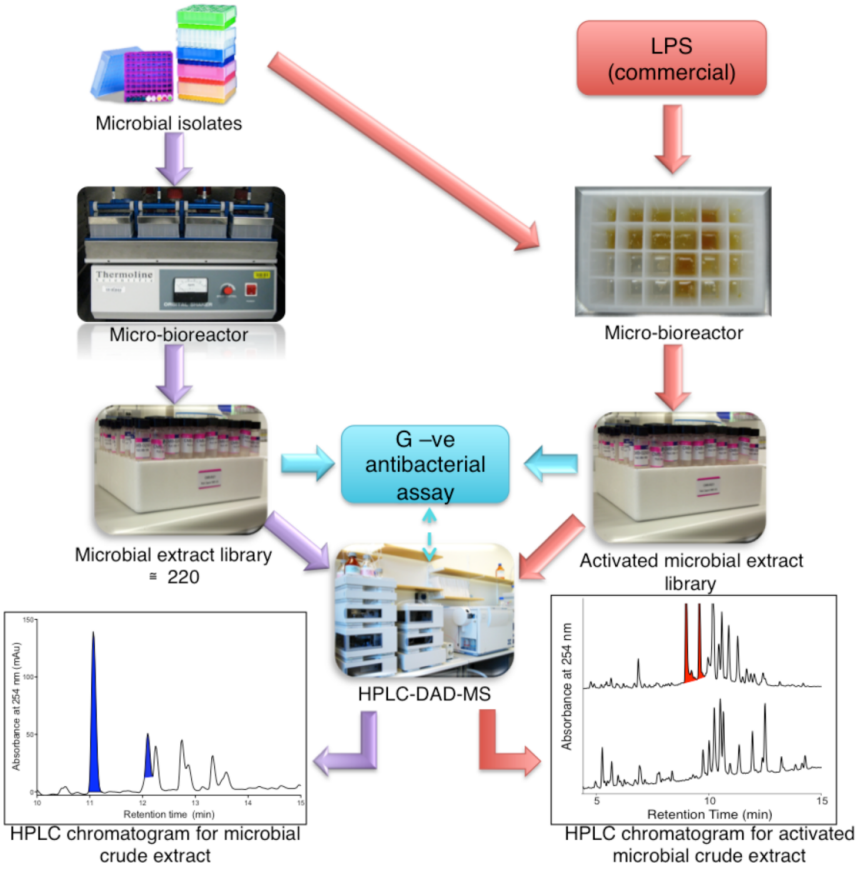

Scheme 3.3. Activation of microbial secondary metabolites by LPS

3.2.4.1 Hits from the activation of microbial metabolites by LPS

According to the scheme described above (Scheme 3.3), different strains including actinomycetes and fungi were tested with LPS in which media broth ISP-2 (1.485 mL) was transferred to all the wells plus LPS (15 µL) to give a final concentration 1 ng/mL plus spores from seed culture cultivated on ISP-2 agar plate. The plates were incubated at 26 °C, 190 rpm for 7 – 10 days. After the incubation period, the broth was extracted by the addition of EtOAc (2 mL) and the organic layer was decanted and dried under N2. The crude extract was dissolved in MeOH (100 µL) and analysed by the HPLC-DAD-MS (Figure 3.4, Figure 3.5 and Figure 3.6). The control wells contain only water. The hits where tested for their antibacterial activity against Gram negative and Gram positive bacteria (Figure 3.7) and they were cultivated on large scale for isolation of the activated metabolites. Figure 3.4, Figure 3.5 and Figure 3.6 are examples for the activation process with LPS.

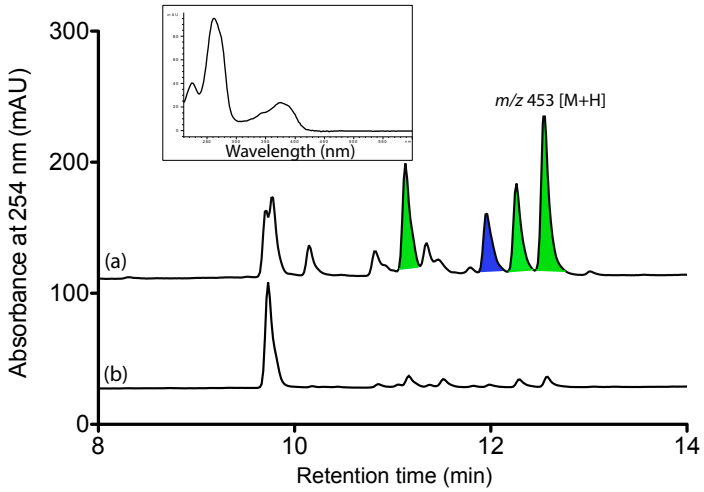

Figure 3.4. HPLC-DAD chromatogram, analytical gradient H_2O/MeCN plus 0.05% HCO_2H using Zorbax C_8 of the crude extract from ACM-165F in the (a) presence and (b) absence of LPS. The highlighted peak represent the enhancement of fungal metabolites while the blue peak represent the activation of fungal metabolites

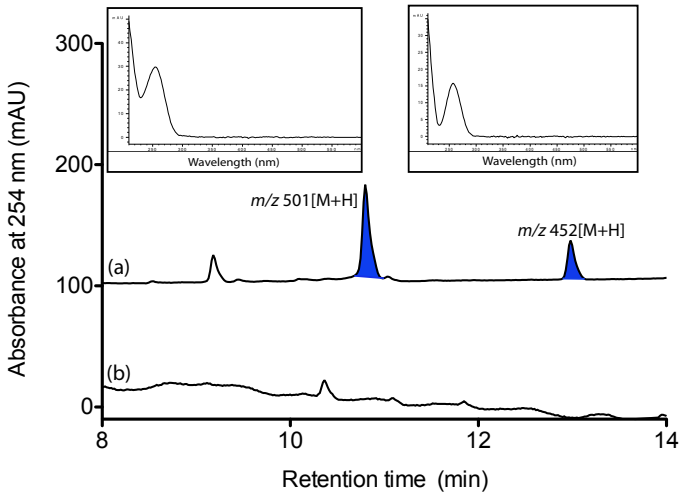

Figure 3.5. HPLC-DAD chromatogram, analytical gradient H_2O/MeCN plus 0.05% HCO_2H using Zorbax C_8 of the crude extract from ACM-194F in the (a) presence and (b) absence of LPS. The highlighted peak (blue) represents the activation of fungal metabolites

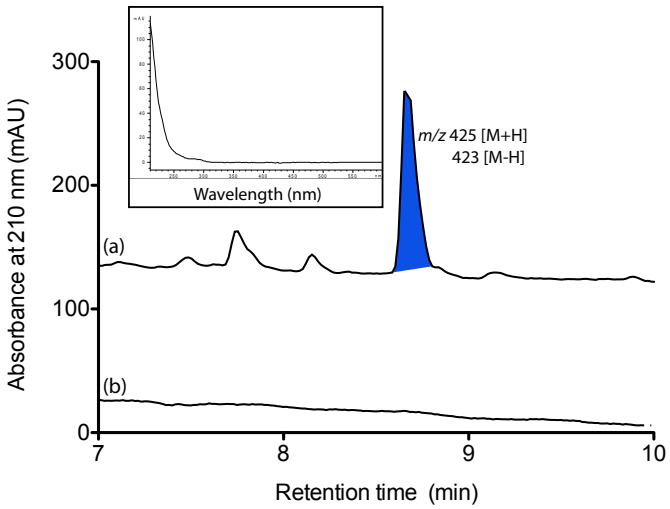

Figure 3.6. HPLC-DAD chromatogram, analytical gradient H_2O/MeCN plus 0.05% HCO_2H using Zorbax C_8 of the crude extract from ACM-4993F in the (a) presence and (b) absence of LPS. The highlighted peak (blue) represents the activation of fungal metabolites

The above figures showed the enhancement of secondary metabolites (Figure 3.4) and activation of metabolites (Figure 3.5 and Figure 3.6). Most of the activated metabolites belong to the class of metabolites as indicated from the UV spectrum.

The antibacterial activity of the activated crude extracts was investigated against Gram-positive bacteria where they showed potent inhibition against *Bacillus subtilis* ATCC 6051 and 6633 (Figure 3.7)

Bacillus subtilis ATCC 6051

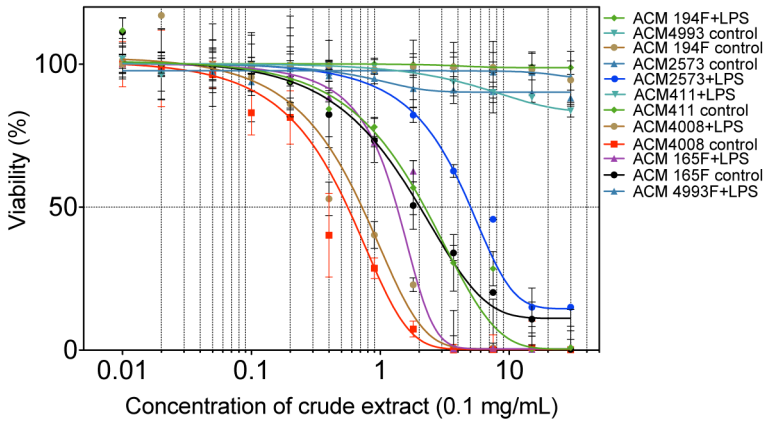

Bacillus subtilis ATCC 6633

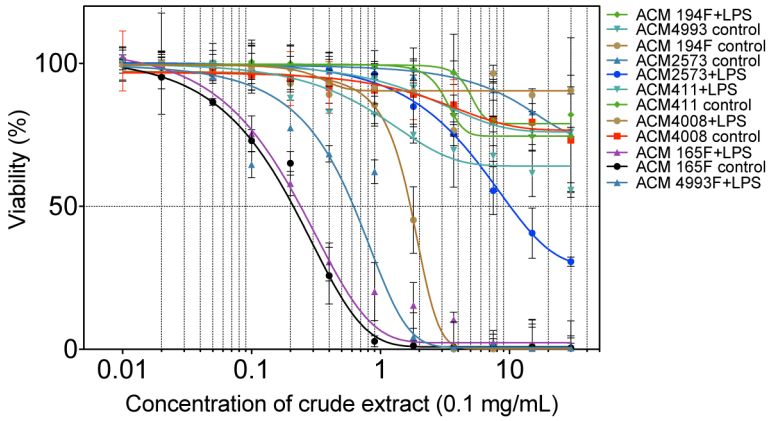

Figure 3.7. Antibacterial assay results showing the effect of the crude extract with LPS compared to the control. The activated crude extract showed activity against *Bacillus subtilis* ATCC 6051/6633

All these promising results prompted us to start looking into the activated crude extracts and investigate the activated secondary metabolites. In the next section, we will focus on four crude extracts that showed good antibacterial activity.

3.2.5 *Streptomyces pseudoechinosporeus* (ACM-2573)

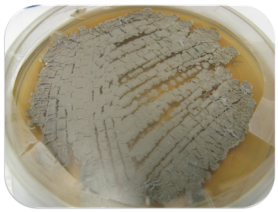

Figure 3.8. *Streptomyces pseudoechinosporeus* (ACM-2573)

3.2.5.1 Analytical cultivation and chemical analysis

A single colony of ACM-2573 was used to inoculate ISP-2 agar media, which was cultivated for a period of 10 days. After cultivation, spores from seed culture were used to inoculate ISP-2 broth (1.48 mL) in the microbioreactor to which LPS (15 μL) was added to give final concentration 0.6 ng/mL. The micro-bioreactor was incubated at 26 °C, 190 rpm for 7 days. After the incubation period, the broth was extracted with EtOAc (2 mL), and the organic extract was dried *in vacuo*. The resulting crude extract was resuspended in MeOH (100 μL) and analysed by HPLC-DAD-MS. The control wells were only inoculated with the bacterial spores. HPLC chromatogram was dominated by a single peak attributed to **3.02**. After the addition of LPS, **3.02** was enhanced and another new metabolite was produced **3.01**. Peaks with the following retention times t_R = 13.1 and 14.8 min exhibited the following *m/z* $[M+H]^+$ 393 (**3.01**) and 377 (**3.02**) as shown in Figure 3.9.

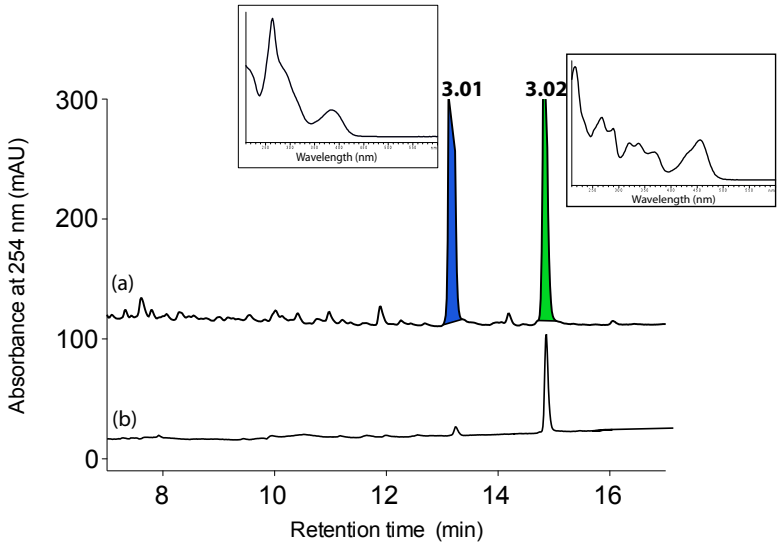

Figure 3.9. HPLC-DAD (254 nm) chromatogram, analytical gradient H_2O/MeCN plus 0.05% HCO_2H using Zorbax C_8 for the crude extract from ACM2573F in the (a) presence and (b) absence of LPS. The highlighted peak (blue) represents the activated metabolite and represents the enhanced metabolite in the presence of LPS

3.2.5.2 Preparative cultivation

A seed culture was prepared by inoculating a 250 mL flask containing liquid medium (80 mL deionized water containing 0.4% starch, 0.2% yeast extract, 1% malt extract) with a single colony of ACM-2573 followed by shaking at 190 rpm for 7 d at 26.5 °C. Aliquots of the seed culture (5 mL) were transferred to two 2 L Fernbach flasks, each containing the same liquid medium (500 mL) and LPS (1 ng/mL), and the flasks were shaken at 190 rpm for 7 d at 26.5 °C. The resulting cultures were each extracted with EtOAc (400 mL) and the combined organic phases concentrated *in vacuo* to yield an extract (60.2 mg). The extract was sequentially triturated with hexane (15 mL) and CH_2Cl_2 (15 mL) to afford, after concentration *in vacuo*, 3.0 and 60.2 mg, respectively. The CH_2Cl_2 fraction was subjected to semi-preparative reversed-phase HPLC (Zorbax C_8 column, 250 × 9.4 mm, 5 μm, 4 mL/min gradient elution 90% H_2O/MeCN to 100% MeCN over 30 min to yield resistoflavin (**3.01**) (t_R = 23.9 min, 1.1 mg, 1.8%) and resistomycin (**3.02**) (t_R = 25.5 min, 0.9 mg, 1.5%) (Scheme 3.4).

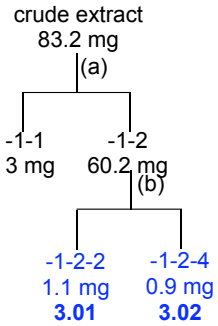

Scheme 3.4. Isolation scheme of ACM-2573 leading to the 2 metabolites. Compounds shaded in blue were isolated and tested against antimicrobial assay. (a) Trituration [hexane (-1-1) and CH_2Cl_2 (-1-2)], (b) Semi-preparative HPLC: Zorbax-C_8, 90-10% H_2O/MeCN, 3 mL/min, 30 min

3.2.5.2.1 Resistoflavin (3.01)

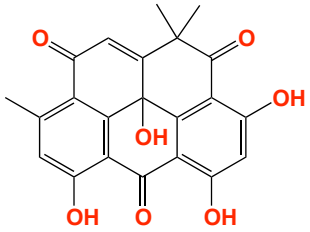

3.01

HRESI(+)MS data for **3.01** revealed a quasi-molecular ion $(M+H)^+$ indicative of a molecular formula $C_{22}H_{16}O_7$ (Δmmu –0.1). The ^1H NMR and 2D NMR ($CDCl_3$) data (Figure 3.11 and Table 3.1) for **3.01** showed the presence of three chelated hydroxyl groups (δ_H 13.52, 12.69 and 12.53), three singlets isolated aromatic resonances at (δ_H 6.94, 6.56 and 6.52), an aromatic methyl (δ_H 2.76) and two aliphatic methyls (δ_H 1.73 and 1.62). The structure elucidation was further supported by 2D NMR data, including HSQC, COSY and HMBC, as outlined in Figure 3.10. On searching the literature with the molecular formula, molecular weight and structure fragment, **3.01** was identified as resistoflavin, an actinomycete metabolite first reported by Eckardt *et al*. in 1970[99] and it was re-isolated with its O-methyl derivative from different terrestrial and marine derived *Streptomyces* sp. (*Streptomyces griseoflavus* and *Streptomyces resistomycificus*).[100-102] Comparison of full experimental and literature data (Table 3.2), including experimental $[\alpha]^{22}_D$ +537 (*c* 0.02, pyridine) and literature $[\alpha]^{23}_D$ –96 (*c* 0.5, pyridine) suggested that we may have the enantiomer of the unknown resistoflavin. The variation in the optical rotation between our candidate and the literature data is due to the high concentration of resistoflavin that has been reported. Resistoflavin was considered as potent cytotoxic against gastric adenocarcinoma and exhibited weak antibacterial activity against Gram-negative and Gram-positive bacteria.[103]

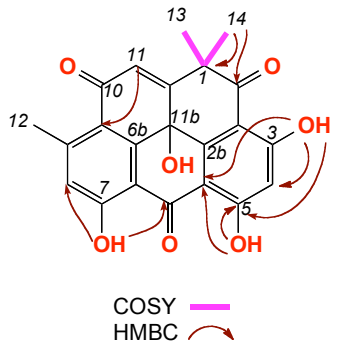

Figure 3.10. Key 2D NMR correlations of resistoflavin (**3.01**)

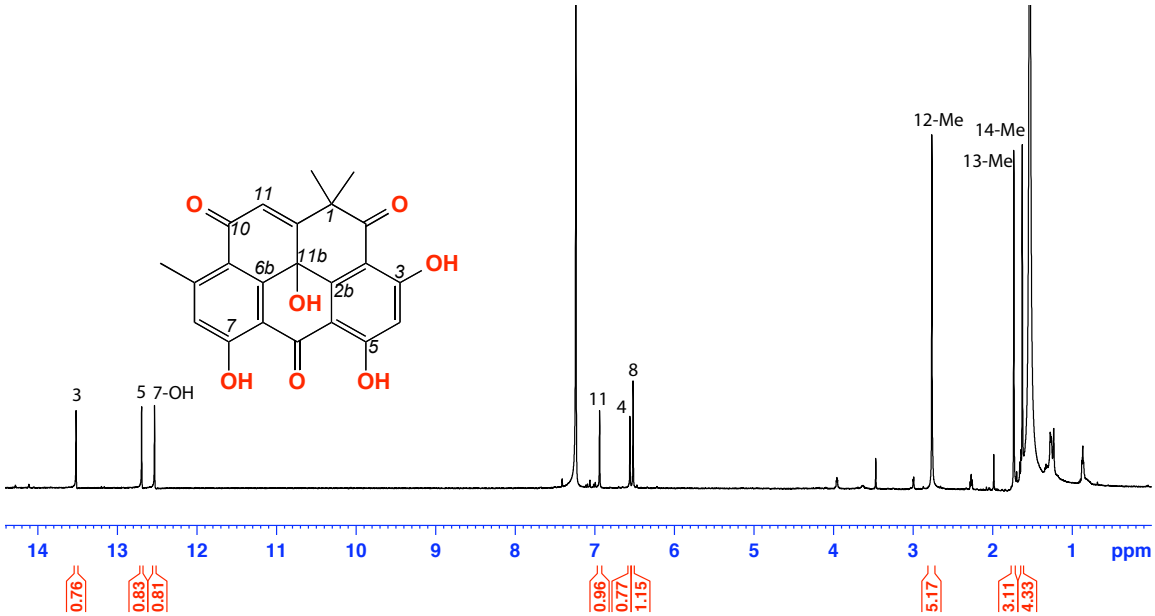

Figure 3.11. ^{1}H NMR (600 MHz, $CDCl_3$) spectrum of resistoflavin (**3.01**)

Table 3.1. NMR (600 MHz, $CDCl_3$) data of resistoflavin (**3.01**)

Pos.	δ_H, mult (*J* in Hz)[a]	δ_C[a]	COSY	^{1}H-^{13}C HMBC
1		47.5		
2		203.1		
2a		109.1		
2b		[b]		
3-OH	13.52, s		13, 14	2a, 4, 5
4	6.56, s	105.5		3
5		169.6		
5-OH	12.69, s			
5a		[b]		
6		165.7		
6a		[b]		
6b		[b]		
7-OH	12.53, s			6, 8
8	6.52, s	128.3	12	9a
9		151.6		
9a		120.2		
10		[b]		
11	6.94, s	123.3		9a
11a		156.3		
11b		[b]		
12-Me	2.76, s	32.6	8	8, 9
13-Me	1.73, s	24.0	3, 14	1, 2, 11a, 14
14-Me	1.62, s	24.8	3, 13	1, 2, 11a,13

(a) ^{13}C assignments obtained from gHSQC and gHMBC data. (b) signals not detected

Table 3.2. ^{1}H NMR (DMSO-d_6) comparison of experimental and literature[103] data of resistoflavine (**3.01**)

Pos	δ_H, mult, (*J* in Hz)[a] experimental	δ_H, mult, (*J* in Hz)[b] literature
4	6.52, s	6.55, s
7-OH	12.35, s	12.37, s
8	6.97, s	7.00, s
11	6.45, s	6.49, s
12-Me	2.65, s	2.69, s
13-Me	1.59, s	1.61, s
14-Me	1.50, s	1.54, s

measured in (a) (600 MHz, DMSO-d_6), (b) (200 MHz, DMSO-d_6)

3.2.5.2.2 Resistomycin (3.02)

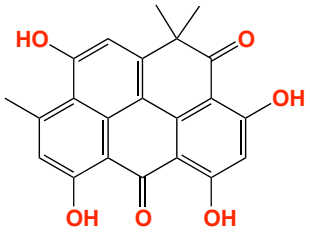

3.02

HRESI(+)MS data for **3.02** revealed a quasi-molecular ion $(M+H)^+$ indicative of molecular formula $C_{22}H_{16}O_6$ (Δmmu –0.6). The ^1H NMR and 2D NMR (MeOH-d_4) data (Figure 3.12, Figure 3.13 and Table 3.3) showed that **3.02** was very similar to **3.01**, but lacking the 11b-OH. The structure elucidation was supported by 2D NMR data, including HSQC, COSY and HMBC, as outlined in Figure 3.12. Literature searching led the known bacterial metabolite resistomycin. Resistomycin (**3.02**) was first reported from *Streptomyces griseoflavus* by Hofle *et al*. in 1983.[101] Analysis of all the NMR data with comparison to literature data (Table 3.3), strongly suggested that **3.02** was the known metabolite resistomycin. Resistomycin is a quinone-related antibiotic with unique structure and exhibited bactericidal and vasoconstrictive activity. In addition, it inhibits RNA and protein synthesis, but have no effect on the DNA synthesis.[104]

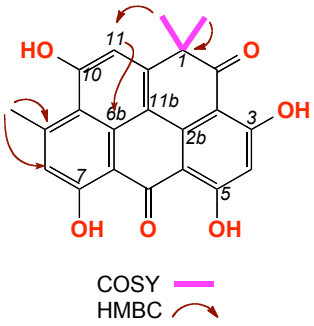

Figure 3.12. Key 2D NMR correlations of resistomycin (**3.02**)

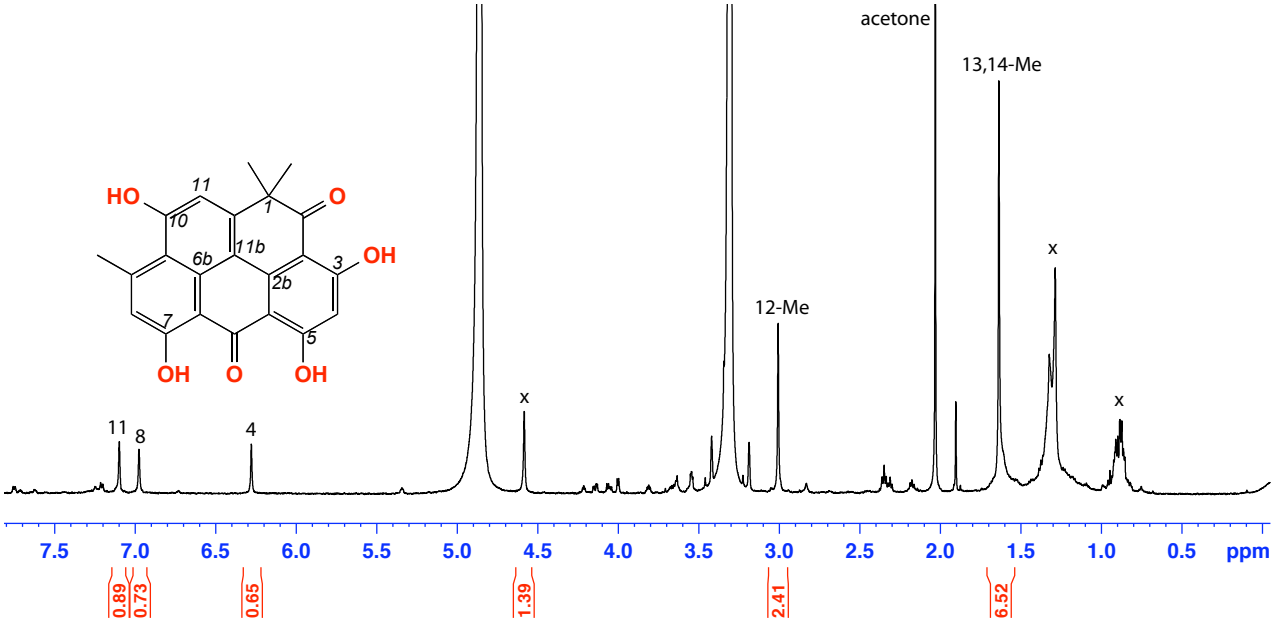

Figure 3.13. ^{1}H NMR (600 MHz, MeOH-d_4) spectrum of resistomycin (**5.02**). (x)- signals for impurities

Table 3.3. NMR (600 MHz, MeOH-d_4) data of resistomycin (**3.02**)

Pos.	δ_H, mult (*J* in Hz)[a]	δ_C[a]	COSY	^{1}H-^{13}C HMBC
1		45.1		
2		205.9		
3		[b]		
4	6.28, s	100.0		
5		[b]		
6b		106.8		
7		[b]		
8	6.97, s	118.3		
9		152.1		
10		[b]		
11	7.09, s	111.7		6b
11a		152.7		
12-Me	3.01, s	24.4	8	8,9
13,14-Me	1.63, s	28.3		1, 2, 11

(a) ^{13}C assignments obtained from gHSQC and gHMBC data. (b) Signals not observed

Table 3.4. ^{1}H NMR (DMSO-d_6) comparison of experimental and literature[105] data of resistomycin (**3.02**)

Pos	δ_H, mult[a] experimental	δ_H, mult[b] literature
3-OH	14.13, s	14.42
4	6.30, s	6.29, s
5-OH	14.39, s	14.30, s
7,10-OH	12.21, s	12.27, s
8	6.97, s	6.93, s
11	7.17, s	7.21, s
12-Me	2.89, s	2.87, s
13,14-Me	1.50, s	1.56, s

measured in (a) (600 MHz, DMSO-d_6), (b) (500 MHz, DMSO-d_6)

3.2.5.2.3 Conclusion

We were able to report that trace levels of LPS added to a culture of *Streptomyces pseudoechinosporeus* (ACM-2573) stimulated the production of resistoflavin (**3.01**) and enhanced the produced of the oxidized analogue of the co-metabolite resistomycin (**3.02**). Recent literature report notes[106] that oxidation of **3.02** into **3.01** is catalyzed by RemO, flavin adenine dinucleotide (FAD) dependent monooxygenase, which uniquely oxidizes the Re face of **3.02** to deliver **3.01** as a single (–) entianmer. By contrast, the sample of resistoflavin produced by LPS activation (during our study) was the (+) enantiomer, a new metabolite. This observation requires further analysis of **3.02** to authetntic resistomycin. Also, this observation suggests that LPS activation stimulates the transcription and/or functionality of RemO[106] or an equivalent monooxygenase, with the opposite enantio selectivity to that reported earlier.

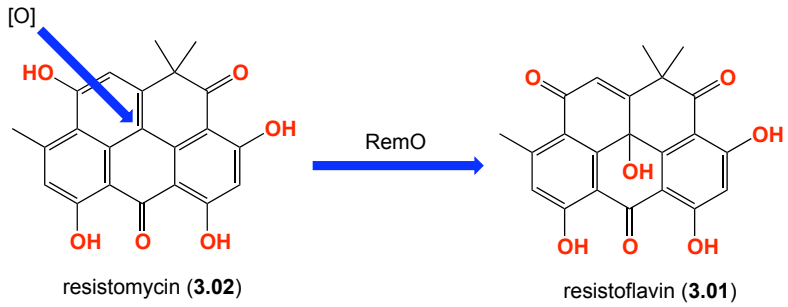

resistomycin (**3.02**) resistoflavin (**3.01**)

3.2.6 CMB-TF411

3.2.6.1 Analytical cultivation and chemical analysis

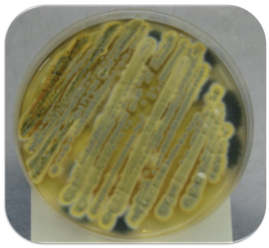

Figure 3.14. Picture of CMB-TF411

Fungal strain (CMB-TF411) was isolated from a terrestrial sample collected from North Stradbroke Island, Brisbane (see Chapter 10). A single colony of CMB-TF411 was used to inoculate a seed culture on ISP-2 agar media, which was cultivated for a period of 10 d. A single colony was used to inoculate ISP-2 broth (1.48 mL) in micro-bioreactor in the presence of LPS (15 μL) to give final concentration (0.6 ng/mL). The micro-bioreactor was incubated at 26 °C, 190 rpm for 7 days. After the incubation period, the broth was extracted with EtOAc (2 mL), and the organic extract was dried under N_2. The resulting crude extract was resuspended in MeOH (100 μL) and analysed by HPLC-DAD-MS. The control wells were only inoculated with the fungal spores. HPLC chromatogram was dominated by a single peak attributed to **3.03**. The addition of LPS, **3.04** was activated. Peaks with the following retention times t_R = 12.2 and 13.9 min exhibited the following *m/z* $[M+H]^+$ 543 (**3.03**) and 539 (**3.04**) as shown in Figure 3.15.

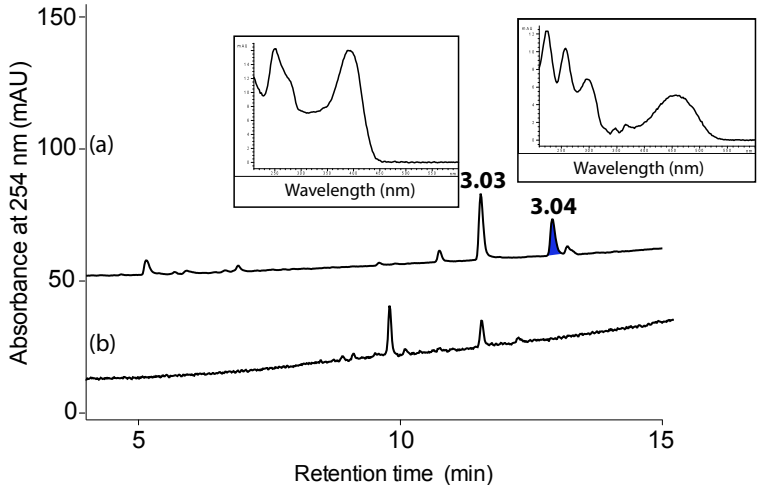

Figure 3.15. HPLC-DAD (254 nm) chromatogram, analytical gradient H_2O/MeCN plus 0.05% HCO_2H using Zorbax C_8 of the crude extract from CMB-TF411 in the (a) presence and (b) absence of LPS cultivated on ISP-2 medium. The highlighted peak represents the activated metabolite in the presence of LPS

3.2.6.2 Preparative cultivation

A seed culture was prepared by inoculating a 250 mL flask containing liquid medium (80 mL deionized water containing 0.4% starch, 0.2% yeast extract, 1% malt extract) with a single colony of CMB-TF411 followed by shaking at 190 rpm for 7 d at 26.5 °C. Aliquots of the seed culture (5 mL) were transferred to two 2 L Fernbach flasks, each containing the same liquid medium (500 mL) and LPS (0.6 ng/mL), and the flasks were shaken at 190 rpm for 7 d at 26.5 °C. The resulting cultures were each extracted with EtOAc (400 mL) and the combined organic phases concentrated *in vacuo* to yield an extract (83.2 mg). The extract was sequentially triturated with hexane (15 mL), CH_2Cl_2 (15 mL) and MeOH (15 mL) to afford, after concentration *in vacuo*, 8, 10 and 45.2 mg fractions, respectively. The MeOH fraction was subsequently subjected to semi-preparative reversed-phase HPLC (Zorbax C_8 column, 250 × 9.4 mm, 5 μm, 3 mL/min gradient elution 90 – 10% H_2O/MeOH over 30 min to yield rugluosin (**3.03**) (t_R = 21.6 min, 0.8 mg, 1.7%) and skyrin (**3.04**) (t_R = 24.5 min, 1.4 mg, 3.1%) (Scheme 3.5).

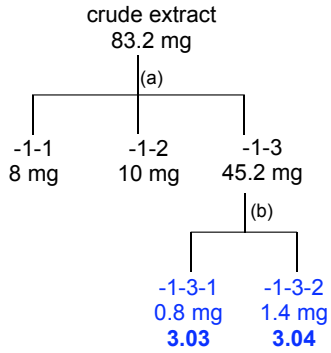

Scheme 3.5. Isolation scheme for CMB-TF411 leading to the 2 metabolites. Compounds shaded in blue were isolated and tested against antimicrobial assay. (a) Trituration [hexane (-1-1), CH_2Cl_2 (-1-2) and MeOH (-1-3)], (b) Semi-preparative HPLC: Zorbax-C_8, 90 – 10% H_2O/MeOH, 3 mL/min, 30 min

3.2.6.2.1 Rugulosin (3.03)

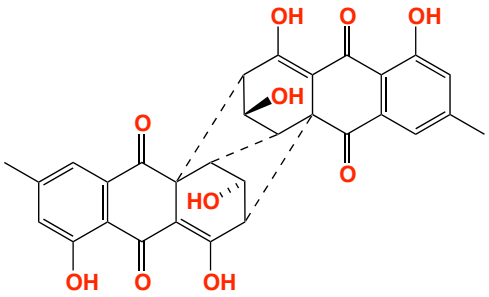

3.03

HRESI(+)MS data of **3.03** revealed a quasi-molecular ion $(M+H)^+$ indicative of molecular formula $C_{30}H_{22}O_{10}$ (Δmmu +0.5). The ^1H NMR and 2D NMR (DMSO-d_6) data (Figure 3.16, Figure 3.17 and Table 3.5) was suggestive of anthraquinone. The structure assignment was supported by 2D NMR data, including HSQC, COSY and HMBC, as outlined in Figure 3.16 and comparison which determined that **3.03** was very likely rugulosin[107]. Comparison of NMR data with literature data (Table 3.6) suggested this assignment, while a comparison of the experimental $[\alpha]^{22}_D$ +68.6 (*c* 0.05, MeOH) and literature $[\alpha]^{30}_D$ +276 (*c* 0.35, MeOH)[108]. The difference in the optical rotation was attributed to the presence of impurities in **3.03**. (+) rugulosin (**3.03**) was first reported from *Penicillium rugulosum*.[107] Rugulosin (**3.03**) has been reported before to possess toxic, mutagenic and insecticidal activities.[109-111]

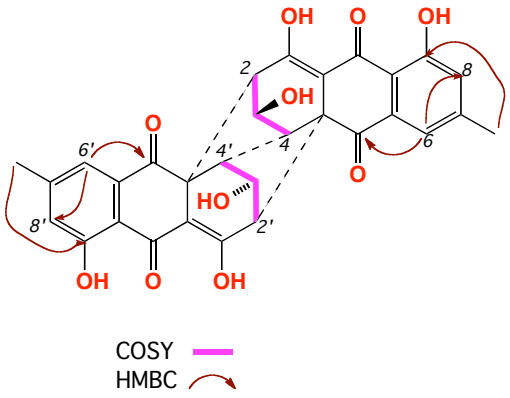

Figure 3.16. Key 2D NMR correlations of rugulosin (**3.03**)

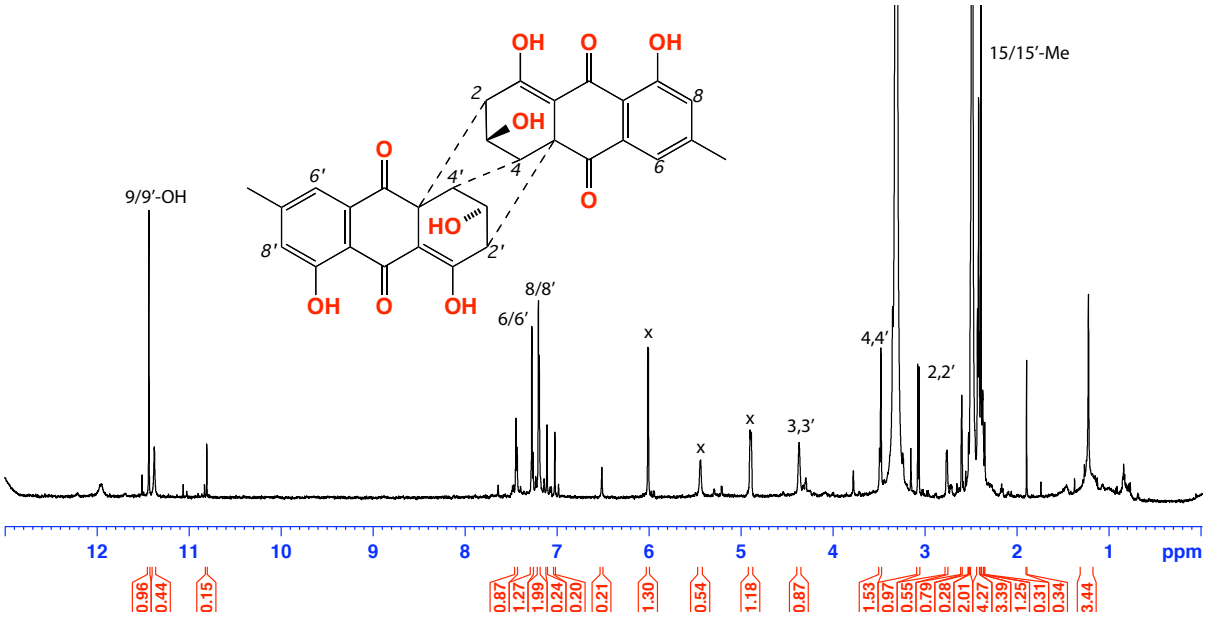

Figure 3.17. ^{1}H NMR (600 MHz, DMSO-d_6) spectrum of rugulosin (**3.03**)

Table 3.5. NMR (600 MHz, DMSO-d_6) data of rugulosin **(3.03)**

Pos.	δ_H, mult (*J* in Hz)[a]	δ_C[a]	COSY	^{1}H-^{13}C HMBC
1,1′-OH	[b]			
2	2.46, d *(4.7)*	58.2	3	
3	4.43, m	58.3	2	
3,3′-OH	6.01, s			
4,4′	3.49, d *(2.6)*	52.2	3,3′	
5,5′	[b]			
6,6′	7.45, d *(8.8)*	122.2	15,15′	8/8′, 13/13′
7,7′		119.2		
8,8′	7.20, d *(4.9)*	124.2	15,15′	6/6′
9,9′		150.3		
9,9′-OH	11.4			11/11′
10,10′		115.2		
11,11′		160.4		
12,12′		[b]		
13,13′		195.1		
14,14′		135.6		
15,15′	2.39, s	135.6	6, 8	
1′-OH	[b]			

(a) ^{13}C assignments obtained from gHSQC and gHMBC data. (b) signals not detected

Table 3.6. ^{1}H NMR (DMSO-d_6) comparison for experimental and literature[112] data of rugulosin (**3.03**)

Pos.	δ_H, mult, (*J* in Hz)[a] experimental	δ_H, mult, (*J* in Hz)[a] literature
1,1′-OH	[b]	14.54, s
2,2′	2.76, d *(4.7)*	2.78, d *(5.5)*
3,3′	4.43, m	4.38, br d *(5.5)*
4,4′	3.48, d *(2.6)*	3.38, brs
6,6′	7.45, d *(1.4)*	7.43, d *(1.2)*
8,8′	7.20, d *(4.9)*	7.16, d *(1.2)*
9,9′	11.4, s	11.37, s
15,15′	2.39, s	2.42, s

measured in (a) (600 MHz, DMSO-d_6), (b) signals not detected

3.2.6.2.2 Skyrin (3.04)

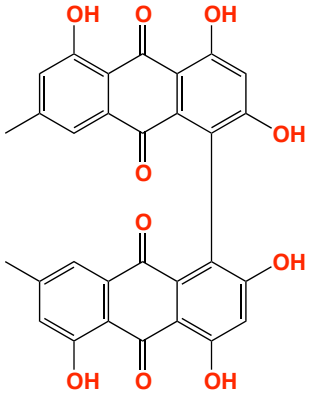

3.04

HRESI(+)MS data for **3.04** revealed a quasi-molecular ion $[M+H]^+$ indicative of molecular formula $C_{30}H_{18}O_{10}$ (Δmmu +0.3). The ^{1}H NMR and 2D NMR (DMSO-d_6) data (Figure 3.19 and Table 3.7) was suggestive of anthraquinone. The structure assignment was supported by 2D NMR data, including HSQC, COSY and HMBC, as outlined in Figure 3.18, and comparison with literature data, which determined that **3.04** was very likely skyrin. Analysis of all the NMR data with comparison to literature data (Table 3.8), strongly suggested that **3.04** was the known metabolite fungal metabolites skyrin.[107] In 1975, Toma *et al*. reported NMR (DMSO-d_6) for the skyrin (**3.04**) isolated from *Penicillium rugulosum*.

Since skyrin has an $[\alpha]_D$ but no chiral centre, it must exist as atropisomers, comparison of the experimental $[\alpha]^{22}_D$ −16 (*c* 0.05, dioxane) and literature $[\alpha]^{13}_D$ +105 (*c* 0.4, dioxane), it may suggest that we have isolated the first reported enantiomer of skyrin. Skyrin (**3.04**) has been reported before to possess toxic, mutagenic activity and skyrin analogues have been claimed for the treatment of Diabetes mellitus.[109,113]

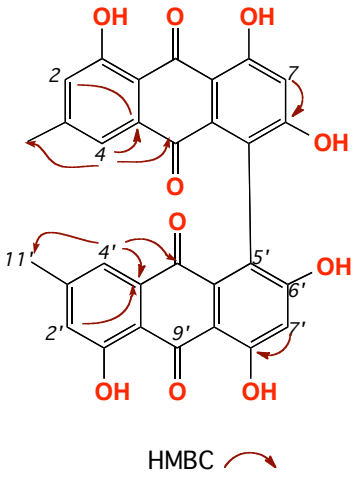

Figure 3.18. Key 2D NMR correlation of skyrin (**3.04**)

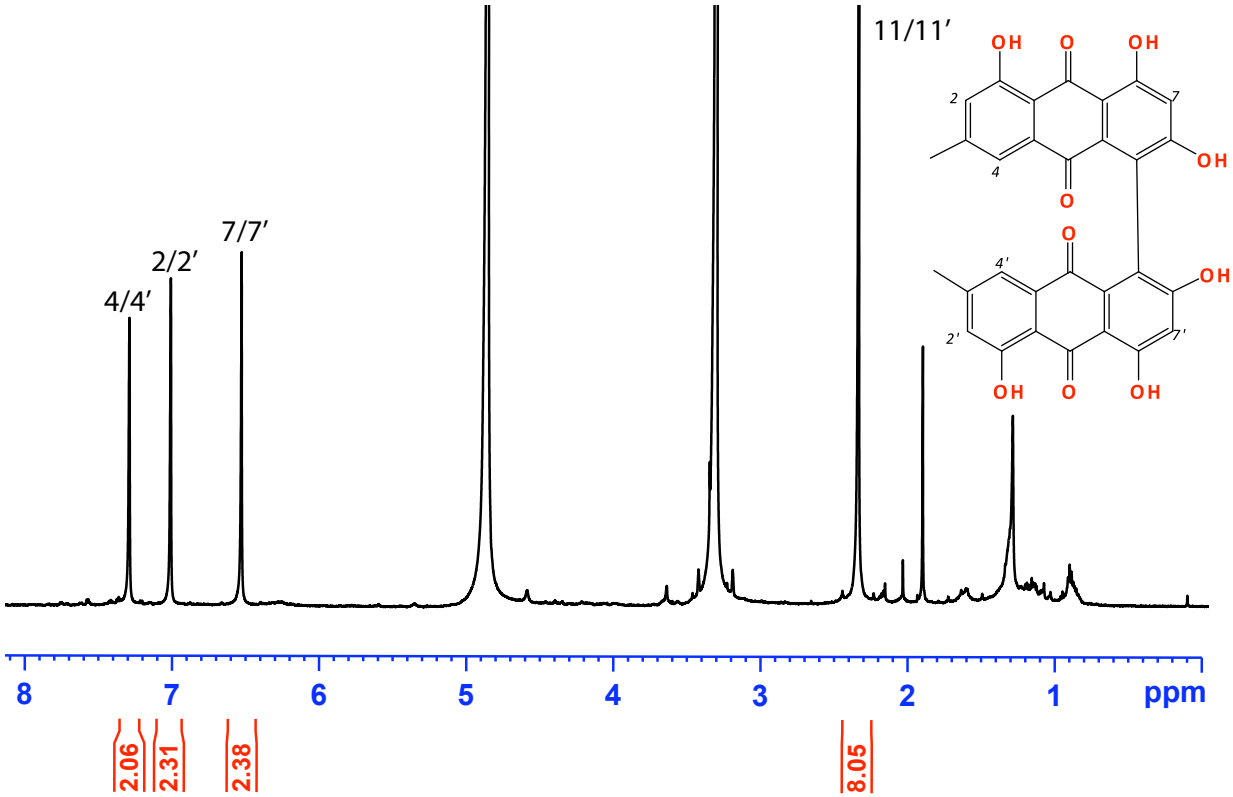

Figure 3.19. ^{1}H NMR (600 MHz, MeOH-d_4) spectrum of skyrin (**3.04**)

Table 3.7. NMR (600 MHz, MeOH-d_4) data of skyrin (**3.04**)

Pos.	δ_H, mult (J in Hz)[a]	δ_C[a]	^{1}H-^{13}C HMBC
1,1′		[b]	
2, 2′	7.02, s	122.3	11/11′
3, 3′		148.5	
4, 4′	7.30, s	120.1	5/5′, 9/9′, 10/10′, 11/11′
5, 5′		124.3	
6, 6′		164.2	
7, 7′	6.56, s	108.4	8/8′
8, 8′		168.2	
9, 9′		[b]	
9a, 9′a		128.4	
10, 10′		182.3	
Me-11, 11′	2.34, s	20.1	3/3′

measured in (a) (600 MHz, MeOH-d_4), (b) signals not detected

Table 3.8. ^{13}C (DMSO-d_6) data comparison of experimental and literature[114] data of skyrin (**3.04**)

Pos	δ_c, mult, (J in Hz) experimental	δ_c, mult, (J in Hz) literature
2,2′	122.2	123.5
3,3′	148.0	148.1
4,4′	119.1	120.4
7,7′	106.5	107.2
Me-11,11′	20.9	21.5

3.2.7 (CMB-M81F)

(CMB-M81F) was isolated from a marine sediment sample collected from Shonecliff, Australia. CMB-M81F was very interested fungus as it showed many metabolites (see chapter 5). In this section, we will discuss only the metabolites that have been activated in the presence of LPS, while the rest of the active metabolites will be discussed in chapter 5.

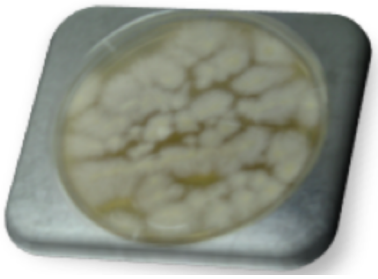

Figure 3.20. Picture of fungus CMB-M81F

3.2.7.1 Analytical cultivation and chemical analysis

Fungal strain (CMB-M81F) was isolated from a marine sample collected from Shorncliffe, Australia by previous PhD student in Capon group. A single colony of CMB-M81F was used to inoculate a seed culture on M1 agar media (0.4% starch, 0.2% yeast extract, 1% peptone and 0.8% agar) prepared in 3.3% artificial ocean sea salt, which was cultivated for a period of 4 weeks. A single colony was used to inoculate M1 broth (0.4% starch, 0.2% yeast extract and 1% peptone) 3.3% artificial ocean sea salt (1.48 mL) in micro-bioreactor in the presence of LPS (15 μL) to give final concentration (0.6 ng/mL). The micro-bioreactor was incubated at 26 °C, 190 rpm for 4 weeks. After the incubation period, the broth was extracted with EtOAc (2 mL), and the organic extract was dried under N_2. The resulting crude extract was resuspended in MeCN (100 μL) and analysed by HPLC-DAD-MS. The control wells were only inoculated with the fungal spores. Peaks with the following retention times t_R = 13.2 min exhibited the following *m*/*z* $[M+H]^+$ 507 (**3.05**) as shown in Figure 3.21.

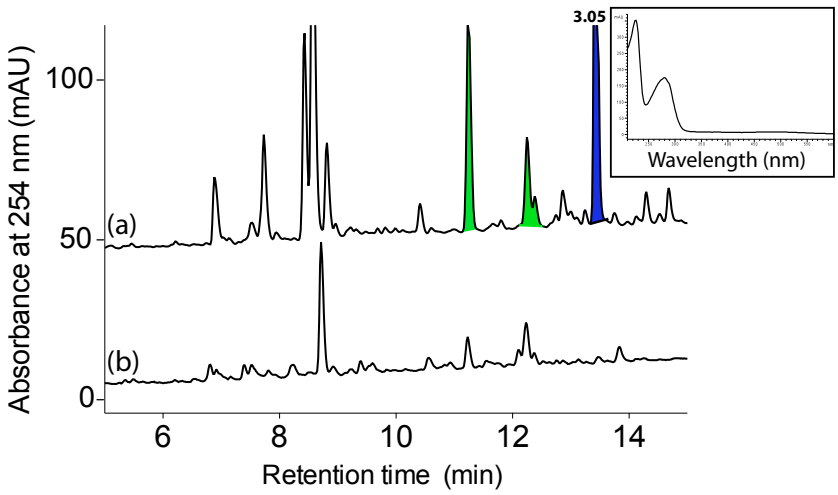

Figure 3.21. HPLC-DAD (254 nm) chromatogram, analytical gradient H_2O/MeCN plus 0.05% HCO_2H using Zorbax C_8 for the crude extract from CMB-M81F in the (a) presence and (b) absence of LPS cultivated on M1 agar medium. The highlighted blue peak represents the activated metabolite **3.05**, while the highlighted green peaks will be discussed in details in chapter 5

3.2.7.2 Preparative cultivation

A seed culture was prepared by inoculating a 250 mL flask containing liquid medium (80 mL deionized water containing 0.4% starch, 0.2% yeast extract, 1% peptone) in the presence of 3.3% artificial ocean sea salt with a single colony of CMB-M81F followed by shaking at 190 rpm for 4 weeks at 26.5 °C. Aliquots of the seed culture (5 mL) were transferred to two 2 L Fernbach flasks, each containing the same liquid medium (400 mL) and LPS (1 ng/mL), and the flasks were shaken at 190 rpm for 4 weeks at 26.5 °C. The resulting cultures were each extracted with EtOAc (400 mL) and the combined organic phases concentrated *in vacuo* to yield an extract (100.5 mg). The extract was sequentially triturated with hexane (15 mL) and DCM (15 mL) to afford, after concentration *in vacuo*, 6.3 and 85.6 mg, respectively. The DCM fraction was subsequently subjected to semi-preparative reversed-phase HPLC (Zorbax C_8 column, 250 × 9.4 mm, 5 μm, 3 mL/min gradient elution 90 – 10% H_2O/MeCN over 30 min to yield neoasterquinone (**3.05**) (t_R = 23.9 min, 1.1 mg, 1.8%) (Scheme 3.6).

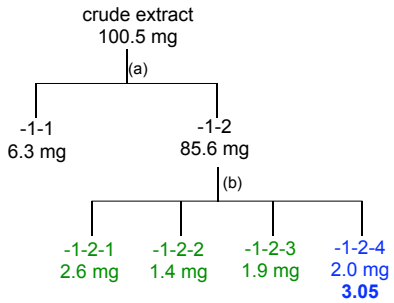

Scheme 3.6. Isolation scheme of CMB-M81F leading to the enhancement of the metabolites listed in below in green and the activation of 1 metabolite in blue (**3.05**). (a) Trituration [hexane (-1-1) and CH_2Cl_2 (-1-2)] and (b) semi-preparative HPLC: Zorbax-C_8, 90 – 10% H_2O/MeCN, 3 mL/min, 30 min

3.2.7.2.1 Neoasterriquinone (3.05)

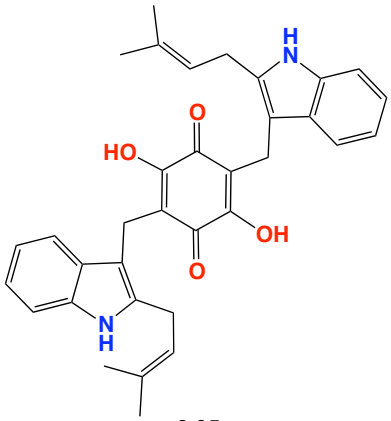

3.05

HRESI(+)MS data for **3.05** revealed a quasi-molecular ion $[M+H]^+$ indicative of molecular formula $C_{32}H_{30}N_2O_4$ (Δmmu +0.4). The ^1H NMR and 2D NMR ($CDCl_3$) data (**Figure 3.23** and **Table 3.9**) showed the presence of quinone moiety. It worth noting that only 13 resonances were observed from the ^{13}C and not 16 resonances which may suggest that **3.05** is symmetrical dimer in which the quinone and the phenolics carbons are missing due to the rapid inter-conversion of two equivalent tautomeric forms of the 2,5-dihydroxyquinone ring system. The structure elucidation was further supported by 2D NMR data, including HSQC, COSY and HMBC, as outlined in **Figure 3.22**, literature comparisons (**Table 3.10**), which determined that **3.05** was very likely neoasterriquinone.[115,116] Neoasterriquinone has been isolated before from the mycelia of *Aspergillus terreus* and they were potent antitumor compounds.[117]

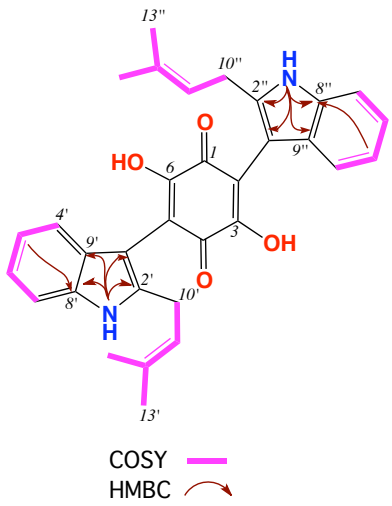

Figure 3.22. Key 2D NMR correlations of neoasterriquinone (**3.05**)

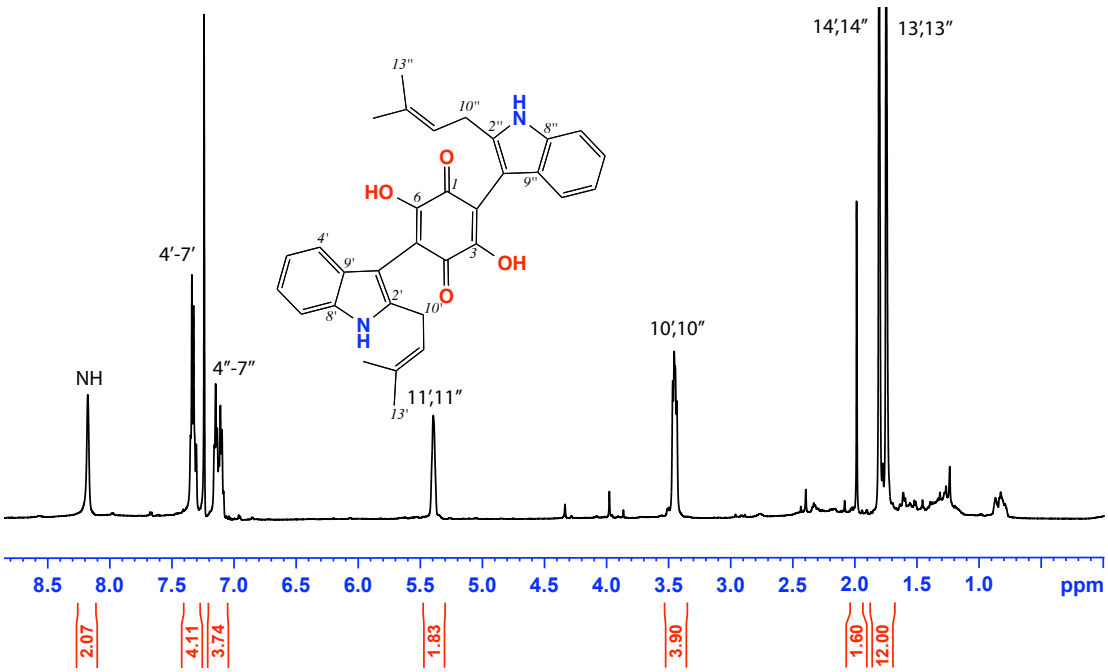

Figure 3.23. ^{1}H NMR (600 MHz, $CDCl_3$) spectrum of neoasterriquinone (**3.05**)

Table 3.9. NMR (600 MHz, $CDCl_3$) data of neoasterriquinone (**3.05**)

Pos.	δ_H, mult (*J* in Hz)[a]	δ_C[a]	COSY	^{1}H-^{13}C HMBC
1		[b]		
2		[b]		
3-OH		[b]		
4		[b]		
5		[b]		
6-OH				
1′,1″	8.17, s			2′, 3′, 8′, 9′
2′,2″		135.4		
3′,3″		100.8		
4′,4″	7.14[b]	121.2		2′/2″,6′/6″
5′,5″	7.10[b]	120.5		7′/7″, 8′/8″
6′,6″	7.31[c]	120.1		7′/7″,8′/8″
7′,7″	7.33[c]	111.1		5′/5″
8′,8″		128.0		
9′,9″		138.6		
10′,10″	3.45, dd *(12.7, 7.2)*	27.1	11′/11″,13′/13″,14′/14″	2′/2″,9′/9″,12′/12″
11′,11″	5.39, br s	120.2	13′/13″,14′/14″	10′/10″, 13′/13″
12′,12″		135.6		
13′,13″	1.74, s	19.6	10′/10″,11′/11″	11′/11″,12′/2″,14′/14″
14′,14″	1.80, s	28.5	10′/10″,11′/11″	11′/11″,12′/12″,13′/13″

*(a) ^{13}C assignments obtained from gHSQC and gHMBC data. (b and c) Overlapping resonances.

Table 3.10. ^{1}H NMR data ($CDCl_3$) comparison of experimental and literature[117] data of neoasterriquinone (**3.05**)

Pos	δ_H, mult, (*J* in Hz) experimental	δ_H, mult, (*J* in Hz) literature
1′,1″	8.17, s	8.20, br s
4′,4″	7.14[b]	7.12 – 7.36
5′,5″	7.10[b]	7.12 – 7.36
6′,6″	7.31[c]	7.12 – 7.36
7′,7″	7.33[c]	7.12 – 7.36
10′,10″	3.45, dd *(12.7, 7.2)*	3.47, d *(7.3)*
11′,11″	5.39, br s	5.42, t *(7.3)*
13′,13″	1.74, s	1.77, s
14′,14″	1.80, s	1.83, s
3,6-OH	[a]	8.07, s

*(a) signals not observed, (b) Overlapping resonances. (c) Overlapping resonances

3.2.8 *Streptomyces afghaniensis* (ACM-4008)

Figure 3.24. *Streptomyces afghaniensis* (ACM-4008)

3.2.8.1 Analytical cultivation and chemical analysis

A single colony of ACM-4008 was used to inoculate a seed culture on ISP-2 agar media (0.4% starch, 0.2% yeast extract, 1% peptone and 0.8% agar), which was cultivated for a period of 10 days. A single colony was used to inoculate ISP-2 broth (0.4% starch, 0.2% yeast extract and 1% peptone) (1.48 mL) in micro-bioreactor in the presence of LPS (15 μL) to give final concentration (0.6 ng/mL). The micro-bioreactor was incubated at 26 °C, 190 rpm for 10 days. After the incubation period, the broth was extracted with EtOAc (2 mL), and the organic extract was dried under N_2. The crude extract was then resuspended in MeOH and analysed by HPLC-DAD-MS. Peaks with the following retention times t_R = 8.9 and 9.8 min exhibited the following *m*/*z* $[M+Na]^+$ 739 (**3.06**) and 693 (**3.07**) as shown in Figure 3.25

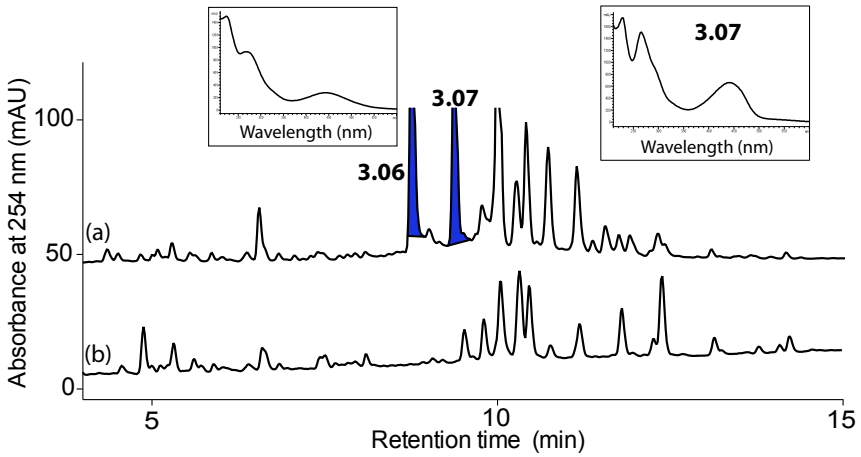

Figure 3.25. HPLC-DAD (254 nm) chromatogram, analytical gradient H_2O/MeCN plus 0.05% HCO_2H using Zorbax C_8 for the crude extract from ACM4008 in the (a) presence and (b) absence of LPS cultivated on ISP-2 broth medium. UV (inset) of **3.06** and **3.07**

3.2.8.2 Preparative cultivation

A seed culture was prepared by inoculating a 250 mL flask containing liquid medium (80 mL deionized water containing 0.4% starch, 0.2% yeast extract, 1% malt extract) with a single colony of ACM-4008 followed by shaking at 190 rpm for 10 d at 26.5 °C. Aliquots of the seed culture (5 mL) were transferred to one 2 L flasks, each containing the same liquid medium (400 mL) and LPS (0.6 ng/mL), and the flasks were shaken at 190 rpm for 10 d at 26.5 °C. The resulting cultures were each extracted with EtOAc (400 mL) and the combined organic phases concentrated *in vacuo* to yield an extract (100 mg). The extract was sequentially triturated with hexane (15 mL) and DCM (15 mL) to afford, after concentration *in vacuo*, 23.2 and 85.6 mg, respectively. The DCM fraction, which was found to be rich in the target metabolites **3.06** and **3.07** was subsequently subjected to semi-preparative reversed-phase HPLC (Zorbax C_8 250 × 9.4 mm, 5 μm column, 3 mL/min gradient elution from 90 – 10% H_2O/MeCN over 40 min with a hold at 100% MeCN for 5 min), to yield julichrome analogue (**3.06**) (t_R = 19.1 min, 1.5 mg, 1.7%) and julichrome $Q_{3.4}$ (**3.07**) (t_R = 22.4 min, 1.2 mg, 1.4%) (Scheme 3.7).

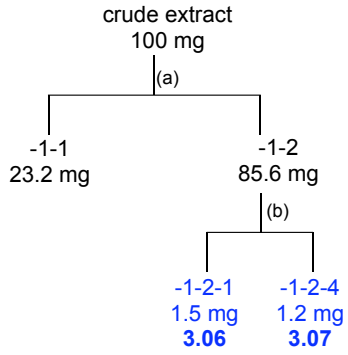

Scheme 3.7. Isolation scheme of the metabolites from crude extract of ACM4008. (a) Trituration [hexane (-1-1) and CH_2Cl_2 (-1-2)] and (b) Semi-preparative HPLC: Zorbax-C_8, 90 – 10% H_2O/MeCN, 3 mL/min, 30 min

3.2.8.2.1 Julichrome $Q_{3.5}$ (3.07)

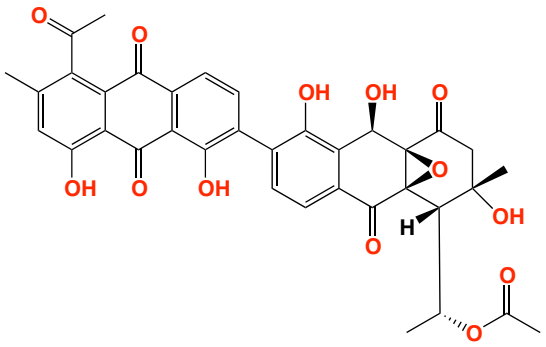

3.07

HRESI(+)MS data of **3.07** revealed an adduct ion $[M+Na]^+$ corresponding to a molecular formula $C_{36}H_{30}O_{13}$ (Δmmu +2.0). The NMR ($CDCl_3$) data of **3.07** showed the presence of five aromatic protons [δ 7.77, d, 7.7 Hz, H-6′; δ 7.89, d, 7.7 Hz, H-5′; δ 7.85, d, 8.0 Hz, H-5; δ 7.48, d, 8.0 Hz, H-6 and δ 7.19, s, H-2′], and two carbonyl at δ 204.7, C-1 and δ 170.8, C-12. All these observations accounted for 20 DBE, while two were not observed; therefore we assume the presence of two another carbonyl groups, which may suggest that **3.07** at least incorporated four rings. Analysis of the HMBC NMR ($CDCl_3$) for **3.07** revealed structure subunits as indicated in Figure 3.26, comprising (i) a correlation from methyl group H-11′ to the carbonyl C-11′; the deshielded methyl H-3′ to H-4′a through H-2′, (ii) 9-OH to C-9a, (iii) the deshielded methylene H-2 to H-13 through H-2 to C1; H-2 to H-4; H-4 to H-11 and H-13 to C-12. The structure elucidation was further supported by 2D NMR data, including HSQC, COSY and HMBC, as outlined in Figure 3.26, Figure 3.27 and Table 3.11. On searching the literature and our database based on the molecular formula, molecular weight and structure fragment, **3.07** was consistent with julichrome $Q_{3.5}$. Analysis of all the NMR data with comparison to literature data (Table 3.12) strongly suggested that **3.07** was the known metabolites julichrome $Q_{3.5}$.[118]

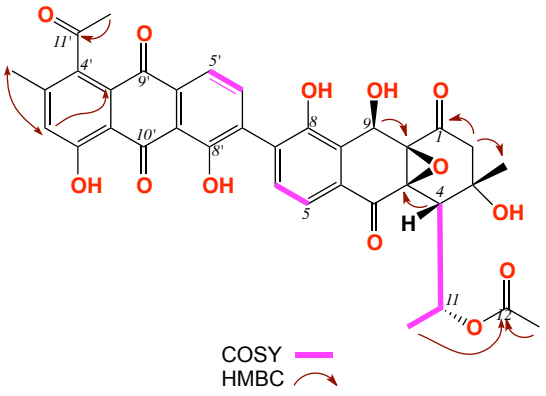

Figure 3.26. Key 2D NMR correlations of julichrome $Q_{3.5}$ (**3.07**)

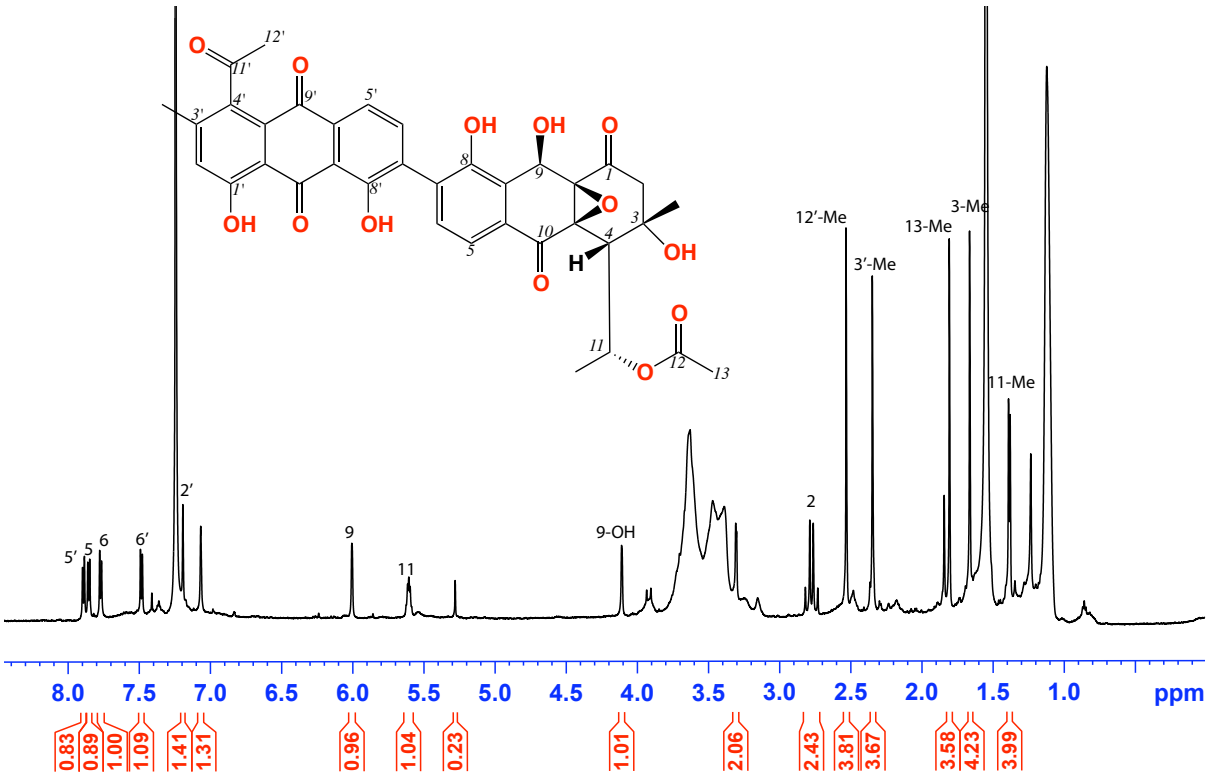

Figure 3.27. ^{1}H NMR (600 MHz, $CDCl_3$) spectrum of julichrome $Q_{3.5}$ (**3.07**)

Table 3.11. NMR (600 MHz, $CDCl_3$) data of julichrome $Q_{3.5}$ (**3.07**)

Pos.	δ_H, mult (*J* in Hz)[a]	δ_C[a]	COSY	^1H-^{13}C HMBC
1		204.7		
2	a 2.77, d (*18.9*)	50.8	3-Me	1, 4
	b 2.73 d (*18.9*)			
3		69.5		
3-Me	1.66, s	34.3	2	2, 3, 4
4	3.31[b]	45.4	11	2, 3, 11, 11-Me
4a		[c]		
5	7.85, d (*8.0*)	120.7	6	7, 8a
6	7.48, d (*8.0*)	132.1	5	8, 10a
7		131.1		
8		153.0		
8a		126.3		
9	6.01, br s	60.8	9-OH	9a
9a		64.5		
10		[c]		
10a		128.8		
11	5.60, m	68.5	4, 11-Me	
11-Me	1.38, d (*6.5*)	22.1	11	4
12		170.8		
13-Me	1.80, s	21.5		12
1′		162.8		
2′	7.19, s	126.5	3′-Me	3′-Me, 4′, 9′a
3′		144.9	2′	
3′-Me	2.34, s	19.9		2′, 3′, 4′
4′		137.5		
5′	7.89, d (*7.7*)	120.7	6′	7′,8′a
6′	7.77, d (*7.7*)	139.5	5′	8′
7′		133.6		
8a′		115.9		
9′		[c]		
9a′		113.3		
11′		204.7		
12′-Me	2.53, s	31.4	11	11′
8-OH	[c]			
1′-OH	12.04, s		1′	
8′-OH	13.02, s			
9-OH	4.15, br s		9	

(a) ^{13}C assignments obtained from gHSQC and gHMBC data. (b) Overlapping resonances. (c) signals not observed

Table 3.12. ^{1}H NMR data ($CDCl_3$) comparison of experimental and literature[118] data of julichrome $Q_{3.5}$ (**3.07**)

Pos	δ_H, mult, (*J* in Hz) experimental	δ_H, mult, (*J* in Hz) literature
2	2.77, d (*18.9*) and 2.73 d (*18.9*)	2.78, d (*18.5*) and 2.74, d (*18.9*)
4	3.31[a]	3.30, d (*3.8*)
5	7.85, d (*8.0*)	7.83, d (*8.1*)
6	7.48, d (*8.0*)	7.46, d (*8.1*)
9	6.01, br s	6.01, s
11	5.60, m	5.60, m
2′	7.19, s	7.17, s
5′	7.89, d (*7.7*)	7.86, d (*7.8*)
6′	7.77, d (*7.7*)	7.75, d (*7.8*)
3-Me	1.66, s	1.65, s
11-Me	1.38, d (*6.5*)	1.38, d (*6.5*)
13-Me	1.80, s	1.80, s
3′-Me	2.34, s	2.33, s
12′-Me	2.53, s	2.52, s
1′-OH	12.04, s	12.08, s
8′-OH	13.02, s	12.88, br s
8-OH	[b]	[b]
3-OH	4.15, br s	4.15, br s

*(a) overlapping resonances, (b) signals not observed

3.2.8.2.2 ACM4008-1-2-1 (3.06)

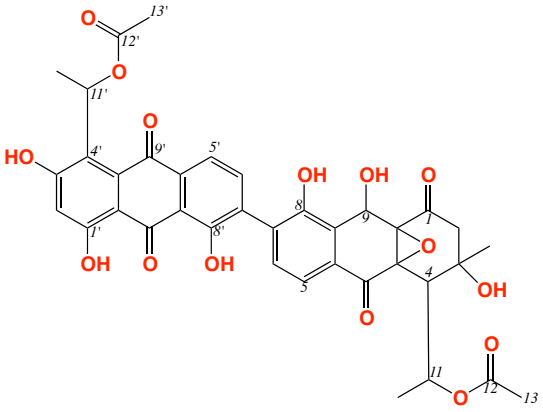

ACM4008-1-2-1 (**3.06**)

ESI(+)MS data of **3.06** revealed a molecular ion $[M+H]^+$ corresponding to a *m/z* 717 [M+H]. The UV spectrum was consistent with julichrome like compounds. The ^{1}H NMR ($CDCl_3$) data for **3.06** was very similar to julichrome $Q_{3.5}$ (**3.07**) with exception for the presence of acetyl group. This compound still under investigation.

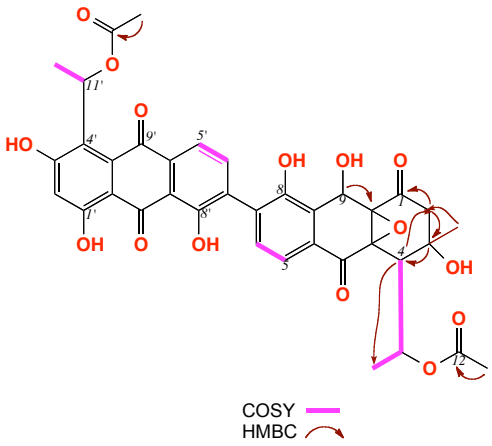

Figure 3.28. Key 2D NMR correlations of ACM-4008-1-2-1 (**3.06**)

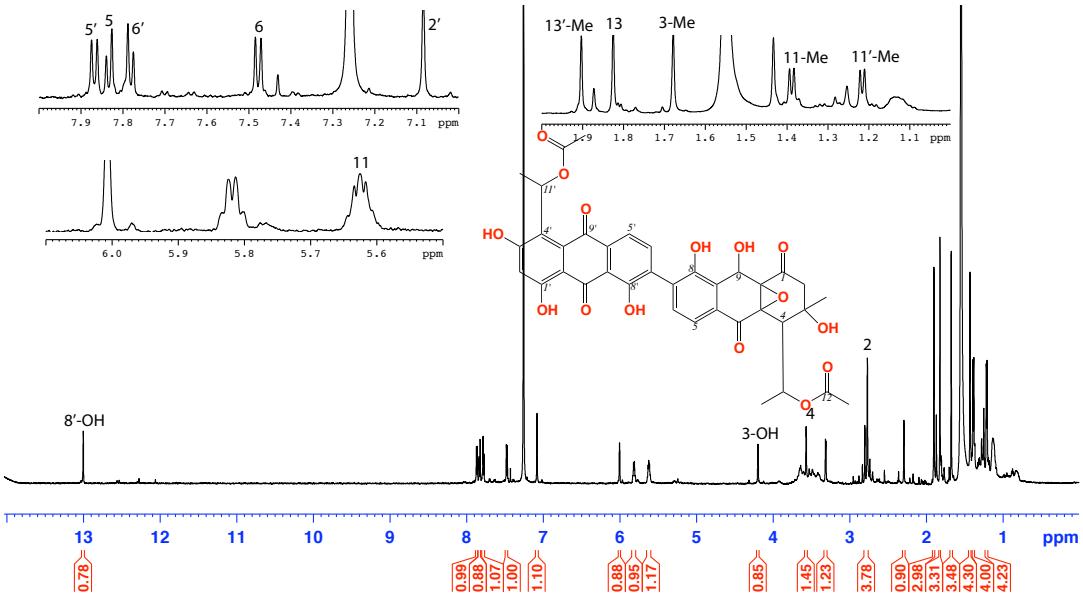

Figure 3.29. ^{1}H NMR (600 MHz, $CDCl_3$) spectrum of ACM-4008-1-2-1 (**3.06**)

Table 3.13. NMR (600 MHz, $CDCl_3$) data of ACM-4008-1-2-1 (**3.06**)

Pos.	δ_H, mult (*J* in Hz)[a]	δ_C[a]	COSY	^1H-^{13}C HMBC
1		204.5		
2	2.64[c], m	53.6	3-Me	1, 4
3		[d]		
3-Me	1.77, s	23.9	2	
4	3.16, d (*4.0*)	49.7	11	2, 3, 11, 11-Me
4a		[d]		
5	7.75[b]	123.3	6	
6	7.68, d (*7.2*)	135.2	5	
7		[d]		
8		[d]		
8a		[d]		
9	6.01, s	61.7		9a
9a		64.4		
10		[d]		
10a		[d]		
11	5.65, q (*6.2*)	72.3	4, 11-Me	
11-Me	1.45, d (*6.2*)	25.1	11	4
12		174.6		
13-Me	1.78, s	20.3		12
1′		[d]		
2′	7.06	121.2		
3′		[d]		
3′-Me	2.51[c]	22.1		
4′		[d]		
4a′		[d]		
5′	7.75[b]	123.3	6′	
6′	7.41, d (*7.2*)	142.1	5′	
7′		[d]		
8′		[d]		
8a′		[d]		
9′		[d]		
9a′		[d]		
10′		[d]		
10a′		[d]		
11′	5.79, br s	72.3		
12′		171.3		
11′-Me	1.25, d (*6.2*)	25.1	11	
13′-Me	1.90, s	24.4		12′

*(a) ^{13}C assignments obtained from gHSQC and gHMBC data. (b) Overlapping resonances. (c) Overlapping resonances. (d) signals not observed

By ^{1}H NMR analysis, it was observed that fragment A in **3.06** and **3.07** are approximately similar in the chemical shifts which may suggests that they can have the same stereochemistry (Table 3.14). Fragment B in 3.06 was quite different than fragment B in **3.07**, in which the COMe has been replace with OAc group (Figure 3.30 and Figure 3.31).

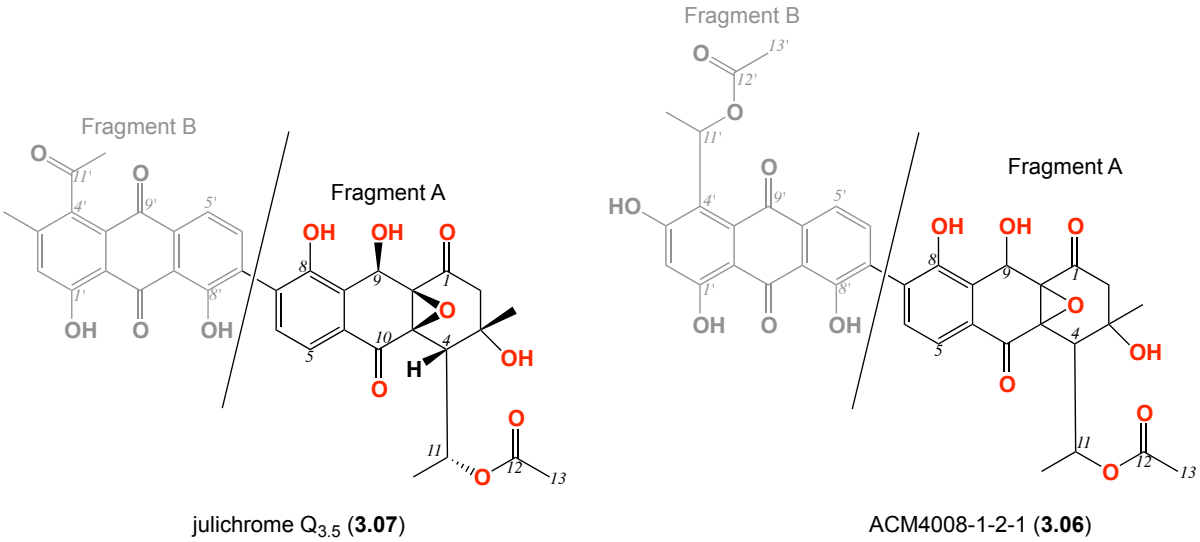

Figure 3.30. Comparison between ACM4008-1-2-1 (**3.06**) and julichrome $Q_{3.5}$ (**3.07**)

Table 3.14. NMR (600 MHz, $CDCl_3$) similarity between **3.06** and **3.07**

Pos.	δ_H, mult (*J* in Hz) (**3.07**)	δ_C[a]	δ_H, mult (*J* in Hz) (**3.06**)	δ_C[a]
1		204.7		204.5
2	2.77, d (*18.9*) and 2.73 d (*18.9*)	50.8	2.64, m	53.6
3		69.5		[c]
3-Me	1.66, s	34.3	1.77, s	23.9
4	3.31[b]	45.4	3.16, d (*4.0*)	49.7
4a		[c]		[c]
5	7.85, d (*8.0*)	120.7	7.75, d *(8.0)*	123.3
6	7.48, d (*8.0*)	132.1	7.68, d (*7.2*)	135.2
7		131.1		[c]
8		153.0		[c]
8a		126.3		[c]
9	6.01, br s	60.8	6.01, s	61.7
9a		64.5		64.4
10		[c]		[c]
10a		128.8		[c]
11	5.60, m	68.5	5.65, q (*6.2*)	72.3
11-Me	1.38, d (*6.5*)	22.1	1.45, d (*6.2*)	25.1
12		170.8		174.6
13-Me	1.80, s	21.5	1.78, s	20.3

*(a) ^{13}C assignments obtained from gHSQC and gHMBC data. (b) Overlapping resonces. (c) signals not observed

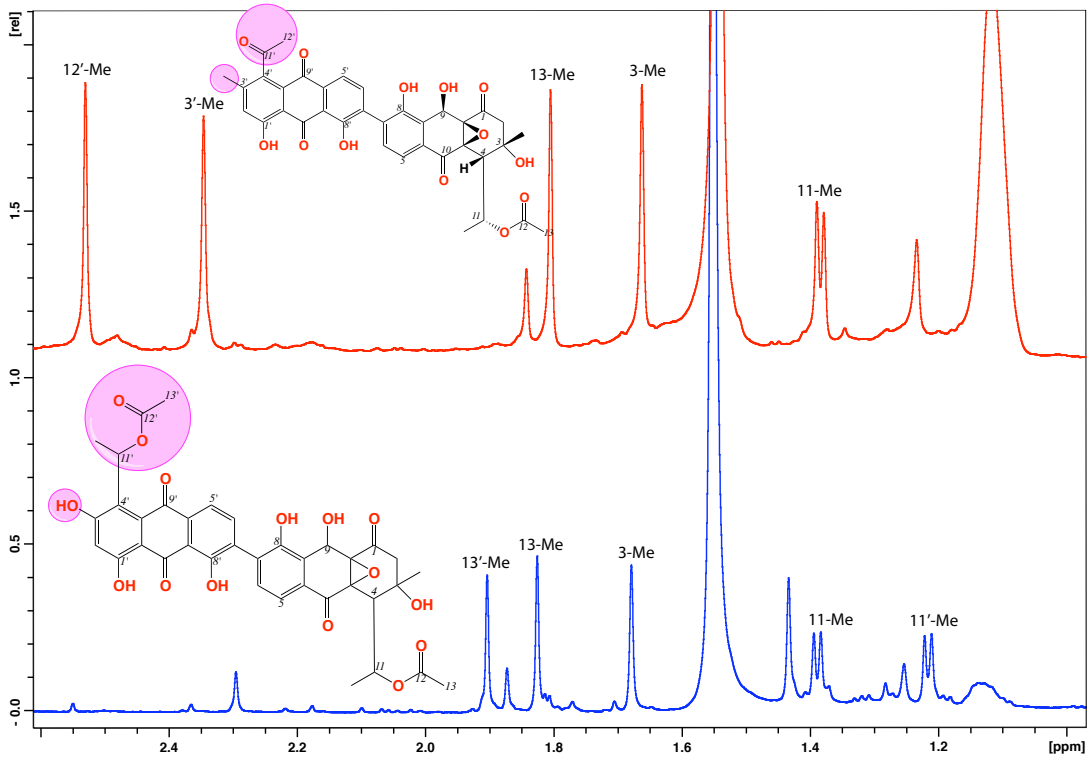

Figure 3.31. ^{1}H NMR (600 MHz, $CDCl_3$) spectrum of both julichrome $Q_{3.5}$ (**3.07**) (red) and (**3.06**) (blue) highlighting the difference between the two structures

3.3 Conclusion

This chapter illustartes a new paradigm for drug discovery to help to overcome the limited laboratory conditions and to establish a new technique to target the production of antibiotics. In order to perform such paradigm, combinatorial chemical libraries were established in order to cover much chemical space to increase the probability of wakening up the silent genes and turning on new secondary metabolites. Therefore, the micro-bioreactor was used to screen large number of microbes against the microbial crude extracts library and pure compounds as well as the LPS from *Escherichia coli*. Activation of silent metabolites was perfomed by the addition of another microbial crude extract and this section is still under investigation. Unfortunately, this approach was not practical as we got only 2 hits from around 300 experiments; therefore we decided to start looking into using LPS.

Lipopolysaccharide (LPS) from Gram-negative bacteria (*Escherichia coli*) was purchased from Sigma and tested for the induction of microbial secondary metabolites that may have antibacterial activity. Different microbes (actinomycetes and fungi) were chosen from the constructed terrestrial microbial library as well as from the ACM and marine collection. All the microbes were screened using the micro-bioreactor in the presence and the absence of LPS. After analysing the crude

extracts using our HPLC/DAD/MS, the hits were screened against antimicrobial assay using both Gram negative and Gram positive bacteria, *Escherichia coli* (ATCC 11775), *Pseudomonaus aeruginosa* (ATCC 10145), *Staphylococcus aureus* (ATCC 25293/9144), *Bacillus subtilis* (ATCC 6051/6633). The hits that showed antibacterial effect against Gram-positive bacteria were further investigated through large-scale cultivation and structural elucidation. Three hits were chosen, which are ACM 2573, CMB-TF411, CMB-M81F and ACM 4008. The first hit was ACM 2573 in which two metabolites were isolated, resistomycin (**3.01**) and activated metabolite resistoflavine (**3.02**). The second hit, CMB-TF411 the known metabolites, rugulosin (**3.03**) and activated metabolite skyrin (**3.04**) were isolated. The third hit was CMb-M81F in which the activated metabolite neoasterriquinone (**3.05**) was isolated. The fourth hit was from ACM 4008, in which the known metabolite julichrome $Q_{3.5}$ (**3.06**) was isolated and another unknown metabolite (**3.07**) in which it is related to the julichrome family because of the similarity of its UV spectrum and ^{1}H NMR of **3.06.** We can conclude that LPS can be considered as a new tool for the access of microbial genome and the activation of microbial secondary metabolites that may have a role as pharmaceutically active agents especially in the antibiotic field.

3.4 Experimental section

resistoflavine (**3.01**): deep purple powder; NMR (600 MHz, $CDCl_3$) see Table 3.1; HRESI(+)MS *m/z* 393.0970 $[M+H]^+$ (calcd for $C_{22}H_{17}O_7$ 393.0969).

resistomycin (**3.02**): deep purple powder; NMR (600 MHz, MeOD d_4) see Table 3.3; HRESI(+)MS *m/z* 377.1026 $[M+H]^+$ (calcd for $C_{22}H_{17}O_6$ 377.1020).

rugulosin (**3.03**): deep yellow oil; $[\alpha]^{23}_D$ +68.4 (*c* 0.05, MeOH); NMR (600 MHz, $CDCl_3$) see Table 3.5; see HRESI(+)MS *m/z* 565.1105 $[M+H]^+$ (calcd for $C_{30}H_{22}O_{10}Na$ 565.1110).

skyrin (**3.04**): deep violet powder; $[\alpha]^{23}_D$ –20.7 (*c* 0.05, $CDCl_3$); NMR (600 MHz, MeOH-d_4) see Table 3.7; HRESI(+)MS *m/z* 539.0970 $[M+H]^+$ (calcd for $C_{30}H_{19}O_{10}$ 539.0973).

neoasterriquinine (**3.05**): deep violet oil; NMR (600 MHz, $CDCl_3$) see Table 3.9; HRESI(+)MS *m/z* 507.2274 $[M+H]^+$ (calcd for $C_{32}H_{31}N_2O_4$ 507.2278).

julichrome analogue (**3.06**): reddish brown powder; $[\alpha]^{23}_D$ –29.8 (*c* 0.05, $CDCl_3$); NMR (600 MHz, $CDCl_3$) seeTable 3.13; ESI(+)MS *m/z* 717 $[M+H]^+$

julichrome $Q_{3.5}$ (**3.07**): reddish brown powder; $[\alpha]^{23}_D$ –30.4 (*c* 0.05, $CDCl_3$); NMR (600 MHz, $CDCl_3$) see Table 3.11; HRESI(+)MS *m/z* 693.1548 $[M+Na]^+$ (calcd for $C_{36}H_{30}O_{13}Na$ 693.1570.

4 Chapter 4: Beach warfare: An *Aspergillus* stimulates antifungal defenses in a *Streptomyces* sp.

4.1 Heronapyrroles

The heronapyrroles A – C (**4.01** – **4.03**) as shown in Figure 4.1 and Figure 4.2 belong to a rare mixed pyrroloterpene structure class bearing the nitro functionality α to the pyrrole nitrogen. These compounds have been isolated from an Australian marine derived-microbe *Streptomyces* sp. (CMB-M0423) obtained from a shallow water (– 1 m) sand sample collected near Heron Island, Queensland, Australia. HPLC-DAD-MS analysis of a small-scale liquid cultivation (100 mL) revealed biosynthetically related yellow pigments [*m/z* 421 (**4.01**), 405 (**4.02**), and 407 (**4.03**)] sharing an unusual polyene-like chromophore [λ_{max} 348] as shown in Figure 4.1. These compounds (Figure 4.2) isolated by a previous PhD student in our group, exhibited promising antibacterial activity against *Staphylococcus aureus* (ATCC 2593 and 9144) and *Bacillus subtilis* (ATCC 6051 and 6633).

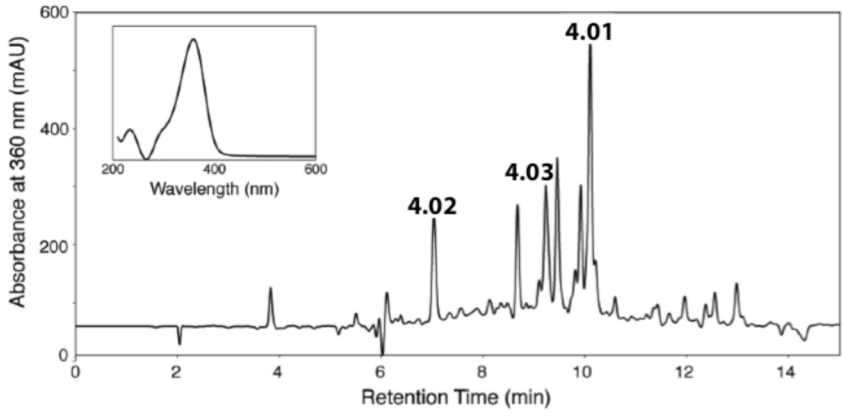

Figure 4.1. HPLC-DAD chromatogram (360 nm) of crude EtOAc extract from *Streptomyces* sp. (CMB-M0423)[119]

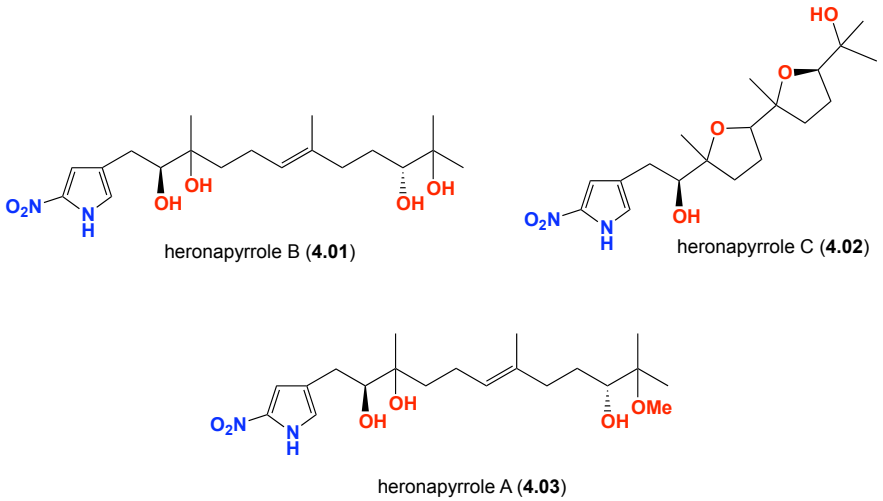

Figure 4.2. Structures of the heronapyrroles

It is also a noteworthy that heronapyrroles belong to the rare family of nitropyrrole natural products, known examples of which are limited to the 3-nitropyrrole pyrrolomycin class of *Streptomyces* antibiotics, pyrrolomycin A (**4.04**) and B (**4.05**).[120] Furthermore, the heronapyrroles are considered as the first documented examples of natural products bearing a 2-nitropyrrole functionality.

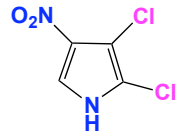

pyrrolomycin A (**4.04**)

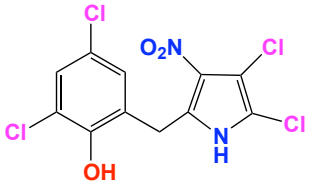

pyrrolomycin B (**4.05**)

Although natural products of mixed biosynthesis featuring terpenoid residues attached to various aromatic/heterocyclic systems are well known across the field of natural products chemistry, pyrroloterpenes are especially rare. The few known examples are limited to the lipid peroxidation inhibitor pyrrolostatin (**4.06**) from a Brazilian soil *Streptomyces chestomyceticus*,[121] and the antimicrobial and anticancer glaciapyrroles A – C (**3.07 – 3.09**) from an Alaskan marine-derived *Streptomyces* sp.[122] Following publication of the heronapyrroles, closely related analogues, nitropyrrolins A – E (**4.10 - 4.14**) were reported by Fenical *et al.* from a marine-derived actinomycete.[123]

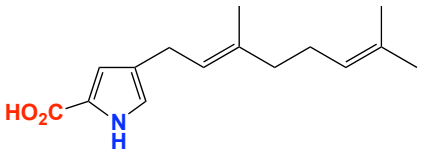

pyrrolostatin (**4.06**)

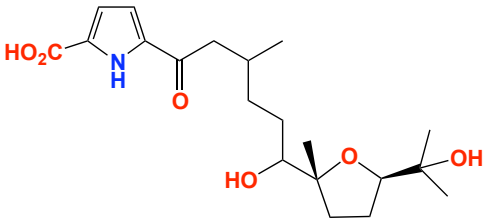

glaciapyrrole A (**4.07**)

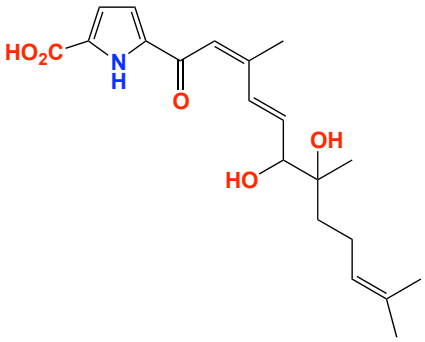

glaciapyrrole B (**4.08**)

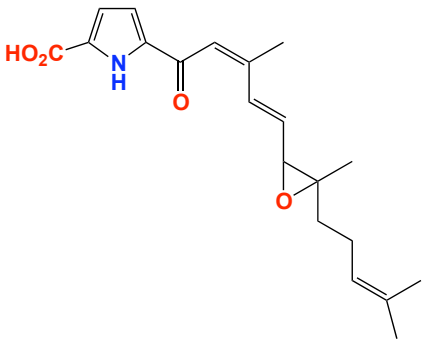

glaciapyrrole C (**4.09**)

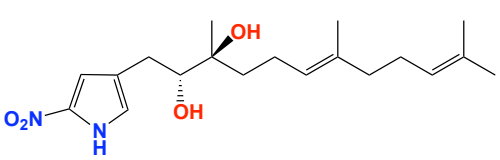

nitropyrrolin A (**4.10**)

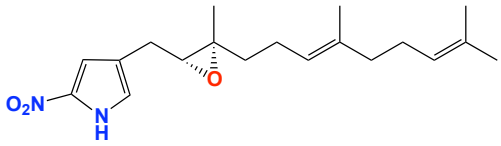

nitropyrrolin B (**4.11**)

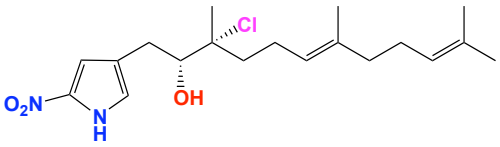

nitropyrrolin C (**4.12**)

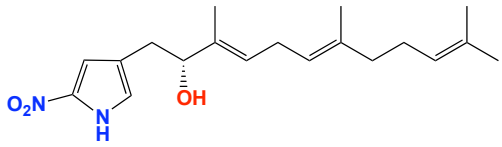

nitropyrrolin D (**4.13**)

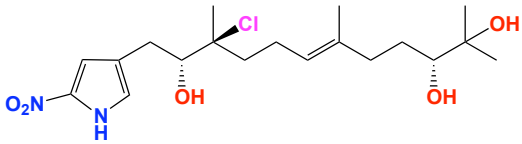

nitropyrrolin E (**4.14**)

4.2 Future of heronapyrroles

A plausible biosynthesis for the heronapyrroles is outlined in Figure 4.3. In this pathway, aromatic substitution of the pyrrole moiety by farnesyl pyrophosphate provided access to the pyrroloterpene carbon framework, further elaborated by nitration, oxidation and nucleophilic ring opening of the epoxide intermediates in which a cascade cyclization provides the full suite of heronapyrroles.[119]

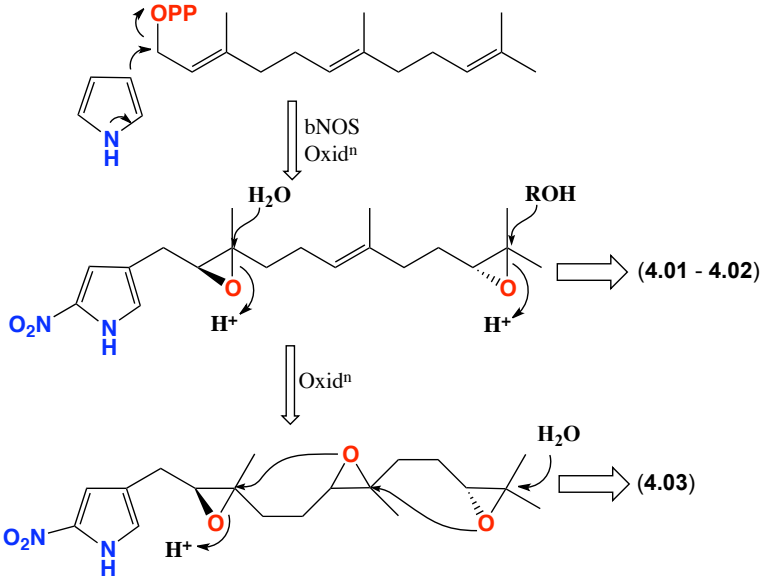

Figure 4.3. Plausible biosynthesis of heronapyrroles

In 2012, Stark *et al.* completed the synthesis of heronapyrrole C (**4.03**) and assigned relative and absolute stereochemistry to heronapyrrole C (**4.03**). This stereochemical assignment suggested that the biosynthetic polyprenalyation of the pyrrole system of the acyclic terpenoid subunit is subjected

to oxidative conversion to a bis-THF sub-structure as shown as in Figure 4.4. This hypothesis requires an alternative (left to right) intramolecular cyclization proposed for **4.03**, with H_2O attack at the first epoxide (Figure 4.4).[124]

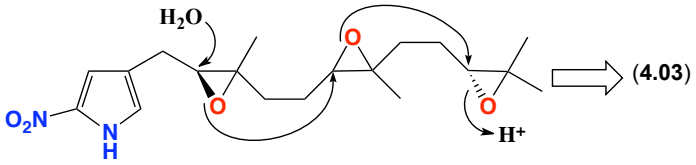

Figure 4.4. New possible biosynthesis of heronapyrrole C (**4.03**)[124]

While our research group had published the heronapyrroles, we were nevertheless interested in pursing their antibacterial properties further. To achieve this goal we needed a secure supply of the three known heronapyrroles (**4.01** - **4.03**) and if possible a selection of biosynthetically related analogues. Taking note of the role that bacterial nitric oxide synthase (bNOS) can play in the nitration of secondary metabolites.[125] We speculated on the involvement of bNOS in heronapyrroles biosynthesis. To test our hypothesis, a series of experiments were designed in which *Streptomyces* sp. (CMB-M0423) was cultivated in the presence of the commercially available NOS inhibitors aminoguanidine (AG) (**4.16**), N^G-methyl-L-arginine (NMMA) (**4.17**) and nitro-L-arginine-methyl ester (NAME) (**4.18**). These studies were designed to inhibit a hypothetical bNOS, with a possible consequence being the production of non-nitrated heronapyrroles analogues. Such unnatural heronapyrroles would be very valuable in the structure activity relationship studies designed to probe the antibacterial properties of this unique structure class. Before proceeding to the results and discussion, it is necessary to pause and reflect on the history and the role of NOS in both mammalian and bacterial systems.

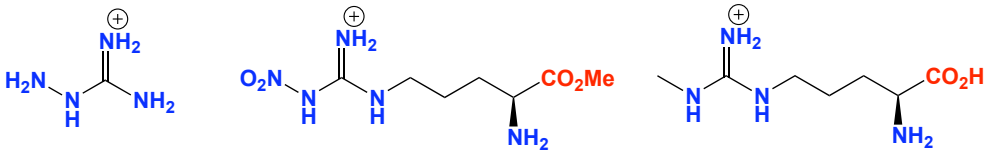

AG (**4.16**) L-NAME (**4.17**) L-NMME (**4.18**)

4.3 Nitric oxide synthase (NOS)

The story of nitric oxide synthase (NOS) is a wonderful example on how an enzyme function can evolve overtime, with its structure and mechanism of action remaining largely intact. In 1967, nitric oxide (NO) was first identified as an important biological product and proved as an intermediate in the denitrification process in the bacterium *Pseudomonas perfectomarinus*.[126] Denitrification is a process in the environmental cycle in which bacteria reduce NO_3^{2-} to NO_2^- and N_2 as an important

process in acquiring energy as well as balancing the redox state during anaerobic respiration.[127] In 1980, NO was discovered as an essential regulator in many biological mechanisms, including cellular signalling and immune responses such as the regulation of blood pressure, control of vascular tone, protection against other pathogens as a defence mechanism and cancer, hormone regulation, nerve cell transmission and angiogenesis.[128-130]

4.3.1 Mammlian NOS

Nitric oxide is a crucial messenger molecule, which has numerous molecular targets such as neurotransmission[131,132], control of vascular tone[133,134] and regulation of gene transcription[135] and mRNA translation[136]. In mammals, NO can be generated by three different isoforms of the enzyme NO synthase (NOS). This important discovery led to the identification of three isoenzymes responsible for the regulation of NO, endothelial nitric oxide synthase (eNOS), inducible NOS (iNOS) and neuronal NOS (nNOS).[137,138] All isoforms utilize L-arginine as the substrate, and molecular oxygen and reduced nicotinamide-adenine-dinucleotide phosphate (NADPH) as co-substrates.[134,139]

Mammalian NO synthases (mNOSs) are complex enzymes that consist of dimeric proteins which contain an amino-terminal haem oxygenase domain (NOS_{oxy}) and a carboxy-terminal flavoprotein reducatse domain (NOS_{red}). The oxygenase domain binds to L-arginine (L-Arg), haem and the redox active cofactor tetrahydrobiopterin, while the reductase domain binds to flavin adenine dinucleotide (FAD), flavin mononucleotide (FMN) and nicotinamide adenine dinucleotide phosphate (NADPH) which later catalyzes the oxidation of L-Arg to NO and citrulline and the molecular signal NO as well as a reductase domain that shuttles electrons to the heme of the oxygenase domain as shown in Figure 4.5.[140]

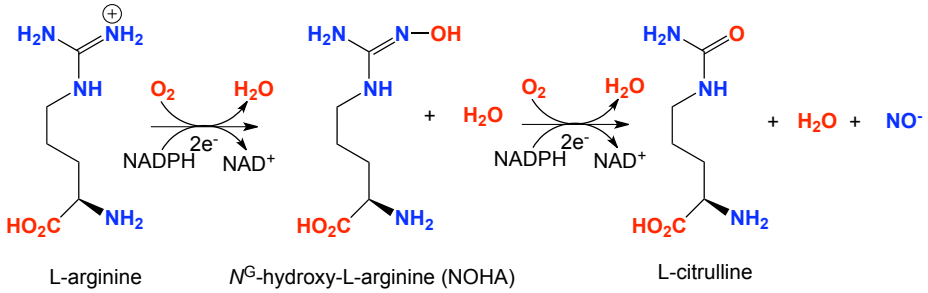

Figure 4.5. Two-step oxidation of L-arginine to L-citrulline and NO. Abbreviation: NOHA, N^G-hydroxy-L-arginine

Neuronal NOS has been implicated in modulating physiological functions such as learning, memory and neurogenesis.[141] Inducible NOS is not usually expressed in the cells, but its expression can be induced by the presence of bacterial lipopolysaccharide, cytokines and other agents. Once

expressed, iNOS is constantly active and not regulated by intracellular Ca^{2+} concentrations.[142] When iNOS is induced in the macrophages, the resulting NO binds to protein-bound iron and inhibits key enzymes that contain iron in their catalytic centres. These effects are considered the basis of the cytostatic and cytotoxic effects of NO on parasitic microorganisms and tumour cells.[143] Endothelial NOS is a homostatic regulator of numerous essential cardiovascular functions in which it dilates all types of blood vessels leading to increase in the blood pressure.[133] NO released towards the vascular lumen helps to inhibit platelet aggregation and therefore aid in the protection from thrombosis.[144]

4.3.2 Bacterial NOS (bNOS)

The genome sequencing for bacterial NOSs has revealed that some bacteria contain genes coding for NOS proteins. This outcome is consistent with studies of NOS-like activities in bacterial extracts. By 2004, bacterial NOS (bNOS) had been found in more than 20 bacterial genera, such as *Bacillus*, *Staphylococcus* and *Deinococcus*.[145] Other studies provided *in vivo* evidence for bNOS dependent NO production in *B. subtilis*, *Rhodococcus* sp. and other *Streptomyces* species.[146,147] Differences between mammalian and bNOSs include the absence of a C-terminal reductase domain in the latter.[148] The first discovery of bNOS activity in 1994 was reported from a *Nocardia* species[149], while the first discovery of biological function came in 2004 from the discovery that bNOS was responsible for the potato scab disease caused by a *Streptomyces* toxin thaxtomin A (**4.15**), which interfered with plant cell wall synthesis. Thaxtomin A (**4.15**) is a dipeptide produced by non-ribosomal peptide synthase, in which a tryptophanyl moiety is nitrated at C-4. The location of a bNOS gene cluster close to the non-ribosomal peptide synthase genes suggested that bNOS may be involved in the nitration process. Kers *et al.*[125] proved that NOS inhibitors such as aminoguandine (AG), nitro-L-arginine methyl ester (NAME) and N^G-methyl-L-arginine (NMMA) suppress bNOS and the production of thaxtomin A (**4.15**) without affecting the bacterial growth. Thaxotamin A (**4.15**) plays a vital role in the cellulose biosynthesis inhibition which is crucial for plant pathogenicity in most pathogenic streptomycetes[150] and it would appear that a functioning bNOS is essential for its biosynthesis.

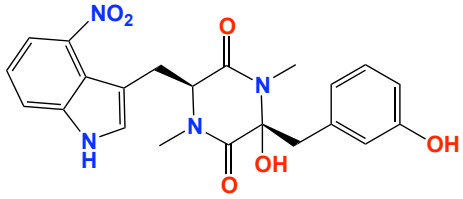

thaxtomin A (**4.15**)

In subsequent studies in 2008, Evan *et al.* proved that bNOS in plant pathogenic *Streptomyces* provides the NO necessary for the production of thaxtomin A (**4.15**). These workers also demonstrated that bNOS is capable of releasing NO *in vivo* and that NO has significant implications for bacterial signalling in which a plant pathogenic *Streptomyces* sp. produce NO at the host-pathogen interface and they proved that NO synthesis is induced by plant cell wall component, cellobiose.[148]

4.3.3 Structural differences between nitric oxide synthases

Key residues in the cofactor and the substrate binding sites are well conserved among different NOS. Still there are notable differences within the oxygenase domain as shown in Table 4.1, Figure 4.6 and Figure 4.7.

Table 4.1. Major differences between mammalian and bacterial NOSs[151]

	Mammlian NOS	Bacterial NOS
Oxygenase/reductase domain moiety	N-terminal oxygenase, C-terminal reductase domains	Oxygenase domain only, multiple reductase partners
Oxygenase domain dimer	Stabilized by Zn^{2+} bound at the dimer interface	Lacks Zn^{2+} binding site but forms stable dimers
Pterin binding site	Closed; can only fit H_4B	Exposed, can carry H_4B and other molecules
Targeting	Isotype specific N-terminal domains	Lack the domains
Regulation	Ca^{2+}/CaM (nNOS, eNOS) Transcriptionally (iNOS)	Unknown mechanism
Roles of NO	Neurotransmission (nNOS), vasodilation (eNOS), host defence (iNOS) and others functions.	antioxidative stress, and UV damage, plays a role in the biosynthesis of different nitrated compounds as well as transcriptional regulation.

*nNOS = neuronal NOS, eNOS = epithelial NOS, iNOS = inducible NOS, H_4B = tetrahydrobiopterin

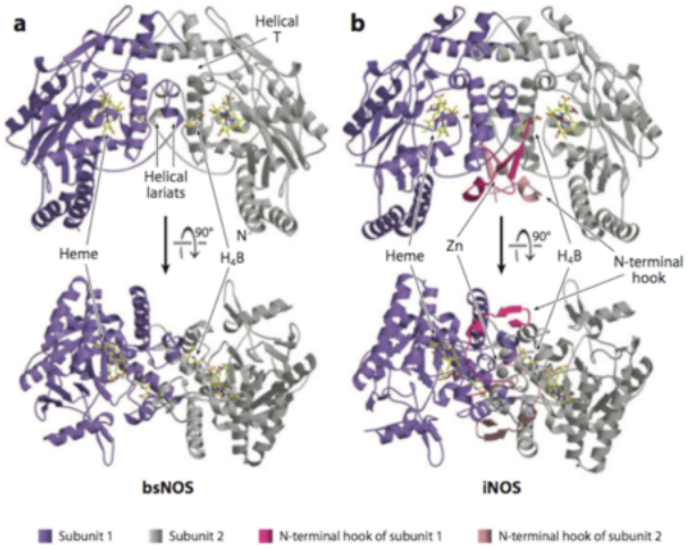

Figure 4.6. Structures of the N-terminal heme oxygenase domains of (a) *B. subtilis* bNOS and (b) human iNOS. The structures are highly similar with the exception of the missing N-terminal hook and zinc-binding regions in bNOS. Figure from Crane *et al.*[152]

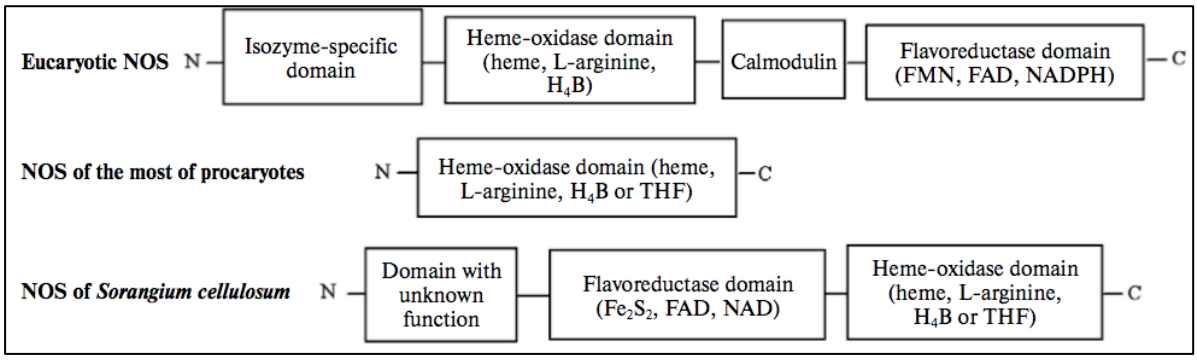

Figure 4.7. Domain structure of NO synthases from different sources. Figure from Filippovich *et al.*[153]

4.3.4 Nitric oxide synthase inhibitors

The understanding of the involvement of NO in physiological processes makes it an important target for the development of many therapeutic agents. The depletion of NO can result in hypertension, angina and impotence, while in other cases the overproduction of NO can lead to shock, sepsis, stroke, inflammatory responses and some neurodegenerative diseases such as Parkinson's Alzheimer's and Huntington's disease.[154] The inhibition of nNOS (neuronal NOS) or iNOS (inducible NOS) could provide effective treatment for many diseases and the selective inhibitors could be a useful tool for investigating the biological functions of NO and the treatment of the involved disease. The last 6 years has been > 60 new patents focusing on NOS inhibitors, as evidence of considerable interest by the pharmaceutical industry. The NOS inhibitors, AG (**4.16**), L-NAME (**4.17**) and L-NMME (**4.18**) are believed to exhibit isoform-selective NOS inhibition, decreasing NO concentration in specific tissues.[155] These three NOS inhibitors will be discussed later in this thesis. Compounds reported as selective nNOS inhibitor are shown in Figure 4.9.[155]

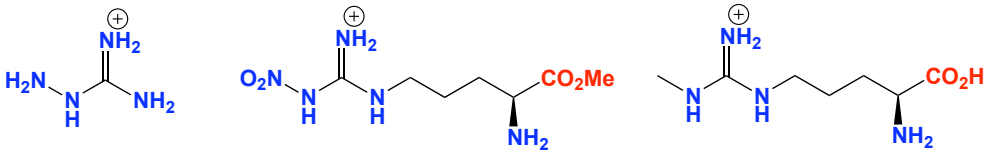

Figure 4.8. Structures of some bNOS inhibitors

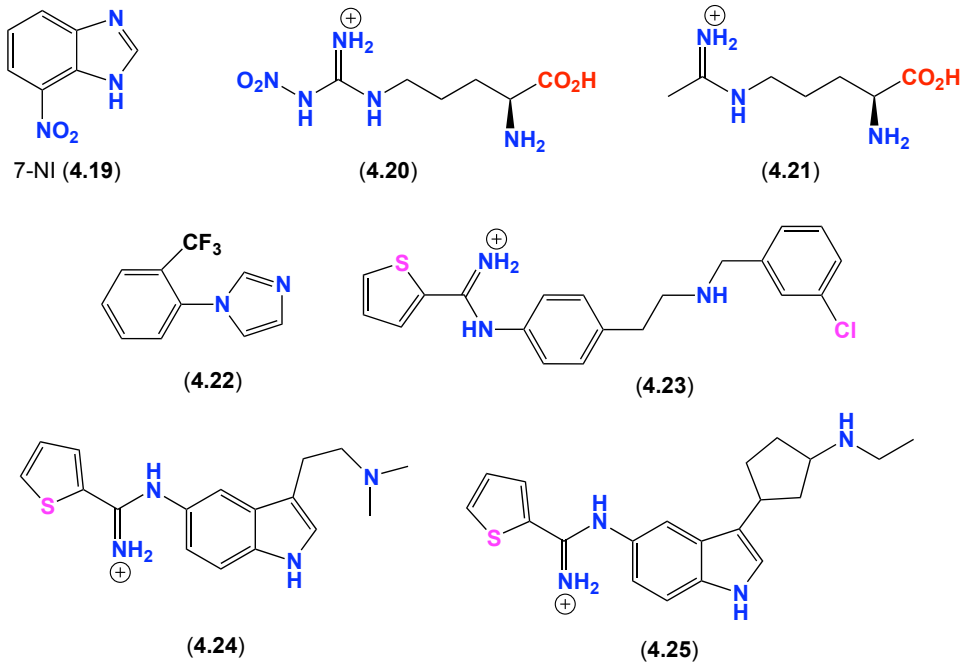

Figure 4.9. Selective nNOS inhibitors

4.3.5 Bacterial nitric oxide synthase and their importance

4.3.5.1 Plant toxin production

Based on the above findings, attempts have been made to find and characterize sources of NOS activity from microbial strains. As discussed earlier, the first indication of bNOS function came from the discovery of a *nos*-like open reading frame in *Streptomyces* sp. that causes potato scab through the production of thaxtomin A (**4.15**).[125] The position of *nos* on the pathogenicity island responsible for thaxtomin A biosynthesis, near the genes encoding non-ribosomal peptide synthase, strongly suggested that bNOS was involved in the nitration of thaxtomin A. Upon the addition of NOS inhibitor, non-nitrated thaxtomin A was not detected. The addition of NOS inhibitors did however lead to a decrease in the production of thaxtomin A without affecting the cell growth, and thereby decreasing the toxic effect.[156]

Wach *et al.*[156] used the NOS inhibitors to provide evidence for the involvement of bNOS in the biosynthesis of thaxtomin A (**4.15**), a toxin produced by the plant pathogen *Streptomyces turgidiscabies* that is responsible for causing potato scab disease. The addition of four NOS inhibitors; AG (**4.16**), NAME (**4.17**), NMMA (**4.18**) and 7-NI (**4.19**), and the NO scavenger 2-(4-carboxyphenyl)-4,4,5,5-tetramethylimidazoline-1-oxyl-3-oxide (CPTIO) (**4.26**), reduced production of **4.15** without affecting bacterial growth.[125] Likewise addition of the NO donors, diethylamino nitric oxide (DEANO) (**4.27**); 3-morpholinosydnonimine (SIN) (**4.28**); and *S*-nitroso-*N*-acetylpenicillamine (SNAP) (**4.29**) to *S. turgidiscabies* with a deleted *nos* gene restored the

production of **4.15**. All these studies provide strong evidence that NO plays a crucial role in the biosynthesis of thaxtomin A (**4.15**) with bNOS being the source of NO. In these studies NOS inhibitors were used at different concentrations, AG (2.7, 27, 270 μM); NAME (32, 320 nM, 3.2, 32, 350 μM); NMME (17, 170, 510 μM), and all NO donors, DEANO, SIN, and SNAP and the NO scavenger CPTIO were all tested at 1 mM.

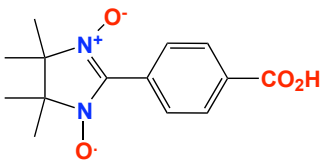

CPTIO (**4.26**)

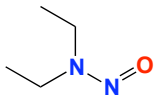

DEANO (**4.27**)

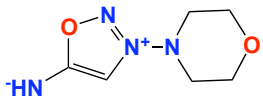

SIN (**4.28**)

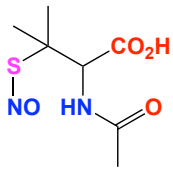

SNAP (**4.29**)

4.3.5.2 NO production and the defence mechanism against oxidative stress

Energy demands of many aerobic organisms require the efficient synthesis of ATP by mitochondrial oxidative phosphorylation. Together with ATP synthesis, the organism is exposed to reactive oxygen species (ROS) that are considered as mitochondrial electron transport chain product. Under the conditions of continuous oxidative production, antioxidant enzymes that are responsible for removing ROS can be overwhelmed, leading to oxidative stress. Oxidative stress has been implicated in different degenerative diseases including carcinogenesis, hemochromatosis, Parkinson's disease, Alzheimer disease and aging. Diseases associated with tissue iron accumulation are of great interest as iron catalyzes the generation of the highly reactive hydroxyl radical, in a process known as the Fenton reaction.[157]

In bacteria, H_2O_2 reacts with free cellular Fe^{2+} to generate OH radical through a Fenton reaction, leading to DNA damage and depletion of Fe^{2+}. Thus to drive the Fenton reaction, Fe^{3+} must be continuously reduced to Fe^{2+} by cellular reductants (Figure 4.10).[158]

$$Fe^{2+} + H_2O_2 \longrightarrow Fe^{3+} + OH^{\bullet} + OH^-$$

Figure 4.10. Fenton's reaction

In 2005, Gusarov *et al.*[146] showed that NO plays a critical role in the adaptation mechanism to the oxidative stress associated with metabolic stress and defending the pathogen against immune oxidative attack. These authors showed that NO protects bacterial cells against reactive oxygen species through suppressing the enzymatic reaction of free cysteine that catalyses the damaging

Fenton reaction. At the same time, NO also reactivates catalase, a major component of antioxidant enzyme that is inhibited by endogenous cysteine.

4.3.5.3 NO production and the defence mechanism against antibiotics

Anon *et al.*[159] showed that NO generated by bNOS increases the resistance of bacteria to a broad spectrum of antibiotics which enable the bacteria to survive and share their environment with antibiotic-producing microorganisms. They proved that *B. subtilis* with *nos* is capable of defending itself against pyocyanin which is considered as one of many natural toxins with broad antimicrobial activity produced by *P. aeruginosa*.

Bacteria use small molecules to communicate with nearby organisms in the surrounding environment. This process called quorum sensing (QS), commonly regulates bioluminescence, biofilm production and virulence. In 2012, Henares *et al.*[160] investigated the effect of NO on the bioluminescence in *Vibrio harveyi*. They showed that NO is involved in QS through LuxU gene cluster in *Vibrio harveyi*, by detecting an NO concentration-dependent increase in bioluminescence.

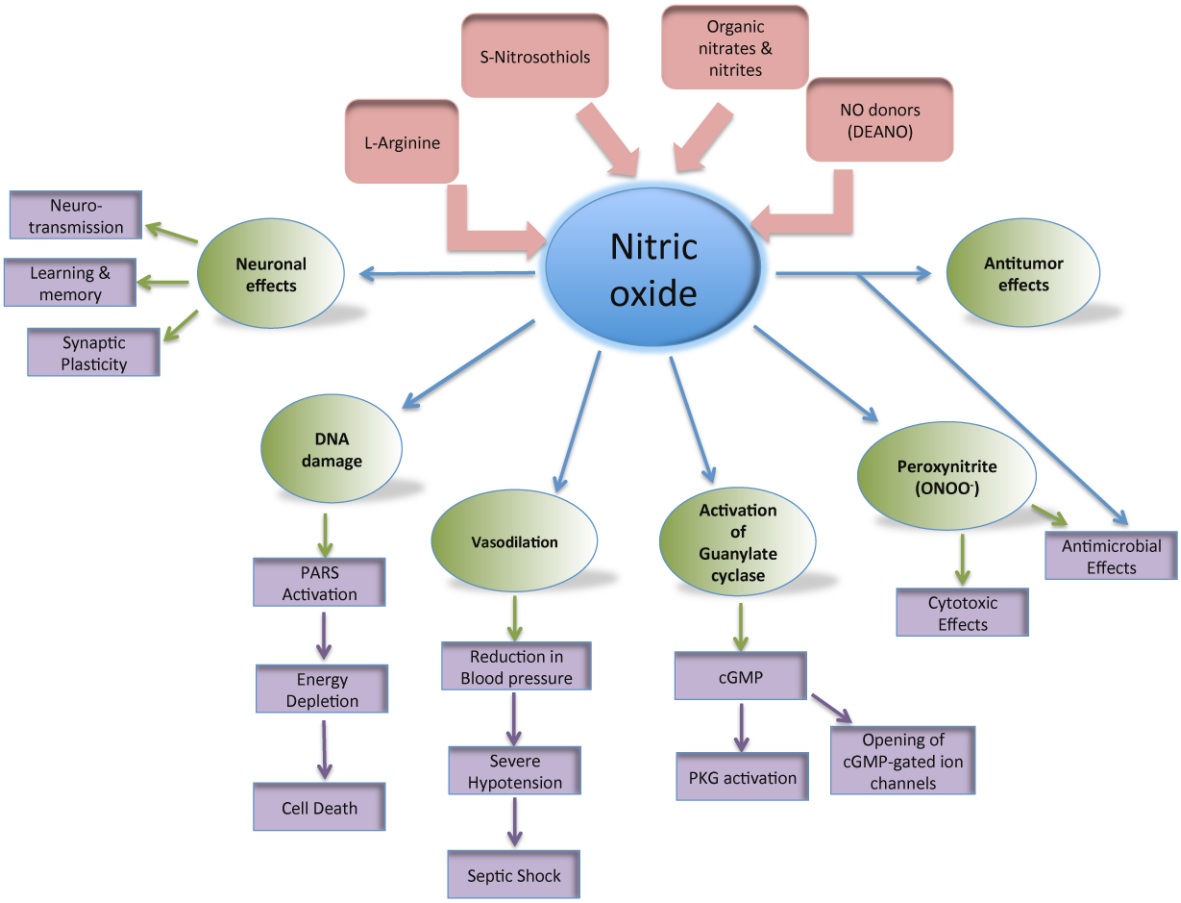

Figure 4.11. Summary of physiological functions of nitric oxide (NO)

4.4 Results and discussion

4.4.1 Cultivation of *Streptomyces* sp. (CMB-M0423) in the micro-bioreactor

Chapter 2 outlined the details of the methodology for cultivation in the micro-bioreactor. Micro-bioreactor cultivation methodology was used to study the secondary metabolites chemical profiling of *Streptomyces* sp. (CMB-M0423). In order to ensure that the *Streptomyces* sp. (CMB-M0423) was not adversely affected by this technology, it was cultivated and analysed in the micro-bioreactor (1.5 mL broth), and a standard shake flask (80 mL broth), in the same M1 3.3% artificial ocean sea salt-based media (Figure 4.12). The results from this experiment suggested that the micro-bioreactor do not affect the secondary metabolites produced by *Streptomyces* sp. (CMB-M0423).

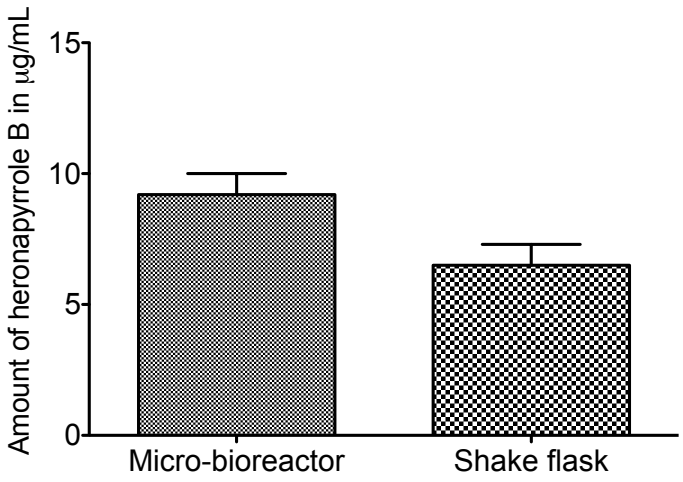

Figure 4.12. Production of heronapyrrole B (**4.02**) in the micro-bioreactor and shake flask (three replicates)

4.4.2 Cultivation of *Streptomyces* sp. (CMB-M0423)

Streptomyces sp. (CMB-M0423) was cultivated in the micro-bioreactor containing M1 broth (1.5 mL) in 3.3% artificial ocean sea salt. The micro-bioreactor was incubated for 7 days at 26.5 °C, 190 rpm. After the incubation period, individual cultures were extracted by the addition of EtOAc (1.5 mL) to each well. The organic layer was decanted, dried *in vacuo*, re-weighed, re-dissolved in MeOH to give final concentration of 1 mg/mL, then analysed using HPLC-DAD-MS. The chemical profiling confirmed that the cryo-recovered strain of *Streptomyces* sp. (CMB-M0423) has ceased production of heronapyrroles A (**4.01**) and C (**4.03**), but had retained the capacity to produce heronapyrrole B (**4.02**) (Figure 4.13).

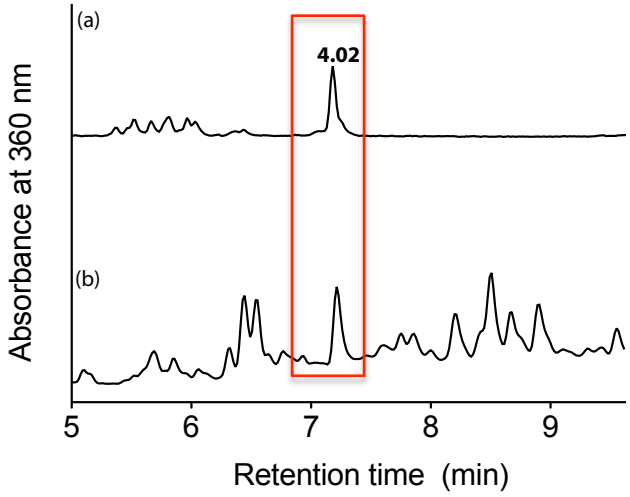

Figure 4.13. HPLC-DAD chromatogram analytical gradient H_2O/MeCN plus HCO_2H on a Zorbax C_8 column of (a) heronapyrrole B standard, (b) crude extract from *Streptomyces* sp. (CMB-M0423) at 360 nm showing the production of heronapyrrole B (**4.02**)

4.4.3 Quantification of heronapyrrole B production

A calibration curve was generated in order to determine the concentration of heronapyrrole B in the crude extract of *Streptomyces* sp. (CMB-M0423). Known concentrations (4 to 0.06 nmol/10 μL) of heronapyrrole B (**4.02**) in MeOH were prepared in two-fold dilutions. The standard solutions were analysed by HPLC-DAD-MS, Zorbax C_8 analytical HPLC column, 5.8 μm, 150 × 4.6 mm, 1 mL/min gradient elution from 90% H_2O/MeCN to 100% MeCN (with a constant 0.05% formic acid/MeCN modifier) over 15 min, monitoring at 210, 254 and 360 nm. The standard calibration curve was plotted using the area under the peak at 360 nm. From the standard calibration curve (Figure 4.14) the concentration of heronapyrrole B in the crude extract from the micro-bioreactor was determined to be 9.2 ± 0.8 μg/mL compared to 6.5 ± 0.7 μg/mL for the shake flask

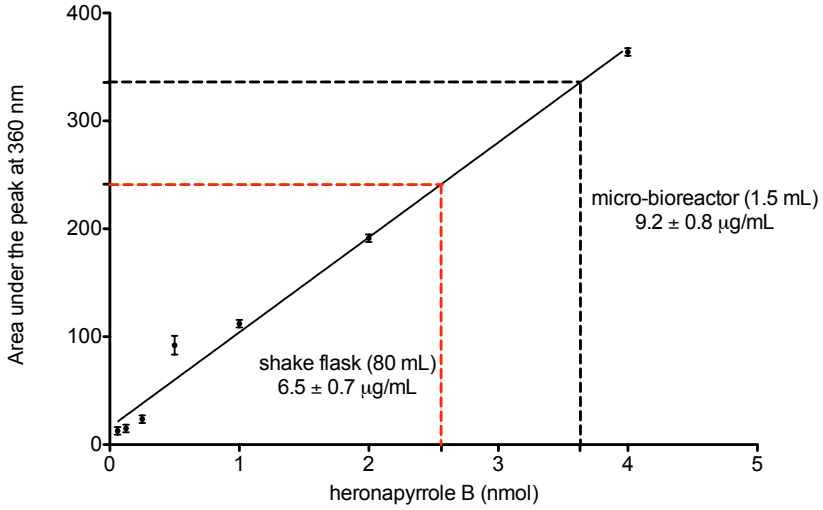

Figure 4.14. Calibration curve (360 nm) of **4.02** with values of 10 μL injection into the HPLC-DAD-MS of both micro-bioreactor (black) and shake flask (red)

Using a calibrated analytical method, the production levels of heronapyrrole B (**4.02**) were confirmed and the concentration of **4.02** in the crude extract from the micro-bioreactor was proved to be 9.2 ± 0.8 μg/mL compares very favourably with the values obtained during shake flask culture 6.7 ± 0.7 μg/mL.

4.4.4 Cultivation of *Streptomyces* sp. (CMB-M0423) in the presence of NOS inhibitors

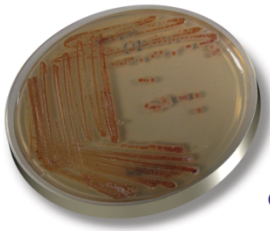

Figure 4.15. *Streptomyces* sp. (CMB-M0423)

We speculated that the addition of NOS inhibitors to the culture medium of *Streptomyces* sp. (CMB-M0423) may provide evidence for the involvement of bNOS in the biosynthesis of heronapyrroles, and may lead to the production of non-nitrated analogues. To test this hypothesis, the effect of three NOS inhibitors on *Streptomyces* sp. (CMB-M0423), AG (**4.16**), L-NAME (**4.17**) and L-NMME (**4.18**) were examined. Taking note of the tested concentrations previously reported for the NOS inhibitors, we chose 4 different concentrations 30, 15, 7.5 and 3.7 μM. From these studies, it was determined that 7.5 μM was optimum concentration to induce secondary metabolites production, and was used in all our future studies.

Streptomyces sp. (CMB-M0423) was cultivated on M1 broth prepared using 3.3% artificial ocean sea salt in the presence of 7.5 μM (1% DMSO) of the NOS inhibitors, AG (**4.16**) or L-NAME (**4.17**) or L-NMME (**4.18**). The resulting EtOAc crude extracts were analysed by HPLC-DAD-MS, to reveal suppression of heronapyrrole B (**4.02**) biosynthesis, and the production of new metabolites with the following retention times t_R = 7.8, 8.1, 8.5, 8.2, 5.2 and 4.8 min exhibited the following *m*/*z* $(M+H)^+$ 432 (**4.30**), 327 (**4.31**), 357 (**4.32**), 380 (**4.33**), 261 (**4.34**) and 345 (**4.35**) respectively, as shown in the case of AG in Figure 4.16.

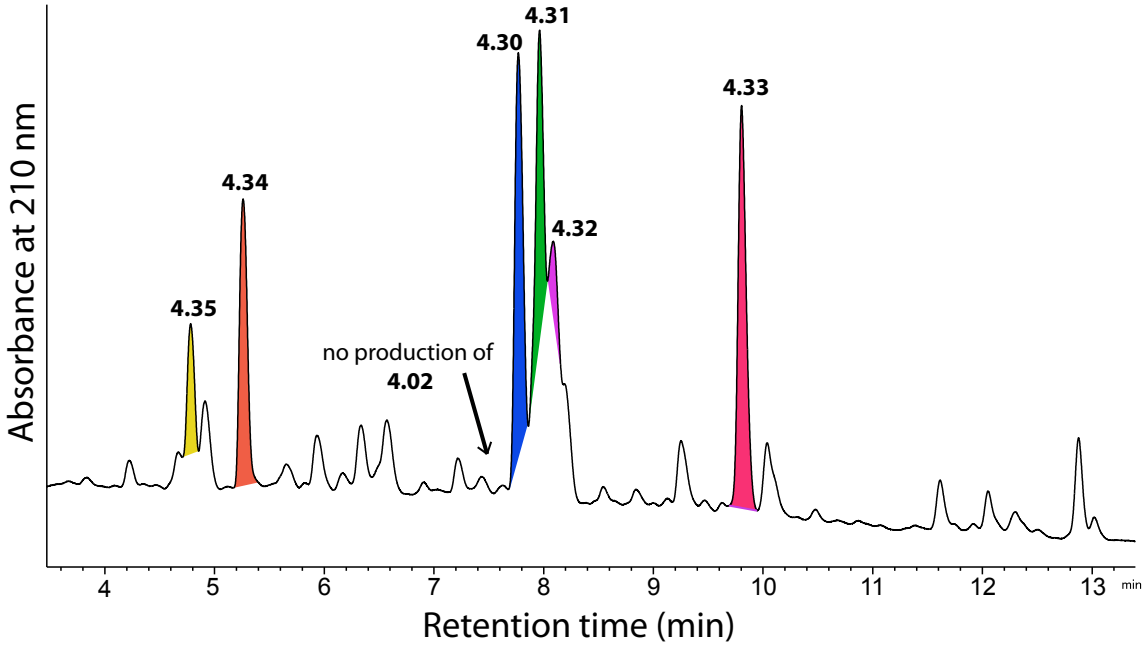

Figure 4.16. HPLC-DAD chromatogram from an analytical gradient H_2O/MeCN plus 0.05% HCO_2H using Zorbax C_8 column at 210 nm of the crude EtOAc extract from *Streptomyces* sp. (CMB-M0423) in the presence of AG (7.5 μM). * no production of **4.02**

Large-scale cultivation followed by fractionation yielded pseurotin A (t_R= 21.3 min; 5.1 mg, 7.3%) (**4.30**), gliotoxin (t_R= 22.0 min; 4.5 mg, 6.4%) (**4.31**), bisdethiobisgliotoxin (t_R= 22.7 min; 3 mg, 4.3%) (**4.32**) and fumitremorgin C (t_R= 25 min; 2.4 mg, 3.4%) (**4.33**) and two diketopiperazines, *cyclo*-(L-Phe-*trans*-4-hydroxy-L-Pro) (t_R= 15.7 min; 3 mg, 3.6%) (**4.34**) and *cyclo*-(L-Phe-L-Pro) (t_R= 17.2 min; 1.5 mg, 2.3%) (**4.35**). [Note - % yields were determined on a mass-to-mass basis against the EtOAc crude extract] (Scheme 4.1).

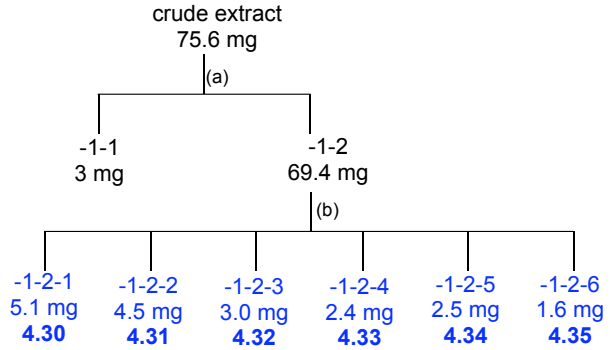

Scheme 4.1. Isolation scheme of *Streptomyces* sp. (CMB-M0423) cultured in the presence of AG (7.5 μM). (a) trituration [hexane (-1-1) and CH_2Cl_2 (-1-2)], (b) semi-preparative HPLC: Zorbax C_8, 90 – 10% H_2O/MeOH, 3 mL/min, 30 min

4.4.5 Pseurotin A_2 (4.30)

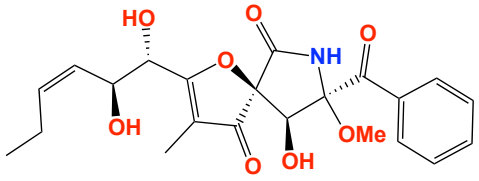

4.30

HRESI(+)MS analysis of **4.30** revealed an adduct ion ($[M+Na]^+$) indicative of the molecular formula $C_{22}H_{25}NO_8$ (Δmmu –0.4). The NMR ($CDCl_3$) data for **4.30** (Figure 4.18 and Table 4.2) showed the presence of a mono-substituted aromatic ring and aliphatic chain with two hydroxyl groups. The structure elucidation was further supported by 2D NMR data, including HSQC, COSY and HMBC, as outlined in Table 4.2. On searching the literature, it was determined that **4.30** was identical to the known fungal metabolite pseurotin A. Analysis of all the NMR data with comparison to literature data, confirmed that **4.30** was identical to the known fungal metabolite pseurotin A_2 (Table 4.3). This assignment was further confirmed by a comparison of the $[\alpha]^{22}_D$ –11.5 (*c* 0.1, MeOH) for **4.30** compared to $[\alpha]^{23}_D$ –4.2 (*c* 0.1, MeOH) for pseurotin A_2.[161-163] (**4.30**) as outlined in Figure 4.17 and Table 4.3.

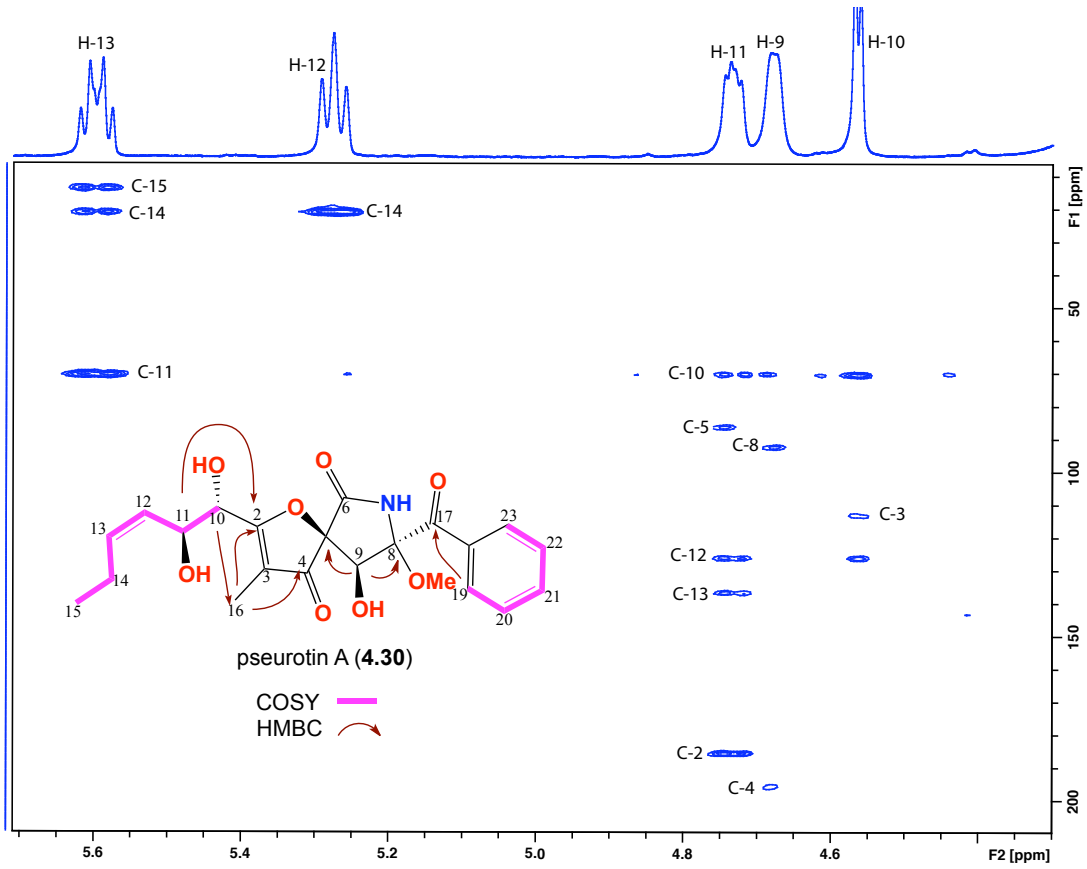

Figure 4.17. HMBC (600 MHz, $CDCl_3$) spectrum and 2D NMR correlations of pseurotin A_2 (**4.30**)

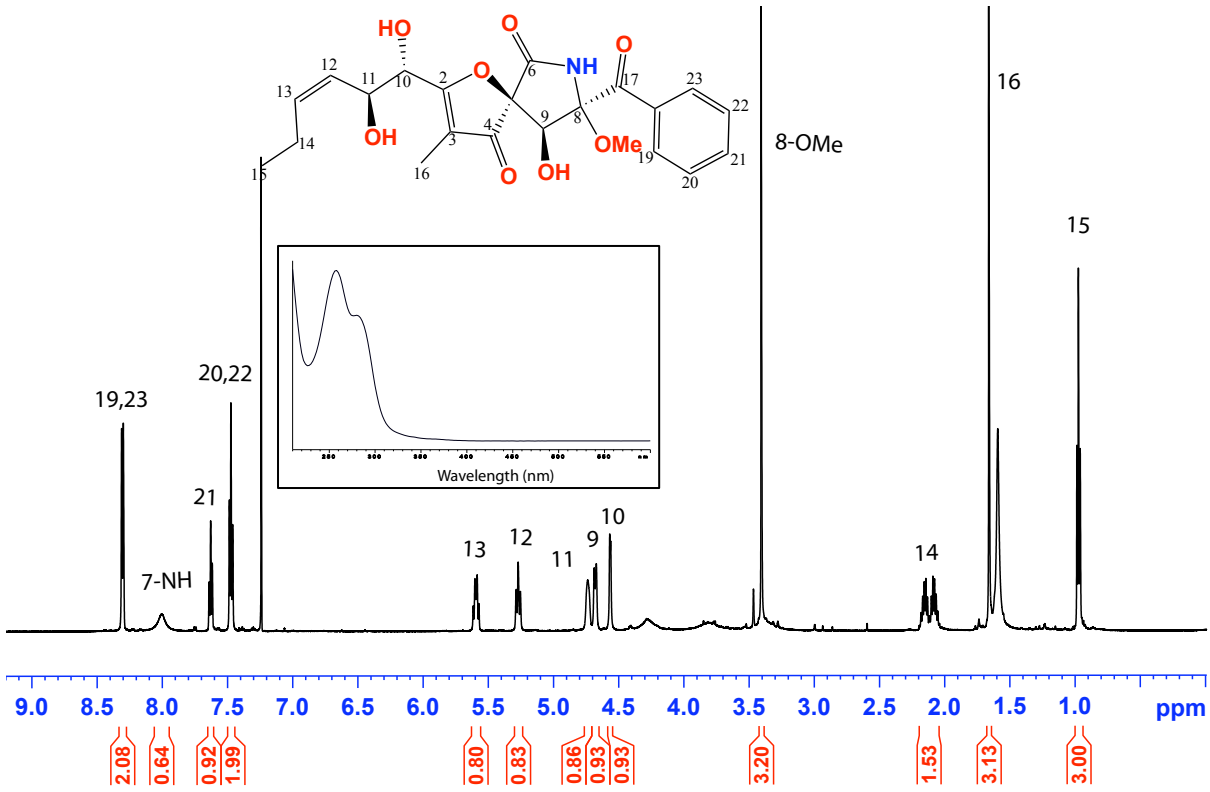

Figure 4.18. ^{1}H NMR (600 MHz, $CDCl_3$) and UV-vis (HPLC-DAD, H_2O/MeCN plus HCO_2H) spectra of pseurotin A_2 (**4.30**)

Table 4.2. NMR (600 MHz, $CDCl_3$) data of pseurotin A_2 (**4.30**)

Pos.	δ_H, mult (*J* in Hz)[a]	δ_C[a]	COSY	^{1}H-^{13}C HMBC
2		186.2		
3		115.1		
4		197.2		
5		92.6		
6		[b]		
7-NH	8.01, br s			
8		93.2		
9	4.68, d *(9.9)*	15.1	9-OH	5, 8
10	4.56, d *(4.4)*	73.5		11, 16
11	4.73, br s	74.4	10, 11	2, 10, 12, 13
12	5.26, dd *(10.5, 9.5)*	130.2	11, 13	11, 13
13	5.59, ddd *(10.5, 7.6, 7.6)*	139.5	12, 14a,b	11, 14a/b, 15
14	a 2.14, ddt *(14.8, 7.6, 7.6)*	24.8	13, 15	12, 13, 15
	b 2.09, ddt *(14.8, 7.6, 7.6)*		13, 15	12, 13, 15
15	0.96, t *(7.6)*	16.7	14a,b	13, 14
16	1.65, s	7.4		2, 3, 4
17		194.8		
18		134.4		
19/23	8.31, d *(8.0)*	133.7	20/22	18, 20/21, 22
20/22	7.47, dd *(8.0, 7.5)*	131.8	19/23, 21	19/23, 20/22
21	7.62, t *(7.5)*	137.6	20, 22	19/23, 20/22
8-OMe	3.41, s	55.1		
9-OH	4.48, br s			
10-OH	[b]			
11-OH	[b]			

*(a) ^{13}C assignments obtained from gHSQC and gHMBC data. (b) signals not observed.

Table 4.3. ^{1}H NMR (DMSO-d_6) data comparison for experimental and literature[162] data of pseurotin A_2 (**4.30**)

Pos.	δ_H, mult, (*J* in Hz) (experimental)	δ_H, mult, (*J* in Hz) literature
9	4.13, m	4.18, d *(9.9)*
10	4.39, m	4.51, t *(5.5)*
11	4.44, m	4.57, ddd *(11.0, 8.4, 5.5)*
12	5.35, m	5.42, dd *(11.0, 8.5)*
13	5.42, m	5.47, dd *(11.0, 7.0)*
14a	2.05, m	2.08, m
14b	2.05, m	2.08, m
15	0.88, dd *(7.6, 7.6)*	0.93, dd *(7.7, 7.3)*
16	1.62, s	1.66, s
19/23	8.24, d *(7.7)*	8.28, d *(7.3)*
20/22	7.52, dd *(7.3, 7.3)*	7.55, dd *(8.0, 7.7)*
21	7.66, t *(7.7)*	7.69, t *(7.3)*
7-NH	9.92, s	9.99, s
8-OMe	3.20, s	3.20, s
9-OH	[a]	6.35, d *(9.9)*
10-OH	[a]	5.87, d *(5.5)*
11-OH	[a]	5.09, d *(5.5)*

*(a) signals not observed

4.4.6 Gliotoxin (4.31)

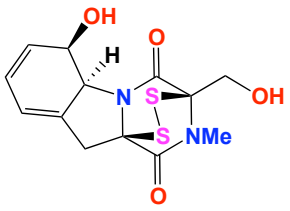

4.31

HRESI(+)MS analysis of **4.31** revealed an adduct ion ($[M+Na]^+$) indicative of the molecular formula $C_{13}H_{14}N_2O_4S_2$ (Δmmu +0.9). The NMR ($CDCl_3$) data of **4.31** (Figure 4.19, Figure 4.20 and Table 4.4) showed the presence of a hydroxyl cyclohexadiene and a possible N-methyl serine residue. The structure elucidation was further supported by 2D NMR data, including HSQC, COSY and HMBC, as outlined in Table 4.4. On searching the literature, it was determined that **4.31** was consistent with gliotoxin. Analysis of all the NMR data with comparison to literature data, confirmed that **4.31** was the known fungal metabolite gliotoxin (Table 4.5). This assignment was further confirmed by a comparison of the $[\alpha]^{22}_D$ –167 (*c* 0.1, MeOH) of **4.31** compared to $[\alpha]^{25}_D$ –440 (*c* 0.1, MeOH) of the reported gliotoxin.[164-166]

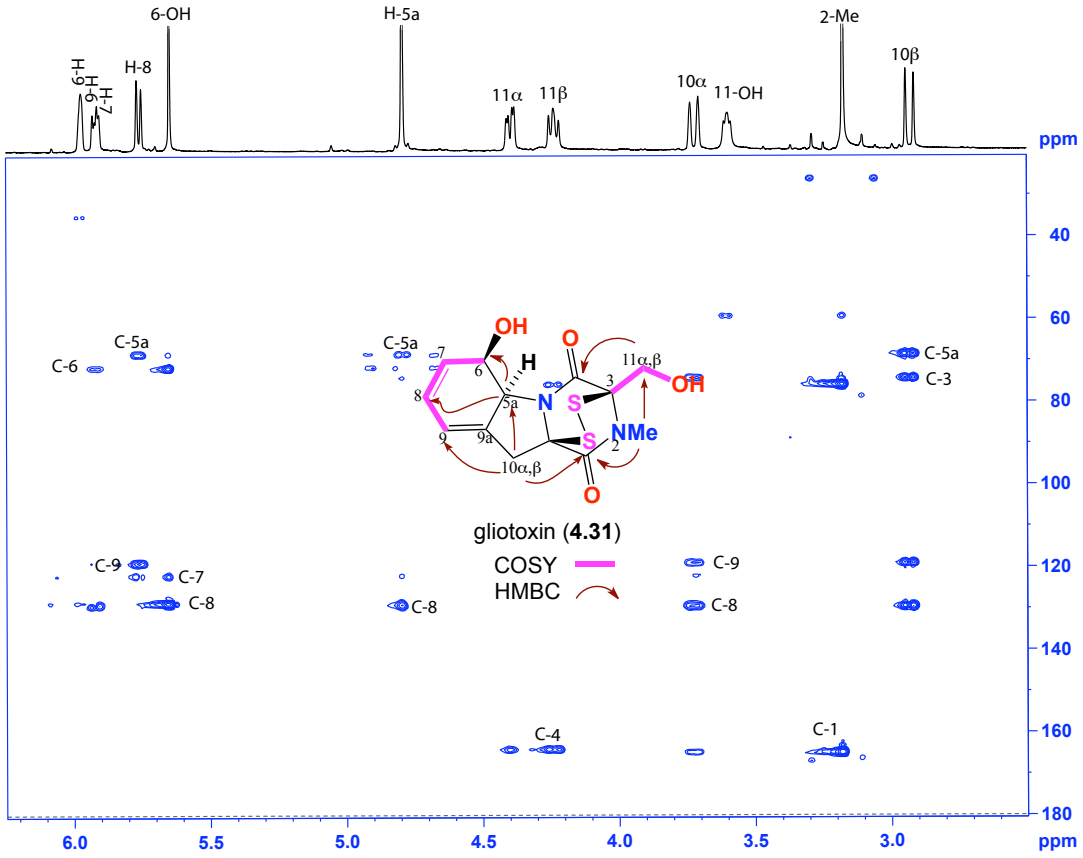

Figure 4.19. HMBC (600 MHz, $CDCl_3$) spectrum and key 2D NMR correlations of gilotoxin (**4.31**)

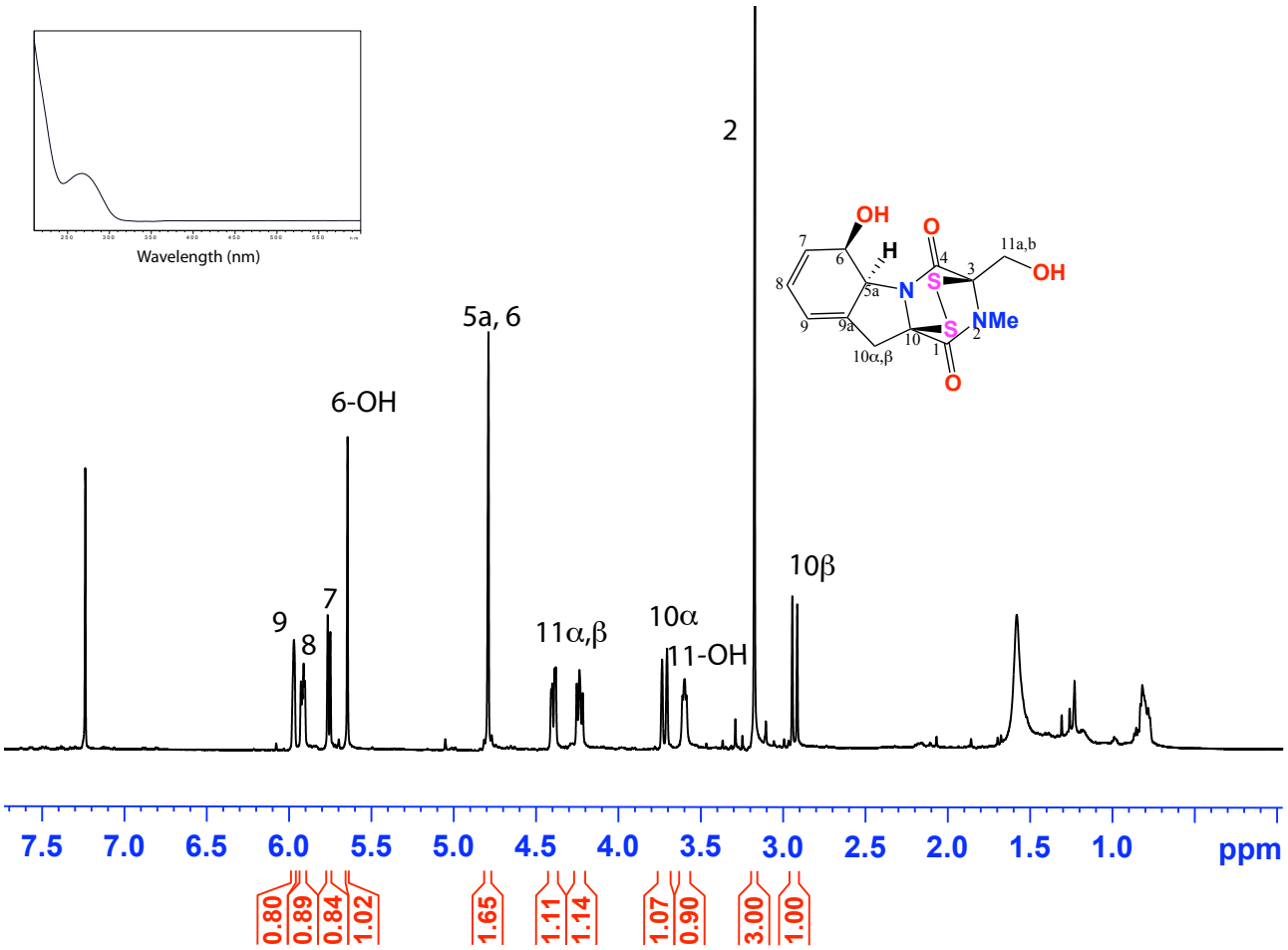

Figure 4.20. ^{1}H NMR (600 MHz, $CDCl_3$) and UV-vis (HPLC-DAD, H_2O/MeCN plus HCO_2H) spectra of gliotoxin (**4.31**)

Table 4.4. NMR (600 MHz, $CDCl_3$) data of gliotoxin (**4.31**)

Pos.	δ_H, mult (*J* in Hz)[a]	δ_C[a]	COSY	^{1}H-^{13}C HMBC
1		166.1		
2-Me	3.17, s	26.7		1, 3, 11
3		74.8		
4		164.1		
5a	4.81[c], s	67.8		6, 8
6	4.81[c], s	71.3		
7	5.76, d *(9.7)*	123.2	8	5a, 8
8	5.92, dd *(9.7, 5.0)*	128.1	7, 9	5a, 6, 9
9	5.97, br	118.9	8	
10a		[b]		
10	α 3.72, d *(20.1)*	35.1	10β	4, 5a, 8, 9
	β 2.93, d *(20.1)*		10α	4, 5a, 8, 9
11	α 4.39, d *(13.2)*	59.1	11β, 11-OH	4
	β 4.23, dd *(13.2, 9.2)*		11α, 11-OH	4
6-OH	5.65, s			5a, 7, 8
11-OH	3.61, br d			11

*(a) ^{13}C assignments obtained from gHSQC and gHMBC data. (b) not observed. (c) overlapping resonances

Table 4.5. ^{1}H NMR ($CDCl_3$) data comparison of experimental and literature[166] data of gliotoxin (**3.31**)

Pos.	δ_H, mult, (*J* in Hz)[a] (experimental)	δ_H, mult, (*J* in Hz)[b] (literature)
2-Me	3.17, s	3.20, s
5a	4.81[c], s	4.81[c], s
6	4.81[c], s	4.81[c], s
7	5.76, d *(9.7)*	5.77, d *(9.5)*
8	5.92, dd *(9.7, 5.0)*	5.93, dd *(9.5, 4.6)*
9	5.97, br	5.98, br
10	α 3.72, d *(20.1)*	3.74, dd *(17.7, 1.5)*
	β 2.93, d *(20.1)*	2.94, d *(17.7)*
11	α 4.39, d *(13.2)*	4.42, dd *(12.5, 6.1)*
	β 4.23, dd *(13.2, 9.2)*	4.24, dd *(12.5, 9.5)*
6-OH	5.65, s	5.69, s
11-OH	3.61, br	3.76, dd *(9.5, 6.1)*

*measured in (a) (600 MHz, $CDCl_3$), (b) (400 MHz, $CDCl_3$), (c) overlapping resonances

4.4.7 Bisdethiobis(methylthio)gliotoxin (4.32)

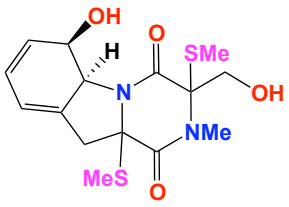

4.32

HRESI(+)MS analysis of **4.32** revealed an adduct ion ($[M+Na]^+$) indicative of the molecular formula $C_{15}H_{20}N_2O_4S_2$ (Δmmu +0.3), consistent with a C_2H_6 homologue of the co-metabolite **4.31**. The NMR ($CDCl_3$) data of **4.32** (Figure 4.21, Figure 4.22 and Table 4.6) were similar to **4.31** except for opening of the disulphide bridge and the addition of two S-Me reasonces. The structure elucidation was further supported by 2D NMR data, including HSQC, COSY and HMBC, as outlined in Table 4.6. On searching the literature, it was determined that **4.32** was consistent with bisdethiobis(methylthio)gliotoxin. Analysis of all the NMR data with comparison to literature data, confirmed that **4.31** was the known fungal metabolite gliotoxin (Table 4.7). This assignment was further confirmed by comparison of the $[\alpha]^{22}_D$ –67.2 (*c* 0.1, MeOH) for **4.32** compared to $[\alpha]^{20}_D$ –51 (*c* 1.0, MeOH) for the reported bisdethiobis(methylthio)gliotoxin strongly suggested the known fungal metabolite bisdethiobis(methylthio)gliotoxin.[164-166]

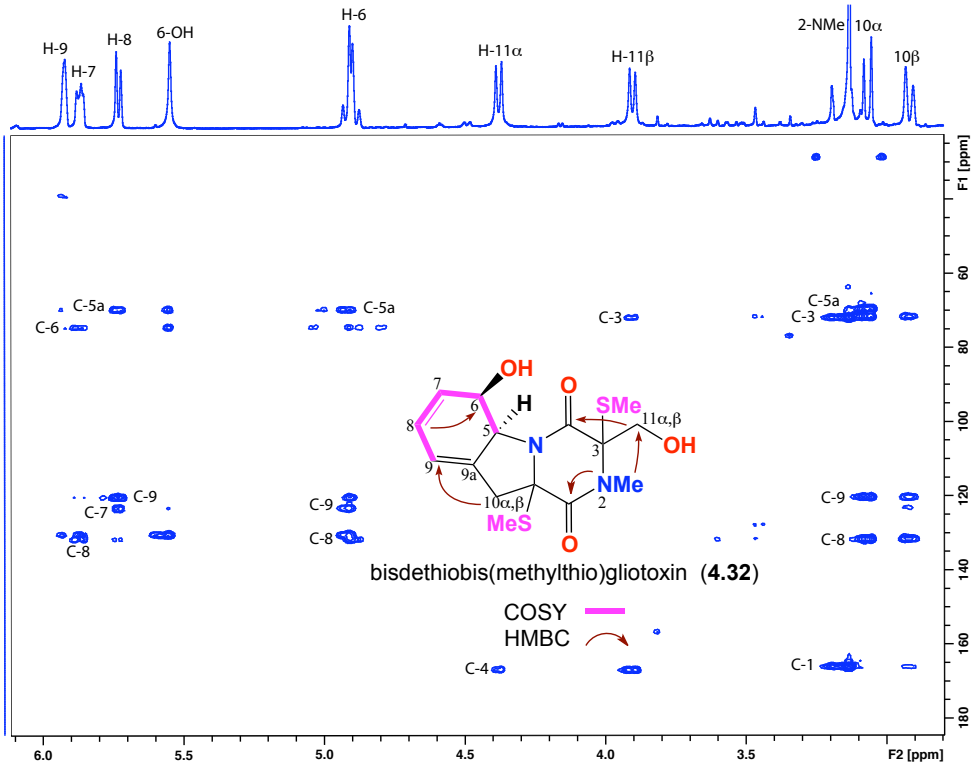

Figure 4.21. HMBC (600 MHz, $CDCl_3$) spectrum and key 2D NMR correlations of bisdethiobis(methylthio)gliotoxin (**4.32**)

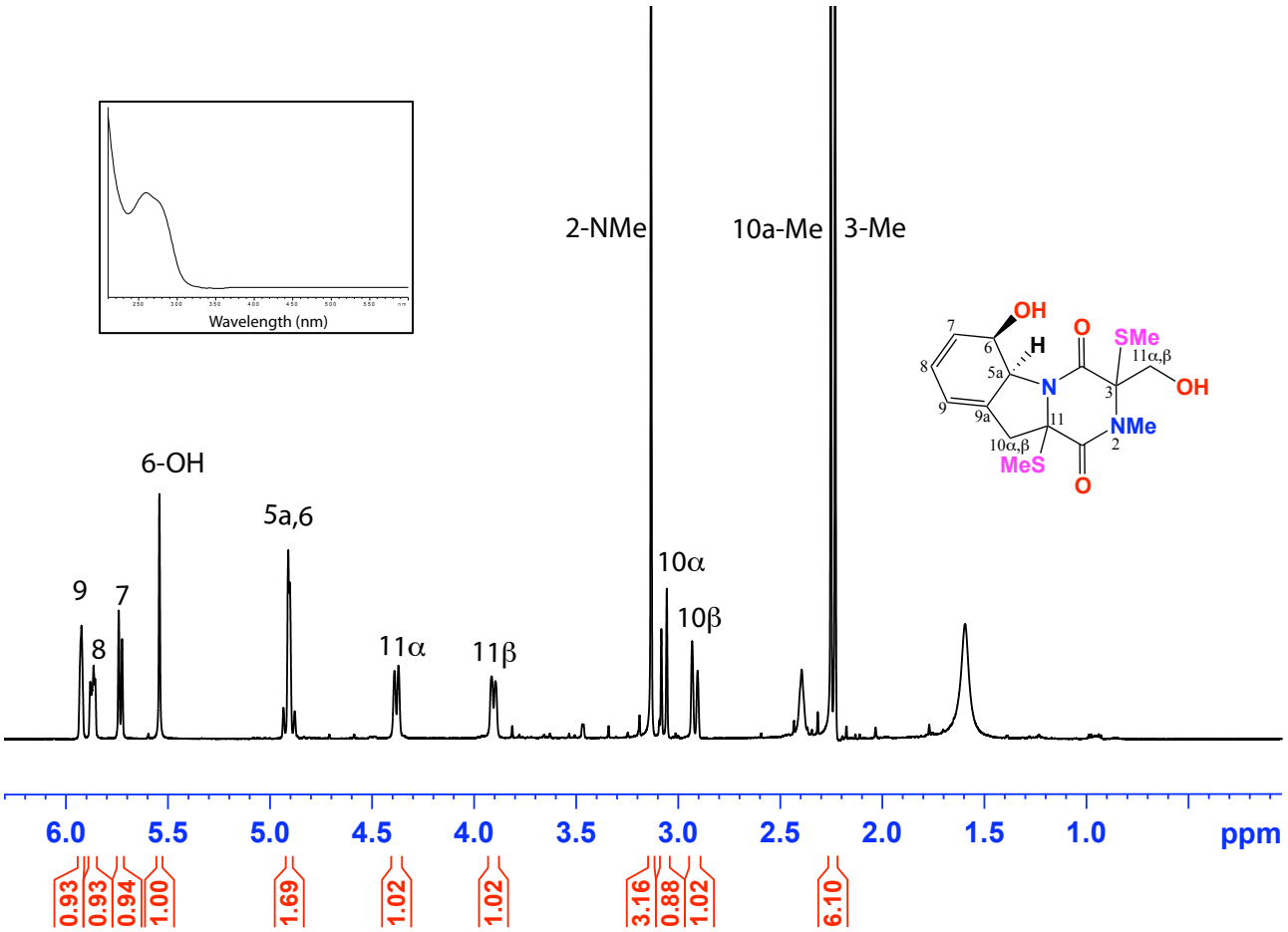

Figure 4.22. ^{1}H NMR (600 MHz, $CDCl_3$) and UV-vis (HPLC-DAD, H_2O/MeCN plus HCO_2H) spectra of bisdethiobis(methylthio)gliotoxin (**4.32**)

Table 4.6. NMR (600 MHz, $CDCl_3$) data of bisdethiobis(methylthio)gliotoxin (**4.32**)

Pos.	δ_H, mult (*J* in Hz)[a]	δ_C[a]	COSY	^{1}H-^{13}C HMBC
1		164.3		
2	3.13, s	29.1		11
3		67.2		
3-Me	2.23, s	14.3		
4		167.4		
5a	4.91[c]	69.4		
6	4.91[c]	74.4	7	5a, 8, 9
7	5.73, d *(9.7)*	130.7		5, 8
8	5.87, m	122.9	7, 9	5a, 6, 7
9	5.93, br s	119.8	8, 10α/β	6, 8, 10a/b
9a		133.2		
10	α 3.07, d *(15.7)*	39.2	10β	1, 8, 9
	β 2.92, d *(15.7)*		10α	1, 8, 9
10a		71.2		
11-Me	2.24, s	14.1		11
11	α 4.38, d *(12.4)*	63.6	11β	4
	β 3.90, d *(12.4)*		11α	3, 4
6-OH	[b]			

*(a) ^{13}C assignments obtained from gHSQC and gHMBC data. (b) Signals not observed. (c) Overlapping resonances

Table 4.7. ^{1}H NMR ($CDCl_3$) comparison for experimental and literature[167] data of bisdethiobis(methylthio)gliotoxin (**4.32**)

Pos.	δ_H, mult, (*J* in Hz)[a] (experimental)	δ_H, mult, (*J* in Hz)[b] (literature)
2-Me	3.13, s	3.15, s
3-Me	2.23, s	2.27, s
5a	4.91[c]	4.88, m
6	4.91[c]	4.92, m
7	5.73, d *(9.7)*	5.73, m
8	5.87, m	5.88, m
9	5.93, br s	5.93, m
10	α 3.07, d *(15.7)*	α 3.05, d *(16.0)*
	β 2.92, d *(15.7)*	β 2.90, d *(16.0)*
11-Me	2.24, s	2.24, s
11	α 4.38, d *(12.4)*	α 4.37, d *(12.0)*
	β 3.90, d *(12.4)*	β 3.92, d *(12.0)*
6-OH	[d]	[d]

*measured in (a) (600 MHz, $CDCl_3$). (b) (300 MHz, $CDCl_3$). (c) overlapping resonances. (d) signals not observed

4.4.8 Fumitremorgin C (4.33)

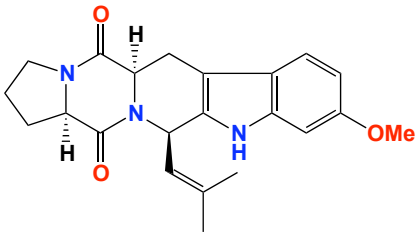

4.33

HRESI(+)MS analysis of **4.33** revealed a quasi molecular ion ($[M+H]^+$) indicative of the molecular formula $C_{22}H_{25}N_3O_3$ (Δmmu −1.3). The NMR ($CDCl_3$) data of **4.33**, (Figure 4.23, Figure 4.24 and Table 4.8) showed the presence of 1,2,4 trisubstituted benzene ring, a diketopiperazine ring, plus prolinyl and isoprenyl units. The structure elucidation was further supported by 2D NMR data, including HSQC, COSY and HMBC, as outlined in Table 4.8, Figure 4.23 and Figure 4.24. On searching the literature, it was determined that **4.33** was consistent with fumitremorgin C. Analysis of all the NMR data with comparison to literature data, confirmed that **4.33** was the known fungal metabolite fumitremorgin C (Table 4.9). This assignment was further confirmed by comparison of the $[\alpha]^{22}_D$ –26.2 (*c* 0.04, MeOH) for **4.33** compared to $[\alpha]^{28}_D$ –13 (*c* 0.53, MeOH) for the reported fumitremorgin C.[168-170]

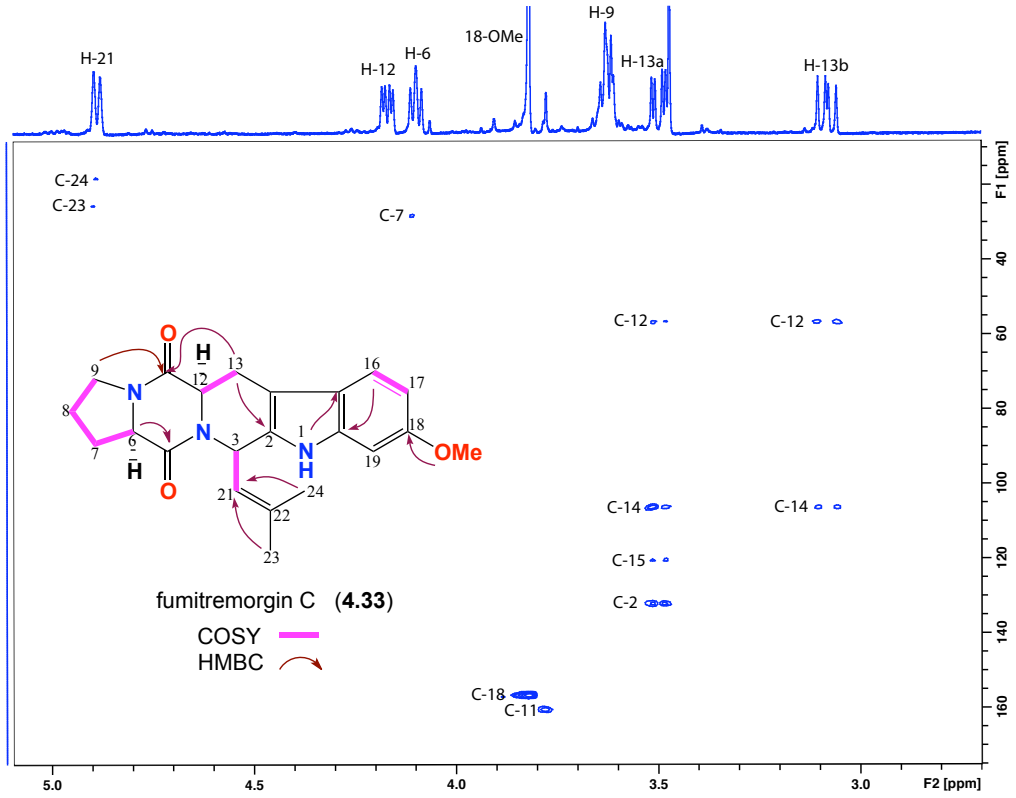

Figure 4.23. HMBC (600 MHz, $CDCl_3$) spectrum and key 2D NMR correlations of fumitremorgin C (**4.33**)

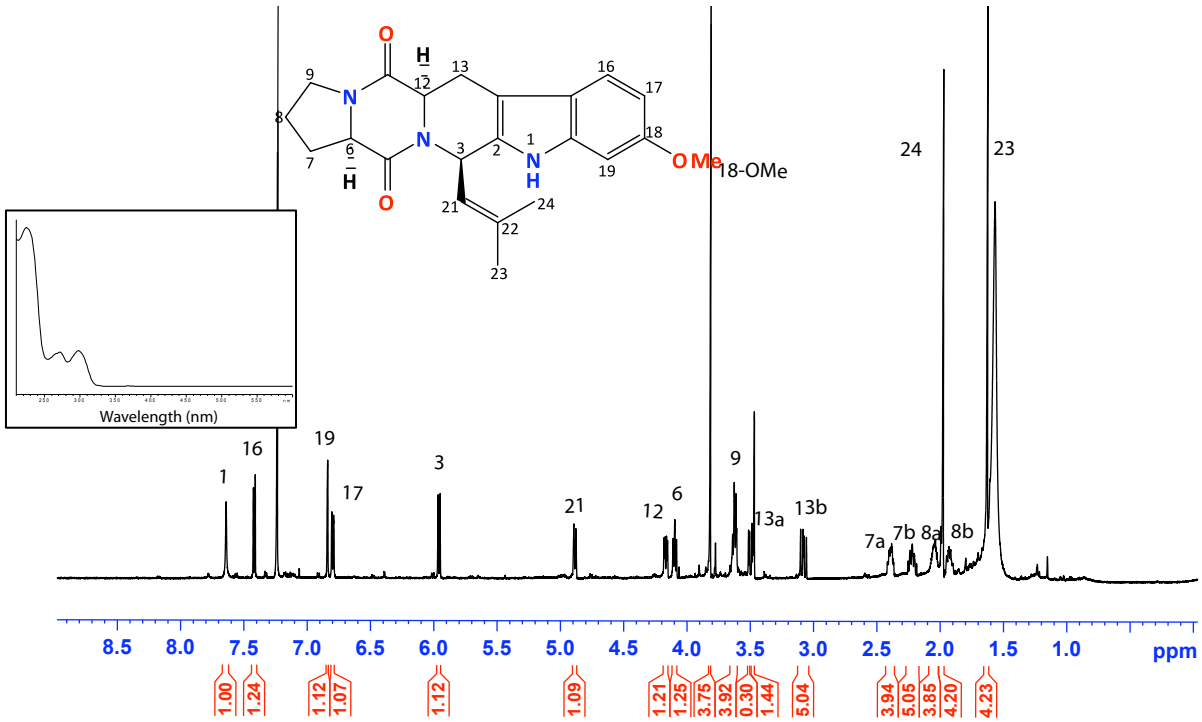

Figure 4.24. ^{1}H NMR (600 MHz, $CDCl_3$) and UV-vis (HPLC-DAD, H_2O/MeCN plus HCO_2H) spectra of fumitremorgin C (**4.33**)

Table 4.8. NMR (600 MHz, $CDCl_3$) data of fumitremorgin C (**4.33**)

Pos.	δ_H, mult (*J* in Hz)[a]	δ_C[a]	COSY	^{1}H-^{13}C HMBC
1-NH	7.64, s			15
2		131.6		
3	5.96, d *(9.6)*	51.1	21	2, 14, 21
4				
5		b		
6	4.09, dd *(9.4, 7.5)*	58.9		7a/b
7	a 2.39, m	28.7	6, 7b, 8b	
	b 2.21, m		6, 7a, 8a	
8	a 2.05, m	23.2	7b, 9	
	b 1.93, m		7a, 9	
9	3.62, m	45.7	8a,b	11
11		160.5		
12	4.17, dd *(16.0, 5.2)*	57.0	13a,b	13a/b
13	a 3.51, dd *(16.0, 5.2)*	21.7	12, 13b	2, 14
	b 3.08, dd *(16.0, 5.2)*		12, 13a	14
14		106.6		
15		120.7		
16	7.42, d *(8.6)*	119.3	17	17, 18, 20
17	6.80, d *(8.6)*	109.7	16	18, 19
18		157.3		
18-OMe	3.82, s	55.1		18
19	6.84, br s	95.3		16, 17, 18
20		137.3		
21	4.88, d *(9.6)*	124.4	3, 23, 24	23, 24
22		134.1		
23	1.63, s	25.6	21	3, 21
24	1.99, s	19.2	21	3, 21

*(a) ^{13}C assignments obtained from gHSQC and gHMBC data. (b) signals not observed

Table 4.9. ^{1}H NMR ($CDCl_3$) data comparison of experimental and literature[168] data of fumitremorgin C (**4.33**)

Pos.	δ_H, mult, (*J* in Hz)[a] (experimental)	δ_H, mult, (*J* in Hz)[b] (literature)
1-NH	7.64, s	7.89, br s
3	5.96, d *(9.6)*	5.98, br d *(9.5)*
6	4.09, dd *(9.4, 7.5)*	4.10, br dd *(9.5, 7.5)*
7a	2.39, m	2.40, m
7b	2.21, m	2.23, m
8	a 2.05, m	2.06, m
	b 1.93, m	1.94, m
9	3.62, m	3.65, m
12	4.17, dd *(16.0, 5.2)*	4.18, br dd *(11.5, 5.0)*
13	a 3.51, dd *(16.0, 5.2)*	3.51, dd *(16.0, 5.0)*
	b 3.08, dd *(16.0, 5.2)*	3.10, ddd *(16.0, 11.5, 1.0)*
16	7.42, d *(8.6)*	7.43, d *(9.0)*
17	6.80, d *(8.6)*	6.81, dd *(9.0, 2.2)*
18-OMe	3.82, s	3.83, s
19	6.84, br s	6.85, d *(2.2)*
21	4.88, d *(9.6)*	4.91, dm *(9.5)*
23	1.63, s	1.64, s
24	1.99, s	1.99, s

*measured in (a) (600 MHz, $CDCl_3$), (b) (500 MHz, $CDCl_3$)

4.4.9 *cyclo*-(L-Phe-*trans*-4-hydroxy-L-Pro) (4.34)

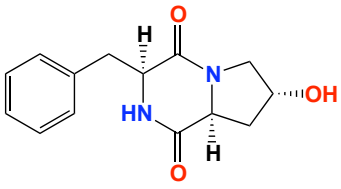

4.34

HRESI(+)MS analysis of **4.34** revealed a quasi-molecular ion ($[M+H]^+$) indicative of the molecular formula $C_{14}H_{16}N_2O_3$ (Δmmu +0.8). The NMR ($CDCl_3$) data of **4.34** (Figure 4.26) revealed the presence of phenylalanine and hydroxyl proline residues, with the molecular formula suggestive of a diketopiperazine. The structure elucidation was further supported by 2D NMR data, including HSQC, COSY and HMBC, as outlined in Table 4.10. On searching the literature, **4.34** was determined to be consistent with *cyclo*-(L-Phe-*trans*-4-hydroxy-L-Pro). Analysis of all the NMR data with comparison to literature data, confirmed **4.34** was the known fungal metabolite *cyclo*-(L-Phe-*trans*-4-hydroxy-L-Pro) (Table 4.11). This assignment was further confirmed by comparison of the $[\alpha]^{22}_D$ – 20.9 (*c* 0.05, MeOH) for **4.34** with the $[\alpha]^{20}_D$ –6.7 (*c* 0.01, MeOH) reported for *cyclo*-(L-Phe-*trans*-4-hydroxy-L-Pro)[168,171,172] and C_3 Marfey's analysis (Figure 4.28 and Figure 4.29).

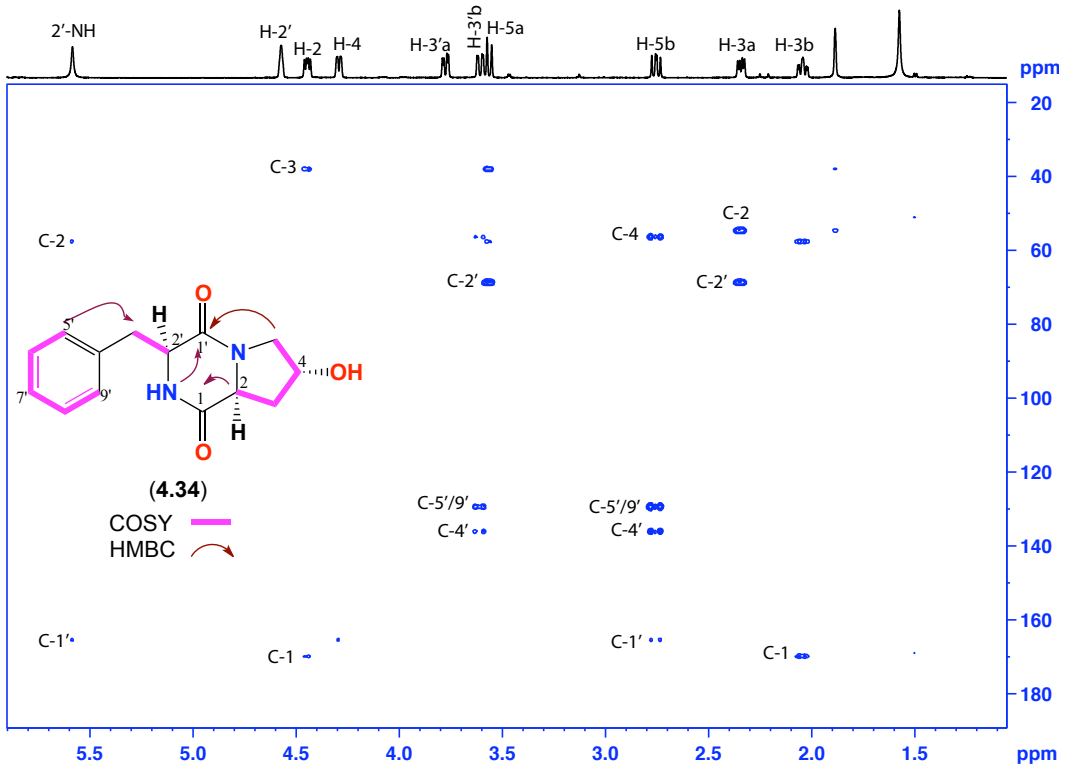

Figure 4.25. HMBC (600 MHz, $CDCl_3$) spectrum and key 2D NMR correlations of *cyclo*-(L-Phe-*trans*-4-hydroxy-L-Pro) (**4.34**)

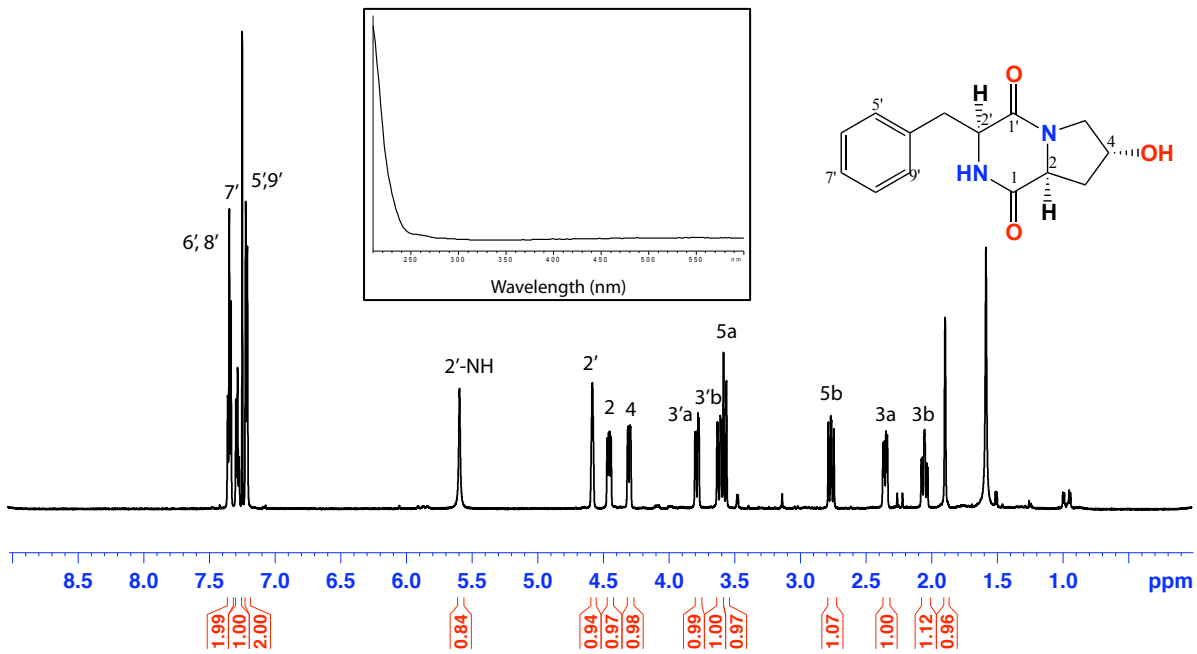

Figure 4.26. ^{1}H NMR (600 MHz, $CDCl_3$) and UV-vis (HPLC-DAD, H_2O/MeCN plus HCO_2H) spectra of *cyclo*-(L-Phe-*trans*-4-hydroxy-L-Pro) (**4.34**)

Table 4.10. NMR (600 MHz, $CDCl_3$) data of *cyclo*-(L-Phe-*trans*-4-hydroxy-L-Pro) (**4.34**)

Pos.	δ_H, mult (*J* in Hz)[a]	δ_C[a]	COSY	^{1}H-^{13}C HMBC	ROESY
hydroxyproline					
1		169.8			
2	4.46, dd *(13.3, 3.8)*	57.7	3a,b	3, 4	2′
3	a 2.34, dd *(13.3, 3.8)*	37.9	2, 4	2	
	b 2.06, dd *(13.3, 3.8)*			2	
4	4.31, d *(13.3, 3.8)*	56.6	5a,b		
5	a 3.58, dd *(13.2, 10.3)*	36.9	4	4	
	b 2.77, dd *(13.2, 10.3)*			4	
4-OH		[b]			
phenylalanine					
1′	--	165.8			
2′-NH	5.57, br s	--		2, 2′	
2′	4.57, br s	68.7	3′a,b		2
3′	a 3.79, dd (*13.3, 4.1*)	54.7	2′	4′	
	b 3.62, d (*13.3*)		2′	2′, 4′, 5′/9′	
4′	--	135.7			
5′, 9′	7.22, d *(7.3)*	129.5	6′, 8′	3′, 7′	
6′, 8′	7.35, t *(7.3)*	129.8	7′	4′, 5′, 9′	
7′	7.29, t *(7.3)*	127.9	6′, 8′	5′, 6′, 10′	

(a) ^{13}C assignments obtained from gHSQC and gHMBC data. (b) signals not observed

Table 4.11. ^{1}H NMR ($CDCl_3$) data comparison for experimental and literature[172] data of *cyclo*-(L-Phe-*trans*-4-hydroxy-L-Pro) (**4.34**)

Pos.	δ_H, mult, (*J* in Hz)[a] (experimental)	δ_H, mult, (*J* in Hz)[b] (literature)
hydroxyproline		
2	4.46, dd *(13.3, 3.8)*	4.47, dd *(11.1, 6.3)*
3	a 2.34, dd *(13.3, 3.8)*	2.36, dd *(13.2, 6.2)*
	b 2.06, dd *(13.3, 3.8)*	2.06, ddd *(13.5, 11.4, 4.2)*
4	4.31, d *(13.3, 3.8)*	4.31, dd *(10.7, 2.6)*
5	a 3.58, dd *(13.3, 10.3)*	3.63, dd *(15.9, 3.9)*
	b 2.77, dd *(13.3, 10.3)*	2.77, dd *(14.6, 10.9)*
4-OH	[c]	[c]
phenylalanine		
2′-NH	5.57, br s	5.89, s
2′	4.57, br s	4.60, t *(4.1)*
3′	a 3.79, dd (*13.3, 4.1*)	3.80, dd *(13.2, 4.5)*
	b 3.62, d (*13.3*)	3.58, d *(13.8)*
5′, 9′	7.22, d *(7.3)*	7.29, br m
6′, 8′	7.35, t *(7.3)*	7.29, br m
7′	7.29, t *(6.9)*	7.29, br m

*measured in (a) (600 MHz, $CDCl_3$), (b) (300 MHz, $CDCl_3$), (c) signals not observed

4.4.9.1 Assigning absolute configurations: C_3 Marfey's method

The Marfey's method[173] is a popular method for the assignments of absolute configuration of amino acids residues in natural products. The method relies on acid hydrolysis followed by derivatisation of amino acid residues with N-α-(2,4-dinitro-5-fluorophenyl)-D/L-alaninamide (FDAA), and resolution of the resulting diastereomers by HPLC-DAD as shown in Figure 4.27. The Marfey's method consists of the following steps:

- **Hydrolysis:** The natural product to be analysed is subjected to acid hydrolysis (6 M HCl) in order to release the amino acid residue(s), and the resulting analyte is concentrated to dryness under nitrogen.
- **Derivatisation:** The hydrolysed amino acid(s) is derivatised with Marfey's reagent (D or L FDAA) under alkaline conditions (1 M $NaHCO_3$).
- **Neutralisation:** The acidic reaction products are neutralized (1 M HCl) and diluted with MeCN (1 mL).
- **Analysis:** The diluted solution is subjected to HPLC-DAD/MS analysis.

The FDAA derivatives of pure amino acids standards are also prepared and analyzed using steps outlined above.

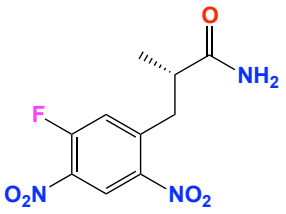

N-α-(2,4-dinitro-5-fluorophenyl)-D-alaninamide
(D-FDAA)

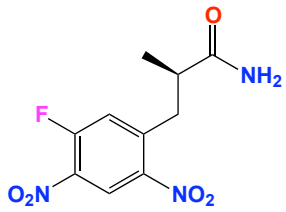

N-α-(2,4-dinitro-5-fluorophenyl)-L-alaninamide
(L-FDAA)

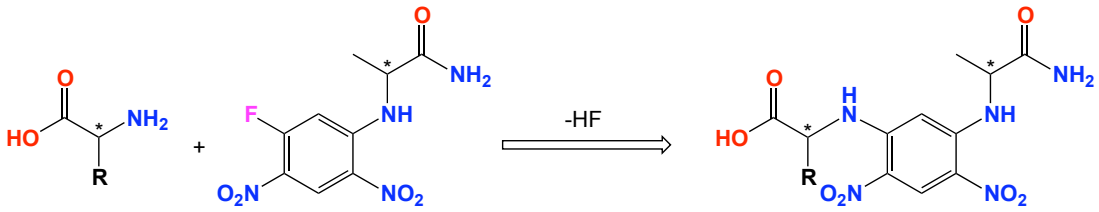

Figure 4.27. Reaction scheme between D/L amino acid with D/L-FDAA to give the diastereomeric derivatised amino acids *- chiral centre

However, some drawbacks have appeared from using C_{18} Marfey's method[174] in that it cannot resolve L-Ile from L-*allo*-Ile, and D-Ile from D-*allo*-Ile, and also it does not transition seamlessly between HPLC-DAD and HPLC-MS detection methodology. The Capon group has refined and optimized the C_{18} Marfey's method to address these limitations, and the refined method is referred to as the C_3 Marfey's method.[45]

The absolute configuration of the **4.34** was confirmed using the C_3 Marfey's method. [45] Standard amino acids, D-Phe, L-Phe, *trans*-4-hydroxy-L-Pro and *trans*-4-hydroxy-D-Pro were derivatised with D-FDAA and analyzed by the HPLC as shown as in Figure 4.28. Absolute configuration of **4.34** was determined by comparing the retention times of standard amino acids with the hydrolysate of **4.34**. The amino acid residues in **4.34** were confirmed to be L-Phe and *trans*-4-hydroxy-L-Pro as shown in Figure 4.28 and Figure 4.29.

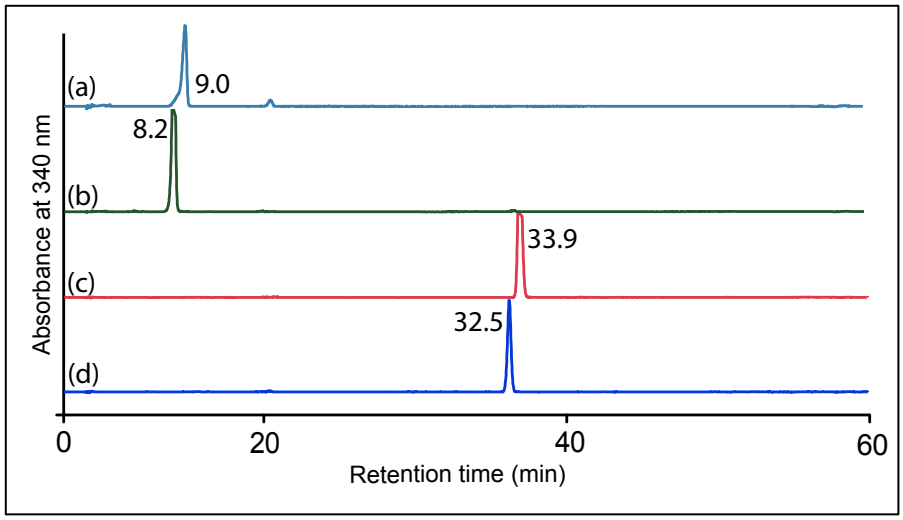

Figure 4.28. C_3 Marfey's analysis of the selected amino acids derivatized with D-FDAA with the retention times. (a) *trans*-4-hydroxy-D-Pro + D-FDAA. (b) *trans*-4-hydroxy-L-Pro + D-FDAA. (c) D-Phe + D-FDAA and (d) L-Phe + D-FDAA.

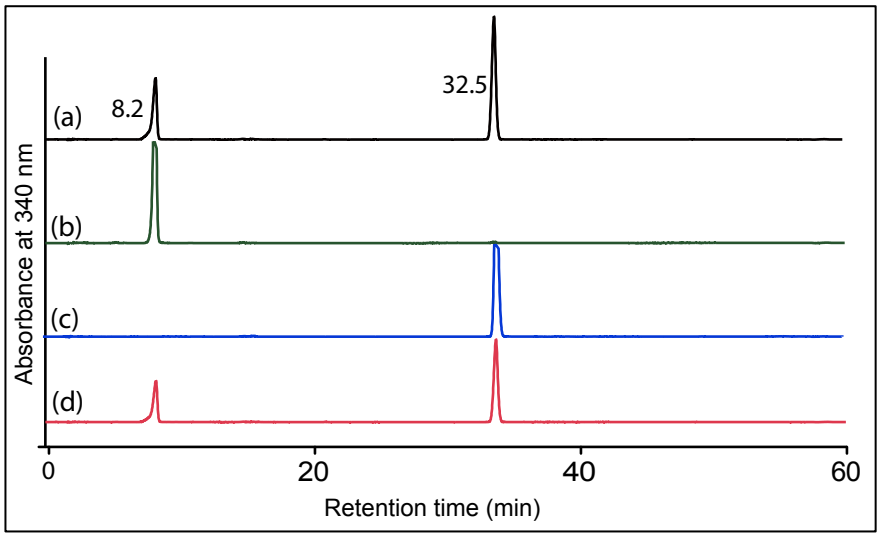

Figure 4.29. HPLC-DAD (340 nm) C_3 Marfey's analysis of *cyclo*-(L-Phe-*trans*-4-hydroxy-L-Pro) (**4.34**). Identity of amino acids was confirmed by retention time and molecular weight. (a) coinjection of hydrolyzed **4.34** + D-FDAA with the standard L-Phe + D-FDAA and *trans*-4-hydroxy-L-Pro + D-FDAA. (b) *trans*-4-hydroxy-L-Pro + D-FDAA. (c) L-Phe + D-FDAA. (d) D-FDAA derivatized hydrolysate of **4.34** showing the presence of L-Phe (t_R = 32.5 min) and *trans*-4-hydroxy-L-Pro (t_R = 8.2 min). HPLC conditions, Zorbax, SB-C_3 column (150 × 4.6 mm, 5 μm), 1 mL/min, gradient of 15 – 60% MeOH/H_2O (isocratic 5% MeCN containing 1% formic acid) over 55 min.

4.4.10 *cyclo*-(L-Phe-L-Pro) (4.35)

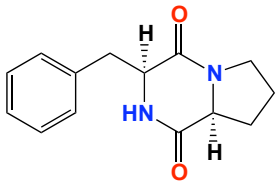

4.35

HRESI(+)MS analysis of **4.35** revealed a quasi-molecular ion ($[M+H]^+$) indicative of a molecular formula $C_{14}H_{16}N_2O_2$ (Δmmu +2.8). The NMR ($CDCl_3$) data of **4.35** (Figure 4.31) were very similar to **4.34** with exception of the replacement of methine H-4 in **4.34** with methylene (δ_H 2.02 and 2.32) in **4.35** suggesting the absence of the hydroxyl moiety. The structure elucidation of **4.35** was further supported by 2D NMR data, including HSQC, COSY and HMBC, as outlined in **Table 4.12**. Analysis of all the NMR data with comparison to literature data, confirmed that **4.35** was the known fungal metabolite *cyclo*-(L-Phe-L-Pro) (**4.35**) (Table 4.13).[168,171] This assignment was confirmed by C_3 Marfey's analysis (**Figure 4.32** and Figure 4.33).

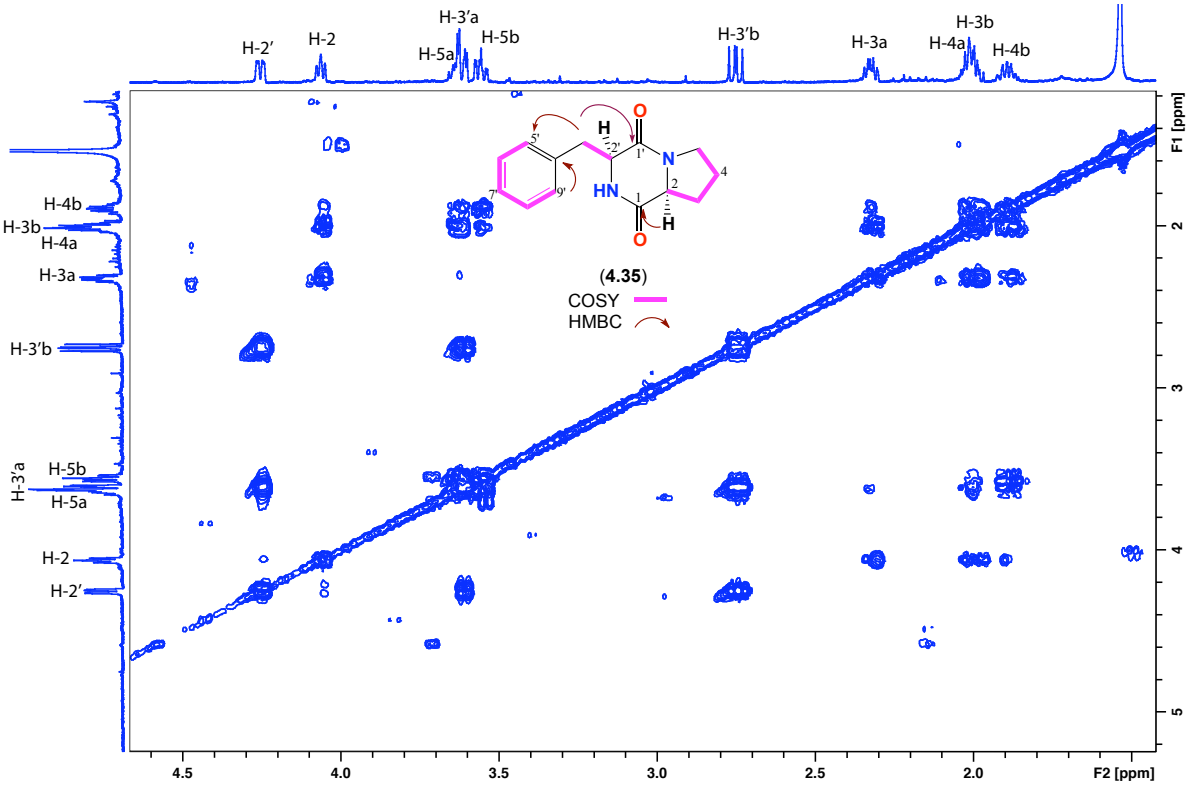

Figure 4.30. COSY (600 MHz, $CDCl_3$) spectrum and key 2D NMR correlations of *cyclo*-(L-Phe-L-Pro) (**4.35**)

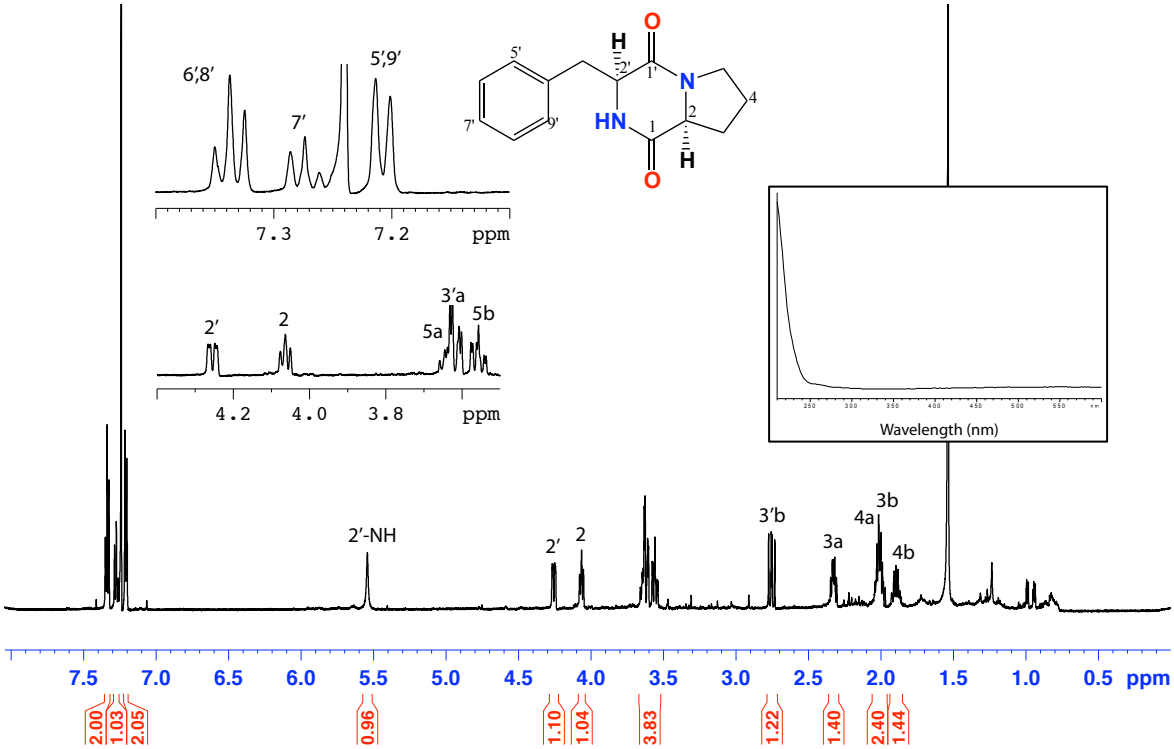

Figure 4.31. ^{1}H NMR (600 MHz, $CDCl_3$) and UV-vis spectrum (HPLC-DAD, H_2O/MeCN plus HCO_2H) spectra of *cyclo*-(L-Phe-L-Pro) (**4.35**)

Table 4.12. NMR (600 MHz, $CDCl_3$) data of *cyclo*-(L-Phe-L-Pro) (**4.35**)

Pos.	δ_H, mult (*J* in Hz)[a]	δ_C[a]	COSY	^{1}H-^{13}C HMBC	ROSEY
proline					
1		165.2			
2	4.06, dd *(7.9, 7.3)*	59.2	5a/b	1, 4	2′
3	a 2.32, m	28.3	3b, 4a/b	5	
	b 2.01[b]		3a, 4a/b	5	
4	a 2.02[b]	22.5	3a/b, 5a/b		
	b 1.89, m		3a/b, 5a/b		
5	a 3.65[c], m	45.5	5b		
	b 3.63 [c], m		5a		
phenylalanine					
1′	--	166.2			
2′-NH	5.54, br s	--			
2′	4.25, dd *(14.7, 10.7)*	56.3	3′a/b	1′, 3′	2
3′	a 3.64 [c], m	36.9	2′, 3′b	1′, 2′, 4′, 5′/9′	
	b 2.75, dd *(14.7, 10.7)*		2′, 3′a	2′, 4′, 5′/9′	
4′	--	136.1			
5′, 9′	7.20, d *(7.6)*	129.5	6′, 8′	3′, 4′	
6′, 8′	7.33, t *(7.6)*	129.6	5′, 9′	7′	
7′	7.27, t *(7.6)*	128.0	6′, 8′	6′/8′	

*(a)^{13}C assignments obtained from gHSQC and gHMBC data. (b and c) Overlapping resonances.

Table 4.13. ^{1}H NMR ($CDCl_3$) data comparison of experimental and published [175] data of *cyclo*-(L-Phe-L-Pro)

Pos.	δ_H, mult, (*J* in Hz)[a] (experimental)	δ_H, mult, (*J* in Hz)[b] (literature)
proline		
2	4.06, t *(7.9)*	4.08, m
3	a 2.32, m	1.90 – 2.10, m
	b 2.02[b]	2.30 – 2.40, m
4	a 2.02[b]	1.90 – 2.10, m
	b 1.89, m	
5	a 3.63[c], m	3.60 – 3.70, m
	b 3.55, m	
phenylalanine		
2′-NH	5.54, br s	5.57, bs
2′	4.25, dd *(10.4, 10.7)*	4.28, dd *(9.2, 2.8)*
3′	a 3.60[c], m	3.60 – 3.70, m
	b 2.75, dd *(14.7, 10.7)*	2.77, dd *(14.4, 9.2)*
5′, 9′	7.20, d *(7.6)*	7.2 – 7.39, m
6′, 8′	7.33, t *(7.6)*	
7′	7.27, t *(7.6)*	

*measured in (a) (600 MHz, $CDCl_3$). (b) (300 MHz, $CDCl_3$). (c) Overlapping resonances

4.4.10.1 C_3 Marfey's analysis of *cyclo*-(L-Phe-L-Pro) (4.35)

Employing the C_3 Marfey's method as previously described, **4.35** was subjected to acid hydrolysis using 6M HCl, derivatized with D-FDAA, and subjected to HPLC analysis to determine the absolute configuration of the Phe and Pro amino acids residues. The absolute configuration of **4.35** was determined by comparing the retention times of standard amino acids with the hydrolysate of **4.35**, to be L-Phe and L-Pro (**Figure 4.32** and Figure 4.33).

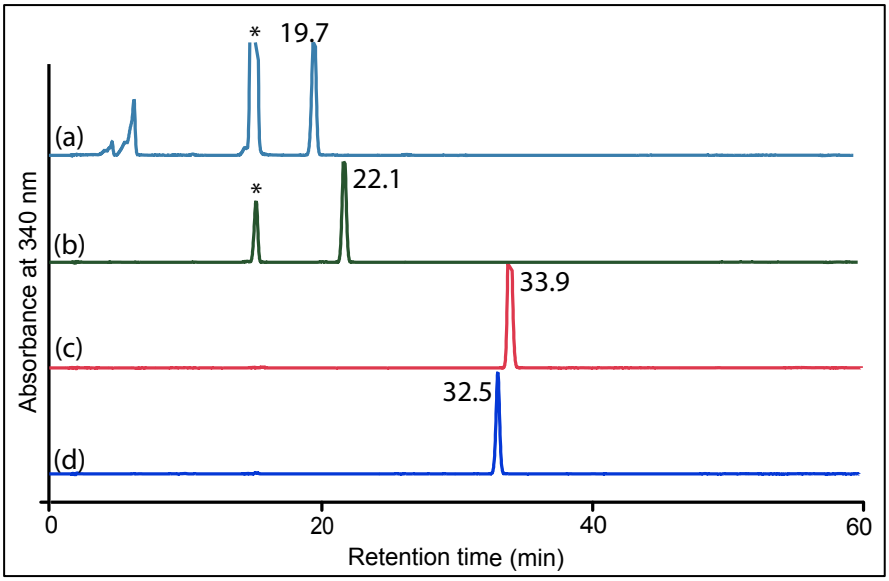

Figure 4.32. C_3 Marfey's analysis of the selected amino acids derivatized with D-FDAA with the retention times. (a) D-Pro + D-FDAA, (b) L-Pro + D-FDAA, (c) D-Phe + D-FDAA and (d) L-Phe + D-FDAA. * residual Marfey's reagent

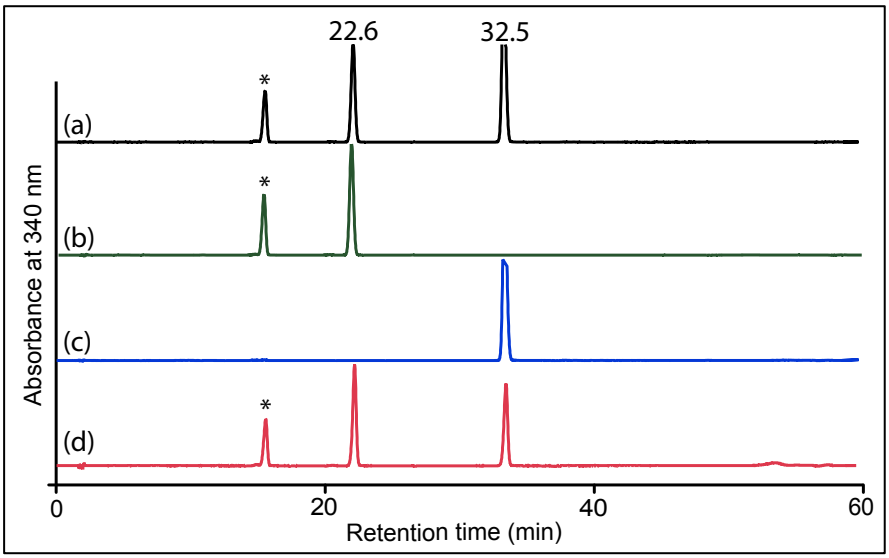

Figure 4.33. HPLC-DAD (340 nm) C_3 Marfey's analysis of *cyclo*-(L-Phe-L-Pro) (**4.35**). Identity of amino acids was confirmed by retention time and molecular weight. (a) coinjection of hydrolyzed **4.35** + D-FDAA with the standard L-Phe + D-FDAA and L-Pro + D-FDAA. (b) L-Pro + D-FDAA. (c) L-Phe + D-FDAA. (d) hydrolyzed of **4.35** showing the presence of L-Phe (t_R = 32.5 min) and L-Pro (t_R = 8.2 min). HPLC conditions, Zorbax, SB-C_3 column (150 × 4.6 mm, 5 μm), 1 mL/min, gradient of 15 - 60% MeOH/H_2O (isocratic 5% MeCN containing 1% formic acid) over 55 min.

4.4.11 Summary for impact of NOS inhibitors

Surprisingly all three NOS inhibitors **4.16 – 4.18** shut down heronapyrrole B (**4.02**) production and resulted in the production of **4.30 – 4.35**, a suite of known fungal metabolites. While our initial hypothesis that heronapyrrole B (**4.02**) biosynthesis was dependent on a functional bNOS has been vindicated, the unexpected appearance of fungal metabolites needs to be addressed.

4.4.12 Detection of an *Aspergillus* in the *Streptomyces* (CMB-M0423)

4.4.12.1 Fungal contamination

In a busy research laboratory, fungal contamination of cultures is always a risk and a concern. While great care is taken to employ sterile technique, it is difficult to completely exclude the possibility of contamination from airborne spores. To test the hypothesis that *Streptomyces* sp. (CMB-M0423) was accidentally contaminated by a fungus, we cultured *Streptomyces* sp. (CMB-M0423) multiple times on separate days in the presence and absence of NOS inhibitors. In the absence of NOS inhibitors, *Streptomyces* sp. (CMB-M0423) always produced heronapyrrole B (**4.02**), while in the presence of NOS inhibitors; *Streptomyces* sp. (CMB-M0423) always produced the fungal metabolites. To further challenge the contamination hypothesis, we recovered cryo-preserved samples of *Streptomyces* sp. (CMB-M0423) and repeated the sequence of cultures with and without the addition of NOS inhibitors. On all occasions the results were the same as the first

study. From these results, we can unambiguously exclude accidental laboratory fungal contamination after accessing the cryopreserved sample.

4.4.12.2 Associated fungus

Having established that the original isolate of *Streptomyces* sp. (CMB-M0423) was not inadvertently contaminated with a fungus during laboratory handling, we hypothesized that the original culture was "naturally" co-inoculated with an "associated" fungus, but that this fungus was suppressed under standard culture conditions, and only appearing on addition of NOS inhibitors. To try to detect and even obtain pure isolates of this "silent" fungus, *Streptomyces* sp. (CMB-M0423) was cultured in the presence of the antibacterial rifampicin (**4.36**), to suppress the growth of the *Streptomyces* sp. (CMB-M0423), and in the presence of the antifungal cycloheximide (**4.37**), to suppress fungal growth. The intent of both studies was to recover pure strains of both the *Streptomyces* and its associated *Aspergillus*.

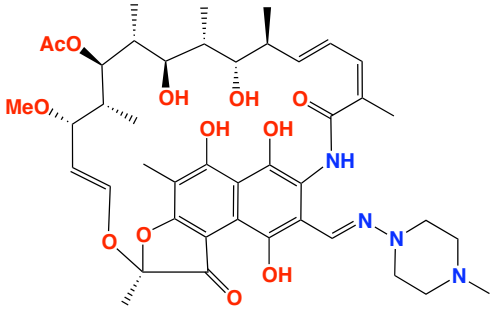

rifampicin (**3.36**)

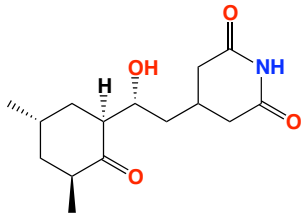

cycloheximide (**3.37**)

The results of these culturing trials are shown in Figure 4.34. When cultured on oatmeal-based media in the presence of rifampicin for 45 days, the original culture of *Streptomyces* sp. (CMB-M0423) displayed a multitude of individual black fungal colonies. These colonies were sub-cultured to deliver a pure fungal isolate, which was subjected to DNA extraction using cetyltrimethylammonium bromide (CTAB) protocol[176] (Appendix). A BLAST search on the resulting 18S rRNA sequence showed 98% homology with a species of the genus *Aspergillus* (Appendix). HPLC-DAD analysis of an extract derived from this pure *Aspergillus* sp. (CMB-M0423) revealed all the fungal metabolites **4.30 – 4.35**. We propose that this "associated fungus" be identified as *Aspergillus* sp. (CMB-M0423) (most likely *Aspergillus fumigatus*). By comparison, cultivation of the original *Streptomyces* sp. (CMB-M0423) isolate on M1 3.3% seawater media in the presence of the antifungal agent cycloheximide yielded a pure actinomycete strain that now can be assigned the correct description, *Streptomyces* sp. (CMB-M0423). To avoid confusion the original *Streptomyces* sp. (CMB-M0423) isolate is now renamed *Aspergillus*/*Streptomyces* sp. (CMB-M0423)

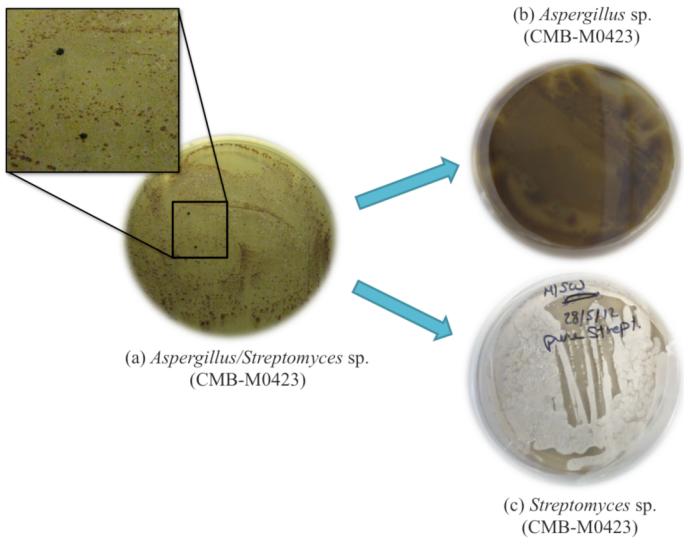

Figure 4.34. Pictures showing the isolation of *Aspergillus* sp. (CMB-M0423) from *Streptomyces* sp. (CMB-M0423). (a) Original *Aspergillus/Streptomyces* sp. (CMB-M0423). The zoom picture of the presence of *Aspergillus* colonies. (b) *Aspergillus* sp. (CMB-M0423), (c) *Streptomyces* sp. (CMB-M0423). Note the difference in the colour between (a) and (c)

4.4.13 Cultivation of *Aspergillus* sp. (CMB-M0423)

Aspergillus sp. (CMB-M0423) was cultivated on M1 broth containing 3.3% artificial ocean sea salt and incubated at 190 rpm, 26.5 °C over 10 d. Over the incubation period *Aspergillus* sp. (CMB-M0423) was capable of producing its fungal metabolites (**4.30** – **4.35**) (Figure 4.35).

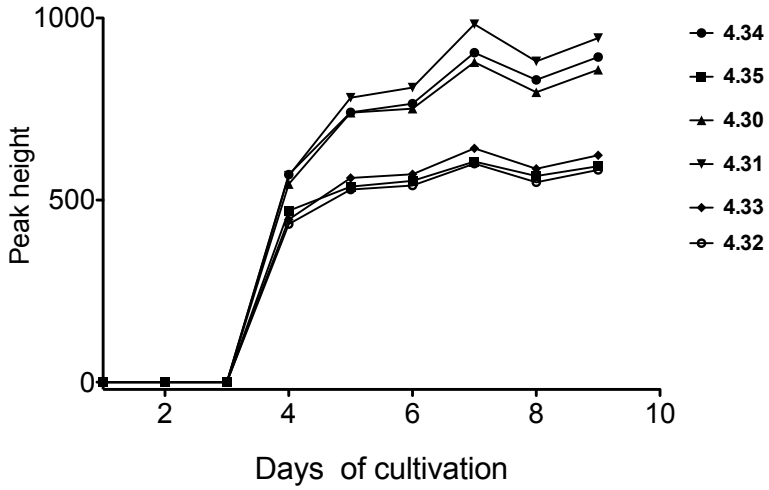

Figure 4.35. Graph showing production of *Aspergillus* sp. (CMB-M0423) secondary metabolites production over 10 d cultivation period. The crude extracts were analysed using HPLC-DAD-MS at 210 nm, analytical gradient H_2O/MeCN plus 0.05% HCO_2H using Zorbax C_8 column at 210 nm. The graph was plotted using the peak height for every fungal metabolite versus days of cultivation.

4.4.14 Cultivation of the pure *Streptomyces* sp. (CMB-M0423)

Streptomyces sp. (CMB-M0423) was cultivated in the microbioreactor on M1 broth containing 3.3% artificial ocean sea salt [composed of 0.5 g starch, 1 g yeast extract, 2 g peptone and 3.3% artificial ocean sea salt per 1 L of distilled water] (1.5 mL), at 26.5 °C for 7 days at 190 rpm. After the incubation period, the broth was extracted by the addition of EtOAc (1.5 mL) and the organic

layer dried under N_2. The organic layer was re-dissolved in MeOH (100 µL) and analyzed by HPLC-DAD-MS. *Streptomyces* sp. (CMB-M0423), to reveal no heronapyrrole B (**4.02**), strongly suggestive that the presence of *Aspergillus* sp. (CMB-M0423) was critical to the induction of heronapyrrole B and related metabolites (Figure 4.36 and Figure 4.37).

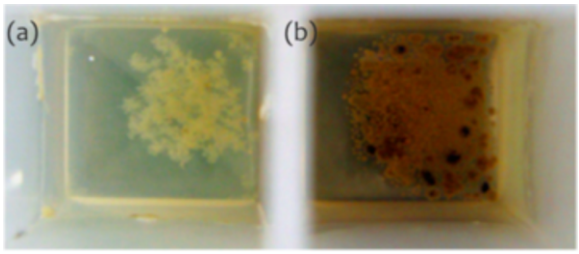

Figure 4.36. Picture showing micro-bioreactor culture of (a) *Streptomyces* sp. (CMB-M0423) and (b) *Aspergillus/Streptomyces* sp. (CMB-M0423)

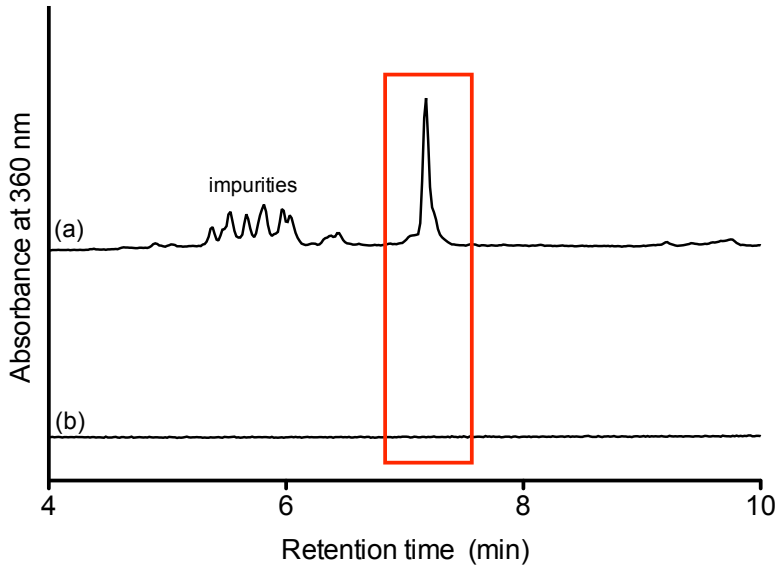

Figure 4.37. HPLC-DAD chromatogram at 360 nm, gradient elution H_2O/MeCN, HCO_2H using Zorbax C_8. (a) authentic heronapyrrole B, (b) crude extract from *Streptomyces* sp. (CMB-M0423) showing no production of heronapyrrole B (or indeed any secondary metabolites).

4.4.15 Co-cultivation of *Streptomyces* sp. and *Aspergillus* sp. (CMB-M0423)

Aspergillus sp. (CMB-M0423) was co-cultivated with *Streptomyces* sp. (CMB-M0423) in the micro-bioreactor (1.5 mL) using M1 broth containing 3.3% artificial ocean sea salt. After 7 days, the broth was extracted with EtOAc (1.5 mL) and re-dissolved in MeOH (100 µL) to give a final concentration of 1 mg/mL and analysed by HPLC-DAD-MS. The chemical profiling for the crude extract from *Streptomyces* sp. (CMB-M0423) showed no signs of heronapyrrole B production, while after co-culturing with *Aspergillus* sp. (CMB-M0423), heronapyrrole B production was observed (Figure 4.38) along with a large number of additional co-metabolites.

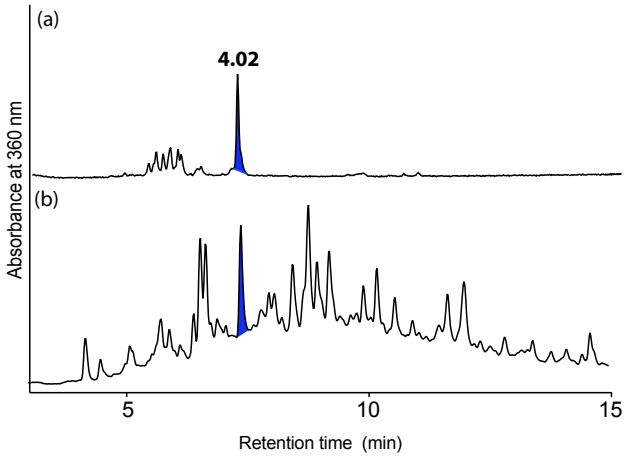

Figure 4.38. HPLC-DAD (360 nm) chromatogram, gradient elution H_2O/MeCN, HCO_2H using Zorbax C_8 for the crude extract in MeOH from mixing the *Aspergillus* sp. (CMB-M0423) and the *Streptomyces* sp. (CMB-M0423). The heronapyrrole B is co-eluted with the standard compound of heronapyrrole B. (a) authentic heronapyrrole B, (b) crude extract for co-culture of *Aspergillus* sp. (CMB-M0423) plus *Streptomyces* sp. (CMB-M0423).

These studies confirm that:

- The original *Streptomyces* sp. (CMB-M0423) isolate was in fact a mixed culture of *Streptomyces* sp. (CMB-M0423) plus quiescent *Aspergillus* sp. (CMB-M0423).
- The presence of the *Aspergillus* sp. (CMB-M0423) is essential for activating *Streptomyces* sp. (CMB-M0423) to produce heronapyrrole B.

4.4.16 Effect of *Aspergillus* chemistry on *Streptomyces* sp. (CMB-M0423)

4.4.16.1 Fungal metabolites as activators of *Streptomyces* sp. (CMB-M0423)

All the fungal metabolites listed above (**4.30** – **4.35**) were individually tested at 10 μM on *Streptomyces* sp. (CMB-M0423) to determine if any induced heronapyrrole B production. Only *cyclo*-(L-Phe-*trans*-4-hydroxy-L-Pro) (**4.34**) was capable on inducing heronapyrrole B production (Figure 4.39). Indeed, addition of **4.34** at 10 μM to a liquid micro-bioreactor culture of *Streptomyces* sp. (CMB-M0423) retrieved a 20.4 μg/mL yield of heronapyrrole B.

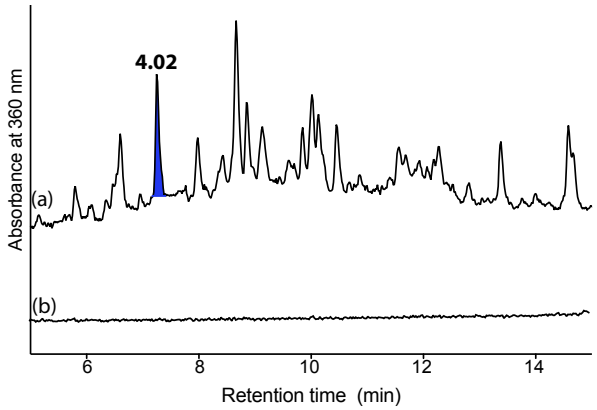

Figure 4.39. HPLC-DAD chromatogram, analytical gradient H_2O/MeCN, HCO_2H at 360 nm using Zorbax, C_8 showing metabolite profile of a micro-bioreactor culture of *Streptomyces* sp. (CMB-M0423) (a) in the presence of **4.34** (10 μM) and (b) in the absence of **4.34**

To further explore the effect of *cyclo*-(L-Phe-trans-4-hydroxy-L-Pro) (**4.34**) on the pure *Streptomyces* sp. (CMB-M0423), a concentration profile had been carried out in which a stock solutions of **4.34** were prepared in 2-fold dilution, ranging from 138 mM to 15 nM in 30% DMSO. An aliquot (15 µL) from each stock solution was transferred to micro-bioreactor wells containing M1 broth in 3.3% artificial ocean sea salt (1.45 mL), to deliver final **4.34** concentrations ranging from 4.6 mM to 0.5 nM plus 1% DMSO per well. After 7 d of incubation period, the broth was extracted with EtOAc (2 mL) and the organic layer dried under N_2. The crude extract was suspended in MeOH (100 µL) and analysed by HPLC-DAD-MS. The results showed that *cyclo*-(L-Phe-*trans*-4-hydroxy-L-Pro) at concentrations ranging from 291 µM to 1.1 µM induced the production of heronapyrrole B in *Streptomyces* sp. (CMB-M0423), with the optimum production of heronapyrrole B occurring at 10 – 40 µM, returning 20 ± 2 µg/mL of heronapyrrole B. Curiously, concentrations of **4.34** above 583 µM and below 0.5 µM failed to induce the production of heronapyrrole B (Figure 4.40 and Figure 4.41). This experiment provided strong evidence that **4.34** is an important regulator molecule for the induction of *Streptomyces* sp. (CMB-M0423) secondary metabolites, including but not limited to heronapyrrole B (**4.02**).

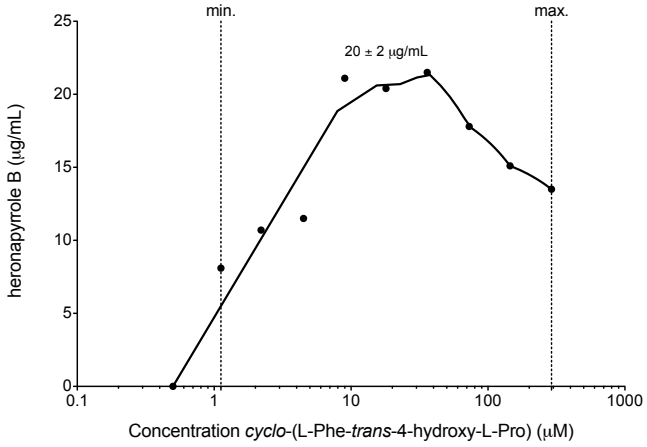

Figure 4.40. Graph showing the effect of different concentrations of *cyclo*-(L-Phe-*trans*-4-hydroxy-L-Pro) (**4.34**) (µM) highlighting min and max concentrations and the production of heronapyrrole B (µg/mL) in *Streptomyces* sp. (CMB-M0423)

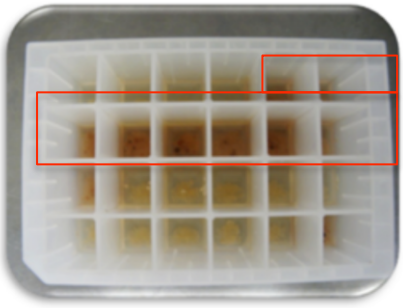

Figure 4.41. Picture of micro-bioreactor showing the effect of *cyclo*-(L-Phe-*trans*-4-hydroxy-L-Pro) (**4.34**) two fold dilution starting with (5.1 mM to 0.3 nM) on the production of heronapyrrole B by *Streptomyces* sp. (CMB-M0423). The brown colour in the wells coincides with the induction of the heronapyrrole B.

Having confirmed the induction of **4.02** by **4.34** in liquid culture, the effect of *cyclo*-(L-Phe-*trans*-4-hydroxy-L-Pro) (**4.34**) was tested on solid phase (agar) culture of *Streptomyces* sp. (CMB-M0423). *Streptomyces* sp. (CMB-M0423) exhibited morphological differences when cultivated on solid phase (agar plates) exposed to **4.34** (10 μM) (Figure 4.42). Figure 4.42 A/B demonstrate the effect of the absence (A) and presence (B) of **4.34** (10 μM) during micro-bioreactor liquid cultivation of *Streptomyces* p. (CMB-M0423). The brown colouration of the latter coincides with activation of heronapyrrole B (**4.02**) production. Figure 4.42C illustrates the growth of *Streptomyces* sp. (CMB-M0423) (white boat shape), riding a brown colouration (sea) caused by addition of **4.34** (DKP) to the lower 20% quadrant of the agar plate. Figure 4.42D represents an alternative representation where **4.34** is applied to the lower quadrant of the agar plate by way of a paper disc (10 μM) with the resulting gradient of **4.34** activating the lower (beard) section of the face cartoon to produce brown colouration – coinciding with production of **4.02** and co-metabolites. Figure 4.42E is an alternate representative where a plate inoculated with *Streptomyces* sp. (CMB-M0423) has been stimulated in the east and west quadrant by addition of **4.34** (10 μM).

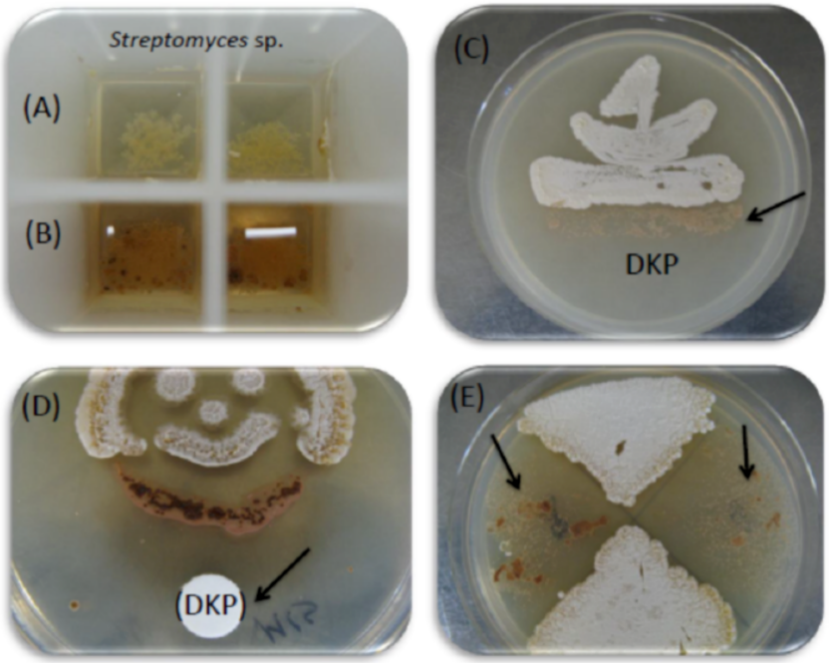

Figure 4.42. Picture shows the effect of *cyclo*-(L-Phe-*trans*-4-hydroxy-L-Pro) (**4.34**) (DKP) on *Streptomyces* sp. (CMB-M0423). (A) *Streptomyces* sp. (CMB-M0423) cultivated in the 24 well microbioreactor in the absence of *cyclo*-(L-Phe-*trans*-4-hydroxy-L-Pro) in M1 broth 3.3% artificial ocean sea salt. (B) *Streptomyces* sp. (CMB-M0423) cultivated in the presence of 0.01 mM *cyclo*-(L-Phe-*trans*-4-hydroxy-L-Pro) (**4.34**) in M1 broth 3.3% ocean sea salt. (D) Cultivation of *Streptomyces* sp. (CMB-M0423) on the M1 3.3% agar in the presence of disc containing 0.01 mM *cyclo*-(L-Phe-*trans*-4-hydroxy-L-Pro) (**4.34**). The inductions of heronapyrroles start to appear towards the disc while the rest of the *Streptomyces* is white in colour. (E) *Streptomyces* sp. (CMB-M0423) cultivated in the whole M1 agar plate containing 3.3% artificial ocean sea salt. The arrows point to the addition of *cyclo*-(L-Phe-*trans*-4-hydroxy-L-Pro) and the induction of the heronapyrrole B.

4.4.17 Detecting the presence of *cyclo*-(L-Phe-*trans*-4-hydroxy-L-Pro) in the crude extract of *Aspergillus*/ *Streptomyces*. sp (CMB-M0423)

Our emerging theory suggests that *cyclo*-(L-Phe-*trans*-4-hydroxy-L-Pro) (**4.34**) is the regulator molecule produced by *Aspergillus* sp. (CMB-M0423) that activates *Streptomyces* sp. (CMB-M0423) to produce heronapyrrole B (**4.02**). This theory has been supported by the observation that *Aspergillus* metabolites, in particular *cyclo*-(L-Phe-*trans*-4-hydroxy-L-Pro) (**4.34**), do indeed activate *Streptomyces* sp. (CMB-M0423) to produce heronapyrrole B (**4.02**). To further confirm this theory required detection and quantification of *cyclo*-(L-Phe-*trans*-4-hydroxy-L-Pro) (**4.34**) in the crude extract of an *Aspergillus*/*Streptomyces* sp. (CMB-M0423) culture. To achieve this, HPLC-DAD-ESI(+)MS data on the crude extracts, were examined by single ion extraction methodology, using the *m/z* 261 $[M+H]^+$ for **4.34**. This approach detected *cyclo*-(L-Phe-*trans*-4-hydroxy-L-Pro) (**4.34**) in the crude extract of an *Aspergillus*/*Streptomyces* sp. (CMB-M0423) culture (Figure 4.43).

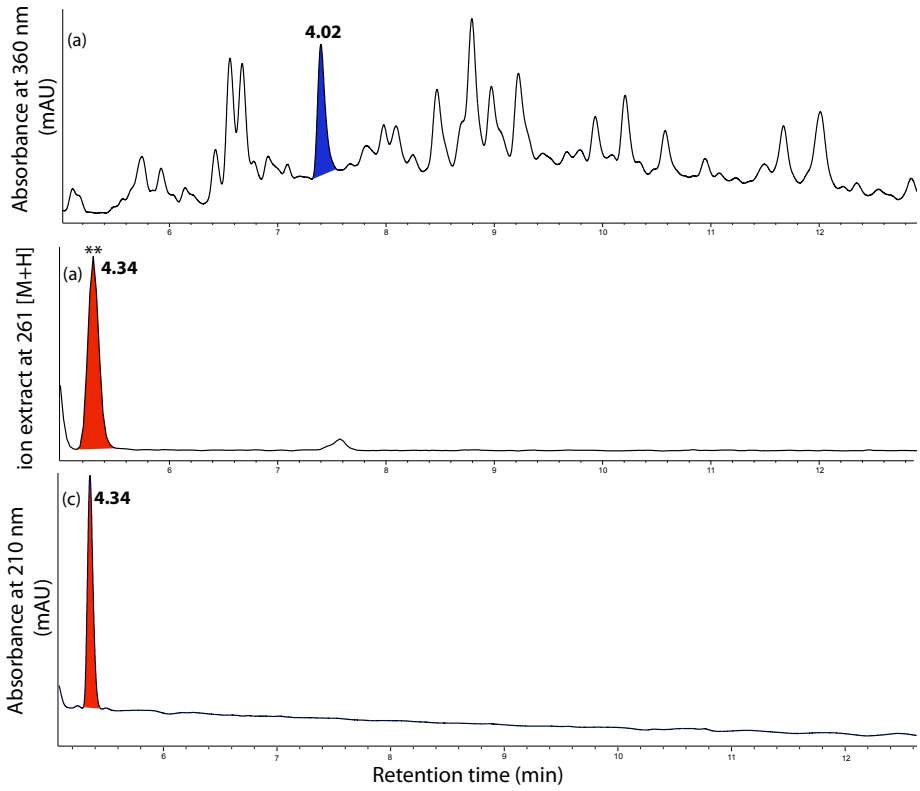

Figure 4.43. Chromatograms showing *Aspergillus*/*Streptomyces* sp. (CMB-M0423) crude extract, (a) HPLC-DAD-MS, gradient elution H_2O/MeCN, HCO_2H using Zorbax C_8 for the crude extract from *Streptomyces* sp. (CMB-M0423) at 360 nm showing the presence of heronapyrrole B (**4.02**). (b) Single ion extraction at 261 [M+H] showing the presence of *cyclo*-(L-Phe-*trans*-4-hydroxy-L-proline) (**4.34**) in the crude extract of *Aspergillus*/*Streptomyces* sp. (CMB-M0423). (c) Authentic *cyclo*-(L-Phe-*trans*-4-hydroxy-L-proline) (**4.34**)

4.4.18 Quantify *cyclo*-(L-Phe-*trans*-4-hydroxy-L-proline) (4.34)

Having demonstrated above that *cyclo*-(L-Phe-*trans*-4-hydroxy-L-proline) (**4.34**) is present in the crude extract of *Aspergillus*/*Streptomyces* sp. (CMB-M0423), we moved on to quantify these levels to establish if they were high enough to initiate heronapyrrole B (**4.02**) biosynthesis. A standard calibration curve was prepared using *cyclo*-(L-Phe-*trans*-4-hydroxy-L-proline) in 2-fold dilution ranging from 7.8 to 0.4 μg/mL in MeOH, in which 10 μL was injected into the HPLC-DAD-MS. The graph was plotted using the area under the peak for the extracted ion 261 $[M+H]^+$ consistent with the molecular weight for *cyclo*-(L-Phe-*trans*-4-hydroxy-L-proline) (Figure 4.44).

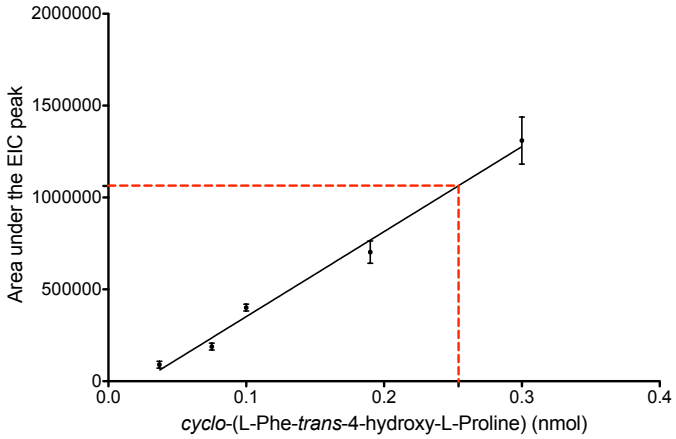

Figure 4.44. Graph showing the standard calibration curve using ion extraction at 261$[M+H]^+$ for standard concentrations of *cyclo*-(L-Phe-*trans*-4-hydroxy-L-Pro) (**4.34**). Red dashed line represents the area under the peak for the extracted ion for **4.34** in the crude extract of *Aspergillus*/*Streptomyces* sp. (CMB-M0423).

Figure 4.44 demonstrated that *cyclo*-(L-Phe-*trans*-4-hydroxy-L-Pro) (**4.34**) has a crucial effect on the induction of heronapyrrole B by *Streptomyces* sp. (CMB-M0423), with the levels of **4.34** in *Aspergillus*/*Streptomyces* sp. (CMB-M0423) crude extract being 0.47 ± 0.07 μg/mL (1.8 ± 0.3 μM) which induces the production of 9.2 ± 0.8 μg/mL of heronapyrrole B in the crude extract.

4.4.19 Effect of *Streptomyces* chemistry on *Aspergillus* sp. (CMB-M0423)

Pure samples of heronapyrrole A (**4.01**), B (**4.02**) and C (**4.03**) were individually added to micro-bioreactor culture wells to give final concentration of 10 μM in 1% DMSO per well, and wells were inoculated with *Aspergillus* sp. (CMB-M0423) in M1 3.3% artificial ocean sea salt. Micro-bioreactor cultures were monitored every day of 12 days, by removing an aliquot (100 μL) from each well and measuring the OD (600 nm). All cultures remained in the stationary phase until day 5. It was also observed that heronapyrrole C (**4.03**) did not affect the growth as OD values continued to increase until day 10. On the other hand, both heronapyrrole A (**4.01**) and B (**4.02**) inhibited the growth at day 7 (Figure 4.47). Simultaneous chemical profiling (HPLC-DAD)

revealed a suppression/loss of secondary metabolite production for all secondary metabolites except **4.34** – the only metabolite critical to activating heronapyrrole biosynthesis in *Streptomyces* sp. (CMB-M0423) (Figure 4.48).

These experiments demonstrated that *Aspergillus* sp. (CMB-M0423) exposed to heronapyrroles experiences retarded cell growth, and an altered secondary metabolite production. These observations suggest that heronapyrroles A (**4.01**) and B (**4.02**) and possibly heronapyrrole C (**4.03**) are fungistatic (**Figure 4.45** and Figure 4.46).

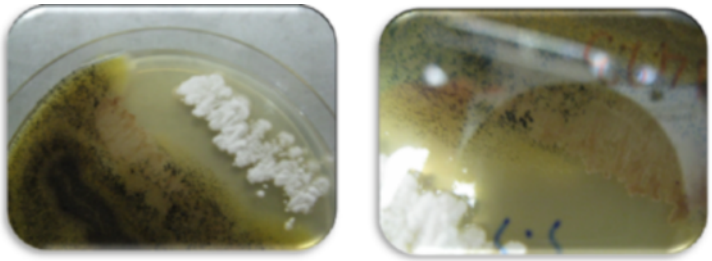

Figure 4.45. Pictures showing co-culture of both the *Aspergillus* sp. (CMB-M0423) and *Streptomyces* sp. (CMB-M0423) on M1 agar plate containing 3.3% ocean sea salt.

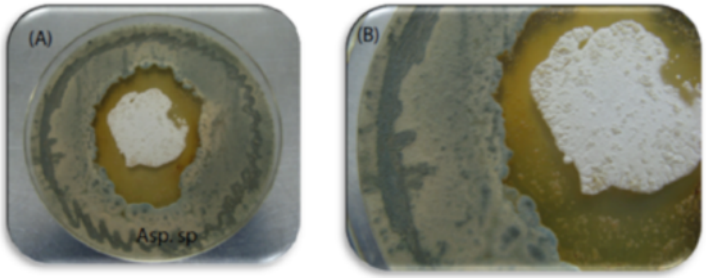

Figure 4.46. (A) Streaking of *Aspergillus* sp. (CMB-M0423) on M1 agar with 3.3% artificial ocean sea salt, and then re-streaking of *Streptomyces* sp. (CMB-M0423). The picture shows that on the edges of the plate the *Aspergillus* sp. (CMB-M0423) starts growing until it reaches *Streptomyces* sp. (CMB-M0423) where it induces heronapyrrole production, which inhibits *Aspergillus* sp. (CMB-M0423). In the middle of the plate *Streptomyces* sp. (CMB-M0423) is completely white in colour. (B) Expanded image illustrating inhibition of *Aspergillus* sp. (CMB-M0423).

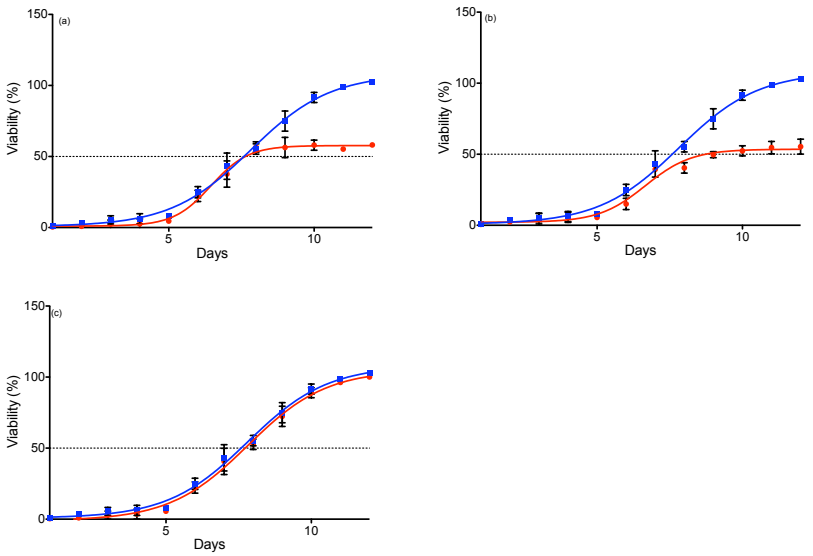

Figure 4.47. Graph showing the effect of (a) heronapyrrole A (**4.01**), (b) heronapyrrole B (**4.02**) and (c) heronapyrrole C (**4.03**) in red at 10 μM on the growth of *Aspergillus* sp. (CMB-M0423) versus control (blue)

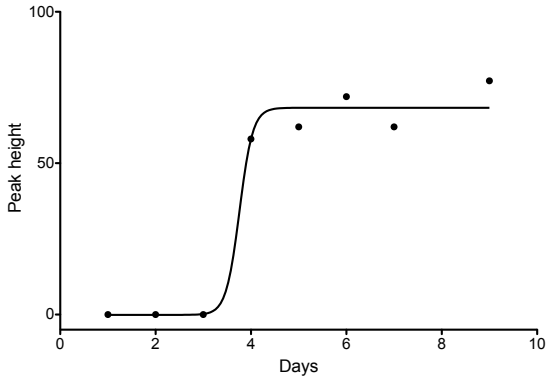

Figure 4.48. Graph showing peak height of **4.34** using HPLC-DAD (254 nm) chromatogram, gradient elution, H_2O/MeCN, HCO_2H using Zorbax C_8 of the crude extract from *Aspergillus* sp. (CMB-M0423) in the presence of heronapyrrole B (10 μM)

4.4.20 The effect of heronapyrrole B on *Aspergillus* sp. (CMB-M0423)

As demonstrated above, 10 μM of heronapyrrole B (**4.02**) is fungistatic towards *Aspergillus* sp. (CMB-M0423). As the levels of heronapyrrole B (**4.02**) in *Aspergillus*/*Streptomyces* sp. (CMB-M0423) cultures was quantified at 9.2 ± 0.8 μg/mL (see Figure 4.14), and as a 10 μM concentration equates to 3.8 μg/mL, we elected to undertake a study into the fungistatic properties of **4.02** on *Aspergillus* sp. (CMB-M0423) across a range of concentrations. Therefore, two-fold dilutions from stock solution of heronapyrrole B were prepared starting from 1800 to 54 μM in 30% DMSO. An aliquot (50 μL) from the stock solutions was transferred to the wells of the microbioreactor plate containing seed culture of *Aspergillus* sp. in M1 broth 3.3% artificial ocean sea salt (1.45 mL) to give a final concentration of 60 – 1.8 μM/1% DMSO per well. The experiment was performed in triplicate. The plate was incubated at 26.5 °C, 190 rpm for 10 days. After the incubation period, an aliquot (200 μL) from the broth was transferred into microtiter plate and the absorbance was measured spectrophotometrically at 600 nm in which IC_{50} of heronapyrrole B against *Aspergillus* sp. (CMB-M0423) was 12.1 μM, while the MIC was between 60 – 30 μM (Figure 4.49).

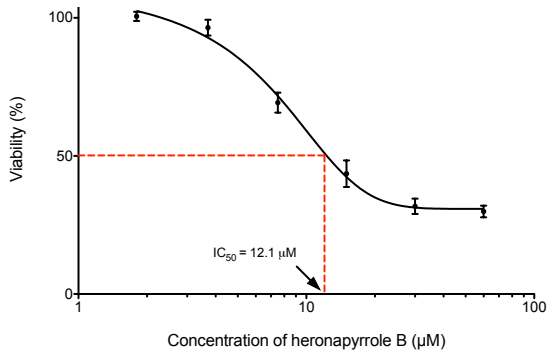

Figure 4.49. Graph showing the fungistatic effect of heronapyrrole B (**4.02**) on *Aspergillus* sp. (CMB-M0423)

4.4.21 Synthesis of diketopiperazine analogue library

The studies discussed above illustrated that *cyclo*-(L-Phe-*trans*-4-hydroxy-L-Pro) (**4.34**) is crucial for the production of heronapyrroles. In order to test if other diketopiperazines (DKPs) have an effect on the production of heronapyrroles, different DKP analogues were synthesized and tested using a fast, simple and convenient microwave approach. To arrive at a large array of synthetic DKPs, we employed a microwave assisted chemical synthesis, which nowadays is becoming increasingly popular and offers a number of significant advantages, by increasing rates and yields.

4.4.22 Synthesis of methyl esters (4.38a – e) and diketopiperazines (4.39a – l)

A series of DKPs **4.39a** – **l** (Table 4.14) were prepared in a 2 steps. Esterification of the amino acids **4.37a** – **d** using standard procedures, followed by microwave irradiation of mixtures of hydrochloride salts of the corresponding methyl esters **4.38a** – **e** in the presence of triethylamine, afforded the diketopiperazines **4.39a** – **l** (Scheme 4.2).

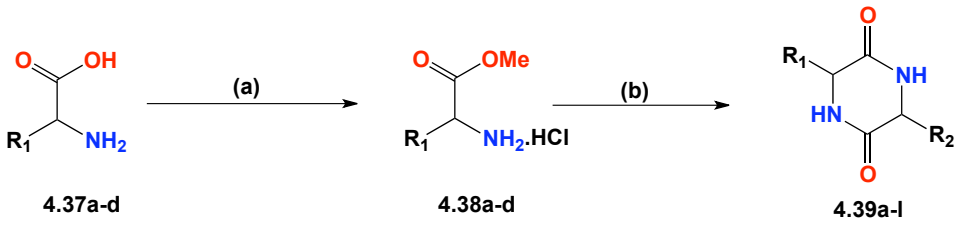

Scheme 4.2. Synthesis of DKPs derivatives. (a) addition of $SOCl_2$ in the presence of MeOH under reflux for 18 h. (b) The reaction mixture was dissolved in H_2O (5 mL), triethylamine (2.5 eq) and heated in the microwave at 140 °C, 300 W for 3 min

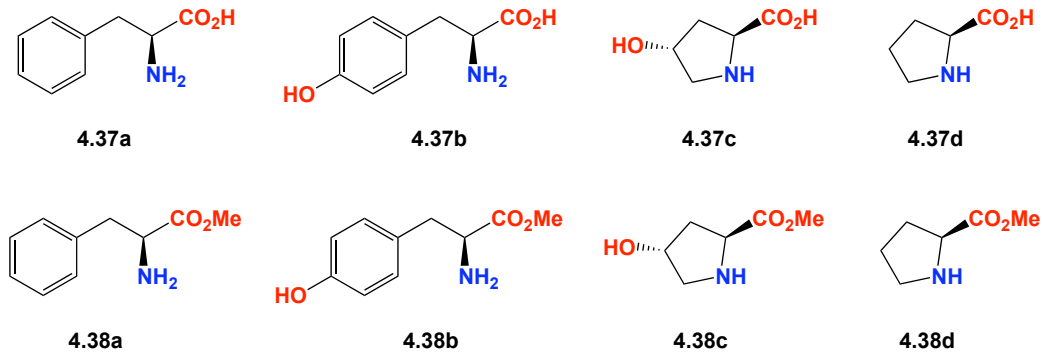

Figure 4.50. Structures of amino acids (**4.37a – d**) and their methyl esters (**4.38a – b**)

Table 4.14. Diketopiperazine derivatives **4.39a – l**

Molecular Structure of synthetic DKPs	
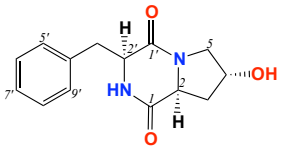 *cyclo*-(L-Phe-*trans*-4-hydroxy-L-Pro) (**4.39a**)	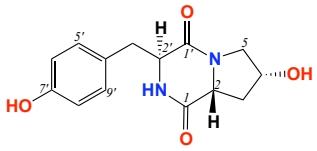 *cyclo*-(L-Tyr-*cis*-4-hydroxy-D-Pro) (**4.39g**)
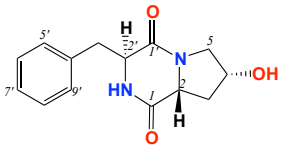 *cyclo*-(L-Phe-*cis*-4-hydroxy-D-Pro) (**4.39b**)	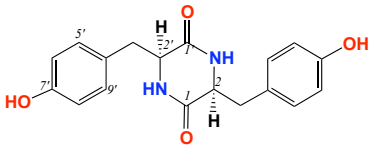 *cyclo*-(L-Tyr-L-Tyr) (**4.39h**)
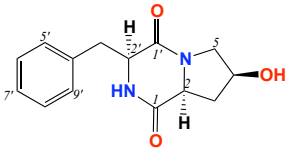 *cyclo*-(L-Phe-*cis*-4-hydroxy-L-Pro) (**4.39c**)	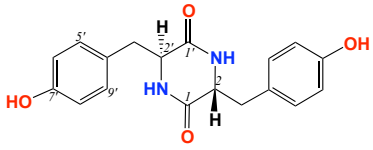 *cyclo*-(L-Tyr-D-Tyr) (**4.39i**)
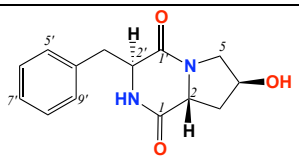 *cyclo*-(L-Phe-*trans*-4-hydroxy-D-Pro) (**4.39d**)	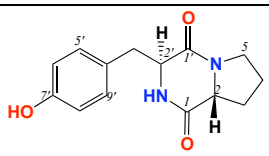 *cyclo*-(L-Tyr-D-Pro) (**4.39j**)
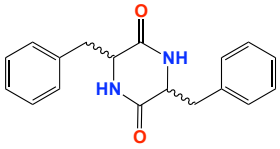 *cyclo*-(Phe-Phe) (**4.39e**)	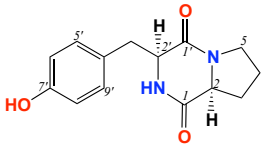 *cyclo*-(L-Tyr-L-Pro) (**4.39k**)
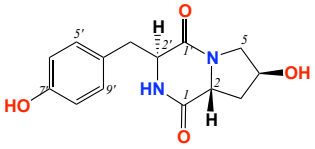 *cyclo*-(L-Tyr-*trans*-4-hydroxy-D-Pro) (**4.39f**)	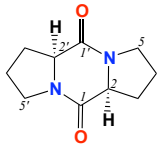 *cyclo*-(L-Pro-L-Pro) (**4.39l**)

4.4.22.1 Stereochemical Equilibrium

Prior literature studies have demonstrated that proline and 4-hydroxy-proline undergo racemization during conversion into DKPs, leading to a mixture of stereoisomers.[177,178] We set out to explore this equilibration, to achieve a larger array of DKP stereoisomers.

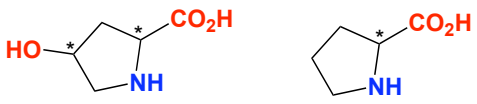

Pro 4-hydroxy-pro

4.4.23 Synthesis of *cyclo*-(Phe-4-hydroxy-Pro) stereoisomers

The reaction was performed by irradiating a 1:1 mixture of L-Phe methyl ester (**4.37a**) with *trans*-4-hydroxy-L-Pro methyl ester (**4.37b**) in H_2O (3 mL) in the presence of triethylamine (2.5 equivalent). The reaction was performed in a microwave reactor at 140 ˚C, 300 WATT for 3 min, the crude product was washed with H_2O, and the H_2O insoluble residue was dried *in vacuo* to recover a product that was analysed by HPLC-DAD-MS as containing multiple diketopiperazines (Figure 4.51 and Scheme 4.3).

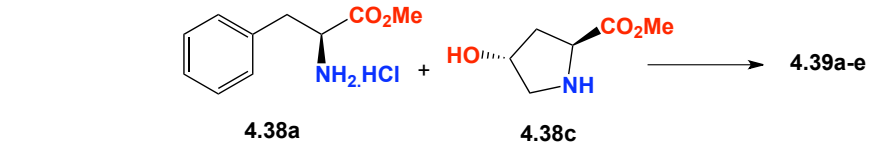

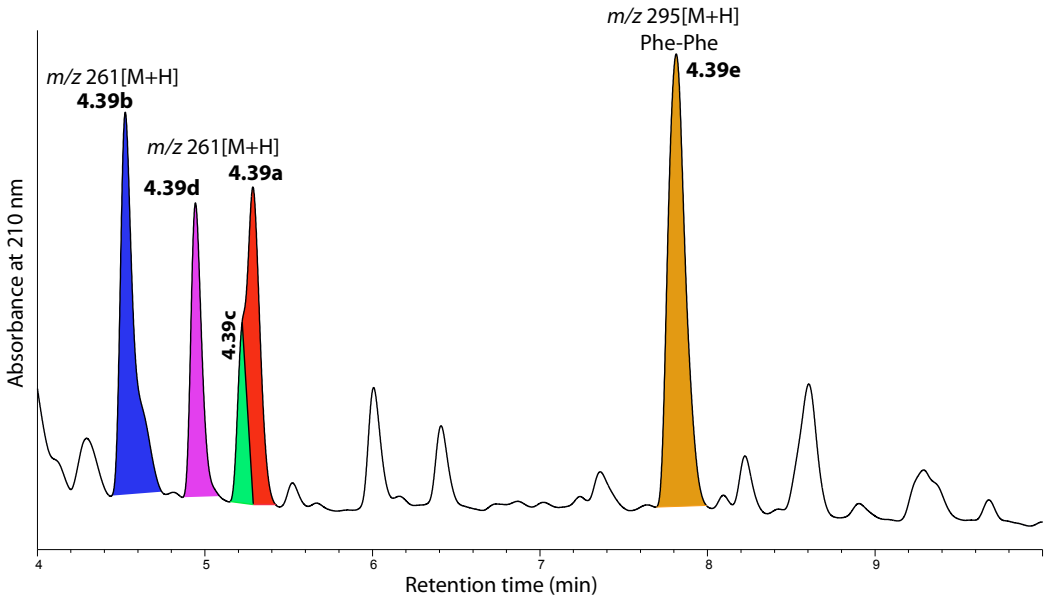

Figure 4.51. HPLC-DAD-MS reaction product of *cyclo*-(L-Phe-4-hydroxy-Pro). Reacting the methyl ester of L-Phe (**4.38a**) with methyl ester of *trans*-4-hydroxy-L-Pro (**4.38c**). The highlighted peaks represent DKPs

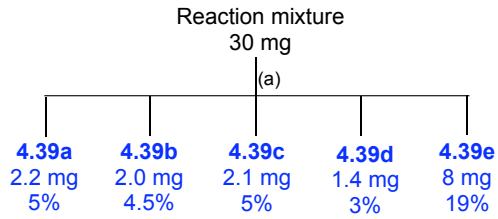

Scheme 4.3. Fractionation scheme of the reaction of methyl ester of L-Phe (**4.38a**) with methyl ester of *trans*-4-hydroxy-L-Pro (**4.38c**). (a) Semi-preparative gradient HPLC: Zorbax-C_8, 90 – 30% H_2O/MeOH, 3 mL/min, 30 min

4.4.23.1 *cyclo*-(L-Phe-*trans*-4-hydroxy-L-Pro) (4.39a)

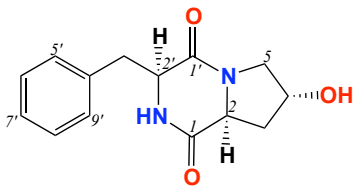

(**4.39a**)

Compound **4.39a** was synthesized as an optically active amorphous white powder ($[\alpha]^{22}_{D}$ −5.5, *c* 0.15, MeOH). HRESI(+)MS showed an adduct ion $(M+Na)^+$ (Δmmu +0.8) consistent with the molecular formula $C_{14}H_{16}N_2O_3$. Optimizing the isolation method, we were able to isolate **4.39a** from **4.39c** (Figure 4.53). The ^{1}H NMR ($CDCl_3$) data, of **4.39a** compared very well with data for the natural product **4.34**, confirming the assigned structure.

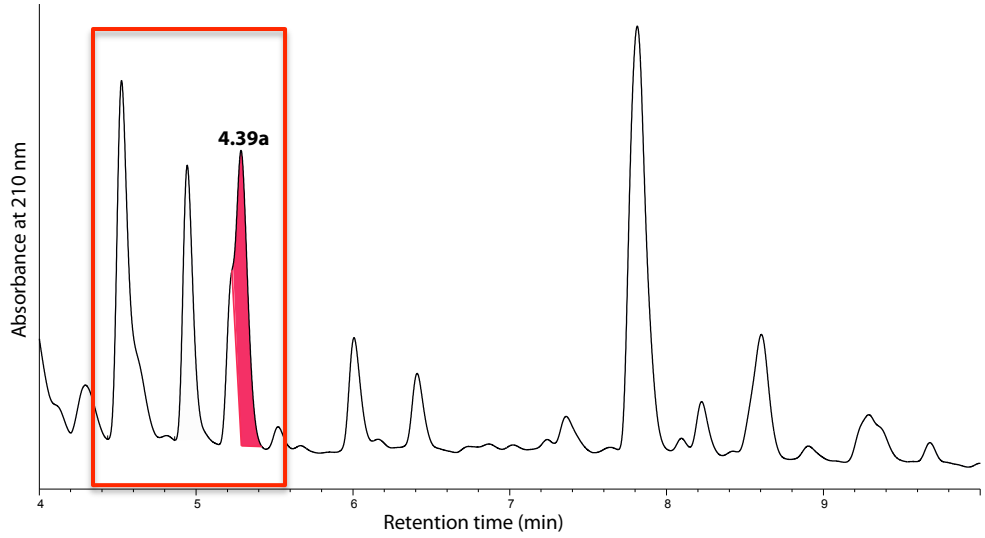

Figure 4.52. HPLC-DAD chromatogram, analytical gradient H_2O/MeCN plus HCO_2H at 210 nm using Zorbax C_8 column of the reaction mixture highlighting **4.39a**

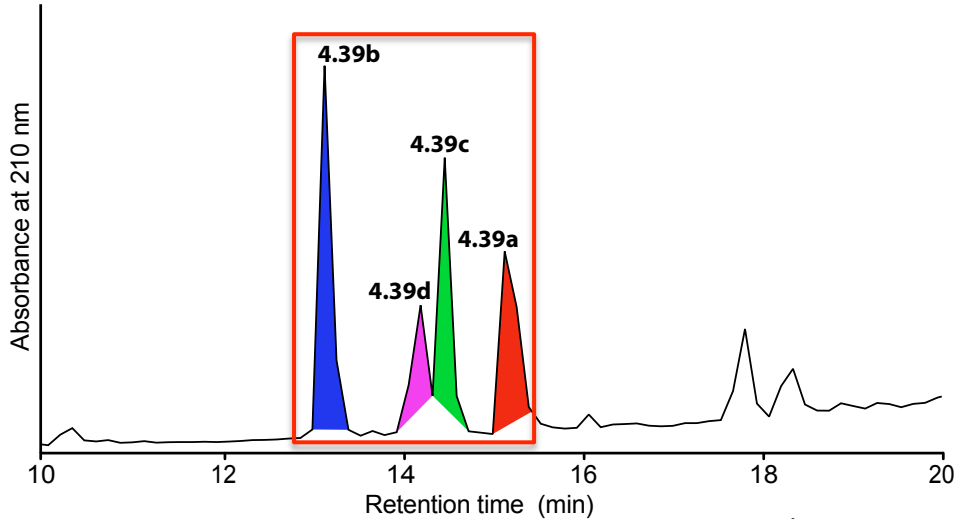

Figure 4.53. Semi-preparative HPLC-DAD chromatogram using H_2O/MeOH at 210 nm using Zorbax C_8 column optimized for resolution of **4.39a** – **d**

Table 4.15. NMR (600 MHz, $CDCl_3$) data of *cyclo*-(L-Phe-*trans*-4-hydroxy-L-Pro) (**4.39a**)

Pos.	δ_H, mult (*J* in Hz)[a]	δ_C[a]	COSY	^{1}H-^{13}C HMBC	ROESY
hydroxyproline					
1		169.8			
2	4.46, dd *(14.1, 3.2)*	57.7	3a,b	3, 4	2′
3	a 2.34, dd *(14.1, 3.2)*	37.9	2	2	
	b 2.06, dd *(14.1, 3.2)*			2	
4	4.31, d *(13.3)*	56.6	5a,b		
5	a 3.58, d *(13.3)*	36.9	4	4	
	b 2.77, dd *(13.3, 10.3)*			4	
4-OH		[b]			
phenylalanine					
1′	--	165.8			
2′-NH	5.57, br	--		2, 2′	
2′	4.57, br	68.7	3′a,b		2
3′	a 3.79, dd (*13.3, 4.1*)	54.7	2′	4′	
	b 3.62, d (*13.3*)		2′	2′, 4′, 5′/9′	
4′	--	135.7			
5′, 9′	7.22, d *(7.3)*	129.5	6′, 8′	3′, 7′	
6′, 8′	7.35, t *(7.3)*	129.8	7′	4′, 5′, 9′	
7′	7.29, t *(7.3)*	127.9	6′, 8′	5′, 6′, 10′	

(a)^{13}C assignments obtained from gHSQC and gHMBC data. (b) signals not observed

The NMR data of both **4.34** and **4.39a** were identical. Further analysis using ROESY data confirmed a *cis* relationship between H-2 and H-2′ (Figure 4.54).

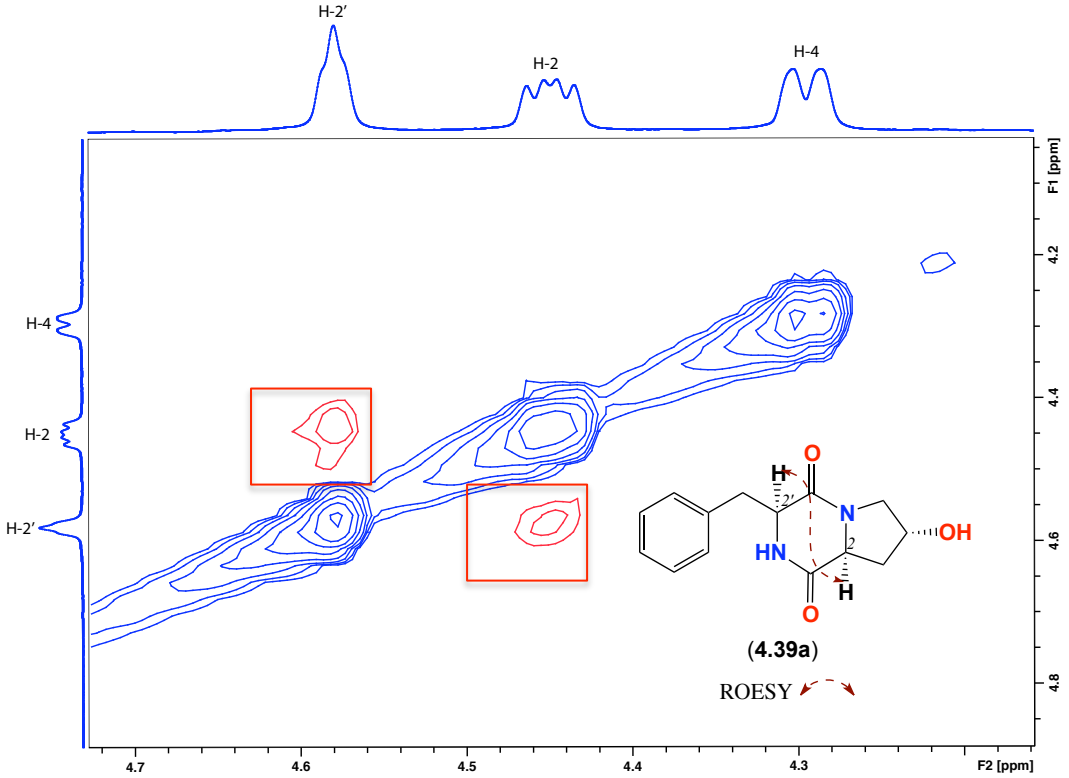

Figure 4.54. ROESY (600 MHz, $CDCl_3$) spectrum showing the correlations of *cyclo*-(L-Phe-*trans*-4-hydroxy-L-Pro) (**4.39a**)

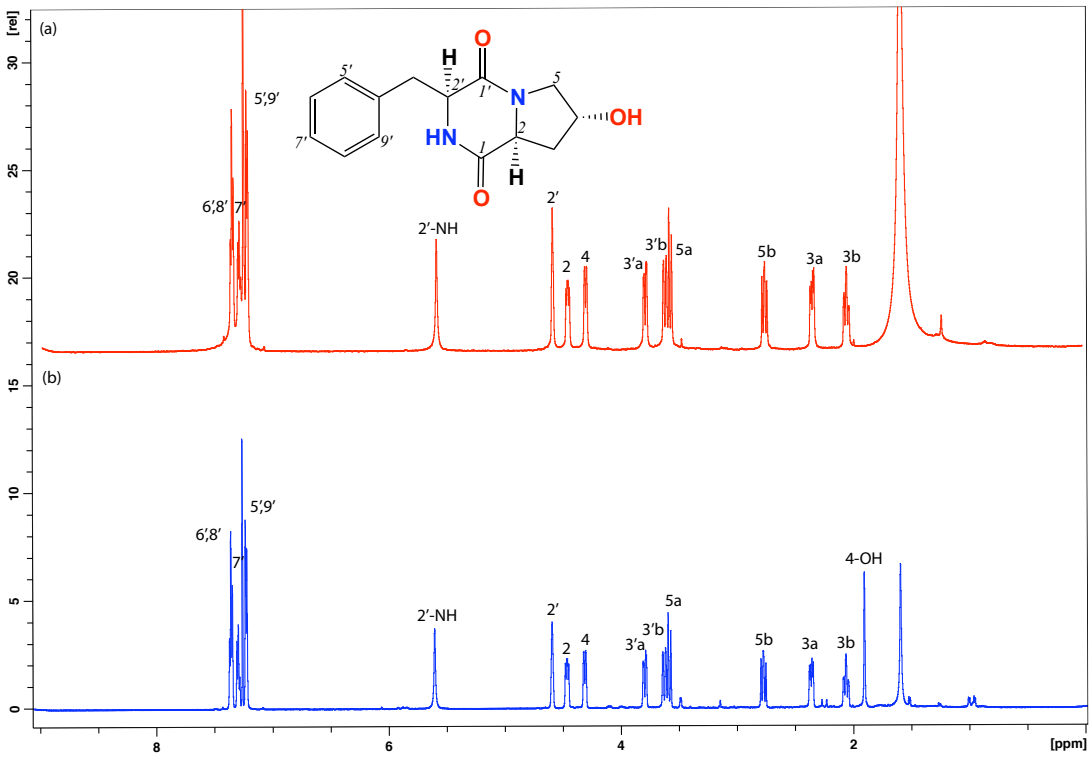

Figure 4.55. Comparison of ^{1}H NMR (600 MHz, $CDCl_3$) of (a) natural metabolite *cyclo*-(L-Phe-*trans*-4-hydroxy-L-Pro) (**4.34**) and (b) synthetic *cyclo*-(L-Phe-*trans*-4-hydroxy-L-Pro) (**4.39a**)

4.4.23.2 *cyclo*-(L-Phe-*cis*-4-hydroxy-D-Pro) (4.39b)

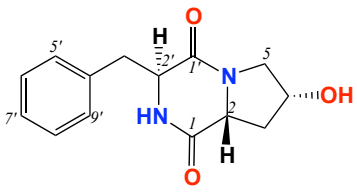

(**4.39b**)

Compound **4.39b** was synthesized as an optically active amorphous white powder ($[\alpha]^{22}_{D}$ −33, *c* 0.06, MeOH). HRESI(+)MS showed a adduct ion $(M+Na)^+$ consistent with the molecular formula $C_{14}H_{16}N_2O_3$ (Δmmu +0.5). The ^{1}H NMR ($CDCl_3$) data of **4.39b** are presented in Figure 4.58 and Table 4.16 and supported the assigned structure. ROESY correlations confirmed a *cis* configuration between H-2 and H-4 as shown as in Figure 4.57 and the absolute configuration of **4.39b** was confirmed by C_3 Marfey's analysis (Figure 4.59 and Figure 4.60).

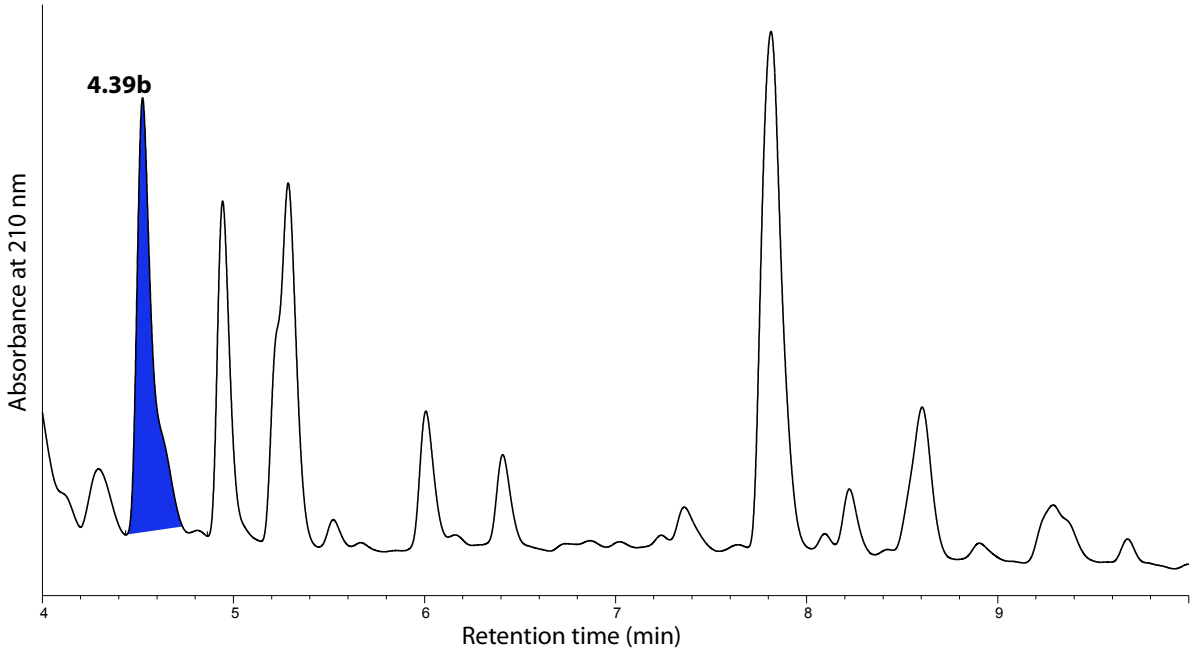

Figure 4.56. HPLC-DAD chromatogram, analytical gradient H_2O/MeCN plus HCO_2H at 210 nm using Zorbax C_8 column of the reaction mixture, highlighting **4.39b**

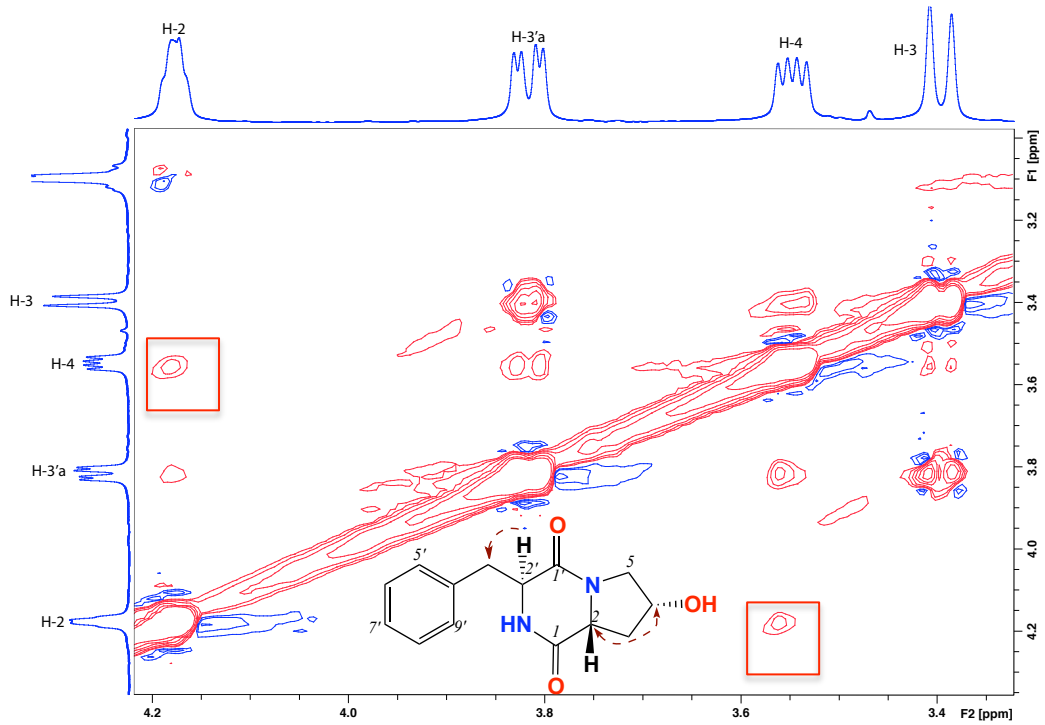

Figure 4.57. ROESY (600 MHz, $CDCl_3$) spectrum showing the correlations of *cyclo*-(L-Phe-*cis*-4-hydroxy-D-Pro) (**4.39b**)

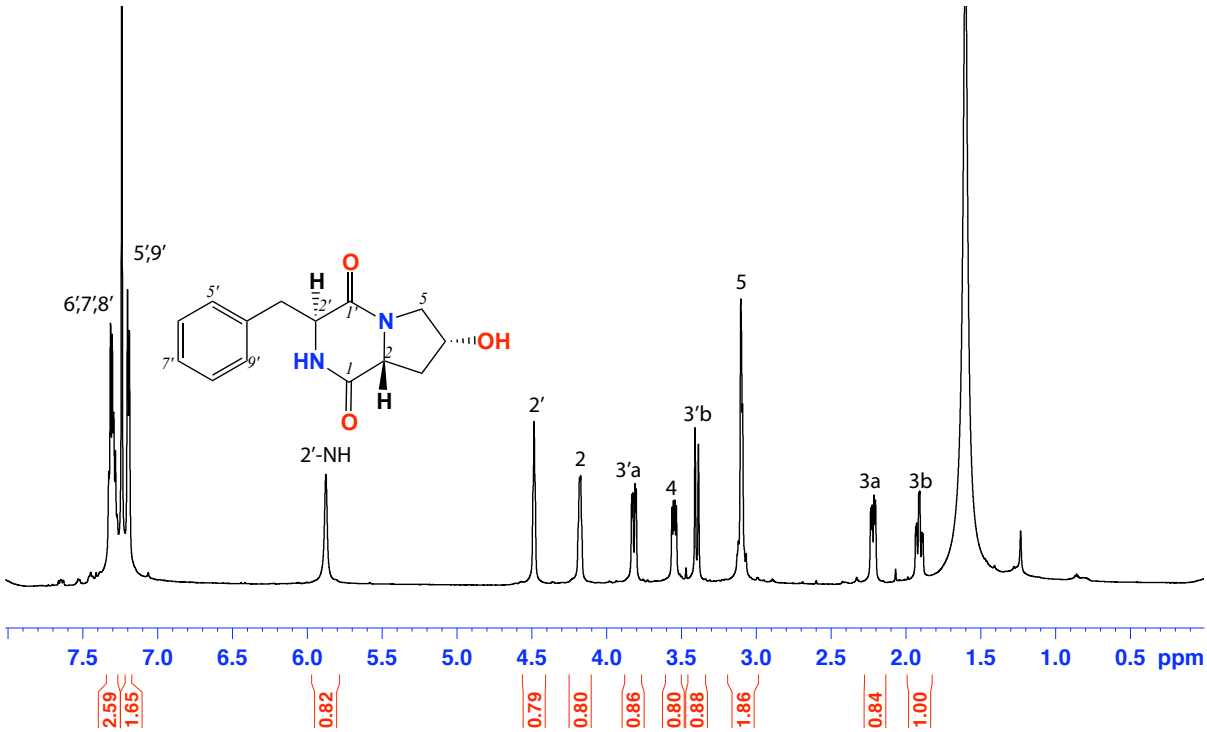

Figure 4.58. ^{1}H NMR (600 MHz, $CDCl_3$) of *cyclo*-(L-Phe-*cis*-4-hydroxy-D-Pro) (**4.39b**)

Table 4.16. NMR (600 MHz, $CDCl_3$) data of *cyclo*-(L-Phe-*cis*-4-hydroxy-D-Pro) (**4.39b**)

Pos.	δ_H, mult (*J* in Hz)[a]	δ_C[a]	COSY	^1H-^{13}C HMBC	ROESY
hydroxyproline					
1		169.6			
2	4.17, br s	59.7	3	1, 1′, 5	2′-NH
3	a 2.21, dd *(13.1, 5.8)*	38.8	2, 4	1	
	b 1.90, ddd *(13.1, 12.5, 5.8)*		2, 4	1	
4	2.54, dd *(13.1, 5.8)*	56.2	5a/b	1	2
5	a 3.09, br	40.7	4	1′, 2	5′a,b
	b 3.08, br		4	5	
4-OH	[c]				
phenylalanine					
1′		165.4			
2′-NH	5.87, brd		2′		
2′	4,48, brd	68.2	3′b		3
3′	a 3.81, dd *(13.1, 4.6)*	56.2	3′b		
	b 3.39, d *(13.1)*		2′, 3′a	3′	
4′		135.4			
5′, 9′	7.19, d *(7.1)*	130.4	6′, 8′	6′,7′,8′	
6′, 8′	7.30[b]	129.6			
7′	7.30[b]	128.3			

(a)^{13}C assignments obtained from gHSQC and gHMBC data. (b) Overlapping resonances. (c) Signals are not observed

4.4.23.2.1 C_3 Marfey's analysis of *cyclo*-(L-Phe-*cis*-4-hydroxy-D-Pro) (4.39b)

Employing the C_3 Marfey's method as previously described, **4.39b** was subjected to acid hydrolysis using 6M HCl, derivatized with D-FDAA, and subjected to HPLC analysis to determine the absolute configuration of the associated amino acids residues. The absolute configuration of **4.39b** was determined by comparing the retention times of derivatized standard amino acids with the derivatized hydrolysate of **4.39b**, as L-Phe and *cis*-4-hydroxy-D-Pro (Figure 4.59 and Figure 4.60).

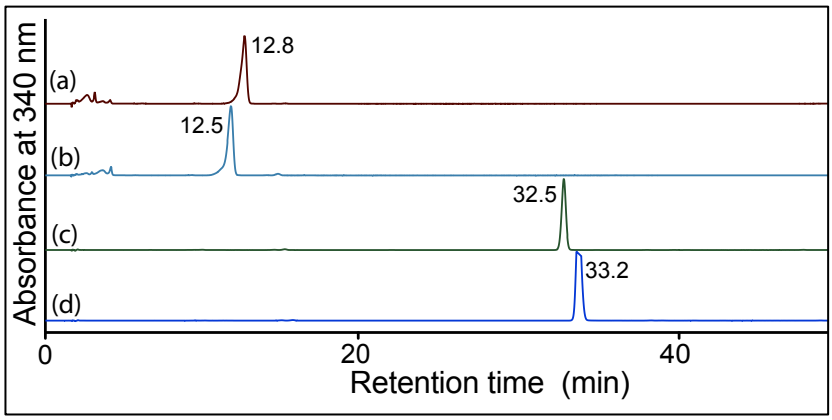

Figure 4.59. HPLC trace (340 nm) from HPLC-DAD-MS C_3 Marfey's analysis of the standard amino acids reacting with D-FDAA. Identity of amino acids was confirmed by retention time and molecular weight. (a) *cis*-4-hydroxy-L-Pro + D-FDAA (t_R = 12.8 min), (b) *cis*-4-hydroxy-D-Pro + D-FDAA (t_R = 12.5 min), (c) L-Phe + D-FDAA (t_R = 32.5 min) and (d) D-Phe + D-FDAA (t_R = 33.2 min). HPLC conditions, Zorbax, SB-C_3 column (150 × 4.6 mm, 5 μm), 1 mL/min, gradient of 15 – 60% MeOH/H_2O (isocratic 5% MeCN containing 1% formic acid) over 55 min

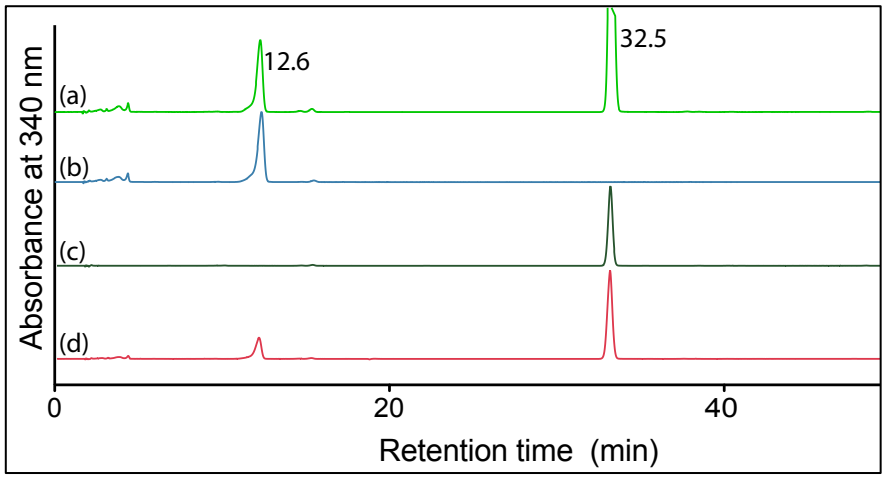

Figure 4.60. HPLC trace (340 nm) from HPLC-MS C_3 Marfey's analysis of *cyclo*-(L-Phe-*cis*-4-hydroxy-D-Pro) (**3.39b**). Identity of amino acids was confirmed by retention time and molecular weight. (a) Co-injection of D-FDAA derivatized hydrolysate of **3.39b** with L-Phe and *cis*-4-hydroxy-D-Pro + D-FDAA, (b) *cis*-4-hydroxy-D-Pro + D-FDAA, (c) L-Phe + D-FDAA, (d) D-FDAA derivatized hydrolyzed of **4.39b** (200 µg) showing the presence of L-Phe (t_R = 32.5 min) and *cis*-4-hydroxy-D-Pro (t_R = 12.6 min). HPLC conditions, Zorbax, SB-C_3 column (150 × 4.6 mm, 5 µm), 1 mL/min, gradient of 15 – 60% MeOH/H_2O (isocratic 5% MeCN containing 1% formic acid) over 55 min

4.4.23.3 *cyclo*-(L-Phe-*cis*-4-hydroxy-L-Pro) (4.39c)

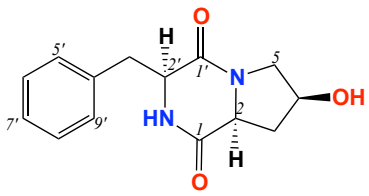

(**4.39c**)

Compound **4.39c** was synthesized as an optically active amorphous white powder ($[\alpha]^{21}_{D}$ −7.6, *c* 0.05, MeOH). HRESI(+)MS showed an adduct ion $(M+Na)^+$ consistent with the molecular formula $C_{14}H_{16}N_2O_3$ (Δmmu +1.5). The ^1H NMR ($CDCl_3$) spectrum and tabulated data of **4.39c** are presented in Figure 4.63 and Table 4.17 respectively. ROESY correlations confirmed the *cis* relationship between H-2′, H-2 and H-4 as shown in Figure 4.62. Marfey analysis was used to confirm the absolute configuration (Figure 4.64 and Figure 4.65).

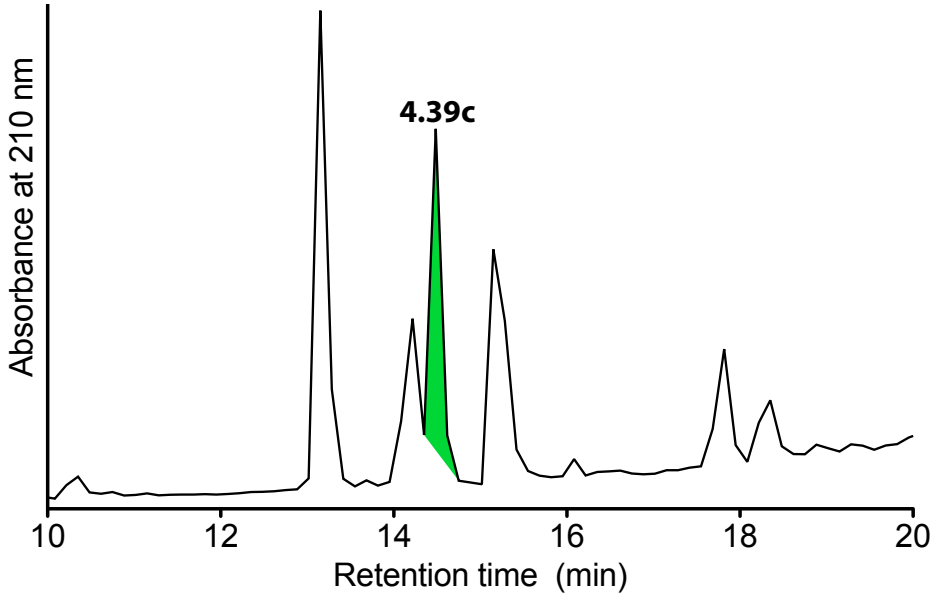

Figure 4.61. Semi-preparative HPLC-DAD chromatogram using H_2O/MeOH at 210 nm using Zorbax C_8 column optimized for resolution of **4.39c**

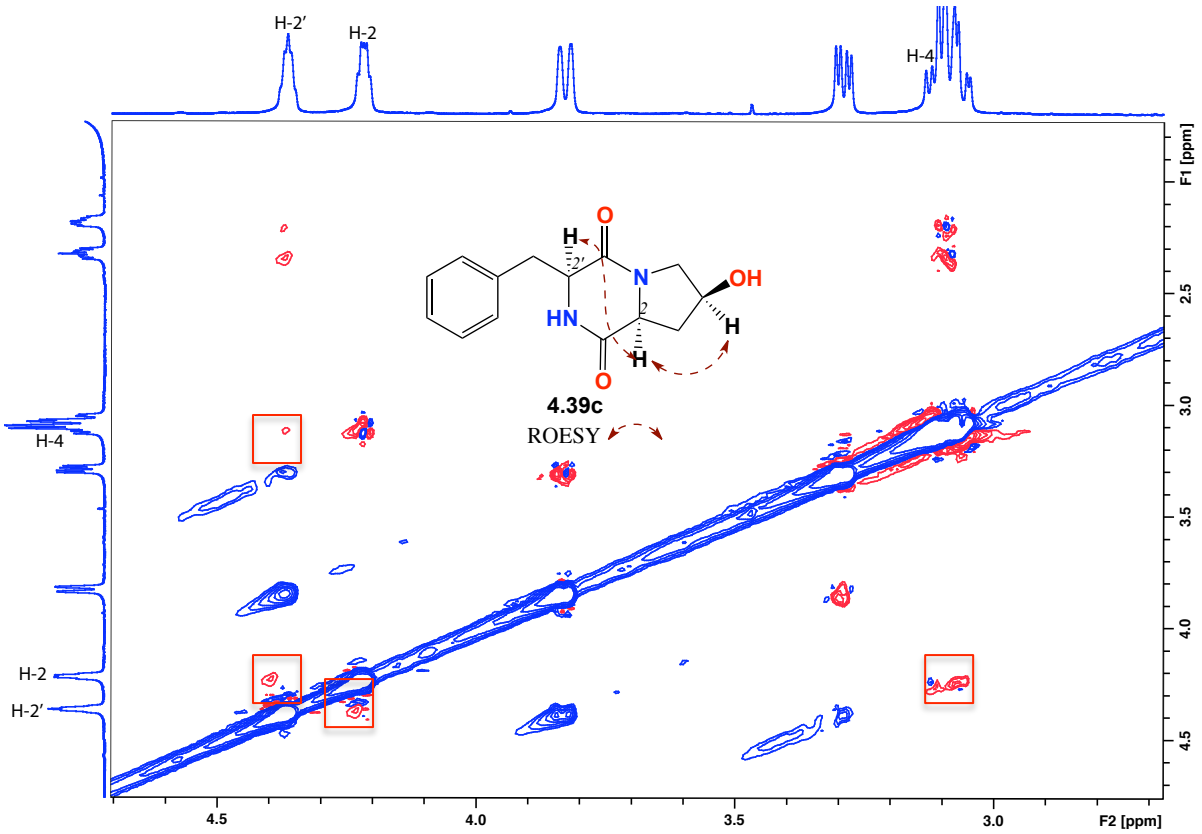

Figure 4.62. ROESY (600 MHz, $CDCl_3$) spectrum showing the correlations of *cyclo*-(L-Phe-*cis*-4-hydroxy-D-Pro) (**4.39c**)

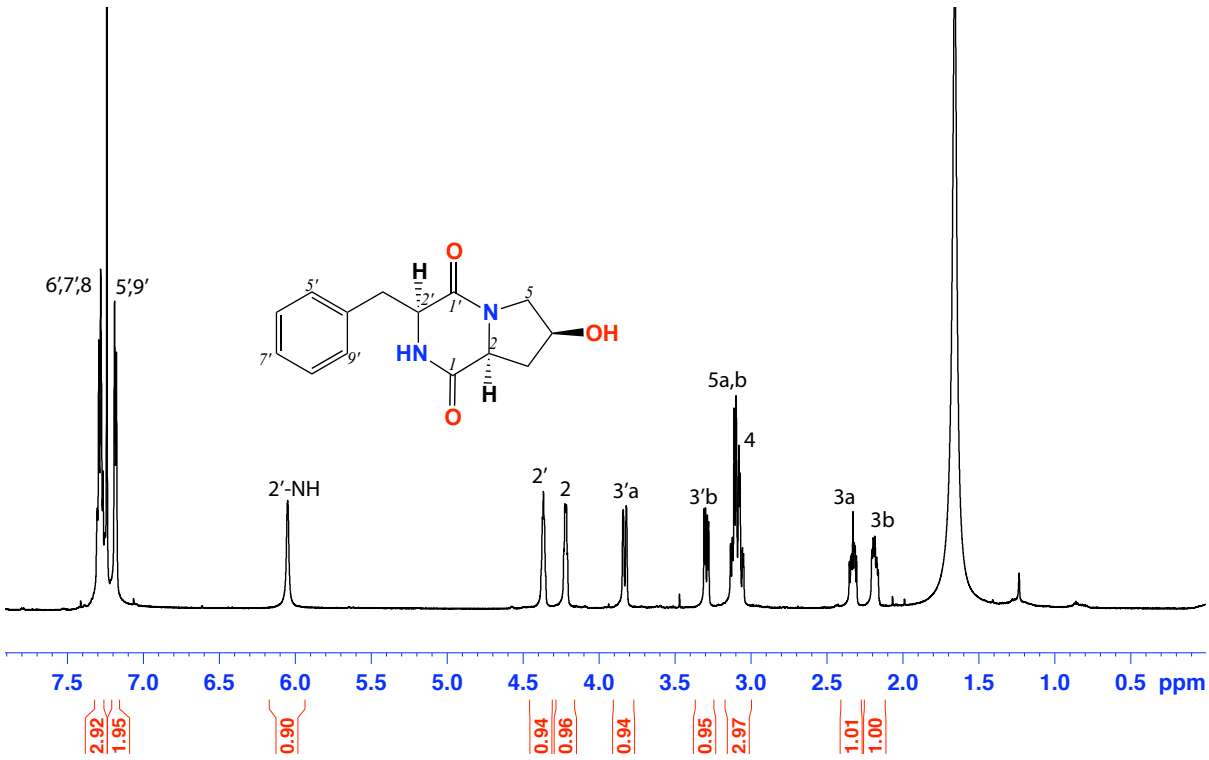

Figure 4.63. ^{1}H NMR (600 MHz, $CDCl_3$) spectrum of *cyclo*-(L-Phe-*cis*-4-hydroxy-D-Pro) (**4.39c**)

Table 4.17. NMR (600 MHz, $CDCl_3$) data of *cyclo*-(L-Phe-*cis*-4-hydroxy-L-Pro) (**4.39c**)

Pos.	δ_H, mult (*J* in Hz)[a]	δ_C[a]	COSY	^1H-^{13}C HMBC	ROESY
hydroxyproline					
1		165.9			
2	4.21, br s	59.7	3a,b	1′, 1	4
3	a 2.32, m	37.8	2, 4	1′	
	b 2.18, m		2, 4	1′	
4	3.08[b],m	56.5		1, 3	2
5	a 3.08[b],m	40.8		1′, 2	
	b 3.07[b],m			1′, 2	
4-OH	[c]				
phenylalanine					
1′		169.1			
2′-NH	6.04, br s		2′		
2′	4.36, m	68.8	2′-NH		
3′	a 3.82, d *(12.6)*	54.1	2′, 3′b	2′	3′b
	b 3.29, dd *(12.6, 4.9)*		2′, 3′a	2′	3′a
4′		127.9			
5′, 9′	7.18, d *(7.1)*	130.5	6′, 8′		
6′, 8′	7,28[b],m	129.7	4′, 5′, 9′		
7′	7.28[b],m	128.5	6′,8′		

(a)^{13}C assignments obtained from gHSQC and gHMBC data. (b) Overlapping resonances. (c) Signals are not observed

4.4.23.3.1 C_3 Marfey's analysis of *cyclo*-(L-Phe-*cis*-4-hydroxy-L-Pro) (4.39c)

Employing the C_3 Marfey's method as previously described, **4.39c** was subjected to acid hydrolysis using 6 M HCl, derivatized with D-FDAA, and subjected to HPLC analysis to determine the absolute configuration of the amino acid residues. The absolute configuration of **4.39c** was determined by comparing the retention times of derivatized standard amino acids with the derivatized hydrolysate of **4.39c** to be L-Phe and *cis*-4-hydroxy-L-Pro (Figure 4.64 and Figure 4.65).

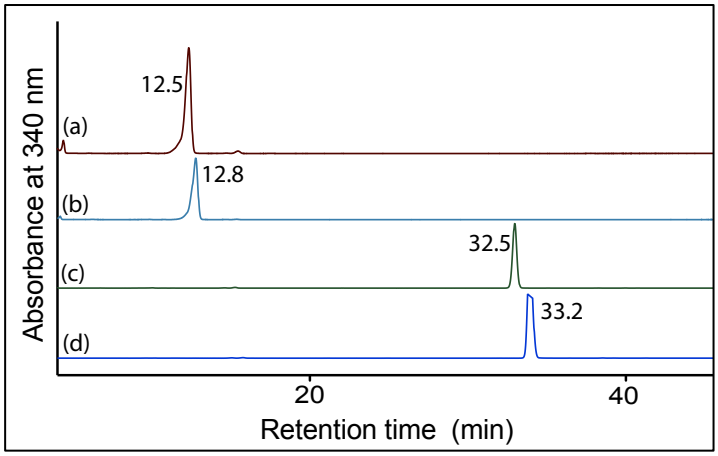

Figure 4.64. HPLC trace (340 nm) from HPLC-DAD-MS C_3 Marfey's analysis of the standard amino acids reacting with D-FDAA. Identity of amino acids was confirmed by retention time and molecular weight. (a) *cis*-4-hydroxy-D-Pro + D-FDAA (t_R = 12.5 min), (b) *cis*-4-hydroxy-L-Pro + D-FDAA (t_R = 12.8 min), (c) L-Phe + D-FDAA (t_R = 32.5 min) and (d) D-Phe + D-FDAA (t_R = 33.2 min). HPLC conditions, Zorbax, SB-C3 column (150 × 4.6 mm, 5 μm), 1 mL/min, gradient of 15 – 60% MeOH/H_2O (isocratic 5% MeCN containing 1% formic acid) over 55 min

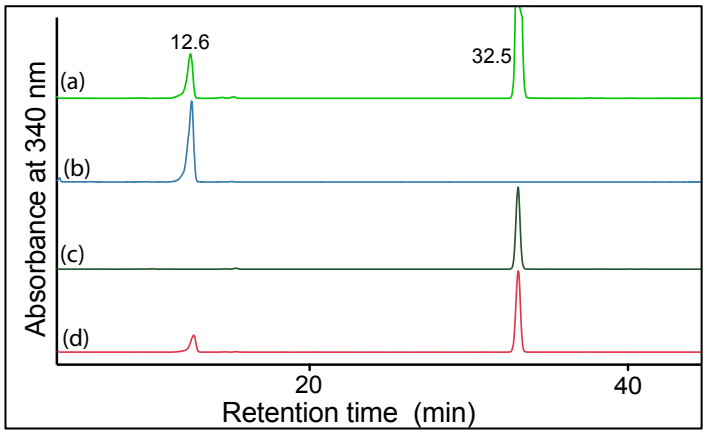

Figure 4.65. HPLC trace (340 nm) from HPLC-DAD-MS C_3 Marfey's analysis of *cyclo*-(L-Phe-*cis*-4-hydroxy-L-Pro) (**4.39c**). Identity of amino acids was confirmed by retention time and molecular weight. (a) Co-injection of D-FDAA derivatized hydrolysate of **4.39c** with L-Phe and *cis*-4-hydroxy-L-Pro + D-FDAA, (b) *cis*-4-hydroxy-L-Pro + D-FDAA, (c) L-Phe + D-FDAA and (d) D-FDAA derivatized hydrolyzed of **4.39c** (200 μg) showing the presence of L-Phe (t_R = 32.5 min) and *cis*-4-hydroxy-L-Pro (t_R = 12.6 min) as well as co-injection of the hydrolysate **4.39c** with the standards. HPLC conditions, Zorbax, SB-C_3 column (150 × 4.6 mm, 5 μm), 1 mL/min, gradient of 15 – 60% MeOH/H_2O (isocratic 5% MeCN containing 1% formic acid) over 55 min

4.4.23.4 *cyclo*-(L-Phe-*trans*-4-hydroxy-D-Pro) (4.39d)

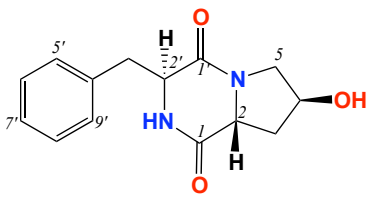

(**4.39d**)

Compound **4.39d** was synthesized as an optically active amorphous white powder ($[\alpha]^{22}_{D}$ −5.4, *c* 0.1, MeOH). HRESI(+)MS showed an adduct ion $(M+Na)^+$ consistent with the molecular formula $C_{14}H_{16}N_2O_3$ (Δmmu +0.5). The ^1H NMR ($CDCl_3$) spectrum and tabulated data of **4.39d** are presented in Figure 4.67, Figure 4.68 and Table 4.18 respectively. The absence of ROESY correlations (Figure 4.67) was consistent with the assigned configuration, which was subsequently confirmed by C_3 Marfey's analysis (Figure 4.69 and Figure 4.70).

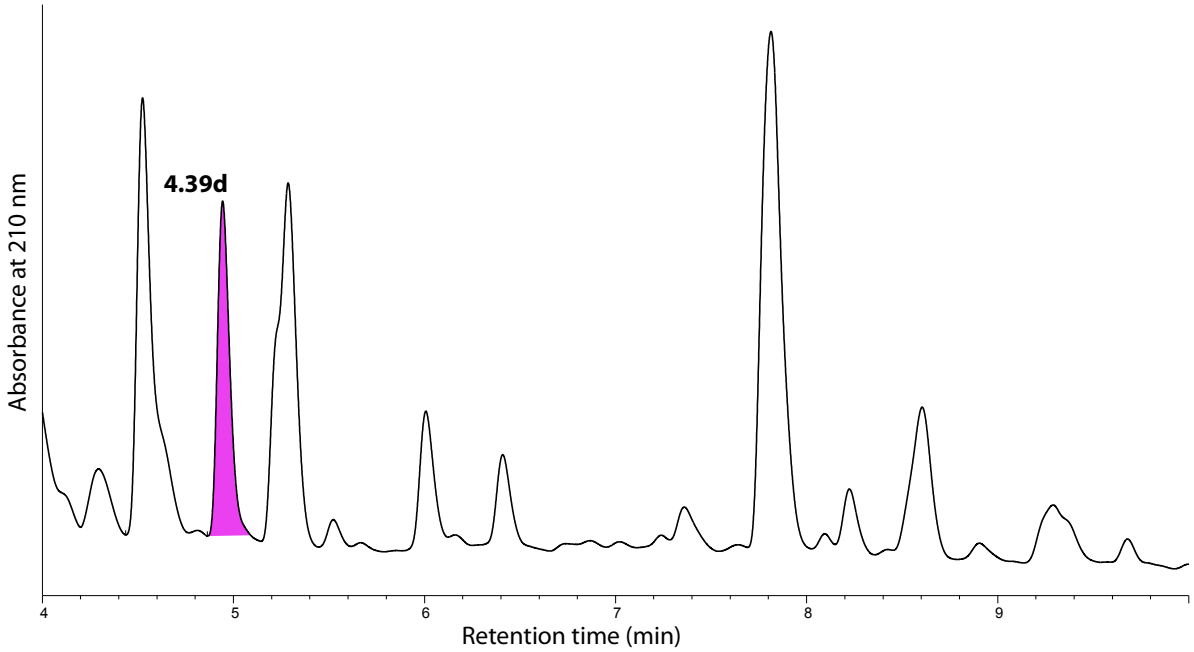

Figure 4.66. HPLC-DAD chromatogram, analytical gradient H_2O/MeCN plus HCO_2H at 210 nm using Zorbax C_8 column of the reaction mixture highlighting **4.39d**

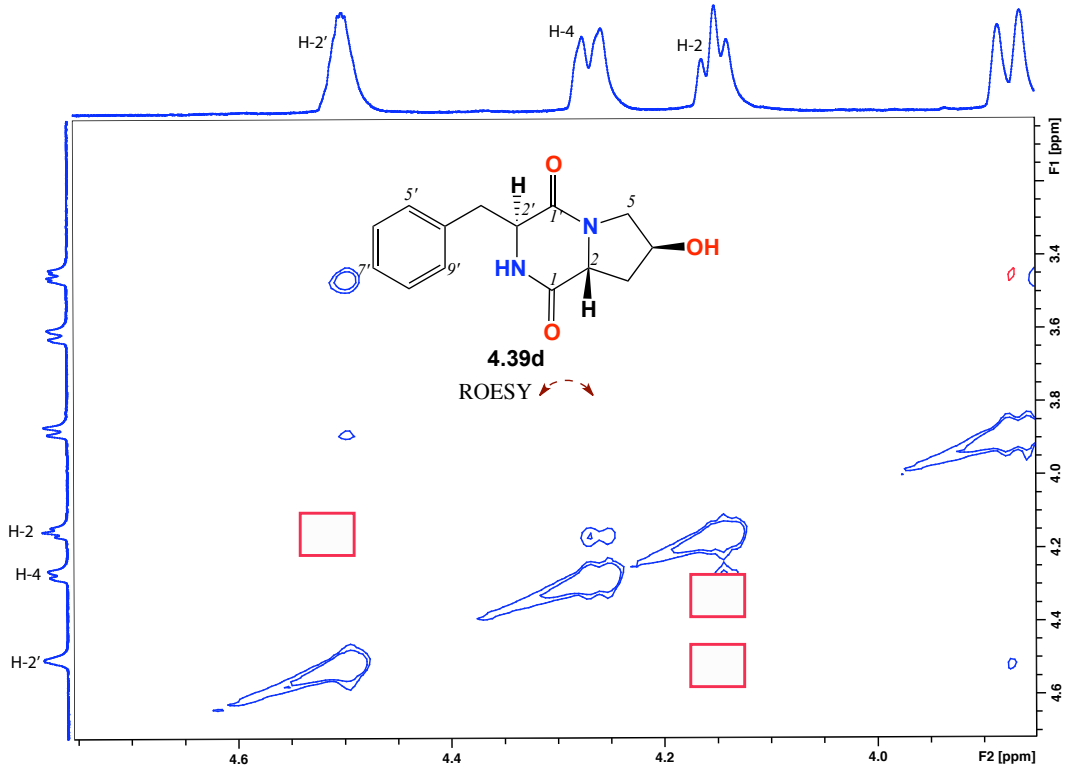

Figure 4.67. ROESY (600 MHz, $CDCl_3$) spectrum showing the absence of key correlations of *cyclo*-(L-Phe-*trans*-4-hydroxy-D-Pro) (**4.39d**)

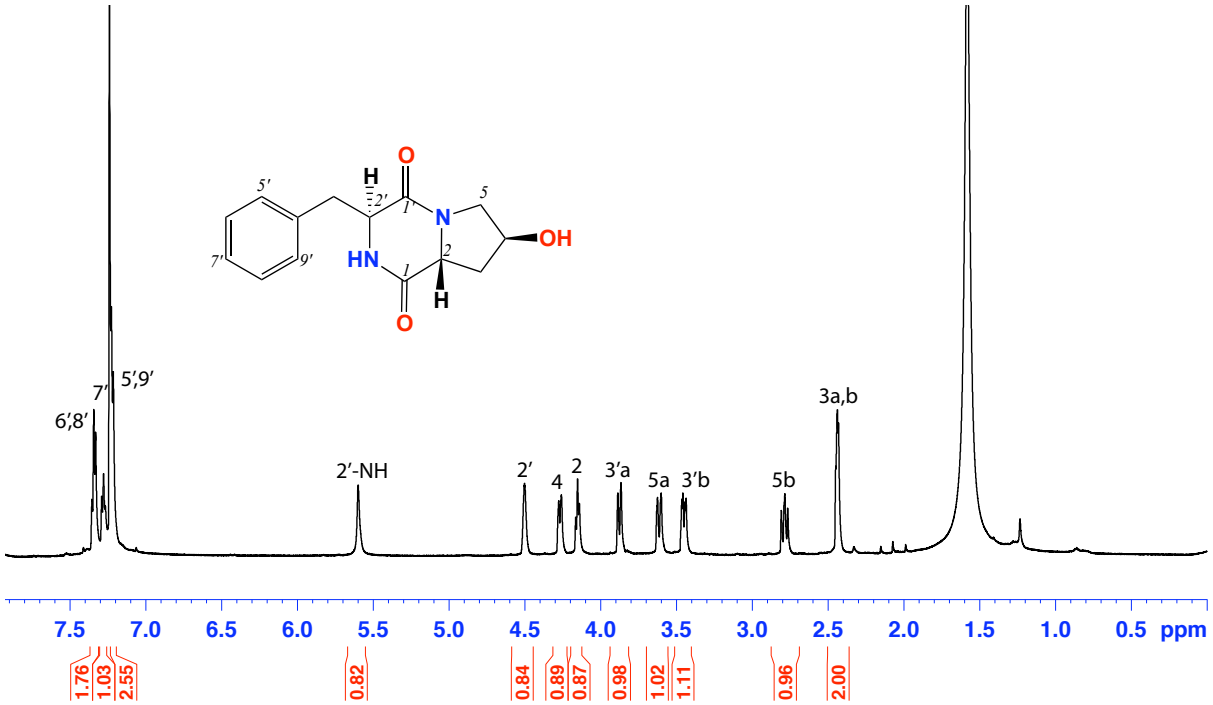

Figure 4.68. ^{1}H NMR (600 MHz, $CDCl_3$) of *cyclo*-(L-Phe-*trans*-4-hydroxy-D-Pro) (**4.39d**)

Table 4.18. NMR (600 MHz, $CDCl_3$) data of *cyclo*-(L-Phe-*trans*-4-hydroxy-D-Pro) (**4.39d**)

Pos.	δ_H, mult (*J* in Hz)[a]	δ_C[a]	COSY	^1H-^{13}C HMBC	ROESY
hydroxyproline					
1		166.7			
2	4.15, t *(7.1)*	57.4	3	1′, 5	
3	2.43, br	36.0	2	2	
4	4.26, d *(11.3, 3.1)*	56.2	5a,b		3′a/b, 5a
5	a 3.61, d *(11.3)*	36.1	4, 5b	2	4
	b 2.78, dd *(11.3, 10.1)*		4, 5a	1, 2, 3	
4-OH	[c]				
phenylalanine					
1′		169.8			
2′-NH	5.59, br s				
2′	4.50, br s	68.6	3′b		3′a,b
3′	a 3.87, d *(12.4)*	53.5	3′b		2′
	b 3.45, dd *(12.4, 4.6)*		2′, 3′a		2′, 4
4′		136.1			
5′, 9′	7.22[b]	129.5	6′, 8′	7′	
6′, 8′	7.33[b],m	129.7	5′, 9′	4′, 5′, 9′	
7′	7.27,t *(7.1)*	128.0	6′, 8′		

(a)^{13}C assignments obtained from gHSQC and gHMBC data. (b) Overlapping resonances. (c) Signals are not observed

4.4.23.4.1 C_3 Marfey's analysis for *cyclo*-(L-Phe-*trans*-4-hydroxy-D-Pro) (4.39d)

Employing the C_3 Marfey's method as previously described, **4.39d** was subjected to acid hydrolysis using 6 M HCl, derivatized with D-FDAA, and subjected to HPLC analysis to determine the absolute configuration of the amino acid residues. The absolute configuration of **4.39d** was determined by comparing the retention times of derivatized standard amino acids with the derivatized hydrolysate of **4.39d**, to be L-Phe and *trans*-4-hydroxy-D-Pro (Figure 4.69 and Figure 4.70).

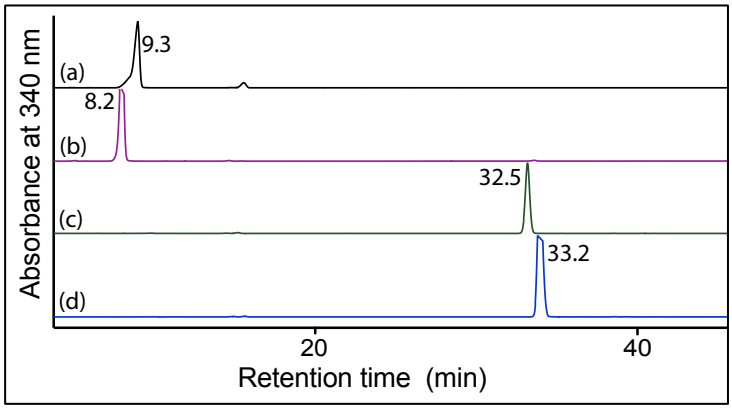

Figure 4.69. HPLC trace (340 nm) from HPLC-DAD-MS C_3 Marfey's analysis of the standard amino acids reacting with D-FDAA. Identity of amino acids was confirmed by retention time and molecular weight. (a) *trans*-4-hydroxy-D-Pro + D-FDAA (t_R = 9.2 min), (b) *trans*-4-hydroxy-L-Pro + D-FDAA (t_R = 8.2 min), (c) L-Phe + D-FDAA (t_R = 32.5 min) and (d) D-Phe + D-FDAA (t_R = 33.2 min). HPLC conditions, Zorbax, SB-C_3 column (150 × 4.6 mm, 5 μm), 1 mL/min, gradient of 15 – 60% MeOH/H_2O (isocratic 5% MeCN containing 1% formic acid) over 55 min

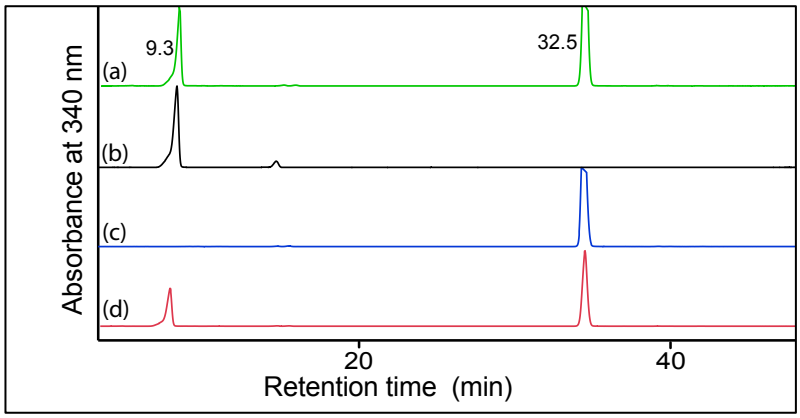

Figure 4.70. HPLC trace (340 nm) from HPLC-MS C_3 Marfey's analysis of *cyclo*-(L-Phe-*trans*-4-hydroxy-D-Pro) (**4.39d**). Identity of amino acids was confirmed by retention time and molecular weight. (a) Co-injection of the D-FDAA derivatized hydrolysate **4.39d** with the standards L-Phe and *trans*-4-hydroxy-D-Pro + D-FDAA, (b) *trans*-4-hydroxy-D-Pro + D-FDAA, (c) L-Phe + D-FDAA and (d) D-FDAA derivatized hydrolyzed of **4.39d** (200 μg) showing the presence of L-Phe (t_R = 32.5 min) and *trans*-4-hydroxy-D-Pro (t_R = 9.3 min). HPLC conditions, Zorbax, SB-C3 column (150 × 4.6 mm, 5 μm), 1 mL/min, gradient of 15 – 60% MeOH/H_2O (isocratic 5% MeCN containing 1% formic acid) over 55 min

4.4.24 *cyclo*-(Phe-Phe) (4.39e)

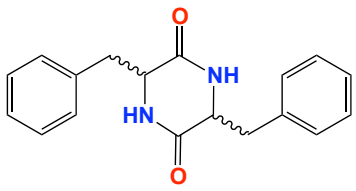

(**4.39e**)

Compound **4.39e** was isolated as a white powder with NMR ($CDCl_3$), ES(+)MS data (*m/z*, 295, $M+H^+$) and ($[\alpha]^{21}_D$ 0, *c* 0.05, MeOH) suggestive of a mixture of *cyclo*-(L-Phe-L-Phe), *cyclo*-(D-Phe-D-Phe) and *cyclo*-(L-Phe-D-Phe). The relatively high yield (19%) of symmetric dimers depletes the availability of L-Phe in the reaction mixture and may (at least in part) explain the low yield of unsymmetric (Phe + Pro) diketopiperazines products. This observation suggests that a change in the ratio of Pro to Phe starting material from 1:1 to 1:10 may improve the yields of Phe-Pro products.

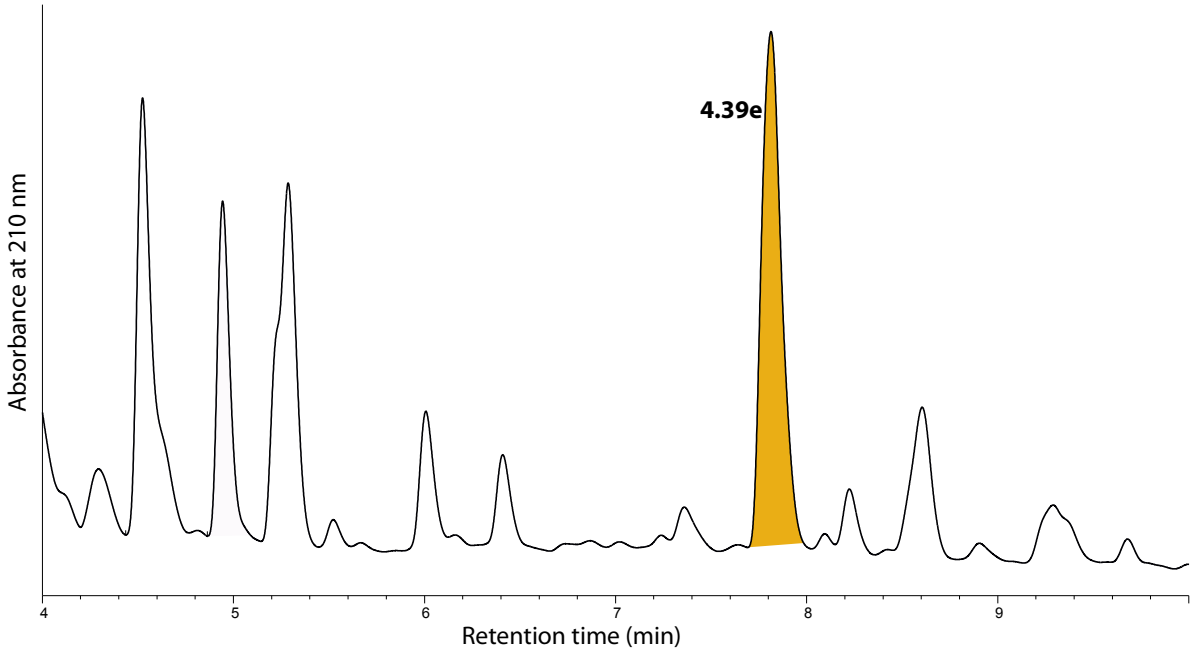

Figure 4.71. HPLC-DAD chromatogram, analytical gradient H_2O/MeCN plus HCO_2H at 210 nm using Zorbax C_8 column of the reaction mixture highlighting **4.39e**

4.4.24.1 Summary for all the *cyclo*-(Phe-4-hydroxy-Pro) stereoisomers

Following a microwave assisted synthetic approach, four stereoisomers of *cyclo*-(Phe-4-hydroxy-Pro) were synthesized (Figure 4.72 and Scheme 4.4). Curiously, the configuration about the L-Phe residue in these diketopiperazines was preserved; where as the configurations about both chiral centres in the *trans*-4-hydroxy-L-Pro residue were racemized. While this synthetic approach may seem inelegant from a synthetic methodology standpoint, in practice it proved to be effective at delivering a suite of stereoisomers for SAR investigations.

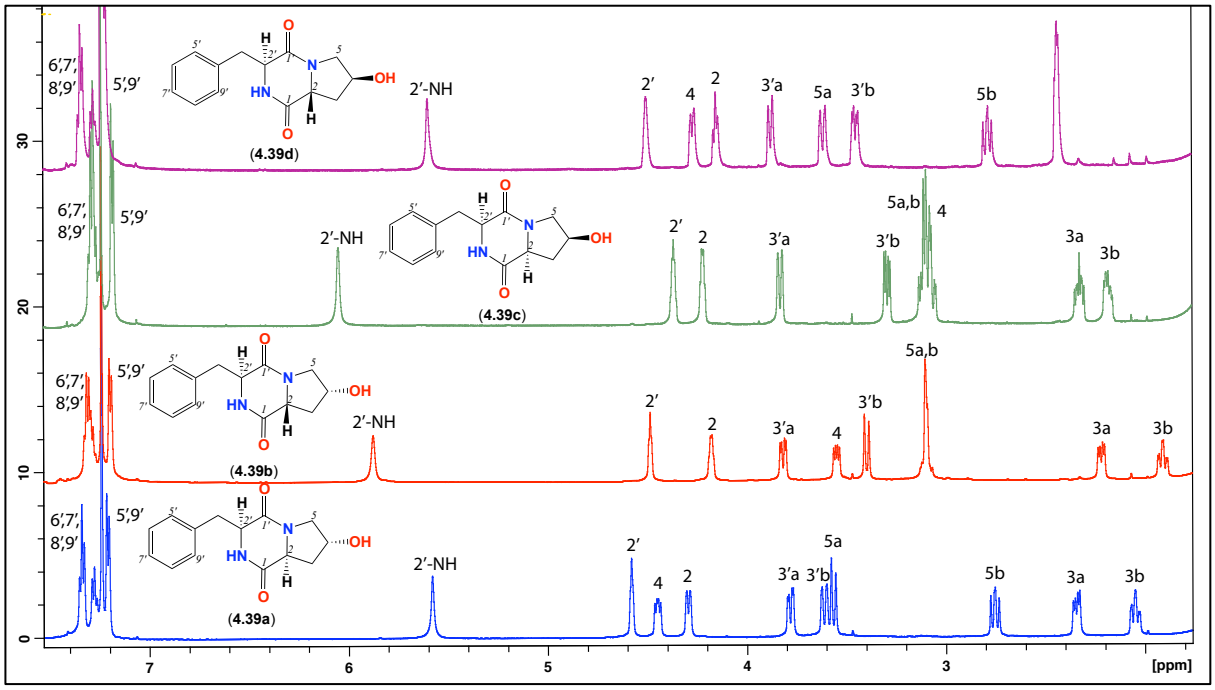

Figure 4.72. ^{1}H NMR (600 MHz, $CDCl_3$) comparison of *cyclo*-(Phe-4-hydroxy-Pro) stereoisomers

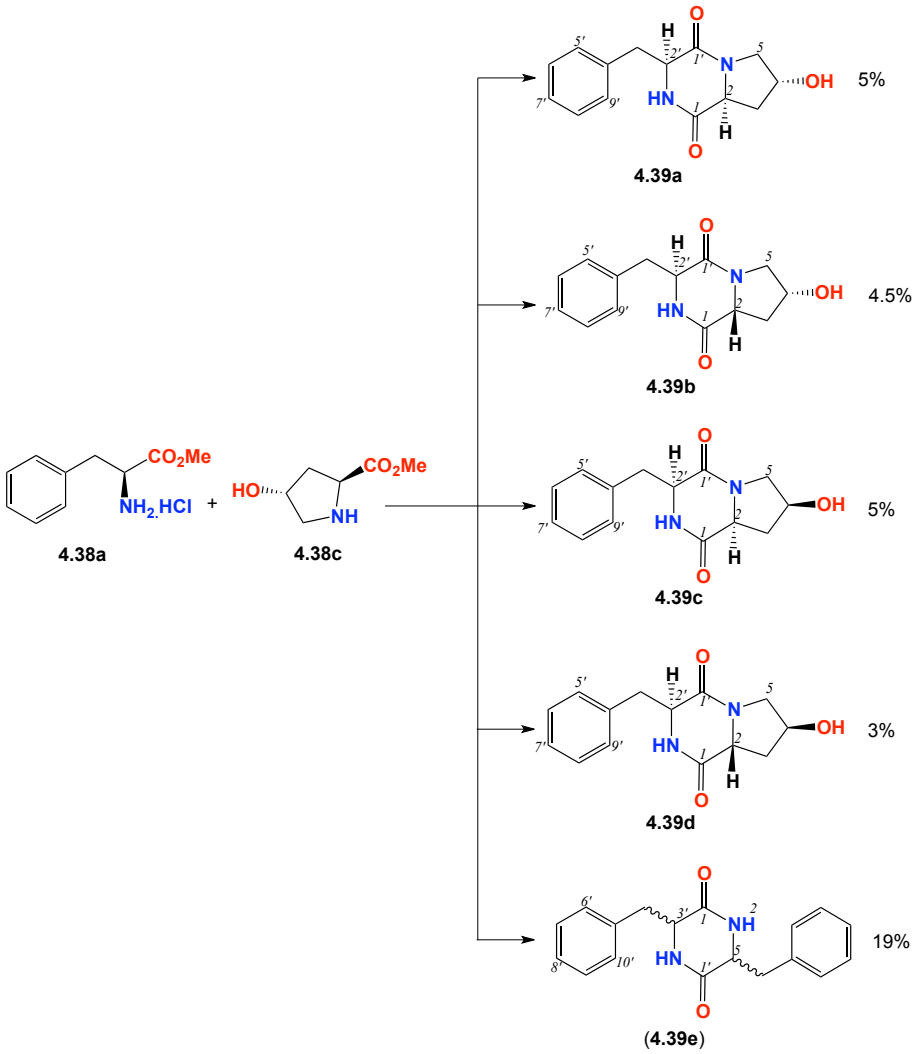

Scheme 4.4. Synthesis of different stereoisomers of *cyclo*-(Phe-4-hydroxy-Pro)

4.4.25 Synthesis of *cyclo*-(Tyr-4-hydroxy-Pro) stereoisomers

The reaction was performed by microwave irradiation of a 1:1 mixture of L-Tyr methyl ester (**4.38b**) and *trans*-4-hydroxy-L-Pro methyl ester (**4.38c**) in H_2O (3 mL) in the presence of triethylamine (2.5 eq) in a microwave reactor at 140 °C, 300 W for 3 min. The dried reaction product was washed with H_2O and the H_2O insoluble residue was dried *in vacuo* to recover a product that analysed by HPLC-DAD-MS as containing multiple diketopiperazines (Figure 4.73).

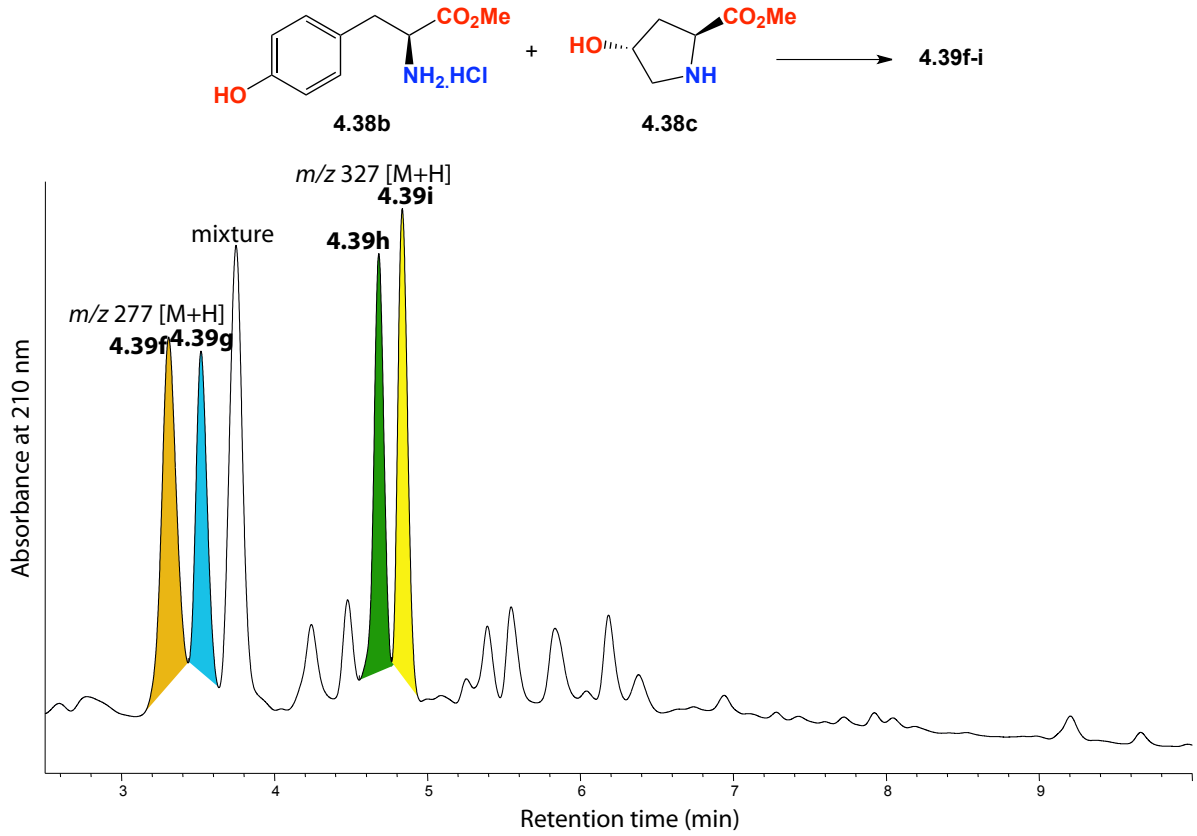

Figure 4.73. HPLC-DAD-MS reaction product of *cyclo*-(Tyr-4-hydroxy-Pro). Reacting the methyl ester of L-Tyr (**4.38b**) with methyl ester of *trans*-4-hydroxy-L-Pro (**4.38c**). The highlighted peaks represent DKPs

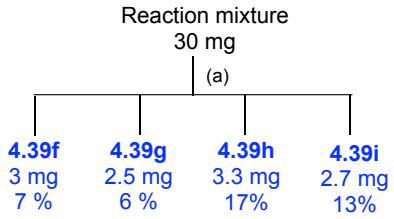

Scheme 4.5. Fractionation scheme for the reaction of methyl ester of L-Tyr (**4.38b**) with methyl ester of *trans*-4-hydroxy-L-Pro (**4.38c**). (a) Semi-preparative gradient HPLC: Zorbax C_8, 90 – 50% H_2O/MeOH, 3 mL/min

The peak in the chromatogram above named "mixture" was isolated as a white powder with NMR ($CDCl_3$), ES(+)MS data (*m/z*, 277, $M+H^+$) suggestive of a mixture of diastereomers of *cyclo*-(L-Tyr-4-hydroxy-Pro).

4.4.25.1 *cyclo*-(L-Tyr-*trans*-4-hydroxy-D-Pro) (4.39f)

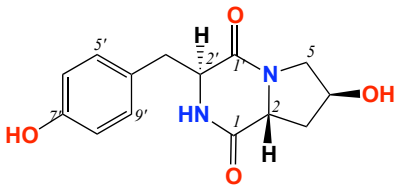

(**4.39f**)

Compound **4.39f** was synthesized as an optically active amorphous white powder ($[\alpha]^{22}_{D}$ −33.9, *c* 0.06, MeOH). HRESI(+)MS showed an adduct ion $(M+Na)^+$ consistent with the molecular formula $C_{14}H_{16}N_2O_3$ (Δmmu −0.1). The ^{1}H NMR (MeOH-d_4) spectum and tabulated data of **4.39f** are presented in **Figure 4.76** and **Table 4.19**. The absence of ROESY correlations between H-2′, H-2 and H-4 (Figure 4.75), was consistent with the proposed configuration, however this assignment was subsequently confirmed by C_3 Marfey's analysis (Figure 4.77 and Figure 4.78).

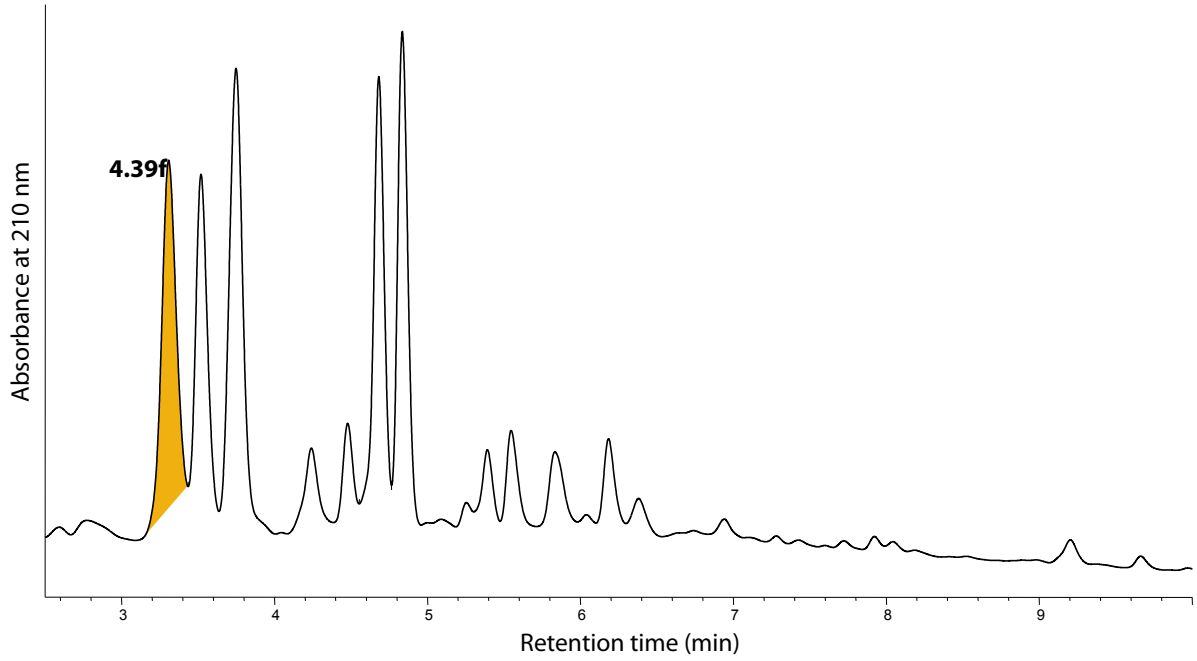

Figure 4.74. HPLC-DAD chromatogram, analytical gradient H_2O/MeCN plus HCO_2H at 210 nm using Zorbax C_8 column of the reaction mixture, highlighting **4.39f**

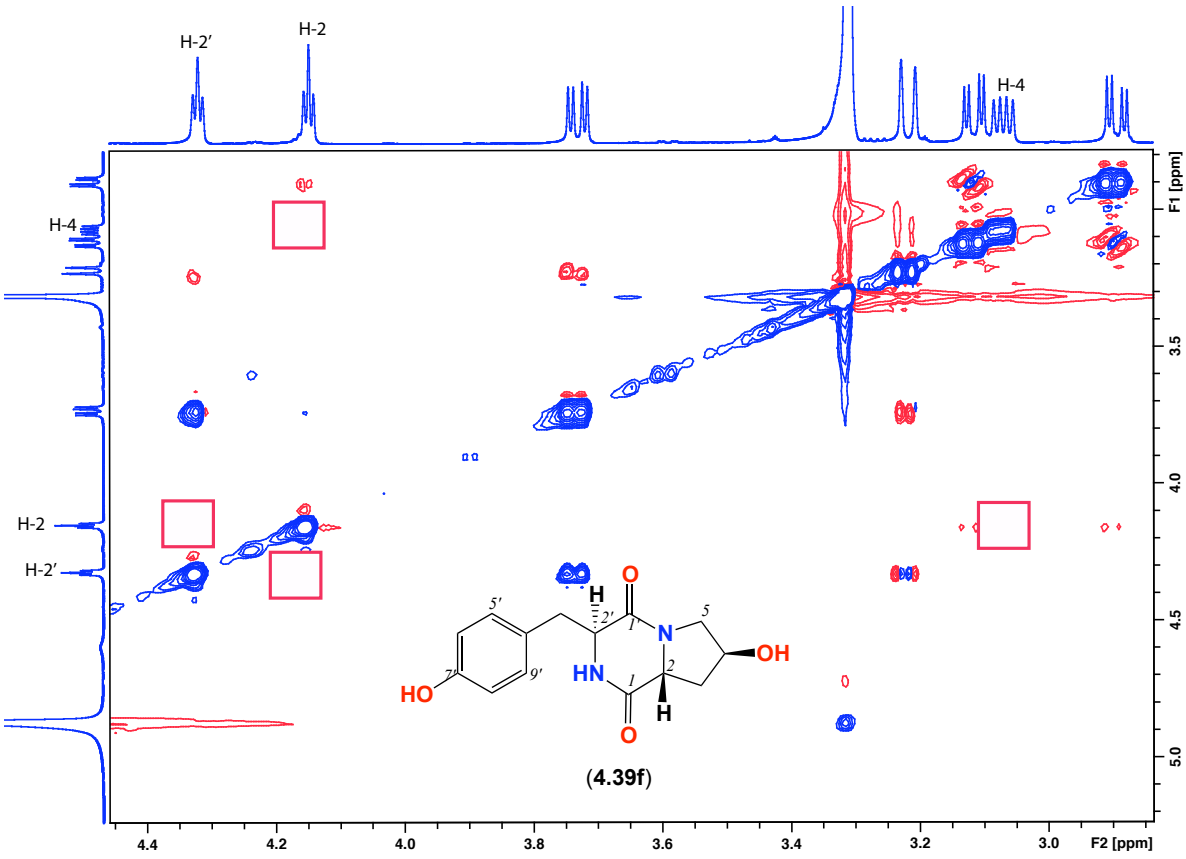

Figure 4.75. ROESY (600 MHz, MeOH-d_4) spectrum of *cyclo*-(L-Tyr-*trans*-4-hydroxy-D-Pro) **(4.39f)** revealing the absence of key correlations

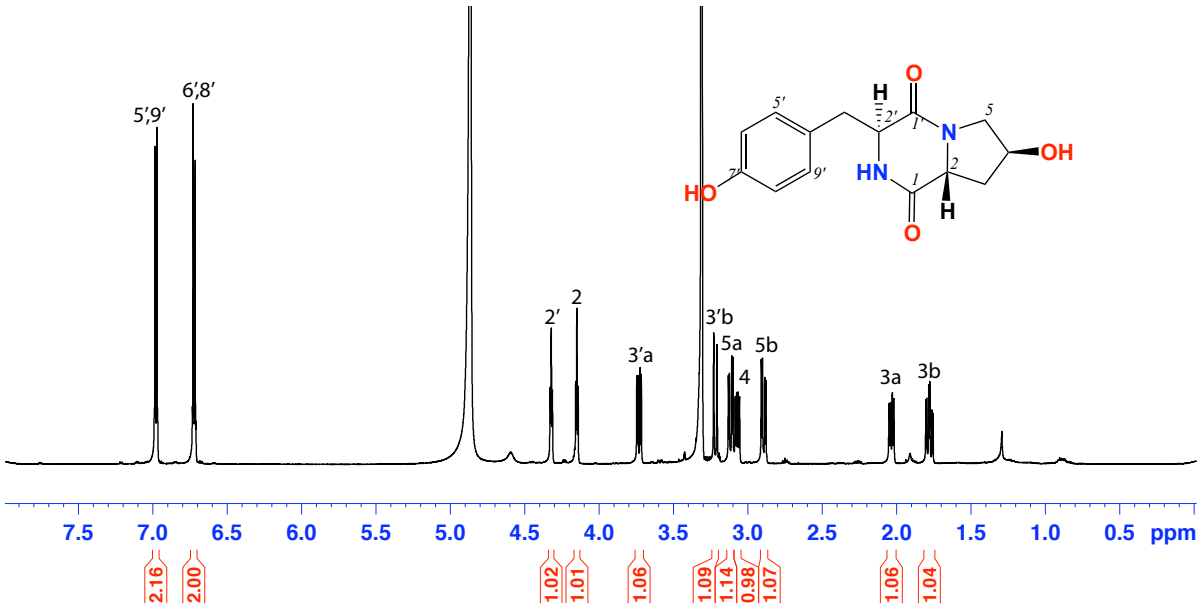

Figure 4.76. ^{1}H NMR (600 MHz, MeOH-d_4) spectrum of *cyclo*-(L-Tyr-*trans*-4-hydroxy-D-Pro) (**4.39f**)

Table 4.19. NMR (600 MHz, MeOH-d_4) data of *cyclo*-(L-Tyr-*trans*-4-hydroxy-D-Pro) (**4.39f**)

Pos.	δ_H, mult (*J* in Hz)[a]	δ_C[a]	COSY	^{1}H-^{13}C HMBC	ROESY
hydroxyproline					
1		167.5			
2	4.14, t (*4.6*)	59.5	3, 5a,b	1, 1′	5a
3	a 2.03, dd (*13.1, 6.0*)	39.0	3b, 4	2′	3b
	b 1.77, ddd *(13.1, 12.1, 6.0)*		3a, 4	1′, 4	3a
4	3.06, dd *(13.1, 6.0)*	57.2	3a,b	1′	3b
5	a 3.11, dd *(13.1, 4.4)*	40.2	2, 5b	1, 2	2, 5b
	b 2.89, dd *(13.1, 4.4)*		2, 5a	1, 2	5a
4-OH	[b]				
tyrosine					
1′		171.8			
2′-NH					
2′	4.32, t *(4.6)*	68.4	3′a	3′	3′a
3′	a 3.72, dd *(13.1, 4.6)*	55.2	2′,3′b	1	2′,3′b
	b 3.21, d *(13.1)*		3′a	2′	3′a
4′		126.8			
5′, 9′	6.97, d *(8.4)*	132.1	6′, 8′	7′	
6′, 8′	6.72, d *(8.4)*	116.3	5′, 9′	4′,7′	
7′		158.1			

(a)^{13}C assignments obtained from gHSQC and gHMBC data. (b) Signals not observed

4.4.25.1.1 C_3 Marfey's analysis for *cyclo*-(L-Tyr-*trans*-4-hydroxy-D-Pro) (4.39f)

Employing the C_3 Marfey's method as previously described, **4.39d** was subjected to acid hydrolysis using 6M HCl, derivatized with D-FDAA, and subjected to HPLC analysis to determine the absolute configuration of the amino acid residues. The absolute configuration of **4.39f** was determined by comparing the retention times of derivatized standard amino acids with the derivatized hydrolysate of **4.39f** to be L-Tyr and *trans*-4-hydroxy-D-Pro (Figure 4.77 and Figure 4.78).

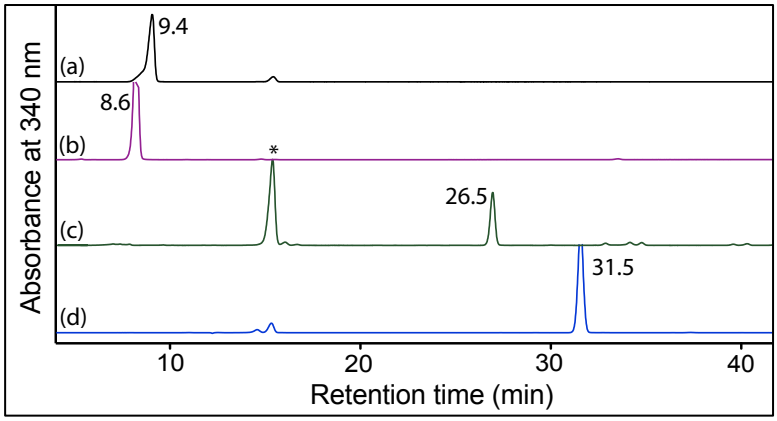

Figure 4.77. HPLC trace (340 nm) from HPLC-DAD-MS C_3 Marfey's analysis of the standard amino acids reacting with D-FDAA. Identity of amino acids was confirmed by retention time and molecular weight. (a) *trans*-4-hydroxy-D-Pro + D-FDAA (t_R = 9.4 min), (b) *trans*-4-hydroxy-L-Pro + D-FDAA (t_R = 8.6 min), (c) D-Tyr + D-FDAA (t_R = 26.5 min) and (d) L-Tyr + D-FDAA (t_R = 31.5 min). HPLC conditions, Zorbax, SB-C_3 column (150 × 4.6 mm, 5 μm), 1 mL/min, gradient of 15 – 60% MeOH/H_2O (isocratic 5% MeCN containing 1% formic acid) over 55 min

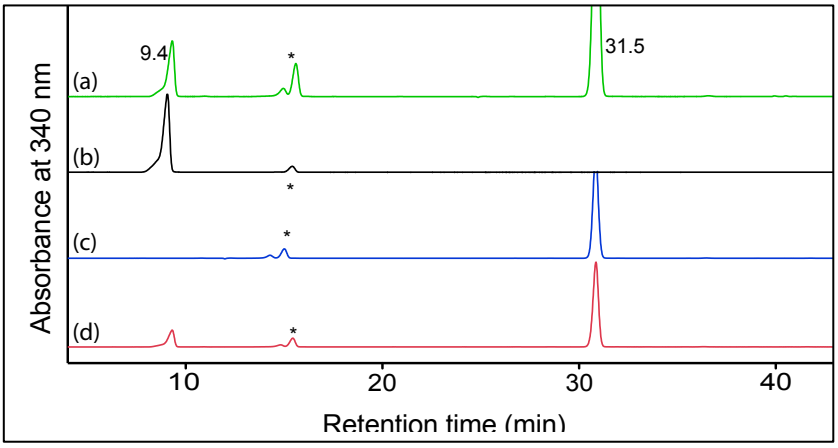

Figure 4.78. HPLC trace (340 nm) from HPLC-DAD-MS C_3 Marfey's analysis of *cyclo*-(L-Tyr-*trans*-4-hydroxy-D-Pro) (**4.39f**). Identity of amino acids was confirmed by retention time and molecular weight. (a) Co-injection of the D-FDAA derivatized hydrolysate **4.39f** with the standards, (b) *trans*-4-hydroxy-D-Pro + D-FDAA, (c) L-Tyr + D-FDAA and (d) D-FDAA derivatized hydrolyzed of **4.39f** (300 μg) showing the presence of L-Tyr (t_R = 31.5 min) and *trans*-4-hydroxy-D-Pro (t_R = 9.4 min). HPLC conditions, Zorbax, SB-C_3 column (150 × 4.6 mm, 5 μm), 1 mL/min, gradient of 15 – 60% MeOH/H_2O (isocratic 5% MeCN containing 1% formic acid) over 55 min.* residual of Marfey's reagent

4.4.25.2 *cyclo*-(L-Tyr-*cis*-4-hydroxy-D-Pro) (4.39g)

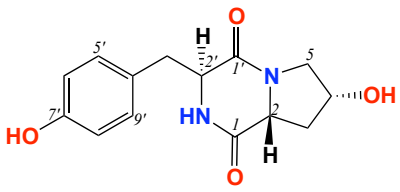

(**4.39g**)

Compound **4.39g** was synthesized as an optically active amorphous white powder ($[\alpha]^{22}_{D}$ −34, *c* 0.06, MeOH). HRESI(+)MS showed an adduct ion $(M+Na)^+$ consistent with the molecular formula $C_{14}H_{16}N_2O_3$ (Δmmu −0.4). The ^{1}H NMR (MeOH-d_4) spectrum and tabulated data for **4.39g** are presented in Figure 4.80 and Table 4.20. ROESY correlations confirmed the *cis* configuration between H-2′, H-2 and H-4 (Figure 4.80), with absolute configurations confirmed by C_3 Marfey's analysis (Figure 4.82 and Figure 4.83).

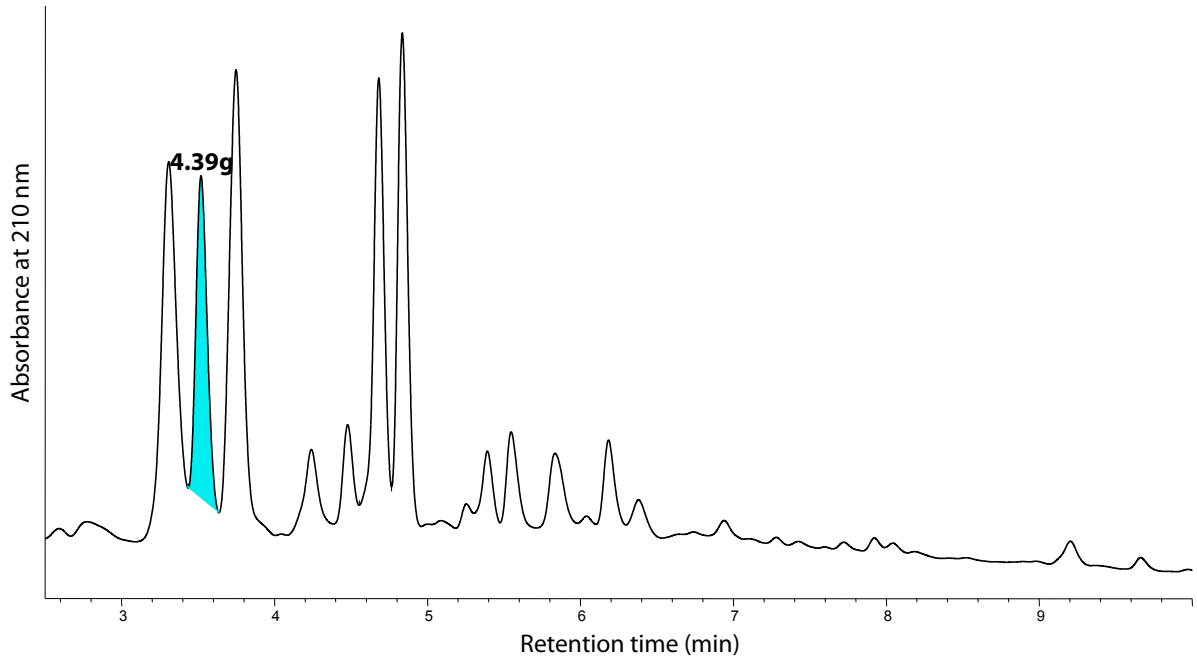

Figure 4.79. HPLC-DAD chromatogram, analytical gradient H_2O/MeCN plus HCO_2H at 210 nm using Zorbax C_8 column of the reaction mixture, highlighting (**4.39g**)

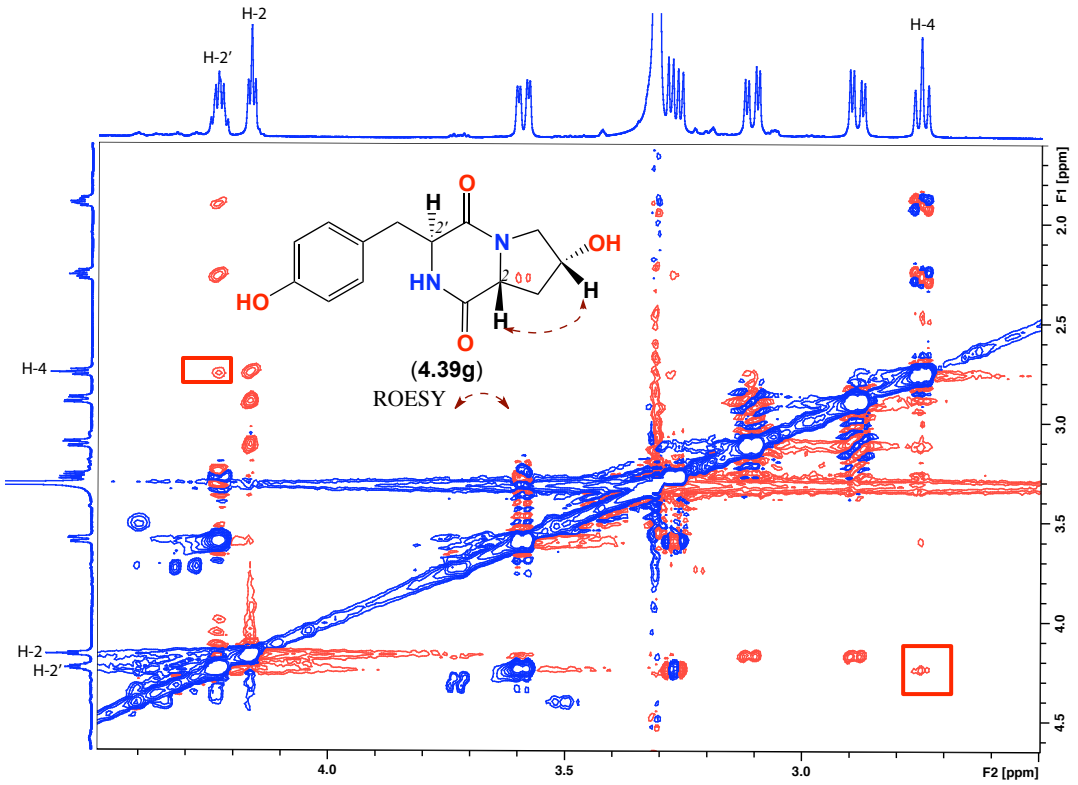

Figure 4.80. ROESY (600 MHz, MeOH-d_4) spectrum showing key correlations of *cyclo*-(L-Tyr-*cis*-4-hydroxy-D-Pro) (**4.39g**)

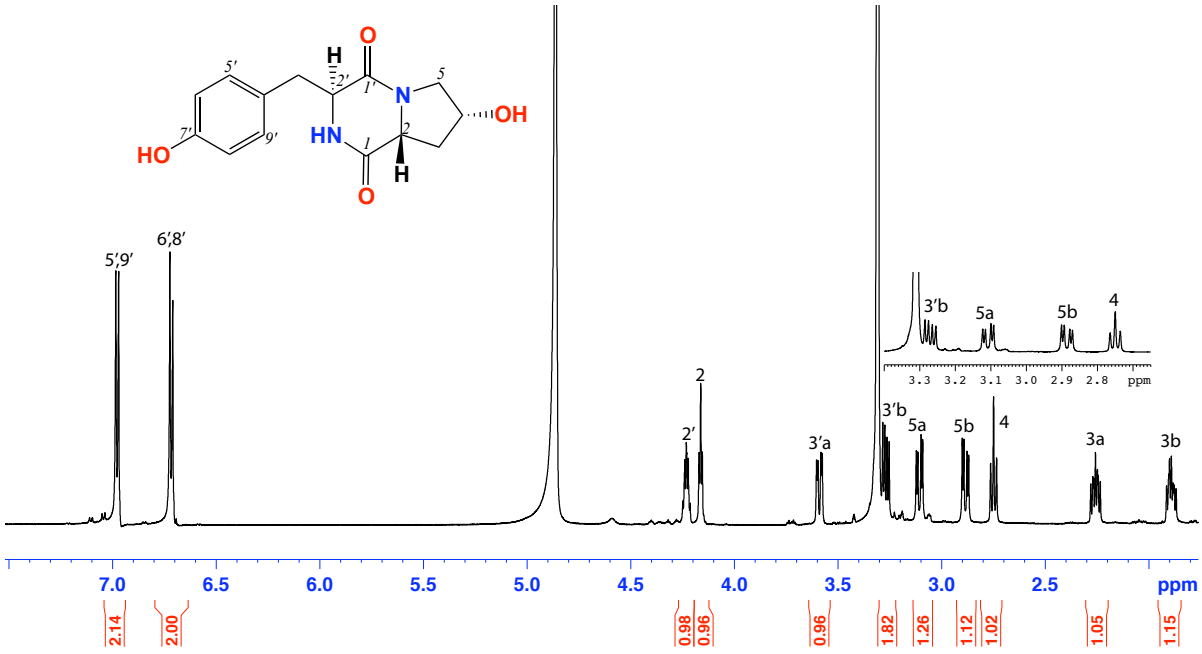

Figure 4.81. ^{1}H NMR (600 MHz, MeOH-d_4) spectrum of *cyclo*-(L-Tyr-*cis*-4-hydroxy-D-Pro) (**4.39g**)

Table 4.20. NMR (600 MHz, MeOH-d_4) data of *cyclo*-(L-Tyr-*cis*-4-hydroxy-D-Pro) (**4.39g**)

Pos.	δ_H, mult (*J* in Hz)[a]	δ_C[a]	COSY	^{1}H-^{13}C HMBC	ROESY
hydroxyproline					
1		167.3			
2	4.16, t *(4.4)*	59.3	5a, b	1, 1′, 4′, 5	4
3	a 2.25, m	37.6	3b, 4	2	
	b 1.89, m		3a, 4	1′, 2′, 2	
4	2.75, t *(4.5)*	57.0	3a, b	1′, 3	2
5	a 3.10, dd *(14.0, 4.5)*	40.3	2, 5b	2, 4	
	b 2.88, dd *(14.0, 4.5)*		2, 5a	1, 2, 4	
4-OH	[b]				
tyrosine					
1′		171.4			
2′-NH					
2′	4.32, m	68.6	3′a, b		
3′	a 3.59, dd *(12.4, 3.4)*	54.3	2′, 3′b	2′	
	b 3.26, dd *(12.4, 3.4)*		2′, 3′a		
4′		127.3			
5′, 9′	6.97, d *(8.3)*	132.2	6′/8′	7′	
6′, 8′	6.71, d *(8.3)*	116.3	5′/9′	7′	
7′		158.3			

(a)^{13}C assignments obtained from gHSQC and gHMBC data. (b) Signals not observed

4.4.25.2.1 C_3 Marfey's analysis for *cyclo*-(L-Tyr-*cis*-4-hydroxy-D-Pro) (4.39g)

Employing the C_3 Marfey's method as previously described, **4.39g** was subjected to acid hydrolysis using 6 M HCl, derivatized with D-FDAA, and subjected to HPLC analysis to determine the absolute configuration of the amino acid residues. The absolute configuration of **4.39g** was determined by comparing the retention times of derivatized standard amino acids with the derivatized hydrolysate of **4.39g** to be L-Tyr and *cis*-4-hydroxy-D-Pro (Figure 4.82 and Figure 4.83).

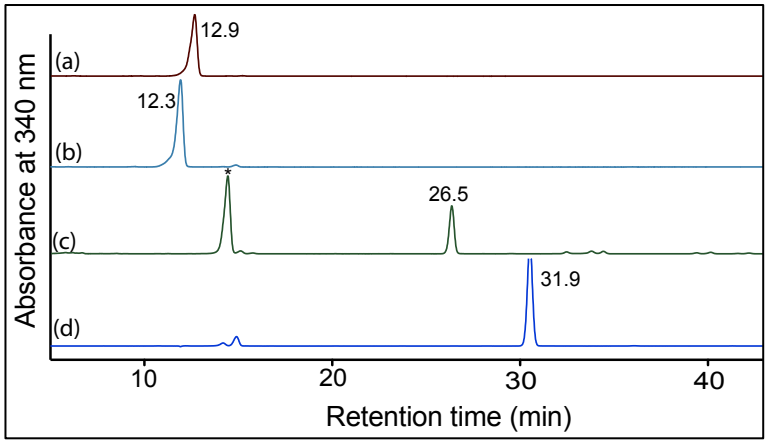

Figure 4.82. HPLC trace (340 nm) from HPLC-DAD-MS C_3 Marfey's analysis for the standard amino acids reacting with D-FDAA. Identity of amino acids was confirmed by retention time and molecular weight. (a) *cis*-4-hydroxy-L-Pro + D-FDAA (t_R = 12.9 min), (b) *cis*-4-hydroxy-D-Pro + D-FDAA (t_R = 12.3 min), (c) D-Tyr + D-FDAA (t_R = 26.5 min) and (d) L-Tyr + D-FDAA (t_R = 31.9 min). HPLC conditions, Zorbax, SB-C_3 column (150 × 4.6 mm, 5 μm), 1 mL/min, gradient of 15 – 60% MeOH/H_2O (isocratic 5% MeCN containing 1% formic acid) over 55 min

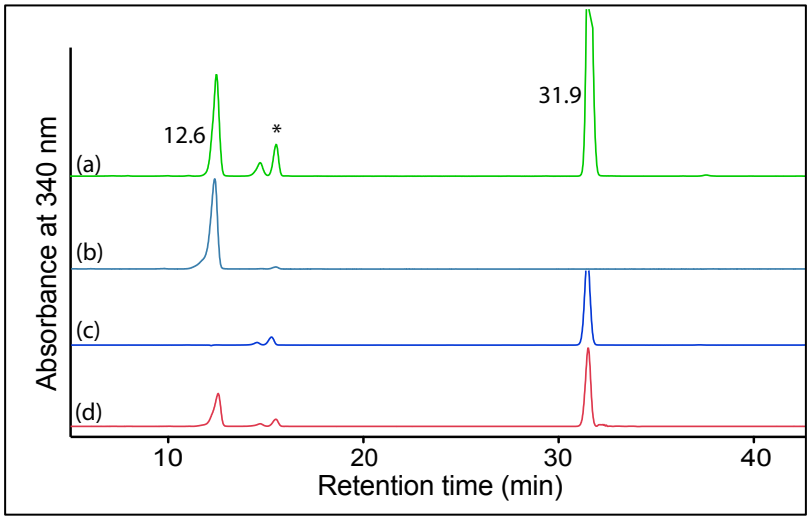

Figure 4.83. HPLC trace (340 nm) from HPLC-DAD-MS C_3 Marfey's analysis of *cyclo*-(L-Tyr-*cis*-4-hydroxy-D-Pro) (**4.39g**). Identity of amino acids was confirmed by retention time and molecular weight. (a) Co-injection of the D-FDAA derivatized hydrolysate **4.39g** with the standards, (b) *cis*-4-hydroxy-D-Pro + D-FDAA, (c) L-Tyr + D-FDAA and (d) D-FDAA derivatized hydrolysate of **4.39g** (300 μg) showing the presence of L-Tyr (t_R = 31.9 min) and *cis*-4-hydroxy-D-Pro (t_R = 12.6 min). HPLC conditions, Zorbax, SB-C_3 column (150 × 4.6 mm, 5 μm), 1 mL/min, gradient of 15 – 60% MeOH/H_2O (isocratic 5% MeCN containing 1% formic acid) over 55 min.* residual of Marfey's reagent

4.4.25.3 *cyclo*-(L-Tyr-L-Tyr) (4.39h)

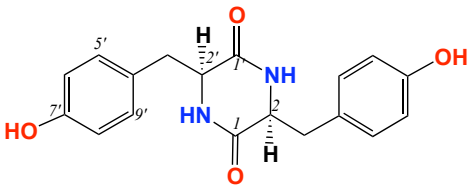

(**4.39h**)

Compound **4.39h** was synthesized as an optically active amorphous white powder ($[\alpha]^{21}_{D}$ −8, *c* 0.08, MeOH). HRESI(+)MS showed an adduct ion $(M+Na)^+$ consistent with the molecular formula $C_{18}H_{18}N_2O_4$ (Δmmu +1.6). The ^{1}H NMR (DMSO-d_6) spectra and tabulated data of **4.39h** are presented in Figure 4.86 and **Table 4.21**. ROESY correlations were not very helpful in the assignment of configuration between H-2 and H-2′, due to symmetry. Absolute configurations were determined by C_3 Marfey's analysis (Figure 4.87).

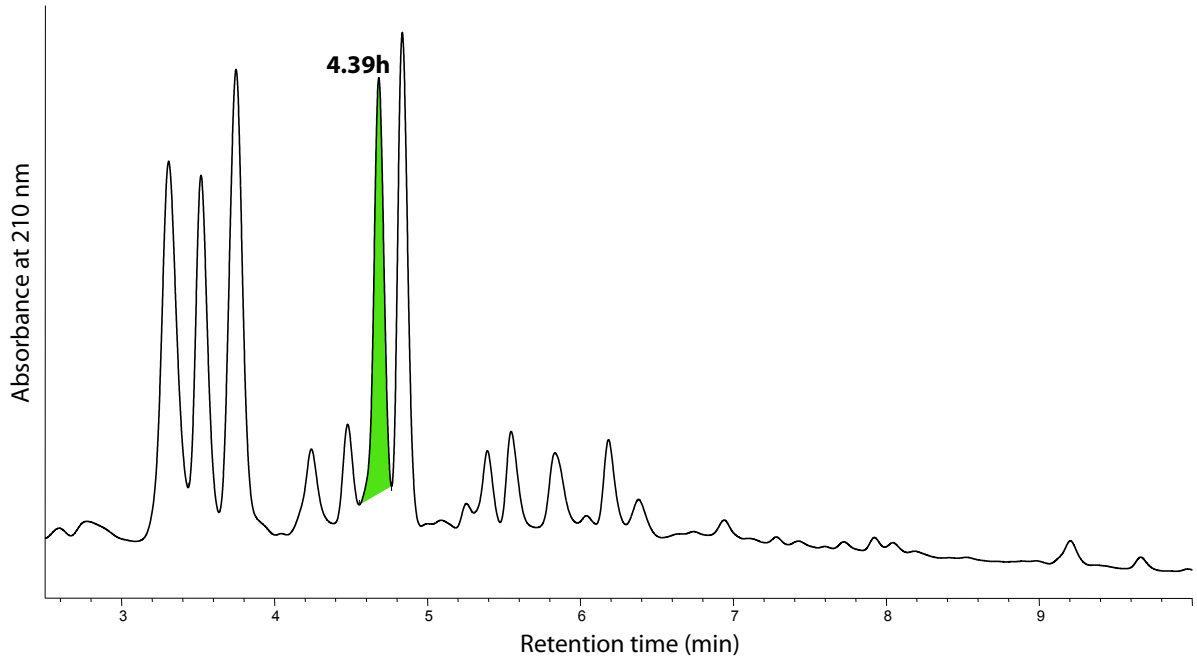

Figure 4.84. HPLC-DAD chromatogram, analytical gradient H_2O/MeCN plus HCO_2H at 210 nm using Zorbax C_8 column of the reaction mixture, highlighting **4.39h**

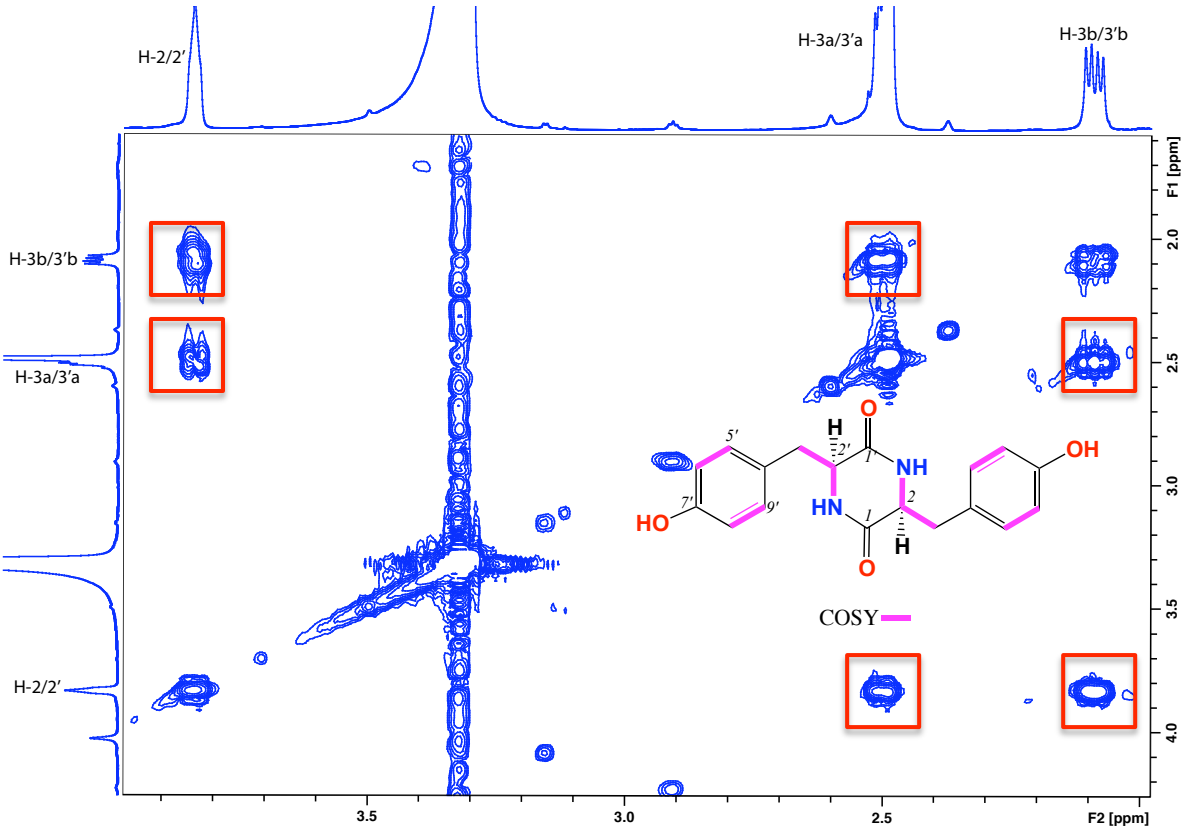

Figure 4.85. COSY (600 MHz, DMSO-d_6) spectrum showing the key correlations of *cyclo*-(L-Tyr-L-Tyr) (**4.39h**)

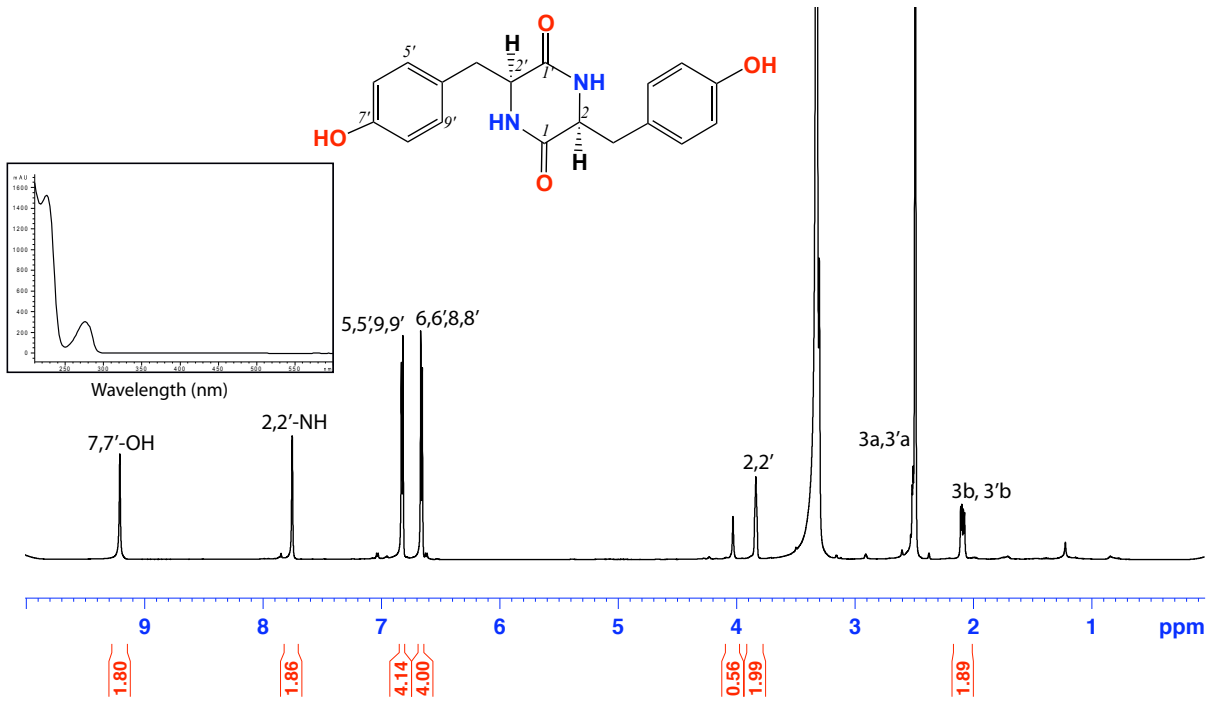

Figure 4.86. ^{1}H NMR (600 MHz, DMSO-d_6) and UV-vis (HPLC-DAD, H_2O/MeCN plus HCO_2H) spectra of *cyclo*-(L-Tyr-L-Tyr) **(4.39h)**

Table 4.21. NMR (600 MHz, DMSO-d_6) of *cyclo*-(L-Tyr-L-Tyr) (**4.39h**)

Pos.	δ_H, mult (*J* in Hz)[a]	δ_C[a]	COSY	^{1}H-^{13}C HMBC	ROESY
tyrosine					
1, 1′		166.7			
2, 2′-NH	7.76, s		2/2′	1/1′, 2/2′	2/2′, 5/5′, 9/9′
2, 2′	3.83, br s	55.9	2/2′NH, 3 /3′	1/1′	5/5′, 9/9′
3, 3′	a 2.51[b]	39.1	2/2′, 3b/3′b		
3, 3′	b 2.09, dd *(13.6, 6.2)*		2/2′, 3a/3′a	1/1′, 2/2′, 4/4′, 5/5′	2/2′
4, 4′		127.6			
5, 5′, 9, 9′	6.82, d *(8.2)*	131.1	6/6′, 8/8′	3/3′, 7/7′	2/2′,3/3′
6, 6′, 8, 8′	6.66, d *(8.2)*	115.7	5/5′, 9/9′	4/4′	
7, 7′		156.2			
7, 7′-OH	9.21, s				6/6′, 8/8′

(a) ^{13}C assignments obtained from gHSQC and gHMBC data. (b) Obscured by the solvent

4.4.25.3.1 C_3 Marfey's analysis for *cyclo*-(L-Tyr-L-Tyr) (4.39h)

Employing the C_3 Marfey's method as previously described, **4.39h** was subjected to acid hydrolysis using 6 M HCl, derivatized with D-FDAA, and subjected to HPLC analysis to determine the absolute configuration of the amino acid residues. The absolute configuration of **4.39h** was determined by comparing the retention times of derivatized standard amino acids with the derivatized hydrolysate of **4.39h** to be L-Tyr (Figure 4.87).

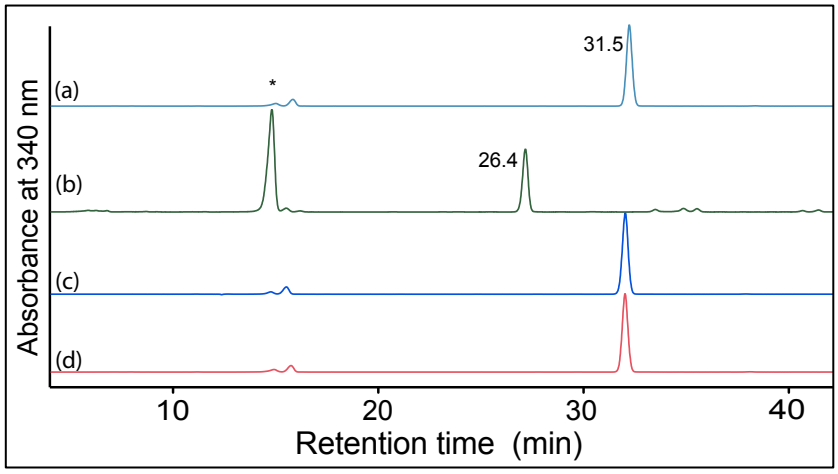

Figure 4.87. HPLC trace (340 nm) from HPLC-DAD-MS C_3 Marfey's analysis of *cyclo*-(L-Tyr-L-Tyr) (**4.39h**). Identity of amino acids was confirmed by retention time and molecular weight. (a) Co-injection of the D-FDAA derivatized hydrolysate **4.39h** with the standards. (b) D-Tyr + D-FDAA, (c) L-Tyr + D-FDAA and (d) D-FDAA derivatized hydrolyzed of **4.39h** (300 μg) showing the presence of L-Tyr (t_R = 31.5 min). HPLC conditions, Zorbax, SB-C_3 column (150 × 4.6 mm, 5 μm), 1 mL/min, gradient of 15 – 60% MeOH/H_2O (isocratic 5% MeCN containing 1% formic acid) over 55 min. * residual of Marfey's reagent

4.4.25.4 *cyclo*-(L-Tyr-D-Tyr) (4.39i)

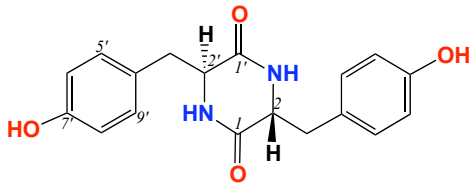

(**4.39i**)

Compound **4.39i** was synthesized as meso amorphous white powder ($[\alpha]^{21}_{D}$ −0, *c* 0.05, MeOH). HRESI(+)MS showed an adduct ion $(M+Na)^+$ consistent with the molecular formula $C_{18}H_{18}N_2O_4$ (Δmmu +2.6). The ^{1}H NMR ($CDCl_3$) spectrum and tabulated data of **4.39i** are presented in Figure 4.90 and Table 4.22. ROESY correlations could not be used to solve the configuration about the two stereocenters, due to symmetry. Absolute configurations were determined by C_3 Marfey's analysis (Figure 4.91).

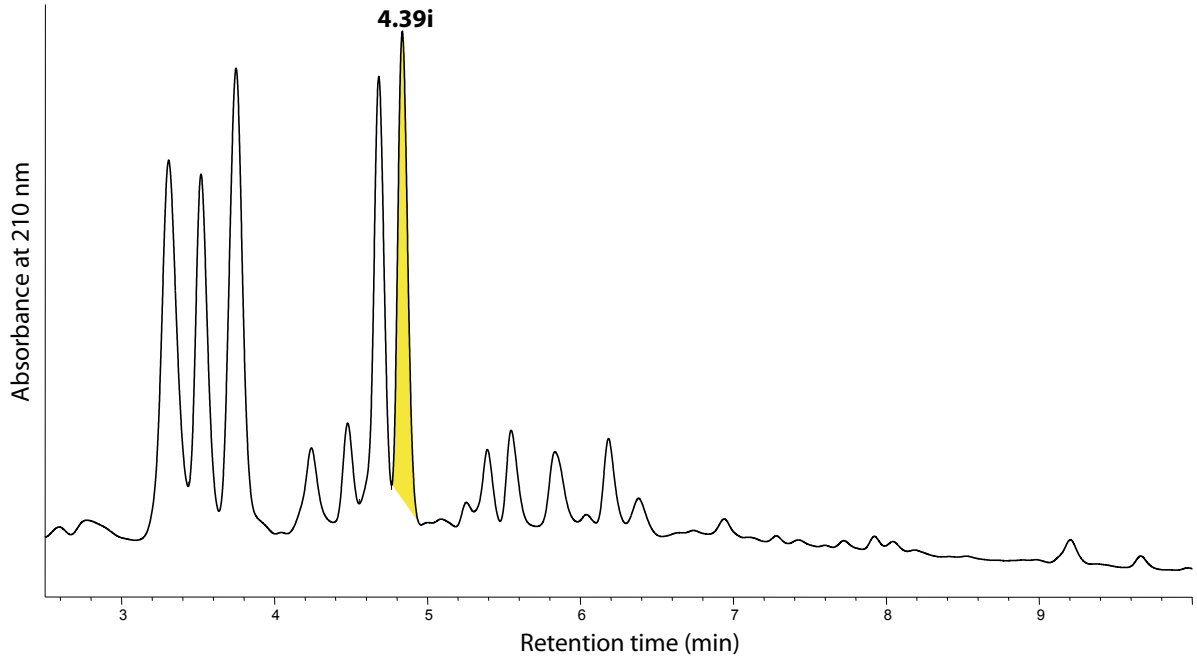

Figure 4.88. HPLC-DAD chromatogram, analytical gradient H_2O/MeCN plus HCO_2H at 210 nm using Zorbax C_8 column of the reaction mixture, highlighting **4.39i**

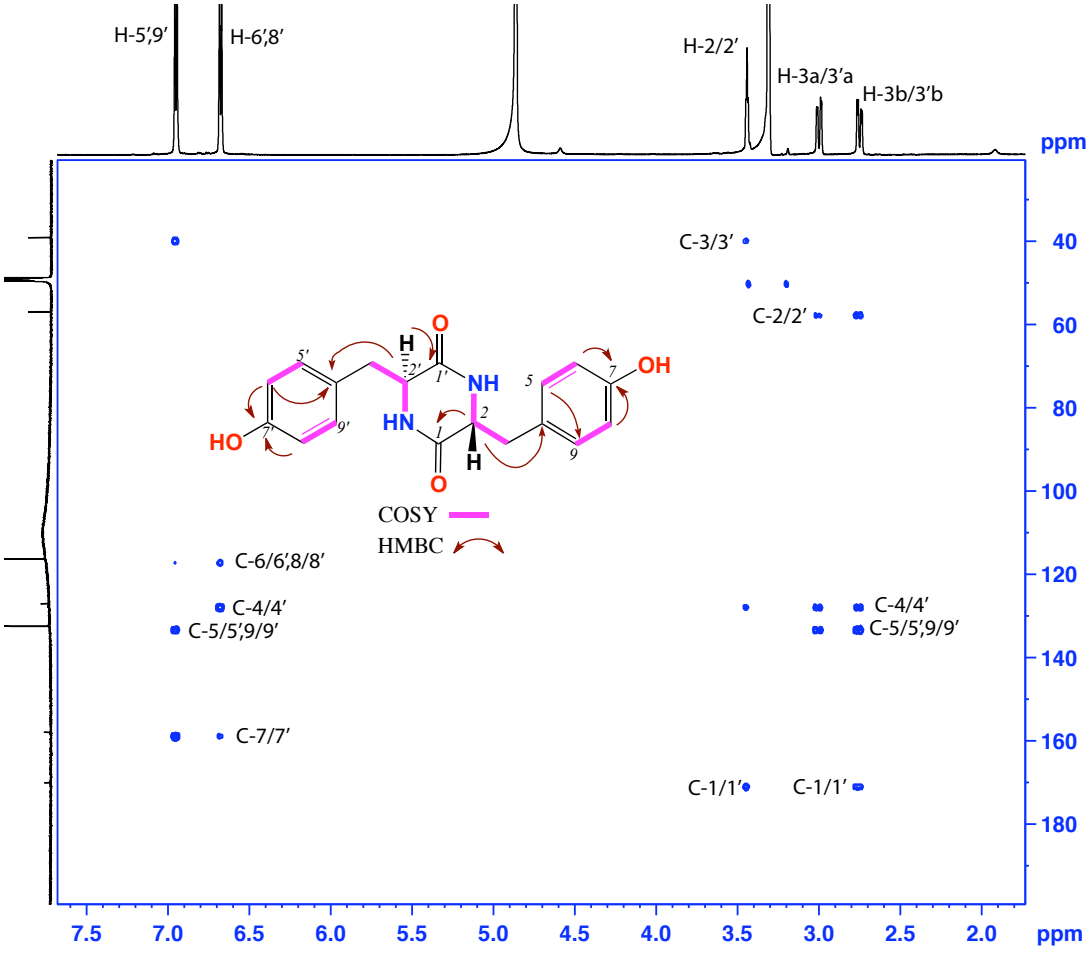

Figure 4.89. HMBC (600 MHz, DMSO-d_6) spectrum showing key correlations of *cyclo*-(L-Tyr-D-Tyr) (**4.39i**)

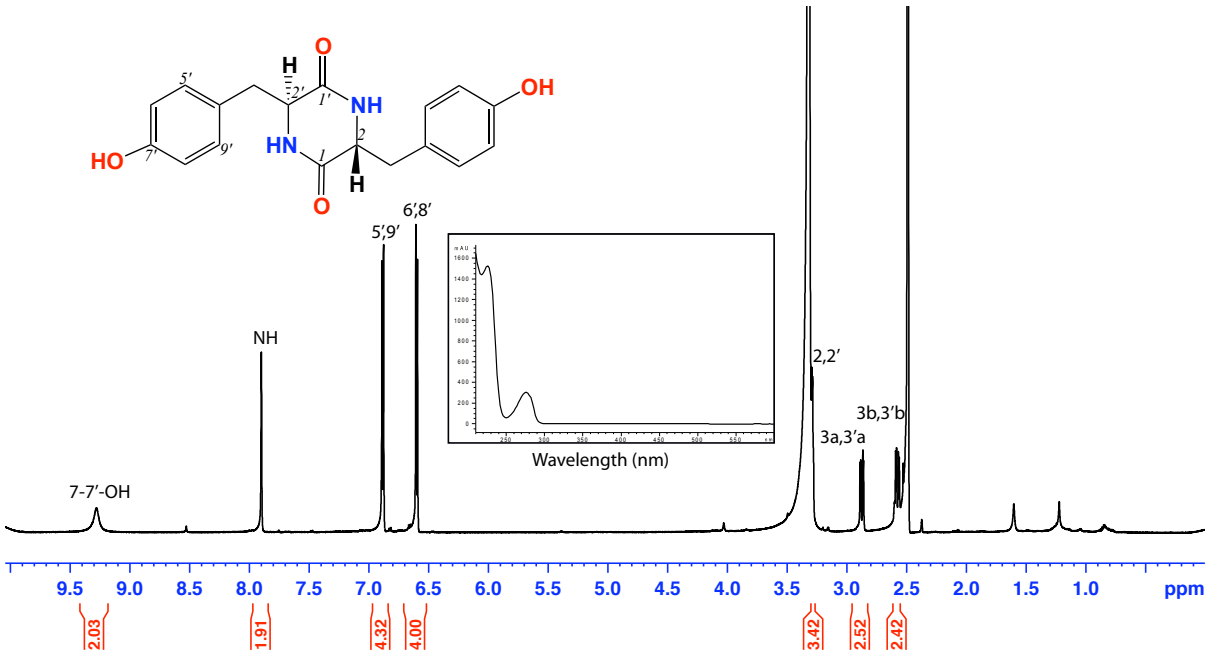

Figure 4.90. ^{1}H NMR (600 MHz, DMSO-d_6) and UV-vis (HPLC-DAD, H_2O/MeCN plus HCO_2H) spectra of *cyclo*-(L-Tyr-D-Tyr) (**4.39i**)

Table 4.22 NMR (600 MHz, DMSO-d_6) of *cyclo*-(L-Tyr-D-Tyr) (**4.39i**)

Pos.	δ_H, mult (*J* in Hz)[a]	δ_C[a]	COSY	^{1}H-^{13}C HMBC	ROESY
tyrosine					
1,1′		171.4			
2, 2′-NH	7.90, br		2/2′		
2, 2′	3.29[b]	57.3	2/2′NH, 3/3′a,b	1/1′, 3/3′, 4/4′	
3, 3′	a 2.87, dd *(13.8, 5.1)*	39.9	2/2′, 3/3′b	2/2′, 4/4′, 5/5′, 9/9′	5/5′, 9/9′
3, 3′	b 2.57, dd *(13.8, 5.1)*		2/2′, 3/3′a	1/1′, 2/2′, 4/4′, 5/5′, 9/9′	5/5′, 9/9′
4, 4′		128.4			
5, 5′, 9, 9′	6.88, d *(8.4)*	133.2	6/6′, 8/8′	3/3′, 7/7′	3/3′a,b
6, 6′, 8, 8′	6.60, d *(8.4)*	117.8	5/5′, 9/9′	4/4′	
7, 7′		158.8			

*(a)^{13}C assignments obtained from gHSQC and gHMBC data. (b) Obscured by the solvent

4.4.25.4.1 C_3 Marfey's analysis for *cyclo*-(L-Tyr-D-Tyr) (4.39i)

Employing the C_3 Marfey method as previously described, **4.39i** was subjected to acid hydrolysis using 6 M HCl, derivatized with D-FDAA, and subjected to HPLC analysis to determine the absolute configuration of the amino acid residues. The absolute configuration of **4.39i** was determined by comparing the retention times of derivatized standard amino acids with the derivatized hydrolysate of **4.39i** to be L-Tyr and D-Tyr (Figure 4.91).

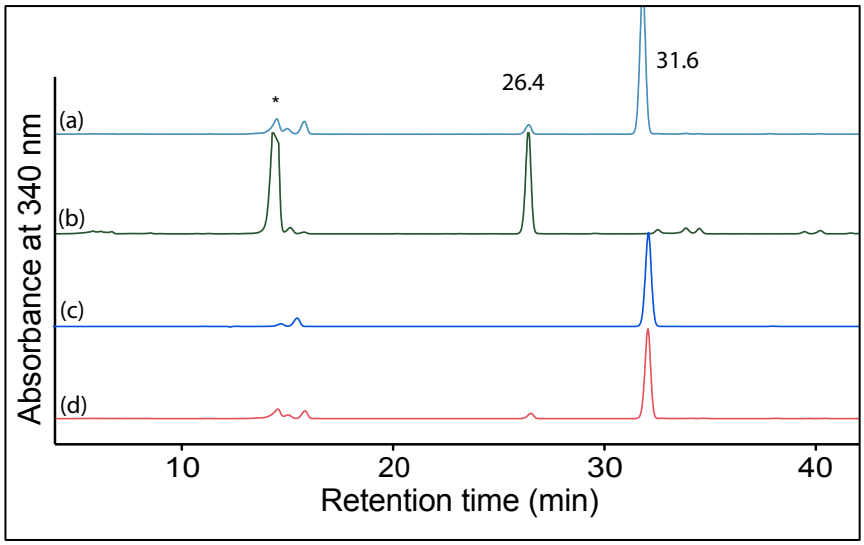

Figure 4.91. HPLC trace (340 nm) from HPLC-DAD-MS C_3 Marfey's analysis of *cyclo*-(L-Tyr-D-Tyr) (**4.39i**). Identity of amino acids was confirmed by retention time and molecular weight. (a) Co-injection of the D-FDAA derivatized hydrolysate **4.39i** with the standards. (b) D-Tyr + D-FDAA, (c) L-Tyr + D-FDAA and (d) D-FDAA derivatized hydrolyzed of **4.39i** (300 µg) showing the presence of L-Tyr (t_R = 31.6 min) and D-Tyr (t_R = 26.4 min). HPLC conditions, Zorbax, SB-C_3 column (150 × 4.6 mm, 5 µm), 1 mL/min, gradient of 15 – 60% MeOH/H_2O (isocratic 5% MeCN containing 1% formic acid) over 55 min. * residual of Marfey's reagent

4.4.25.5 Summary for all the *cyclo*-(Tyr-4-hydroxy-Pro) stereoisomers

In this part, we were able to synthesise different stereoisomers of *cyclo*-(Tyr-4-hydroxy-Pro) as shown in Figure 4.92 and Figure 4.93.

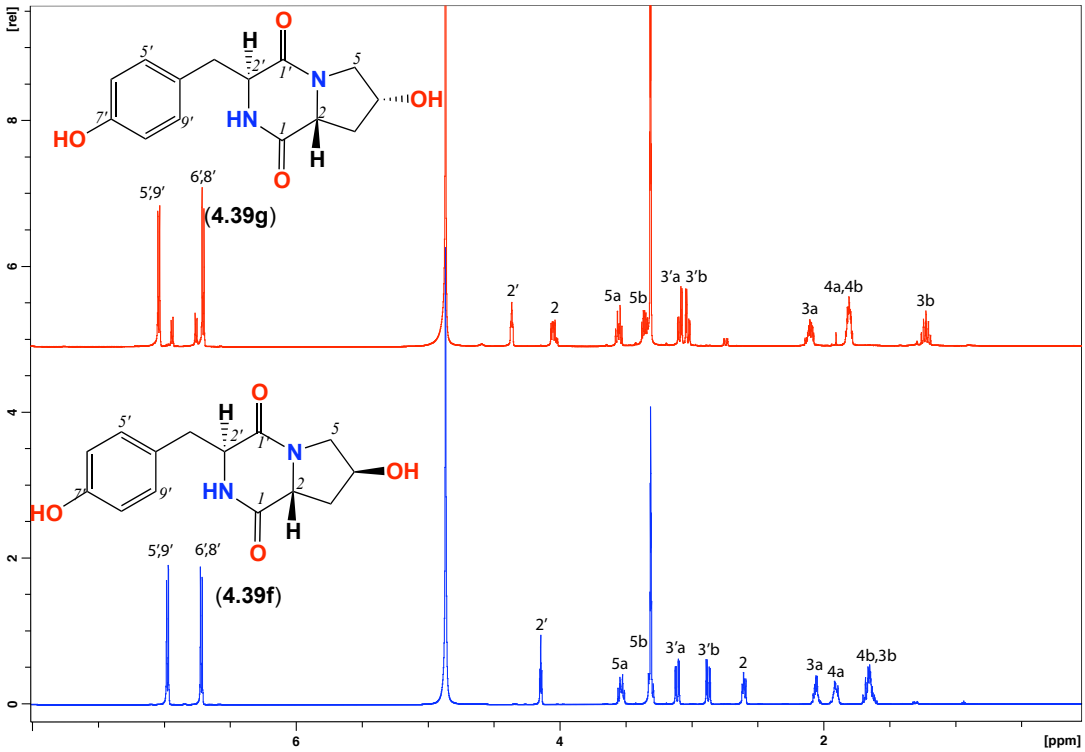

Figure 4.92. Comparison of ^{1}H NMR (600 MHz, MeOH-d_4) spectrum of *cyclo*-(L-Tyr-*cis*-4-hydroxy-D-Pro) (**4.39g**) and *cyclo*-(L-Tyr-*trans*-4-hydroxy-D-Pro) (**4.39f**)

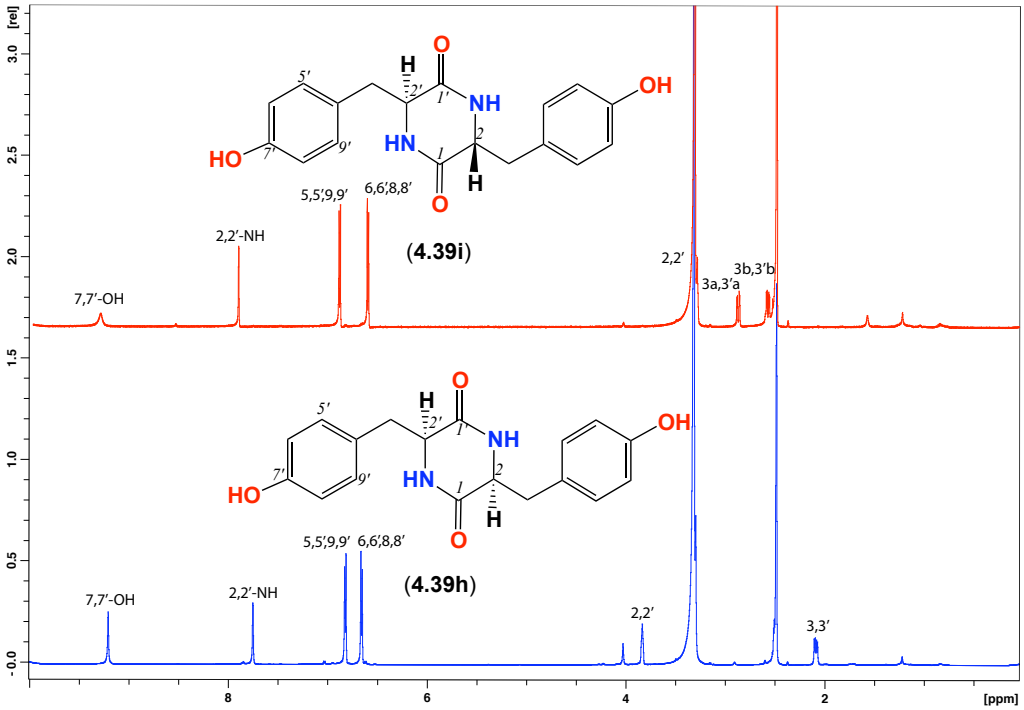

Figure 4.93. Comparison for ^{1}H NMR (600 MHz, DMSO-d_6) of *cyclo*-(L-Tyr-L-Tyr) (**4.39i**) and *cyclo*-(L-Tyr-D-Tyr) (**4.39h**)

As with the microwave-assisted synthesis of Phe and hydroxyl-Pro diketopiperazines, the product mixture from microwave assisted reaction of Tyr and hydroxyl-Pro features significant yields of Tyr/Tyr diketopiperazines (Scheme 4.6). These latter products deplete the pool of available Tyr thereby reducing product yields of Tyr and hydroxyl-Pro diketopiperazines. Future efforts to optimize yields would benefit from increasing the ratio of Tyr to hydroxyl-Pro from 1:1 to 10:1.

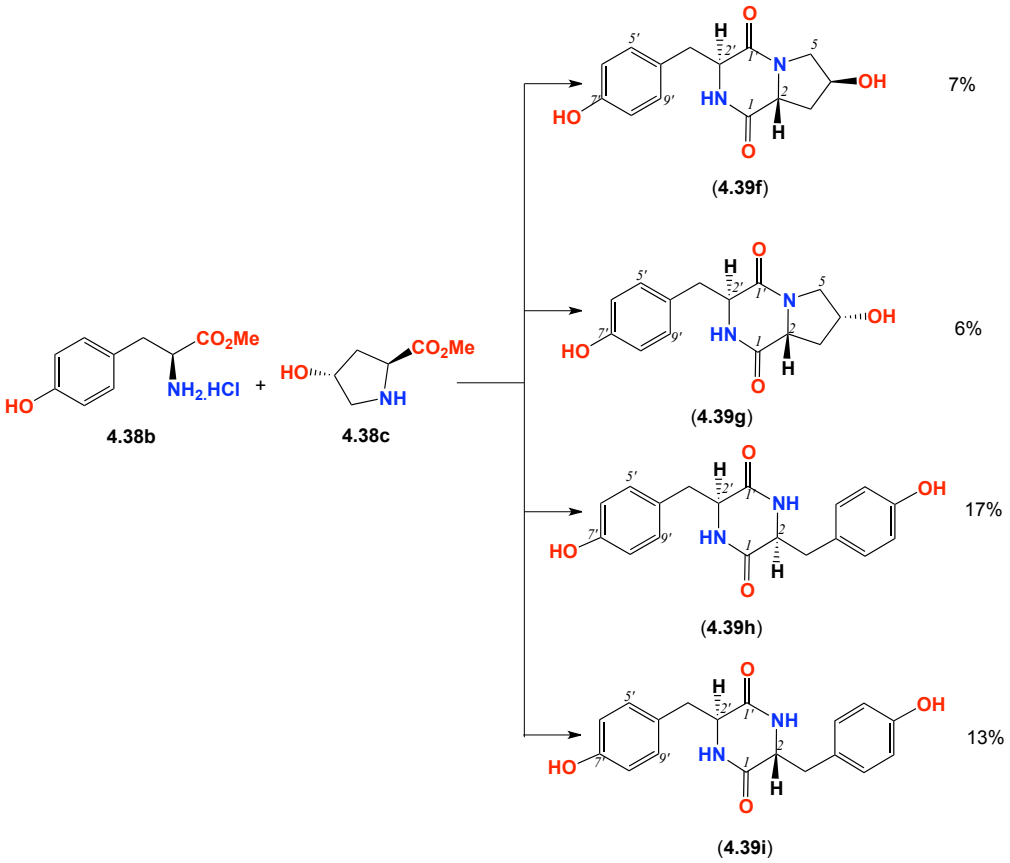

Scheme 4.6. Synthesis of different stereoisomers of *cyclo*-(Tyr-4-hydroxy-Pro)

4.4.26 Synthesis of *cyclo*-(L-Tyr-Pro) stereoisomers

The reaction was performed by irradiating L-Tyr and L-Pro methyl esters (**4.38b** and **4.38d**) respectively in H_2O (3 mL) in the presence of triethylamine (2.5 eq.), in a microwave reactor at 140 ˚C, 300 W for 3 min. The recovered dried reaction product was washed with H_2O and dried *in vacuo* to yield a MeOH soluble product that was analysed by HPLC-DAD-MS (Figure 4.94 and Scheme 4.7).

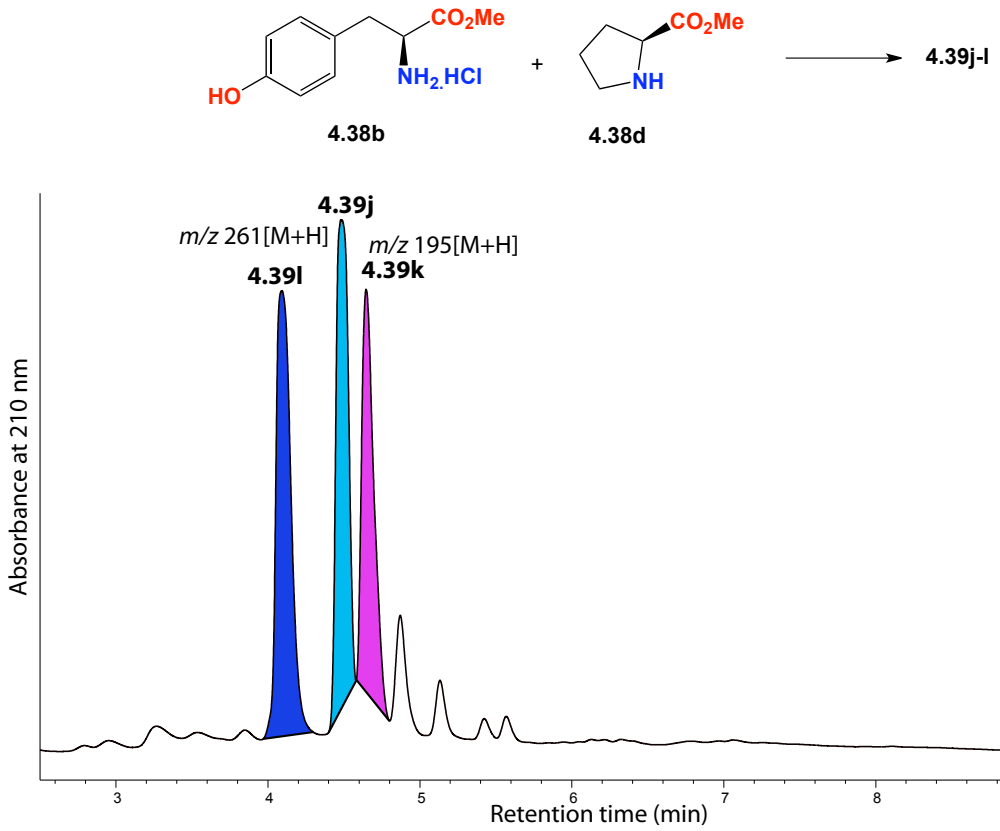

Figure 4.94. HPLC-DAD-MS reaction product for *cyclo*-(Tyr-Pro). Reacting the methyl ester of L-Tyr (**4.38b**) with methyl ester of L-Pro (**4.38d**). The highlighted peaks represent DKPs

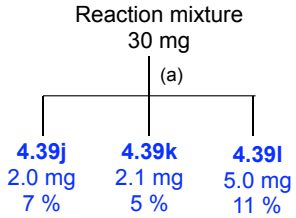

Scheme 4.7. Fractionation scheme of the reaction of methyl ester of L-Tyr (**4.38b**) with methyl ester of L-Pro (**4.38d**). (a) Semi-preparative gradient HPLC: Zorbax C_8, 90 – 50% H_2O/MeOH, 3 mL/min

4.4.26.1 *cyclo*-(L-Tyr-D-Pro) (4.39j)

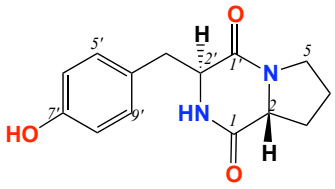

(**4.39j**)

Compound **4.39j** was synthesized as an optically active amorphous white powder ($[\alpha]^{22}_{D}$ −2.2, *c* 0.1, MeOH). HRESI(+)MS showed an adduct ion $(M+Na)^+$ consistent with the molecular formula $C_{14}H_{16}N_2O_3$ (Δmmu +0.3). The ^{1}H NMR (MeOH-d_4) spectrum and tabulated data of **4.39j** are presented Figure 4.97 and Table 4.23. The ROESY data showed no correlations between H-2 and H-2′ (Figure 4.96), consistent with a *trans* relationship, however the absolute configuration of **4.39i** was confirmed by C_3 Marfey's analysis (Figure 4.98 and Figure 4.99).

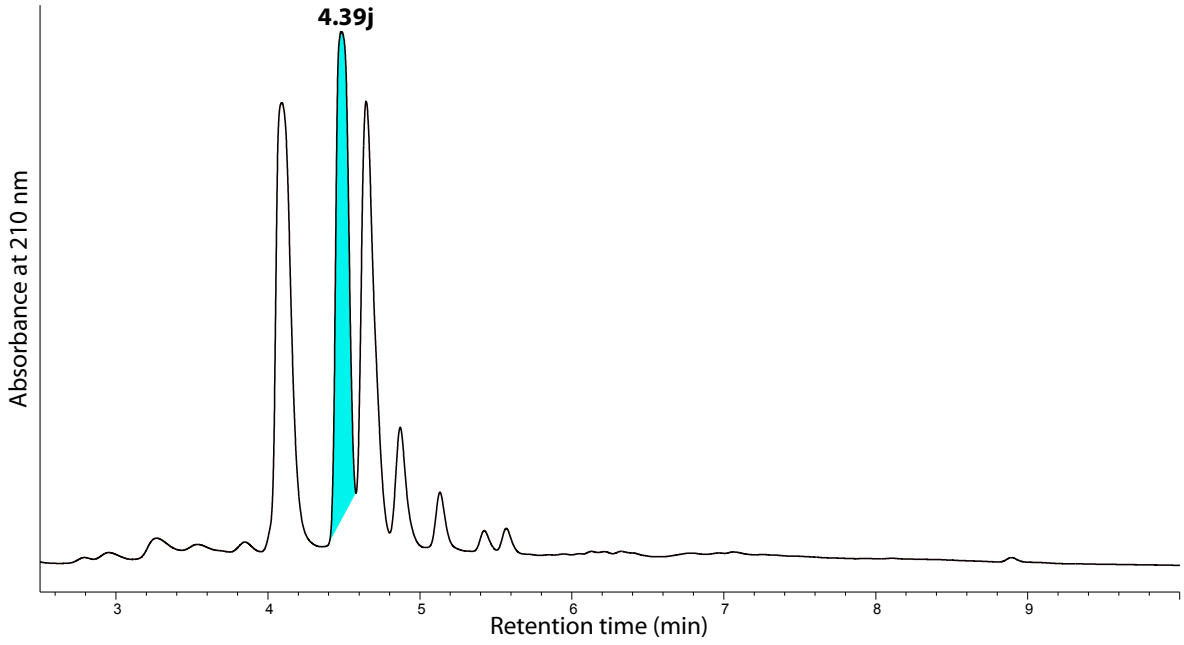

Figure 4.95. HPLC-DAD chromatogram, analytical gradient H_2O/MeCN plus HCO_2H at 210 nm using Zorbax C_8 column of the reaction mixture, highlighting **4.39j**

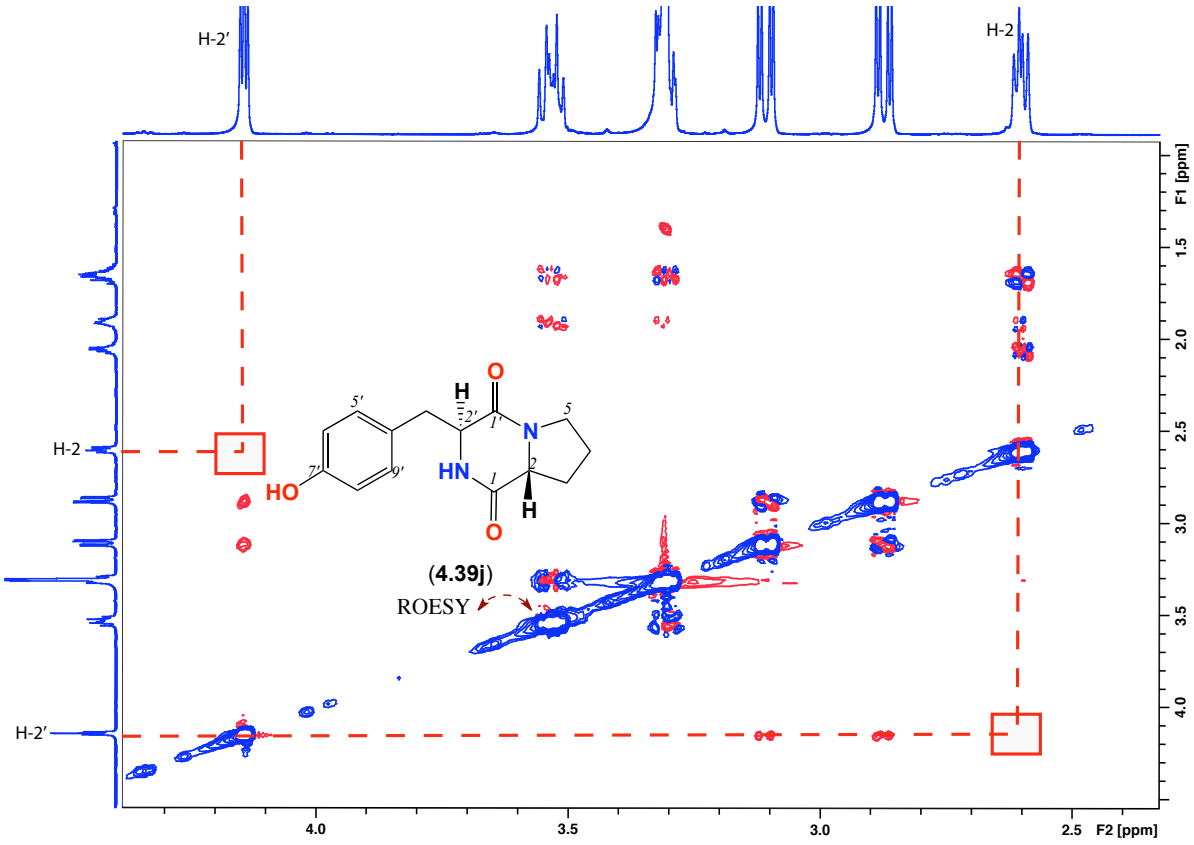

Figure 4.96. ROESY (600 MHz, $CDCl_3$) spectrum showing the absence of key correlations of *cyclo*-(L-Tyr-D-Pro) (**4.39j**)

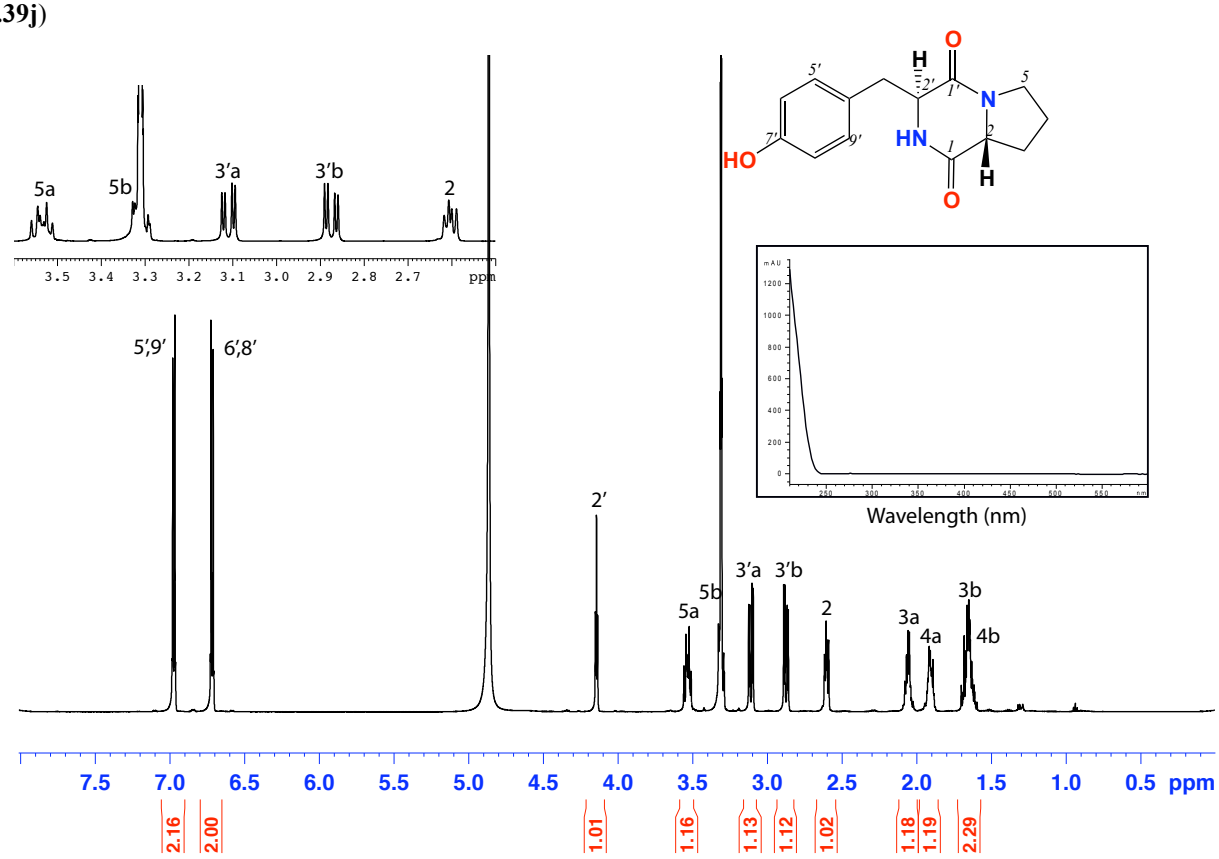

Figure 4.97. ^{1}H NMR (600 MHz, MeOH-d_4) and UV-vis (HPLC-DAD, H_2O/MeCN plus HCO_2H) spectra of *cyclo*-(L-Tyr-D-Pro) (**4.39j**)

Table 4.23. NMR (600 MHz, MeOH-d_4) of *cyclo*-(L-Tyr-D-Pro) (**4.39j**)

Pos.	δ_H, mult (*J* in Hz)[a]	δ_C[a]	COSY	^{1}H-^{13}C HMBC	ROESY
proline					
1		167.5			
2	2.60, dd *(10.4, 6.2)*	58.6	3a/b	1′	
3	a 2.05, m	29.4	2, 4a,3b	2, 4, 5	
	b 1.65[b], m		3a		
4	a 1.91, m	22.1	3a/b, 4b		
	b 1.65[b],m	22.1	5a/b		
5	a 3.53, m	45.6	4a/b, 5b	4	
	b 3.33[c]		4a/b, 5a	3, 4	
tyrosine					
1′		171.7			
2′-NH	[d]				
2′	4.14, t *(4.4)*	59.3	3′a/b	4′	3′a/b
3′	a 3.10, dd *(14.0, 4.4)*	39.8	2′,3′b	1,2′,4′ 5′/9′	2′, 5/9′
	b 2.87, dd *(14.0, 4.4)*	39.8	2′,3′a	1,2′,4′ 5′/9′	
4′	--	126.8			
5′, 9′	6.97, d *(8.4)*	132.5	6′,8′	3′, 6′/8′, 7′	3′a/b
6′, 8′	6.71, d *(8.4)*	116.3	5′,9′	4′,5′/9′, 7′	
7′		158.0			

*(a)[13]C assignments obtained from gHSQC and gHMBC data. (b) Overlapping resonances. (c) Obscured by the solvent. (d) Not observed

4.4.26.1.1 C_3 Marfey's analysis for *cyclo*-(L-Tyr-D-Pro) (4.39j)

Employing the C_3 Marfey method as previously described, **4.39j** was subjected to acid hydrolysis using 6 M HCl, derivatized with D-FDAA, and subjected to HPLC analysis to determine the absolute configuration of the amino acid residues. The absolute configuration of **4.39j** was determined by comparing the retention times of derivatized standard amino acids with the derivatized hydrolysate of **4.39j** to be L-Tyr and D-Pro (Figure 4.98 and Figure 4.99).

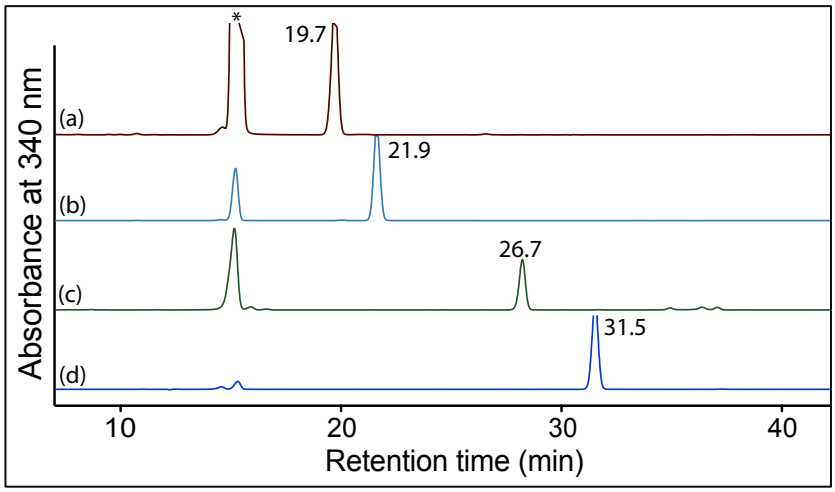

Figure 4.98. HPLC trace (340 nm) from HPLC-DAD-MS C_3 Marfey's analysis of the standard amino acids reacting with D-FDAA. Identity of amino acids was confirmed by retention time and molecular weight. (a) D-Pro + D-FDAA (t_R = 19.7 min), (b) L-Pro + D-FDAA (t_R = 21.9 min), (c) D-Tyr + D-FDAA (t_R = 26.7 min and (d) L-Tyr + D-FDAA (t_R = 31.5 min). HPLC conditions, Zorbax, SB-C_3 column (150 × 4.6 mm, 5 μm), 1 mL/min, gradient of 15 – 60% MeOH/H_2O (isocratic 5% MeCN containing 1% formic acid) over 55 min

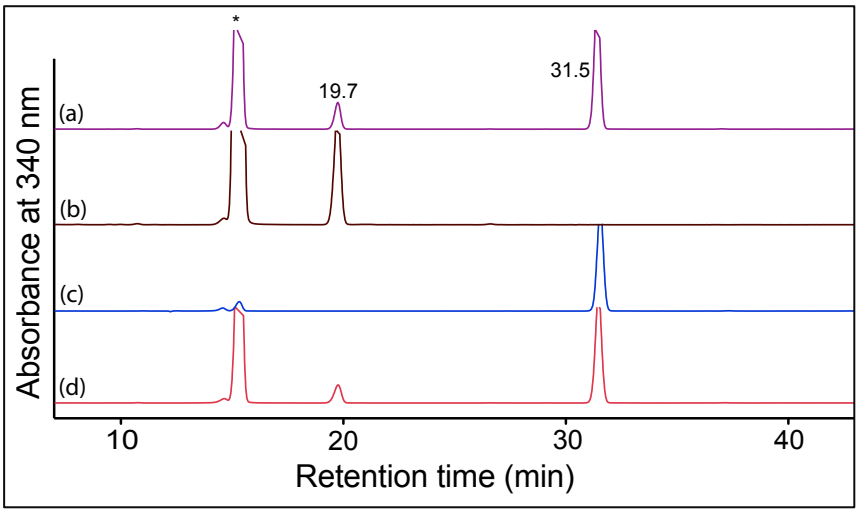

Figure 4.99. HPLC trace (340 nm) from HPLC-DAD-MS C_3 Marfey's analysis of *cyclo*-(L-Tyr-D-pro) (**4.39j**). Identify of amino acids was confirmed by retention time and molecular weight. (a) co-injection of the D-FDAA derivatized hydrolysate **4.39j** with the standards, (b) D-Pro + D-FDAA, (c) L-Tyr + D-FDAA and (d) D-FDAA derivatized hydrolyzed of **4.39j** (300 μg) showing the presence of L-Tyr (t_R = 31.6 min) and L-Tyr (t_R = 31.5 min) and D-Pro (t_R = 19.7 min). HPLC conditions, Zorbax, SB-C_3 column (150 × 4.6 mm, 5 μm), 1 mL/min, gradient of 15 – 60% MeOH/H_2O (isocratic 5% MeCN containing 1% formic acid) over 55 min. * residual of Marfey's reagent

4.4.26.2 *cyclo*-(L-Tyr-L-Pro) (4.39k)

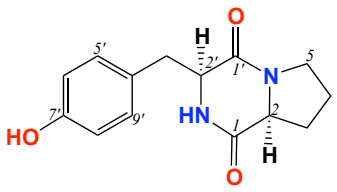

(**4.39k**)

Compound **4.39k** was synthesized as an optically active amorphous white powder ($[\alpha]^{22}_{D}$ −6.8, *c* 0.06, MeOH). HRESI(+)MS showed an adduct ion $(M+Na)^+$ consistent with the molecular formula $C_{14}H_{16}N_2O_3$ (Δmmu +0.2). The ^{1}H NMR (MeOH-d_4) spectrum and tabulated data of **4.39k** are presented in Figure 4.102 and Table 4.24. The ROESY data confirmed the *cis* relationship between H-2 and H-2′ as shown in Figure 4.101. The absolute configurations were assigned by C_3 Marfey's analysis (Figure 4.103 and Figure 4.104).

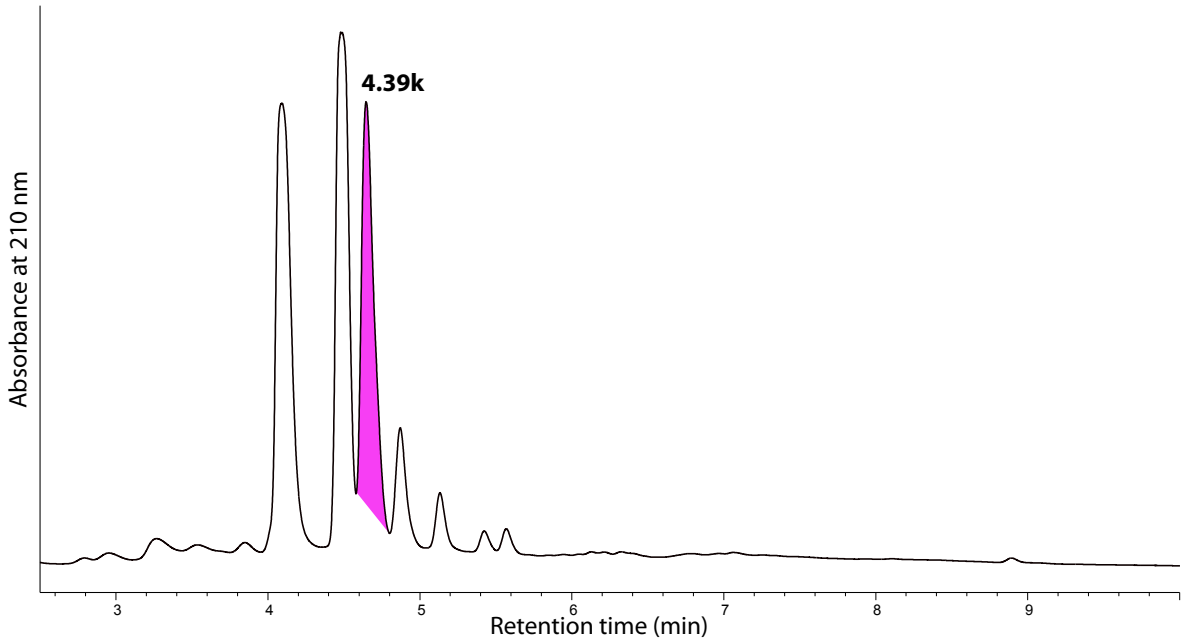

Figure 4.100. HPLC-DAD chromatogram, analytical gradient H_2O/MeCN plus HCO_2H at 210 nm using Zorbax C_8 column of the reaction mixture, highlighing **4.39k**

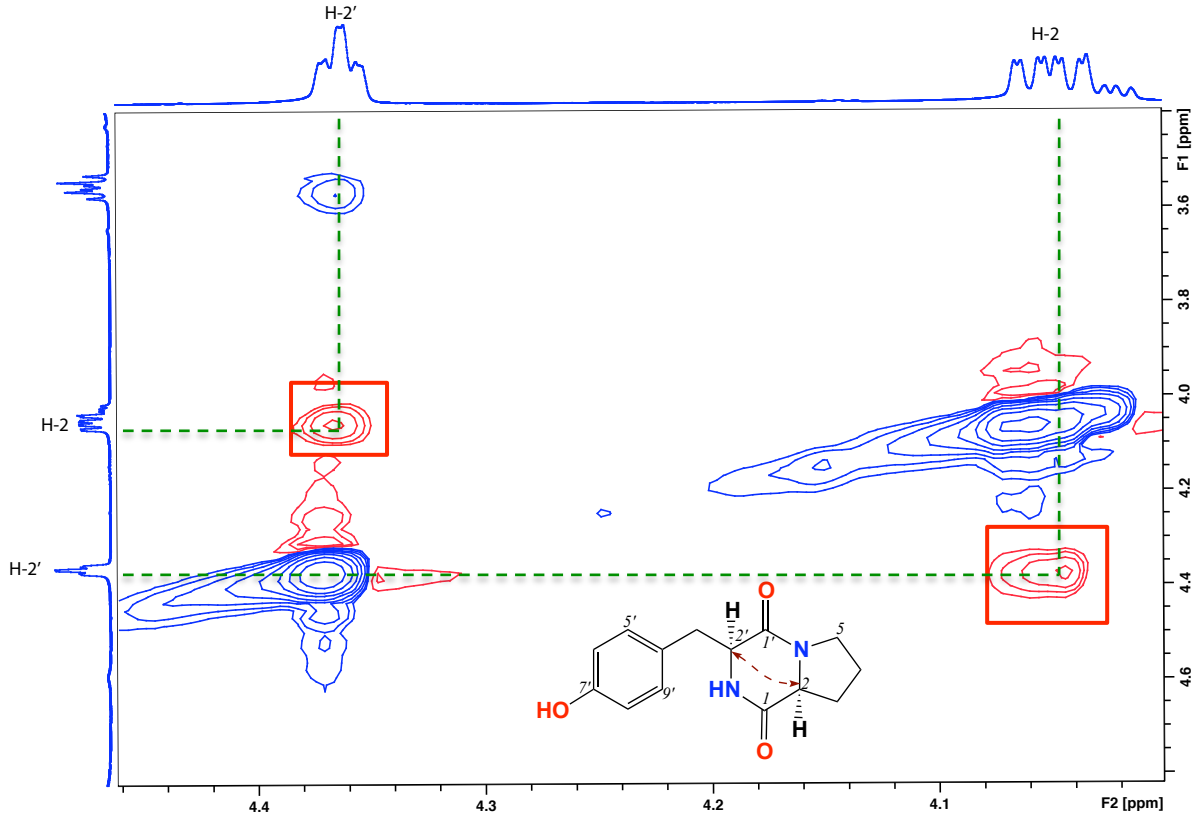

Figure 4.101. ROESY (600 MHz, MeOH-d_4) spectrum showing key correlations of *cyclo*-(L-Tyr-L-Pro) (**4.39k**)

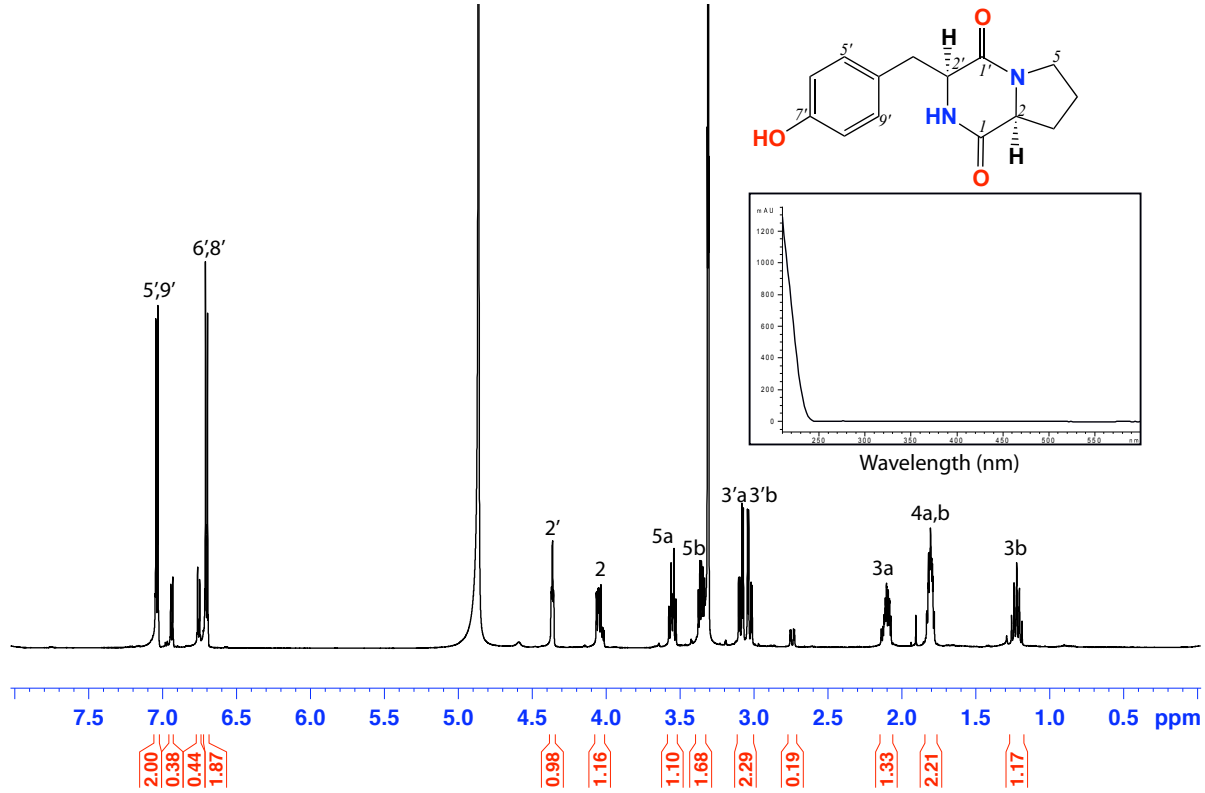

Figure 4.102. ^{1}H NMR (600 MHz, MeOH-d_4) and UV-vis (HPLC-DAD, H_2O/MeCN plus HCO_2H) spectra of *cyclo*-(L-Tyr-L-Pro) (**4.39k**)

Table 4.24. NMR (600 MHz, MeOH-d_4) of *cyclo*-(L-Tyr-L-Pro) (**4.39k**)

Pos.	δ_H, mult (*J* in Hz)[a]	δ_C[a]	COSY	^{1}H-^{13}C HMBC	ROESY
proline					
1		166.3			
2	4.04, m	59.6	3a/b	1′, 3	2′
3	a 2.10, m	28.3	2, 3b, 4a/b	1′, 5	
	b 1.22, q *(10.3)*		2, 3a, 4a/b	1′, 5	
4	a 1.80[b], m	22.1	3b, 5a/b	3	
	b 1.80[b], m		3b, 5a/b	3	
5	a 3.55, ddd (*16.7, 11.9, 7.8*)	45.3	4a/b, 5b	3, 4	
	b 3.35, ddd (*16.7, 11.9, 7.8*)		4a/b, 5a	3, 4	
tyrosine					
1′		170.5			
2′-NH	[c]				
2′	4.36, br s	57.3	3′a/b	1, 3′,4′	2
3′	a 3.05, ddd *(15.3, 13.6, 5.1)*	37.6	2′, 3′b	1,2′, 4′, 5′/9′	
	b 3.01, ddd *(15.3, 13.6, 5.1)*	37.6	2′, 3′a	1, 2′, 4′, 5′/9′	
4′		127.5			
5′, 9′	7.03, d *(8.2)*	132.1	6′, 8′	3′, 7′	
6′, 8′	6.70, d *(8.2)*	115.8	5′, 9′	4′	
7′		156.8			

(a) ^{13}C assignments obtained from gHSQC and gHMBC data. (b) Overlapping resonances. (c) Not observed

4.4.26.2.1 C_3 Marfey's analysis for *cyclo*-(L-Tyr-L-Pro) (4.39k)

Employing the C_3 Marfey's method as previously described, **4.39k** was subjected to acid hydrolysis using 6 M HCl, derivatized with D-FDAA, and subjected to HPLC analysis to determine the absolute configuration of the amino acids residues. Absolute configuration for **4.39k** were determined by comparing the retention times of derivatized standard amino acids with the derivatized hydrolysate of **4.39k**, to be L-Tyr and L-Pro (Figure 4.103 and Figure 4.104).

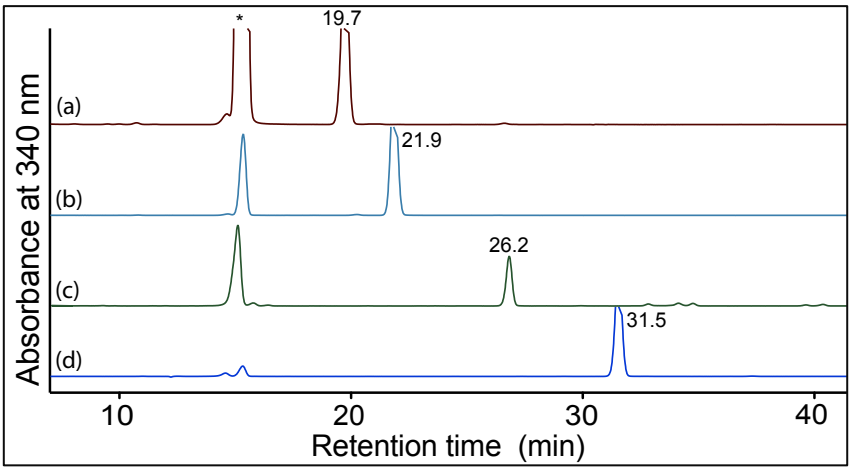

Figure 4.103. HPLC trace (340 nm) from HPLC-DAD-MS C_3 Marfey's analysis of the standard amino acids reacting with D-FDAA. Identity of amino acids was confirmed by retention time and molecular weight. (a) D-Pro + D-FDAA (t_R = 19.7 min), (b) L-Pro + D-FDAA (t_R = 21.9 min), (c) D-Tyr + D-FDAA (t_R = 26.2 min) and (d) L-Tyr + D-FDAA (t_R = 31.5 min). HPLC conditions, Zorbax, SB-C_3 column (150 × 4.6 mm, 5 µm), 1 mL/min, gradient of 15 – 60% MeOH/H_2O (isocratic 5% MeCN containing 1% formic acid) over 55 min

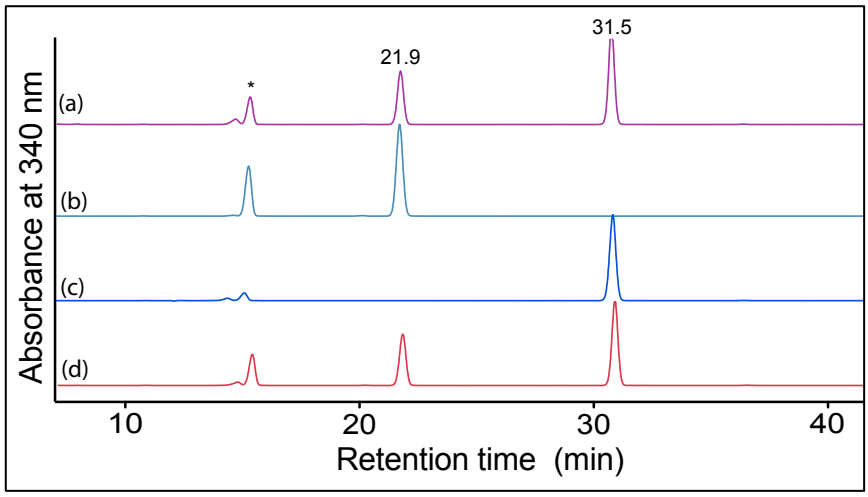

Figure 4.104. HPLC trace (340 nm) from HPLC-DAD-MS C_3 Marfey's analysis of *cyclo*-(L-Tyr-L-Pro) (**4.39k**). Identity of amino acids was confirmed by retention time and molecular weight. (a) co-injection of the D-FDAA derivatized hydrolysate **4.39k** with the standards, (b) L-Pro + D-FDAA, (c) L-Tyr + D-FDAA and (d) D-FDAA derivatized hydrolyzed of **4.39k** (200 μg) showing the presence of L-Tyr (t_R = 31.5 min) and L-Pro (t_R = 21.9 min). HPLC conditions, Zorbax, SB-C_3 column (150 × 4.6 mm, 5 μm), 1 mL/min, gradient of 15 – 60% MeOH/H_2O (isocratic 5% MeCN containing 1% formic acid) over 55 min. * residual of Marfey's reagent

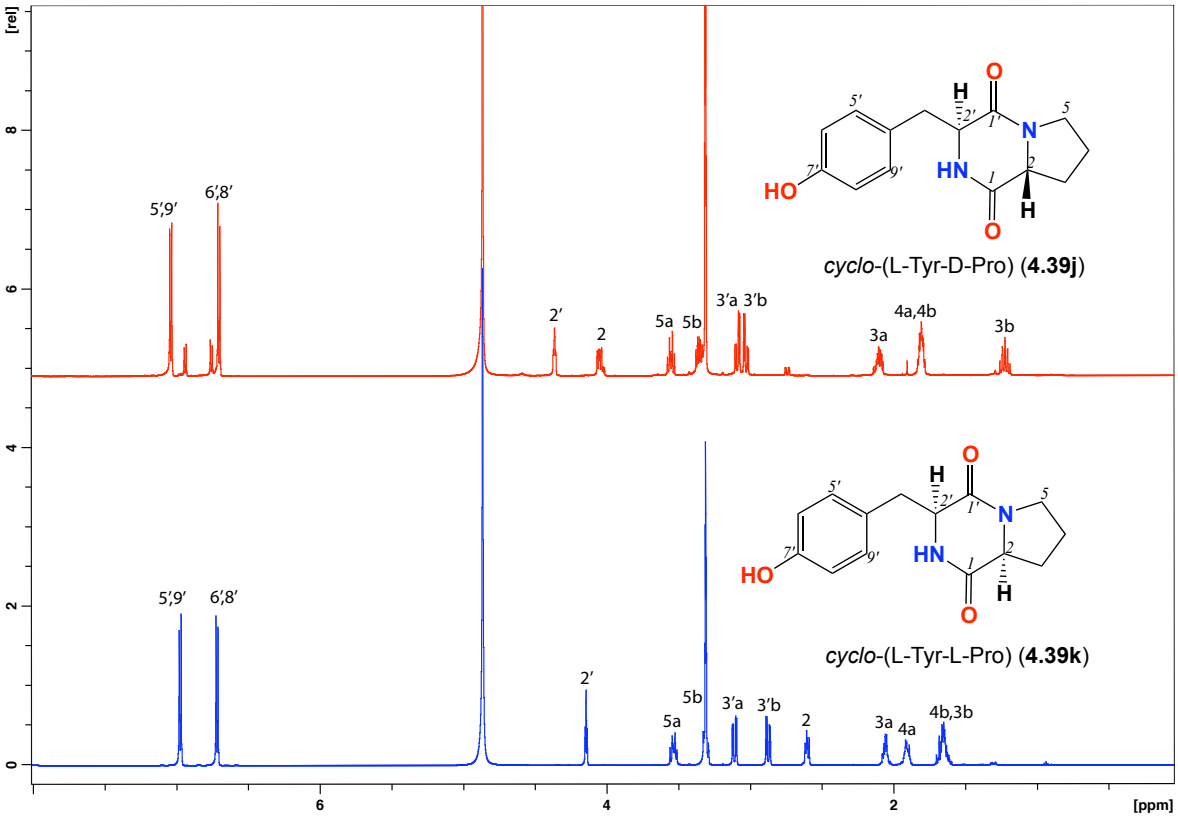

Figure 4.105. Comparison for ^{1}H NMR (600 MHz, MeOH-d_4) of *cyclo*-(L-Tyr-D-Pro) (**4.39j**) and *cyclo*-(L-Tyr-L-Pro) (**4.39k**)

4.4.26.3 *cyclo*-(L-Pro-L-Pro) (4.39l)

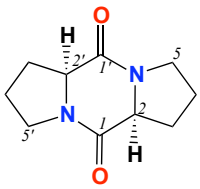

(**4.39l**)

Compound **4.39l** was synthesized as an optically active amorphous white powder ($[\alpha]^{22}_{D}$ −5.9, *c* 0.1, MeOH). HRESI(+)MS showed an adduct ion $(M+Na)^+$ consistent with the molecular formula $C_{10}H_{14}N_2O_2$ (Δmmu +2.0). The ^{1}H NMR (MeOH-d_4) spectrum and tabulated data of **4.39l** are presented in Figure 4.107, Figure 4.108 and Table 4.25. ROESY correlations could not be used to assign the stereochemistry of the two chiral centres H-2 and H-2′ due to symmetry. The absolute configuration of *cyclo*-(L-Pro-L-Pro) was determined by application of the C_3 Marfey's analysis (Figure 4.109).

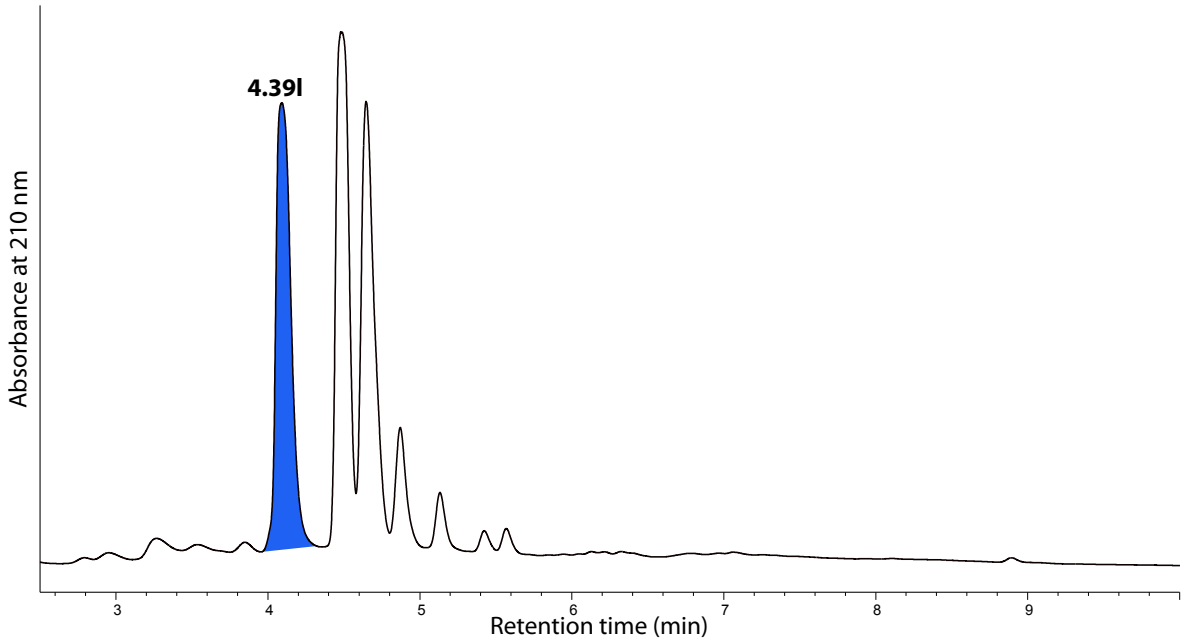

Figure 4.106. HPLC-DAD chromatogram, analytical gradient H_2O/MeCN plus HCO_2H at 210 nm using Zorbax C_8 column of the reaction mixture, highlighting **4.39l**

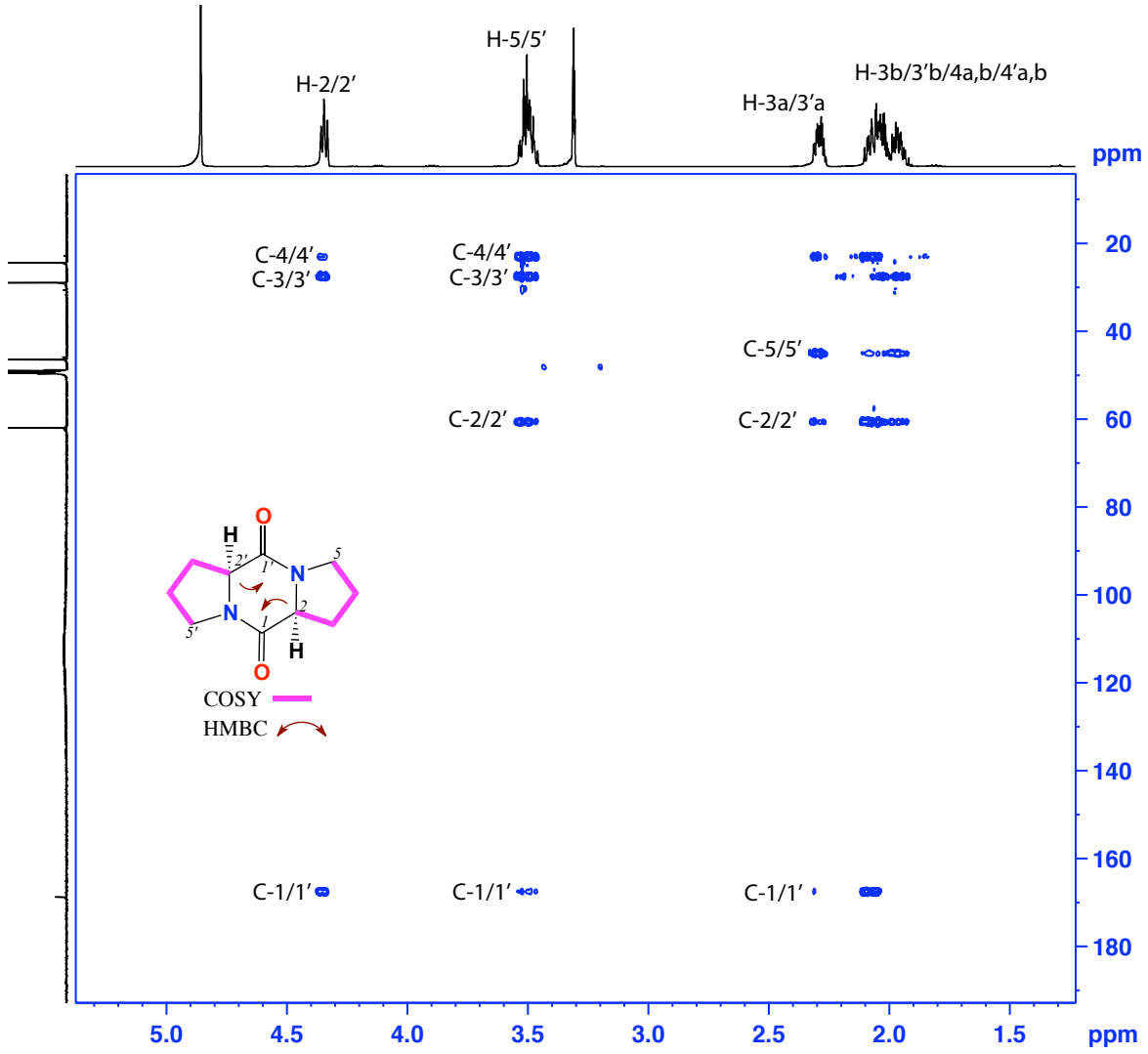

Figure 4.107. HMBC (600 MHz, MeOH-d_4) spectrum and key correlations of *cyclo*-(L-Pro-L-Pro) (**4.39l**)

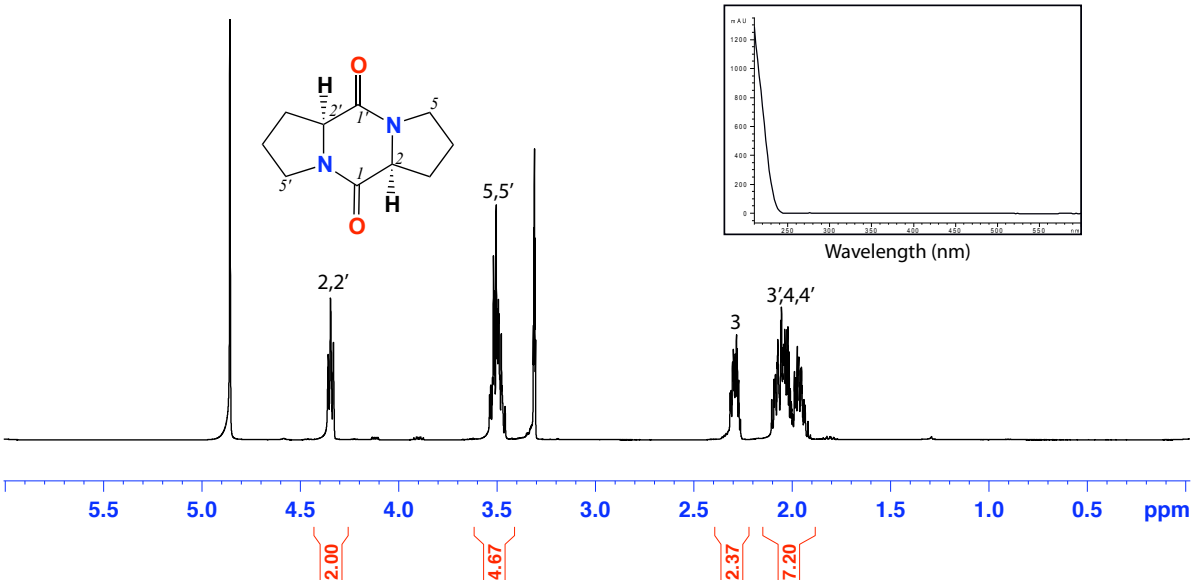

Figure 4.108. ^{1}H NMR (600 MHz, MeOH-d_4) and UV-vis (HPLC-DAD, H_2O/MeCN plus HCO_2H) spectra of *cyclo*-(L-Pro-L-Pro) (**4.39l**)

Table 4.25. NMR (600 MHz, MeOH-d_4) of *cyclo*-(L-Pro-L-Pro) (**4.39l**)

Pos.	δ_H, mult (*J* in Hz)[a]	δ_C[a]	COSY	^{1}H-^{13}C HMBC	ROESY
proline					
1,1′		167.5			
2, 2′	4.34,t *(7.2)*	60.6	3/3′	1/1′, 3/3′	5/5′
3, 3′	a 2.29, m	27.5	4/4′	1/1′, 2/2′	
	b 2.06[b], m	27.5			
4, 4′	a 2.04[b], m	22.9		2/2′	
	b 1.96, m	22.9			
5, 5′	3.50, m	45.1	3/3′	1/1′, 2/2′	2/2′

(a)^{13}C assignments obtained from gHSQC and gHMBC data. (b) Overlapping resonances.

4.4.26.3.1 C_3 Marfey analysis for *cyclo*-(L-Pro-L-Pro) (4.39l)

Employing the C_3 Marfey's method as previously described, **4.39k** was subjected to acid hydrolysis using 6 M HCl, derivatized with D-FDAA, and subjected to HPLC analysis to determine the absolute stereochemistry of the three chiral centres H-2 and H-2′. Absolute configuration of **4.39k** was determined by comparing the retention times of derivatized standard amino acids with the derivatized hydrolysate of **4.39k**, to be L-Tyr and L-Pro (Figure 4.109).

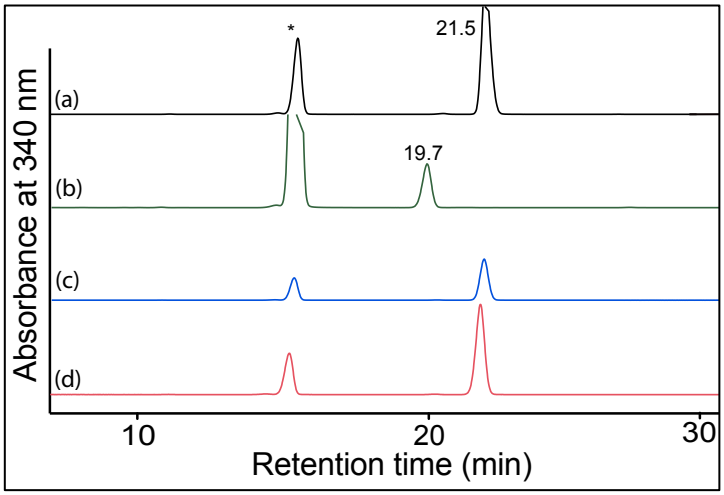

Figure 4.109. HPLC trace (340 nm) from HPLC-DAD-MS C_3 Marfey's analysis of *cyclo*-(L-Pro-L-Pro) (**4.39l**). Identity of amino acids was confirmed by retention time and molecular weight. (a) co-injection of the D-FDAA derivatized hydrolysate **4.39l** with the standards, (b) D-Pro + D-FDAA, (c) L-Pro + D-FDAA and (d) D-FDAA derivatized hydrolyzed of **4.39l** (100 μg) showing the presence of L-Pro (t_R = 21.5 min). HPLC conditions, Zorbax, SB-C_3 column (150 × 4.6 mm, 5 μm), 1 mL/min, gradient of 15 – 60% MeOH/H_2O (isocratic 5% MeCN containing 1% formic acid) over 55 min. * residual of Marfey's reagent

4.4.26.4 Summary for the *cyclo*-(Tyr-Pro) reaction

The microwave reaction leading to the *cyclo*-(Tyr-Pro) afforded 3 compounds (Scheme 4.8), **4.39j** (yield 5%), **4.39k** (yield 5%) and **4.39l** (yield 11%). The high yield of **4.39l**, 11% could possibly be avoided in the future by increasing the ratio of the Pro versus the Tyr from 1:1 to 10:1

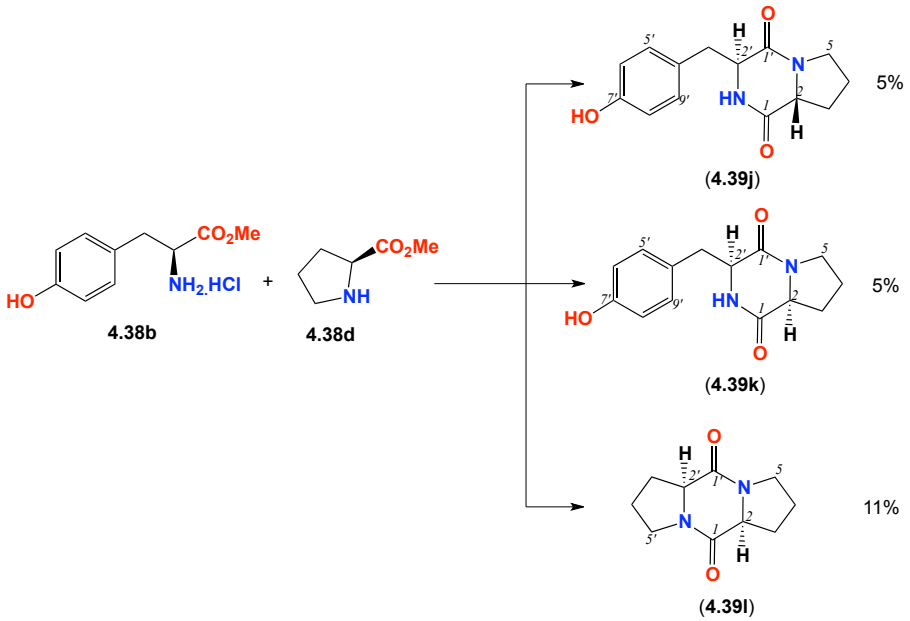

Scheme 4.8. Synthesis of different stereoisomers of *cyclo*-(Tyr-Pro)

4.4.27 Summary for the different synthetic diketopiperazines analogues

#	Name	H-2′	H-2	H-4	Yield %
4.39a	*cyclo*-(L-Phe-*trans*-4-hydroxy-L-Pro)	*S*	*S*	*R*	5
4.39b	*cyclo*-(L-Phe-*cis*-4-hydroxy-D-Pro)	*S*	*R*	*R*	4.5
4.39c	*cyclo*-(L-Phe-*cis*-4-hydroxy-L-Pro)	*S*	*S*	*S*	5
4.39d	*cyclo*-(L-Phe-*trans*-4-hydroxy-D-Pro)	*S*	*R*	*S*	3
3.39e	*cyclo*-(Phe-Phe)				19

#	Name	H-2′	H-2	H-4	Yield %
4.39f	*cyclo*-(L-Tyr-*trans*-4-hydroxy-D-Pro)	*S*	*R*	*S*	7
4.39g	*cyclo*-(L-Tyr-*cis*-4-hydroxy-D-Pro)	*S*	*R*	*R*	6
4.39h	*cyclo*-(L-Tyr-L-Tyr)	*S*	*S*	--	17
4.39i	*cyclo*-(L-Tyr-D-Tyr)	*S*	*R*	--	13

#	Name	H-2′	H-2	H-4	Yield %
4.39j	*cyclo*-(L-Tyr-D-Pro)	*S*	*R*	--	5
4.39k	*cyclo*-(L-Tyr-L-Pro)	*S*	*S*	--	5
4.39l	*cyclo*-(L-Pro-L-Pro)	*S*	*S*	--	11

All these diketopiperazines analogues were tested in the following sections on *Streptomyces* sp. (CMB-M0423) to determine if they were capable of activating the biosynthesis of heronapyrrole B (**4.02**).

4.4.28 Effect of DKPs on *Streptomyces* sp. (CMB-M0423) secondary metabolism

The observation that the *Aspergillus* sp. (CMB-M0423) diketopiperazine **4.34** stimulated *Streptomyces* sp. (CMB-M0423) to produce heronapyrrole B (**4.02**) (and other metabolites) raises the intriguing question as to how specific is this structure activity relationship (SAR), and could other DKPs also act as activators of *Streptomyces* sp. (CMB-M0423) secondary metabolism. With a library of synthetic DKPs in hand, we set out to test this hypthesis.

DKPs stock solutions were prepared in 2-fold dilution ranging from 138 mM to 15 nM in 30% DMSO/H_2O. An aliquot (15 μL) from each stock solution was transferred to micro-bioreactor wells containing 1.45 mL M1 broth in 3.3% artificial ocean sea salt to give a final DKP concentrations

ranging from 4.6 mM to 0.5 nM in 1% DMSO per well. The positive control micro-bioreactor wells were inoculated with *Aspergillus*/*Streptomyces* sp. (CMB-M0423) seed culture (15 μL), while the negative control micro-bioreactor wells were inoculated with *Streptomyces* sp. (CMB-M0423). Both positive and negative controls were treated with 1% DMSO/H_2O per well. Micro-bioreactor wells containing DKPs were inoculated with *Streptomyces* sp. (CMB-M0423) seed culture (15 μL). All micro-bioreactor plates were incubated at 27 °C for 10 days at 190 rpm, after which the broth was extracted *in situ* with EtOAc (2 mL), and the decanted organic layer dried under N_2. The resulting crude EtOAc extract was resuspended in MeOH (100 μL) and analysed using HPLC-DAD-MS. All the diketopiperazines **4.39a – l** were tested on *Streptomyces* sp. (CMB-M0423), but only **4.39a**, which corresponds to **4.34**, activated production of heronapyrrole B (**4.02**). This data provides compelling evidence of a very specific DKP SAR requirement, confirming that *Aspergillus* sp. (CMB-M0423) possesses a unique ability to activate *Streptomyces* sp. (CMB-M0423) secondary metabolism.

4.4.29 Effect of 4.34 on the activation of bNOS in *Streptomyces* sp. (CMB-M0423)

Having established that **4.34** possessed a unique ability to activate heronapyrrole B (**4.02**) biosynthesis, and having established that heronapyrrole B (**4.02**) biosynthesis was dependent on a functioning bNOS, we hypothesized that **4.34** was a regulator/activator of bNOS. To test this hypothesis required experimental evidence of a link between the addition of **4.34** and activation of bNOS. To acquire this evidence, we employed two independent but complementary approaches. The first approach set out to determine if **4.34** activation of *Streptomyces* sp. (CMB-M0423) could be suppressed by co-incubation with a NOS inhibitor. The second approach set out to detect the levels of NO in *Streptomyces* sp. (CMB-M0423) cultures that had and had not been exposed to **4.34**.

4.4.29.1 Approach #1: NOS inhibitor inactivation of 4.34

Replicate micro-bioreactor cultures of *Streptomyces* sp. (CMB-M0423) were treated with **4.34** (10 μM) in 1% DMSO on day 0, and on day 2 were treated with NOS inhibitor AG (**4.16**) (7.5 μM). After 7 days incubation the cultures were extracted *in situ* with EtOAc (2 mL) and the organic layer decanted, dried under N_2, re-dissolved in MeOH (100 μL) and analysed by HPLC-DAD-MS. This study demonstrated that activation of heronapyrrole B (**4.02**) production could be successfully inhibited by addition of AG (**4.16**) to the culture media. This result strongly suggests that **4.34**

activated bNOS, which in turn is essential for the production of heronapyrrole B (and other metabolites) (Figure 4.110).

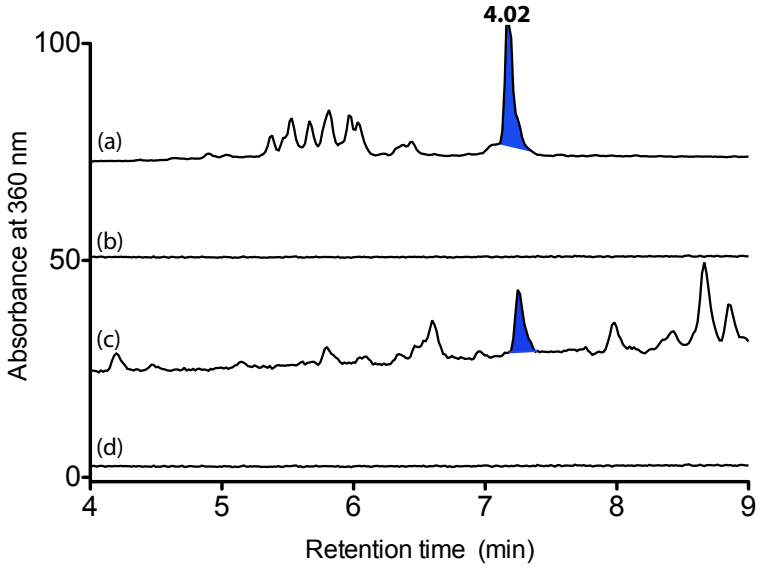

Figure 4.110. HPLC-DAD (360 nm) chromatogram of (a) standard heronapyrrole B (**4.02**). (b) *Streptomyces* sp. (CMB-M0423) exposed to **4.34** plus AG (7.5 μM), (c) *Streptomyces* sp. (CMB-M0423) exposed to **4.34** (d) *Streptomyces* sp. (CMB-M0423) only (control)

4.4.29.2 Approach #2: Measuring NO levels

As prior studies had demonstrated that *Streptomyces* sp. (CMB-M0423) exposed to **4.34** undergo bNOS mediated activation of heronapyrrole B biosynthesis, we set out to independently confirm this association by detecting and correlating NO production with heronapyrrole B production. To achieve this we employed a commercial fluorescent, nitric oxide quantification kit (total nitric oxide assay kit, assay designs, Enzo life Sciences, Ann Arbor, MI). This kit contained a proprietary dye(s) that fluoresced in the presence of NO. This commercial kit was developed to assist the revisualization and quantification of NO levels in mammalian cells, using fluorescence microscopy, so before applying the kit to *Streptomyces* sp. (CMB-M0423) it was necessary to first confirm that that the kit can work on mammalian cells. The kit was successfully trailed on mammalian cells KB-3-1 (adherent epithelial like, human cervix carcinoma) and SW620 (adherent epithelial like, human colorectal carcinoma) stimulated by LPS, with NO levels clearly visible by fluorescence microscopy – employing an BD pathway 855 high content screening confocal microscope (Olympus IX81 OEM, plan Apo 40x/0.90 LWD) (see Appendix 2).

With a functional, albeit mammalian NO fluorescence detection kit in hand, we turned our attention to *Streptomyces* sp. (CMB-M0423). Replicate micro-bioreactor cultures of *Streptomyces* sp. (CMB-

M0423) were cultured (a) without **4.34** activation, (b) with **4.34** activation (10 μM) and (c) with addition of **4.34** (10 μM) and the NOS inhibitor AG (7.5 μM). After 10 days incubation, cells of these cultures were prepared for fluorescence microscopy by treatment with the NO dye kit. Simultaneous to these studies, EtOAc extracts were prepared and analysed by HPLC-DAD. The results from these studies as illustrated in Figure 4.111, clearly indicate that in the absence of **4.34** *Streptomyces* sp. (CMB-M0423) does not produce either NO or heronapyrrole B (**4.02**) or any other co-metabolites, but that on addition of **4.34** secondary metabolism is activated as is NO production. Finally and fully consistent with our theory, addition of both **4.34** and AG (**4.16**) result in no NO and no heronapyrrole B production.

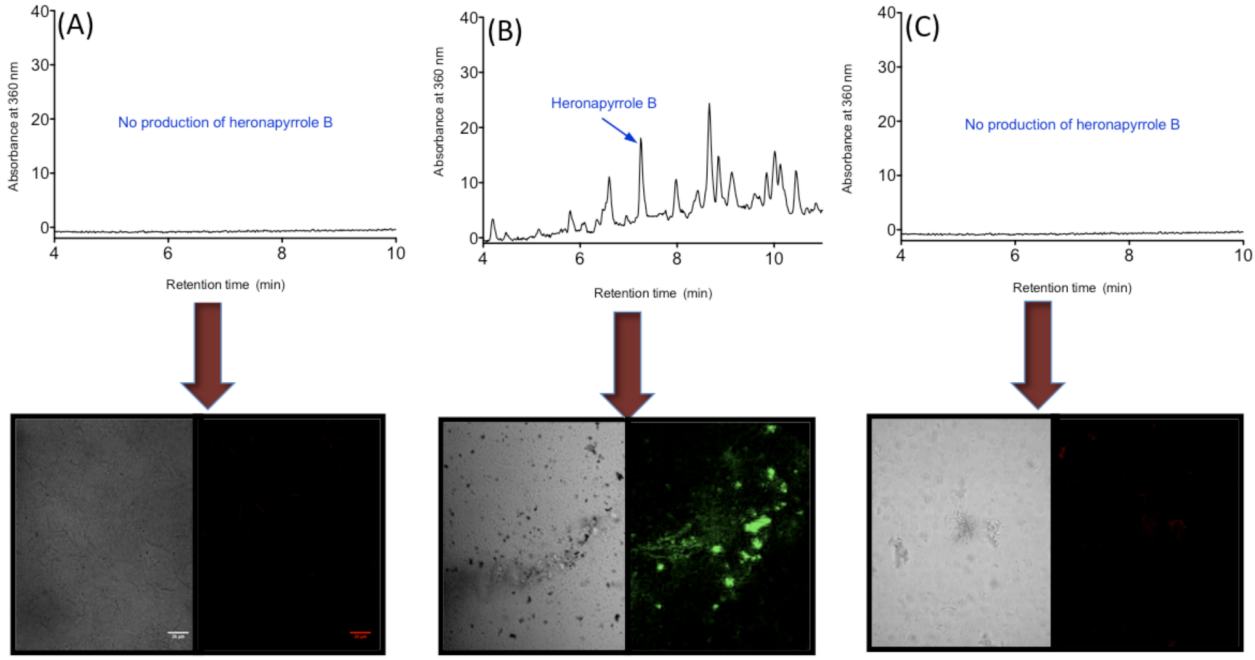

Figure 4.111. (Top) HPLC-DAD-MS chromatograms and (bottom) fluorescence images. (A) *Streptomyces* sp. (CMB-M0423), (B) *Streptomyces* sp., (CMB-M0423) with **4.34** (10 μM). (C) *Streptomyces* sp. (CMB0423) with **4.34** (10 μM) and AG (7.5 μM). Left hand images are visible light microscopy of cell cultures, while right hand images show commercial dye kit fluorescence activation of NO levels. Scale bar are 26 μm

The results of both approach #1 and #2 clearly confirm that **4.34** activates the *Streptomyces* sp. (CMB-M0423) bNOS, which subsequently produces NO, and heronapyrrole B (and the other co-metabolites).

4.4.30 The relationship between NO and heronapyrrole B production

As noted above, **4.34** activates *Streptomyces* sp. (CMB-M0423) to produce both NO and heronapyrrole B (**4.02**) (and other co-metabolites). Likewise, activation by **4.34** can be suppressed (quenched) by the addition of the NOS inhibitor AG (**4.16**). These observations support the hypothesis that, "Heronapyrrole biosynthesis is independent on a functioning bNOS delivering

NO". While the data assembled to date is strongly supportive of this hypothesis, it is necessary to challenge the possibility that **4.34** activation of NOS and heronapyrrole B are parallel and mutual exclusive events. To test this we employed two complementary approaches. In the first approach, we challenged *Streptomyces* sp. (CMB-M0423) cultures with **4.34** and the NO scavenger, 2-(4-carboxyphenyl)-4,4,5,5-tetramethylimidazoline-1-oxyl-3-oxide (CPTIO) (**4.26**), and in the second approach we challenged *Streptomyces* sp. (CMB-M0423) with the NO donor dimethylamine nitric oxide (DEANO) (**4.27**).

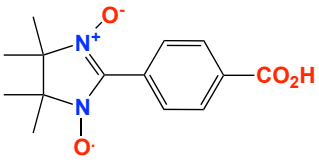

CPTIO (**4.26**)

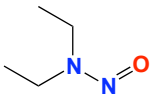

DEANO (**4.27**)

4.4.30.1 Approach #1: NO scavenger CPTIO (4.26)

A stock solution (30 mM in 30% DMSO) of CPTIO (**4.26**) was prepared and an aliquot (50 μL) transferred to micro-bioreactor wells containing 1.45 mL of M1 broth (3.3% artificial ocean sea salt and seed culture from *Streptomyces* sp. (CMB-M0423)) and **4.34** (10 μM) to deliver a final CPTIO concentration of 1 mM in 1% DMSO per well. To establish the appropriate time to add CPTIO (**4.26**) to the culture, separate trials were undertaken with addition at days 1, 5 and 6, with the cultures being extracted *in situ* with EtOAc (2 mL) on day 10 and analysed by HPLC-DAD-MS. All studies were carried out in duplicate, and delivered the same result. Despite the addition of **4.34**, addition of the NO scavenger CPTIO (**4.26**) had the effect of suppressing the production of heronapyrrole B (**4.02**). This results supports the theory that heronapyrrole B biosynthesis is dependent on NO.

4.4.30.2 Approach #2: NO donor DEANO (4.27)

A stock solution of DEANO (**4.27**) was prepared as outlined above for CPTIO (**4.26**). Aliquots (50 μL) of these stock solutions were added to three different cultures (I-III).

(I) *Streptomyces* sp. (CMB-M0423) in the absence of activation by **4.34**.

(II) *Streptomyces* sp. (CMB-M0423) activated by **4.34** (10 μM) on day 0, with NO production quenched by addition of AG (**4.16**) (7.5 μM) on day 2.

(III) *Aspergillus*/*Streptomyces* sp. (CMB-M0423) in the presence of AG (**4.16**) (7.5 μM).

In all cases (I-III), the 50 μL aliquot of the NO donor DEANO (**4.27**) was added on day 5, and the culture extracted with EtOAc (2 mL) on day 10, and the extract analysed by HPLC-DAD-MS. Despite failure to activate bNOS (I), or quenching of NO production (II-III), all these cultures produced detectable levels of heronapyrrole B (**4.02**). In the case of (III) this also coincided with suppression of *Aspergillus* sp. (CMB-M0423) secondary metabolism. This studies support the theory that heronapyrrole B biosynthesis is dependent on NO (Figure 4.114 and Figure 4.115).

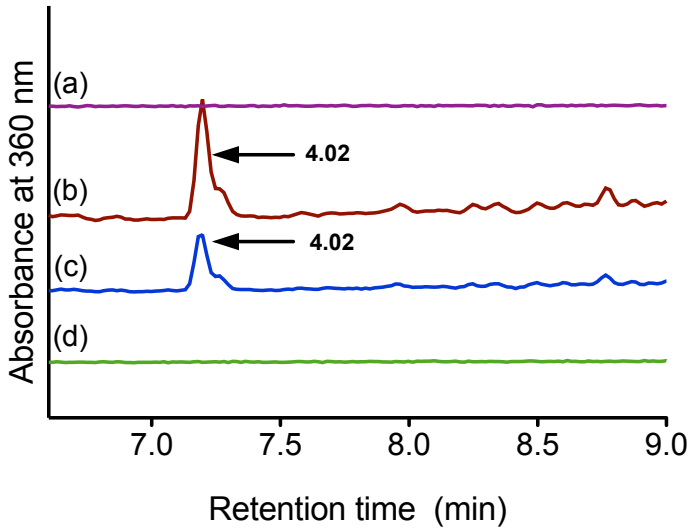

Figure 4.112. HPLC-DAD chromatograms at 360 nm for the microbial extract from *Streptomyces* sp. (CMB-M0423) in the absence/presence of **4.34**, CPTIO (**4.26**) and DEANO (**4.27**). (a)- **4.34** (10 μM) plus CPTIO (**4.26**) (1 mM). (b)- **4.34** (10 μM) plus AG (7.5 μM) plus DEANO (1 mM) showing the production of heronapyrrole B (5.7 ± 0.5 μg/mL) , (c)- *Streptomyces* sp. (CMB-M0423) plus DEANO (**4.27**) (1 mM) showing the production of heronapyrrole B (7.5 ± 0.7 μg/mL), (d)- *Streptomyces* sp. (CMB-M0423) only

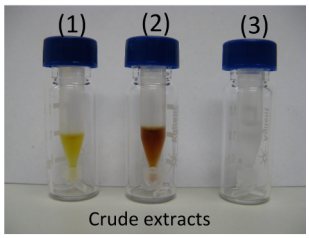

Figure 4.113. (1) *Aspergillus*/*Streptomyces* sp. (CMB-M0423) in the presence of AG (**4.16**) (7.5 μM) with no heronapyrrole B production. (2) *Streptomyces* sp. (CMB-M0423) in the presence of DEANO (**4.27**) (1mM) with heronapyrrole production. (3) *Streptomyces* sp. (CMB-M0423) with no heronapyrrole production

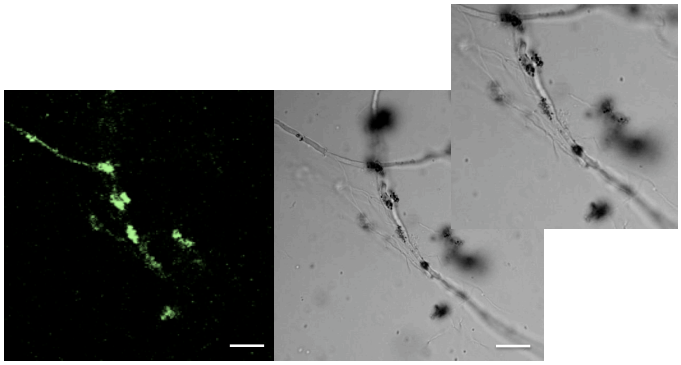

Figure 4.114. Visualization of NO production in *Aspergillus*/ *Streptomyces* sp. (CMB-M0423)

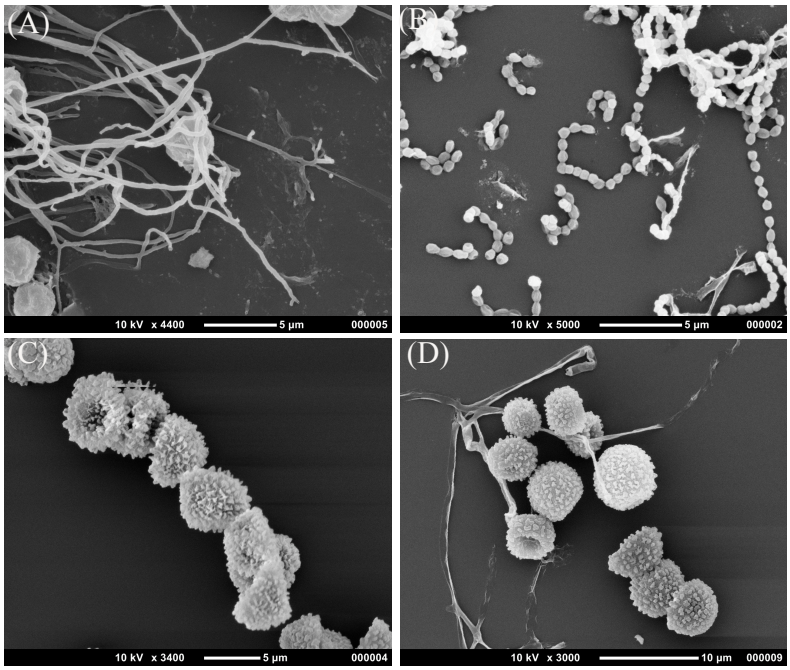

Figure 4.115. Electron microscope images. (A)- *Aspergillus* sp./*Streptomyces* sp. (CMB-M0423). (B)- *Streptomyces* sp. (CMB-M0423). (C and D)- *Aspergillus* sp. (CMB-M0423)

4.4.31 Precursor directed biosynthesis

Having established a relationship between heronapyrrole B (**4.02**), **4.34** and bNOS, the original objective of this investigation had been the manipulation of *Streptomyces* sp. (CMB-M0423) biosynthesis to deliver new (unnatural) heronapyrroles, that could be used in SAR studies to probe antibacterial properties and potentials. Unfortunately, the use of NOS inhibitors did not deliver such analogues. Nevertheless, with newfound knowledge of heronapyrrole biosynthesis we elected to expose *Streptomyces* sp. (CMB-M0423) micro-bioreactor cultures that had not been activated by addition of **4.34**, with the plausible natural biosynthetic precursor 2-nitropyrrole. The rationale behind this study was that if 2-nitropyrrole (**4.40**) could initiate heronapyrrole biosynthesis, we could then challenge *Streptomyces* sp. (CMB-M0423) cultures with a range of unnatural precursors, such as 3-nitropyrrole (**4.41**) and other nitro aromatics. The hypothesis to be tested was: addition of nitro aromatics to cultures of *Streptomyces* sp. (CMB-M0423) will yield new unnatural heronapyrroles. Before this study could proceed we first had to acquire samples of the target nitro aromatics.

4.4.32 Synthesis of 2 and 3- nitropyrrole

Samples of 2 and 3-nitropyrrole were prepared according the method described by Iranpoor *et al*. to afford 2-nitropyrrole (t_R= 10 min, 1.5 mg, 3%) (**4.40**) and 3-nitropyrrole (t_R= 12 min, 1.1 mg, 2%) (**4.41**)[179] as shown in Figure 4.116

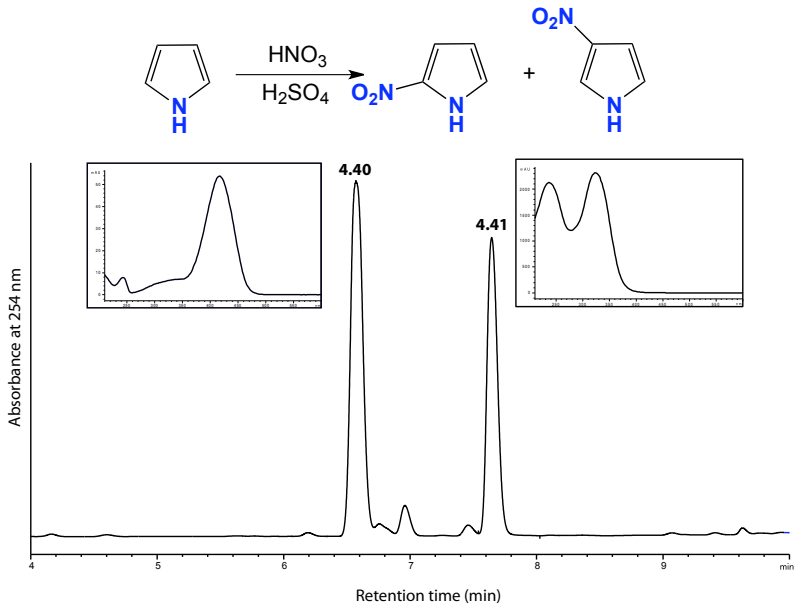

Figure 4.116. HPLC-DAD-MS chromatogram and UV-vis spectrum, analytical gradient H_2O/MeCN plus 0.05% HCO_2H using Zorbax C_8 of the nitration of pyrrole to yield 2-nitropyrrole (**4.40**) and 3-nitropyrrole (**4.41**)

4.4.32.1 2-nitropyrrole (4.40)

Compound **4.40** was synthesized as pale yellow oil, which was purified by semi-preparative gradient HPLC, 10-50% MeOH over 30 min, 3 mL/min. HRESI(+)MS showed an adduct ion $(2M+Na)^+$ consistent with the molecular formula $C_4H_4N_2O_2$ (Δmmu +0.7). The ^1H NMR ($CDCl_3$) data, for 2-nitropyrrole (**4.40**) (Figure 4.117 and Table 4.26).

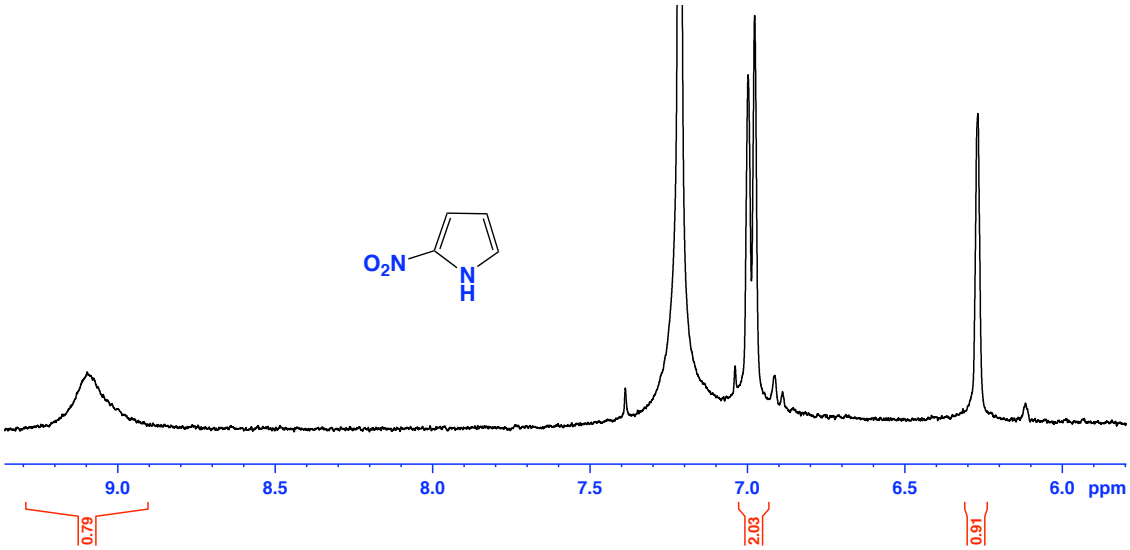

Figure 4.117. ^1H NMR (600 MHz, $CDCl_3$) spectrum of 2-nitropyrrole (**4.40**)

Table 4.26. Comparison of ^1H NMR (600 MHz, $CDCl_3$) of experimental and published[180] data of 2-nitropyrrole (**4.40**)

Pos.	δ_H, mult (*J* in Hz) **4.40** (experimental)	δ_H, mult (*J* in Hz) (published)
1-NH	9.09, br s	
2	6.99, br s	7.05, s
3-NO_2	--	--
4	6.97, br s	7.13, s
5	6.27, s	6.29, s

4.4.32.2 3-nitropyrrole (4.41)

Compound **4.41** was synthesized as pale yellow oil which was purified by semi-preparative gradient HPLC, 10-50% MeOH over 30 min, 3 mL/min. HRESI(+)MS showed an adduct ion $(2M+Na)^+$ consistent with the molecular formula $C_4H_4N_2O_2$ (Δmmu +0.6). The ^1H NMR ($CDCl_3$) data for 3-nitropyrrole (**4.41**) (Figure 4.118 and Table 4.27).

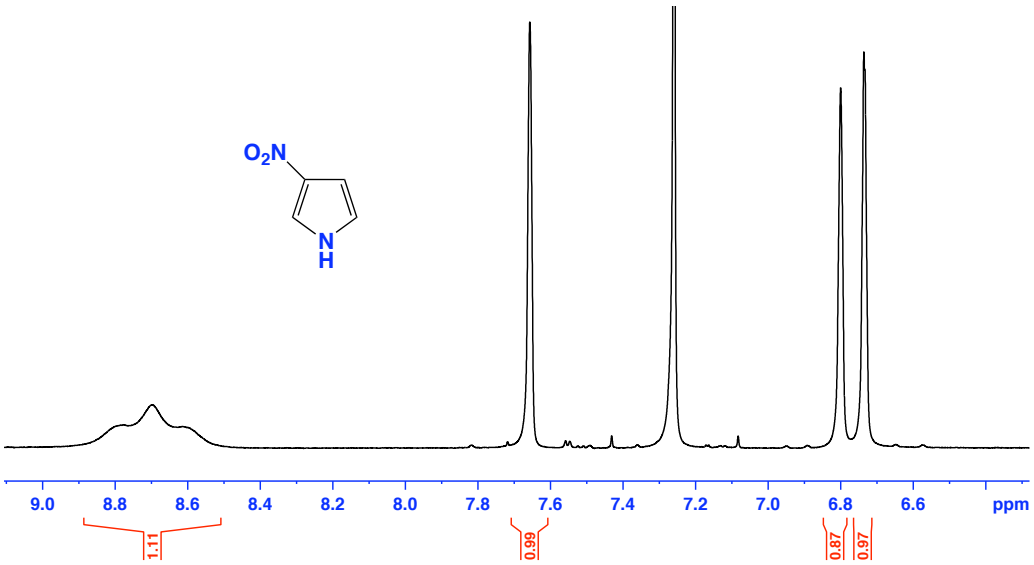

Figure 4.118. ^{1}H NMR (600 MHz, $CDCl_3$) spectrum of 3-nitropyrrole (**4.41**)

Table 4.27. Comparison of ^{1}H NMR (600 MHz, $CDCl_3$) for experimental and published[180] data of 3-nitropyrrole (**4.41**)

Pos.	δ_H, mult (*J* in Hz) (experimental)	δ_H, mult (*J* in Hz) (published)
1-NH	8.69, br	
2	7.65, br s	7.66, br s
3-NO_2		
4	6.80, br s	6.75, br s
5	6.73, d *(2.4)*	6.75 d *(2.1)*

4.4.33 Assembly of an analogue library for precursor directed biosynthesis

Different nitro-aromatics and nitrogen heterocycles were chosen as substrates for precursor directed the heronapyrrole biosynthesis in *Streptomyces* sp. (CMB-M0423) as shown in Figure 4.119. All these nitro aromatics were commercially available.

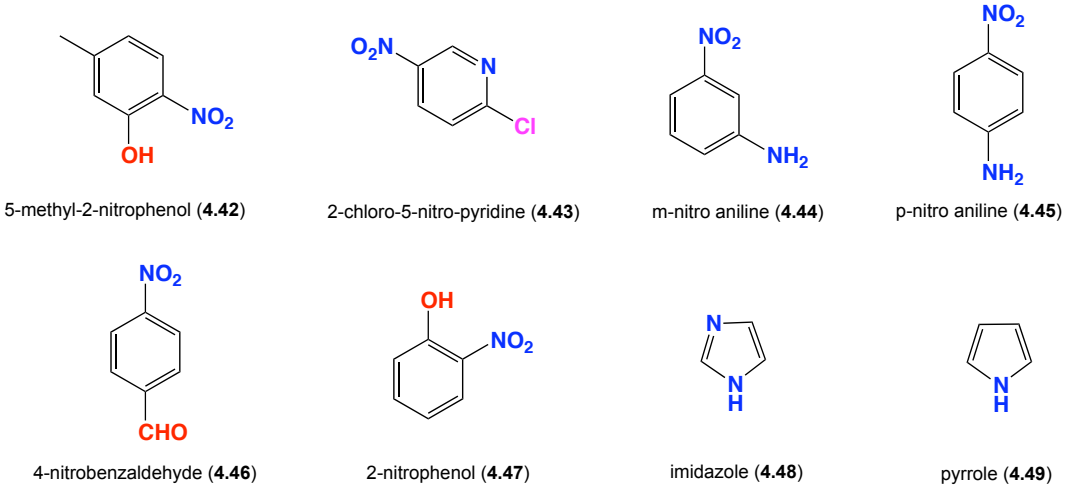

Figure 4.119. Structures of the different nitro aromatics substrates

4.4.34 Addition of 2-nitropyrrole to *Streptomyces* sp. (CMB-M0423)

This study tested the hypothesis that addition of the putative heronapyrrole biosynthetic precursor 2-nitropyrrole to a culture of *Streptomyces* sp. (CMB-M0423), which has not been activated for heronapyrrole biosynthesis, will nevertheless lead to the production of heronapyrroles with 2-nitropyrrole being incorporated into the biosynthetic pathway.

Micro-bioreactor cultures (1.45 mL) of *Streptomyces* sp. (CMB-M0423) were incubated for 10 days in the presence of 2-nitropyrrole (0.25 μM) (**4.40**). The absence of **4.34** from the culture media was designed to "ensure" that bNOS was not activated, that NO was not available, and that normal heronapyrrole biosynthesis was not activated. HPLC-DAD-MS analysis of the EtOAc extracts from these cultures confirmed the production of heronapyrrole B (**4.02**) albeit at low levels (1.1 μg/mL) (Figure 4.120). At the first glance this observation appeared to validate the hypothesis shown above, that the addition of 2-nitropyrrole provides a critical substrate essential to (re) activate heronapyrrole biosynthesis.

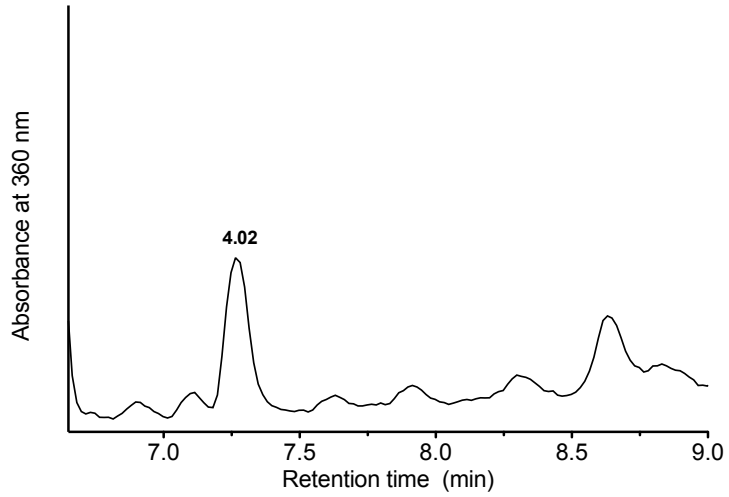

Figure 4.120. HPLC-DAD (360 nm) chromatogram of the crude extract from *Streptomyces* sp. (CMB-M0423) showing the production of heronapyrrole B (**4.02**) in the presence of 2-nitropyrrole (**4.40**) (0.25 μM)

4.4.35 Addition of 3-nitropyrrole to *Streptomyces* sp. (CMB-M0423)

Following the approach outlined above for 2-nitropyrrole (**4.40**), a culture of *Streptomyces* sp. (CMB-M0423) was challenged with 3-nitropyrrole (**4.41**). Much to our surprise addition of **4.41** to the culture media did not lead to the production of unnatural heronapyrroles isomers, rather it (re)activated the production of heronapyrrole B (**4.02**) (1.1 μg/mL). This observation suggests that **4.41** did not act as an "artificial" precursor, but rather, acted as an activator (Figure 4.121), and raises the possibility that the same was true for **4.40**.

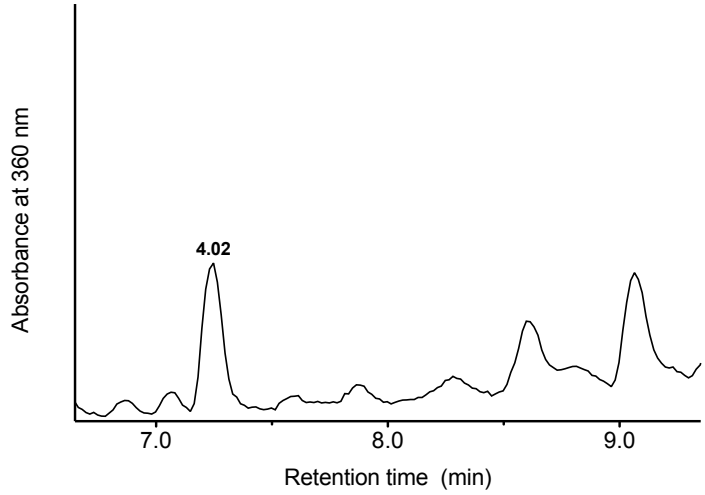

Figure 4.121. HPLC-DAD (360 nm) chromatogram of the crude extract from *Streptomyces* sp. (CMB-M0423) showing the production of heromapyrrole B (**4.02**) in the presence of 3-nitropyrrole (**4.41**) (0.25 μM)

4.4.36 Addition of other nitroaromatics to pure *Streptomyces* sp. (CMB-M0423) culture

Micro-bioreactor cultures (1.5 mL) of *Streptomyces* sp. (CMB-M0423) were incubated for 10 days in triplicate in the presence of five different concentrations (1 μM, 0.5 μM, 0.25 μM, 0.1 μM and 0.05 μM) of six nitro aromatics (5-methyl-2-nitrophenol (**4.42**), 2-chloro-5-nitropyridine (**4.43**), m-nitroaniline (**4.44**), p-nitroaniline (**4.45**), 4-nitrobenzaldehyde (**4.46**), 2-nitrophenol (**4.47**), as well as imidazole (**4.48**) and pyrrole (**4.49**). HPLC-DAD-MS analysis of the EtOAc extracts from these cultures determined that over the concentration range 0.1 to 0.5 μM, all six nitro aromatics activated production of heronapyrrole B (**4.02**) with yields ranging from 0.7 to 1.2 μg/mL. Heronapyrrole B production was not activated at either the highest (1 μM) or lowest (0.05 μM) concentration, nor was it activated by the unnitrated substrates pyrrole and imidazole. No incorporation of the nitroaromatics analogues **4.42** to **4.47** into heronapyrrole analogues was observed. These observations suggest that rather than acting as substrate for heronapyrrole biosynthesis, nitroaromatics are weak activators of bNOS, and deliver modest yields of heronapyrrole B (**4.02**).

A second round of experiments validated this hypothesis where microbioreactor cultures (1.5 mL) of *Streptomyces* sp. (CMB-M0423) were cultured in the presence of each of the nitroaromatics **4.42** to **4.47**, with and without 7.5 μM of AG (**4.16**). HPLC-DAD-MS analysis of the resulting EtOAc extracts confirmed that NOS inhibitor AG (**4.16**) quenched the ability of **4.42** to **4.47** to stimulate heronapyrrole biosynthesis (Figure 4.122).

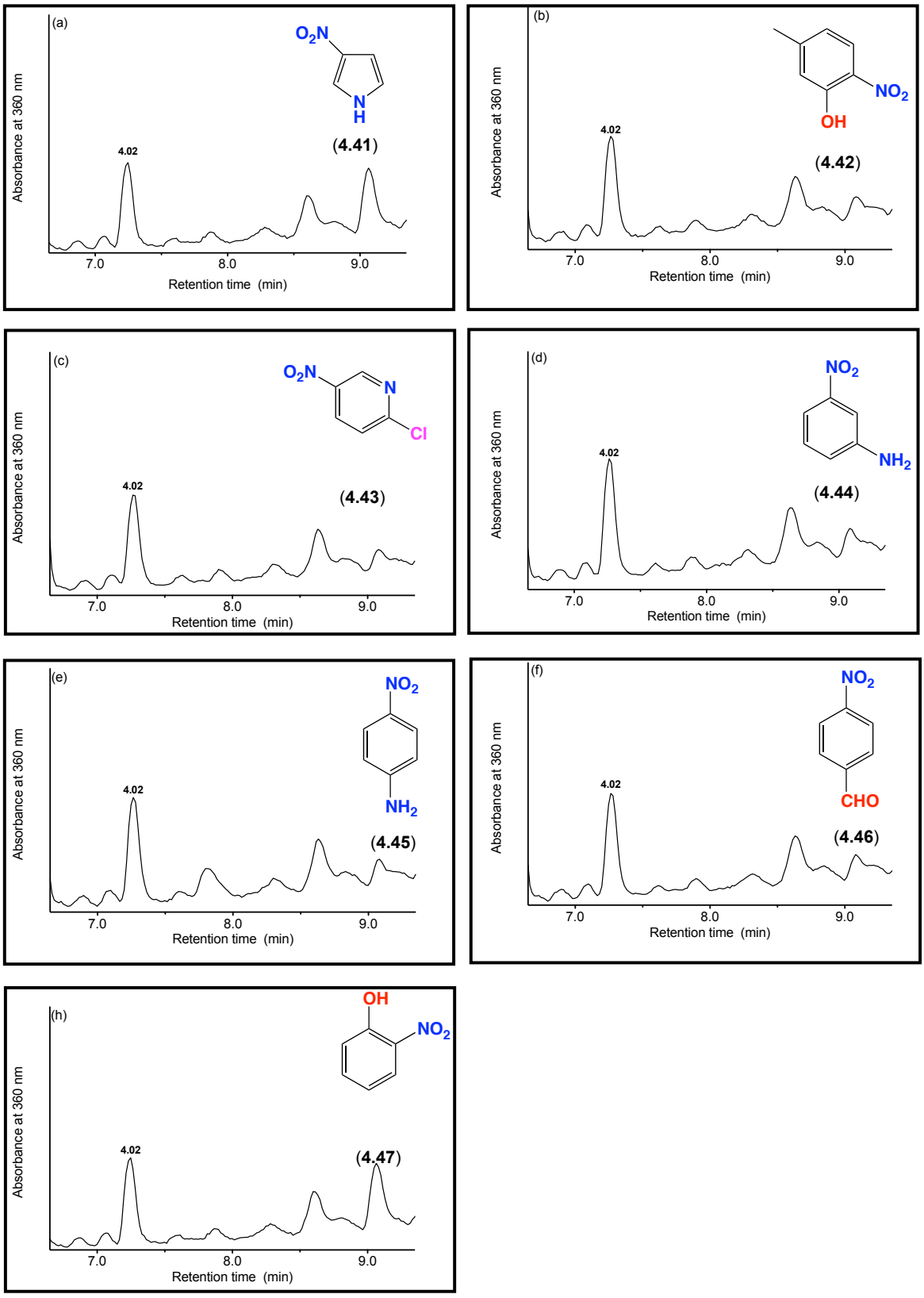

Figure 4.122. HPLC-DAD (360 nm) chromatograms of EtOAc extracts derived from *Streptomyces* sp. (CMB-M0423) culture treated with nitroaromatics (0.25 μM), yield heronapyrrole B (**4.02**) (μg/mL) (a) 1.1, (b) 0.9, (c) 0.6, (d) 1.2, (e) 0.7, (f) 0.9 and (h) 0.6 μg/mL

4.4.37 Endogenous nitroaromatic activates bNOS

The unexpected observation that nitroaromatics can act as activators of bNOS, much like **4.34**, raises the possibility that *Streptomyces* sp. (CMB-M0423) may be stimulated by DKP **4.34** to produce an endogenous nitroaromatic as an internal bNOS activator. To test this hypothesis we analysed *Streptomyces* sp. (CMB-M0423) extracts activated by **4.34**, and *Aspergillus* /*Streptomyces* sp. (CMB-M0423) extracts, using HPLC-DAD-MS single ion extraction methodology. This methodology operates by first acquiring a full HPLC-DAD-MS data set, and then selectively displaying only ions for a specific *m/z* value. As the identity of possible endogenous nitroaromatic bNOS activation was unknown, we speculated on a range of possible simple nitroaromatics, and extracted *m/z* ions accordingly.

Using this approach we determine that both extracts contained low levels of 2,4-dinitrophenol (2,4-DNP) (**4.50**). Although **4.50** is a well-known environmental pollutant associated with the manufacture of 2,4,6-trinitrotoluene (TNT) (**4.51**), to the best of our knowledge, this is the first occasion where it has been detected as a natural product (Figure 4.123).

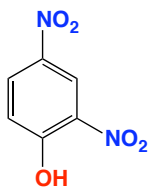

2,4-dinitrophenol (**4.50**)

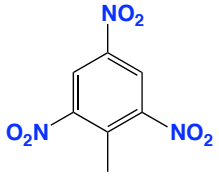

2,4,6-trinitrotoluene (**4.51**)

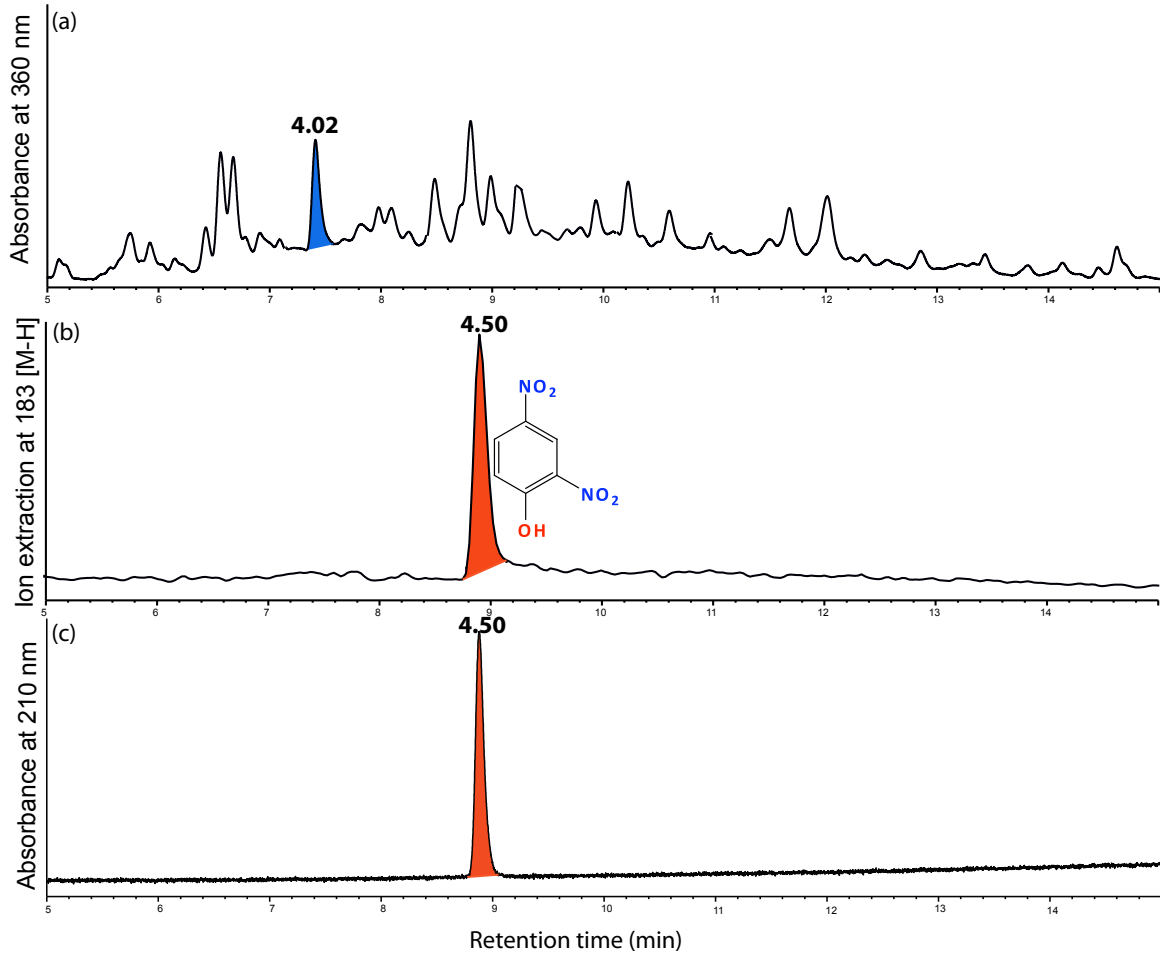

Figure 4.123. (a) HPLC-DAD-MS of the crude extract from *Aspergillus*/*Streptomyces* sp. (CMB-M0423) at 360 nm showing the presence of heronapyrrole B (**4.02**). (b) Ion extract at *m/z* 183 [M-H] showing the presence of 2,4-DNP in the crude extract of *Aspergillus*/*Streptomyces* sp. (CMB-M0423). (c) Authentic sample 2,4-DNP co-eluted at the same retention time

4.4.38 Quantify the amount of 2,4-DNP levels in the microbial culture

Based on the HPLC-DAD-MS analysis, it was clear that the concentration of 2,4-DNP (**4.50**) in microbial extracts was well below the threshold of DAD detection. Consequently, in order to quantify the levels of **4.50** in these extracts we developed a calibration curve based on HPLC-MS analysis of a series of known concentrations of an authentic sample of **4.50**. Stock solutions of **4.50** were prepared in two-fold dilutions ranging from 0.8 µM to 0.05 µM. An aliquot (10 µL) from each was then analysed using HPLC-DAD-MS. In these analyses the target ion of *m/z* 183 was extracted from the total ion using the technique of single ion extraction, and the area under the peak quantified electronically. The measurements were plotted over the range 0.008, 0.004, 0.002, 0.001 and 0.0005 nmoles (Figure 4.124) generating a linear response curve that permitted quantification of the levels of 2,4-DNP (**4.50**) in both the *Aspergillus* sp./*Streptomyces* sp. (CMB-M0423) (4.5 ± 0.1 ng/mL or 2.4 ± 0.5 nM) and **4.34** (10 µM) activated *Streptomyces* sp. (CMB-M0423) at 470 ±

0.1 ng/mL or 2.6 ± 0.5 μM). Analysis of extracts derived from *Streptomyces* sp. (CMB-M0423) and *Aspergillus* sp. (CMB-M0423) failed to detect **4.50**. These results confirm that activation of bNOS either in the co-culture *Aspergillus*/*Streptomyces* sp. (CMB-M0423), or in *Streptomyces* sp. (CMB-M0423) activated by **4.34**, leads to production of detectable levels of 2,4-DNP (**4.50**). Expectedly, where bNOS is not activated, **4.50** was not detected. This study does not however establish whether **4.50** is itself an activator of *Streptomyces* sp. (CMB-M0423) bNOS, and as such heronapyrrole biosynthesis. The detection of 2,4-DNP (**4.50**) raises the possibility that **4.50** is an internal autoregulator of bNOS, produced by *Streptomyces* sp. (CMB-M0423) in response to **4.34** activation, but capable of independent and sustained activation of bNOS and heronapyrrole biosynthesis. To test this hypothesis we exposed micro-bioreactor cultures of *Streptomyces* sp. (CMB-M0423) to a range of concentrations of **4.50**, and analysed the resulting extracts by HPLC-DAD-MS to detect heronapyrrole B (**4.02**).

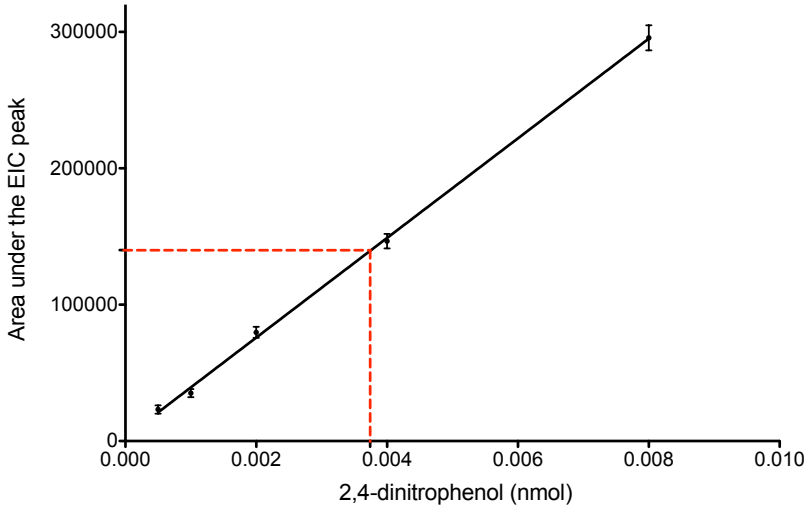

Figure 4.124. Calibration curve for 2,4-DNP (**4.50**) based on single ion extraction of m/z 183 [M-H] from the HPLC-DAD-MS chromatograph. Red dashed line equals concentration of **4.50** in an *Aspergillus*/*Streptomyces* sp. (CMB-M0423) extract

4.4.39 Study on the effect of 2,4-DNP on *Streptomyces* sp. (CMB-M0423)

Stock solutions of 2,4-DNP (**4.50**) were prepared ranging from 153 mM to 1.1 μM. An aliquot (50 μL) of each was transferred to the wells of the micro-bioreactor containing M1 broth in 3.3% artificial ocean sea salt (1.45 mL) to give final concentrations 5100 μM to 0.03 μM. All experiments were performed in duplicate. Micro-bioreactor plates were incubated at 26.5 °C for 10 days, after which the broth was extracted *in situ* with EtOAc (2 mL) and the crude extract dried under N_2. The crude residue was dissolved in MeOH (100 μL). An aliquot (10 μL) analysed using HPLC-DAD-MS. At the highest test concentration of 5100 μM and 2500 μM the production of the heronapyrrole B (**4.02**) was completely suppressed, whereas from 637 μM to 0.03 μM

heronapyrrole biosynthesis was successfully activated, with maximum production at 0.03 μM. This observation indicates that even at extremely low concentrations, 2,4-DNP (**4.50**) is capable of activating production of heronapyrrole B (Figure 4.125).

Heronapyrrole B levels in the crude extract were quantified according to the standard calibration curve reported in section 4.4.3.

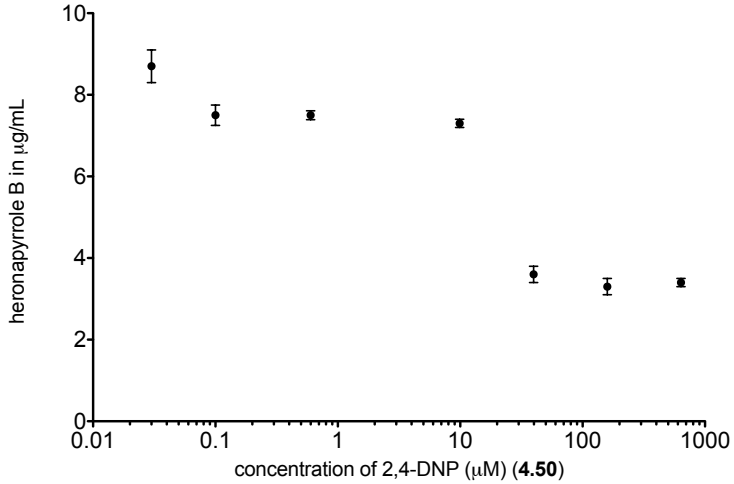

Figure 4.125. Graph showing the effect of different concentrations of 2,4-DNP (**4.50**) on the production of heronapyrrole B in *Streptomyces* sp. (CMB-M0423)

From these studies, 2,4-DNP (**4.50**) when added to *Streptomyces* sp. (CMB-M0423) in the absence of **4.34**, was able to activate the production of heronapyrrole B. Quantification of these studies confirm the 2,4-DNP (**4.50**) (3 nM) activates *Streptomyces* sp. (CMB-M0423) to produce heronapyrrole B (**4.02**) (8.1 μg/mL), a concentration 600 times lower than that required for **4.34** (1.8 μM) to deliver heronapyrrole B (8.7 μg/mL). Importantly, **4.34** activation actually initiates 2,4-DNP (**4.50**) activation.

Our investigations into the biosynthesis of heronapyrroles by what was originally believed to be *Streptomyces* sp. (CMB-M0423), but later transpired to be *Aspergillus*/*Streptomyces* sp. (CMB-M0423), has been a complex but rewarding adventure. Rather than delivering a few non-nitrated heronapyrroles with which to probe antibacterial SAR's, we uncovered an exquisite example of kingdom co-evolution. Along the way we discovered and quantified the potency of two new (first) classes of small molecule bNOS activators – one of which (2,4-DNP) appears to be an internal *Streptomyces* sp. (CMB-M0423) autoregulator of bNOS. We have proved and tested many hypotheses, and have assembled a remarkable picture of a biosynthetic regulatory system. Scheme 4.9 represents an attempt to draw all these discoveries into a single illustration of the molecular

relationships reaching from *Aspergillus* sp. (CMB-M0423) to *Streptomyces* sp. (CMB-M0423), inclusive of activators, autoregulators, bNOS, NO and heronapyrrole biosynthesis.

We have determined that *Aspergillus* sp. (CMB-M0423) releases the chemical cue **4.34**, which triggers *Streptomyces* sp. (CMB-M0423) to activate its "silent" bNOS. The resulting flux of NO leads to the production of 2,4-DNP (**4.50**), which acts as an internal regulator (an amplifier) sustaining the activation event. The need for such an amplifier presumably is in the fact that **4.34** also activate the biosynthesis of the heronapyrrole B (**4.02**) that is selectively fungistatic (12.1 μM) against *Aspergillus* sp. (CMB-M0423). As the *Aspergillus* sp. (CMB-M0423) cell density is suppressed by heronapyrrole B (**4.02**), the levels of **4.34** drop below their activation threshold. It is at this point that the amplifier properties of 2,4-DNP (**4.50**) emerge, sustain the activation event to ensure prolonged suppression of *Aspergillus* sp. (CMB-M0423) by *Streptomyces* sp. (CMB-M0423).

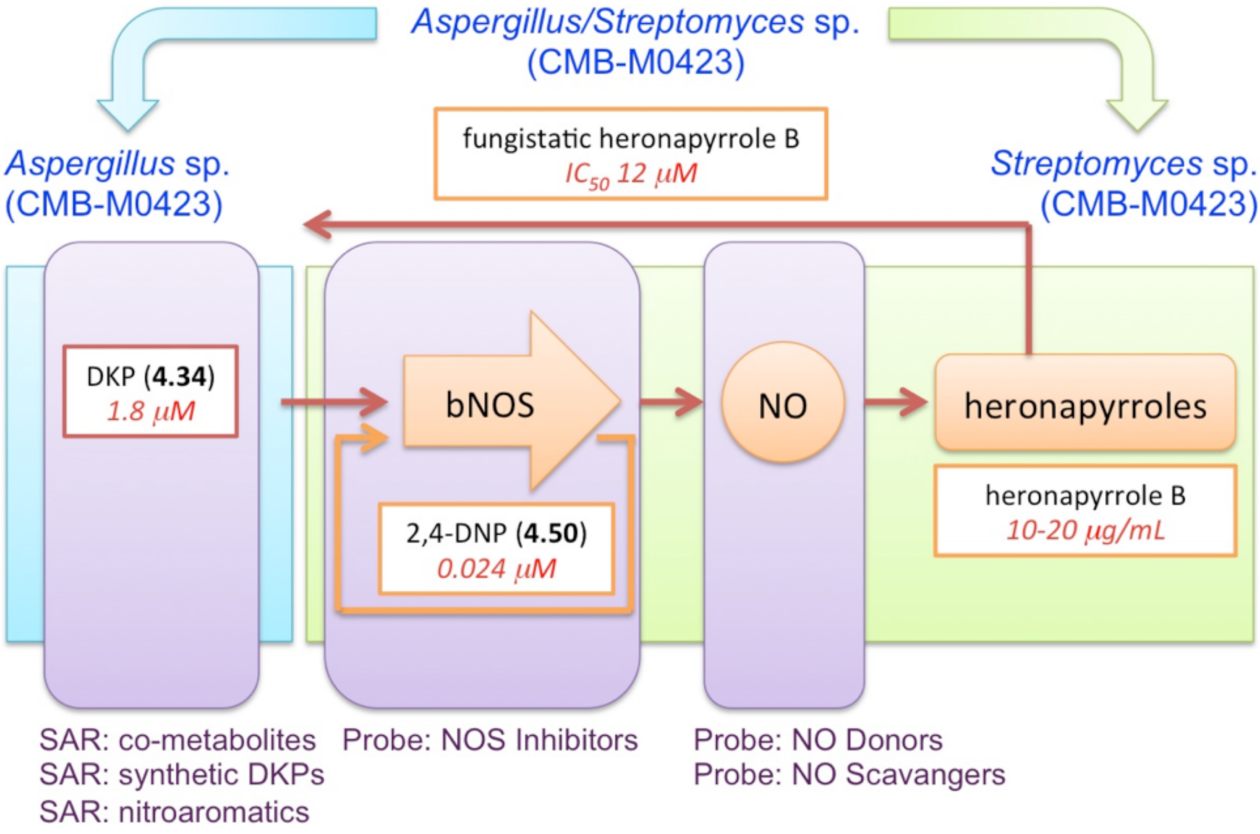

Scheme 4.9. Scheme showing the biosynthetic pathway for heronapyrrole B production

4.4.40 Heronapyrrole co-metabolites

During this study, we noticed that the heronapyrrole B (**4.02**) was always co-activated with many other metabolites, and that while it was yellow in colour the activated extracts were consistently reddish brown in colour. Semi-preparative gradient HPLC permitted the isolation and identification of the red brown pigment **4.53**, as a new member of the marinone class meroterpene (Figure 4.126 and Figure 4.127), as well as new heronapyrrole, **4.52**.

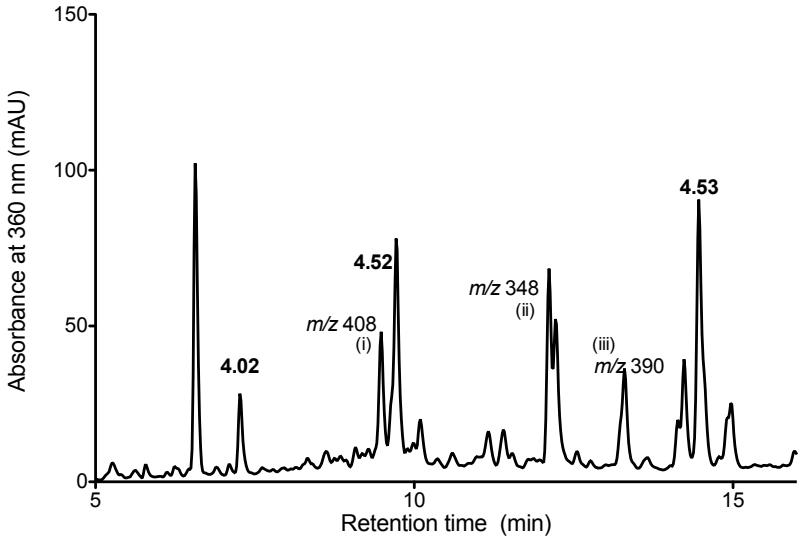

Figure 4.126. HPLC-DAD chromatogram, analytical gradient H_2O/MeCN plus 0.05% HCO_2H using Zorbax C_8 at 360 nm of the crude extract from *Aspergillus*/*Streptomyces* sp. (CMB-M0423)

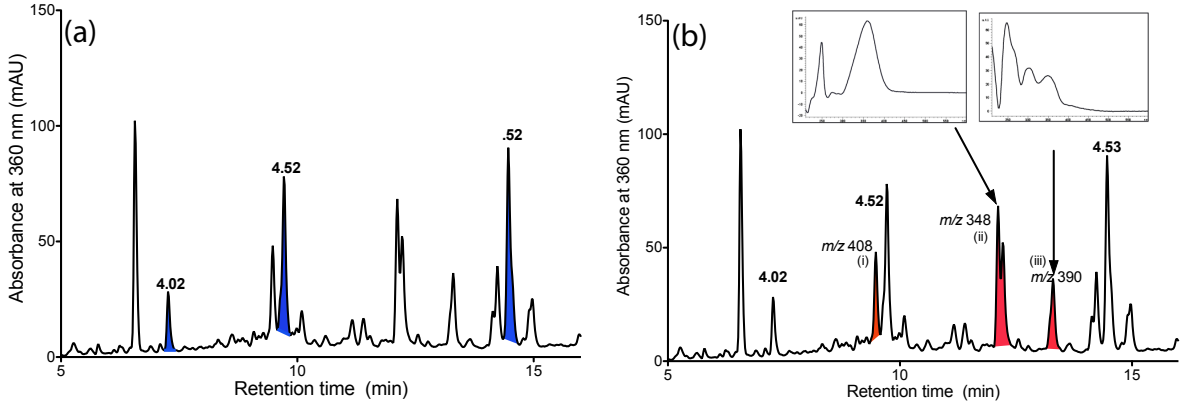

Figure 4.127. HPLC-DAD chromatogram, analytical gradient H_2O/MeCN plus 0.05% HCO_2H using Zorbax C_8 at 360 nm of the crude extract from *Aspergillus*/*Streptomyces* sp. (CMB-M0423). (a) Highlighting the metabolites that had been isolated and identified. (b) Highlighting the metabolites that are still under investigation.

4.4.40.1 Heronapyrrole D (4.52)

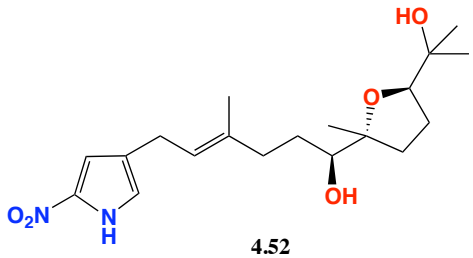

4.52

During the process of the isolating the co-metabolites produced with heronapyrrole B (**4.02**), we were able to isolate a new heronapyrrole metabolite "heronapyrrole D" (**4.52**). HRESI(+)MS analysis of **4.52** revealed a adduct molecular ion ([M+Na], *m/z* 389) that corresponds to a molecular formula ($C_{20}H_{26}N_6O_1$, Δmmu –0.2) Unfortunately, the yield of **4.52** was insufficient to acquire clear and full NMR data. Fortunately, our collaborators Prof. Stark *et al*., have synthetized **4.52** during their efforts at the synthesis of heronapyrrole C (**4.03**). Comparing both synthetic and natural samples of **4.52** by HPLC-DAD-MS (Figure 4.128) and optical rotation for synthetic heronapyrrole D $[\alpha]^{21}_D$ +82.4 (*c* 0.02, MeOH) compared to natural heronapyrrole D (**4.52**) $[\alpha]^{21}_D$ +172.4 (*c* 0.01, MeOH). The variation in the optical roataion measurement was attributed to due some impurities that were present in heronapyrrole D (**4.52**). All these data allowed us to unambiguously identify heronapyrrole D (**4.52**).

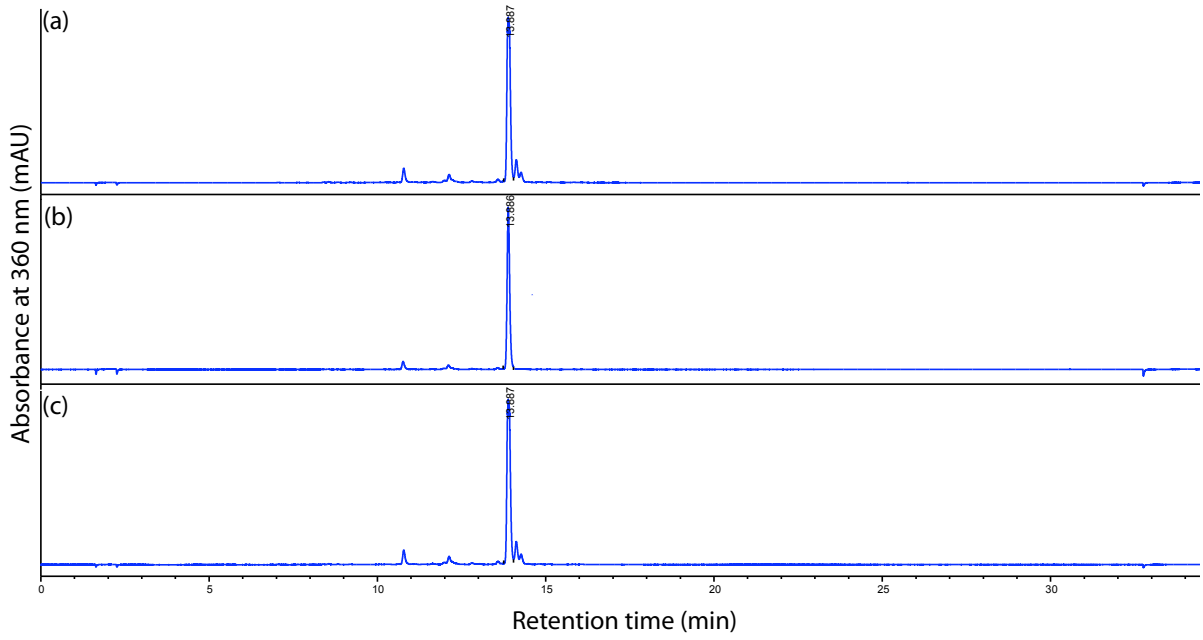

Figure 4.128. HPLC-DAD chromatogram, analytical gradient H_2O/MeCN plus 0.05% HCO_2H using Zorbax C_8 at 360 nm. (a) Natural product heronapyrrole D (**4.52**). (b) Synthetic heronapyrrole D (**4.52**). (c) co-injection of natural and synthetic heronapyrrole D (**4.52**)

4.4.40.2 Debromomarinone (4.53)

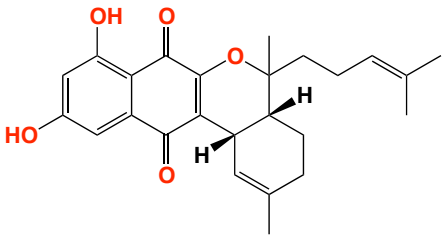

4.53

HRESI(–)MS analysis of **4.53** revealed a quasi-molecular ion ([M–H]$^-$, *m/z* 408) that corresponds to a molecular formula ($C_{25}H_{28}O_5$, Δmmu –0.25) requiring eleven double bond equivalents. Consistent with the red-brown colour and UV-vis spectrum (λ_{max} 268, 312, 386 and 440) and 1D NMR ($CDCl_3$) data for **4.53** revealed a highly conjugated aromatic system, rich in quaternary sp^2 carbons (**Table 4.28**). Furthermore, although **4.53** possessed 25 carbons, only 22 of these could be detected from the HMBC data. Notwithstanding the incomplete characterization of the 1D NMR data, analysis of 2D NMR data (Figure 4.129, Figure 4.130, Figure 4.131 and **Table 4.28**) revealed a number of diagnostic correlations corresponding to: (a) an isoprenyl side chain spanning C-17 to C-22, inclusive of C-23 and C-24; and (b) a methyl cyclohexenyl C-11 to C-16, inclusive of C-25, and pendant to the aromatic quaternary C-10. Further analysis for all the 2D data strongly suggested that **4.53** was the known bacterial metabolite debromomarinone (Table 4.29).

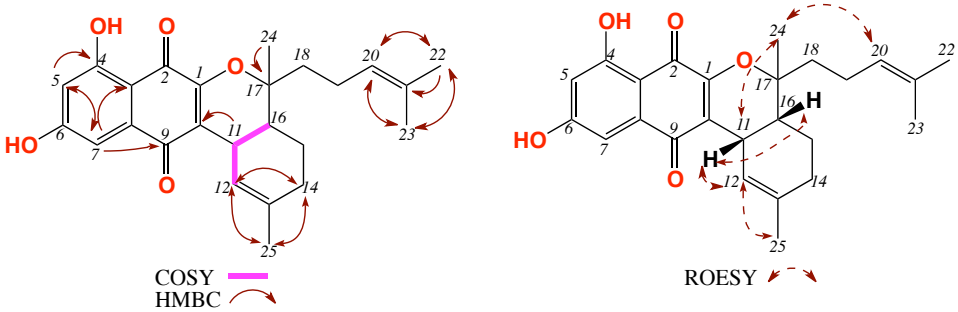

Figure 4.129. COSY, HMBC and ROESY (600 MHz, $CDCl_3$) key correlations of debromomarinone **(4.53)**

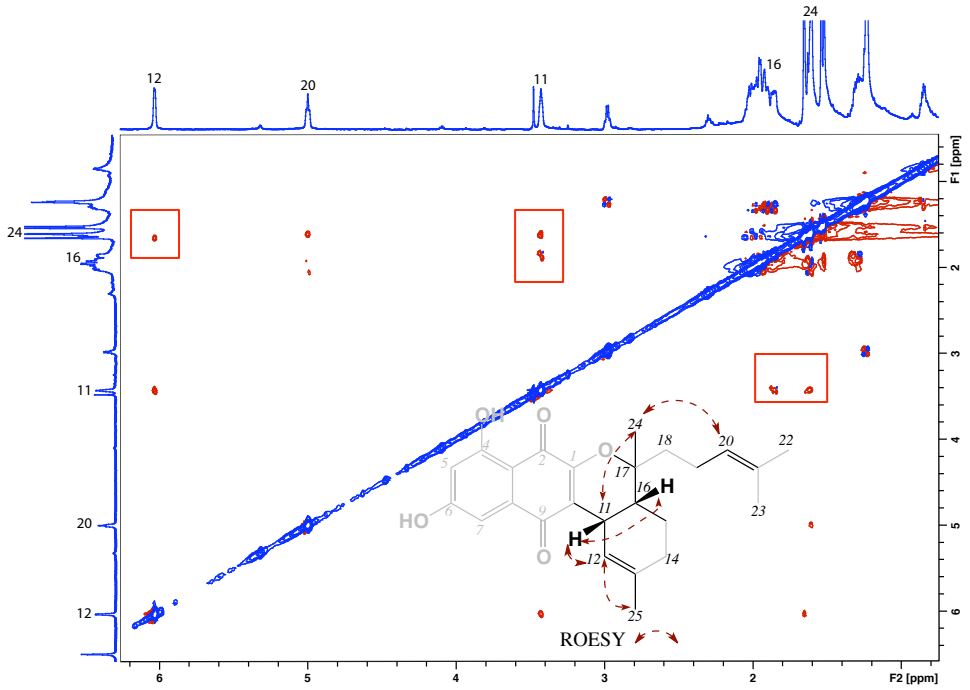

Figure 4.130. ROESY (600 MHz, $CDCl_3$) spectrum of debromomarinone (**4.53**)

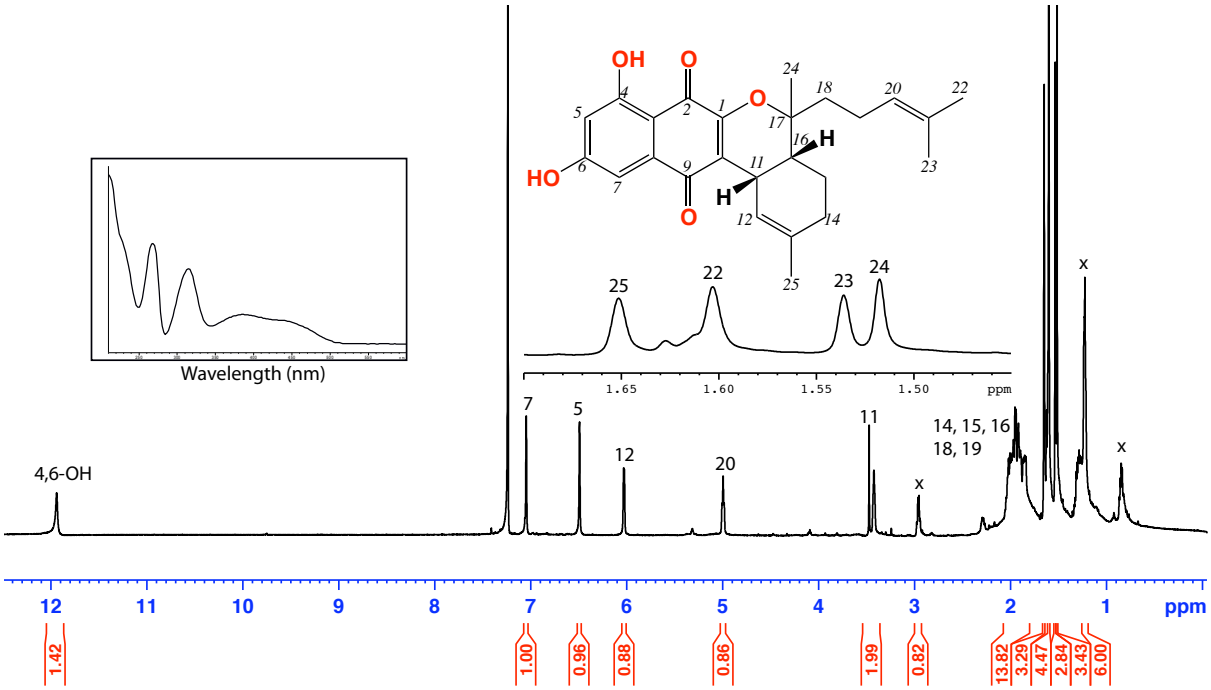

Figure 4.131. ^{1}H NMR (600 MHz, $CDCl_3$) and UV-vis (HPLC-DAD, H_2O/MeCN plus HCO_2H) spectra of debromomarinone (**4.53**)

Table 4.28. NMR (600 MHz, $CDCl_3$) data of debromomarinone (**4.53**)

Pos.	δ_H, mult (*J* in Hz)[a]	δ_C[a]	COSY	ROESY	^1H-^{13}C HMBC
1		[c]			
2		[c]			
3		108.9			
4		164.1			
5	6.49, s	107.4	7		3, 4, 7
6		163.8			
7	7.04, s	109.7	5		3, 5, 9
8		[c]			
9		184.0			
10		124.3			
11	3.43, br	31.3	12, 16	24	10
12	6.03, br	120.6	11	11, 25	11, 14, 25
13		136.0			
14	1.95[b], m	30.1			12, 25
15	1.89[b], m	20.7			
16	1.86[b], m	37.9			
17		83.1			
18	1.61[b], m	37.1			
19	1.95 – 2.02[b], m	22.7			
20	4.99, t *(6.3)*	124.1		24	22, 23
21		132.9			
22	1.60, s	26.3	23		20, 21, 23
23	1.53, s	17.8	22		20, 22
24	1.51, s	22.9			17, 20
25	1.65, s	24.2			12, 13, 14

(a)^{13}C assignments obtained from gHSQC and gHMBC data. (b) Overlapping resonances. (c) signals not observed

Table 4.29. Comparison for ^{13}C (150 MHz, $CDCl_3$) of experimental and published[181] data of debromomarinone (**4.53**)

Pos.	δ_c for (experimental)	δ_c (published)
1	[a]	153.0
2	[a]	182.5
3	108.9	109.0
4	164.1	165.1
5	107.4	106.9
6	163.8	164.4
7	109.7	107.8
8	[a]	134.5
9	184.0	184.0
10	124.3	123.8
11	31.3	30.7
12	120.6	119.9
13	136.0	135.9
14	30.1	29.6
15	20.7	20.0
16	37.9	37.2
17	83.1	82.9
18	37.1	36.5
19	22.7	22.0
20	124.1	123.0
21	132.9	132.3
22	18.0	25.4
23	23.0	17.4
24	25.8	22.4
25	23.9	23.3

(a) signals not observed

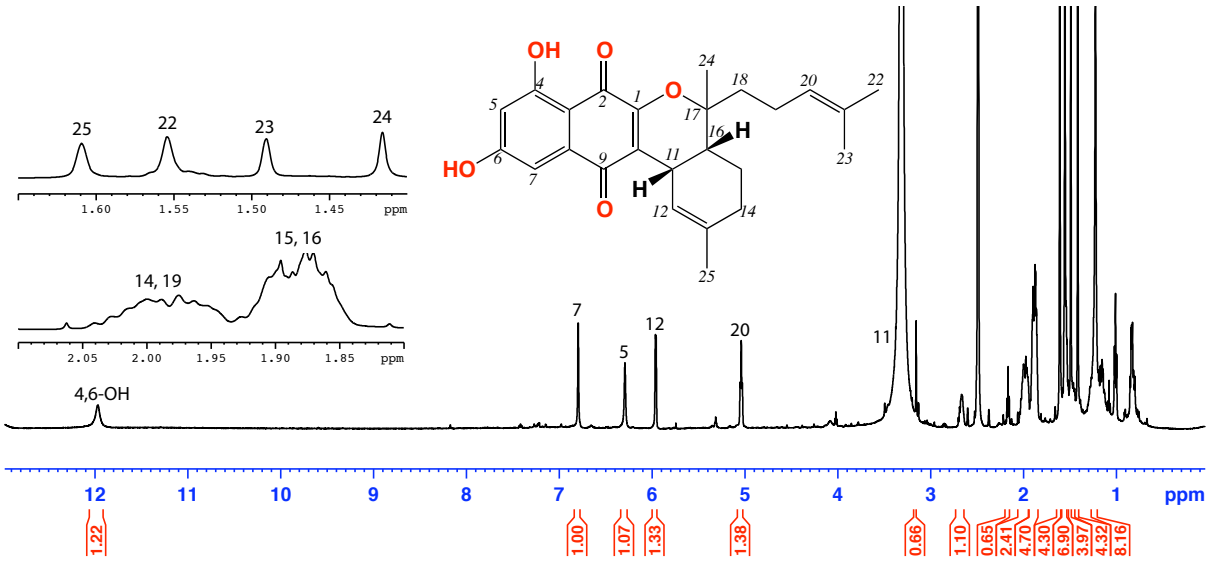

Figure 4.132. ^1H NMR (600 MHz, DMSO-d_6) spectrum of debromomarinone (**4.53**)

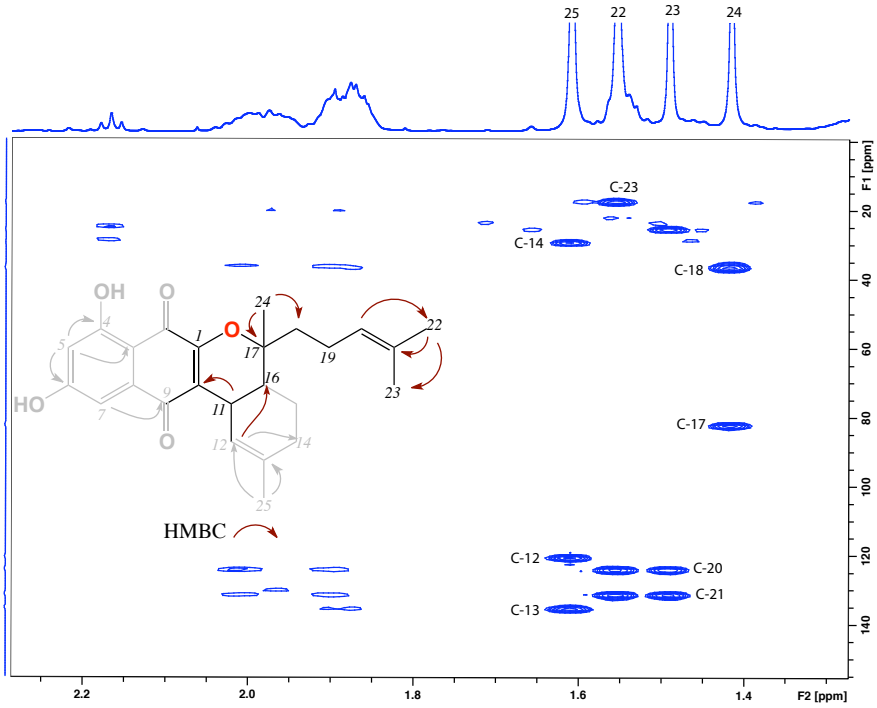

Figure 4.133. HMBC (600 MHz, DMSO-d_6) spectrum of debromomarinone **(4.53)**

Table 4.30. ^{1}H NMR (600 MHz, DMSO d_6) data of debromomarinone (**4.53**)

Pos.	δ_H, mult (J in Hz)[a]	δ_C[a]	COSY	ROESY	^{1}H-^{13}C HMBC
1		[c]			
2		[c]			
3		[c]			
4		[c]			
5	6.29, s	106.2	7		7
6		163.7			
7	6.81, s	110.1	5		5, 9
8		[c]			
9		183.8			
10		122.8			
11	3.33[c]	30.6	16	16	10
12	5.96, s	120.6			14, 16, 25
13		135.3			
14	1.89, 1.96[b], m	29.7			12, 25
15	1.85[b], m	20.1			
16	1.86[b], m	37.2	11	11	
17		82.4			
18	1.54[b]	36.3			
19	1.89, 2.00[b], m	22.1			
20	5.03, br	124.5			
21		131.3			
22	1.55, s	25.6	23		20, 21, 23
23	1.48, s	17.6	22		20, 21, 22
24	1.41, s	22.4		11	17, 18
25	1.61, s	23.9		12	12, 13, 14
4/6-OH	11.82, br s				

*(a)^{13}C assignments obtained from gHSQC and gHMBC data. (b) Overlapping resonances. (c) Obstructed by solvent

Debromomarinone (**4.53**) belongs to the meroterpenoid class of natural product, defined as mixed polyketide-terpenoid scaffold (sesquiterpenoid naphthoquinone). Members of this group include naptherpine (**4.54**)[182] and (–)-furaquinocin C (**4.55**)[183]. In 1992, Fenical *et al.*[184] reported marinone (**4.56**) and the debrominated marinone analogues (**4.57** and **4.58**) from a marine actinomycete, noting that they exhibited antibacterial activity against *Bacillus subtilis* (MIC = 1 μg/mL) with debromomarione (**4.53**) exhibiting antibacterial activity against *Staphylococcus aureus*, *Streptococcus epidermis* and *Streptococcus pyogenes* (MIC = 1 – 2 μg/mL). In 2000, Fenical *et al.*[185] reported neomarinone (**4.57**) and several other derivatives of the marionone class of the naphthoquinone (**4.56** – **4.61**) from another marine actinomycete, noting modest cytotoxicity towards human cancer cells. Although debromomarione has been reported, insufficient data exists to provide a definitive structure proof. Re-isolation of debromomarinone from **4.34** activation from *Streptomyces* sp. (CMB-M0423) offers an opportunity (for other research students in the Capon group) to revisit and confirm/revise the assigned structure.

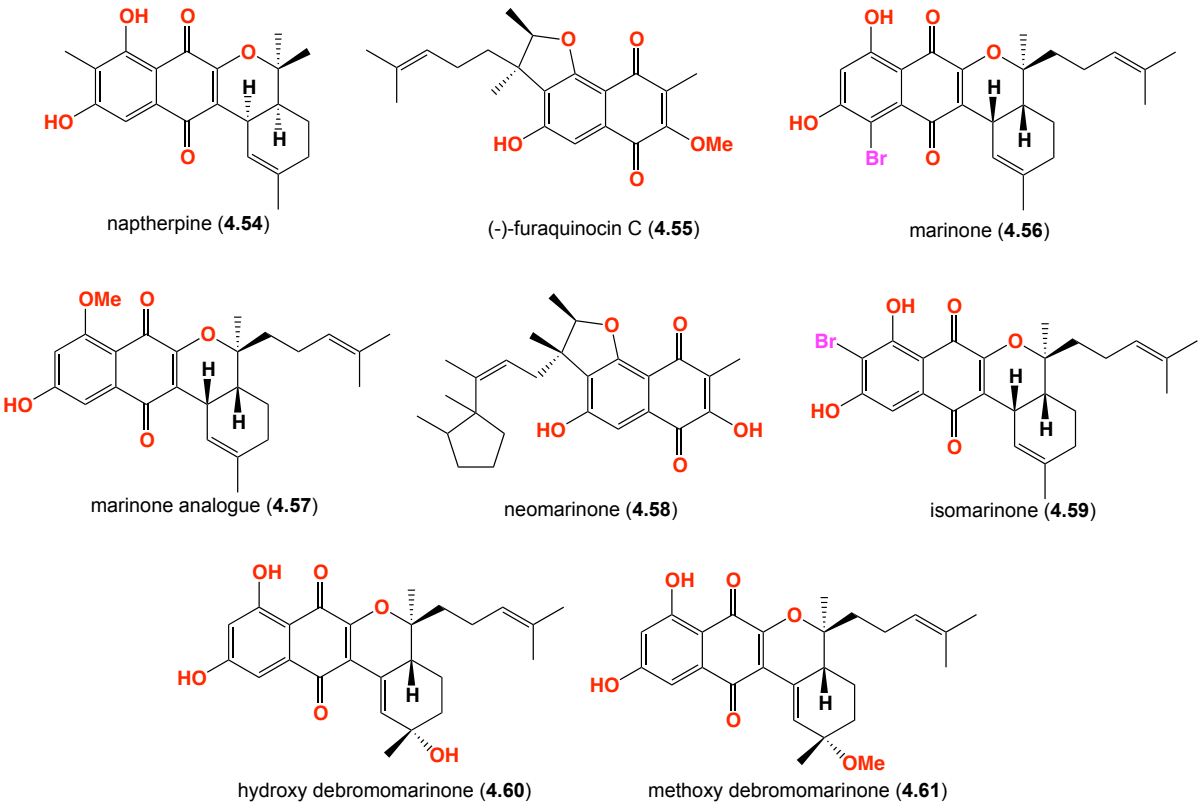

Figure 4.134. Different structures of marinone analogues

4.5 Conclusion

This chapter reports the attempts of activating the production of non-nitrated metabolites through the addition of NOS inhibitor on *Streptomyces* sp. (CMB-M0423). During a chemical investigation

into the Australian marine derived *Streptomyces* sp. (CMB-M0423), five different fungal metabolites including two low molecular weight diketopiperazines molecules have been isolated. In revisiting *Streptomyces* sp. (CMB-M0423), it was observed the presence of *Aspergillus* sp. (CMB-M0423). Many attempts had been made to separate and isolate the *Aspergillus* sp. (CMB-M0423) and *Streptomyces* sp. (CMB-M0423) in which the isolated *Streptomyces* sp. (CMB-M0423) completely lost the ability to produce its secondary metabolites. From a pharmacological standpoint, the five known fungal metabolites were assessed for the ability to induce secondary metabolites production in *Streptomyces* sp. (CMB-M0423) and it was observed that only diketopiperazine *cyclo*-(L-Phe-*trans*-4-hydroxy-L-Pro) was capable of restoring the production of secondary metabolites. From an ecological standpoint, the observations made above draw our attention to the importance of synthesis of library of different diketopiperazines to understand and compare the effect of the synthetic DKPs and the natural product (**4.34**). Results suggested that the natural DKP (**4.34**) was, in particular, the only molecule that is capable on inducing secondary metabolites in *Streptomyces* sp. (CMB-M0423). To the best of our knowledge, this is the first instance for bacterial-fungal coevolution in which intimate fungal metabolite triggers the biosynthesis of bacterial secondary metabolites.

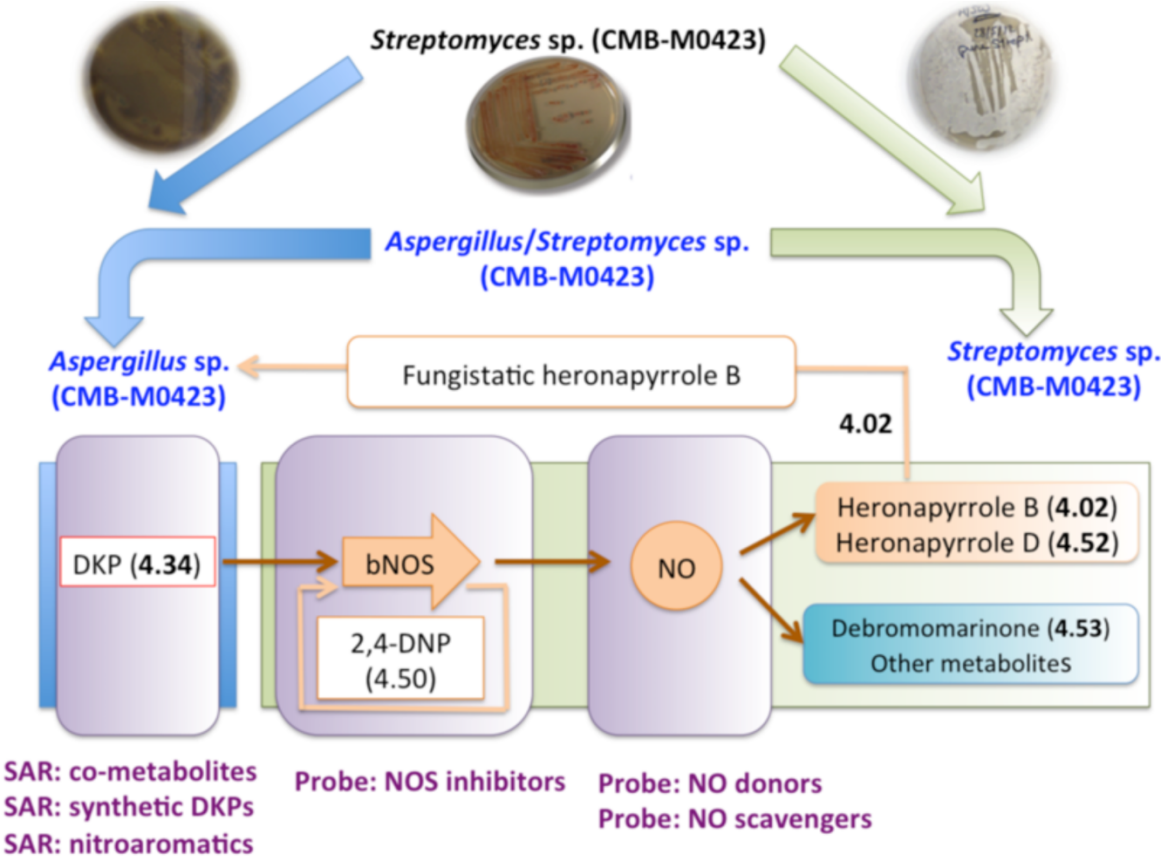

Figure 4.135. General Scheme for the NOS project

4.6 Future Directions

- Although we originally assessed heronapyrroles as not exhibiting any antifungal properties (against Candida), it appears that they may be selectively fungistatic towards *Aspergillus*. As *Aspergillus* sp. are important human pathogens, particularly in cystic fibrosis patients, this opens the possibility that heronapyrroles can be developed as an antifungal agents.
- To the best of our knowledge *Streptomyces* sp. (CMB-M0423) is unique in its ability to "indicate" the activation of bNOS. This strain is currently being developed within our research group as a screening tool to search for other small molecule activators of bNOS.
- The DKP (**4.34**) and 2,4-DNP (**4.50**) represent new tools to probe other microbes, and are currently being employed within our group to screen isolate libraries, to activate bNOS and related silent secondary metabolites.
- The full array of activated secondary metabolites in *Streptomyces* sp. (CMB-M0423) (see Figure) need to be studied. These include but are not limited to heronapyrroles and marinones.
- As both heronapyrroles and marinones depend on farnesyltransferases to farnesylate aromatic residues, its possible that the activation pathway (DKP - bNOS) triggers transcriptions/activation of prenyltransferases, which may be novel in their own right.

4.7 Experimental section

4.7.1 Analytical and Preparative cultivation of CMB-M423 in presence of AG

A single colony of strain CMB-M0423 was used to inoculate a seed culture composed of M1 media (100 mL in a 250 mL Schott flask) prepared using 3.3% artificial Ocean Nature Sea Salt. Aminoguanidine was added to the culture medium to give final concentration of 7.5 μM in 1% DMSO. The strains were shaken at 190 rpm for 7 days at 27 °C, extracted with EtOAc (2 × 50 mL per flask), and the organic phases concentrated *in vacuo* to yield a crude extract of 5.6 mg. The crude extracts were redissolved in MeOH generating a concentration of 1 mg/mL and analysed by HPLC-DAD-ESI(±) MS (Zorbax C_8 column, 150 × 4.6 mm, 5 μm, 1 mL/min gradient from 90% H_2O to 10% MeCN (isocratic 0.05% formic acid) over 15 min, with a hold at 100% MeCN for 5 min). Analysis of the small-scale saline liquid cultivation revealed biosynthetically related yellow pigments with the following retention times t_R = 7.8, 8.1, 8.5, 8.2, 5.2 and 4.8 min exhibited the following *m/z* $(M+H)^+$ 432 (**4.30**), 327 (**4.31**), 357 (**4.32**), 380 (**4.33**), 261 (**4.34**) and 245 (**4.35**) respectively.

For large scale cultivation, six Erlenmeyer flasks (2 L) containing M1 marine broth (500 mL; 1% starch, 0.4 % yeast extract and 0.2% peptone) were inoculated with a starter culture (5 mL) of *Streptomyces* sp. (CMB-M0423) and incubated at 27 °C on a rotary shaker at 190 rpm for 7 days. The flasks were then extracted EtOAc (2 × 250 mL per flask) and the organic phases were combined and concentrated *in vacuo* to yield a combined EtOAc extract (95.6 mg). The EtOAc extract was sequentially triturated (25 mL aliquots) to recover hexane (5.3 mg), CH_2Cl_2 (60 mg) and MeOH (3 mg) soluble materials. The CH_2Cl_2 partition was further fractionated by HPLC (Zorbax C_8 column, 250 × 9.4 mm, 5 μm, 3 mL/min, gradient elution from 90% H_2O/MeOH to 100% MeOH over 30 min) monitoring at 210, 254 and 360 nm to afford pure compounds pseurotin A (t_R= 21.3 min; 5.1 mg, 7.3%) (**4.30**), gliotoxin (t_R= 22.0 min; 4.5 mg, 6.4%) (**4.31**), bisdethiobis gliotoxin (t_R= 22.7 min; 3 mg, 4.3%) (**4.32**) and fumitremorgin C (t_R= 25 min; 2.4 mg, 3.4%) (**4.33**) and two diketopiperazines, *cyclo*-(L-Phe-*trans*-4-hydroxy-L-Pro) (t_R= 15.7 min; 3 mg, 3.6%) (**4.34**) and *cyclo*-(L-Phe-L-Pro) (t_R= 17.2 min; 1.5 mg, 2.3%) (**4.35**).[Note - % yields are determined on a mass-to-mass basis against the EtOAc crude extract].

Pseurotin A (**4.30**): yellowish oil; $[\alpha]^{23}_D$ −178 (*c* 0.10, $CDCl_3$); ^{1}H NMR (600 MHz, $CDCl_3$) see **Table 4.2**; HRESI(+)MS *m/z* 454.1476 $[M+Na]^+$ (calcd for $C_{22}H_{25}NO_8Na$ 454.1472).

Gliotoxin (**4.31**): yellowish oil; $[\alpha]^{22}_{D}$ −167.2 (*c* 0.05, MeOH) ;^{1}H NMR (600 MHz, $CDCl_3$) see **Table 4.4**; HRESI(+)MS *m/z* 349.0278 $[M+Na]^+$ (calcd for $C_{13}H_{14}N_2O_4Na$ 349.0287).

Bisdethiobis(methylthio)gliotoxin (**4.32**): yellowish oil; $[\alpha]^{22}_{D}$ −67.2 (*c* 0.1, MeOH) ;^{1}H NMR (600 MHz, $CDCl_3$) see **Table 4.6**; HRESI(+)MS *m/z* 379.0753 $[M+Na]^+$ (calcd for $C_{15}H_{20}N_2O_4S_2Na$ 379.0757).

Fumitremorgin C (**4.33**): yellowish oil; $[\alpha]^{22}_{D}$ −26.2 (*c* 0.04, MeOH) ;^{1}H NMR (600 MHz, $CDCl_3$) see **Table 4.8**; HRESI(+)MS *m/z* 402.1801 $[M+Na]^+$ (calcd for $C_{22}H_{25}N_3O_3Na$ 402.1788).

cyclo-(L-Phe-*trans*-4-hydroxy-L-Pro) (**4.34**): yellowish oil; $[\alpha]^{22}_{D}$ −20.9 (*c* 0.05, MeOH);^{1}H NMR (600 MHz, $CDCl_3$) see **Table 4.10**; HRESI(+)MS *m/z* 283.1045 $[M+Na]^+$ (calcd for $C_{14}H_{16}N_2O_3Na$ 283.1053).

cyclo-(L-Phe-L-Pro) (**4.35**): yellowish oil; $[\alpha]^{22}_{D}$ − 6.2 (*c* 0.07, MeOH);^{1}H NMR (600 MHz, $CDCl_3$) see **Table** 4.12; HRESI(+)MS *m/z* 267.1075 $[M+Na]^+$ (calcd for $C_{14}H_{16}N_2O_2Na$ 267.1104).

debromomarinone (**4.53**): reddish brown; $[\alpha]^{22}_{D}$ − 98.8 (*c* 0.02, MeOH);^{1}H NMR (600 MHz, $CDCl_3$) see **Table** 4.28; HRESI(−)MS *m/z* 407.1866 $[M-H]^-$ (calcd for $C_{25}H_{27}O_5$ 407.1864).

heronapyrrole D (**4.52**): yellow oil; $[\alpha]^{21}_{D}$ +172.4 (*c* 0.01, MeOH); HRESI(+)MS *m/z* 389.2063 $[M+Na]^+$ (calcd for $C_{20}H_{26}N_6O_1Na$ 389.2060)

4.7.2 Isolation of *Aspergillus* sp. (CMB-M0423) from *Streptomyces* sp. (CMB-M0423)

Streptomyces sp. (CMB-M423) was streaked several times on agar containing M1 3.3% artificial ocean sea salt and 1 μg/mL rifampicin and the plate was incubated at 26.5 °C for 10 d. The plate was re-cultivated continuously for 45 d (around 10 d each). After the incubation period (45 d), small dark colonies start to appear on the plate. These colonies were sub-cultivated on oatmeal agar (72 g/L) plate and incubated at 27.5 °C for another 10 d. Fungal Genomic DNA extraction: DNA extraction was performed using cetyltrimethylammonium bromide (CTAB) protocol[176](Appendix).

4.7.3 The effect of heronapyrroles A - C on the growth of *Aspergillus* sp. (CMB-M0423)

Heronapyrrole A (**4.01**), B (**4.02**) and C (**4.03**) were added to the wells of a microtiter plate to give final concentration of 0.1 μM, 1% DMSO per well. The plate was inoculated with the seed culture of *Aspergillus* sp. (CMB-M0423) (15 μL) in M1 3.3% artificial ocean sea salt (1.45 mL). The plate was shaken for 12 d at 190 rpm, 26.5 °C. An aliquot (300 μL) from each well was withdrawn each

day and the optical density was measured at 600 nm using microtiter plate reader. After the incubation period (7 d), the wells were extracted by the addition of EtOAc (2 mL) and concentrated to dryness under N_2. The crude extracts were dissolved in MeOH (100 μL) and analysed by HPLC-DAD-MS using Zorbax SB-C_8 analytical HPLC column, 5.8 μM, 150 × 4.6 mm, 1 mL/min gradient elution from 90% H_2O/MeCN to 100% MeCN (with a constant 0.05% formic acid/MeCN modifier) over 15 min monitoring at 210, 254 and 360 nm.

4.7.4 Study on the production of *Aspergillus* metabolites

Aspergillus sp. (CMB-M0423) was cultivated in M1 broth containing 3.3% artificial ocean sea salt in a 24-well micro-bioreactor plate over 10 d at 190 rpm, 26.5 °C. Each day, one well was extracted with EtOAc (2 mL). The organic layer was dried down under N_2, re-dissolved in MeOH (300 μL) and analysed using the HPLC-DAD-MS using Zorbax SB-C_8 analytical HPLC column, 5.8 μM, 150 × 4.6 mm, 1 mL/min gradient elution from 90% H_2O/MeCN to 100% MeCN (with a constant 0.05% formic acid/MeCN modifier) over 15 min monitoring at 210, 254 and 360 nm. The *Aspergillus* co-metabolites start to appear from day 4 and continue to day 6 in which it produces compound **4.30** – **4.35**.

4.7.5 The effect of the fungal metabolites on the heronapyrroles production of *Streptomyces* sp.

All the fungal metabolites listed above **4.30** – **4.35** were tested on the culture broth of *Streptomyces* sp. Compounds **4.30** – **4.35** were prepared in 2-fold dilutions starting from 5.1 mM to 0.1 nM in 30% DMSO. An aliquot (15 μL) of each dilution was transferred to a well of the microbioreactor containing M1 broth with 3.3% artificial sea salt (1.45 mL) to give final concentration 0.05 mM to 0.001 nM in 1% DMSO and seed culture from *Streptomyces* sp. (15 μL). The microbioreactor plate was incubated for 10 d, 190 rpm, 26.5 ˚C. After the incubation period, the wells were extracted by the addition of EtOAc (2 mL) and the whole microbioreactor was shaken for 1 h at 100 rpm. The organic layer was dried down under N_2 and the crude extracts were dissolved in MeOH (100 μL) and analysed using the HPLC-DAD-MS using Zorbax SB-C_8 analytical HPLC column, 5.8 μM, 150 × 4.6 mm, 1 mL/min gradient elution from 90% H_2O/MeCN to 100% MeCN (with a constant 0.05% formic acid/MeCN modifier) over 15 min monitoring at 210, 254 and 360 nm. The optical density (400 nm) of each crude extract was also recorded using a microtiter plate reader.

4.7.6 Standard curve for heronapyrrole B (4.02)

A solution of heronapyrrole B in MeOH was diluted from 0.4 mM to 0.006 µM in MeOH. An aliquot (10 µL) of each dilution was injected in HPLC-DAD-MS using Zorbax SB-C_8 analytical HPLC column, 5.8 µM, 150 × 4.6 mm, 1 mL/min gradient elution from 90% H_2O/MeCN to 100% MeCN (with a constant 0.05% formic acid/MeCN modifier) over 15 min monitoring at 210, 254 and 360 nm. The area under the peak for each concentration of heronapyrrole B was determined from the extracted chromatogram as shown below

The equation for the area under the peak:

$$y = 88.02x + 16.06$$

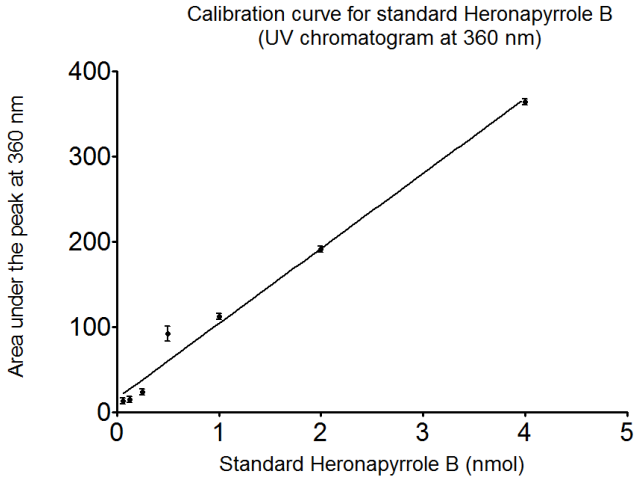

Conc of Stock Heronapyrrole B (mM)	10 µL of Stock (nmol)	Area under the peak (reference 1)	Area under the peak (reference 2)	Average	STDEV	SEM
0.4	4	366	362	364	3	2
0.2	2	194	189	191	4	3
0.1	1	114	111	112	2	1
0.05	0.5	101	83	92	12	9
0.02	0.25	23	24	24	1	0
0.01	0.125	15	16	15	1	1
0.006	0.06	12	13	13	1	0

4.7.7 Standard curve for *cyclo*-(L-Phe-*trans*-4-OH-L-Pro)

A solution of *cyclo*-(L-Phe-*trans*-4-OH-L-Pro) in MeOH was diluted from 5 mM to 0.6 µM in MeOH. An aliquot (10 µL) of each dilution was injected in HPLC-DAD-MS using Zorbax SB-C_8 analytical HPLC column, 5.8 µM, 150 × 4.6 mm, 1 mL/min gradient elution from 90% H_2O/MeCN to 100% MeCN (with a constant 0.05% formic acid/MeCN modifier) over 15 min monitoring at 210, 254 and 360 nm. The area under the peak for each concentration of *cyclo*-(L-Phe-*trans*-4-OH-L-Pro) was determined from the extracted chromatogram as shown below

The equation for the area under the peak is:

$$y = 4.049\times10^{6}x - 49991$$

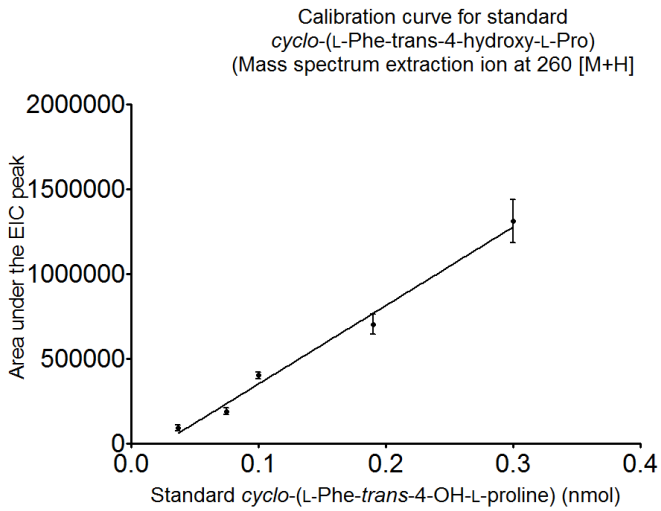

Conc of Stock DKP (mM)	10 µL of Stock (nmol)	Area under the peak (reference 1)	Area under the peak (reference 2)	Average	STDEV	SEM
0.03	0.3	1181662	1437600	1309631	180975	127969
0.02	0.19	763678	641878	702778	86125	60900
0.01	0.1	409338	391917	400627	12318	8710
0.007	0.075	189694	187505	188600	1548	1095
0.003	0.037	87973	92252	90112	3025	2139

4.7.8 Standard curve for 2,4-dinitrophenol

A solution of 2,4-DNP in MeOH was diluted from 0.008 nM to 0.0005 nM in MeOH. An aliquot (10 µL) of each dilution was injected in HPLC-DAD-MS using Zorbax SB-C_8 analytical HPLC column, 5.8 µM, 150 × 4.6 mm, 1 mL/min gradient elution from 90% H_2O/MeCN to 100% MeCN (with a constant 0.05% formic acid/MeCN modifier) over 15 min monitoring at 210, 254 and 360 nm. The area under the peak for each concentration of 2,4-DNP was determined from the extracted chromatogram as shown below

$$y = mx + b$$

$$y = 3.65\times10^{7}\,x + 2807$$

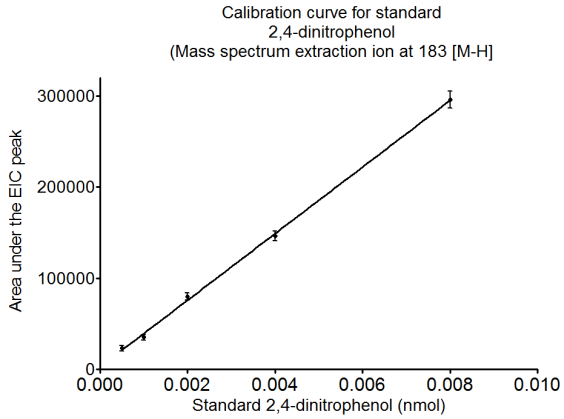

Conc of Stock 2,4-DNP (μM)	10 μL of Stock (nmol)	Area under the peak (reference 1)	Area under the peak (reference 2)	Area under the peak (reference 2)	Average	STDEV	SEM
0.8	0.008	313059	281974	291988	295674	15867	9161
0.4	0.004	148425	136600	154681	146569	9183	5302
0.2	0.002	73414	78677	87152	79748	6932	4002
0.1	0.001	34843	34720	35845	35136	618	357
0.05	0.0005	25418	21682	22373	23158	1987	1147

4.7.9 Synthesis of 2- and 3- nitropyrrole

A solution of HNO_3 (36%, 1 mL, 18 mmol) in acetic anhydride (6 mL) was cooled to 0 °C and added dropwise over 90 min to a solution of pyrrole (200 μL, 0.3 mmol) in acetic anhydride (6 mL) at − 50 ˚C. The mixture was stirred at −50 ˚C for a further 90 min and then allowed to return to room temperature over 1 h. The mixture was then poured over ice and the product was extracted into diethyl ether (4 × 100 mL). The organic layer was washed with H_2O (4 × 100 mL) and 10% aqueous Na_2CO_3 (4 × 100 mL) and concentrated *in vacuo*. The resulting mixture was purified by HPLC Zorbax 5 μm C_8, 250 × 9.4 mm column, 3 mL/min gradient elution from 90% H_2O/MeOH to 100% MeOH over 30 min) to afford 2-nitropyrrole (t_R= 10 min, 1.5 mg, 3%) and 3-nitropyrrole (t_R= 12 min, 1.1 mg, 2%) [179]

2-nitropyrrole (**4.40**): yellow oil; ^{1}H NMR (600 MHz, $CDCl_3$) see **Table 4.26**; HRESI(+)MS *m/z* 247.0431 $[2M+Na]^+$ (calcd for $C_8H_8N_4O_4Na$ 247.0438).

3-nitropyrrole (**4.41**): yellow oil; ^{1}H NMR (600 MHz, $CDCl_3$) see Table 4.27; HRESI(+)MS *m/z* 247.0418 $[2M+Na]^+$ (calcd for $C_8H_8N_4O_4Na$ 247.0438).

4.7.10 General method for the preparation of the methyl ester of the amino acids 10a-e

In a dry round bottom flask (100 mL), amino acids 10a-e (5 mmol) was dissolved in MeOH (15 mL). Thionyl chloride (0.76 mL, 9.08 mmol) was added to the solution dropwise at 0 ^{o}C under argon atmosphere. The reaction mixture was refluxed for 3 h then evaporated under N_2. Toluene (2 × 5 mL) was added and evaporated *in vacuo* to afford the hydrochloride salt of methyl ester of amino acids 11a-e.

4.7.11 General method for the preparation of the diketopiperazine compounds

Two methylester of amino acids **4.38a-e** (20 mg) were dissolved in water (3-5 mL) in the presence of triethylamine (2.5 eq.). The reaction mixture was heated in the microwave at 140 °C and 300 W for 3 min. The reaction mixture was filtered and the precipitate was washed 2 – 3 times with water and dried *in vacuo*. The crude extract was further purified using HPLC-DAD, Zorbax 5 μm C_8, 250 × 9.4 mm column, 3 mL/min gradient elution from 90% H_2O/MeOH to 50% MeOH over 20 min) to afford different diketopiperazines **4.39a-l**.

4.7.12 General Marfey analysis for the synthetic diketopiperazine compounds

Preparation of the standards: In the 2 mL vial, 50 μL of 50 mM amino acid was added to 20 μL 1N $NaHCO_3$ followed by 50 μL 1% (w/v) D-FDAA in acetone. The two vials were heated for 60 min at 40°C. This was followed by the addition of 20 μL 1N HCl and the whole solution was diluted to 1 mL with MeCN.

Preparation of Natural product: 200 μL 6M HCl was added to 100 - 200 μg of pure compound and heated overnight at 110 °C. In following day, the sample was dried under N_2. 20 μL 1N $NaHCO_3$ and 50 μL 1% (w/v) D-FDAA in acetone were added and heated for 60 min at 40°C. This was followed by the addition of 20 μL 1N HCl.

C_3 Marfey's method: A 5 μL aliquot of the 2 standards and the natural product were injected onto a Zorbax C_3 HPLC column maintained at 50°C with flow rate 1 mL/min, consisting of mobile phase A: H_2O; mobile phase B: MeOH 15%-60% over 55 min. Mobile phase C: 1% HCO_2H in MeCN was maintained at 5% linear gradient. DAD was detected at 340 nm.[45]

cyclo-(L-Phe-*cis*-4-hydroxy-D-Pro) (**4.39b**): white powder; $[\alpha]^{22}_{D}$ −34 (*c* 0.06, MeOH); ^{1}H NMR (600 MHz, CDCl3) and ^{13}C (150 MHz, $CDCl_3$) see **Table 4.16**. HRESI(+)MS *m/z* 283.1048 $[M+Na]^+$ (calcd for $C_{14}H_{16}N_2O_3Na$ 283.1053).

cyclo-(L-Phe-*cis*-4-hydroxy-L-Pro) (**4.39c**): white powder; ; $[\alpha]^{21}_{D}$ −7.6 (*c* 0.05, MeOH), ^{1}H NMR (600 MHz, $CDCl_3$) and ^{13}C (150 MHz, $CDCl_3$) see **Table 4.17**. HRESI(+)MS *m/z* 283.1038 $[M+Na]^+$ (calcd for $C_{14}H_{16}N_2O_3Na$ 283.1053).

cyclo-(L-Phe-*trans*-4-hydroxy-D-Pro) (**4.39d**): white powder; ;$[\alpha]^{22}_{D}$ −5.4 (*c* 0.1, MeOH); ^{1}H NMR (600 MHz, $CDCl_3$) and ^{13}C (150 MHz, $CDCl_3$) see **Table 4.18**. HRESI(+)MS *m/z* 283.1047 $[M+Na]^+$ (calcd for $C_{14}H_{16}N_2O_3Na$ 283.1053).

cyclo-(L-Tyr-*trans*-4-hydroxy-D-Pro) (**4.39e**): white powder; ;$[\alpha]^{22}_{D}$ −33.9 (*c* 0.06, MeOH); ^{1}H NMR (600 MHz, MeOH-d_4) and ^{13}C (150 MHz, MeOH-d_4) see **Table** 4.19. HRESI(+)MS *m/z* 299.1003 $[M+Na]^+$ (calcd for $C_{14}H_{16}N_2O_4Na$ 299.1002).

cyclo-(L-Tyr-*cis*-4-hydroxy-D-Pro) (**4.39g**):white powder; $[\alpha]^{22}_{D}$ + 11.2 (*c* 0.05, MeOH); ^{1}H NMR (600 MHz, MeOH-d_4) and ^{13}C (150 MHz, MeOH-d_4) see **Table 4.20**. HRESI(+)MS *m/z* 299.1006 $[M+Na]^+$ (calcd for $C_{14}H_{16}N_2O_4Na$ 299.1002).

cyclo-(L-Tyr-L-Tyr) (**4.39h**): white powder; ;$[\alpha]^{21}_{D}$ −8.2 (*c* 0.08, MeOH); ^{1}H NMR (600 MHz, DMSO-d_6) and ^{13}C (150 MHz, DMSO-d_6) see **Table** 4.21. HRESI(+)MS *m/z* 349.1142 $[M+Na]^+$ (calcd for $C_{18}H_{18}N_2O_4Na$ 349.1159).

cyclo-(L-Tyr-D-Tyr) (**4.39i**): white powder; ;$[\alpha]^{22}_{D}$ 0 (*c* 0.05, MeOH);^{1}H NMR (600 MHz, DMSO-d_6) and ^{13}C (150 MHz, MeOH-d_4) see **Table 4.22**. HRESI(+)MS *m/z* 349.1133 $[M+Na]^+$ (calcd for $C_{18}H_{18}N_2O_4Na$ 349.1159).

cyclo-(L-Tyr-D-Pro) (**4.39j**): white powder; $[\alpha]^{22}_{D}$ −2.2 (*c* 0.1, MeOH); ^{1}H NMR (600 MHz, MeOH-d_4) and ^{13}C (150 MHz, MeOH-d_4) see **Table 4.23**. HRESI(+)MS *m/z* 283.1050 $[M+Na]^+$ (calcd for $C_{14}H_{16}N_2O_3Na$ 283.1053).

cyclo-(L-Tyr-L-Pro) (**4.39k**): white powder; $[\alpha]^{22}_{D}$ −6.8 (*c* 0.06, MeOH); ^{1}H NMR (600 MHz, MeOH-d_4) and ^{13}C (150 MHz, MeOH-d_4) see **Table 4.24**. HRESI(+)MS *m/z* 283.1051 $[M+Na]^+$ (calcd for $C_{14}H_{16}N_2O_3Na$ 283.1053).

cyclo-(L-Pro-L-Pro) (**4.39l**): white powder;$[\alpha]^{21}_{D}$ −5.9 (*c* 0.1, MeOH); ^{1}H NMR (600 MHz, MeOH-d_4) and ^{13}C (150 MHz, MeOH-d_4) see **Table 4.25**. HRESI(+)MS *m/z* 217.0927 $[M+Na]^+$ (calcd for $C_{10}H_{14}N_2O_2Na$ 217.0947).

4.7.13 The effect of nitro aromatic compounds on the secondary metabolites production of the pure *Streptomyces* sp.

Seed culture from *Streptomyces* sp. (CMB-M423) was cultivated in M1 broth containing 3.3% artificial sea salt for 10 d, 190 rpm, 26.5 °C. Seed culture (15 μL) was transferred to the wells of the microbioreactor plate containing 1.45 mL M1 broth containing 3.3% artificial sea salt and aminoguanidine (AG) (10 nM). The microbioreactor was incubated for 2 d at 190 rpm, 26.5 °C. In the third day, an aliquot (15 μL) of 10 nitro compounds 0.1 mg/mL (2-nitrophenol, 2-chloro-5-nitropyridine, 4-nitrobenzaldehyde, 5-methyl-2-nitrophenol, 3-nitroaniline, 4-nitroaniline, 2- and 3-nitropyrrole *trans*-2-nitrocinnamaldehyde), as well as pyrrole and imidazole were added to the wells. The plates were incubated for another 7 d, 190 rpm, 26.5 °C. After the incubation period, the wells were extracted by the addition of EtOAc (2 mL) and the plates were shaken for 1 h at 100 rpm. The organic layer was dried down under N_2, the crude extract was dissolved in MeOH (100 μL) and analysed using HPLC-DAD-MS using Zorbax SB-C_8 analytical HPLC column, 5 μM, 150 × 4.6 mm, 1 mL/min gradient elution from 90% H_2O/MeCN to 100% MeCN (with a constant 0.05% formic acid/MeCN modifier) over 15 min monitoring at 210, 254 and 360 nm.

4.7.14 Study on the effect of 2,4-DNP on the induction of heronapyrroles

Table 4.31. Average production of heronapyrrole B in the presence of different concentrations of 2,4-DNP

Concentration of 2,4-DNP (μM)	Average amount of heronapyrrole B ± 0.7 (μg/mL)
637	3.4
159	3.3
39.8	3.6
9.9	7.3
2.5	5.3
0.6	7.4
0.1	7.4
0.03	8.7

4.7.15 NO donor and scavenger assays

Four plates were set for the NO donor and NO scavenger studies. At the onset of of heronapyrrole production, after approximately 4 – 5 days, NO donor or scavenger were added to the cultures, dissolved in 30% DMSO. The cultures were returned to the shaker and were futhur incubated for another 4 – 5 additional days. During this incubation period, a sample (200 μL) where withdrawn everyday for extraction with EtOAc (200 μL) and then dried down under N_2 and the colorimetric absorbance was measured at 400 nm spectrophotometrically. Also, another sample (200 μL) was

withdrawn to measured at 600 nm spectrophotometrically as described above. Each experiment consisted of two to three replicates and each experiment was independently repeated twice.

4.7.16 The effect of synthetic diketopiperazines on the induction of NO in cancer cells and pure *Streptomyces* sp.

Nitric oxide detection kit consists of NO detection reagent (red), NO inducer (L-arginine) as positive control, NO scavenger (c-PTIO) and wash buffer.

4.7.16.1 Reagents preparation according to manufacturer's instructions:

1. Dilution of NO detection reagent: An aliquot of the NO detection reagent (2.5 μL) was diluted 1:400 with pre-warmed culture medium (1 mL) immediately prior to use.

2. Positive control: The NO inducer (L-arginine) was supplied as a stock (100 mM) in deionized water. A final concentration per well is 1 mM. Therefore 2 μL of the stock was transferred to 198 μL of the cell culture medium.

3. Negative control: The NO Scavenger (c-PTIO) was supplied as lyophilized powder, which was dissolved in dry DMF (100 μL) to produce a stock solution of 4 mM.

4. 1× Wash buffer: The wash buffer was supplied as a 10× solution, which was diluted 1/10 with deionized water to give a 1× working concentration.

4.7.16.2 Cell Preparations

Two cell lines were chosen for the assay, KB-3-1 (adherent epithelial like, human cervix carcinoma) and SW620 (adherent epithelial like, human colorectal carcinoma). Both cells, KB-3-1 and SW620 were cultivated in 96 well plates 3 d prior to the experimental day to ensure 50-70% confluency in the day of the experiment. The cells were seeded in the plates in 2 different concentrations. KB-3-1 was seeded in plates to give final concentration 8000 cells/well, while SW620 was seeded in the plates to give final concentration 8000 cells/well. The plates were incubated at 37 °C for 3 d. On the day of the experiment, KB-3-1, 8000 cells/well gave confluency around 60% and for SW620, 8000 cells/well gave approx. confluency of 70% and the media used were DMEM for KB-3-1 and RPMI1640 for SW620 supplemented with L-glutamine and no phenol red.

4.7.17 BD microscope

The KB-3-1 and SW620 cells were loaded with the pre-diluted NO detection reagent (50 μL) to ensure that the reagent covered the monolayers of the cells and the plates were incubated for 2 h. After 1 h and half, NO Scavenger (2 μL) was added to the negative control wells. After the incubation period, the NO reagent was removed carefully and the cells were washed with 50 μL of 1× wash buffer. Fresh medium without phenol red (DMEM for KB-3-1 and RPMI1640 for SW620) supplemented with L-glutamine, was added to all wells (198 μL). KB-3-1 and SW620 cells were treated with experimental test agents (L-arginine, lipopolysaccharide (LPS) from *Escherichia coli* O111:B4 purchase from Sigma-aldrich, *cyclo*-(L-Phe-*trans*-4-hydroxy-L-Pro), 2,4-dinitrophenol. Stock solutions (100 mM) of each agent were prepared in DMF and serially diluted to give a final concentration (two fold dilution) per well 1 mM to 0.001 μM. An aliquot (2 μL) of each dilution was transferred to the wells of 96 well Nunc microtiter plate. LPS solution was prepared in two-fold dilution in water to give final concentration 2 μg to 2.5 ng per well. Other DKPs were tested at only one concentration (1 mM/1% DMF). After the addition of the compounds, the plates were incubated at 37 °C, 5% CO_2 for another 20 min. After the incubation period, the cells were washed twice with 1X wash buffer (50 μL). The plates were observed using BD microscope using objective 10X Olympus. *Streptomyces* sp. (CMB-M0423) was cultivated in MatTek plates (Coverglass bottom culture dishes, 12 mm well, ProSciTech Pty Ltd, Australia) in 200 μL M1 broth containing 3.3% artificial ocean sea salt. An aliquot (2 μL) from *cyclo*-(L-Phe-*trans*-4-hydroxy-L-Pro) to give a final concentration 0.6 mM, 0.1 mM, 0.03 mM, 9.9 μM and 0.3 μM in 1% DMSO of each was added to the plates and the plates were incubated at 26.5 ˚C, 190 rpm for 10 d.

4.7.18 Electron Microscope

4.7.18.1 Sample processing and imaging

Coverslips coated with poly-L-lysine (1 mg/mL) were inverted onto plates, then left for 5 min for samples to adhere. Coverslips were then immersed in 3% glutaraldehyde in 0.1 M sodium cacodylate buffer for 1 h before being washed twice in the same buffer for 5 min. Samples were then dehydrated in a series of ethanols before being dried in a critical point dryer (Autosamdri-815, Tousimis) according to manufacturer's instructions. Coverslips were attached to stubs with double-sided carbon tabs and coated with gold using an SPI-Module sputter coater (SPI) following manufacturer's instructions. Samples were imaged in a Jeol Neoscope JCM 5000 at an accelerating voltage of 10kV.

5 Chapter 5: Rare marine-derived fungal alkaloids reveal diketomorpholines as inhibitors of P-glycoprotein-mediated multi-drug resistance in cancers, and a promising new scaffold for medicinal chemistry

5.1 Introduction

The diketopiperazine (DKP) motif is well represented among natural products, particularly fungal metabolites, with structural diversity inclusive of fused heterocycles, prenylation, polythio bridging, dimerization, nitration, halogenation, oxidation and far more. Commonly assumed to be produced by nonribosomal peptide synthases,[186] the recent discovery of a DKP cyclase suggests a more complex biosynthetic landscape.[187] The potent (and selective) biological properties displayed by many natural DKPs,[175] combined with their ready availability from fungal cultivation, and the ease with which they can be synthesized and manipulated, has made the DKP scaffold an attractive and valuable resource for drug discovery.[188] It is therefore surprising that, given the diverse and extensive literature surrounding DKPs, the sister diketomorpholine (DKM) scaffold has attracted so little attention. Accounts of DKM natural products are rare, being largely limited to only a handful of fungal metabolites. To our knowledge, the first instance diketomorpholine natural product was reported in 1959, when Abe *et al*.[189] isolated ergosecalinine (**5.01**) from the ergot *Calviceps purpurea*. In 1993, Hasumi *et al*.[190] isolated lateritin (**5.02**) from the mycelia of *Gibberella lateritium* as a new inhibitor of acyl-CoA: cholesterol acetyl transferase (ACAT). In 2010, further studies were carried out on lateritin (**5.02**), documentating its cytotoxic activity against different human cancer cell lines (pancreas, breast, CNS, lung, colon and prostate), antimicrobial activity against Gram positive bacteria (*Staphylococcus aureus* ATCC 29213, *Enterococcus faecalis* ATCC 29212 and *Streptococcus pneumonia* ATCC 6303) and antifungal activity against *Candida albicans* ATCC 90028 and *Micrococcus luteus*)[191] In 1995, Kagamizono *et al*.[192] isolated bassiatin (**5.03**) from *Beauveria bassiana* (K-717), and demonstrated its inhibitory effect against platelet aggregation. The structure of bassiatin was proved by chemical synthesis and X-ray crystallography.

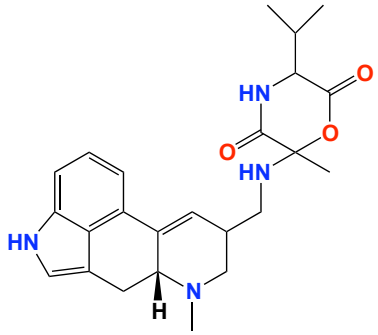

ergosecalinine (**5.01**)

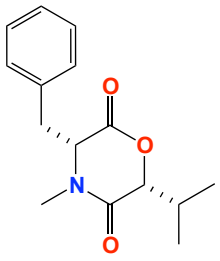

lateritin (**5.02**)

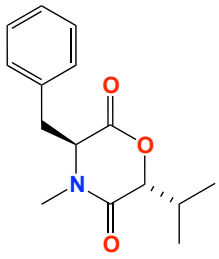

bassiatin (**5.03**)

In 1997, two new diketomorpholines, mollenine A (**5.04**) and B (**5.05**) were isolated from *Eupenicillium molle* in which mollenine A (**5.04**) exhibited moderate cytotoxicity and antibacterial activity.[193] Another example of diketomorpholines are PF1233A (**5.06**) and B (**5.07**), which were isolated from *Asperigllus niveus*. These two substances are voltage-dependent sodium channel blockers, useful for the control of local anesthesia, arrhythmia, epilepsy, pain and psychiatric disorder.[194] In 2005, Suntornchashwej *et al*. isolated another diketomorpholine (**5.08**) from the Thai sea hare *Bursatella leachii*.[195]

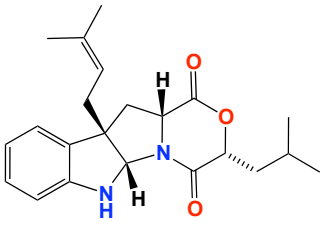

mollenine A (**5.04**)

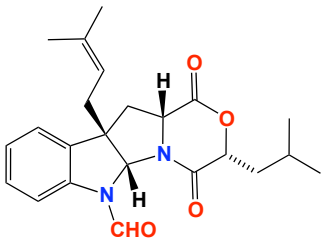

mollenine B (**5.05**)

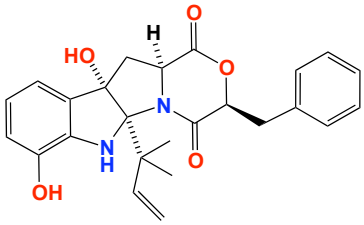

PF1233A (**5.06**)

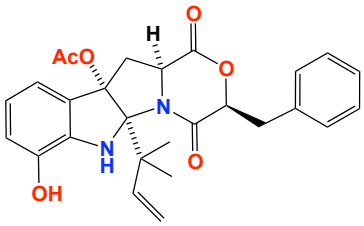

PF1233B (**5.07**)

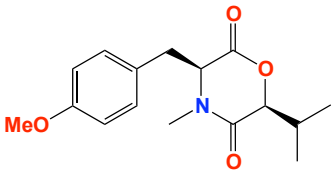

5.08

In 2006, Nakadate *et al*.[196] isolated two diketomorpholine derivatives, javanicunines A (**5.09**) and B (**5.10**) from the fungus *Eupenicillium javanicum*. These compounds possessed strong antifungal activity against *Asperigllus fumigatus* and were structural related to fructigenine B, also known as verrucofortine (**5.11**)[197] which has previously been isolated from *Penicillium verrucosum* and *Penicillium fructigenum*.[197]

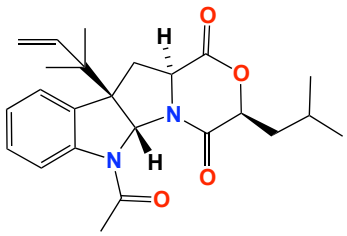

javanicunine A (**5.09**)

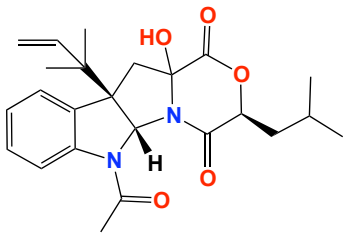

javanicunine B (**5.10**)

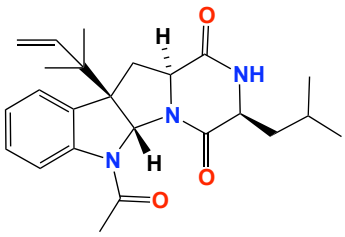

fructigenine (**5.11**)

In 2011, the three diketomorpholines **5.12** – **5.14** were isolated from a pathogenic fungus, *Fusarium sporotrichioides*.[198]

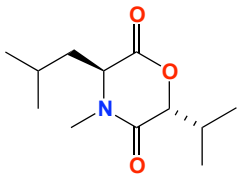

5.12

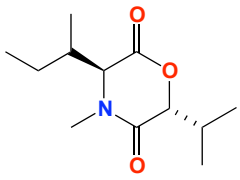

5.13

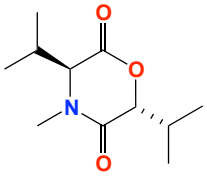

5.14

A previous PhD student in our group isolated the methyl ester **5.15** from marine derived fungus CMB-M081F isolated from marine sediment sample collected from Shorncliffe, Australia. After structure elucidation of **5.15**, it was proposed that it is an artefact due to methanolysis process that occurred during handling. We speculated that diketomorpholine (DKM) ring structure (**5.16**) consisting of the hydroxy phenyl group and the prenylated tryptophan undergoing lactone solvolysis in MeOH generating **5.15** as an artefact. This was further reinforced by the fact that the crude extract was stored in MeOH for a long time and supported by HPLC-DAD-MS studies. (Figure 5.1)

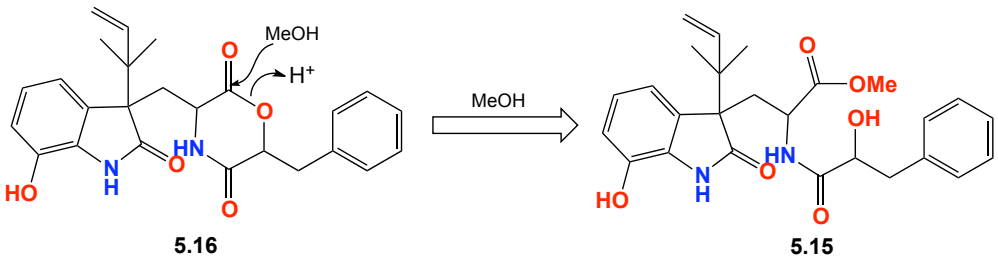

5.16 **5.15**

Figure 5.1. Proposed methanolysis of a putative natural product **5.16** to yield the artefact **5.15**

5.2 Results and discussion

5.2.1 Prior chemistry

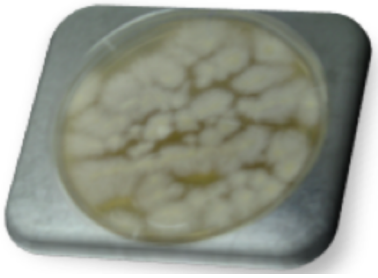

Figure 5.2. CMB-M081F

CMB-M81F was isolated from a marine sediment sample collected from Shorncliffe, QLD, Australia. A previous student studying CMB-M081F isolated and identified **5.15**. As the student made extensive use of MeOH during isolation and handling, this raised concern that the methyl ester **5.15** was an artefact caused by methanolysis. These concerns prompted a careful re-investigation of the chemistry of CMB-M81F, avoiding the use of MeOH.

5.2.2 Analytical cultivation and chemical analysis

A single colony of CMB-M81F was used to inoculate a seed culture on M1 agar media in the presence of 3.3% artificial ocean sea salt, which was cultivated for a period of 30 days. After the initial cultivation the whole agar was extracted with EtOAc (25 mL), the EtOAc extract dried *in vacuo* to yield a crude extract (10 mg), and the crude extract was resuspended in MeCN and analysed by HPLC-DAD-MS. Noteworthy peaks were observed at 11.1 min (*m/z* 435, **5.16**), 12.2 min (*m/z* 485, **5.17**), 12.4 min (*m/z* 469, **5.18**) and 12.8 min (*m/z* 499, **5.19**) (Figure 5.3).

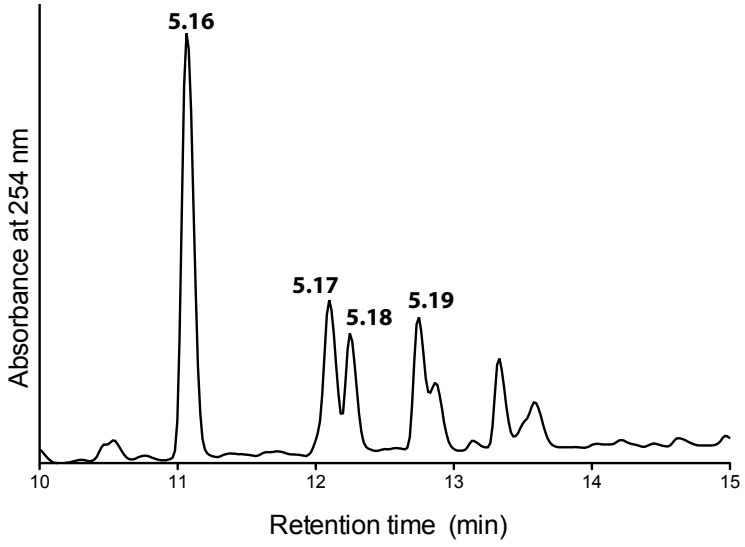

Figure 5.3. HPLC-DAD chromatogram from an analytical gradient H_2O/MeCN plus 0.05% HCO_2H using Zorbax C_8 (254 nm) of the crude extract from CMB-M81F

5.2.3 Preparative cultivation and isolation

A single colony of CMB-M81F was sub-sampled onto ten seawater M1 agar plates (300 mL of 3.3% Ocean Nature seawater, 1% starch, 0.4% yeast extract and 0.2% peptone) and incubated at 27 °C for 4 weeks. The resulting agar plates were extracted in EtOAc (500 mL) for 24 h and the organic phase concentrated *in vacuo* to yield an extract (60.2 mg). The extract was sequentially triturated with hexane (8 mL) and CH_2Cl_2 (8 mL) to afford, after concentration *in vacuo*, hexane (2 mg) and CH_2Cl_2 (60 mg) soluble fractions. The CH_2Cl_2 fraction was subsequently subjected to semi-preparative reversed-phase HPLC (Zorbax C_8 column, 250 × 9.4 mm, 5 μm, 4 mL/min gradient elution 90% H_2O/MeCN to 100% MeCN over 30 min) to yield shornephine A (**5.16**) (t_R = 23.9 min, 2 mg, 1.8%), 15b-β-hydroxy-5-*N*-acetylardeemin (**5.17**) (t_R = 25.5 min, 1.5 mg, 2.2%), 5-*N*-acetylardeemin (**5.18**) (t_R = 27.0 min, 1.9 mg, 2.5%) and 15b-β-methoxy-5-*N*-acetylardeemin (**5.19**) (t_R = 28.0 min, 1.5 mg, 3.0%) (Scheme 5.1).

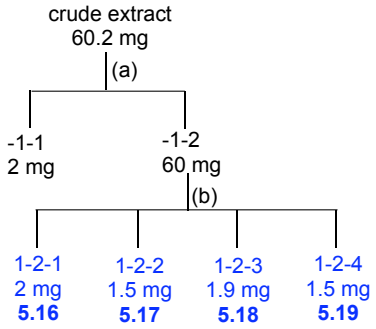

Scheme 5.1. Isolation scheme of crude extract from CMB-M081F (a) Trituration [hexane (-1-1) and CH_2Cl_2 (-1-2)], (b) Semi-preparative HPLC: Zorbax-C_8, 90 – 0% H_2O/MeCN, 3 mL/min, 30 min.

5.2.4 Structure Elucidation of fungal metabolites

5.2.4.1 *seco*-shornephine A (5.15)

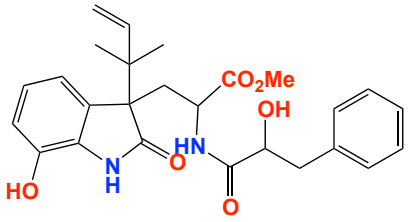

5.15

HRESI(+)MS analysis of *seco*-shornephine A (**5.15**) returned a molecular formula ($C_{26}H_{30}N_2O_6$) requiring thirteen DBE. The NMR (DMSO-d_6) data (Figure 5.5 and Table 5.1) for **5.15** revealed three ester/amide carbonyls C-10, C-1 and C-1′ (δ_C 179.7, 172.5 and 173.5) and a further fourteen sp^2 resonances (δ_C 115.6 to 143.5), accounting for ten DBE and requiring that **5.15** incorporate 3 rings. The ^{1}H and COSY NMR data indicated the presence of two isolated aromatic spin systems, the first with coupled protons H-5 (δ_H 6.56), H-6 (δ_H 6.78) and H-7 (δ_H 6.70) indicative of a 1,2,3-trisubstituted benzene system. HMBC correlations were observed from H-4 to the quaternary carbon C-4 (δ_C 55.8) and C-8a (δ_C 131.0); H-6 to the quaternary carbon C-4a (δ_C 130.0) followed by the COSY spectrum indicating a –CH-CH_2- sequence, H-2 (δ_H 3.79) and H_2-3 (δ_H 2.32, 2.24), the methlyene from this sequence H_2-3 showed HMBC correlations to the quaternary carbons C-4, C-4a, C-10 (δ_C 179.7), C-1 (δ_C 172.5) and C-11 (δ_C 42.3); and the methine H-2 to C-3 (δ_C 32.8), C-1 and C-1′ (δ_C 173.5).

This defined a C-1 to C-10 substituted tryptophan system. The carbonyl C-1 was confirmed to be a methyl ester based on HMBC correlations from the methoxy H_3-1 (δ_H 3.38) to C-1. Furthermore a monosubstituted olefin system with coupled protons signals H-13a (δ_H 5.07) and H-13b (δ_H 4.99) on the carbon C-13 (δ_C 113.8) and the third proton H-12 (δ_H 6.04, δ_C 143.5) showed coupling to a quaternary carbon C-11 (δ_C 42.3). Also observed was the HMBC correlations for the two singlet methyls H_3-14 (δ_H 1.01) and H_3-15 (δ_H 0.93) to the same quaternary carbon C-11 defining an isoprene moiety C-11 – C-15. In addition, the methyl singlets H_3-14 and H_3-15 showed HMBC correlations to the quaternary carbon C-4 to which the methylene H_2-3 and the aromatic proton H-5 also showed coupling, allowing for the construction of fragment A. The second set of aromatic signals H-5′ (δ_H 7.22), H-6′ (δ_H 7.26), H-7′ (δ_H 7.18), H-8′ (δ_H 7.26) and H-9′ (δ_H 7.22) was suggestive of a monosubstituted benzene system, an extension of this system was confirmed from the second set of methylene signals H_2-3′ (δ_H 2.79, 2.61) showing HMBC correlations to C-4′ (δ_C 138.8), C-5′ (δ_C 129.7) and C-9′ (δ_C 129.7). The COSY correlation defined a second –CH-CH_2-

system, H-2′ (δ_H 3.90) and H_2-3′. The downfield characteristic of C-2′ (δ_H 72.5) indicated a hydroxy attachment, with reconfirmation of a COSY correlation of 2′-OH (δ_H 5.53) to H-2′. The following correlation was indicative of a hydroxy phenylalanine representing structural fragment B of **5.15** (Figure 5.4). This accounted for the molecular formula lacking in a hydroxy functionality that was positioned at C-8 of the first aromatic system. The complete planar structure of **5.15** was achieved by the key HMBC correlation of the amide (δ_H 7.35) to C-2 and C-1′ linking the two fragments together.

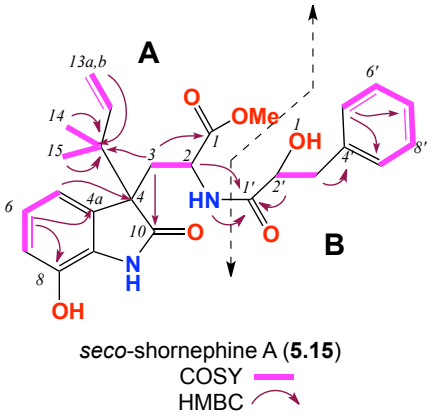

Figure 5.4. Key 2D NMR (600 MHz, DMSO-d_6) correlations of *seco*-shornephine A (**5.15**)

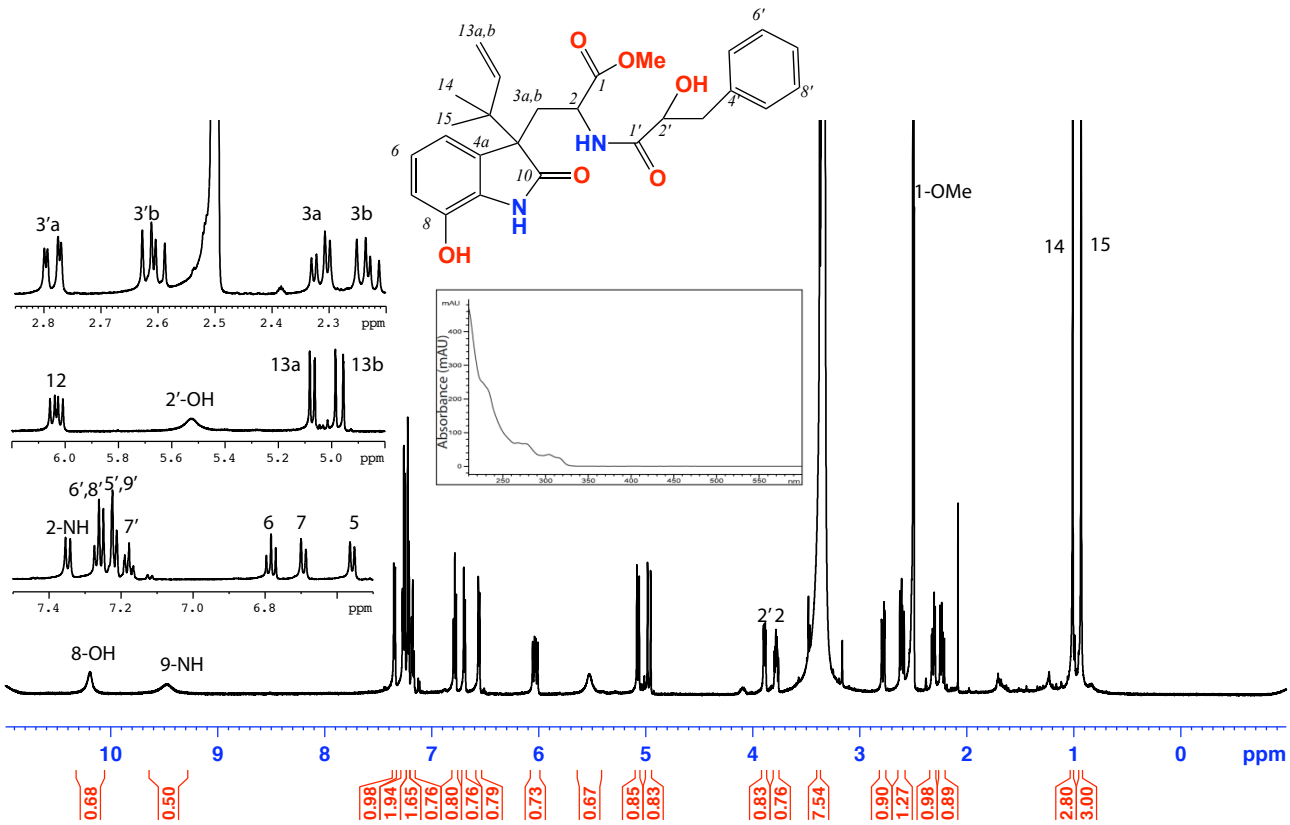

Figure 5.5. ^{1}H NMR (600 MHz, DMSO-d_6) and UV-vis (HPLC-DAD, H_2O/MeCN plus HCO_2H at 254 nm) spectra of *seco*-shornenine A (**5.15**)

Table 5.1. NMR (600 MHz, DMSO-d_6) data of *seco*-shornephine (**5.15**)

Pos.	δ_H, mult, (*J* in Hz)	δ_C[a]	COSY	ROESY	$^1H - ^{13}C$ HMBC
1		172.5			
2	3.79, ddd, (*13.8*, *9.6*, *4.8*)	49.8	3a/b, 2-NH	5, 2-NH	3, 1, 1′
3	a 2.32, dd, (*13.8*, *4.8*)	32.8	3b, 2	5	10, 4a, 4, 2, 1, 11
	b 2.24, dd, (*13.8*, *9.6*)		3a, 2	2-NH	10, 4, 4a, 2, 1, 11
4		55.8			
4a		130.0			
5	6.56, d, (*7.8*)	117.0	6	3a, 2, 12, 14, 15	4, 7, 8a
6	6.78, t, (*7.8*)	121.4	5, 7		4a, 8
7	6.70, d, (*8.4*)	115.6	6		5, 8, 8a
8		141.5			
8a		131.0			
9	9.50, br s				
10		179.7			
11		42.3			
12	6.04, dd, (*17.4*, *10.8*)	143.5	13a/b	5, 14, 15	11, 15
13	a 5.07, dd, (*10.8*, *0.6*)	113.8	12		11
	b 4.99, dd, (*17.4*, *0.6*)		12		11, 12
14	1.01, s	22.1		5, 12	4, 11, 12, 15
15	0.93, s	21.8		5, 12	4, 11, 12, 14
1′		173.5			
2′	3.90, dd, (*9.6*, *3.6*)	72.5	3′a/b	2-NH	1′
3′	a 2.79, dd, (*13.8*, *3.6*)	40.4	2′, 3′b		2′, 4′, 5′/9′
	b 2.61, dd, (*13.8*, *9.6*)		2′, 3′a		2′, 4′, 5′/9′
4′		138.8			
5′	7.22, d[b], (*7.2*)	129.7[c]	6′		7′, 5′/9′
6′	7.26, dd, (*7.2*, *0.6*)	128.2[c]	5′/9′, 7′		4′, 6′/8′
7′	7.18, dd, (*7.2*, *0.6*)	126.3	6′/8′		5′/9′
8′	7.26, dd, (*7.2*, *0.6*)	128.2[c]	7′, 5′/9′		4′, 6′/8′
9′	7.22, d, (*7.2*)	129.7[c]	6′/8′		5′/9′, 7′
1-OMe	3.38, s	52.1			1
2-NH	7.35, d, (*7.8*)		2	3b, 2, 2′	2, 1′
8-OH	10.2, br s				
2′-OH	5.53, br s		2′		

*(a) assignments supported by HSQC and HMBC. (b) Overlapping resonances. (c) Interchangeable resonances

5.2.4.2 Shornephine A (5.16)

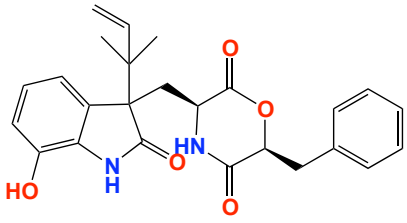

(5.16)

HRESI(+)MS analysis of shornephine A (**5.16**) revealed a quasi-molecular ion $[M+H]^+$ corresponding to a molecular formula ($C_{25}H_{26}N_2O_5$, Δmmu +0.3) requiring 14 double bond equivalents (DBE). The 1D and 2D NMR ($CDCl_3$) data for **5.16** revealed a number of diagnostic resonances and correlations that could be assembled into significant structure fragments. For example, COSY correlation sequences from H-2′ to H-3′, and from H-7′ to H-8′ to H-9′ (inclusive of H-5′ and H-6′ due to symmetry), supported by HMBC correlations from H_2-3′ to C-1′, C-4′ and C-5′/9′, together with deshielded ^{13}C NMR resonances for C-2′ (δ_C 78.5) and carbonyl C-1′ (δ_C 167.2) consistent with oxymethine, and suggestive of phenyl lactic acid residue (Fragment A) (Figure 5.6). Likewise, COSY correlation sequences from H-5 to H-6 to H-7, and diastereotopic methylene H_2-3 to H_1-2 supported by HMBC correlations from H-6 to C-8 (δ_C 141.4) and from H-5 to C-4a (136.3) and H-2 to C-1 (δ_C 167.7) suggestive of tryptophane residue (Fragment B). In addition, COSY correlation sequences from H-12 to H-13 supported by HMBC correlation from H_3-14/15 to C-12 (δ_C 144.1) suggesting isoprene residue (Fragment C) (Figure 5.6). All these data supported by the previous data from *seco*-shornephine A (**5.15**) strongly suggest the structure of shornephine A (**5.16**) (Figure 5.7 and Figure 5.8).

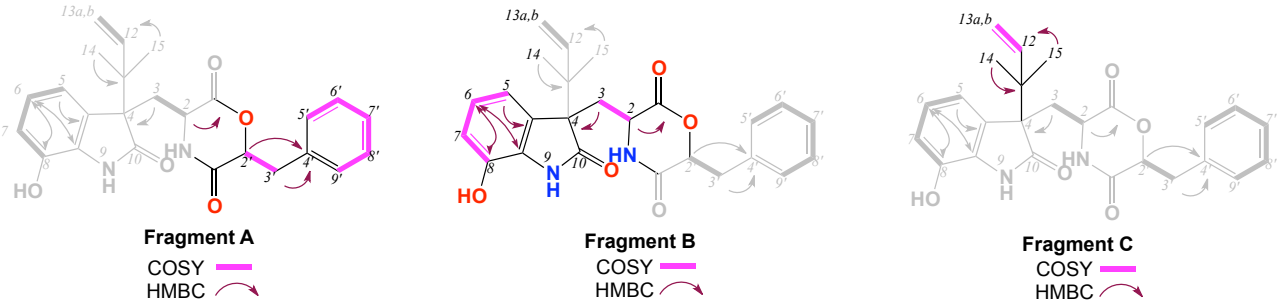

Figure 5.6. Key 2D NMR (600 MHz, $CDCl_3$) correlations of shornephine A (**5.16**) for fragment A, B and C

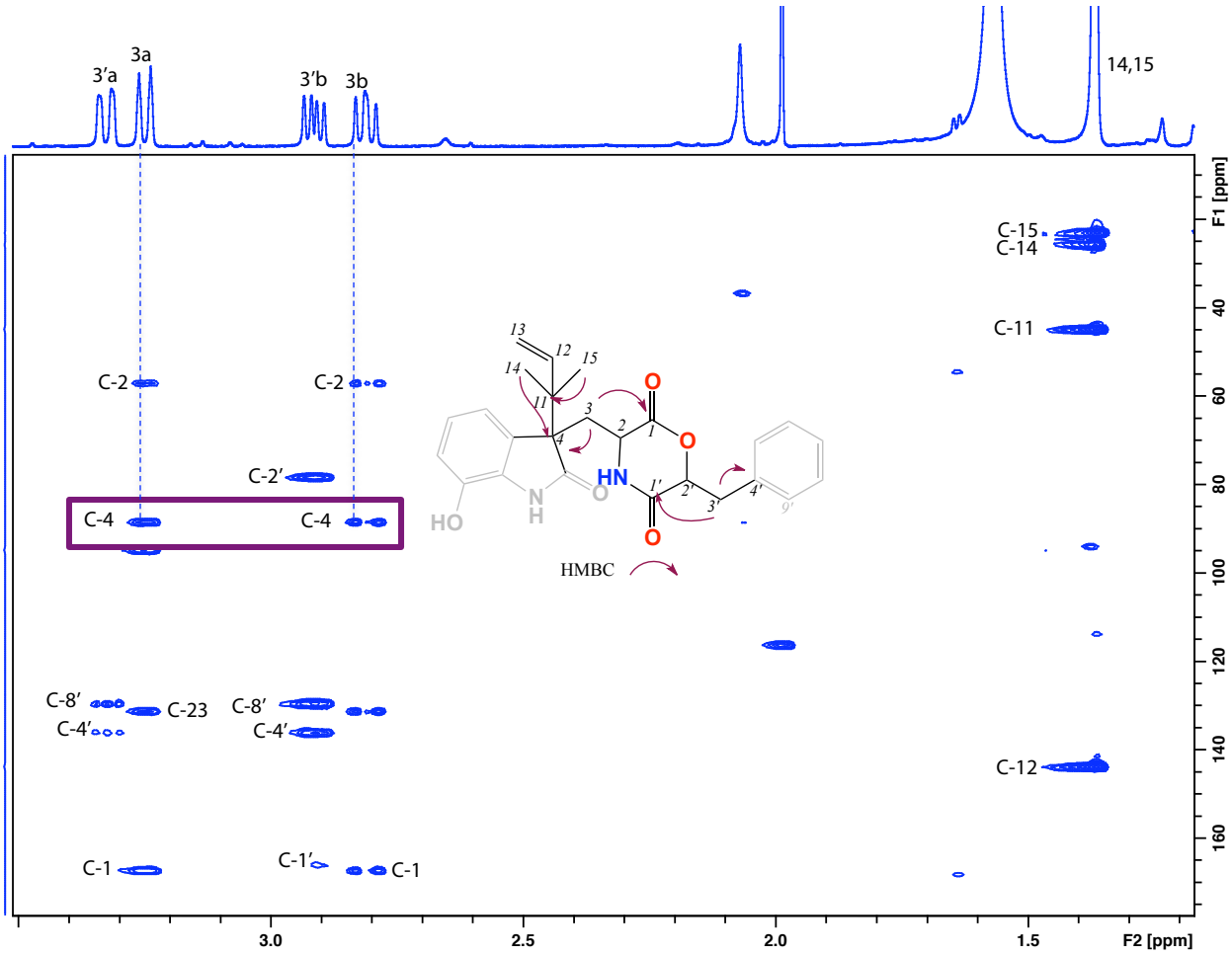

Figure 5.7. HMBC (600 MHz, $CDCl_3$) spectrum of shornephine A (**5.16**)

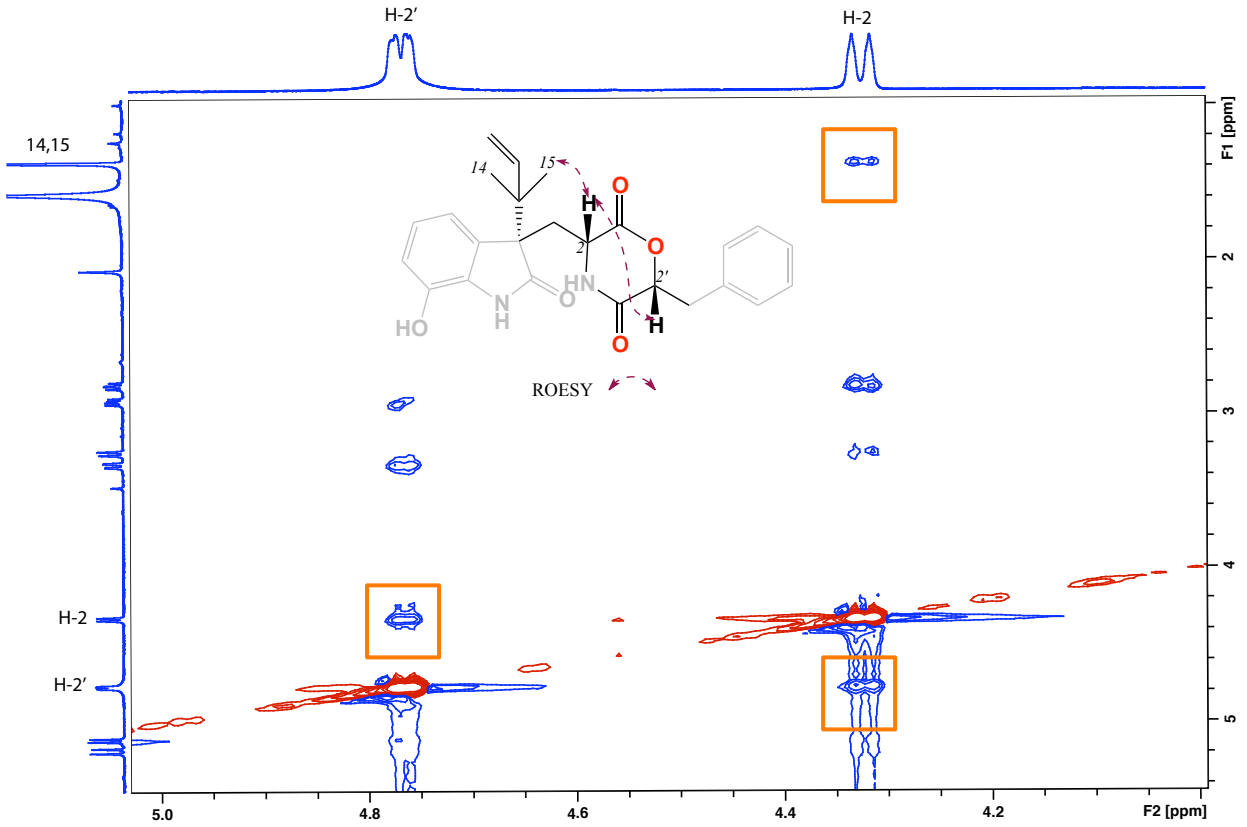

Figure 5.8. ROESY (600 MHz, $CDCl_3$) spectrum of shornephine A (**5.16**)

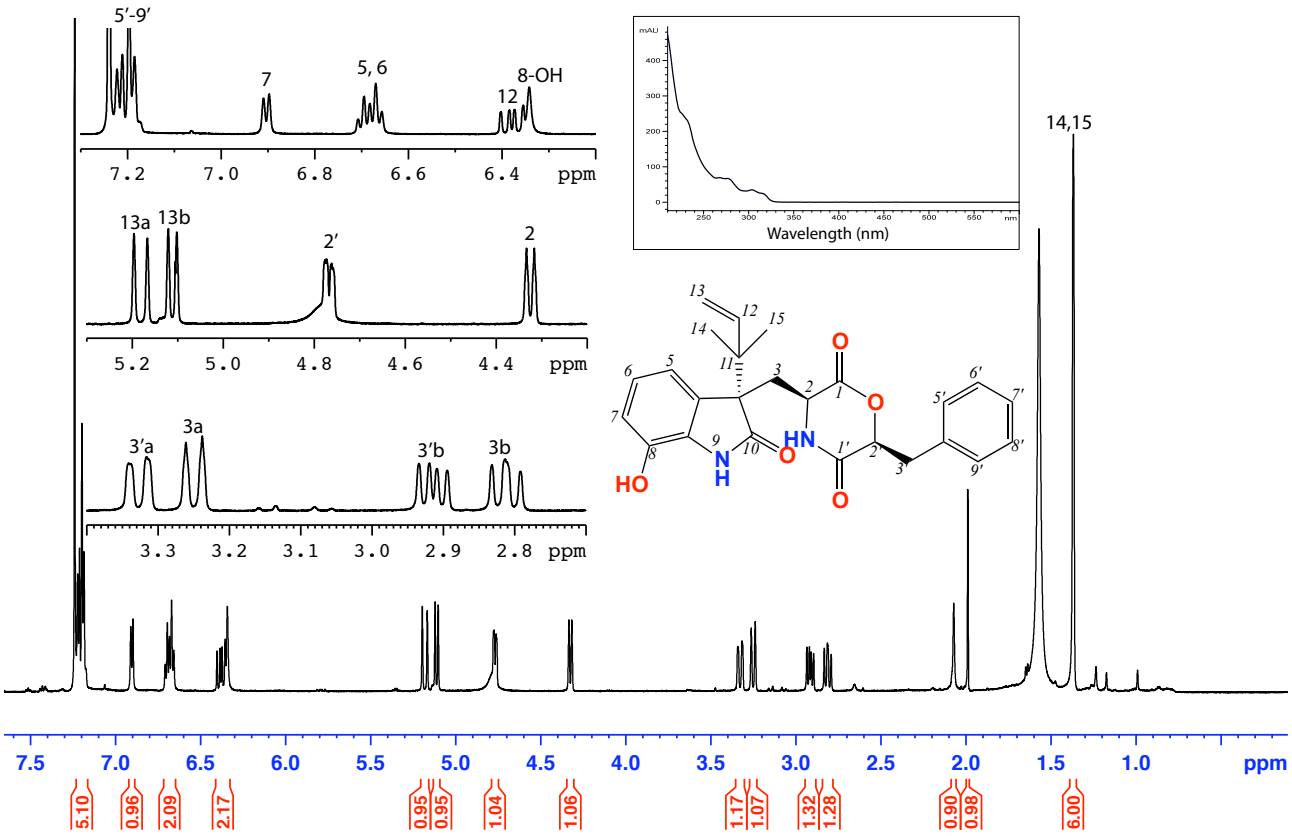

Figure 5.9. ^{1}H NMR (600 MHz, $CDCl_3$) and UV-vis (HPLC-DAD, H_2O/MeCN plus HCO_2H) spectra of shornephine A (**5.16**)

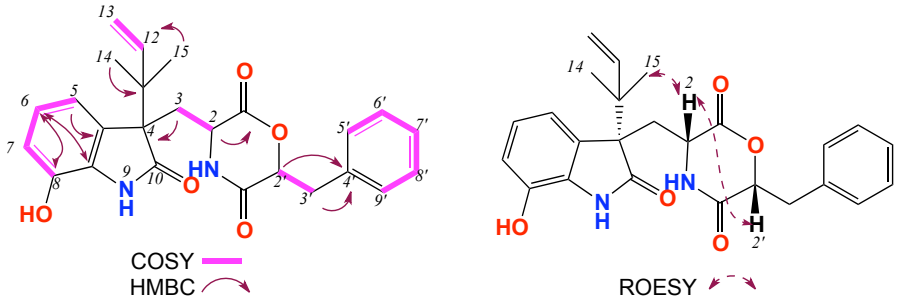

Figure 5.10. Key 2D NMR (600 MHz, $CDCl_3$) correlations of shornephine A (**5.16**)

Table 5.2. ^{1}H NMR (600 MHz, $CDCl_3$) data of shornephine A **(5.16)**

Pos.	δ_H, mult (*J* in Hz)[a]	δ_C[a]	COSY	ROESY	^{1}H-^{13}C HMBC
1		167.7			
2	4.32, d *(13.7)*	57.3	3a/b	2′, 14/15	1, 3, 4
3	a 3.26, d *(13.7)*	36.9	2		1, 2, 4, 8a
	b 2.89, dd *(13.7,11.1)*		2		1, 2, 4, 8a
4		88.5			
4a		136.3			
5	6.67[b], m	117.3[d]	6		4a, 7
6	6.69[b], m	121.2[d]	5, 7		8, 8a
7	6.91, d *(7.7)*	117.1	6		4, 5/6
8		141.4			
8a		130.9			
10		[c]			
11		44.9			
12	6.39, dd *(17.3,10.6)*	144.1	13a/b		11, 14, 15
13	a 5.18, d *(17.3)*	113.1	12		11, 12
	b 5.11, d *(17.3)*				11, 12
1′		165.9			
2′	4.76, dd *(8.8, 1.6)*	78.5	3′a/b	2	3′, 4′
3′	a 3.27, d *(15.1)*	34.4	2′, 3′b		4′, 5′/9′
	b 2.92, dd *(15.1, 8.8)*		2′, 3′a		1′, 2′, 4′, 5′/9′
4′		136.2			
5′	7.20[b]	126.7[d]			
6′	7.20[b]	129.3[d]			
7′	7.20[b]	128.5[d]			
8′	7.20[b]	126.7[d]			
9′	7.20[b]	126.7[d]			
2-NH	[c]				
9-NH	[c]				
8-OH	6.34, s		7		4, 8a
14-Me	1.38, s	22.6	12	2	11, 12, 13, 14/15
15-Me	1.38, s	22.6	12	2	11, 12, 13, 14/15

*(a)^{13}C assignments obtained from gHSQC and gHMBC data. (b) overlapping resonances. (c) signals not observed. (d) interchangeable signals

5.2.4.2.1 Mosher ester derivation

To assign an absolute configuration to shornephine A (**5.16**), mosher ester derivatives were prepared according to protocol published by Hoye *et al.*[199] Shornephine A (**5.16**) was subjected to acid hydrolysis to release phenyllactic acid residue, which was derivatized with (*R*)-α-methoxy-α-trifluoromethylphenylacetic acid (*R*-(+)-MTPA) to yield the corresponding *R* Mosher ester. Authentic samples of (*S*)-(–)-phenyllactic acid were also derivatized in this manner with *R*-(+)-MTPA and *S*-(+)-MTPA to yield the corresponding *R* and *S* Mosher esters respectively and the reactions were analysed using HPLC-DAD-MS using a 60 – 15% H_2O/MeCN plus 0.05% HCO_2H, gradient elution on a Zorbax Eclipse XDB-C_8 column.

Mosher ester derivatives were separated, *R*-(+)-MTPA + (*S*)-(–)-3-phenyl lactic acid showed t_R= 15.7 min and *S*-(+)-MTPA + (*S*)-L-(-)-phenyllactic acid showed t_R= 16.2 min. Retention times of the two standards *R*-(+)-MTPA and *S*-(+)-MTPA reacted to (*S*)-L-(–)-phenyllactic acid compared to the reaction of *R*-(+)-MTPA + hydrolyzed shornephine A (**5.16**) (15.7 min), confirming the 2*S* and 2′*S* configuration of shornephine A (**5.16**) (Figure 5.11).

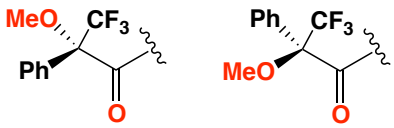

S-MTPA *R*-MTPA

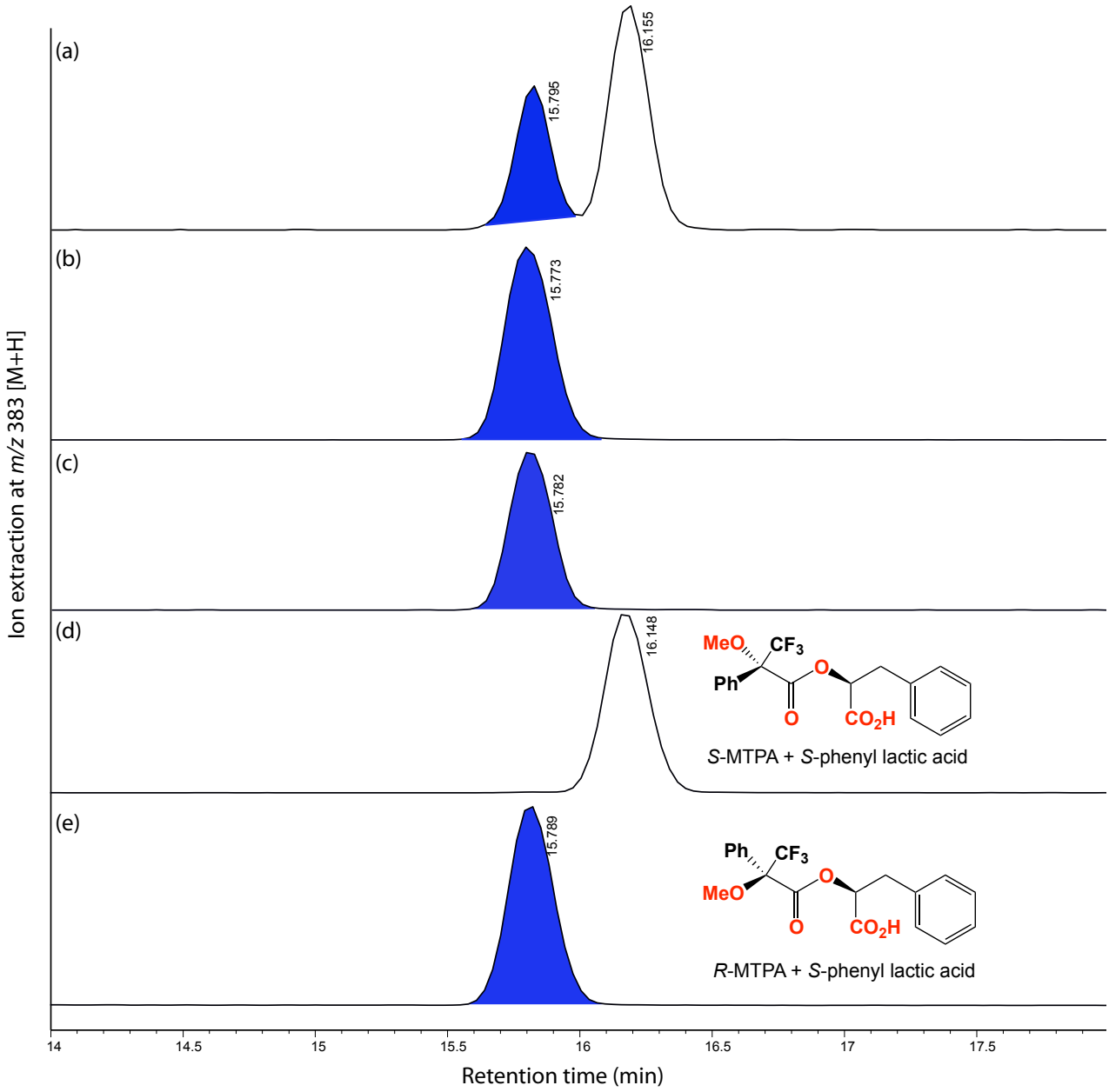

Figure 5.11. Chromatogram showing Mosher analysis for **5.16**. LCMS condition: Zorbax Eclipse C_8 analytical column, 150 × 4.6 mm, eluting with 1.0 mL/min 60% H_2O/MeCN to 15 H_2O/MeCN (0.05% HCO_2H modifier) over 40 min, then held for 5 min and detecting at extract ions 383 [M+H]/381 [M-H]. (a) coinjection of *R*-(+)-MTPA-OH + (*S*)-(−)-3-phenyl lactic acid and *S*-(+)-MTPA-OH + (*S*)-(−)-3-phenyl lactic acid, (b) co-injection of *R*-(+)-MTPA-OH + (*S*)-(−)-3-phenyl lactic acid and *R*-(+)-MTPA-OH + shornephine A (**5.16**) , (c) *R*-(+)-MTPA-OH + shornephine A (**5.16**), (d) *S*-(+)-MTPA-OH + (*S*)-(−)-3-phenyl lactic acid and (e) *R*-(+)-MTPA-OH + (*S*)-(−)-3-phenyl lactic acid

ROSEY correlations between H-2 and H-2′ (Figure 5.8) as well as Mosher analysis unambiguously confirmed the absolute configuration of H-2 and H-2′ as *S* configuration. Unfortunately, assignment of the absolute configuration of the remaining stereocentre C-4 of isoprene unit was undetermined. Chem 3D model studies could not give a definitive answer due to flexibility of the molecule. However, it can be tentatively inferred that the absolute configuration of C-4 in **5.16** can be based on the biosynthetic grounds of the other co-metabolites that will be discussed in the next sections.

5.2.4.3 15b-β-hydroxy-5-*N*-acetylardeemin (5.17)

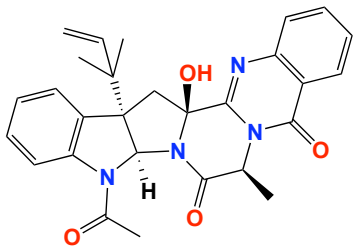

(**5.17**)

HRESI(+)MS data for **5.17** revealed an adduct ion $(M+Na)^+$ corresponding to a molecular formula ($C_{28}H_{28}N_4O_8$, Δmmu −1.3). The ^1H NMR ($CDCl_3$) data of **5.17** (Figure 5.14 and Table 5.3) suggested the presence of indole, isoprene, piperazine and quinazoline residues, further supported by 2D NMR data, including HSQC, COSY and HMBC (Figure 5.12). On searching the literature, **5.17** was determined to be consistent with the known fungal metabolite 15b-β-hydroxy-5-*N*-acetylardeemin. Analysis of all the NMR data with comparison to literature data (Table 5.4), confirmed that **5.17** was 15b-β-hydroxy-5-*N*-acetylardeemin. This assignment was further supported by a comparison of the $[\alpha]^{23}_D$ −18 (*c* 0.09, MeOH) for **5.17** compared to $[\alpha]^{25}_D$ − 245 (*c* 0.2, MeOH) for the reported 15b-β-hydroxy-5-*N*-acetylardeemin.[200] The wide difference in the optical rotation of both compounds can be attributed to the possibility of other issues such as high concentration of the reported 15b-β-hydroxy-5-*N*-acetylardeemin. Karwowski *et al*., isolated 15b-β-hydroxy-5-*N*-acetylardeemin from *Aspergillus fischerai* as a novel heterocyclic compound which reverses multidrug resistance in tumour cells.[201]

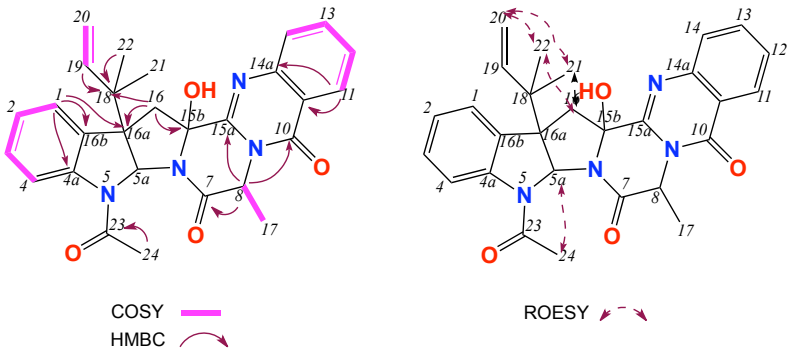

Figure 5.12. Key 2D NMR correlations of 15b-β-hydroxy-5-*N*-acetylardeemin (**5.17**)

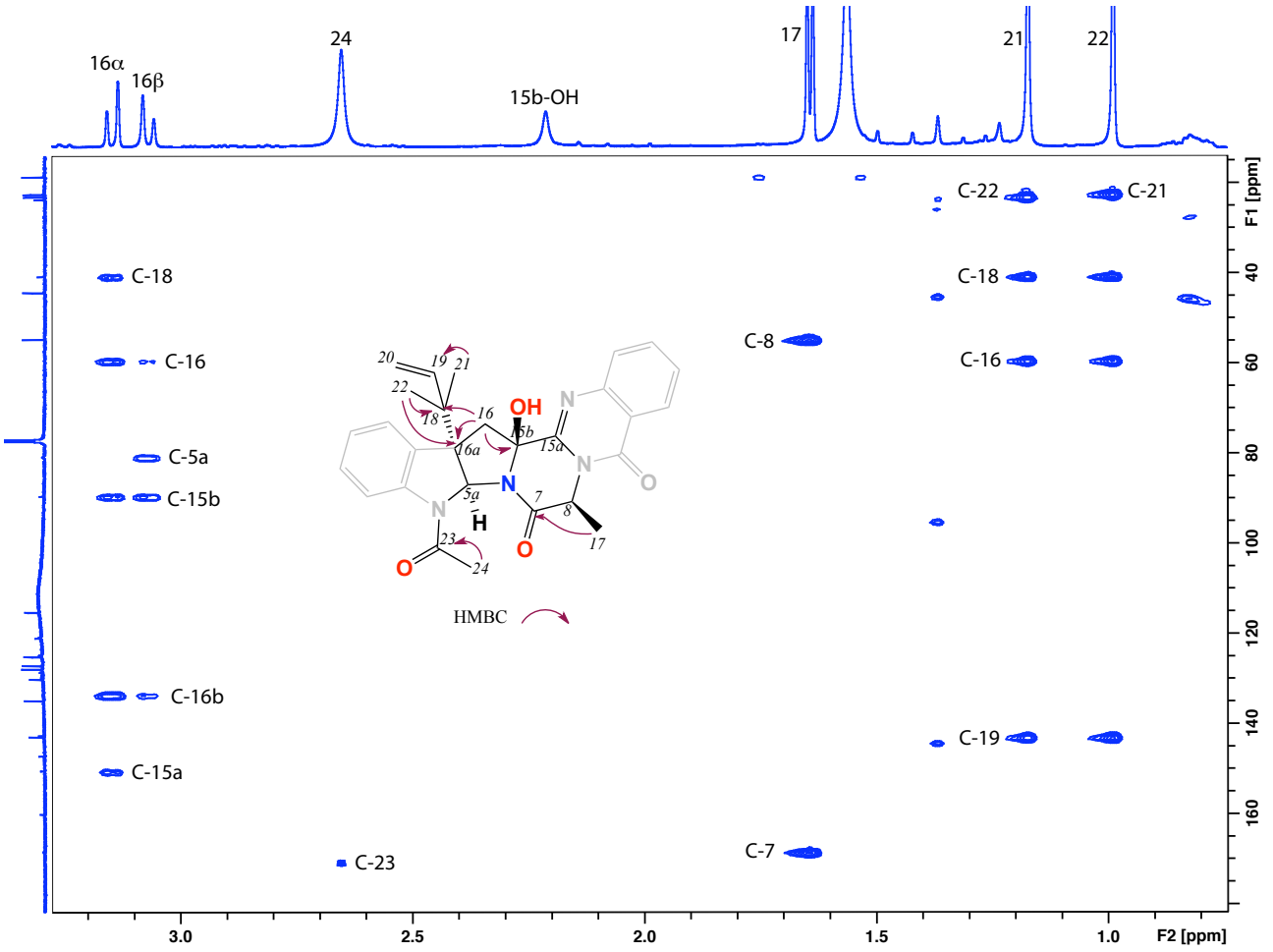

Figure 5.13. HMBC (600 MHz, $CDCl_3$) spectrum of 15b-β-hydroxy-5-*N*-acetylardeemin (**5.17**)

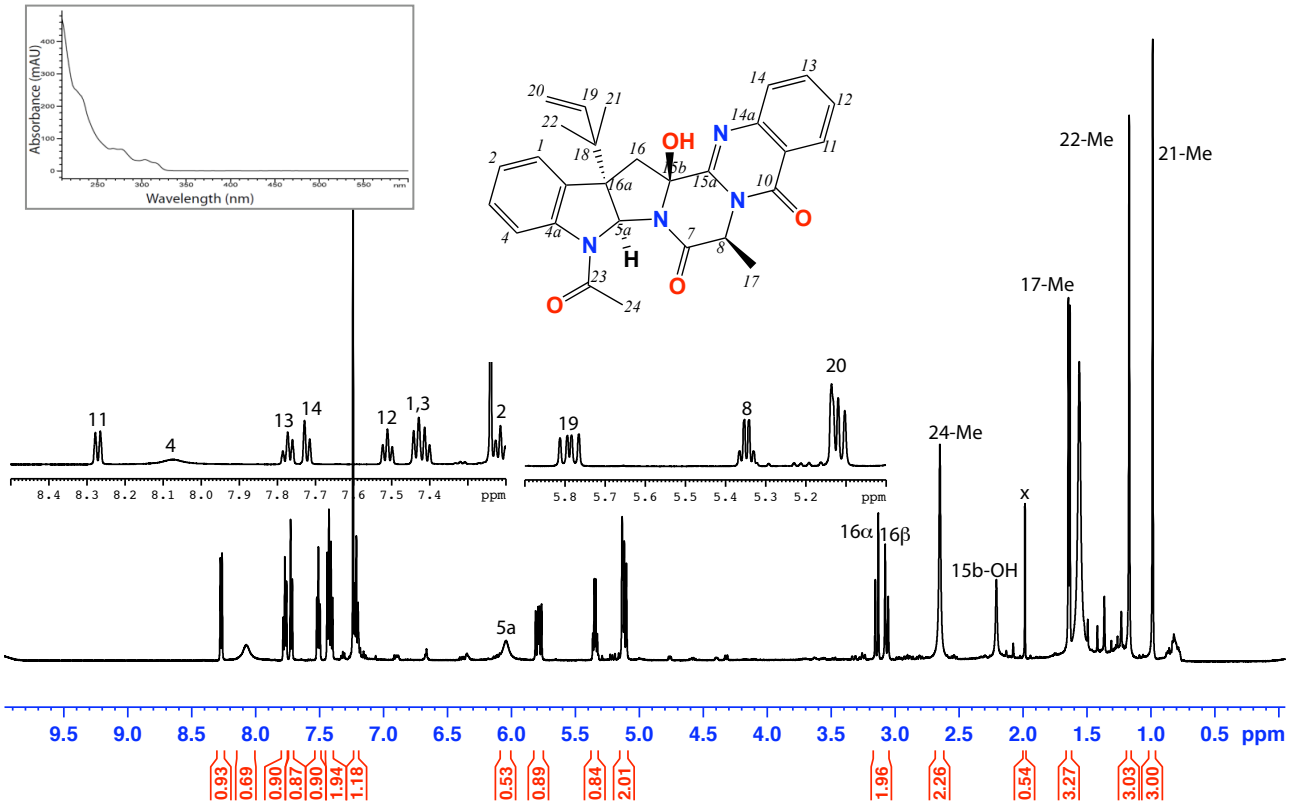

Figure 5.14. ^{1}H NMR (600 MHz, $CDCl_3$) and UV-vis spectrum (HPLC-DAD, H_2O/MeCN plus HCO_2H at 254 nm) spectra of 15b-β-hydroxy-5-*N*-acetylardeemin (**5.17**)

Table 5.3. NMR (600 MHz, $CDCl_3$) of 15b-β-hydroxy-5-*N*-acetylardeemin (**5.17**)

Pos.	δ_H, mult, (*J* in Hz)[a]	δ_C[a]	COSY	ROESY	HMBC
1	7.42, d *(7.5)*	124.4	2		3, 16α, 16β
2	7.21, t *(7.5)*	124.9	1, 3		1, 3, 4, 4a, 16β
3	7.45, t *(7.5)*	130.2	2, 4		1, 16b
4	8.07, br d	[b]	3		
4a		142.5			
5a	6.04, br	80.2		21, 22, 24	
7		168.4			
8	5.34, dd *(14.1, 7.1)*	53.5	17		7, 10, 15a, 17
10		160.1			
10a		120.7			
11	8.27, d *(7.5)*	127.1	12, 13		10, 12, 14a
12	7.77, t *(7.5)*	128.3	11, 12		10a, 11
13	7.51, t *(7.5)*	134.9	11, 13, 14		11, 14a
14	7.72, d *(8.1)*	127.8	13		10, 10a, 13
15a		150.6			
15b		89.2			
16	α 3.15, d *(14.8)*	43.8		21, 22	15a, 15b, 16α, 16β, 18
	β 3.06, d *(14.8)*			21, 22	5a, 15b, 16β
16a		59.4			
16b		133.3			
17	1.64, d *(7.1)*	18.3	8		7, 8
18		40.5			
19	5.78, dd *(17.4, 10.8)*	143.4	20α,β	16α, 21, 22	18, 22
20	α 5.13, br d	115.9	19	21, 22	18, 19
	β 5.11, d *(17.4)*			21, 22	18, 19
21	0.98, s	22.6	22	5a, 19	16α, 18, 19, 22
22	1.17, s	22.8	21	5a, 19	16α, 18, 19, 21
23		170.8			
24	2.65, br s	23.6		21, 22	23
15b-OH	2.21, br s				15a

(a)^{13}C assignments obtained from gHSQC and gHMBC data. (b) signals not observed

Table 5.4. ^{1}H NMR (600 MHz, DMSO-d_6) data comparison of experimental and literature[200] data of 15b-β-hydroxy-5-*N*-acetylardeemin (**5.17)**

Pos.	δ_H, mult, (*J* in Hz)[a] (experimental)	δ_H, mult, (*J* in Hz)[b] (literature)
1	7.42, d *(7.5)*	7.41, dd, (*7.8*, *1.2*)
2	7.21, t *(7.5)*	7.13, td, (*7.8*, *0.8*)
3	7.45, t *(7.5)*	7.24, td, (*7.8*, *1.2*)
4	8.07, br	7.80, br s
5a	6.04, br s	6.04, br s
8	5.34, dd *(14.1, 7.1)*	5.03, q, (*7.0*)
11	8.27, d *(7.5)*	8.18, dd, (*8.2*, *1.6*)
12	7.77, t *(7.5)*	7.58, br dd, (*8.2*, *7.1*)
13	7.51, t *(7.5)*	7.87, ddd, (*8.1*, *7.1*, *1.6*)
14	7.72, d *(8.1)*	7.76, br d, (*8.1*)
16	α 3.15, d *(14.8)*	α 3.09, d, (*13.7*)
	β 3.06, d *(14.8)*	β 2.97, d, (*13.7*)
17	1.64, d *(7.1)*	1.51, d, (*7.0*)
19	5.78, dd *(17.4, 10.8)*	5.83, dd, (*17.6*, *11.0*)
20	α 5.13, br d	α 5.08, br d, (*11.0*)
	β 5.11, d *(17.4)*	β 5.05, br d, (*17.6*)
21	0.98, s	0.91, s
22	1.17, s	1.08, s
24	2.21, br s	2.55, br s

*measured in (a) (600 MHz, DMSO-d_6), (b) (500 MHz, DMSO-d_6).

5.2.4.4 5-*N*-acetylardeemin (5.17)

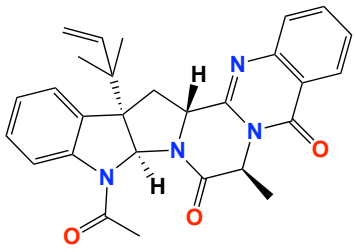

(**5.18**)

HRESI(+)MS data for **5.18** revealed an adduct ion $(M+Na)^+$ corresponding to a molecular formula ($C_{28}H_{28}N_4O_4$, Δmmu +0.4). The ^1H NMR ($CDCl_3$) data for **5.18** were closely related to **5.17** with exception for the replacement of 15b-OH group in **5.17** with 15b-H in **5.18**. The structure elucidation was further supported by 2D NMR data, including HSQC, COSY and HMBC (Figure 5.15). On searching the literature **5.18** was determined to be consistent with 5-*N*-acetylardeemin. Analysis of all the NMR data with comparison to literature data (**Table 5.6**), confirmed that **5.17** was the known metabolite 5-*N*-acetylardeemin. This assignment was further confirmed by a comparison of the $[\alpha]^{23}_D$ –9.7 (*c* 0.05, MeOH) for **5.18** compared to $[\alpha]^{25}_D$ –33 (*c* 0.7, MeOH) for the reported 5-*N*-acetylardeemin.[200] Karwowski *et al*., isolated 5-N-acetylardeemin as a co-metabolite with 15b-β-hydroxy-5-*N*-acetylardeemin from *Aspergillus fischerai* as a novel heterocyclic compound, which reverses multidrug resistance in tumour cells.[201] An X-ray determination of 5-*N*-acetylardeemin assigned the relative configuration and confirmed the structure.[200]

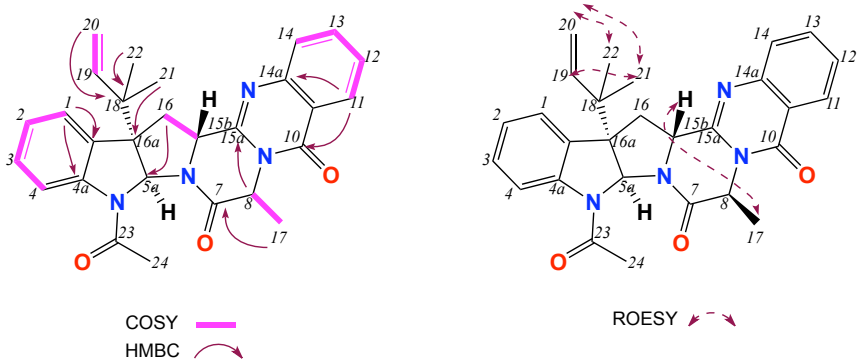

Figure 5.15. Key 2D NMR correlations of 5-*N*-acetylardeemin (**5.18**)

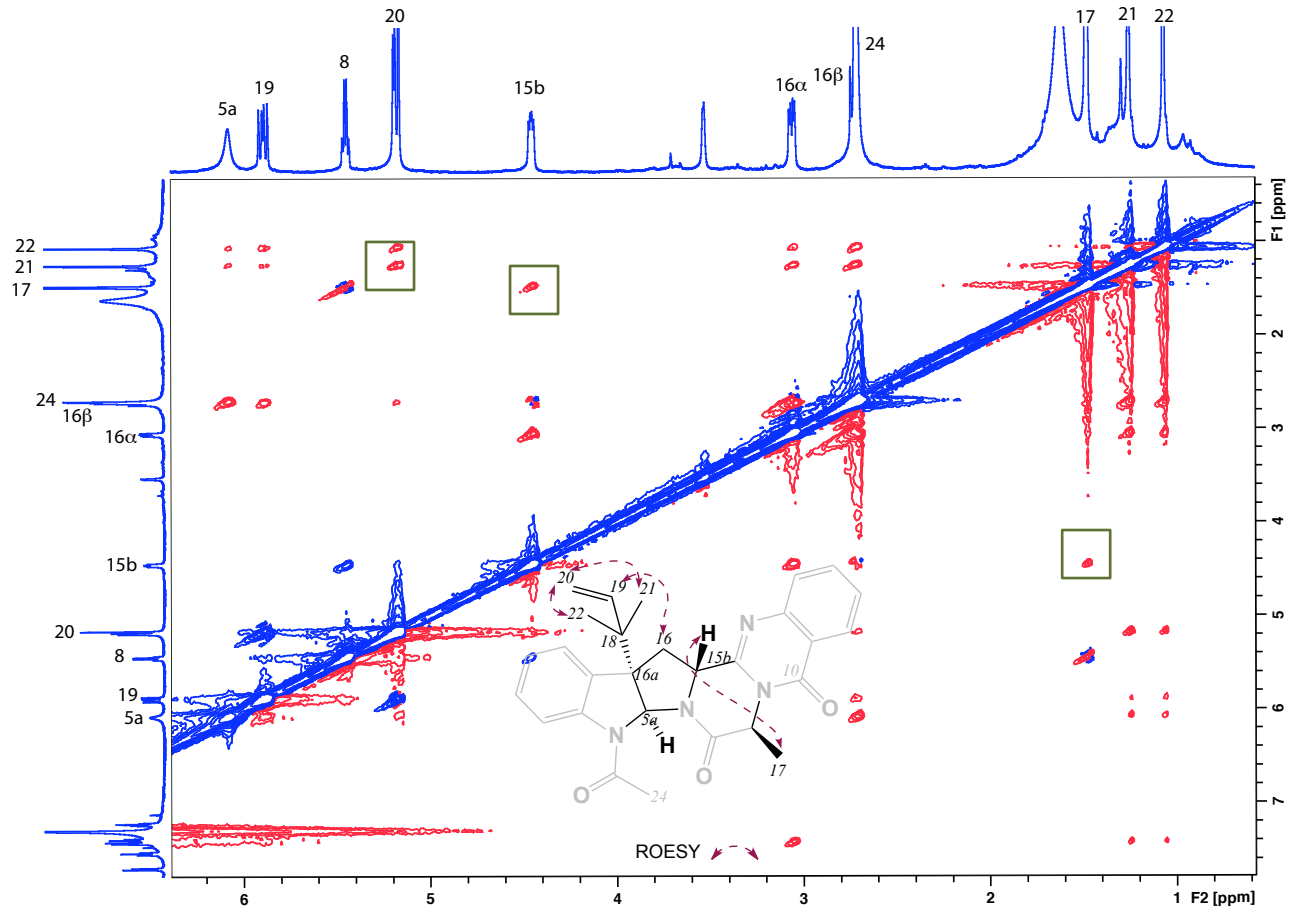

Figure 5.16. ROESY (600 MHz, $CDCl_3$) spectrum of 5-*N*-acetylardeemin (**5.18**)

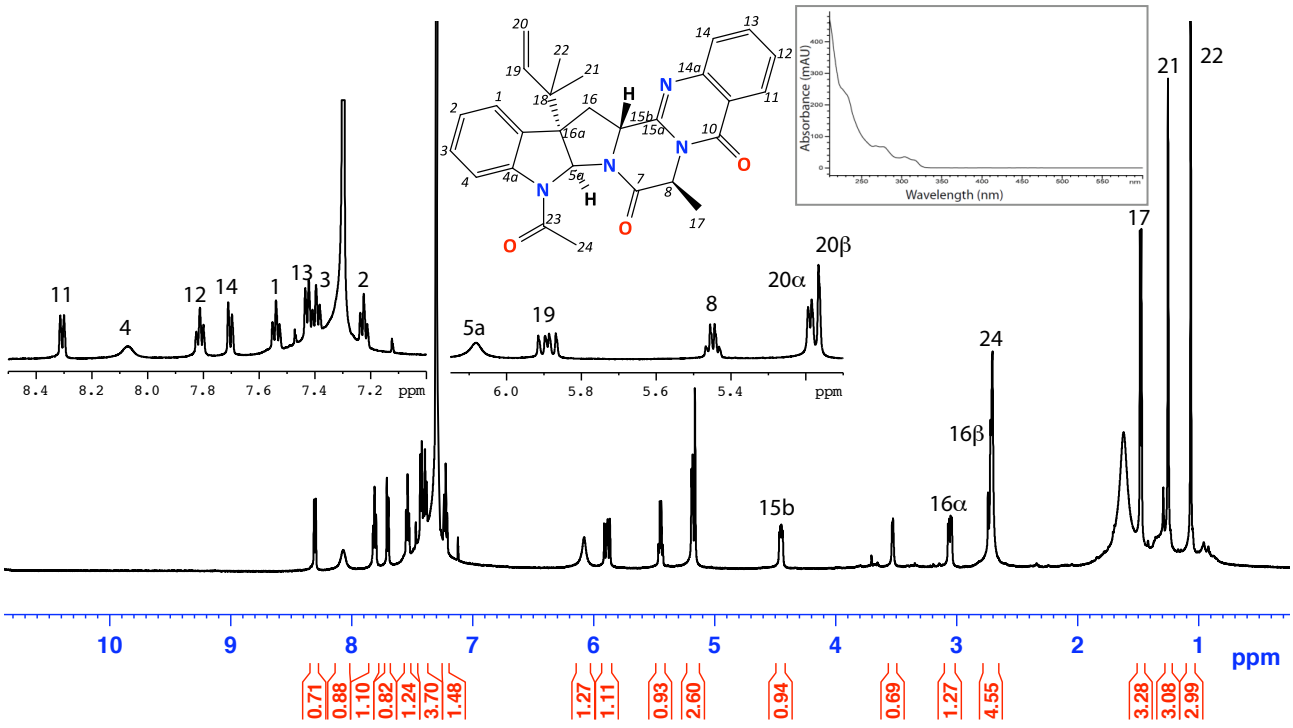

Figure 5.17. ^1H NMR (600 MHz, $CDCl_3$) and UV-vis (HPLC-DAD, H_2O/MeCN plus HCO_2H at 254 nm) spectra of 5-*N*-acetylardeemin (**5.18**)

Table 5.5. NMR (600 MHz, $CDCl_3$) of 5-*N*-acetylardeemin (**5.18**)

Pos.	δ_H, mult, (*J* in Hz)[a]	δ_C[a]	COSY	ROESY	HMBC
1	7.39, d, (*7.8*)	124.7	2		4, 16
2	7.18, t, (*7.8*)	124.5	1, 3		4
3	7.36, dd, (*7.8*, *7.2*)	130.1	2, 4		1, 4a
4	8.03, br s	121.2	3		2
4a		142.2			
5a	6.04, br s	81.2		16β, 21, 22	16, 18
7		169.1			
8	5.41, q, (*7.2*)	53.6	17		7
10		160.1			
10a		121.2			
11	8.27, d, (*7.8*)	127.8	12		
12	7.50, dd, (*7.8*, *7.2*)	127.5	11, 13		10a
13	7.72, ddd, (*8.4*, *7.2*, *1.2*)	135.2	12, 14		14a
14	7.66, d, (*8.4*)	126.3	13		
14a		149.4			
15a		151.1			
15b	4.41, dd, (*10.2*, *5.4*)	90.2	16a,b	16α,b, 17	15a
16a		60.1			
16b		132.3			
16	α 3.02, dd, (*12.6*, *10.8*)	59.2	15b, 16β		18
	β 2.69, dd, (*12.6*, *10.8*)		15b, 16α		18
17	1.44, d, (*7.2*)	19.1	8	15b	
18		41.2			
19	5.85, dd, (*17.4*, *10.2*)	145.3	20a, b	16β, 21, 22	
20	α 5.13, d, (*16.8*)	115.1	19, 20β	21, 22	21, 22
	β 5.15, d, (*16.8*)		19, 20α		21, 22
21	1.21, s	22.1	22		4a, 16α, 18, 20
22	1.03, s	22.3	21		4a, 16α, 18, 20
23		171.4			
24	2.67, s	23.6			

(a)^{13}C assignments obtained from gHSQC and gHMBC data.

Table 5.6. ^{1}H NMR data comparison of experimental and literature[200] data of 5-*N*-acetylardeemin (**5.18)**

Pos.	δ_H, mult, (*J* in Hz)[a] (experimental)	δ_H, mult, (*J* in Hz)[b] (literature)
1	7.39, d, (*7.8*)	7.38, br d, (*7.6*)
2	7.18, t, (*7.8*)	7.17, br t, (*7.6*)
3	7.36, dd, (*7.8*, *7.2*)	7.34, dd, (*8.1*, *7.6*)
4	8.03, br s	8.00, br s
5a	6.04, br s	6.08, br s
8	5.41, q, (*7.2*)	5.37, q, (*7.1*)
11	8.27, d, (*7.8*)	8.24, dd, (*8.1*, *1.5*)
12	7.50, dd, (*7.8*, *7.2*)	7.47, dd, (*8.1*, *7.1*)
13	7.72, ddd, (*8.4*, *7.2*, *1.2*)	7.76, ddd, (*8.1*, *7.1*, *1.5*)
14	7.66, d, (*8.4*)	7.65, d, (*8.1*)
15b	4.41, dd, (*10.2*, *5.4*)	4.41, dd, (*10.7*, *5.6*)
16	α 3.02, dd, (*12.6*, *10.8*)	3.01, dd, (*12.7*, *5.6*)
	β 2.69, dd, (*12.6*, *10.8*)	2.67, d, (*12.7*, *10.7*)
17	1.44, d, (*7.2*)	1.42, d, (*7.1*)
19	5.85, dd, (*17.4*, *10.2*)	5.84, dd, (*17.3*, *10.7*)
20	α 5.13, d, (*16.8*)	5.11, d, (*10.7*)
	β 5.15, d, (*16.8*)	5.15, d, (*17.3*)
21	1.21, s	1.20, s
22	1.03, s	1.01, s
24	2.67, s	2.63, s

*measured in (a) (600 MHz, $CDCl_3$), (b) (500 MHz, $CDCl_3$).

5.2.4.5 15b-β-methoxy-5-*N*-acetylardeemin (5.19)

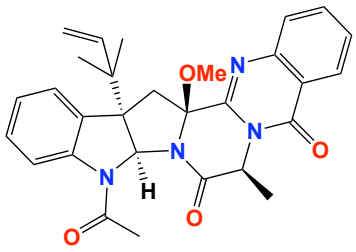

(**5.19**)

HRESI(+)MS data of **5.19** revealed an adduct ion $(M+Na)^+$ corresponding to a molecular formula ($C_{29}H_{30}N_4O_4$, Δ mmu −0.4). The ^1H NMR ($CDCl_3$) data of **5.19** was very closely related to **5.17** with exception for the replacement of 15b-OH in **5.17** with OMe in **5.19** (Figure 5.20, Figure 5.21, **Table 5.7** and Table 5.8) Additional HSQC, COSY, HMBC and ROESY NMR data (Figure 5.18 and **Table 5.7**) provided further evidence to support the assigned structure (Figure 5.18). $[\alpha]^{22}_D$ −16 (*c* 0.05, MeOH). On searching the literature **5.19** was determined to be new analogue to ardeemin family.

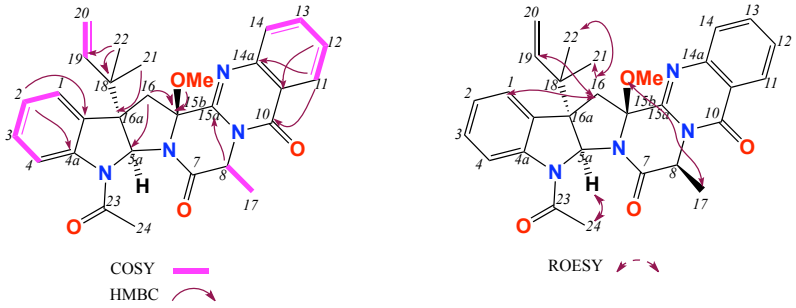

Figure 5.18. Key 2D NMR correlations of 15b-β-methoxy-5-*N*-acetylardeemin (**5.19**)

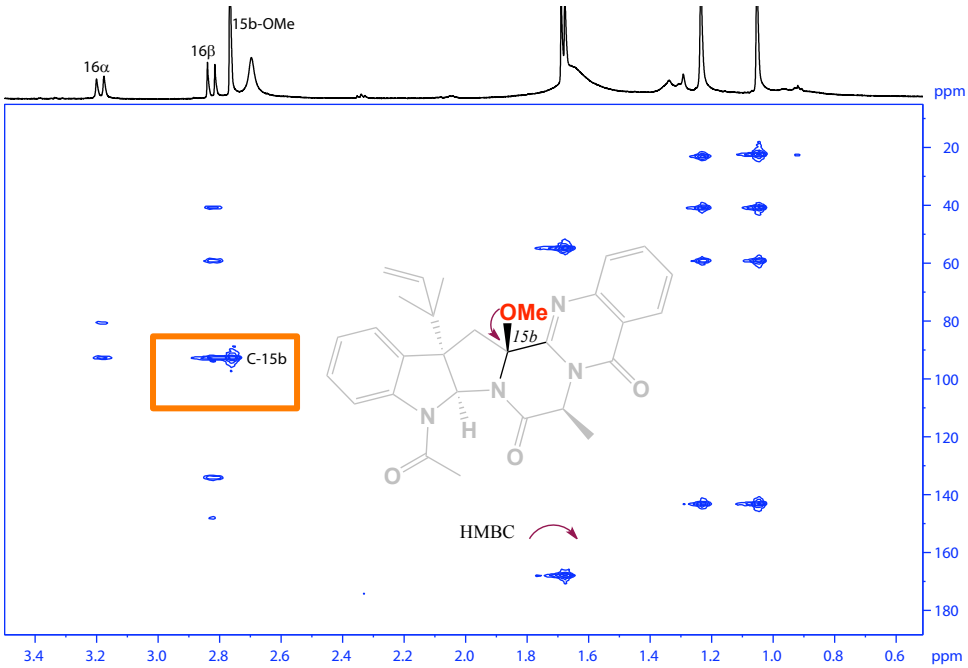

Figure 5.19. HMBC (600 MHz, $CDCl_3$) spectrum of 15b-β-methoxy-5-*N*-acetylardeemin (**5.19**)

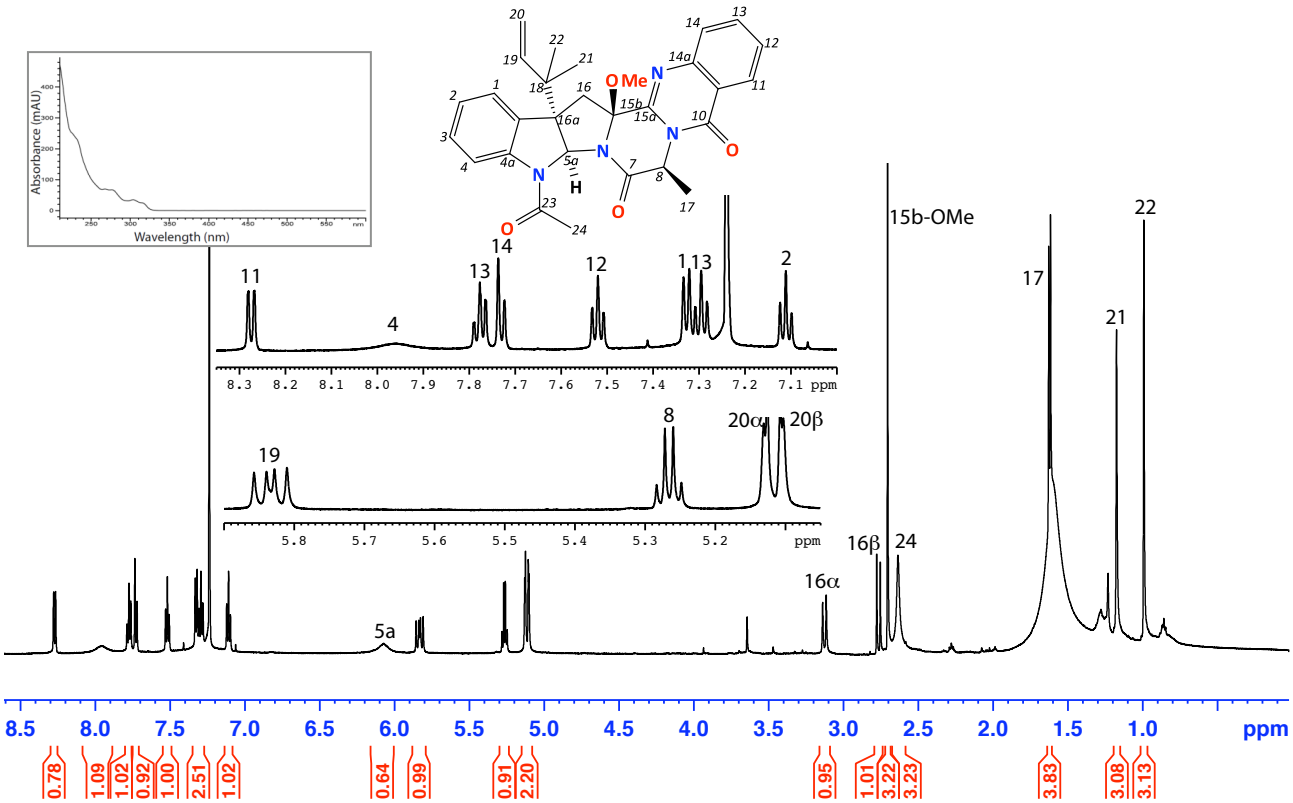

Figure 5.20. ^{1}H NMR (600 MHz, $CDCl_3$) and UV-vis (HPLC-DAD, H_2O/MeCN plus HCO_2H at 254 nm) spectra of 15b-β-methoxy-5-*N*-acetylardeemin (**5.19**)

Table 5.7. NMR (600 MHz, $CDCl_3$) data of 15b-β-methoxy-5-*N*-acetylardeemin (**5.19**)

Pos.	δ_H, mult, (*J* in Hz)	δ_C*	COSY	ROESY	^{1}H – ^{13}C HMBC
1	7.35, d, (*7.8*)	123.8	2	16β	3, 4a
2	7.13, dd, (*7.8*, *0.6*)	123.9	1, 3		4, 16β
3	7.31, dd, (*7.8*, *0.6*)	128.5	2, 4		1, 4a
4	7.98, br d	119.5	3		
4a		143.0			
5a	6.10, br	80.5		24	
7		168.0			
8	5.29, q, (*6.6*)	54.9	17		7, 15a, 17
10		160.0			
10a		120.8			
11	8.29, d, (*7.8*)	126.9	12		10, 13, 14a
12	7.54, dd, (*7.8*, *1.8*)	127.9	11, 13		10a, 14
13	7.80, dd, (*7.8*, *1.8*)	134.8	12, 14		11, 14a
14	7.75, d, (*7.8*)	127.9	13		10a, 12
14a		146.3			
15a		148.1			
15b		92.7			
16	α 3.15, d, (*14.4*)	37.4	16β	1, 21, 22	5a, 15b
	β 2.79, d, (*14.4*)		16α	19	15a, 16α, 16β, 18
16a		59.1			
16b		134.2			
17	1.64, d, (*6.6*)	18.9	8	15b-OMe	7, 8
18		40.9			
19	5.85, dd, (*16.8*, *11.4*)	143.3	20α, β	16b	
20	α 5.15, d, (*16.8*)	114.9	19		18
	β 5.13, d, (*16.8*)		19		18
21	1.20, s	22.6		16α	16α, 18, 19, 22
22	1.01, s	23.3		16α	16α, 18, 19, 21
23					
24	2.66, br s	23.9		5a	
15b-OMe	2.73, s	51.7		17	15b

*(a)^{13}C assignments obtained from gHSQC and gHMBC data

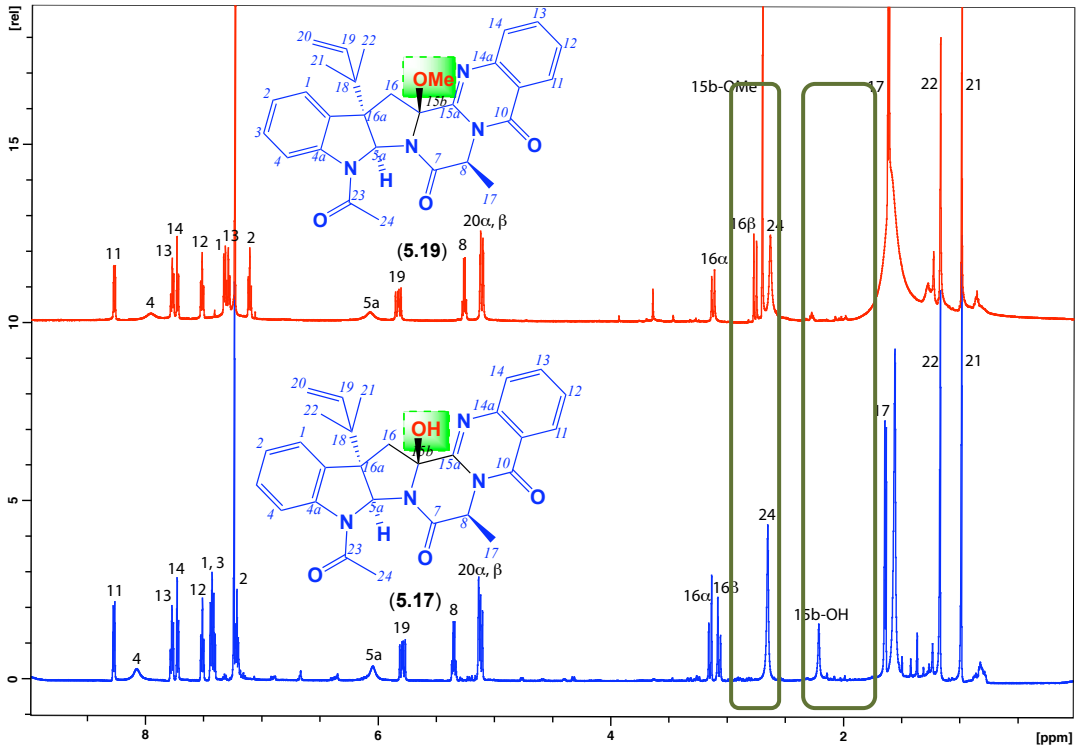

Figure 5.21. ^{1}H NMR (600 MHz, $CDCl_3$) spectra of 15b-β-hydroxy-5-*N*-acetylardeemin (**5.17**) (blue) and 15b-β-methoxy-5-*N*-acetylardeemin (**5.19**) (red)

Table 5.8. NMR (600 MHz, $CDCl_3$) data comparison of 15b-β-hydroxy-5-*N*-acetylardeemin (**5.17**) and 15b-β-methoxy-5-*N*-acetylardeemin (**5.19**)

Pos.	δ_H, mult, (*J* in Hz)[a] of **5.17**	δ_C[a]	Pos.	δ_H, mult, (*J* in Hz)[a] of **5.19**	δ_C[a]
1	7.42, d *(7.5)*	124.4	1	7.35, d, (*7.8*)	123.8
2	7.21, t *(7.5)*	124.9	2	7.13, dd, (*7.8*, *0.6*)	123.9
3	7.45, t *(7.5)*	130.2	3	7.31, dd, (*7.8*, *0.6*)	128.5
4	8.07, br	[b]	4	7.98, br s	119.5
4a		142.5	4a		143.0
5a	6.04, br	80.2	5a	6.10, br s	80.5
7		168.4	7		168.0
8	5.34, dd *(14.1, 7.1)*	53.5	8	5.29, q, (*6.6*)	54.9
10		160.1	10		160.0
10a		120.7	10a		120.8
11	8.27, d *(7.5)*	127.1	11	8.29, d, (*7.8*)	126.9
12	7.77, t *(7.5)*	128.3	12	7.54, dd, (*7.8*, *1.8*)	127.9
13	7.51, t *(7.5)*	134.9	13	7.80, dd, (*7.8*, *1.8*)	134.8
14	7.72, d *(8.1)*	127.8	14	7.75, d, (*7.8*)	127.9
14a			14a		146.3
15a		150.6	15a		148.1
15b		89.2	15b		92.7
16	α 3.15, d *(14.3)*	43.8	16	α 3.15, d, (*14.4*)	37.4
	β 3.06, d *(14.3)*			β 2.79, d, (*14.4*)	
16a		59.4	16a		59.1
16b		133.3	16b		134.2
17	1.64, d *(7.1)*	18.3	17	1.64, d, (*6.6*)	18.9
18		40.5	18		40.9
19	5.78, dd *(17.1, 10.8)*	143.4	19	5.85, dd, (*16.8*, *11.4*)	143.3
20	α 5.13, br	115.9	20	α 5.15, d, (*16.8*)	114.9
	β 5.11, d *(10.1)*			β 5.13, d, (*16.8*)	
21	0.98, s	22.6	21	1.20, s	22.6
22	1.17, s	22.8	22	1.01, s	23.3
23		170.8	23		[b]
24	2.65, br s	23.6	24	2.66, br s	23.9
15b-OH	2.21, br s		15b-OMe	2.73, s	51.7

*(a)^{13}C assignments obtained from gHSQC and gHMBC data. (b) signals not observed

5.2.5 Plausible biosynthetic pathway linking shornephine A and ardeemins

As shornephine A (**5.16**) and DKPs **5.17** – **5.19** are structurally related co-metabolites, it seems likely that they share common biosynthetic precursors and transformations. One such plausible biosynthetic relationship would have both sharing a common isoprenylated tryptophan precursor (Figure 5.22). Given that the α orientation of the isoprenyl moiety in **5.17** - **5.19** is conserved, and has been unambiguously assigned,[200] on biosynthetic grounds we *tentatively* assign the same configuration to **5.16** – albeit acknowledging that this assignment would best be resolved by total synthesis. Give the above, the complete structures for shornephine A (**5.16**) and *seco*-shornephine A (**5.15**), inclusive of absolute configurations are assigned as *S* configuration.

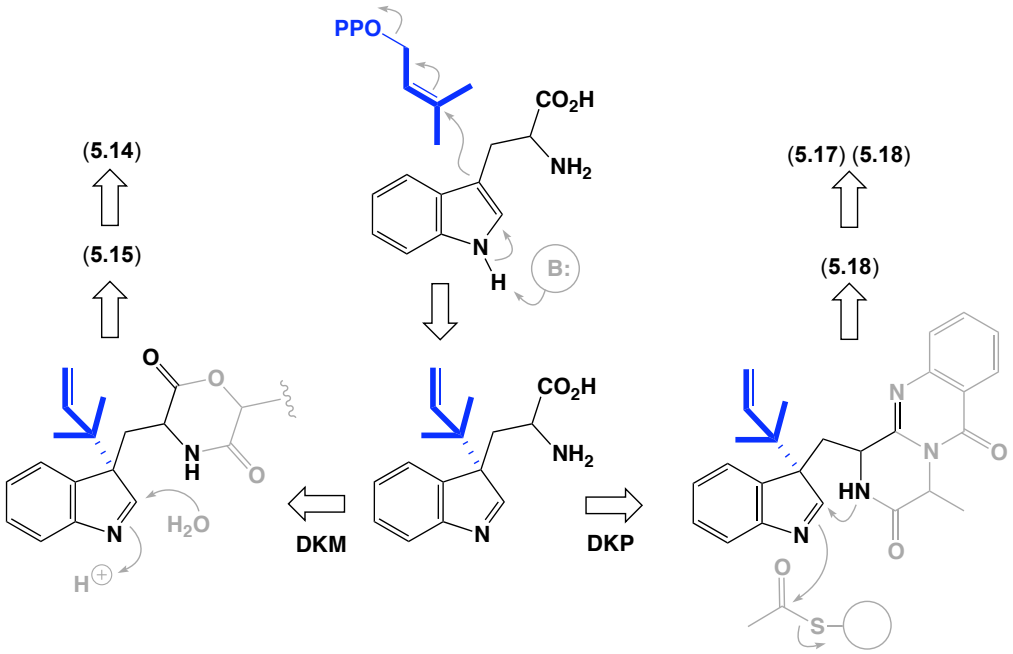

Figure 5.22. A plausible biosynthetic pathway linking shornephine A (DKM) and ardeemins (DKP)

5.2.6 Synthesis of diketomorpholines (DKMs) derviatives

Shornephine A (**5.16**) and ardeemins (**5.17** – **5.19**) were tested in cytotoxic and antibacterial assay and were inactive. However, they showed good inhibitory effects against P-glycoprotein (discussed in Section 1.10). Therefore, a selection of DKMs analogues were synthesised (Figure 5.24) to test the hypothesis that DKM scaffold possesses P-gp inhibitory activity. The hydrochloride salts of methyl ester of amino acids **5.2a** – **d** were prepared from refluxing **5.1a** – **d** with $SOCl_2$ in methanol in a quantitative yield (Scheme 5.2).

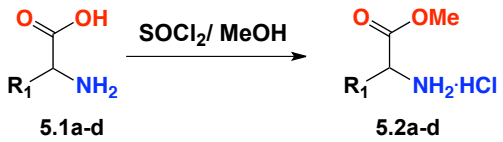

5.1a-d **5.2a-d**

Scheme 5.2. Synthesis of amino acids methyl esters (**5.2a** – **d**). Addition of $SOCl_2$ in the presence of MeOH under reflux for 18 h.

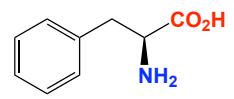

L-phenylalanine (**5.1a**)

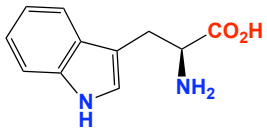

L-tryptophan (**5.1b**)

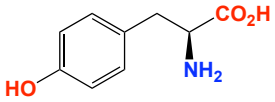

L-tyrosine (**5.1c**)

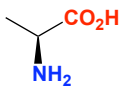

L-alanine (**5.1d**)

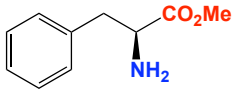

L-phenylalanine methyl ester (**5.2a**)

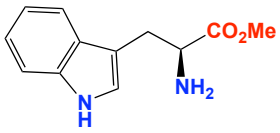

L-tryptophan methyl ester (**5.2b**)

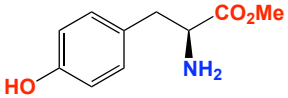

L-tyrosine methyl ester (**5.2c**)

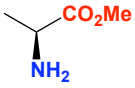

L-alanine methyl ester (**5.2d**)

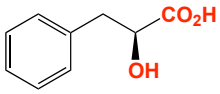

L-phenyllactic acid (**5.3a**)

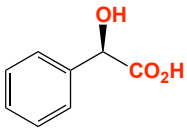

L-mandelic acid (**5.3b**)

Figure 5.23. Structures of amino acids and their methyl esters

The methyl ester of the dipeptides **5.4a** – **h** were synthesized by coupling the α-hydroxycarboxylic acid, L-phenyllactic acid (**5.3a**) and L-mandelic acid (**5.3b**) with the methyl esters of the hydrochloride salts of **5.2a** – **d** using HBTU and DIPEA in good yields (Table 5.9 and Scheme 5.3). Methyl ester of the dipeptides **5.4a** – **h** were heated in the microwave at 140 ^{o}C for 3 min in presence of p-toluene sulphonic acid as a catalyst to afford DKMs derivatives **5.5a** – **h** (Table 5.10, Scheme 5.3).

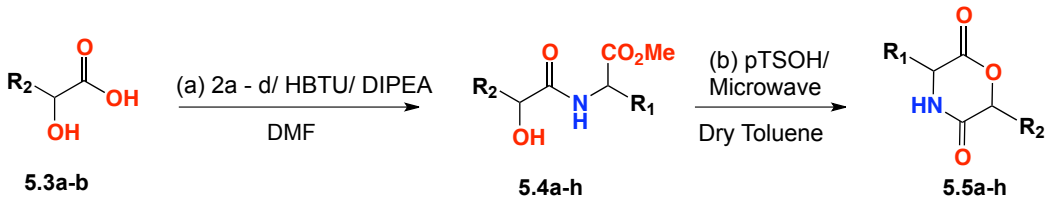

Scheme 5.3. Synthesis of morpholine derivatives **(5.5a – h).** (a)-addition of HBTU/DIPEA in the presence of dry DMF under argon for 3 h. (b)-The reaction mixture was dissolved in 5 mL dry toleune, pTSOH and heated in the microwave at 140 °C, 300 W for 3 min

Table 5.9. Methyl ester of the dipeptides 5.4a – h

Compound No.	R_1	R_2	Yield %
5.4a	Bn	Bn	85
5.4b	Bn	Ph	82
5.4c	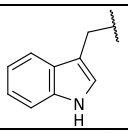	Bn	85
5.4d	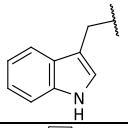	Ph	85
5.4e	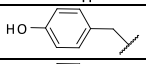	Bn	85
5.4f	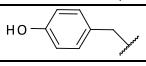	Ph	84
5.4g	Me	Bn	86
5.4h	Me	Ph	85

Table 5.10. DKM derivatives 5.5a – h

Compound No.	R_1	R_2	Yield %
5.5a	Bn	Bn	75
5.5b	Bn	Ph	72
5.5c	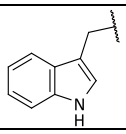	Bn	75
5.5d	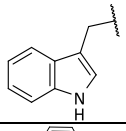	Ph	75
5.5e	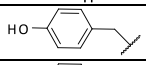	Bn	69
5.5f	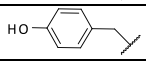	Ph	65
5.5g	Me	Bn	62
5.5h	Me	Ph	69

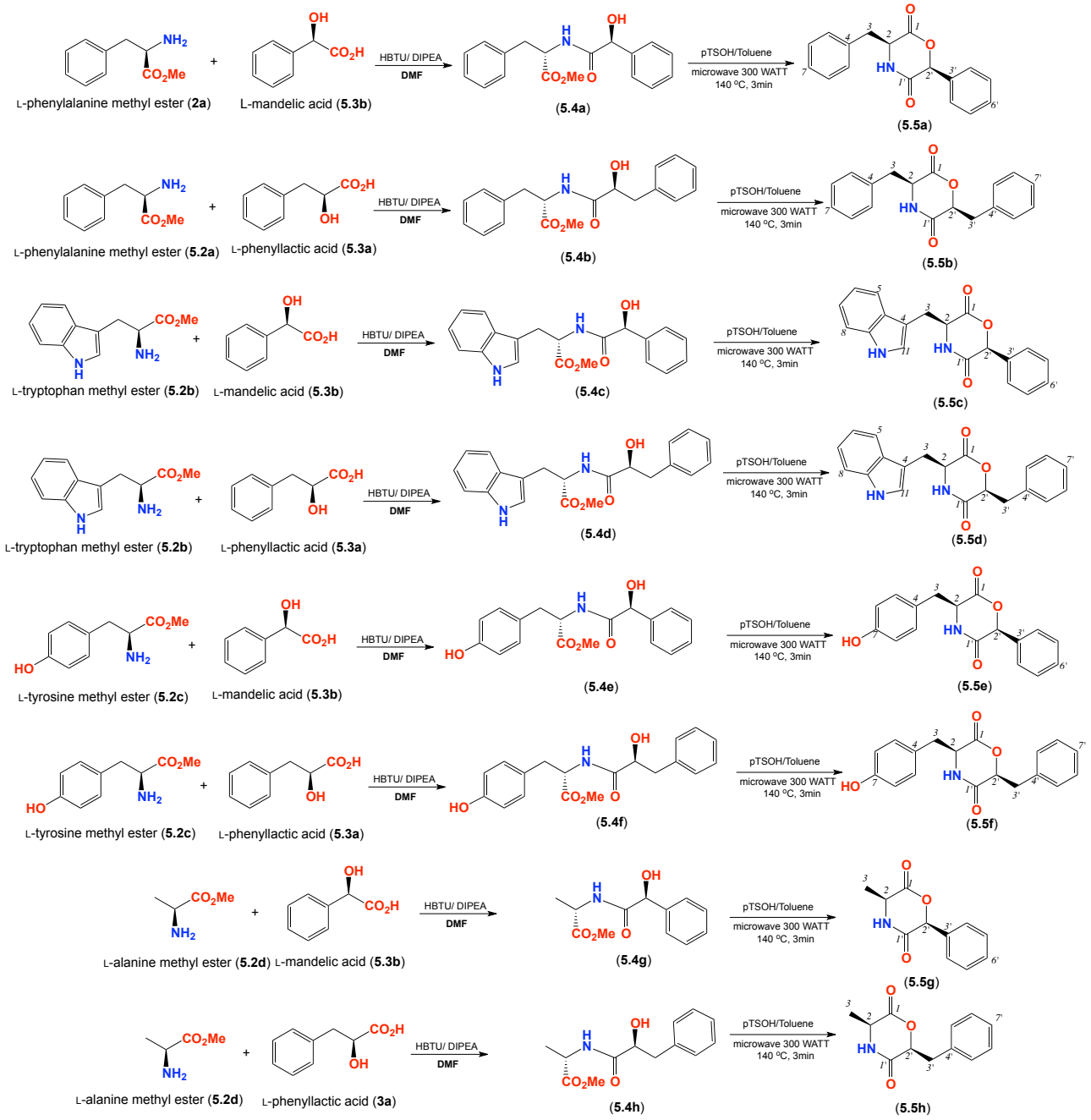

Figure 5.24. Diagram that shows the synthesis of 8 different dioxomorpholine derivatives through the formation of 8 different dipetides intermediates

5.2.6.1 *(S)*-Methyl 2-((*S*)-2-hydroxy-2-phenylacetamido)-3-phenylpropanoate (5.4a)

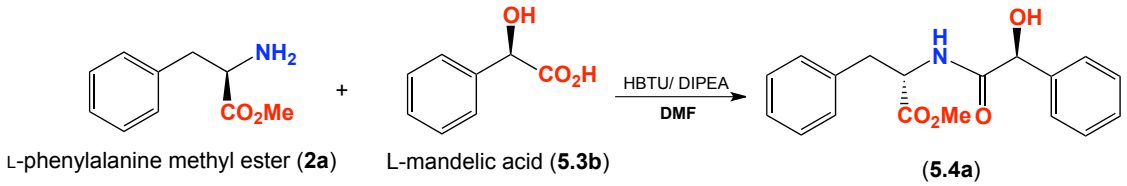

L-phenylalanine methyl ester (**2a**) L-mandelic acid (**5.3b**) (**5.4a**)

The crude product was purified using flash column chromatography (10 – 60% EtOAc/hexane) to yield compound **5.4a** as a white crystals (250 mg, 85%); $[\alpha]_D^{22}$ +914.7 (*c* 0.05, $CHCl_3$); R_f:0.29 (10 –70% EtOAc/hexane and $KMnO_4$ dip). ESIMS, *m/z*: 314 $[M + H]^+$. HRESI(+)MS calculated for $C_{18}H_{19}N_1NaO_4$ 336.1206, found 336.1252. ^{1}H NMR (600 MHz, $CDCl_3$) δ_H 7.24 (2H, m), 7.18 (5H, m), 6.99 (1H, d, *8.1*), 6.93 (2H, m), 4.91 (1H, d, *2.3*), 4.76 (1H, dd, *13.6, 6.6*), 3.90 (1H, brd), 3.63 (3H, s), 3.06 (1H, dd, *13.6, 6.6*), 2.95 (1H, dd, *13.6, 6.6*); ^{13}C NMR (150 MHz, $CDCl_3$) δ_C 172.1, 171.9, 139.1, 135.7, 129.3, 128.7, 128.6, 128.5, 127.1, 126.7, 74.3, 52.9, 52.5, 37.7.

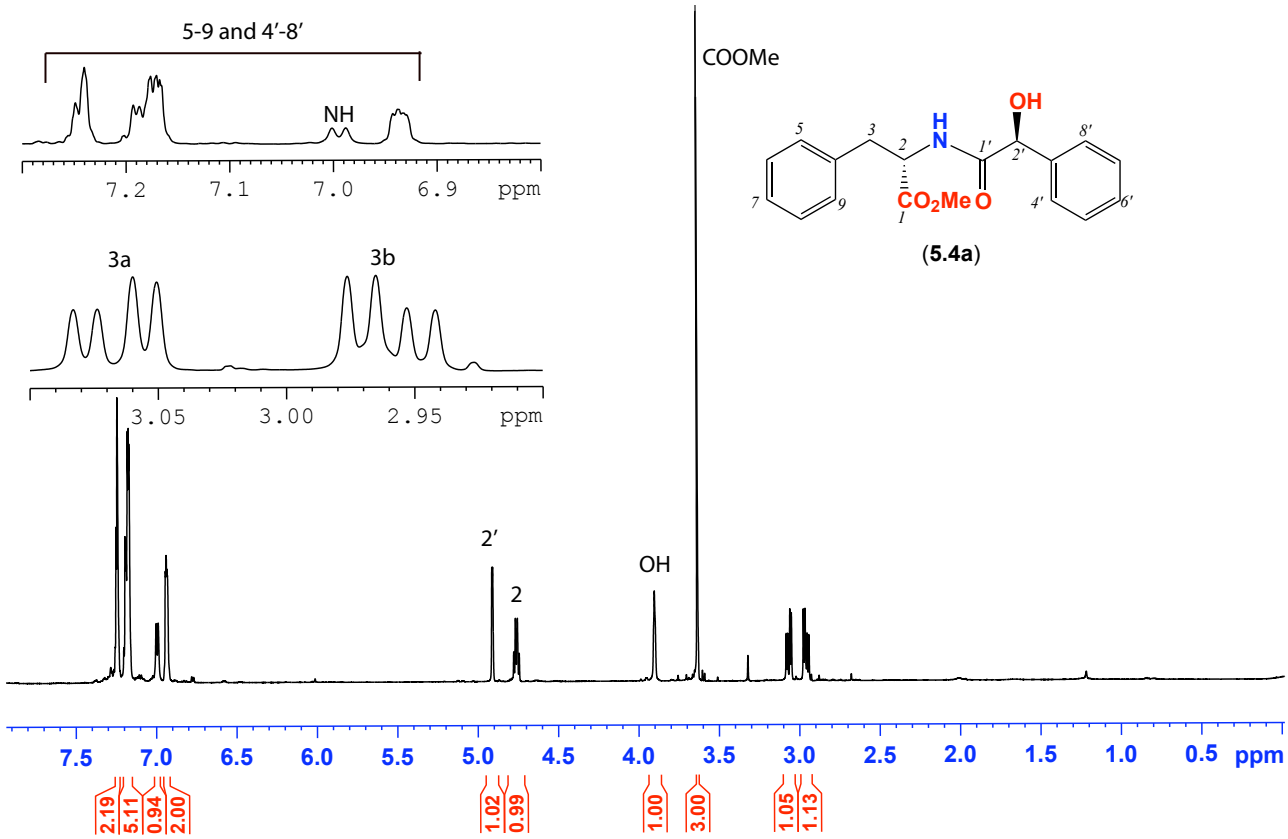

Figure 5.25. ^{1}H NMR (600 MHz, $CDCl_3$) of *(S)*-Methyl-2-((*S*)-2-hydroxy-2-phenylacetamido)-3-phenylpropanoate **(5.4a)**

5.2.6.2 (*S*)-Methyl 2-((*S*)-2-hydroxy-3-phenylpropanamido)-3-phenylpropanoate (5.4b)

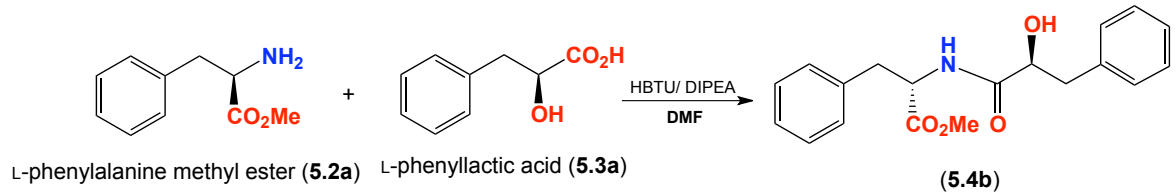

L-phenylalanine methyl ester (**5.2a**) L-phenyllactic acid (**5.3a**) (**5.4b**)

The crude product was purified using flash column chromatography (10 – 60% EtOAc/hexane) to yield compound **5.4b** as white crystals (200 mg, 82%); $[\alpha]_D^{22}$ +60.7 (*c* 0.25, $CHCl_3$); R_f:0.31 (10-70% EtOAc/hexane and $KMnO_4$ dip). ESIMS, *m/z*: 328 $[M + H]^+$. HRESI(+)MS calculated for $C_{19}H_{22}N_1O_4$ 328.1543, found 328.1550. ^{1}H NMR (600 MHz, $CDCl_3$) δ_H 7.28 (2H, t, *7.4*), 7.21 (6H, m), 7.06 (1H, d, *8.0*), 6.92 (2H, d, *8.0*), 4.83 (1H, ddd, *14.8, 8.0, 6.8*), 4.25 (1H, dd, *8.0, 6.8*), 3.64 (3H, s), 3.29 (1H, br d), 3.08 (1H, dd, *8.0, 6.8*), 2.99 (2H, dd, *8.0, 6.8*), 2.77 (1H, dd, *14.8, 6.8*); ^{13}C NMR (150 MHz, $CDCl_3$) δ_C 174.2, 173.4, 138.5, 137.2, 131.3, 130.8, 130.1, 130.1, 128.6, 128.4, 74.2, 54.1, 53.9, 42.1, 39.6. (Figure 5.26)

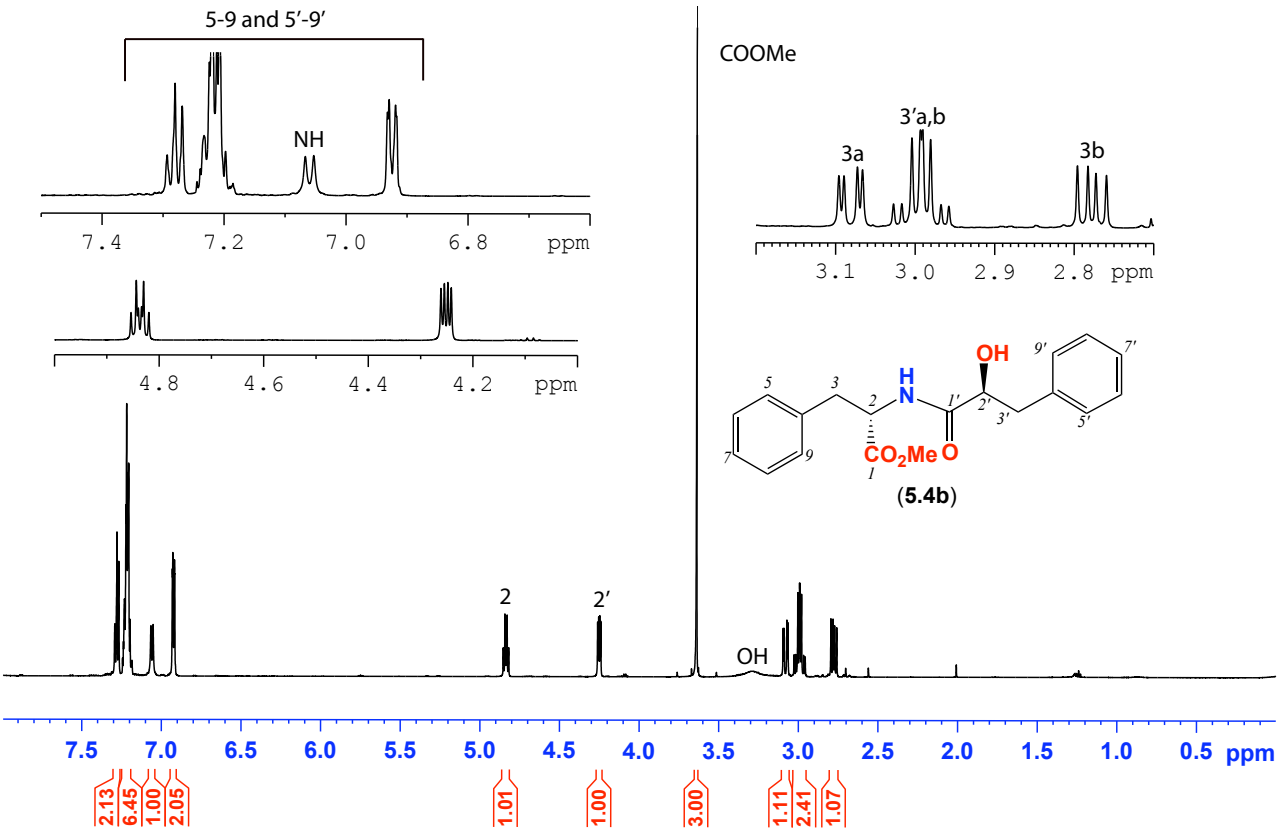

Figure 5.26. ^{1}H NMR (600 MHz, $CDCl_3$) spectrum of (*S*)-Methyl-2-((*S*)-2-hydroxy-3-phenylpropanamido)-3-phenylpropanoate **(5.4b)**

5.2.6.3 (*S*)-Methyl 2-((*S*)-2-hydroxy-2-phenylacetamido)-3-(1H-indol-3-yl)propanoate (5.4c)

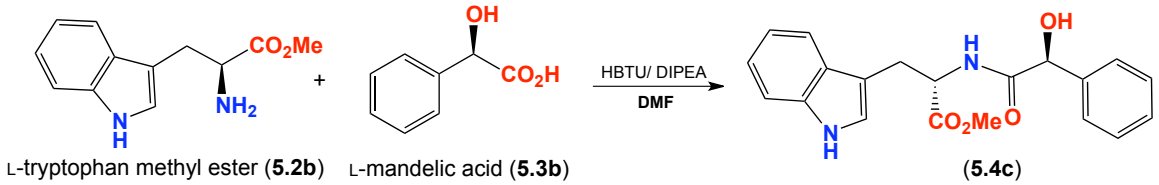

L-tryptophan methyl ester (**5.2b**) L-mandelic acid (**5.3b**) (**5.4c**)

The crude product was purified using flash column chromatography (10-60% EtOAc/hexane) to yield compound **5.4c** as white oil (210 mg, 83%); $[\alpha]_D^{22}$ +20.5 (*c* 0.05, $CHCl_3$); R_f*:* 0.28 (10 – 70% EtOAc/hexane and $KMnO_4$ dip). ESIMS, *m/z*: 367 $[M + H]^+$. HRESI(+)MS calculated for $C_{21}H_{23}N_2O_4$ 367.1652, found 367.1628. ^{1}H NMR (600 MHz, $CDCl_3$) δ_H 7.87 (1H, brd), 6.99 (1H, d, *8.0*), 6.76 (4H, m), 6.69 (3H, m), 6.61 (2H, dd, *15.3, 7.8*), 6.28 (1H, s), 4.43 (1H, s), 4.38 (1H, ddd, *13.5, 8.0, 5.8*), 3.50 (1H, br d), 3.13 (3H, s), 2.78 (2H, d, *5.8*); ^{13}C NMR (150 MHz, $CDCl_3$) δ_C 172.3, 139.1, 136.2, 128.7, 128.4, 127.5, 126.7, 123.1, 122.2, 119.7, 118.5, 111.5, 109.4, 74.1, 52.8, 52.5, 27.5. (Figure 5.27).

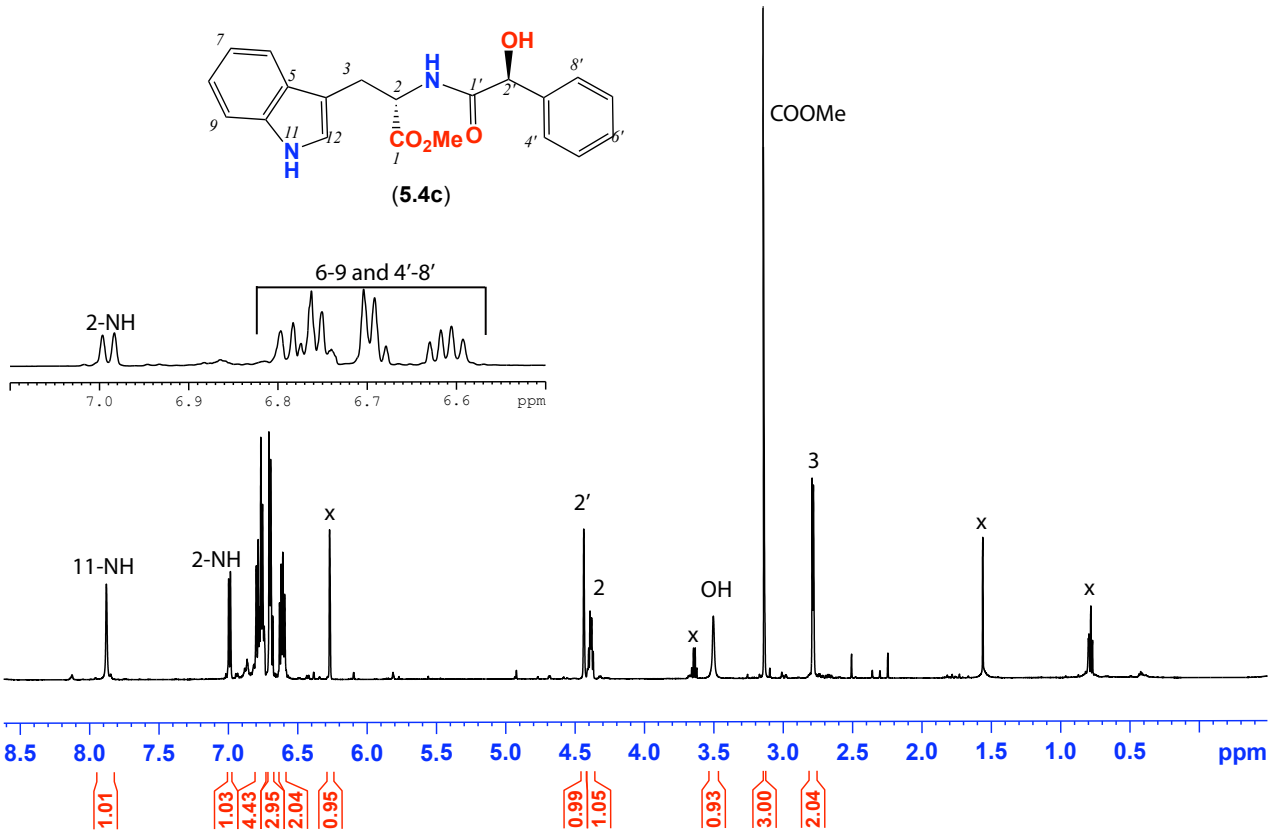

Figure 5.27. ^{1}H NMR (600 MHz, $CDCl_3$) spectrum of (*S*)-Methyl-2-((*S*)-2-hydroxy-2-phenylacetamido)-3-(1H-indol-3-yl)propanoate (**5.4c**). (x) impurities + EtOAc traces

5.2.6.4 (*S*)-Methyl 2-((*S*)2-hydroxy-3-phenylpropanamido)-3-(1H-indol-3-yl) propanoate (5.4d)

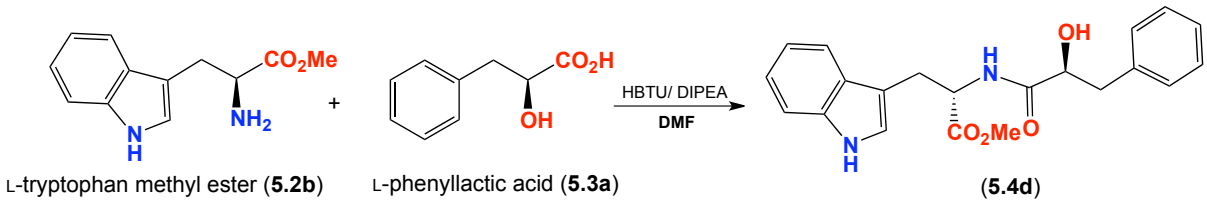

L-tryptophan methyl ester (**5.2b**) L-phenyllactic acid (**5.3a**) (**5.4d**)

The crude product was purified using flash column chromatography (10 – 60% EtOAc/hexane) to yield compound **5.4d** as white oil (150 mg, 85%); $[\alpha]_D^{22}$ +180.4 (*c* 0.05, $CHCl_3$); R_f*:* 0.29 (10-70% EtOAc/hexane and $KMnO_4$ dip). ESIMS, m/z: 367 $[M + H]^+$. HRESI(+)MS calculated for $C_{21}H_{22}N_2NaO_4$ 389.1472, found 389.1475. ^{1}H NMR (600 MHz, $CDCl_3$) δ_H 7.55 (1H, d, *8.0*), 7.30 (2H, t, *8.3*), 7.27 (2H, t, *8.3*), 7.17 (3H, m), 7.10 (2H, d, *7.6*), 6.99 (1H, d, *8.2*), 6.89 (1H, t, *7.6*), 6.53 (1H, s), 6.17 (1H, d, *7.6*), 4.76 (1H, ddd, *12.4, 8.0, 5.2*), 4.66 (1H, ddd, *13.1, 7.6, 5.8*), 4.06 (1H, dd, *7.6, 4.1*), 3.61 (3H, s), 3.25 (1H, dd, *13.1, 5.8*), 3.15 (1H, dd, *13.1, 5.8*), 3.09 (1H, dd, *14.8, 5.5*), 3.02 (1H, dd, *13.9, 10.1*), 2.98 (1H, dd, *12.4, 8.0*), 2.75 (1H, dd, *12.4, 8.0*); ^{13}C NMR (150 MHz, $CDCl_3$) δ_C 172.8, 171.9, 170.7, 129.8, 128.8, 127.2, 123.7, 123.2, 120.0, 119.7, 119.2, 118.7, 111.3, 111.2, 72.7, 53.3, 52.8, 52.5, 40.4, 27.9, 27.4 (Figure 5.28). **5.4d** was not pure and was contaminated with the starting material(s).

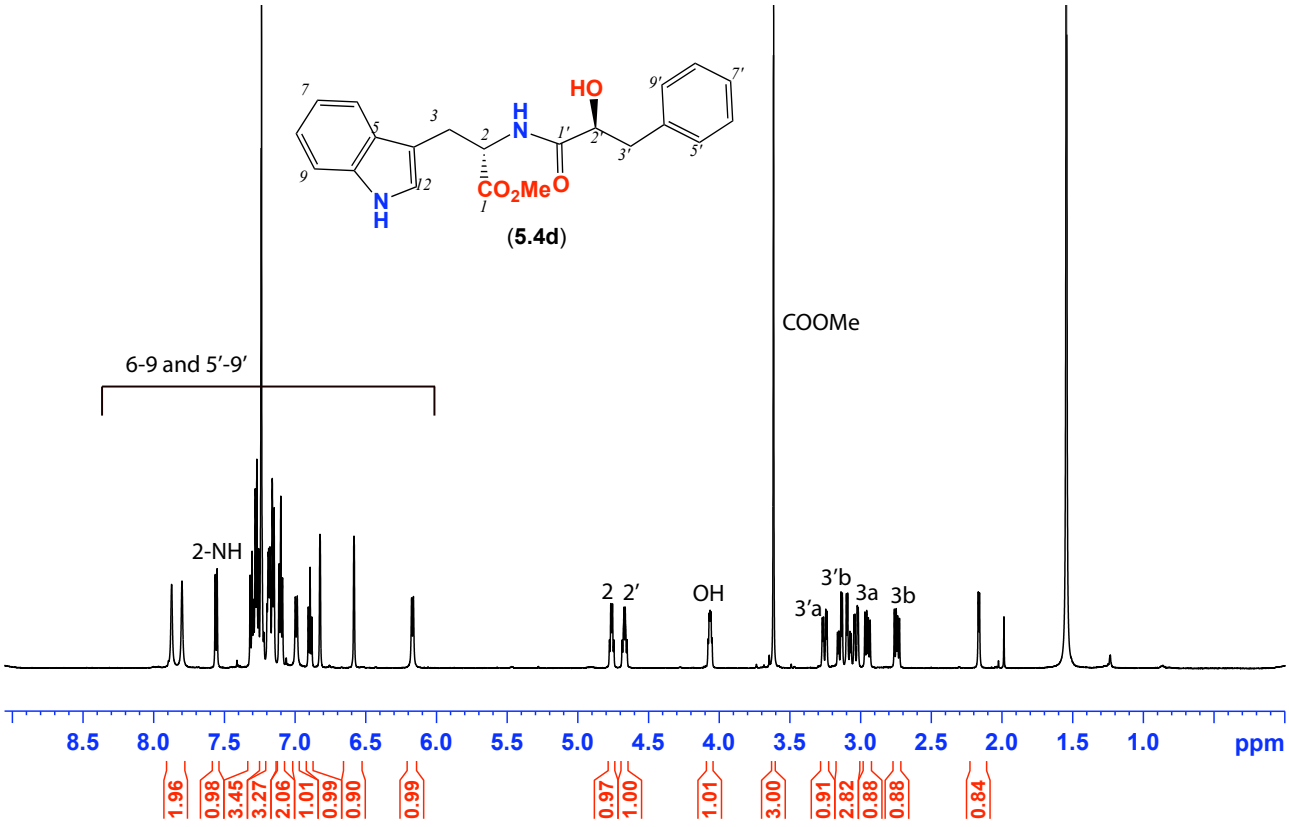

Figure 5.28. ^{1}H NMR (600 MHz, $CDCl_3$) spectrum of (*S*)-Methyl 2-((*S*)2-hydroxy-3-phenylpropanamido)-3-(1H-indol-3-yl) propanoate (**5.4d**)

5.2.6.5 (*S*)-Methyl-2-((*S*)-2-hydroxy-2-phenylacetamido)-3-(4-hydroxyphenyl)propanoate (5.4e)

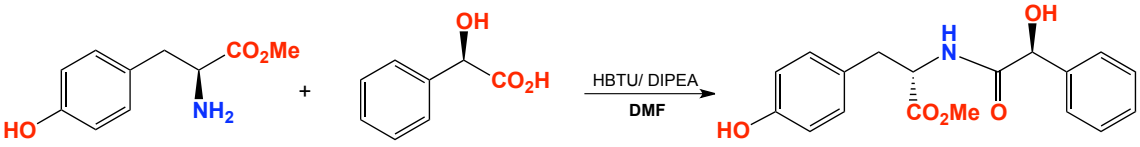

L-tyrosine methyl ester (**5.2c**) L-mandelic acid (**5.3b**) (**5.4e**)

The crude product was purified using flash column chromatography (10 – 70% EtOAc/hexane) to yield compound **5.4e** as a white powder (150 mg, 85%); $[\alpha]_D^{22}$ +167.5 (*c* 0.15, $CHCl_3$); R_f*:* 0.29 (10-70% EtOAc/hexane and $KMnO_4$ dip). ESIMS, m/z: 330 $[M + H]^+$. HRESI(+)MS calculated for $C_{18}H_{20}N_1O_5$ 330.1336, found 330.1320. ^{1}H NMR (600 MHz, $CDCl_3$) δ 7.22 (2H, m), 7.16 (2H, m), 7.11 (1H, d *7.7*), 6.93 (1H, brd), 6.76 (2H, d, *7.7*), 6.52 (1H, d, *7.7*), 4.92 (1H, brd), 4.75 (1H, dd, *14.1, 6.9*), 3.93 (2H, br s), 3.63 (3H, s), 3.01 (1H, dd, *14.1, 6.9*), 2.89 (1H, dd, *14.1, 6.9*); ^{13}C NMR (150 MHz, $CDCl_3$) δ 172.5, 172.3, 155.4, 138.8, 130.3, 128.8, 126.8, 115.7, 74.4, 53.1, 52.7, 37.0. (Figure 5.29).

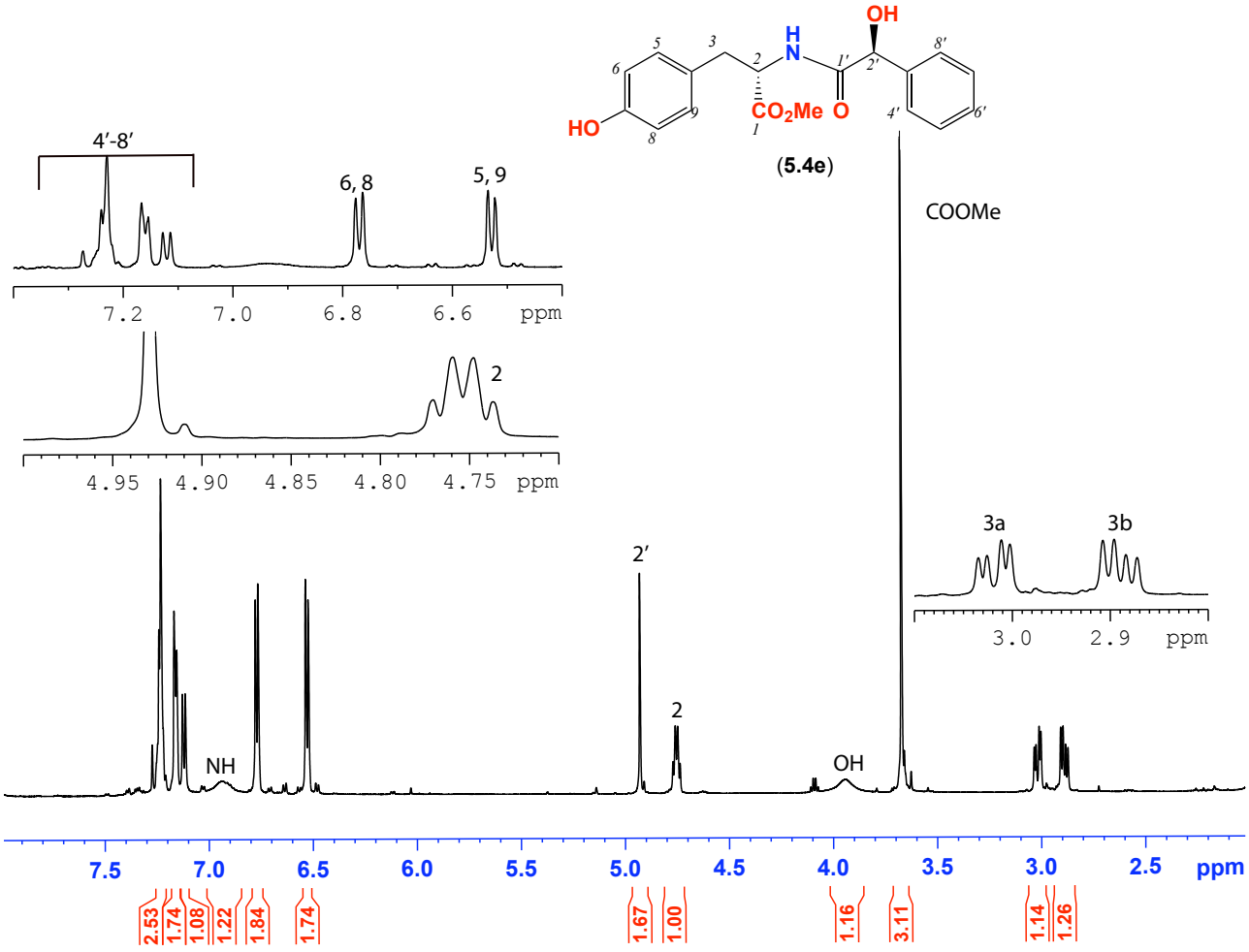

Figure 5.29. ^{1}H NMR (600 MHz, $CDCl_3$) spectrum of (*S*)-Methyl-2-((*S*)-2-hydroxy-2-phenylacetamido)-3-(4-hydroxyphenyl) propanoate (**5.4e**)

5.2.6.6 (*S*)-Methyl-2-(*S*)-2-hydroxy-3-phenylpropanamido)-3-(4-hydroxyphenyl) propanoate (5.4f)

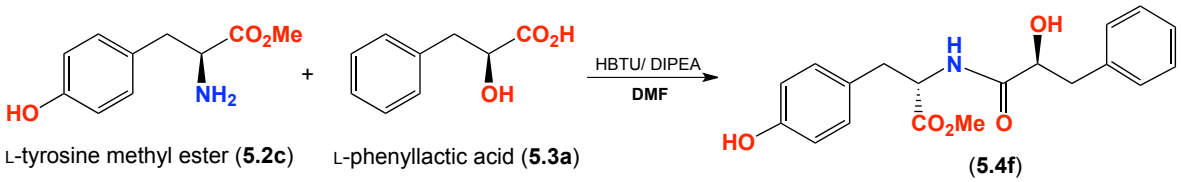

L-tyrosine methyl ester (**5.2c**) L-phenyllactic acid (**5.3a**) (**5.4f**)

The crude product was purified using flash column chromatography (10-70% EtOAc/hexane) to yield compound **5.4f** as a white powder (150 mg, 85%); $[\alpha]_D^{22}$ +167.5 (*c* 0.15, $CHCl_3$); R_f*:* 0.29 (10-70% EtOAc/hexane and $KMnO_4$ dip). ESIMS, *m/z*: 343 $[M + H]^+$. HRESI(+)MS calculated for $C_{19}H_{22}N_1O_5$ 344.1492, found 344.1481. ^{1}H NMR (600 MHz, $CDCl_3$) δ_H 7.28 - 7.19 (5H, m), 7.04 (1H, d, *7.7*) 6.76 (2H, d, *7.7*), 6.65 (1H, d, *7.7*), 4.82 (1H, dd, *13.8, 6.4*), 4.27 (1H, dd, *13.9, 5.9*), 3.69 (3H, s), 3.10 (1H, dd, *13.8, 6.4*), 2.95 (1H, dd, *13.9, 5.9*), 2.90 (1H, dd, *13.9, 5.9*), 2.78 (1H, dd, *13.8, 6.4*); ^{13}C NMR (150 MHz, $CDCl_3$) δ_C 174.5, 173.8, 156.9, 138.2, 131.8, 131.2, 130.1, 128.5, 117.1, 78.8, 78.6, 78.4, 74.2, 54.2, 54.0, 42.0, 38.7 (Figure 5.30).

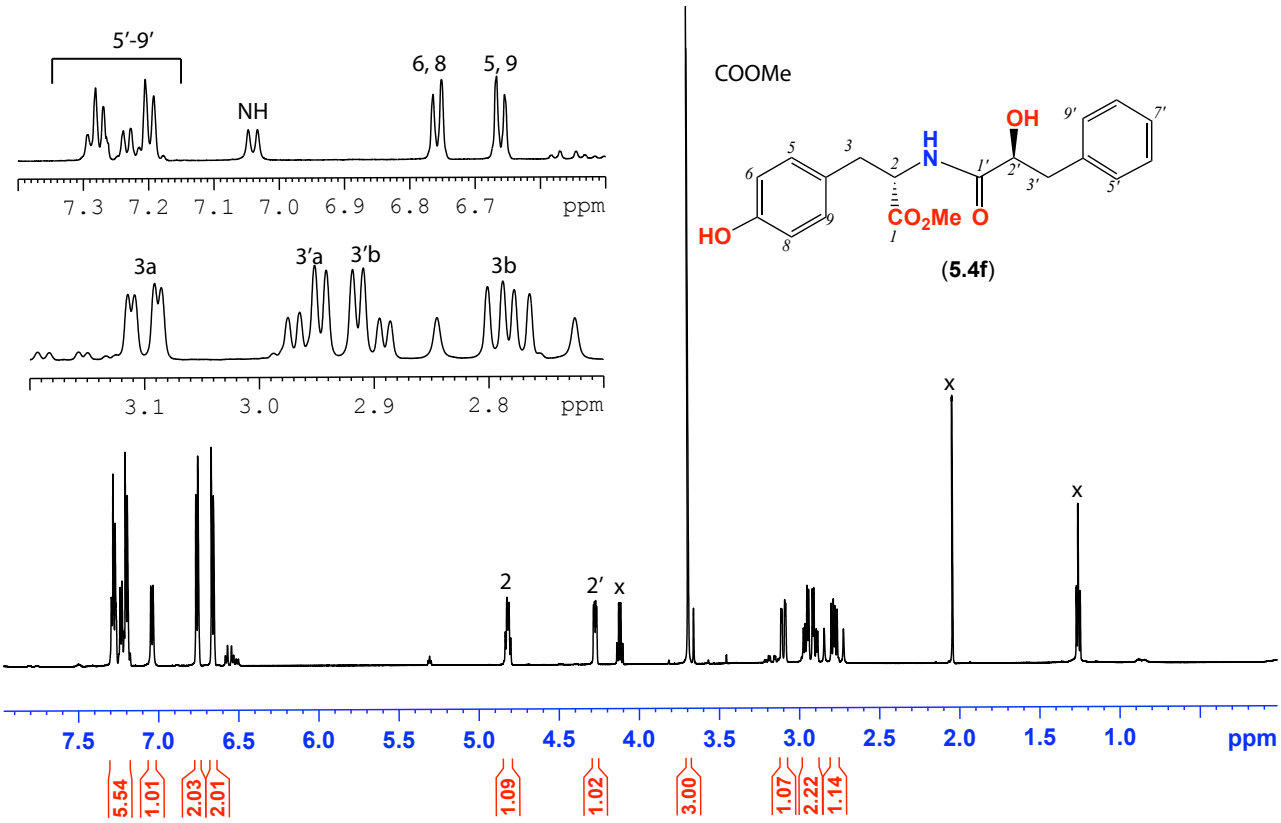

Figure 5.30. ^{1}H NMR (600 MHz, $CDCl_3$) spectrum of (*S*)-Methyl-2-(*S*)-2-hydroxy-3-phenylpropanamido)-3-(4-hydroxyphenyl) propanoate (**5.4f**). (x) traces of EtOAc

5.2.6.7 (*S*)-Methyl 2-((*S*)-2-hydroxy-2-phenylacetamido)propanoate (5.4g)

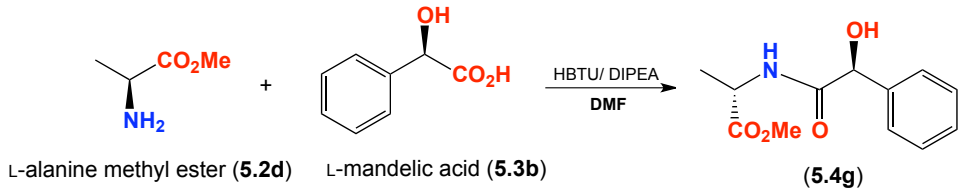

L-alanine methyl ester (**5.2d**) L-mandelic acid (**5.3b**) (**5.4g**)

The crude product was purified using flash column chromatography (10-70% EtOAc/hexane) to yield compound **5.4g** as colourless oil (200 mg, 86%); $[\alpha]_D^{22}$ –161.7 (*c* 0.25, $CHCl_3$); R_f*:* 0.26 (10-70% EtOAc/hexane in and $KMnO_4$ dip). ESIMS, m/z: 238 $[M + H]^+$. HRESI(+)MS calculated for $C_{12}H_{15}N_1NaO_4$ 260.0893, found 260.0899. ^{1}H NMR (600 MHz, $CDCl_3$) δ_H 6.92 - 6.55 (5H, m), 6.54 (1H, br d, *7.1*), 4.55 (1H, s), 4.06 (1H, dd, *14.5, 7.1*), 3.59 (1H, brd), 3.23, (3H, s), 0.90 (3H, d, *7.1*); ^{13}C NMR (150 MHz, $CDCl_3$) δ_C 173.3, 172.2, 139.2, 128.8, 128.6, 126.8, 74.1, 52.6, 48.1, 18.2. (Figure 5.31).

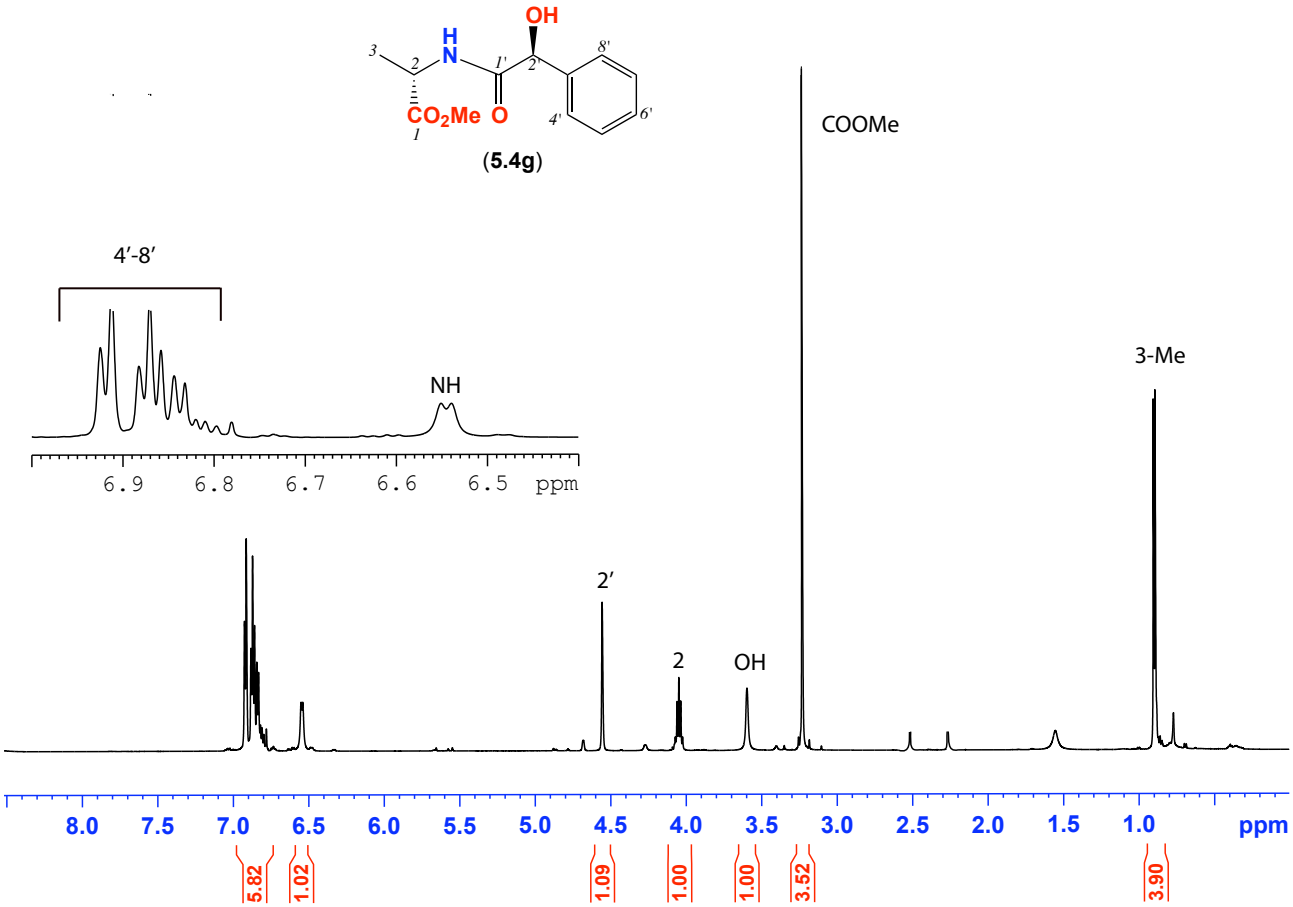

Figure 5.31. ^{1}H NMR (600 MHz, $CDCl_3$) spectrum of (*S*)-Methyl 2-((*S*)-2-hydroxy-2-phenylacetamido)propanoate **(5.4g)**

5.2.6.8 (*S*)-Methyl 2-((*S*)-2-hydroxy-3-phenylpropanamido)propanoate (5.4h)

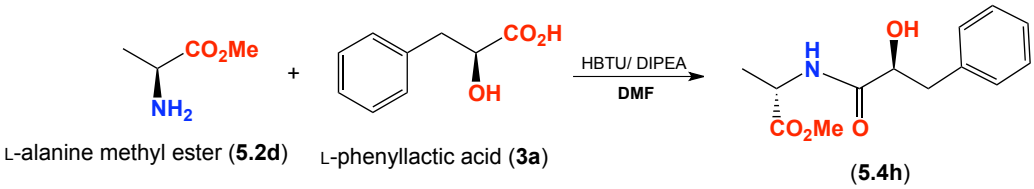

L-alanine methyl ester (**5.2d**) L-phenyllactic acid (**3a**) (**5.4h**)

The crude product was purified using flash column chromatography (10-70% EtOAc/hexane) to yield compound **5.4h** as colourless oil (200 mg, 85%); $[\alpha]_D^{22}$ −160.7 (*c* 0.25, $CHCl_3$); *R_f:* 0.16 (10-70% EtOAc/hexane and $KMnO_4$ dip). ESI MS, *m/z*: 252 $[M + H]^+$. HRESI(+)MS calculated for $C_{13}H_{18}NO_4$ 252.1230, found 252.1253. ^{1}H NMR (600 MHz, $CDCl_3$) δ_H 7.25 – 7.13 (6H, m), 4.47 (1H, q, *7.3*), 4.27 (1H, br), 3.97 (1H, d, *4.6*), 3.63 (3H, s), 3.10 (1H, dd, *13.9, 4.6*), 2.85 (1H, dd, *13.9, 4.6*), 1.24 (3H, d, *7.3*); ^{13}C NMR (150 MHz, $CDCl_3$) δ_C 174.8, 174.7, 138.6, 131.2, 129.8, 128.2, 74.1, 54.0, 49.1, 42.1, 19.5. (Figure 5.32).

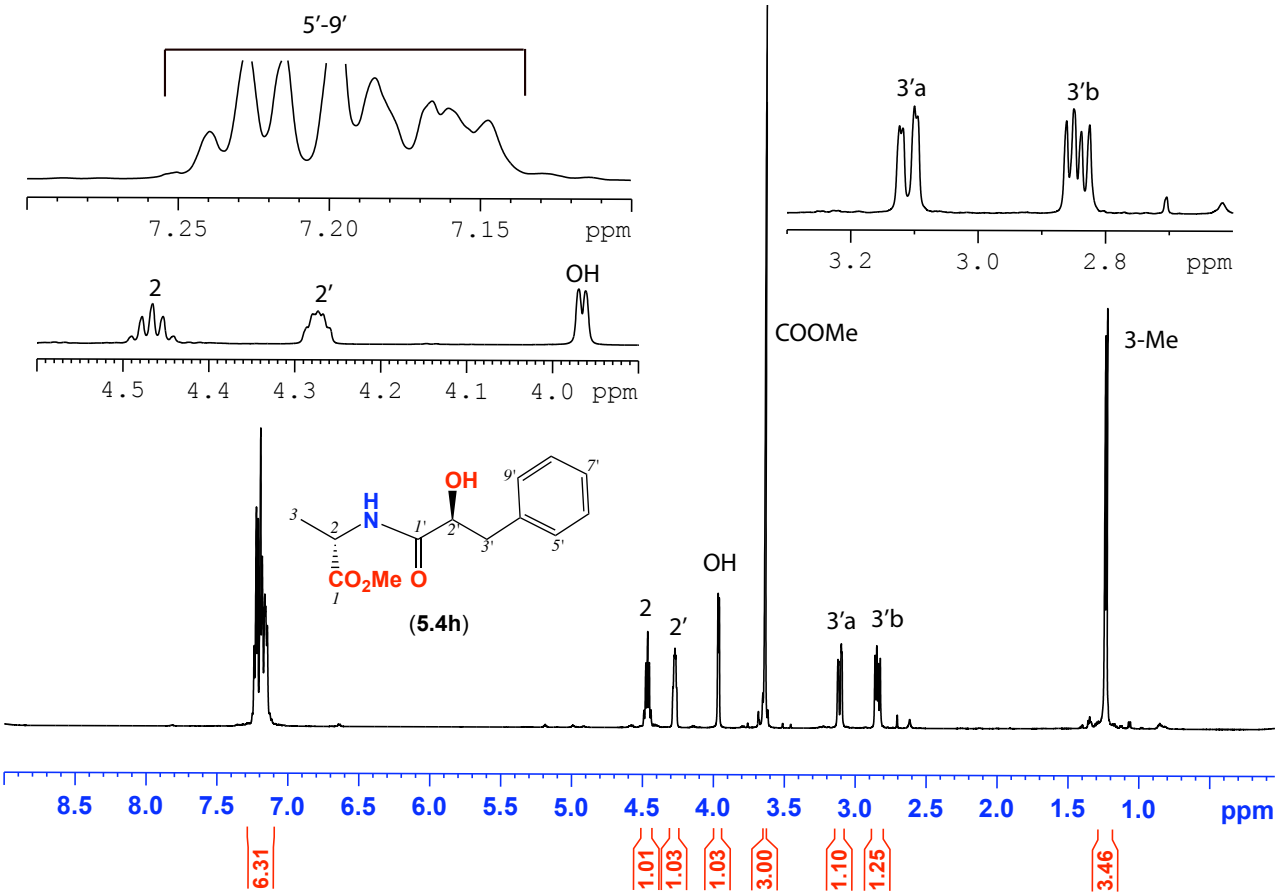

Figure 5.32. ^{1}H NMR (600 MHz, $CDCl_3$) spectrum of (*S*)-Methyl 2-((*S*)-2-hydroxy-3-phenylpropanamido)propanoate **(5.4h)**

5.2.7 General method for the preparation of the morpholine compounds 5.5a – h

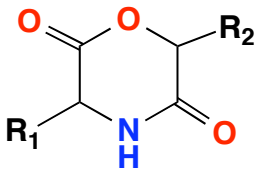

The dipeptides **5.4a – h** (50 mg) were dissolved in anhydrous toluene (5 mL) in the presence of para toluene sulfonic acid (0.10 mg). The reaction was put in the microwave at 300 W, 140 °C for 10 min. The reaction mixture was dried *in vacuo*. The crude extract was further purified using HPLC.

5.2.7.1 (3*S*,6*S*)-3-benzyl-6-phenylmorpholine-2,5-dione (5.5a)

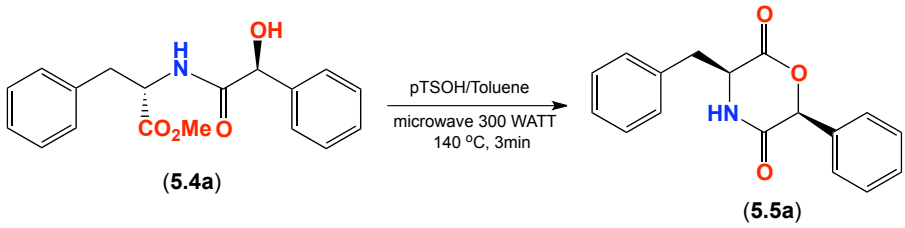

HRESI(+)MS analysis of **5.5a** returned a molecular formula ($C_{17}H_{15}N_1O_3$, Δ mmu +0.7). The crude product was purified using HPLC (10 – 70% MeCN/H_2O) over 30 min, 3 mL/min using Zorbax C_8 to yield compound **5.5a** as a colourless oil (3 mg, 75%); $[\alpha]_D^{22}$ –73.9 (*c* 0.04, $CHCl_3$); R_f: 0.19 (10-60% EtOAc/hexane and $KMnO_4$ dip) (Figure 5.33 and Table 5.11).

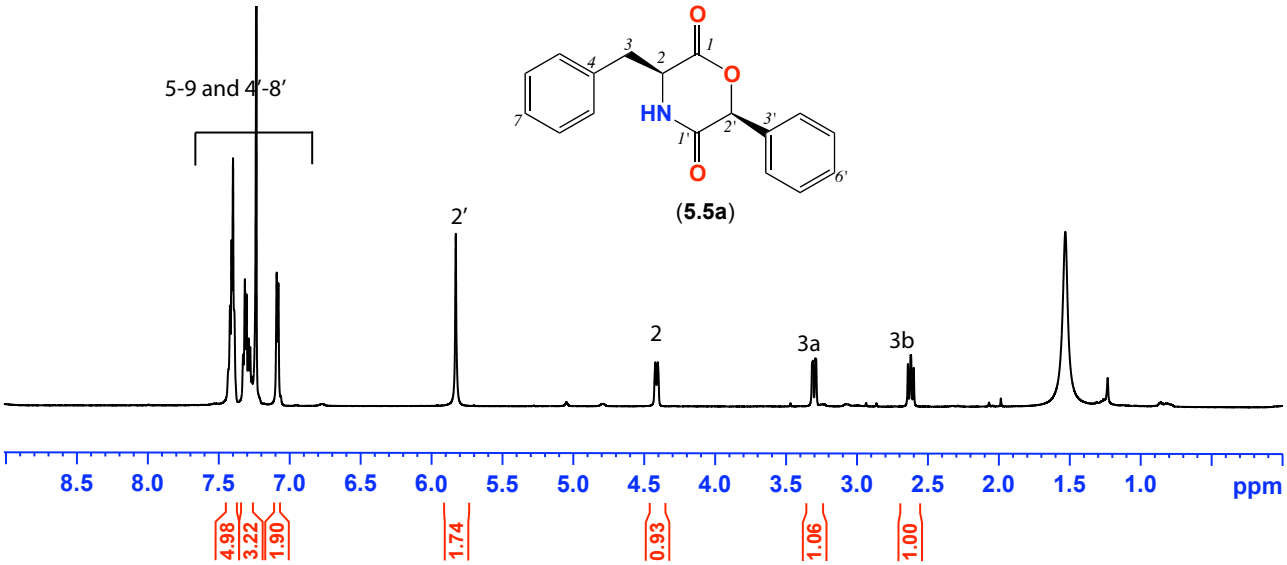

Figure 5.33. ^{1}H NMR (600 MHz, $CDCl_3$) spectrum of (3*S*,6*S*)-3-benzyl-6-phenylmorpholine-2,5-dione **(5.5a)**

Table 5.11. NMR (600 MHz, $CDCl_3$) data of **5.5a**

Pos.	δ_H, mult, (*J* in Hz)	δ_C[a]	COSY	$^1H - ^{13}C$ HMBC	ROESY
1		162.3			
2	5.56, s	55.4	3a,b	1	2′
2-NH	[c]				
3	a 3.30, dd *(13.3, 2.7)*	39.3	2, 3b		
	b 2.62, dd *(13.3, 2.7)*		2, 3a		
4		129.5			
5	7.35[b], m	129.5[d]	8	7	
6	7.10[b], m	128.0[d]	7, 9	5	
7	7.35[b], m	129.5[d]			
8	7.10[b], m	128.0[d]			
9	7.35[b], m	129.5[d]			
1′		162.2			
2′	4.48, d *(13.3)*	79.7		1′	2
3′		129.3			
4′	7.40[b], m	129.4[d]			
5′	7.40[b], m	126.5[d]			
6′	7.40[b], m	126.5[d]			
7′	7.40[b], m	126.5[d]			
8′	7.40[b], m	129.4[d]			

*(a) assignments supported by HSQC. (b) Overlapping reasonces. (c) Signals not observed. (d) Interchangeable resonances

5.2.7.2 (3*S*,6*S*)-3,6-dibenzylmorpholine-2,5-dione (5.5b)

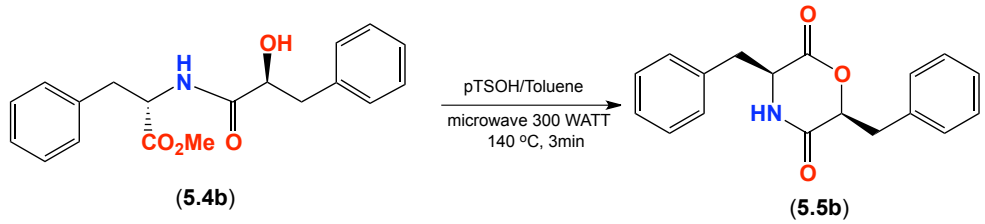

(**5.4b**) (**5.5b**)

HRESI(+)MS analysis of **5.5b** returned a molecular formula ($C_{18}H_{17}N_1O_3$, Δmmu +0.4). The crude product was purified using HPLC (10 – 70% MeCN/H_2O) over 30 min, 3 mL/min using Zorbax C_8 to yield compound **5.5b** as white crystals (2.5 mg, 72%); $[\alpha]_D^{22}$ –446.1 (*c* 0.05, $CHCl_3$); R_f *:* 0.16 (10 – 60% EtOAc/hexane and $KMnO_4$ dip) (Figure 5.34 and Table 5.12).

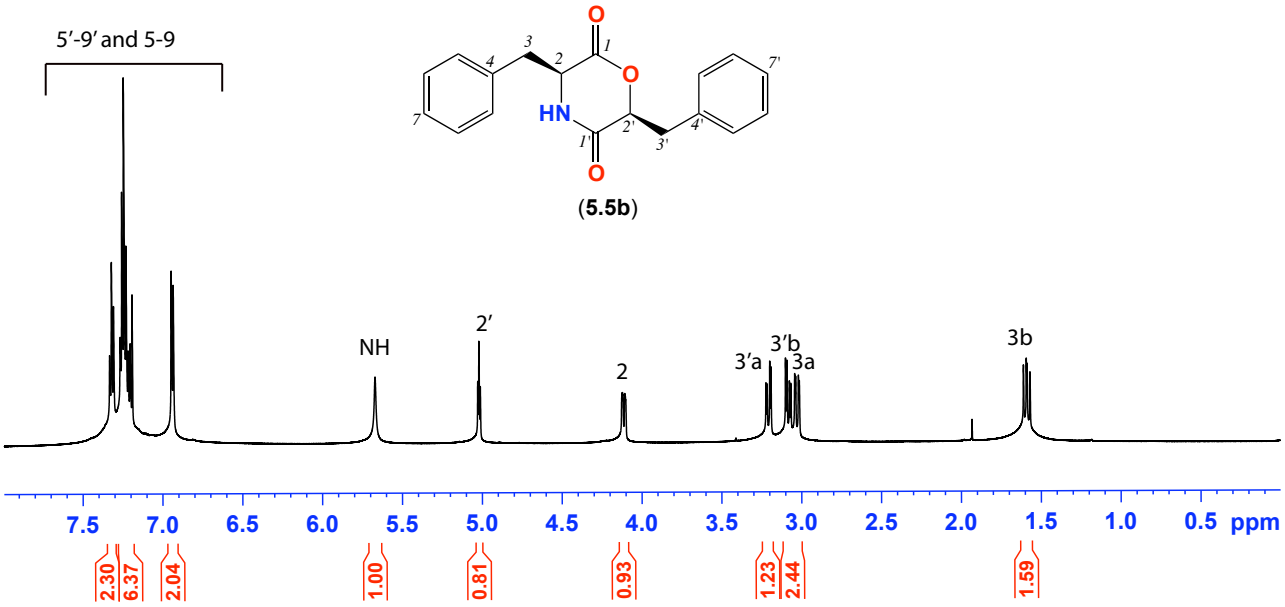

Figure 5.34. ^{1}H NMR (600 MHz, $CDCl_3$) of (3*S*,6*S*)-3,6-dibenzylmorpholine-2,5-dione (**5.5b**)

Table 5.12. NMR (600 MHz, $CDCl_3$) data of **5.5b**

Pos.	δ_H, mult, (*J* in Hz)	δ_C[a]	COSY	^{1}H – ^{13}C HMBC	ROESY
1		167.1			
2	4.11, d *(10.5)*	54.7	3a,b	1	2′
2-NH	5.67, br s			1′	
3a	3.02, dd *(13.9, 3.8)*	39.0	2	1, 4	
3b	1.58, dd *(13.9, 3.8)*	39.0	2	1, 4	
4		130.8			
5-9	7.31[b], m	128.3[d]			
1′		166.9			
2′	5.02, t *(5.2)*	78.1	3′a,b	1′	2
3′	a 3.20, dd *(15.8, 5.2)*	38.1	2′	5′/9′	
	b 3.08, dd *(15.8, 5.2)*	38.1	2′	5′/9′	
4′		132.1			
5′-9′	6.93[b], d *(7.1)*	128.8[d]		3′	
6′-8′	7.23[b], m	127.4[d]			

*(a) assignments supported by HSQC. (b) Overlapping reasonaces. (c) Signals not observed. (d) Interchangeable resonances

5.2.7.3 (3*S*,6*S*)-3-((1H-Indol-3-yl)methyl)-6-phenylmorpholine-2,5-dione (5.5c)

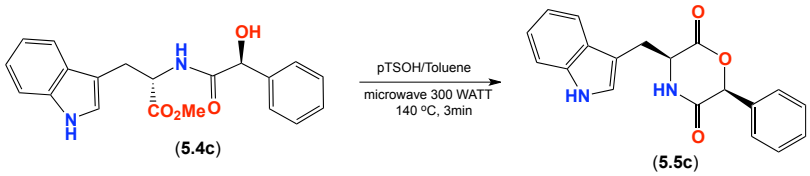

HRESI(+)MS analysis of **5.5c** returned a molecular formula ($C_{19}H_{15}N_2O_3$, Δ mmu −0.2). The crude product was purified using HPLC (10 – 70% MeCN/H_2O) over 30 min, 3 mL/min using Zorbax C_8 to yield compound **5.5c** as a colourless oil (4 mg, 75%); $[\alpha]_D^{22}$ −4.2 (*c* 0.14, $CHCl_3$); R_f: 0.15 (10 – 60% EtOAc/hexane and $KMnO_4$ dip.) (Figure 5.35 and Table 5.13). This compound was to an extent contaminated with the starting material.

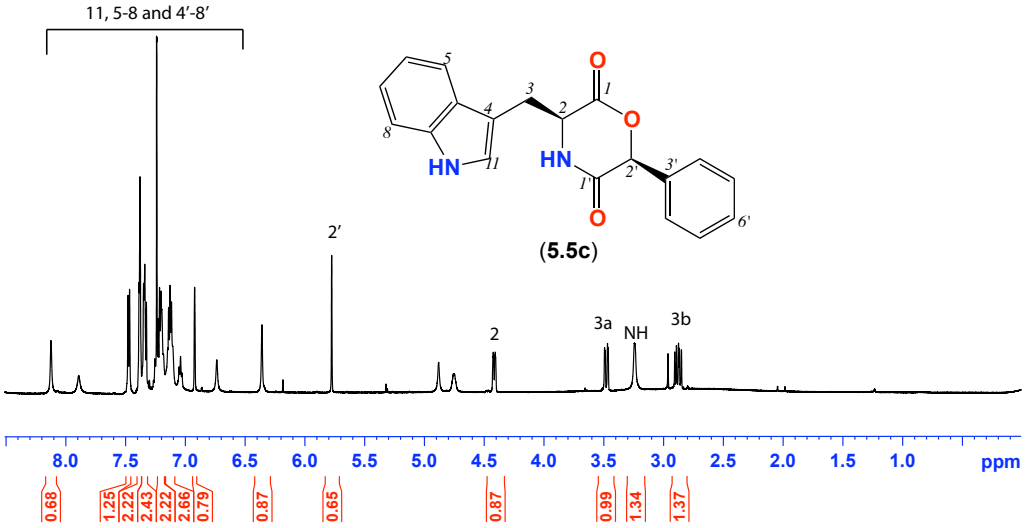

Figure 5.35. ^1H NMR (600 MHz, $CDCl_3$) spectrum of (3*S*,6*S*)-3-((1H-Indol-3-yl)methyl)-6-phenylmorpholine-2,5-dione (**5.5c**)

Table 5.13. NMR (600 MHz, $CDCl_3$) data of **5.5c**

Pos.	δ_H, mult, (*J* in Hz)	δ_C[a]	COSY	^1H – ^{13}C HMBC	ROESY
1		167.1			
2	4.41, t *(8.7)*	54.7	2-NH, 3a,b	1	2′
2-NH	3.24, br s		2		
3	a 3.47, dd *(14.8, 8.4)*	29.4	2	4, 11	
	b 2.87, dd *(14.8, 8.4)*	29.4	2	4, 11	
4		136.6			
4a		133.9			
5	7.37[b], m	128.7[c]			
6	7.34[b], m	128.8[c]			
7	7.34[b], m	129.0[c]			
8	7.47[b], d *(8.4)*	129.5[c]			
9		136.1			
10-NH	8.12, br s		11		
11	7.47[b], d *(8.4)*	118.6[c]			
1′		166.5			
2′	5.77, s	79.5		1′	2
3′		136.6			
4′	7.20[b], m	126.8[c]			
5′	7.12[b], m	128.7[c]			
6′	7.12[b], m	124.0[c]			
7′	7.12[b], m	123.3[c]			
8′	7.12[b], m	122.9[c]			

*(a) assignments supported by HSQC. (b) Overlapping resonances. (c) Interchangeable resonances

5.2.7.4 (3*S*,6*S*)-3-((1H-Indol-3-yl)methyl)-6-benzylmorpholine-2,5-dione (5.5d)

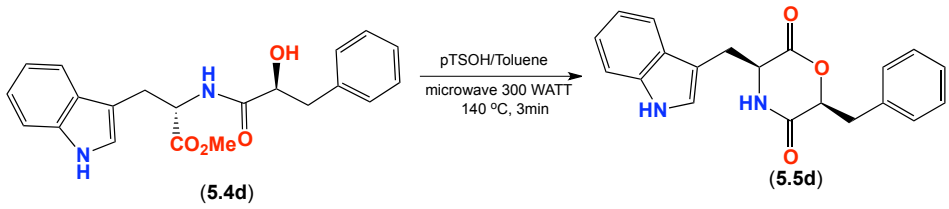

HRESI(+)MS analysis of **5.5d** returned a molecular formula ($C_{20}H_{18}N_2O_3$, Δmmu +1.4). The crude product was purified using HPLC (10 – 70% MeCN/H_2O) over 30 min, 3 mL/min using Zorbax C_8 to yield compound **5.5d** as a colourless oil (4 mg, 75%); $[\alpha]_D^{22}$ –75.6 (*c* 0.05, $CHCl_3$); R_f *:* 0.25 (10-60% EtOAc/hexane and $KMnO_4$ dip) (Figure 5.36 and Table 5.14).

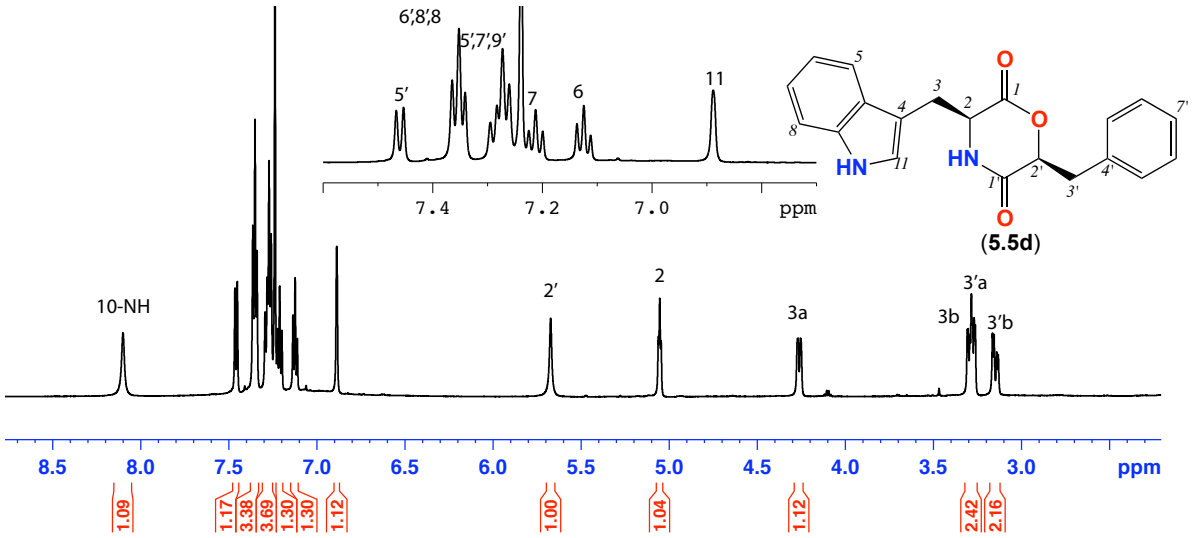

Figure 5.36. ^{1}H NMR (600 MHz, $CDCl_3$) spectrum of (3*S*,6*S*)-3-((1H-indol-3-yl)methyl)-6-benzylmorpholine-2,5-dione (**5.5d**)

Table 5.14. NMR (600 MHz, $CDCl_3$) data of **5.5d**

Pos.	δ_H, mult, (*J* in Hz)	δ_C[a]	COSY	^{1}H – ^{13}C HMBC	ROESY
1		167.1			
2	5.07, t *(11.1)*	53.9	2-NH, 3a,b	1	2′
2-NH	[c]				
3	a 4.28, d *(11.1)*	38.1	2′	4	3
	b 3.31, m		2′	4	
4		135.3			4
5	7.29[b], m	128.5[c]			5
6	7.14, t *(6.9)*	121.2			6
7	7.23, t *(6.9)*	123.8			7
8	7.37[b], t *(7.3)*	124.1[c]			8
9		135.5			9
10-NH	8.12, br				10-NH
1′		165.9			
2′	5.59, br	79.9	3′a,b	1′, 4′	2
3′	a 3.28, m	29.5	2′	4′, 5′	
	b 3.15, dd *(18.1, 6.0)*		2′	4′, 5′	
4′		131.3			
5′	7.41, d *(8.0)*	119.3	6′		
6′	7.37[b], t *(7.3)*	112.5[d]	5′		
7′	7.29[b], m	129.6[d]			
8′	7.37[b], t *(7.3)*	128.6[d]			
9′	7.29[b], m	131.5[d]			

*(a) assignments supported by HSQC. (b) Overlapping resonances. (c) signals not observed. (d) Interchangeable resonaces

5.2.7.5 (3*S*,6*S*)-3-(4-Hydroxybenzyl)-6-phenylmorpholine-2,5-dione (5.5e)

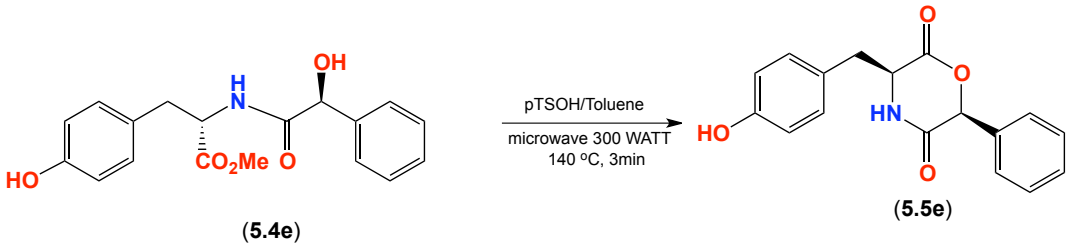

(**5.4e**) (**5.5e**)

HRESI(+)MS analysis of **5.5e** returned a molecular formula ($C_{17}H_{15}N_1O_4$, Δ mmu +0.3). The crude product was purified using HPLC (10 – 70% MeCN/H_2O) over 30 min, 3 mL/min using Zorbax C_8 to yield compound **5.5e** as a colourless oil (2.5 mg, 69%); $[\alpha]_D^{22}$ +0.5 (*c* 0.11, $CHCl_3$); R_f: 0.28 (10-60% EtOAc/hexane and $KMnO_4$ dip) (Figure 5.37 and Table 5.15).

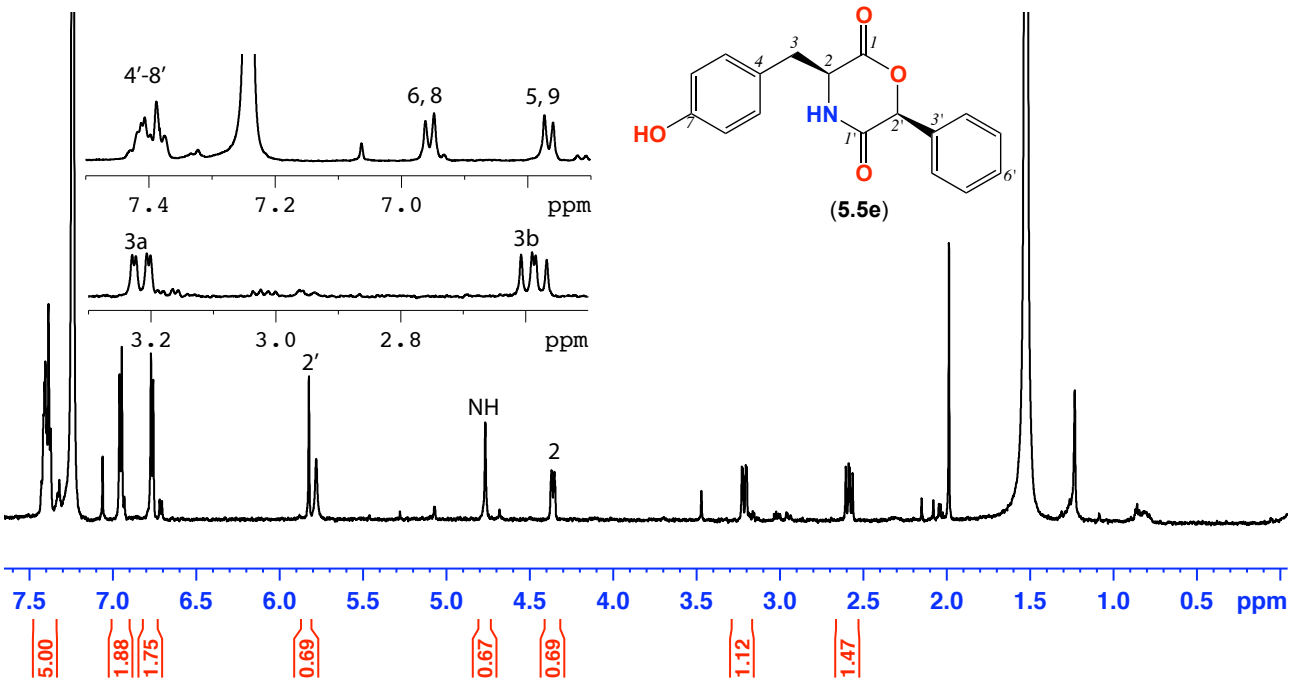

Figure 5.37. ^{1}H NMR (600 MHz, $CDCl_3$) spectrum of (3*S*,6*S*)-3-(4-Hydroxybenzyl)-6-phenylmorpholine-2,5-dione (**5.5e**)

Table 5.15. NMR (600 MHz, $CDCl_3$) data of **5.5e**

Pos.	δ_H, mult, (*J* in Hz)	δ_C[a]	COSY
1		166.5	
2	4.36, dd *(14.1, 10.4)*	55.4	3a,b
2-NH	4.72, br d		
3	a 3.21, dd *(14.1, 10.4)*	38.8	2
	b 2.57, dd *(14.1, 10.4)*	[c]	2
4		[c]	
5, 9	6.76, d *(8.1)*	116.6	
6, 8	6.95, d *(8.1)*	131.1	
7		[c]	
1′		165.1	
2′	5.82, s	79.5	
3′		[c]	
4′-8′	7.38 - 7.41[b], m	129.9	

(a) assignments supported by HSQC. (b) Overlapping resonances. (c) Signals not observed

5.2.7.6 (3*S*,6*S*)-6-Benzyl-3-(4-hydroxybenzyl)morpholine-2,5-dione (5.5f)

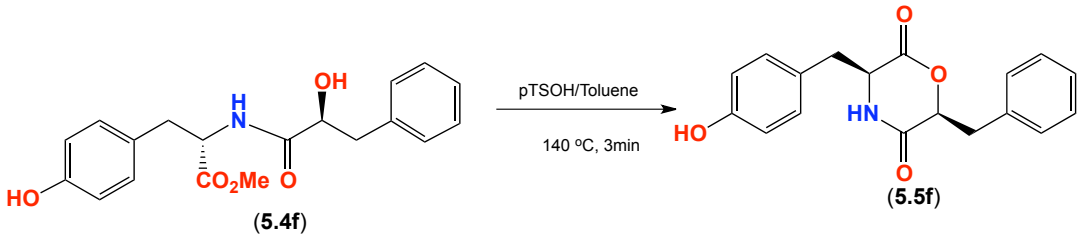

HRESI(+)MS analysis of **5.5f** returned a molecular formula ($C_{18}H_{17}N_1O_4$, Δ mmu +0.5). The crude product was purified using HPLC (10 – 70% MeCN/H_2O) over 30 min, 3 mL/min using Zorbax C_8 to yield compound **5.5f** as a colourless oil (3.1 mg, 65%); $[\alpha]_D^{22}$ –89.4 (*c* 0.1, $CHCl_3$); R_f: 0.25 (10 – 70% EtOAc/hexane and $KMnO_4$ dip) (Figure 5.38 and Table 5.16).

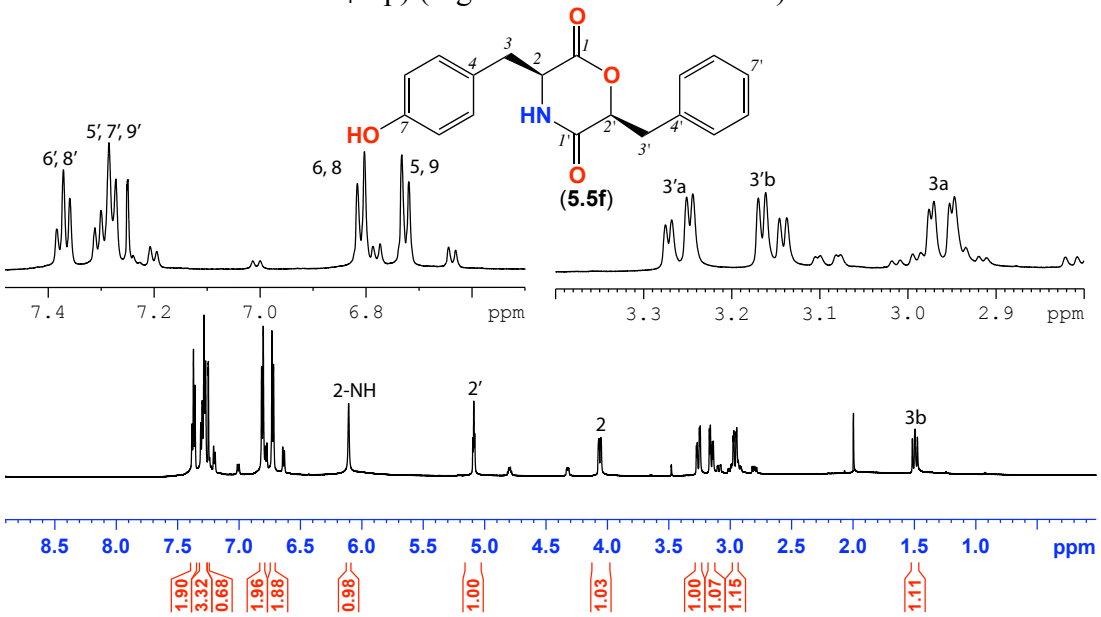

Figure 5.38. ^1H NMR (600 MHz, $CDCl_3$) spectrum of (3*S*,6*S*)-6-Benzyl-3-(4-hydroxybenzyl)morpholine-2,5-dione (**5.5f**)

Table 5.16. NMR (600 MHz, $CDCl_3$) data of **5.5f**

Pos.	δ_H, mult, (*J* in Hz)	δ_C[a]	COSY	^1H – ^{13}C HMBC	ROESY
1		178.3			
2	4.09, dd *(13.3, 10.7)*	58.9	3a,b	1	2′
2-NH	6.12, br				
3	a 2.99, dd *(13.3, 10.7)*	42.7		1	
	b 1.53, dd *(13.3, 10.7)*			1	
4		138.9			
5, 9	6.75, d *(8.1)*	120.4		6/8, 7	
6, 8	6.84, d *(8.1)*	134.8		5/9, 7	
7		159.9			
1′		170.0			
2′	5.11, t *(4.3)*	82.6	3′a,b	1′, 4′	2
3′	a 3.29, dd *(15.3, 4.3)*	42.3	2′	1′, 4′	
	b 3.18, dd *(15.3, 4.3)*		2′	1′, 4′	
4′		138.8			
5′	7.33[b]	132.1[c]			
7′	7.30[b]	134.9[c]			
9′	7.31[b]	132.7[c]			
6′, 8′	7.40, t *(7.1)*	133.1			

*(a) assignments supported by HSQC. (b) Overlapping resonances. (c) Interchangeable resonances

5.2.7.7 (3*S*,6*S*)-3-Methyl-6-phenylmorpholine-2,5-dione (5.5g)

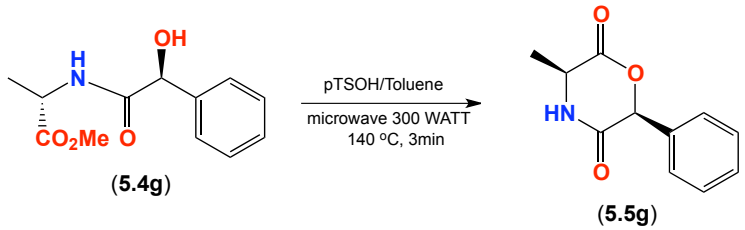

HRESI(+)MS analysis of **5.5g** returned a molecular formula ($C_{11}H_{11}NO_3$, Δmmu –0.7). The crude product was purified using HPLC (20 – 60% MeCN/H_2O) over 30 min, 3 mL/min using Zorbax C_3 to yield compound **5g** as a colourless oil (2.5 mg, 62%); $[\alpha]_D^{22}$ +28.5 (*c* 0.05, $CHCl_3$); R_f: 0.19 (10 – 60% EtOAc/hexane and $KMnO_4$ dip) (Figure 5.39 and Table 5.17).

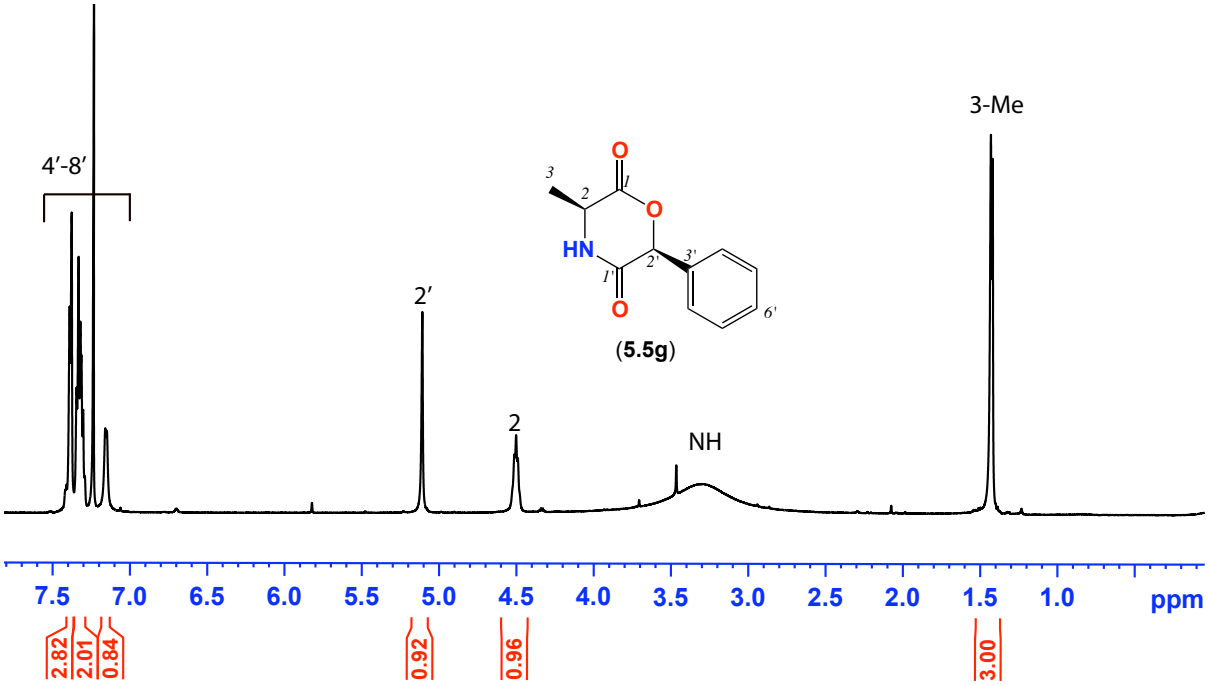

Figure 5.39. ^{1}H NMR (600 MHz, $CDCl_3$) spectrum of (3*S*,6*S*)-3-Methyl-6-phenylmorpholine-2,5-dione (**5.5g**)

Table 5.17. NMR (600 MHz, $CDCl_3$) data of **5.5g**

Pos.	δ_H, mult, (*J* in Hz)	δ_C[a]	COSY	^{1}H – ^{13}C HMBC	ROESY
1		174.8			
2	4.50, m	49.7	3-Me, 2-NH	1	2′
3-Me	1.48, d *(6.8)*	19.1	2		
2-NH	3.42, br				
1′		174.8			
2′	5.11, s	75.7		1′, 3′	2
3′		140.1			
4′	7.43[b], m	130.3			
5′	7.42[b], m	130.2			
6′	7.33[b], m	128.2			
7′	7.32[b], m	128.2			
8′	7.32[b], m	128.2			

(a) assignments supported by HSQC and HMBC. (b) Overlapping resonances.

5.2.7.8 (3*S*,6*S*)-6-Benzyl-3-methylmorpholine-2,5-dione (5.5h)

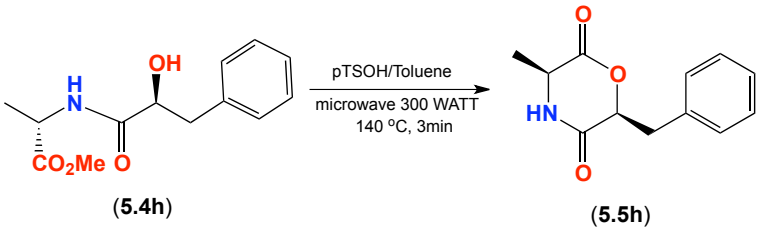

(**5.4h**) (**5.5h**)

HRESI(+)MS analysis of **5.5h** returned a molecular formula ($C_{12}H_{13}NO_3$, Δ mmu −0.8). The crude product was purified using HPLC (20 – 60% MeCN/H_2O) over 30 min, 3 mL/min using Zorbax C_3 to yield compound **5.5h** as a colourless oil (3.1 mg, 69%); $[\alpha]_D^{22}$ +85.4 (*c* 0.05, $CHCl_3$); R_f: 0.17 (10 – 60% EtOAc/hexane and $KMnO_4$ dip) (Figure 5.40 and Table 5.18).

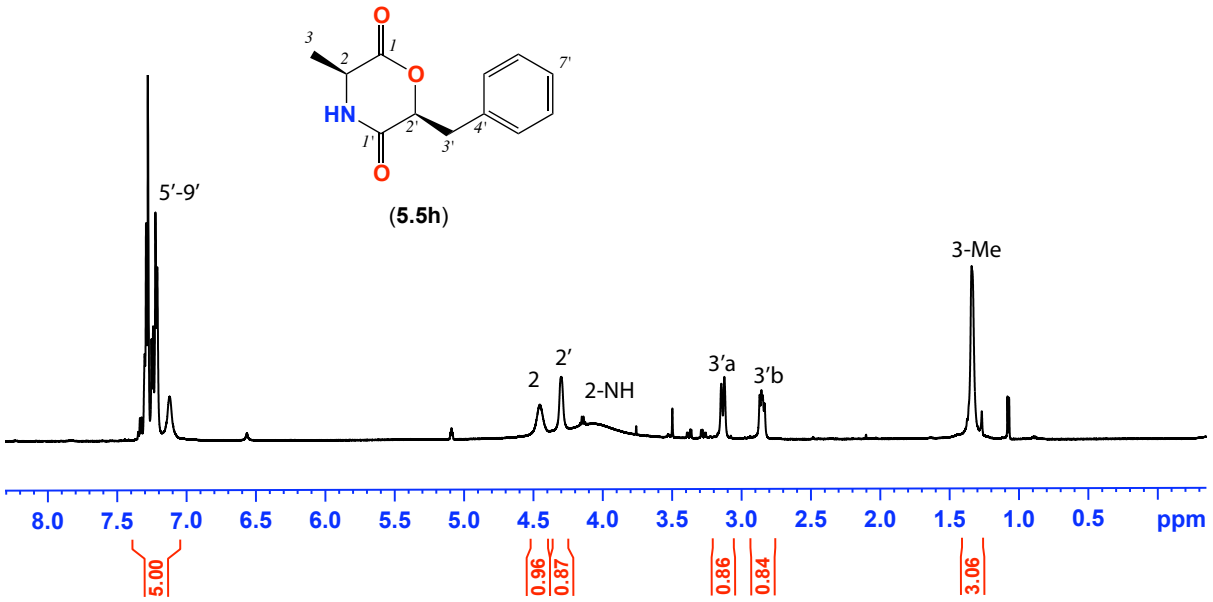

Figure 5.40. ^{1}H NMR (600 MHz, $CDCl_3$) spectrum of (3*S*,6*S*)-6-Benzyl-3-methylmorpholine-2,5-dione (**5.5h**)

Table 5.18. NMR (600 MHz, $CDCl_3$) data of **5.5h**

Pos.	δ_H, mult, (*J* in Hz)	δ_C[a]	COSY	^{1}H – ^{13}C HMBC	ROESY
1		174.7			
2	4.45, br	72.8	3-Me		2′
3-Me	1.33, br	17.5	2	1	
2-NH	4.22, br				
1′		174.5			
2′	4.29, br	50.2	3′a,b	1′	2
3′	a 3.14, d *(13.3)*	40.5	2′	4′	
	b 2.85, dd *(13.3, 7.6)*	40.5	2′	4′	
4′		136.9			
5′, 9′	7.42[b], m	129.7[c]	6′/8′	4′	
6′, 8′	7.33[b], m	127.0[c]	5′/9′	7′	
7′	7.23[b], m	128.6[c]	6′/8′		

(a) assignments supported by HSQC. (b) Overlapping resonances. (c) Interchangeable resonances

5.2.8 Biological assays

The natural product shornephine A (**5.16**) and DKPs (**5.17** – **5.19**), and synthetic DKMs **5.5a** – **5.5f**, displayed no antibiotic activity against the Gram negative bacteria *Escherichia coli* (ATCC 11775) and *Pseudomonas aeruginosa* (ATCC 10145), or the Gram positive bacteria *Staphylococcus aureus* (ATCC 9144 and ATCC 25923) and *Bacillus subtilis* (ATCC 6633 and ATCC 6051), or the fungus *Candida albicans* (ATCC 90028). Likewise, these same compounds failed to exhibit cytotoxicity (IC_{50} >30 μM) against the human colon cancer cell line SW620, or its doxorubicin selected P-gp over-expressing daughter cell line SW620 Ad300, or the human cervical carcinoma cell line KB-3-1, or its vinblastine selected P-gp over-expressing daughter cell line KB-V1.

Given the above it seems likely that if the natural products **5.16** – **5.19** were capable of providing CMB-M081F with a survival advantage, it must act via a mechanism other than direct cytotoxicity. Alternative strategies could include (a) inhibiting the ability of competing microbes to release defensive (antifungal) natural products into the environment, thereby rendering them ineffective, or (b) inhibiting the ability of competing microbes to defend against offensive (antibiotic) natural products produced by other organisms, thereby accentuating their potency. Both these objectives could be achieved by inhibiting ABC transporter mediated efflux system in competing microbes.

5.2.8.1 Diketomorpholine Chemotype as a P-glycoprotein inhibitor

Human cancers are often treated by systemic administration of chemotherapeutic agents (anticancer drugs), a process that relies on the ability of highly cytotoxic drugs to penetrate and selectively kill cancer cells. While this approach has proven to be clinically successful, many cancer cells exhibit either intrinsic or acquired resistance to multiple chemotherapeutic agents. A number of factors can contribute to multi-drug resistance (MDR), prominent among them being accelerated drug efflux by high levels of membrane spanning, adenosine triphosphate binding cassette[175] transporter proteins. Discovered in 1976 by Ling *et al.*,[202] the function, distribution and substrate specificity of the first MDR ABC transporter protein, P-glycoprotein (P-gp, ABCB1), has attracted much attention. P-gp plays an important role in many tissues and organs, including the blood brain barrier, regulating cellular exposure to xenotoxins and cytotoxins.[203] While invaluable to natural cellular defences, over expression of P-gp can prove counter productive, leading to the premature efflux of many important drugs, including anticancer, antibiotic, antidepressant, antiepileptic, analgesic and antiviral agents.[204] Inhibitors of P-gp have potential application as anticancer therapeutics that operate by modulation of MDR mediated by P-gp and ABC transporters.[205,206] In 1994, Zacherl *et al.* demonstrated that verapamil (**5.20**) inhibits P-gp mediated efflux of

doxorubicin (**5.21**), daunorubicin (**5.22**), vinblastine (**5.23**) and taxol (**5.24**) in the monolayer cultures of intestinal adenocarcinoma.[204] With respect to P-gp inhibition and multidrug resistance, Golstein *et al.* demonstrated in 1999 that glibenclamide (**5.25**) and another two synthetic compounds (**5.26** and **5.27**) inhibits the P-gp mediated efflux in vinblastine-selected tumour cell line (VBL600) selected from a human T-cell line (CEM) derived from an acute leukaemia; and an epithelial cell line derived from colchicine-selected rat colonic adenocarcinoma (CC531^{mdr+}).[207] While inhibition of P-gp mediated drug efflux represents an attractive strategy for dealing with MDR, no P-gp inhibitors have yet to advance to the clinic.

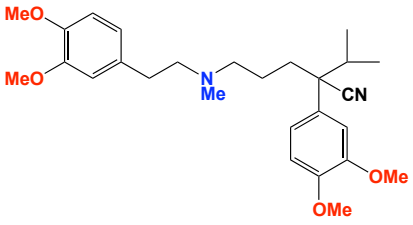

verapamil
5.20

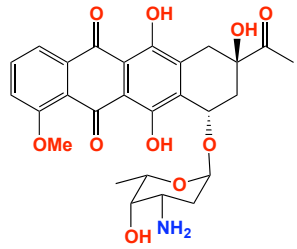

daunorubicin
5.22

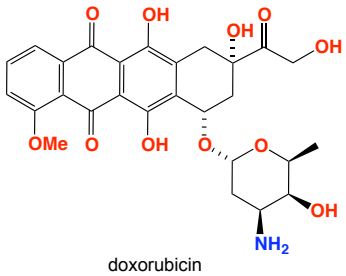

doxorubicin
5.21

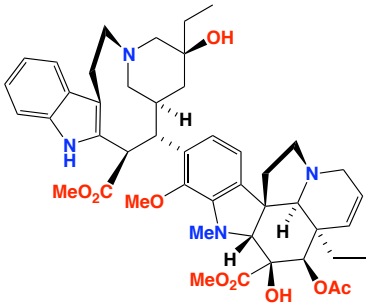

vinblastine
5.23

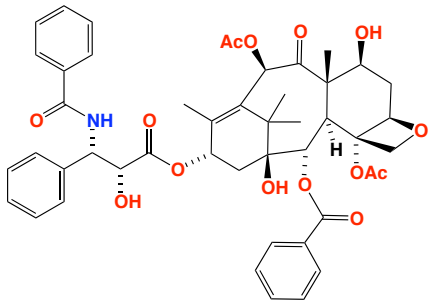

taxol
5.24

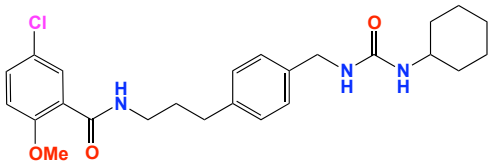

glibenclamide
5.25

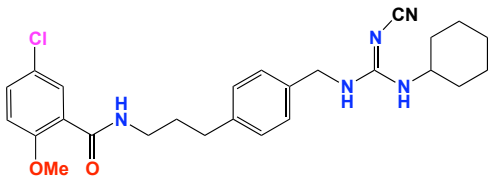

BM-208
5.26

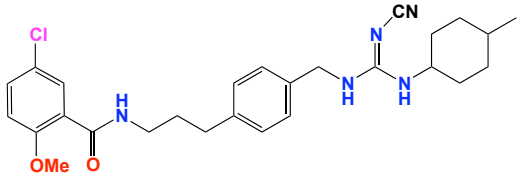

BM-223 (cis-trans)
5.27

5.2.8.2 Investigation on the interaction of DKMs with P-glycoprotein

High intrinsic or acquired expression of membrane spanning, adenosine triphosphate binding cassette[175] transporter proteins, such as P-glycoprotein (P-gp), in cancers represents a major impediment to chemotherapy, with accelerated drug efflux leading to multi-drug resistance (MDR). Although P-gp inhibitors offer the prospect of reversing the MDR phenotype, no inhibitors have advanced to the clinic. Because very few marine natural products have been assessed/reported to inhibit P-gp mediated drug efflux associated with multi-drug resistance, we employed a range of cytotoxicity and MDR reversal assay, together with flow cytometry to discover the interaction of DKMs with P-gp.

To better explore and understand the chemistry and biology of the CMB-M081F metabolites **5.16** - **5.19**, DKMs **5.5a** – **5.5h** (as shown above) and DKP *cyclo*-(L-Trp-L-Phe) (**5.28**) (Figure 5.41) were synthesised, employing standard synthetic methodology[208]. As predicted, whereas the *cyclo*-(L-Trp-L-Phe) (**5.28**) was stable to methanolysis, the DKMs **5.5a** – **5.5h** underwent rapid and quantitative ring opening after even brief room temperature exposure to MeOH.

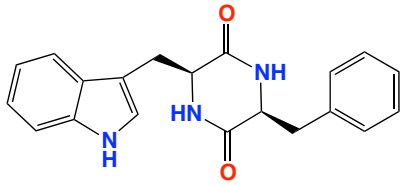

5.28

Figure 5.41. *cyclo*-(L-Trp-L-Phe)

5.2.8.3 Effect of DKMs on accumulation of calcein AM: identification of P-gp inhibitors

In order to determine if DKMs inhibit P-gp mediated efflux of increase intracellular accumulation of P-gp substrate; flow cytometry was employed to examine their effect on the accumulation of acetomethyoxy derivative of calcein (calcein AM). This assay operates on the basis that the non-fluorescent reagent calcein AM diffuses into the cellular cytoplasm of a doxorubicin selected P-gp over-expressing human colon cancer (SW620 Ad300) cell line, where it undergoes hydrolysis by esterases to yield the fluorescent dye calcein. Importantly, calcein AM is a P-gp substrate and the hydrolysed product calcein is not. In the presence of functioning P-gp calcein AM is (largely) effluxed prior to hydrolysis, resulting in low levels of intracellular fluorescence. In the presence of a P-gp inhibitor, calcein AM efflux is (partially or completely) blocked and calcein AM undergoes hydrolysis to calcein, leading to higher levels of intracellular fluorescence. Intracellular calcein fluorescence is quantified by cell flow cytometry to arrive at a fluorescence arbitrary ratio (FAR),

which measures intracellular calcein (hydrolysed from calcein AM) fluorescence in P-gp overexpressing cell line exposed to a P-gp inhibitor, with that from the same cell line not exposed to an inhibitor. The larger the FAR value then (in principle) the more effective the P-gp inhibitor. Verapamil, a calcium channel blocker, which inhibits P-gp and decreases the export of the substrates of P-gp, was employed to be a positive control. In this round of screening (Calcein AM), the P-gp inhibitory activities of 20 μM **5.16** – **5.19** and **5.5a** – **5.5h**, as well as **5.4d**, **5.4h** and **5.4g**, were assessed by brief exposure (0.5 h) to SW620 Ad300 cells followed by immediate quantification of the intracellular (calcein) fluorescence by cell flow cytometry. After compensating for the baseline levels of the intracellular fluorescence and standardizing to the positive control verapamil (20 μM), three natural metabolites **5.16**, **5.17**, **5.19** (fluorescence arbitrary ratio FAR of 35.5, 30.3 and 27.0 respectively, Table 5.19 and Figure 5.42a, b and c) and three synthetic compounds **5.5c**, **5.5e** and **5.5f** (fluorescence arbitrary ratio FAR of 52.9, 41.5 and 40.5 respectively, Table 5.19 and Figure 5.42d, e and f) showed a strong activity while **5.18** and the rest of the synthetic DKMs analogues only achieved very weak accumulation of calcein (~ 2.3-fold) (Figure 5.42, Figure 5.43 and Table 5.19).

5.2.8.4 Effect of DKMs on the sensitivity of chemotherapeutic agents in the drug-selected cancer cells

While a very useful discovery tool, the flow cytometry calcein AM assay is limited in that it measures inhibition of the P-gp mediated efflux of calcein AM, not an anticancer chemotherapeutic agent, and that the measurement (cell cultivation) window is only half an hour duration. As our objective was the discovery of new inhibitors capable of reversing P-gp mediated efflux of anticancer drugs and **5.5c**, **5.5e**, **5.5f**, **5.16**, **5.17** and **5.18** exerted promising inhibition on P-gp mediated efflux of calcein AM, we set out to establish if co-incubation (72-hour incubation) of MDR cells with active DKMs and clinical anticancer agents (eg vinblastine, doxorubicin, or paclitaxel) would lead to reversal of the MDR phenotype. Prior to undertaking these studies we determined (Table 5.19) that all DKMs exhibited very low cytotoxicity towards a P-gp–overexpressing human colon adenocarcinoma cell line SW620 Ad300 and its parental cell line SW620, and another P-gp overexpressing human cervical carcinoma cell line KB-3-1 and the corresponding parental cell line KV-1 (IC_{50} > 30 μM).

Due to the over-expressing of P-gp, SW620 Ad300 exhibits cross-resistance to a range of anti-cancer agents such as vinblastine, doxorubicin or taxol in the absence of any modulator (14.2-, 22.5- and 1410-fold, compared to parental SW620). Verapamil was employed to be a positive control. When co-administered with verapamil (10 μM), SW620 Ad300 resistance to vinblastine,

doxorubicin and paclitaxel was significantly reduced (17.3-, 11.8- and 638-fold respectively). **5.5c**, which is the most potent inhibitor among DKMs and has similar effect as verapamil on the accumulation of calcein AM in flow cytometry, has the comparable ability to decrease the resistance of SW620 Ad300 to vinblastine (15.9-fold). However, the capacity of 5c to sensitize doxorubicin or paclitaxel to SW620 Ad300 (3.27- or 41.1-fold, respectively) was much inferior to that of verapamil. Another two potent P-gp inhibitors, **5.5e** and **5.5f** exhibited the similar weak ability to decrease the resistance of SW620 Ad300 to not only to doxorubicin and paclitaxel, but also to vinblastine (Table 5.19) The reduced ability of inhibiting P-gp mediated efflux of anticancer drug, which was not proportional to that in flow cytometry assay, was also discovered in another three P-gp inhibitors (**5.16**, **5.17** and **5.19**). Overall, the finding confirmed the proposition that these six DKMs are partially capable of reversing P-gp mediated MDR associated with the clinical anticancer agents vinblastine, doxorubicin and paclitaxel. Although there were many factors such as different experiment methods or substrates that could be contributable to the inconsistency between the result from MDR reversal assay and calcein AM flow cytometry assay, the possible instability of any of these DKMs during long time incubation (72 h) raised our attention and led to further investigation.

Table 5.19. Diketomorpholine interaction with P-glycoprotein

#[a]	IC_{50} (μM)				MDR reversal GS [d]			Calcein FAR[e]
	SW620[b]	SW620 Ad300[b]	KB-3-1[c]	KB-V1[c]	Vinblastine	Doxorubicin	Taxol	
(5.5c)	>30	>30	>30	>30	15.9	3.27	41.1	52.9
(5.19)	>30	>30	>30	>30	4.76	1.40	14.4	27.0
(5.5e)	>30	>30	>30	>30	4.28	1.44	14.5	41.5
(5.5f)	>30	>30	>30	>30	3.56	2.15	9.04	40.5
(5.16)	>30	>30	>30	>30	3.85	1.74	9.71	35.5
(5.17)	>30	>30	>30	>30	5.86	4.63	43.1	30.3
(5.4h)	>30	>30	>30	>30	--	--	--	17.5
5.28	>30	>30	>30	>30	--	--	--	9.2
(5.5b)	>30	>30	>30	>30	--	--	--	1.9
(5.18)	>30	>30	>30	>30	--	--	--	2.3
(5.4d)	>30	>30	>30	>30	--	--	--	2.0
(5.5d)	>30	>30	>30	>30	--	--	--	1.1
(5.5a)	>30	>30	>30	>30	--	--	--	1.2
(5.5h)	>30	>30	>30	>30	--	--	--	1.1
(5.4g)	>30	>30	>30	>30	--	--	--	0.8
(5.5g)	>30	>30	>30	>30	--	--	--	0.9
PBS	--	--	--	--	--	--	--	1.0
Verapamil	--	--	--	--	17.3	11.8	638	72.7

*(a) Tested compound number. (b) Cytotoxicity (MTT) assay against human colon carcinoma. (c) Cytotoxicity (MTT) assay against human cervix carcinoma (d) MDR reversal assay against SW620 Ad300 where GS (gain in sensitivity) = IC_{50} of anti-cancer drug (vinblastine, doxorubicin or taxol) without compound)/IC_{50} of (vinblastine, doxorubicin or taxol) with compound (10 μM). IC_{50} of vinblastine without compound was 0.38 μM, IC_{50} of doxorubicin without compound was 3.59 μM, IC_{50} of taxol without compound was 14.7 μM. (e) Cell flow cytometry analysis of intracellular calcein fluorescence: FAR (fluorescence arbitrary ratio) = calcein fluorescence intensity (Geo mean) in the presence of compound at 20 μM/calcein fluorescence intensity (Geo mean) in the presence of PBS, expressed as a ratio. Positive control is verapamil at 20 μM which FAR = 72.7.

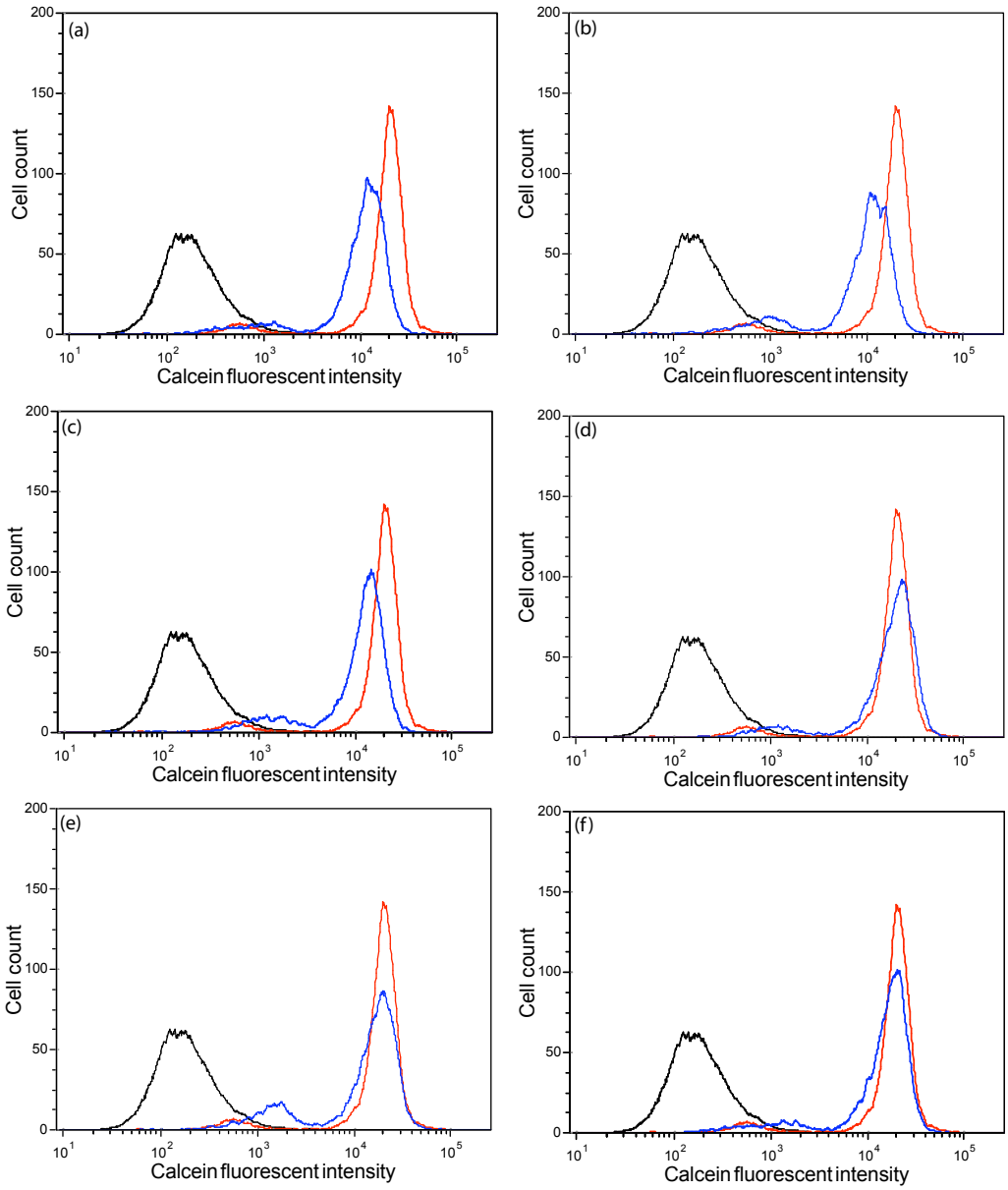

Figure 5.42. Cell flow cytometry of DKMs at 30 μM through inhibiting P-gp in SW20 Ad300. PBS (black) and verapamil (red). (a) shornephine (**5.16**), (b) 15b-β-hydroxy-5-*N*-acetylardeemin (**5.17**), (c) 15b-β-methoxy-5-*N*-acetylardeemin (**5.19**), (d) L-tryptophan-L-mandelic diketomorpholine (**5.5c**), (e) L-tyrosine-L-mandelic diketomorpholine (**5.5d**) and (f) L-tyrosine- L-phenyllactic acid diketomorpholine (**5.5f**)

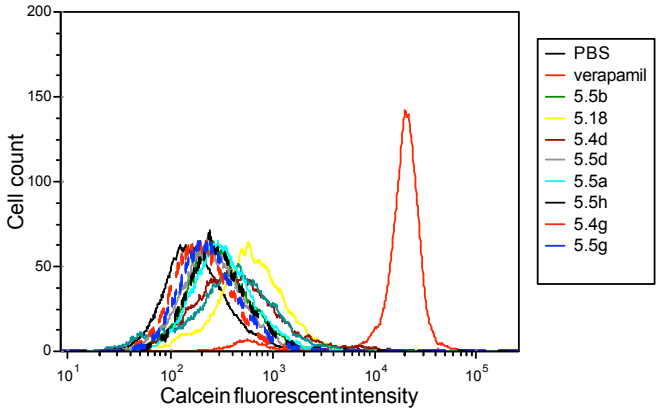

Figure 5.43. Cell flow cytometry of the other synthetic DKMs at 30 μM through inhibiting P-gp in SW20 Ad300. PBS (black) and verapamil (red)

As we have demonstrated that natural product shornephine A (**5.16**), is prone to solvolysis, we speculated that the inability of DKM to reverse MDR was due to premature solvolysis/degradation during the assay.

5.2.9 The stability of the diketomorpholines

The six compounds, (3*S*,6*S*)-3-((1H-indol-3-yl)methyl)-6-phenylmorpholine-2,5-dione (**5.5c**), ((3*S*,6*S*)-3-(4-hydroxybenzyl)-6-phenylmorpholine-2,5-dione (**5.5e**), ((3*S*,6*S*)-6-benzyl-3-(4-hydroxybenzyl) morpholine-2,5-dione (**5.5f**), shornephine A (**5.16**) and 15b-β-hydroxy-5-*N*-acetylardeemin (**5.17**) and 15b-β-methoxy-5-*N*-acetylardeemin (**5.19**) that exhibited P-gp inhibition were tested in the media to determine their stability. Each compound (10 μM) was added to the wells of the microtiter plate containing RPMI medium and the plate was incubated at 37 °C, 5% CO_2 for 3 days. After the incubation period the wells were extracted with EtOAc (100 μL) and the organic layer was dried *in vacuo*. The crude extract was dissolved in MeCN (50 μL) and analysed using the HPLC-DAD-MS. The three synthetic compounds (**5.5c**, **5.5e** and **5.5f**) undergo hydrolysis to give the acid form of the diketomorpholine, which explains the fluctuation in the MDR reversal results. On the other hand the two natural products, shornephine A (**5.16**) and 15b-β-hydroxy-5-*N*-acetylardeemin (**5.17**) were largely stable in the media (Figure 5.44 and Figure 5.45).

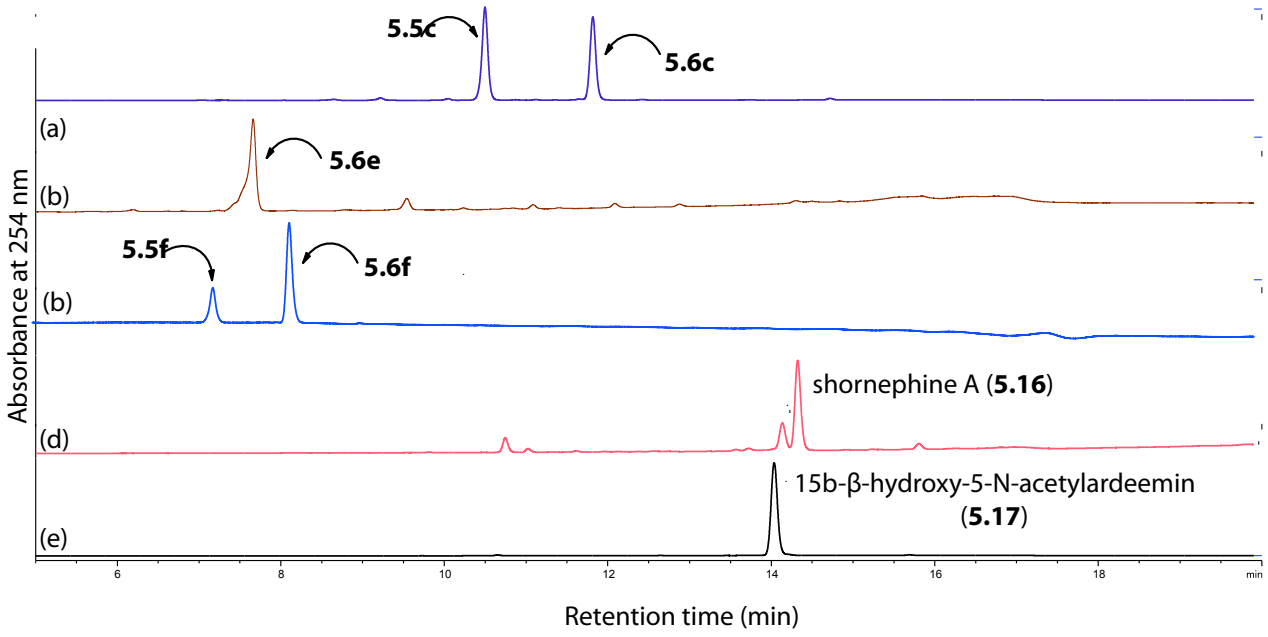

Figure 5.44. HPLC-DAD chromatograms of the tested compounds in MeOH (a) (3*S*,6*S*)-3-((1H-Indol-3-yl)methyl)-6-phenylmorpholine-2,5-dione (**5.5c**), (b) (3*S*,6*S*)-3-(4-hydroxybenzyl)-6-phenylmorpholine-2,5-dione (**5.5e**), (c) (3*S*,6*S*)-6-benzyl-3-(4-hydroxybenzyl)morpholine-2,5-dione (**5.5f**), (d) shornephine A (**5.16**) and (e) 15b-β-hydroxy-5-*N*-acetylardeemin (**5.17**)

The SAR data analysis proved that P-gp inhibition strongly correlates with the presence of diketomorpholine scaffold and the activity was lost with the diketopiperazine analogue. Also of a note, synthetic diketomorpholine analogues were non cytotoxic to parenteral cells and **5.5c** was the most active compound and non-cytotoxic in the same time followed by **5.5e** and **5.5f** as well as the two natural products, shornephine A (**5.16**) and 15b-β-hydroxy-5-*N*-acetylardeemin (**5.17**).

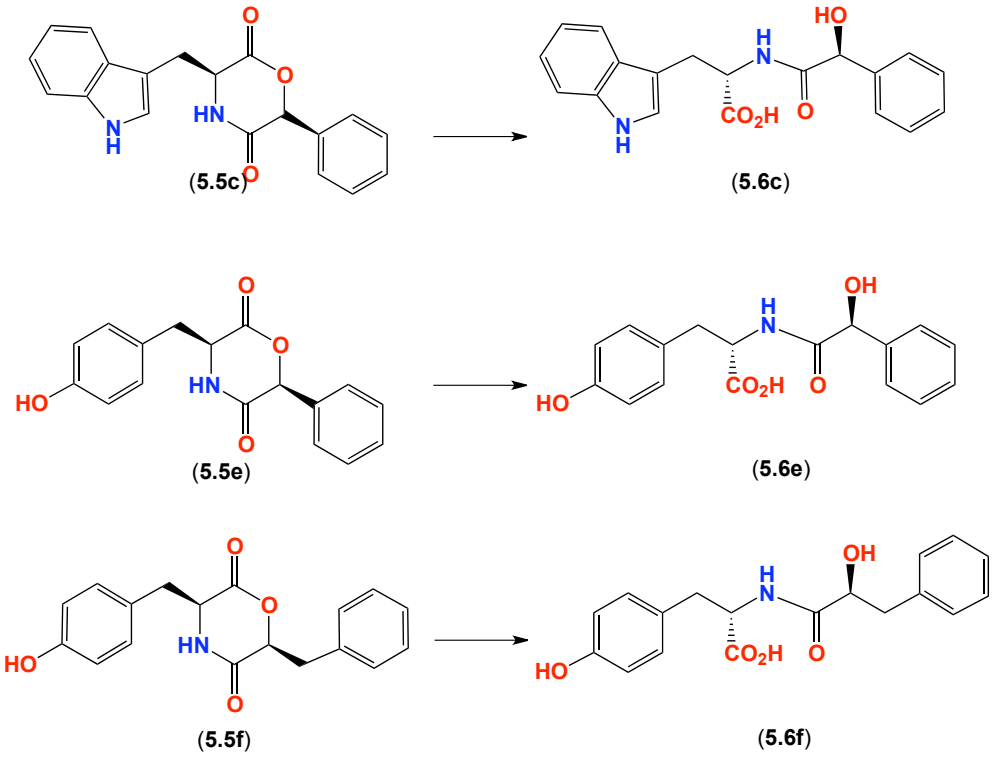

Figure 5.45. Diagram showed the hydrolysis of the synthetic products to give the acid form that has the following molecular weights (**5.6c**) *m/z* 321[M+H], (**5.6e**) *m/z* 316[M+H] and (**5.6f**) *m/z* 312[M+H]

5.3 Conclusion

Chemical analysis of fungal isolate (CMB-M081F), isolated from a sediment sample collected near Shornecliff, Queensland, Australia, yielded the new DKM shornephine A (**5.16**), its methanolysis artifact *seco*-shornephine A (**5.15**), and two known and one new DKP, 15b-β-hydroxyl-5-*N*-acetyladreemin (**5.17**), 5-*N*-acetyladreemin (**5.18**) and 15b-β-methoxy-5-*N*-acetyladreemin (**5.19**) respectively. Two of these metabolites **5.16** and **5.19** were inhibitors of P-glycoprotein, a critical determinant in many multidrug-resistant cancers, responsible for efflux of many clinically important chemotherapeutics. These results directed us to the synthesis of additional diketomorpholines (DKMs), to probe the structure activity relationship (SAR) associated with the P-gp inhibitors pharmacophore. To achieve these objectives, we applied a new method for the synthesis of DKMs using microwave approach, to prepare 14 DKMs analogues, three of which exhibited P-gp inhibitory properties comparable with that of the positive control verapamil. Although the DKMs inhibitors were effective in the P-gp inhibitor assay; they were less effective in a reversal multidrug resistance assay (MDR). The failure to reverse multidrug resistance was attributed to poor *in vivo* stability, and prompted consideration to enhance stability, including a closer analysis of the natural product shornephine A (**5.16**)

5.4 Future work

Curiously, and contrary to our experience with shornephine A (**5.16**), prior published DKM natural products were not prone to methanolysis. Given the ease with which shornephine A (**5.16**) undergoes solvolysis, and being keen to explain how prior published DKM natural products avoided this fate, we noted that the latter fall into two distinct structural groups – inclusive of a common structural feature that differentiates them from shornephine A (**5.16**). The first, consisting of DKMs incorporating a tryptophan moiety (eg. mollenines, javanicunines and PF1233 A and B), all possess a fused A – D heterocyclic scaffold in common with the ardeemins **5.17** – **5.19**. Importantly, this heterocyclic scaffold features fully substituted DKM amide nitrogen. The second, comprising all other known DKM natural products, features an *N*-methylated DKM amide. Based on these observations we speculate that *N*-substitution (heterocycle or methylation) stabilizes the DKM lactone towards solvolysis, greatly simplifying isolation, characterization and structure elucidation, compared to **5.16** which features a free 2-*NH*. This hypothesis may also explain the historic biodiscovery bias, which has failed to document more unstable (reactive) DKMs such as **5.16**.

5.5 Experimental section

5.5.1 Isolation and identification of strain CMB-M081F

The marine derived fungus strain CMB-M81F was isolated from a marine sediment sample collected from Shonecliff, Australia. The fresh sediment sample was transferred to the laboratory in a sealed 50 mL Falcon tube at room temperature (24 h), where it is stored in the dark at −30 °C for one week. Approximately, 1 g of the thawed terrestrial sample was suspended in 8 mL sterile 0.9% saline solution and then subjected to heat-shock at 60 °C for 30 min after which 100 μL was serially diluted to 10^{-1}, 10^{-2} and 10^{-3} and transferred into 1000 μL sterile saline solution by means of sterile micro titre pipette. Furthermore, 50 μL from each diluted portion was dispersed across agar plates comprising into agar medium in artificial ocean sea salt (3.3%, 25 mL), starch (1%), yeast extract (0.4%), peptone (0.2%) and agar (2%) and 0.0005% rifampicin); incubated at 27 °C for 4 weeks. The resulting agar plate was incubated at 27 °C for three weeks. Pure strains of individual colonies were obtained by standard microbiological techniques, and were grown to dense colonies on a single agar plate.

5.5.2 Chemical profiling:

A single colony of CMB-M81F was sub-sampled into agar medium in artificial ocean sea salt (3.3%, 25 mL), starch (1%), yeast extract (0.4%), peptone (0.2%) and agar (2%) and incubated at 27 °C for 4 weeks. The agar plate was soaked into EtOAC (100 mL), and shake on the rotary shaker at 100 rpm overnight. The organic phase was concentrated *in vacuo* to yield an extract that was subsequently analysed by HPLC-DAD-ESI(±)MS and NMR.

5.5.3 Analytical cultivation and chemical analysis

A single colony of strain CMB-M81F was used to inoculate a seed culture composed of M1 agar medium in seawater including artificial ocean seawater (3.3%, 100 mL), starch (1%), yeast extract (0.4%), peptone (0.2%) and agar (2%), which was cultivated for a period of 4 weeks. After the initial cultivation timeline the whole agar plates were extracted with EtOAc, which was then dried *in vacuo* yielding a crude extract of 50.1 mg that was subsequently analysed by HPLC-DAD-MS with conditions set as follows (Zorbax C_8 column, 150 × 4.6 mm, 5 μm, 1 mL/min, gradient from 90 – 10 % H_2O/MeCN (isocratic 0.05% formic acid) over 15 min. Peaks with the following retention times The crude extract was then resuspended in MeCN and analysed by HPLC-DAD-

MS. Peaks with the following retention times t_R = 11.1, 12.2, 12.4 and 12.8 min exhibited the following *m*/*z* $[M+H]^+$ 435 (**5.16**), 485 (**5.17**), 469 (**5.18**) and 499 (**5.19**)

5.5.4 Large-scale cultivation and extraction of strain CMB-M81F:

A single colony of CMB-M81F was sub-sampled onto ten seawater M1 agar plates (300 mL of Ocean Nature seawater, 1% starch, 0.4% yeast extract and 0.2% peptone) with dimensions 150 × 120mm and incubated at 27 °C for 4 weeks. The resulting agar plates were sliced up and soaked in EtOAc (500 mL) for 24 h and the organic phase concentrated *in vacuo* to yield an extract (60.2 mg). The extract was sequentially triturated with 8 mL each of hexane and CH_2Cl_2 to afford, after concentration *in vacuo*, 2 and 60 mg fractions, respectively. The DCM fraction was analysed by HPLC-DAD-ESI(±)MS and NMR which was found to be rich in the secondary metabolites, was subsequently subjected to semi-preparative reversed-phase HPLC (Zorbax C_8 250 × 9.4 mm, 5 μm column, 3 $mLmin^{-1}$ gradient elution from 10% H_2O/MeCN to 100% MeCN over 30 min with a hold at 100% MeCN for 5 min), to yield shornephine A (**5.16**) (t_R = 23.9 min, 2 mg, 1.8%), 15b-β-hydroxy-5-*N*-acetylardeemin (**5.17**) (t_R = 25.5 min, 1.5 mg, 2.2%), 5-*N*-acetylardeemin (**5.18**) (t_R = 27.0 min, 1.9 mg, 2.5%) and 15b-β-methoxy-5-*N*-acetylardeemin (**5.19**) (t_R = 28.0 min, 1.5 mg, 3.0%). [Note - % yields are determined on a mass-to-mass basis against the weight of EtOAc crude extract].

5.5.5 Cell Lines and Cell Culture

Two cancer cell pairs were employed. One pair includes parental cell line SW620 (American Type Culture Collection, Manassasm VA, CCL-227) and subline SW620 Ad300. SW620 is a human colon cell line that was originated from a lymph node metastasis in the patient with primary adenocarcinoma of the colon. The multi-drug resistant (MDR) cell line, SW620 Ad300, which over-expresses Permeable-glycoprotein (P-gp), was selected from SW620 by growth in the presence of increasing concentrations of doxorubicin. SW620 and SW620 Ad300 were grown in RPMI medium 1640 as adherent mono-layer in flasks supplemented with 10% foetal bovine serum, 0.1 mM non-essential amino acids (NEAA), 2 mM L-glutamine, 100 unit/mL penicillin and 100 μg/mL streptomycin in a humidified incubator containing of 5% CO_2 at 37 °C. After SW620 Ad300 exhibited stable phenotype of P-gp, the cells were maintained in 300 ng/mL doxorubicin. Another cancer cell pair includes KB-3-1 and KB-V1. These human cervix cancer cells were grown in DMEM as adherent mono-layer in flasks supplemented with 10% foetal bovine serum, 0.1 mM NEAA, 2 mM L-glutamine and 100 unit/mL penicillin and 100 μg/mL streptomycin in a humidified incubator containing of 5% CO_2 at 37 °C. KB-3-1 is the parental cancer cell line and sensitive to

anticancer agent, the sub line, KB-V1 was vinblastine selected from KB-3-1 and is maintained in 0.1 μg/mL vinblastine. These two cell lines were kindly provided from Dr. M.M. Gottesman in NIH (Bethesda, MD). The cytototxic drug was routinely removed from the sub-line cells 2 weeks in advance before any assay was performed.

5.5.6 MDR Reversal (Vinblastine, doxorubicin and taxol) Assay

Reversal of resistance of SW620 Ad300 cells to anti-cancer drug (doxorubicin, vinblastine or taxol) assay was performed as described for the standard cytotoxicity assay (above). Instead of measuring the cytotoxicity of dioxomorpholines, this assay was applied to measure the cytotoxicity of vinblastine, doxorubicin and taxol against SW620 Ad300, in the presence or absence of natural and synthetic compounds at concentrations that were non-cytotoxic to SW620 Ad300. The amount of medium containing cells per well was adjusted to 160 μL at the beginning and the addition 20 μL of either PBS, compound (designated concentration) or verapamil (10 μM) was dispensed to the well 1 h before addition of an anticancer drug (doxorubicin, vinblastine or taxol) dilution series.
Gain in sensitivity (GS) was calculated according to GS=IC_{50} of vinblastine, doxorubicin and taxol without dioxomorplines/IC_{50} of vinblastine or doxorubicin or taxol with dioxomorpholines (test concentration in μM is shown in parentheses). The IC_{50} value without dioxomorpholines for vinblastine was 0.38 μM, doxorubicin 3.59 μM and taxol 14.7 μM, verapamil 2.5 μM was used as a positive control (GS = 6.23)

5.5.7 Flow Cytometry (Calcein AM assay)

The flow cytometry assay was based on that described previously.[209] Briefly, cells that overexpress P-gp (SW620 Ad300) were harvested with trypsin, resuspended in completed medium to give a final concentration of 50 × 10^4 cells/mL. Cells were then washed twice with cold PBS and pre-incubated with tested compound (20 μM) or verapamil (20 μM) for 30 min at 37 °C under 5% CO_2. Subsequently, cells were incubated with 2.5 μM calcein AM (calcein acetoxymethyl ester) for 1 h before measurement followed by washing twice with cold PBS. Samples were then analysed on a BD FACSCanto™ II flow cytometer (Becton Dickinson, San Jose, CA). Calcein fluorescence was detected with a 488 nm argon laser and a 530 nm band pass filter. The data were analysed by using FCSexpress 3 (De Novo Software, Los Angeles, CA). 10000 events were collected from each sample. Inhibition was evaluated using the following equation: FAR (fluorescence arbitrary ratio) = calcein fluorescence intensity (Geo mean) in the presence of tested compounds at 20 μM /calcein

fluorescence intensity (Geo mean) in the presence of PBS. Verapamil at 20 μM was used as positive control (FAR=43.1) Reversal MTT assay

5.5.8 Mosher ester derivatives of shornephine A (5.17)

Mosher ester derivatives were prepared according to protocol published by Hoye *et al.*[199] Shornephine A (50 μg) (**5.16**) was transferred into 2 mL glass vial with a Teflon-coated magnetic stir bar, to this was added 200 μL 6 M HCl and the reaction were heated overnight at 110 °C. The solution was dried down under N_2 and Teflon magnetic stir bar was added to the vial. Briefly, to a stirred solution of (*S*)-(+)-phenyllactic acid (1 eq in 150 μL dry DCM) in a 2 mL vial, (*R)*-(+)-MTPA-OH (3 eq in 150 μL dry DCM) or (*S)*-(−)-MTPA-OH (3 eq in 150 μL dry DCM) was added, followed by DCC (3 eq in 100 μL dry DCM) and DMAP (3 eq in 100 μL dry DCM). The reaction was left overnight at room temperature, after which it was filtered and dried under N_2 at 40 °C. The product was dissolved in MeOH and was analysed with HPLC-ESIMS, 60 – 15% H_2O/MeCN, 0.05% HCO_2H using Zorbax Eclipse XDB C_8 column. Amount of compounds derivatized: (+)-shornephine A (**5.16**), 0.1 mg (0.23 μmol)

seco-Shornephine A (**5.14**): pale yellow oil; $[\alpha]^{23}_D$ −73 (*c* 0.08, $CHCl_3$); UV (MeOH) λ_{max} (log ε) 218 (4.36), 248 (3.89), 306 (3.96); NMR (600 MHz, $CDCl_3$) see Table 5.1; HRESI(+)MS *m/z* 489.2015 $[M+Na]^+$ (calcd for $C_{26}H_{30}N_2O_6Na$ 489.2009).

Shornephine A (**5.16**): pale yellow oil; $[\alpha]^{22}_D$ +21.8 (*c* 0.05, $CHCl_3$); NMR (600 MHz, $CDCl_3$) see Table 5.2; HRESI(+)MS *m/z* 457.1731 $[M+Na]^+$ (calcd for 457.1734)

15b-β-hydroxyl-5-*N*-acetyladreemin (**5.17**): pale yellow oil; $[\alpha]^{22}_D$ −18.7 (*c* 0.09, $CHCl_3$); NMR (600 MHz, $CDCl_3$) see Table 5.4; HRESI(+)MS *m/z* 507.2016 $[M+Na]^+$ (calcd for $C_{28}H_{28}N_4O_4Na$ 507.2003)

5-*N*-acetyladreemin (**5.18**): pale yellow oil; $[\alpha]^{23}_D$ −20.7 (*c* 0.05, $CHCl_3$); NMR (600 MHz, $CDCl_3$) see Table 5.6; HRESI(+)MS *m/z* 491.2050 $[M+Na]^+$ (calcd for $C_{28}H_{28}N_4O_3Na$ 491.2054)

15b-β-methoxy-5-*N*-acetyladreemin (**5.19**): pale yellow oil; $[\alpha]^{23}_D$ −16.0 (*c* 0.07, MeOH); UV ($CDCl_3$) λ_{max} (log ε) 208 (4.03), 223 (4.06), 262 (3.59), 274 (3.57), 303 (3.17); NMR (600 MHz, $CDCl_3$) see **Table 5.7**; HRESI(+)MS *m/z* 521.2163 $[M+Na]^+$ (calcd for 521.2159)

(3*S*,6*S*)-3-benzyl-6-phenylmorpholine-2,5-dione (**5.5a**): white oil (3 mg, 75%); $[\alpha]_D^{22}$ –73.9 (*c* 0.04, $CHCl_3$); HRMS calculated for $C_{17}H_{16}N_1O_3$ 282.1125, found 282.1117. ^{1}H NMR (600 MHz, $CDCl_3$) see Figure 5.33 and Table 5.11.

(3*S*,6*S*)-3,6-dibenzylmorpholine-2,5-dione (**5.5b**): white crystals (2.5 mg, 72%); $[\alpha]_D^{22}$ – 446.1 (*c* 0.05, $CHCl_3$); HRMS calculated for $C_{18}H_{18}N_1O_3$ 296.1281, found 296.1277. ^{1}H NMR (600 MHz, $CDCl_3$) and ^{13}C NMR (150 MHz, $CDCl_3$) see Figure 5.34 and Table 5.12.

(3*S*,6*S*)-3-((1H-Indol-3-yl)methyl)-6-phenylmorpholine-2,5-dione (**5.5c**): colourless oil (4 mg, 75%); $[\alpha]_D^{22}$ –4.2 (*c* 0.14, $CHCl_3$); HRMS calculated for $C_{19}H_{16}N_2NaO_3$ 343.1053, found 343.1055. ^{1}H NMR (600 MHz, $CDCl_3$) and ^{13}C NMR (150 MHz, $CDCl_3$) see Figure 5.35 and Table 5.13.

(3*S*,6*S*)-3-((1H-Indol-3-yl)methyl)-6-benzylmorpholine-2,5-dione (**5.5d**): colourless oil (4 mg, 75%); $[\alpha]_D^{22}$ –75.6 (*c* 0.05, $CHCl_3$); HRMS calculated for $C_{20}H_{19}N_2O_3$ 335.1390, found 335.1376. ^{1}H NMR (600 MHz, $CDCl_3$) and ^{13}C NMR (150 MHz, $CDCl_3$) see Figure 5.36 and Table 5.14.

(3*S*,6*S*)-3-(4-Hydroxybenzyl)-6-phenylmorpholine-2,5-dione (**5.5e**): colourless oil (2.5 mg, 69%); $[\alpha]_D^{22}$ +2.1 (*c* 0.11, $CHCl_3$); HRMS calculated for $C_{17}H_{16}N_1O_4$ 298.1074, found 298.1072.^{1}H NMR (600 MHz, $CDCl_3$) and ^{13}C NMR (150 MHz, $CDCl_3$) see Figure 5.37 and Table 5.15.

(3*S*,6*S*)-6-Benzyl-3-(4-hydroxybenzyl)morpholine-2,5-dione (**5.5f**): colourless oil (3.1 mg, 65%); $[\alpha]_D^{22}$ –89.4 (*c* 0.1, $CHCl_3$); HRMS calculated for $C_{18}H_{17}N_1NaO_4$ 334.1050, found 334.1044.^{1}H NMR (600 MHz, $CDCl_3$) and ^{13}C NMR (150 MHz, $CDCl_3$) see Figure 5.38 and Table 5.16.

(3*S*,6*S*)-3-Methyl-6-phenylmorpholine-2,5-dione (**5.5g**): colourless oil (2.5 mg, 62%); $[\alpha]_D^{22}$ +28.5 (*c* 0.05, $CHCl_3$); HRMS calculated for $C_{11}H_{12}NO_3$ 206.0812, found 206.0819. ^{1}H NMR (600 MHz, $CDCl_3$) and ^{13}C NMR (150 MHz, $CDCl_3$) see Figure 5.39 and Table 5.17.

(3*S*,6*S*)-6-Benzyl-3-methylmorpholine-2,5-dione (**5.5h**): colourless oil (3.1 mg, 69%); $[\alpha]_D^{22}$ +85.4 (*c* 0.05, $CHCl_3$); HRMS calculated for $C_{12}H_{14}NO_3$ 220.0968, found 220.0976. ^{1}H NMR (600 MHz, $CDCl_3$) and ^{13}C NMR (150 MHz, $CDCl_3$) see Figure 5.40 and Table 5.18.

cyclo-(L-Trp-L-Phe) (**5.28**): This compound was synthesised as reported[208] in quantitative yield to afford pale yellow oil; (45 mg, 98.6%), $[\alpha]^{23}{}_D$ –20.7 (*c* 0.05, $CHCl_3$); ESIMS, *m/z* 334 [M+H] ^{1}H

NMR (600 MHz, DMSO-d_6); 10.87 (1H, s), 7.88 (1H, br s), 7.68 (1H, br s), 7.47 (1H, d, *7.8*), 7.30 (1H, d, *8.1*), 7.15 (2H, m), 7.05 (1H, t, *7.5*), 6.97 (1H, d, *7.5*), 6.95 (1H, d, *7.5*), 6.69 (1H, d, *7.5*), 3.95 (1H, br s), 3.83 (1H, br s), 2.79 (1H, dd, *14.4, 4.2*), 2.51 (1H, d, *6.1*), 2.45 (1H, dd, *13.4, 4.7*), 1.84 (1H, dd, *13.4,7.1*); ^{13}C (150 MHz, DMSO d_6); 168.8, 168.1, 138.5, 138.0, 131.7, 130.1, 130.0, 129.5, 128.3, 126.4, 122.8, 120.7, 120.4, 113.3, 110.8, 81.2, 80.9, 80.7, 57.6, 57.2, 31.7

6 Chapter 6: Desotamides: New cyclic hexapeptides with inhibitory activity against *Mycobacterium bovis*

6.1 Introduction

As part of an ongoing collaboration between the Capon research group and the Australian microbial biodiscovery company, Microbial Screening Technologies (MST), we routinely receive novel microbial metabolites for spectroscopic analysis, structure elucidation and biological evaluation. This chapter describes one study, involving known and new examples of a rare class of cyclic hexapeptides, the desotamides.

6.2 History

To date the scientific literature records only one natural product characterized as a desotamide, first reported in 1997, by Miao *et al*.[210] from a soil isolate of *Streptomyces* sp. Structure elucidation was achieved by NMR analysis including HSQC, COSY, HMBC, TOCSY and NOE, and the absolute configuration assigned by Marfey analysis and total synthesis of the two stereoisomers. Desotamide has not been reported to exhibit any biological activity.

6.3 Desotamides from MST

Studies into the secondary metabolites produced by *Streptomyces* sp. (MST-1150688), led MST researchers to isolate a selection of peptidic metabolites collectively identified as “desotamides”, as outlined in Scheme 6.1.

6.4 Desotamides

The desotamides metabolites were provided from Microbial Screening technology (MST) for structure elucidation and biological assay. Primary screening on HPLC-DAD-MS showed the presence of interesting metabolites as shown in Figure 6.1 and Figure 6.2.

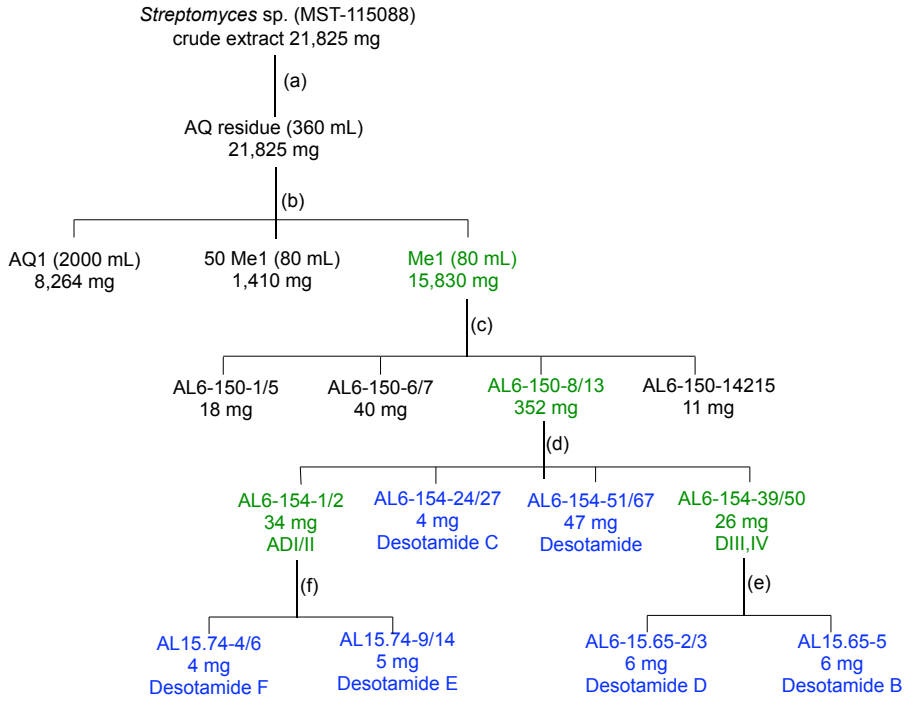

Scheme 6.1. Isolation scheme for desotamide (**6.01 – 6.06**). (a) rotatory evaporation. (b) diluted to 2L with H_2O and purified using C_{18}. (c) 500 mg sub-sample LH-20, 2.5 × 100 cm CH_2Cl_2/MeOH ratio 50:50. (d) mega preparative HPLC, LUNA 65% MeOH, 0.01% TFA, 60 mL/min. (e) preparative HPLC, LUNA 55% MeOH, 0.01% TFA, 10 mL/min. (f) preparative HPLC, LUNA 50% MeOH, 0.01% TFA, 10 mL/min.

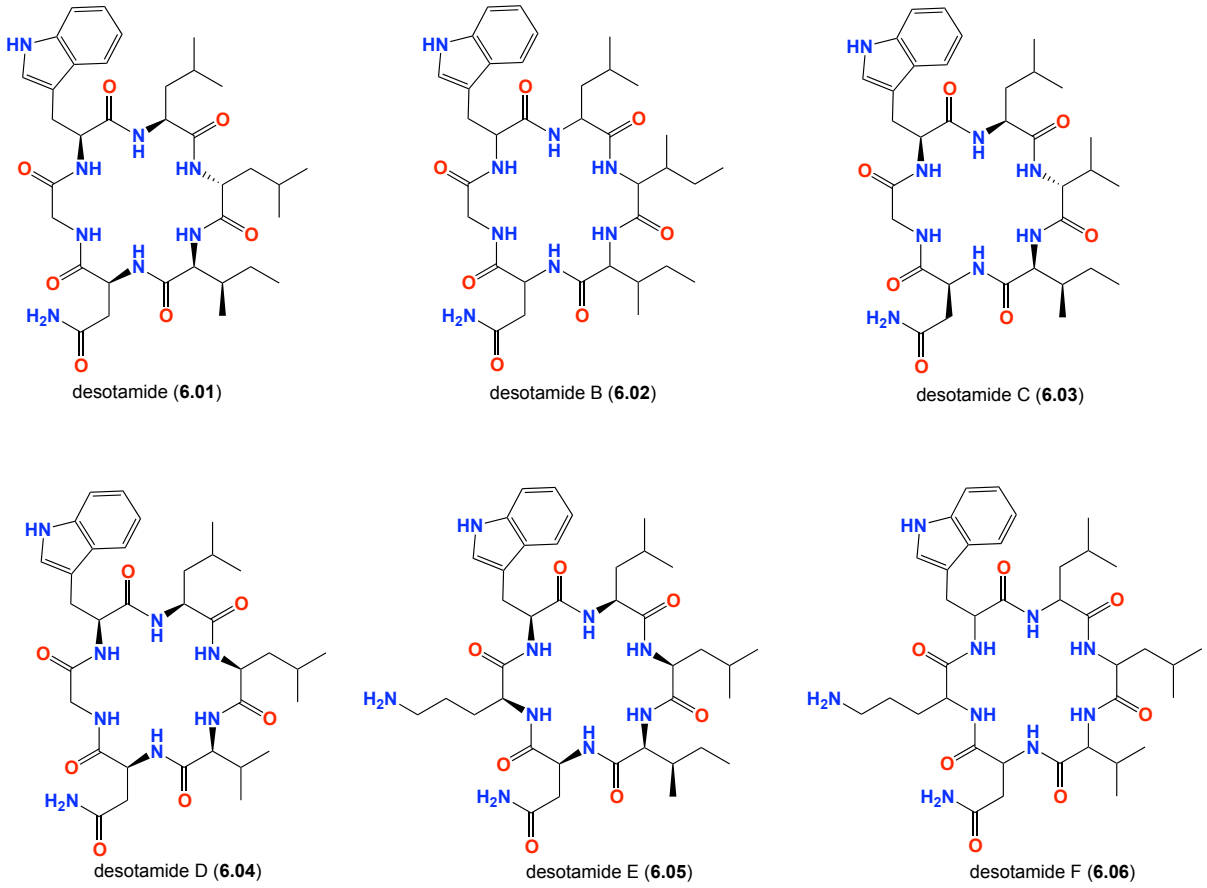

Figure 6.1. Desotamides (**6.01** - **6.06**). *Marfey's analysis of **6.02** and **6.06** is still under progress

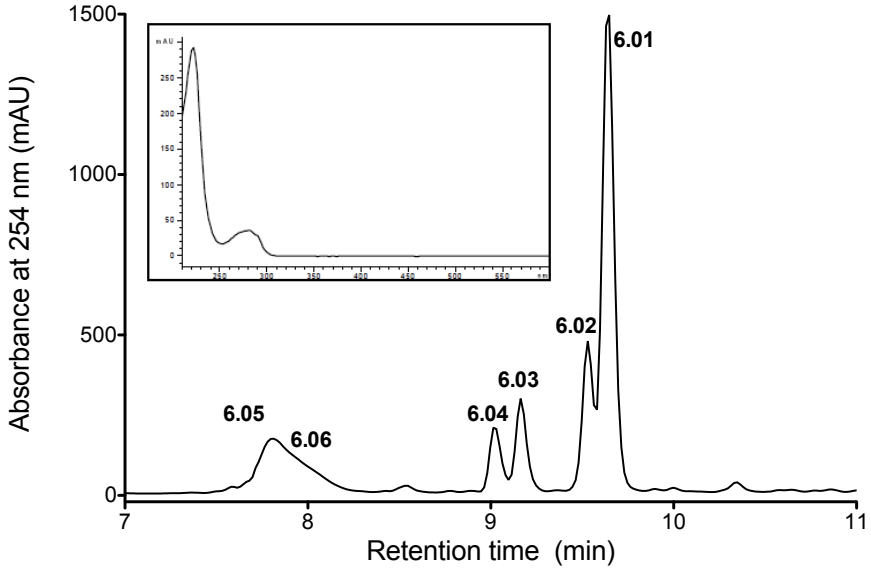

Figure 6.2. HPLC-DAD (254 nm) chromatogram and UV-vis spectrum from analytical gradient H_2O/MeCN with 0.05% HCO_2H using Zorbax C_8 of the crude extract from *Streptomyces* sp. (MST-1150688) of the desotamides (**6.01** – **6.06**)

6.4.1 Desotamide (6.01)

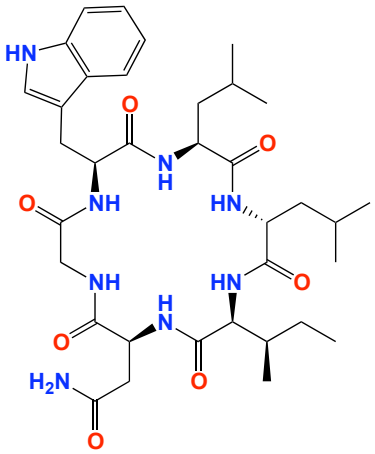

desotamide (**6.01**)

HRESI(+)MS analysis of desotamide (**6.01**) returned an adduct ion $[M+Na]^+$ corresponding to a molecular formula ($C_{35}H_{52}N_8O_7$, Δmmu −0.6). Careful analysis of the 1D and 2D NMR (DMSO-d_6) data for **6.01** suggested a cyclohexapeptide structure inclusive of a Trp residue. A C_3 Marfey's analysis of **6.01** supported this hypothesis, and detected the presence of L-Trp, L-Leu, D-Leu, L-*allo*-Ile, L-Asn and Gly (Figure 6.3 and Figure 6.4), while a literature search suggested that **6.01** $[\alpha]^{22}_D$ – 29.3 (*c* 0.05, MeOH) was the known microbial cyclohexapeptide desotamide $[\alpha]^{23}_D$ –6.7 (*c* 0.35, MeOH) (Table 6.2). Desotamide was first reported in 1997 by Miao *et al.*[210] from a soil isolate of *Streptomyces* sp. To confirm the structure assignment, Miao *et al*. synthesized five closely related co-metabolites. To confirm our reisolation of desotamide (**6.01**), a full spectroscopic and Marfey's analysis was carried out (Figure 6.3, Figure 6.4, **Figure 6.5**, Table 6.1 and Table 6.2).

6.4.1.1 C_3 Marfey's analysis

A Marfey's analysis was performed according to the method described by Miao *et al.*[173,210], **6.01** was subjected to acid hydrolysis using 6 M HCl/5% thioglycolic acid, derivatized with D-FDAA, and subjected to HPLC analysis, using our modified C_3 Marfey's analysis which enable the differentiation between D-Ile from D-*allo*-Ile, or L-Ile from L-*allo*-Ile[45] to determine the absolute stereochemistry of the amino acids. Absolute configuration of **6.01** was determined by comparing the retention times of standard amino acids with the hydrolysate of **6.01**. The amino acids of **6.02** was confirmed to be L-Trp, L-Leu, D-Leu, L-*allo*-isoLeu, L-Asn and Gly consistent with the reported desotamide (Figure 6.3 and Figure 6.4).

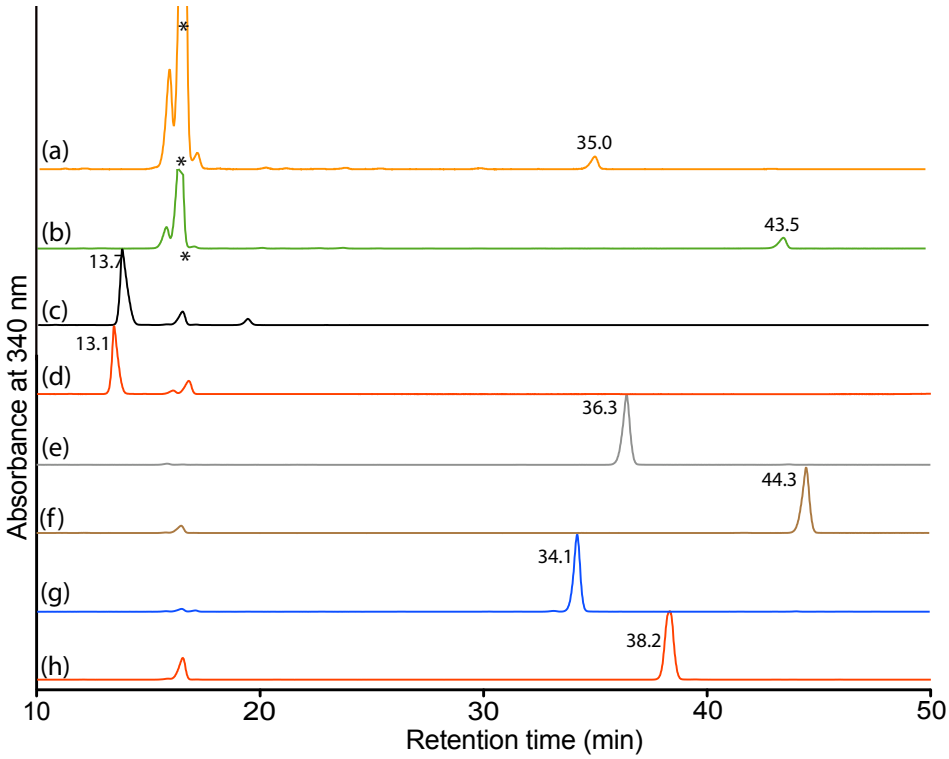

Figure 6.3. HPLC trace (340 nm) from HPLC-DAD-MS C_3 Marfey's analysis of the standard amino acids reacting with D-FDAA. Identity of amino acids was confirmed by retention time and molecular weight. (a) L-*allo*-Ile + L-FDAA (t_R = 35.0 min), (b) L-*allo*-Ile + D-FDAA (t_R = 43.5 min), (c) L-Asn + D-FDAA (t_R = 13.7 min), (d) D-Asn + D-FDAA (t_R = 13.1 min), (e) D-Leu + D-FDAA (t_R = 36.3 min), (f) L-Leu + D-FDAA (t_R = 44.3 min), (g) L-Trp + L-FDAA (t_R = 34.1 min) and (h) L-Trp + D-FDAA (t_R = 38.2 min). HPLC conditions, Zorbax, SB-C_3 column (150 × 4.6 mm, 5 μm), 1 mL/min, gradient of 15 – 60% MeOH/H_2O (isocratic 5% MeCN containing 1% formic acid) over 55 min

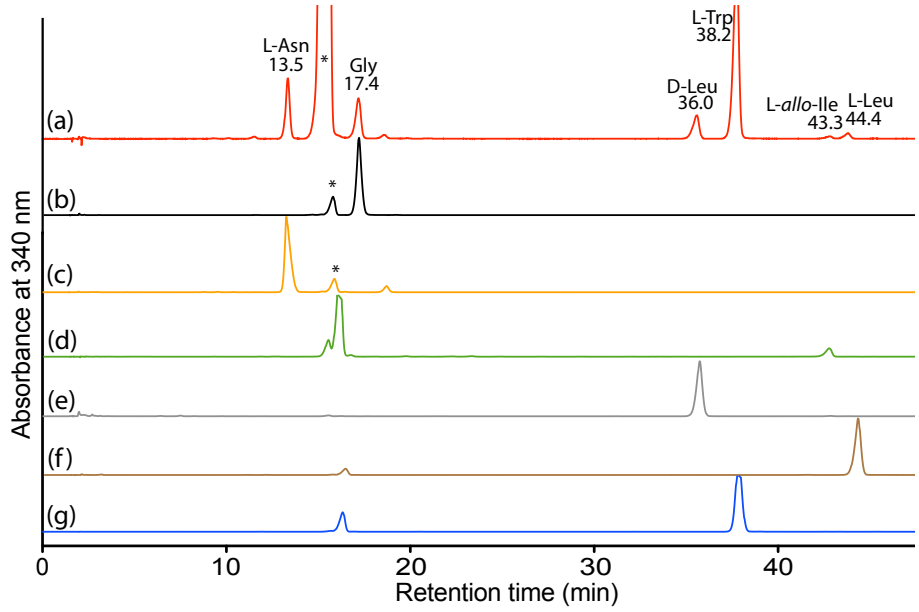

Figure 6.4. HPLC trace (340 nm) from HPLC-DAD-MS C_3 Marfey's analysis of desotamide (**6.01**). Identity of amino acids was confirmed by retention time and molecular weight. (a) Co-injection of hydrolysate of **6.01** (200 μg) with L-Asn, Gly, D -Leu, L-Leu, L-Trp, L-*allo*-Ile + D-FDAA, (b) Gly + D-FDAA, (c) L-Asn + D-FDAA, (d) L-*allo*-Ile + D-FDAA, (e) D-Leu + D-FDAA, (f) L-Leu + D-FDAA and (g) L-Trp + D-FDAA. HPLC conditions, Zorbax, SB-C_3 column (150 × 4.6 mm, 5 μm), 1 mL/min, gradient of 15 – 60% MeOH/H_2O (isocratic 5% MeCN containing 1% formic acid) over 55 min.

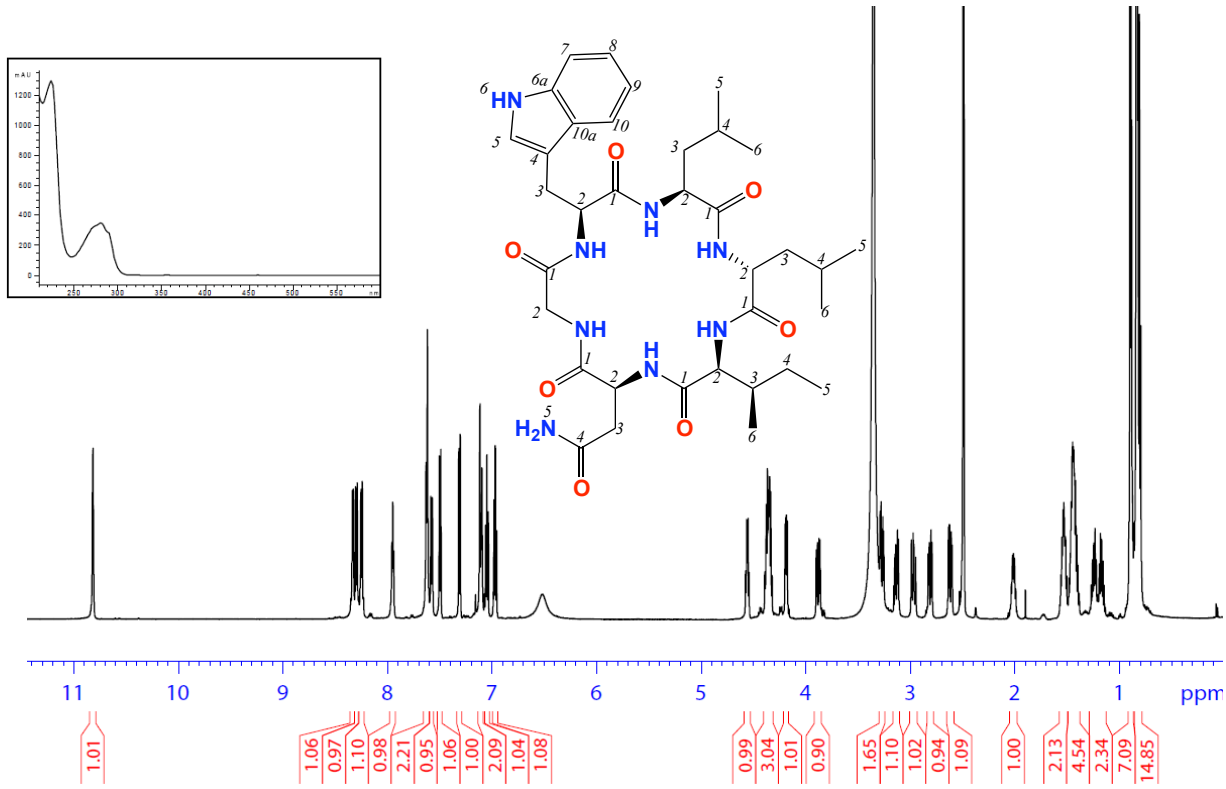

Figure 6.5. ^{1}H NMR (600 MHz, DMSO-d_6) and UV-vis (inset) spectra of desotamide (**6.01**)

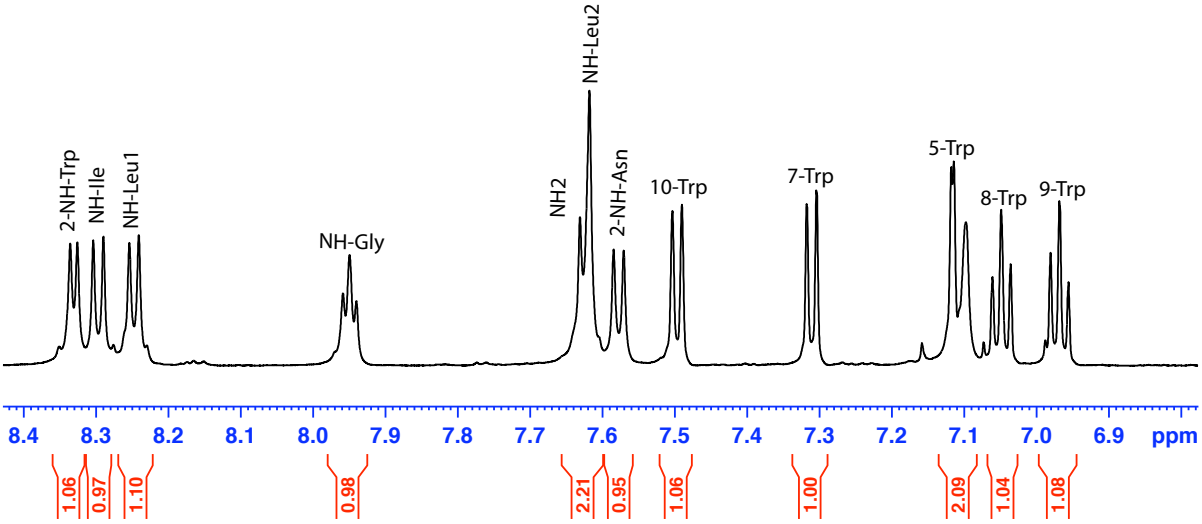

Figure 6.6. ^{1}H NMR (600 MHz, DMSO-d_6) spectrum of desotamide (**6.01**)

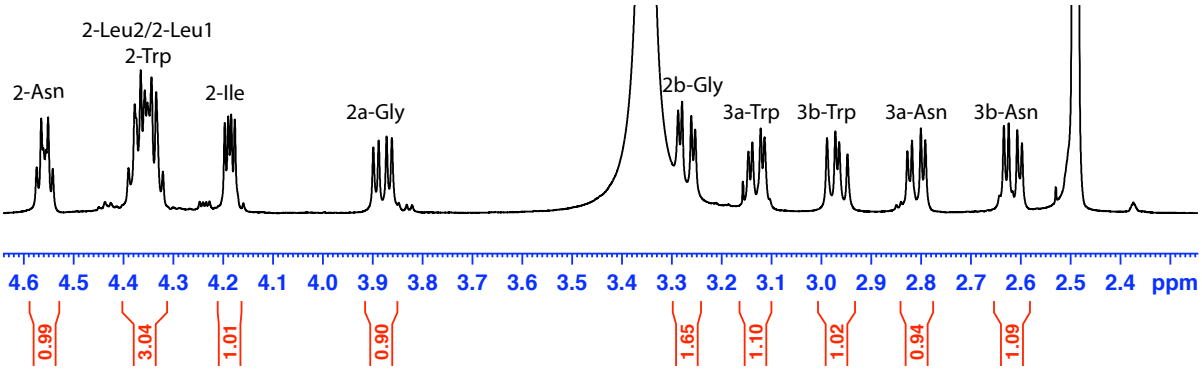

Figure 6.7. ^{1}H NMR (600 MHz, DMSO-d_6) spectrum of desotamide (**6.01**)

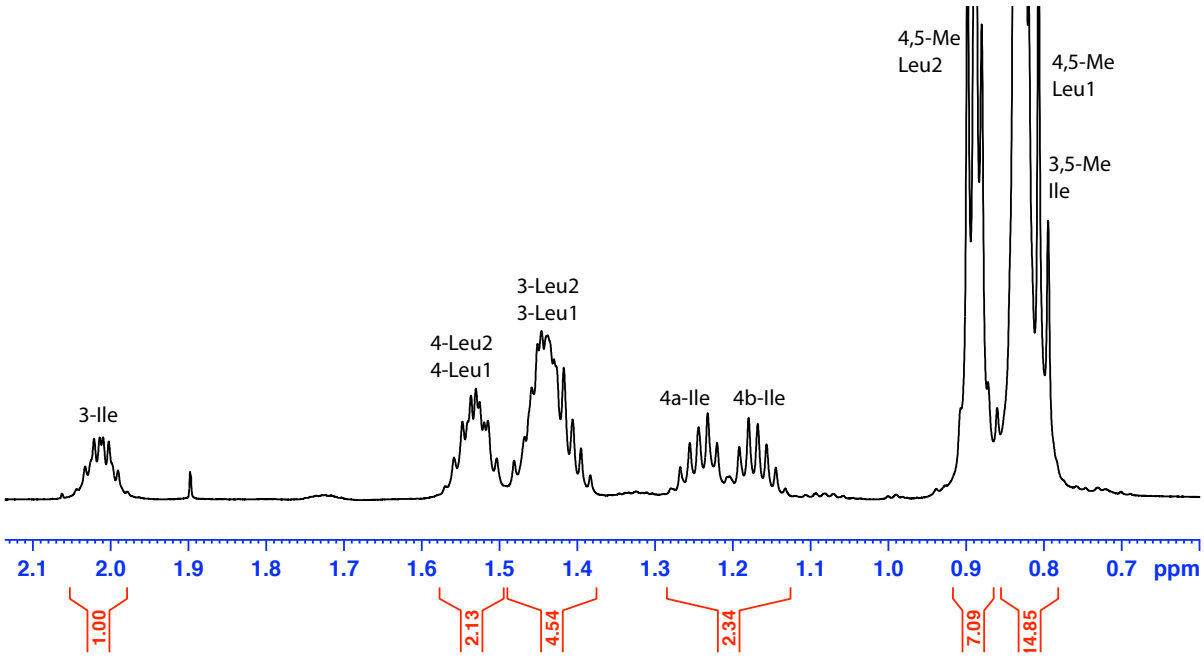

Figure 6.8. ^{1}H NMR (600 MHz, DMSO-d_6) spectrum of desotamide (**6.01**)

The C_3 Marfey's analysis unambiguously confirmed the presence of all the amino acid residues and allowed the assignment of *allo*-Ile without the need for the synthesis of different stereoisomers – as shown in the literature. To assist positioning these residues in **6.01** it was necessary to assign key 1D NMR resonances, and identify key 2D NMR correlations linking adjacent amino acids.

Six amino acid peptide fragment:

L-Trp #1: Analysis of the COSY NMR (DMSO-d_6) data for **6.01** revealed diagnostic correlation sequences consistent with the structure fragment (i) H-7 to H-8 to H-9 to H-10, (ii) 2-NH to H-2 to H_2-3, and (iii) H-5 to 6-NH (see Figure 6.9 and Table 6.1). Key HMBC correlation permitting assignment of the quaternary carbons included (i) H_2-3 and 2-NH to C-1, (ii) H_2-3 and H-10 to C-4 and C-10a, and (iii) 6-NH and H-8 to C-6a

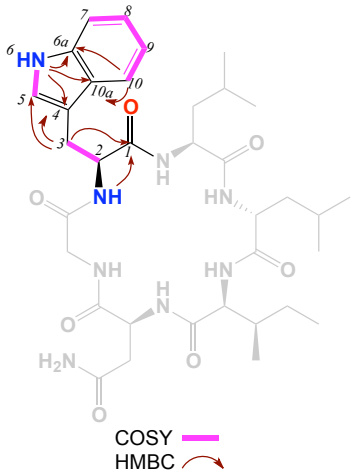

Figure 6.9. Key 2D NMR correlations of desotamide (**6.01**)

L-Leu and D-Leu: As NMR cannot distinguish between amino acid enantiomers, the following assignments of NMR resonances to Leu residues merely characterizes the two independent Leu residues, but does not go to the issue of assignment of their absolute configuration.

Leucine #2: COSY NMR (DMSO-d_6) correlations readily identified the sequence 2-NH to H-2 to H_2-3 to H-4 to H_3-5/H_3-6, while HMBC correlations linked H-2 to C-1

Leucine #3: As above COSY NMR (DMSO-d_6) correlation established the sequence 1-NH to H-2 to H_2-3 to H-4 to H_3-5/H_3-6, while HMBC correlation linked 2-NH to C-1 (Figure 6.10).

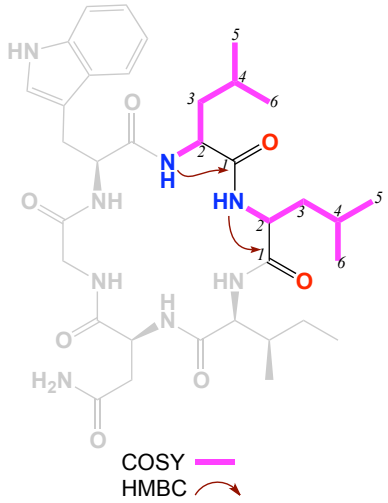

Figure 6.10. Key 2D NMR correlations of desotamide (**6.01**)

L-*allo*-isoleucine #4: Our C_3 Marfey's analysis has the ability to distinguish between *allo*-isoleucine and isoleucine. Analysis of the COSY NMR (DMSO-d_6) data of **6.01** identified the sequence 2-NH to H-2 to H-3/H_3-3 to H_2-4 to H_3-5, while HMBC correlations linked H-2 to C-1 (Figure 6.11).

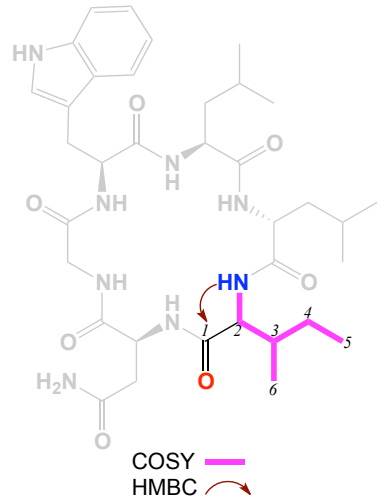

Figure 6.11. Key 2D NMR correlations of desotamide (**6.01**)

L-Asn #5: COSY NMR (DMSO-d_6) correlations readily identified the sequence 2-NH to H-2 to H_2-3, while HMBC correlations linked NH_2 to C-4, H_2-3 to C-1, H-2 and 2-NH to C-1 (Figure 6.12).

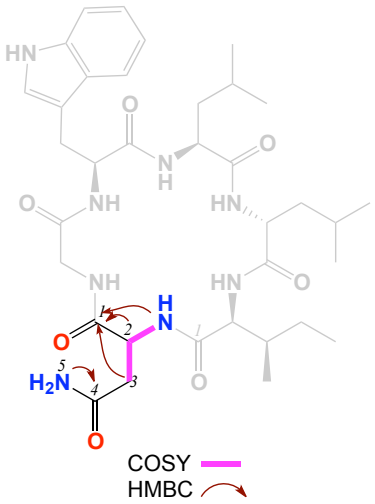

Figure 6.12. Key 2D NMR correlations of desotamide (**6.01**)

Gly #6: COSY NMR (DMSO-d_6) correlations readily identified the sequence 2-NH to H-2, while HMBC correlations linked 2-NH and H_2-2 to C-1 (Figure 6.13).

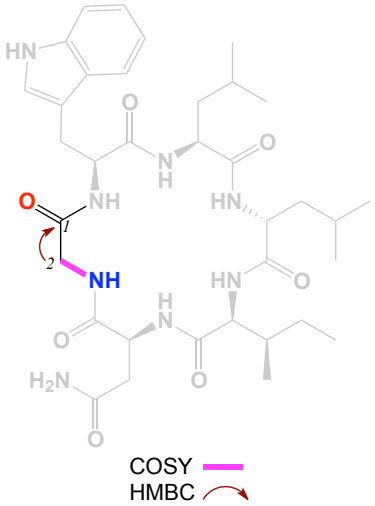

Figure 6.13. Key 2D NMR correlations of desotamide (**6.01**)

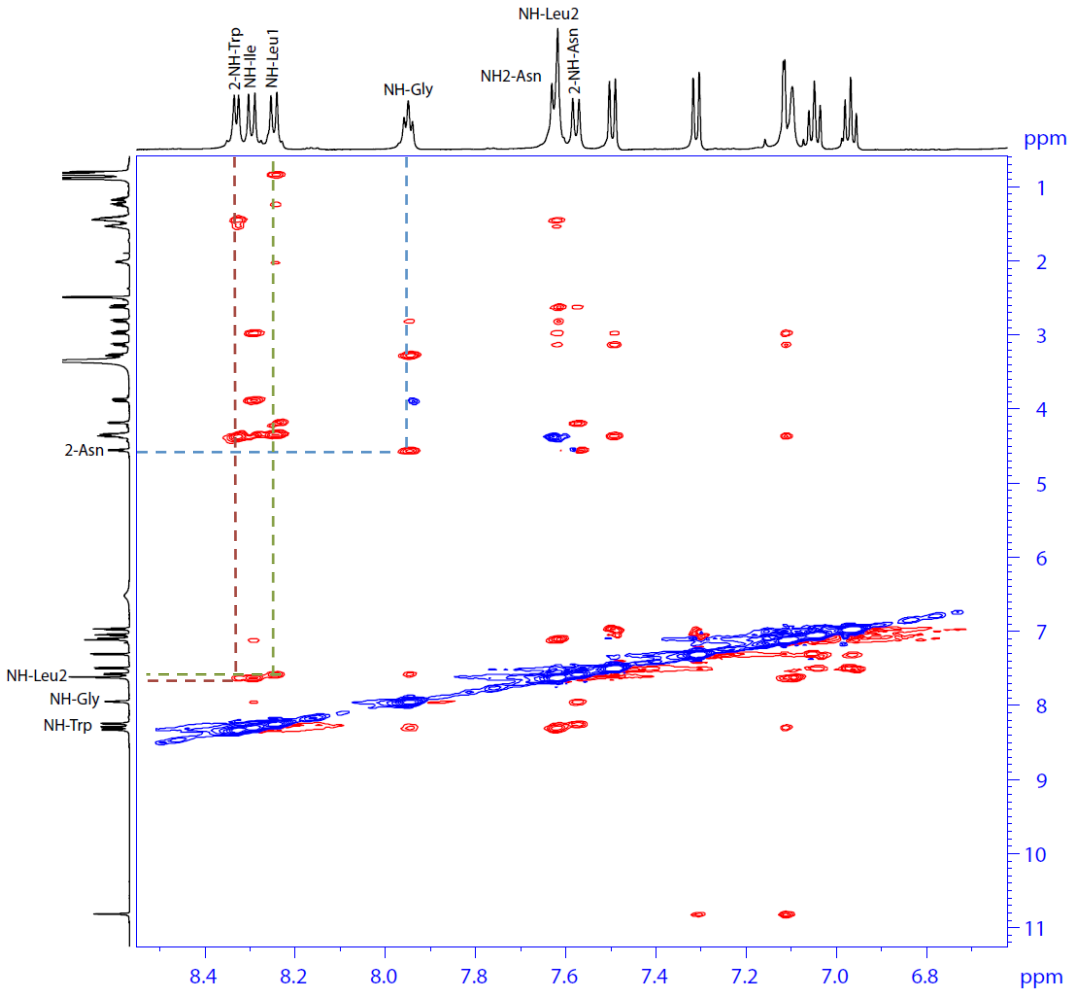

Figure 6.14. ROESY (600 MHz, DMSO-d_6) spectrum showing key correlations of desotamide (**6.01**)

Table 6.1. NMR (600 MHz, DMSO-d_6) data of desotamide (**6.01**)

#	Pos.	δ_H, mult (*J* in Hz)[a]	δ_C[a]	COSY	^{1}H-^{13}C HMBC	ROESY
Trp.	1		171.4			
	2	4.35[b]	54.3	3		
	3	a 3.12, dd (*14.6, 10.1*)	27.0	3b, 2, 2-NH	1, 2, 4, 5, 10a	
		b 2.96, dd (*14.6, 10.1*)		3a, 2, 2-NH	2, 4, 5, 10a	
	4		109.4			
	5	7.11, d (*1.8*)	123.1	6	3, 4, 6a, 10a	2, 3
	6a		135.6			
	7	7.31, d (*8.0*)	110.9	8	10, 10a	6-NH
	8	7.04, t (*8.0*)	120.5	7, 9	6a, 10	
	9	6.96, t (*8.0*)	117.9	8, 10	7, 10a	
	10	7.49, d (*8.0*)	118.2	9	4, 8, 6a, 10a	2, 3
	10a		126.7			
	2-NH	8.29, d (*8.6*)		2	1, 2, 3	2-Gly,2- Leu2
	6-NH	10.81, s		5	4, 5, 6a, 10a	5
Gly.	1		168.9			
	2	a 3.88, dd (*15.8, 6.5*)	42.9	2b, NH	1	2-NH-Trp
		b 3.26, dd (*15.8, 6.5*)		2a, NH	1	2-NH-Trp
	NH	7.94, t (*5.9*)		2a,b		2-Asn,NHAsn
Asn.	1		171.2			
	2	4.55, m	48.9	2-NH, 3	1, 3	NH-Gly
	3	a 2.80, dd (*16.2, 5.5*)	36.5	2, 3b	1, 2	
		b 2.61, dd (*16.2, 5.5*)	36.5	2, 3a	1, 2	
	4		172.0	3a,b		
	2-NH	7.57, d (*8.6*)		2	1, 3	2-*allo*-Ile, NH-Ile
	NH_2	7.62, br s			4	3
allo-Ile	1		170.9			
	2	4.18, dd (*7.8, 4.3*)	56.1	2-NH	1, 3, 6-Me	3-Me,NH-Asn
	3	2.01, m	34.9	2, 6-Me, 4	6-Me, 5-Me	
	4	1.17-1.23, m	25.3	3, 5	2	
	5-Me	0.81[b]	11.1	4		
	6-Me	0.81[b]	14.3	3		
	2-NH	8.24, d (*8.6*)		2	1	
Leu#1	1		173.1			
	2	4.35[b], m	51.3	3, NH	1, 4	NH-Leu#1
	3	1.53, m	39.3	2, 5/6-Me		
	4	1.53[b]	23.7	3, 5/6-Me	2, 5/6-Me	
	5-Me	0.82[b]	22.1[c]		3, 4	
	6-Me	0.82[b]	22.1[c]		3, 4	
	2-NH	8.29, d (*8.6*)			1, 2, 3	NH-Leu#2
Leu#2	1		172.2			
	2	4.35[b], m	50.3	3, NH	1	
	3	1.43, m	41.3	4	2	
	4	1.53[b], m	24.1	3, 5-Me	2	
	5-Me	0.88[b], d (*6.9*)	22.1[c]	6-Me	3	
	6-Me	0.87[b], d (*6.9*)	22.1[c]	5-Me	3	
	2-NH	7.62[b]			2	4, NH-Leu#1

(a) ^{13}C assignments obtained from gHSQC and gHMBC data. (b) Overlapping resonances. (c) Interchangeable resonances

Table 6.2. NMR (DMSO-d_6) data comparison of experimental and literature[210] data of desotamide (**6.01**)

#	Pos.	δ_H, mult (*J* in Hz)[a] (experimental)	δ_c	δ_H, mult (*J* in Hz)[b] (literature)	δ_c
Trp.	1		171.4		170.9
	2	4.35[b]	54.3	4.36, m	55.4
	3	a 3.12, dd (*14.6, 10.1*)	27.0	3.31, dd (*14.7, 5.0*)	27.3
		b 2.96, dd (*14.6, 10.1*)		2.96, dd (*14.7, 10.1*)	
	4		109.4		110.0
	5	7.11, br s	123.1	7.11, s	123.5
	6a		135.6		136.1
	7	7.31, d (*8.0*)	110.9	7.30, d (*8.1*)	111.3
	8	7.04, t (*8.0*)	120.5	7.04, t (*7.7*)	120.9
	9	6.96, t (*8.0*)	117.9	6.96, t (*7.7*)	118.3
	10	7.49, d (*8.0*)	118.2	7.49, d (*7.7*)	118.1
	10a		126.7		127.1
	2-NH	8.29, d (*8.6*)		8.24, d (*8.3*)	
	6-NH	10.81, s		10.76, s	
Gly.	1		168.9		169.1
	2	a 3.88, dd (*15.8, 6.5*)	42.9	3.89, dd (*15.8, 6.2*)	43.3
		b 3.26, dd (*15.8, 5.4*)		3.28, dd (*15.8, 4.6*)	
	NH	7.94, t (*5.9*)		7.90, t (*5.5*)	
Asn.	1		171.2		171.0
	2	4.55, m	48.9	4.56, m	49.4
	3	a 2.80, dd (*16.2, 5.5*)	36.5	2.79, dd (*16.0, 5.5*)	36.9
		b 2.61, dd (*16.2, 5.5*)		2.61, dd (*16.0, 5.5*)	
	4		172.0		172.0
	2-NH	7.57, d (*8.6*)		7.59, d (*8.4*)	
	NH_2	7.62, br s		7.56, s	
Ile	1		170.9		171.0
	2	4.18, dd (*7.8, 4.3*)	56.1	4.16, dd (*7.5, 4.5*)	56.6
	3	2.01, m	34.9	2.00, h (*7.0*)	35.2
	4	1.17-1.23, m	25.3	1.2, m	25.6
	5-Me	0.81[c]	11.1	0.82, t (*7.0*)	11.5
	6-Me	0.81[c]	14.3	0.81, t (*7.0*)	14.5
	NH	8.24, d (*8.6*)		8.19, d (*7.5*)	
Leu#1	1		173.1		173.3
	2	4.35, m	51.3	4.34, m	51.8
	3	1.53, m	39.3	1.45, m	39.3
	4	1.53[c]	23.7	1.54, m	24.2
	5-Me	0.88[c]	22.1[d]	0.82, d (*7.0*)	22.1[d]
	6-Me	0.88[c]	22.1[d]	0.82, d (*7.0*)	22.4[d]
	2-NH	7.09, br s		8.20, d (*6.0*)	
Leu#2	1		172.2		171.9
	2	4.35, m	50.3	4.35, m	50.8
	3	1.53, m	41.3	1.45, m	41.4
	4	1.53	24.1	1.54, m	24.4
	5-Me	0.88[c]	22.1[d]	0.88, d (*7.0*)	22.5[d]
	6-Me	0.87[c]	22.1[d]	0.88, d (*7.0*)	22.6[d]
	2-NH	7.64, d (*7.6*)		7.65, d (*7.8*)	

*(a) ^{1}H NMR at 600 MHz. (b)^{1}H NMR at 400 MHz. (c) Overlapping resonances. (d) Interchangeable resonances

6.4.2 Desotamide B (6.02)

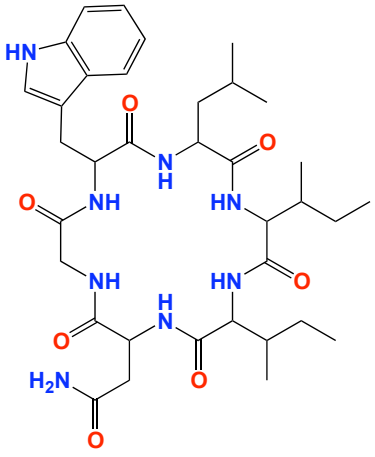

desotamide B (**6.02**)

HRESI(+)MS analysis of **6.02** returned an adduct ion $[M+Na]^+$ consistent with a molecular formula $C_{35}H_{52}N_8O_7$ (Δmmu +1.6). Examination of the NMR (DMSO-d_6) data (Table 6.3 and Figure 6.16) revealed a close similarity to desotamide (**6.01**). As the ESI(+)MS data (*m/z*, 695, $M+H^+$) was the same as **6.01**, the structure elucidation was performed using 2D NMR spectra including HSQC, COSY and HMBC correlation outline in Figure 6.16 and Table 6.3. NMR data showed the presence of Trp, Leu, Ile × 2, Asn and Gly residues. A C_3 Marfey's analysis is still under investigation to prove the presence of the amino acid residues and determine the absolute stereochemistry of the amino acids. The sequence of amino acid residues is tentatively proposed as indicated, but will be addressed towards the end of this chapter.

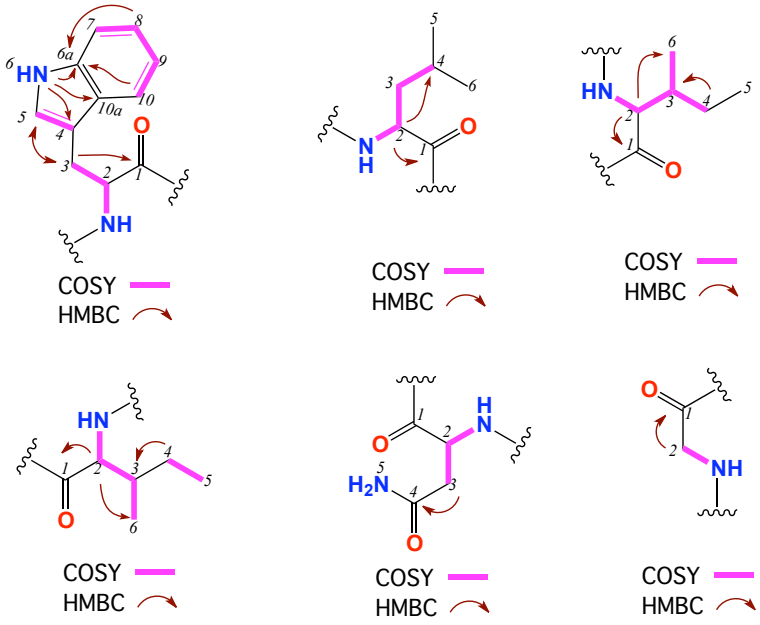

Figure 6.15. Key 2D NMR correlations for amino acids residues of desotamide B (**6.02**)

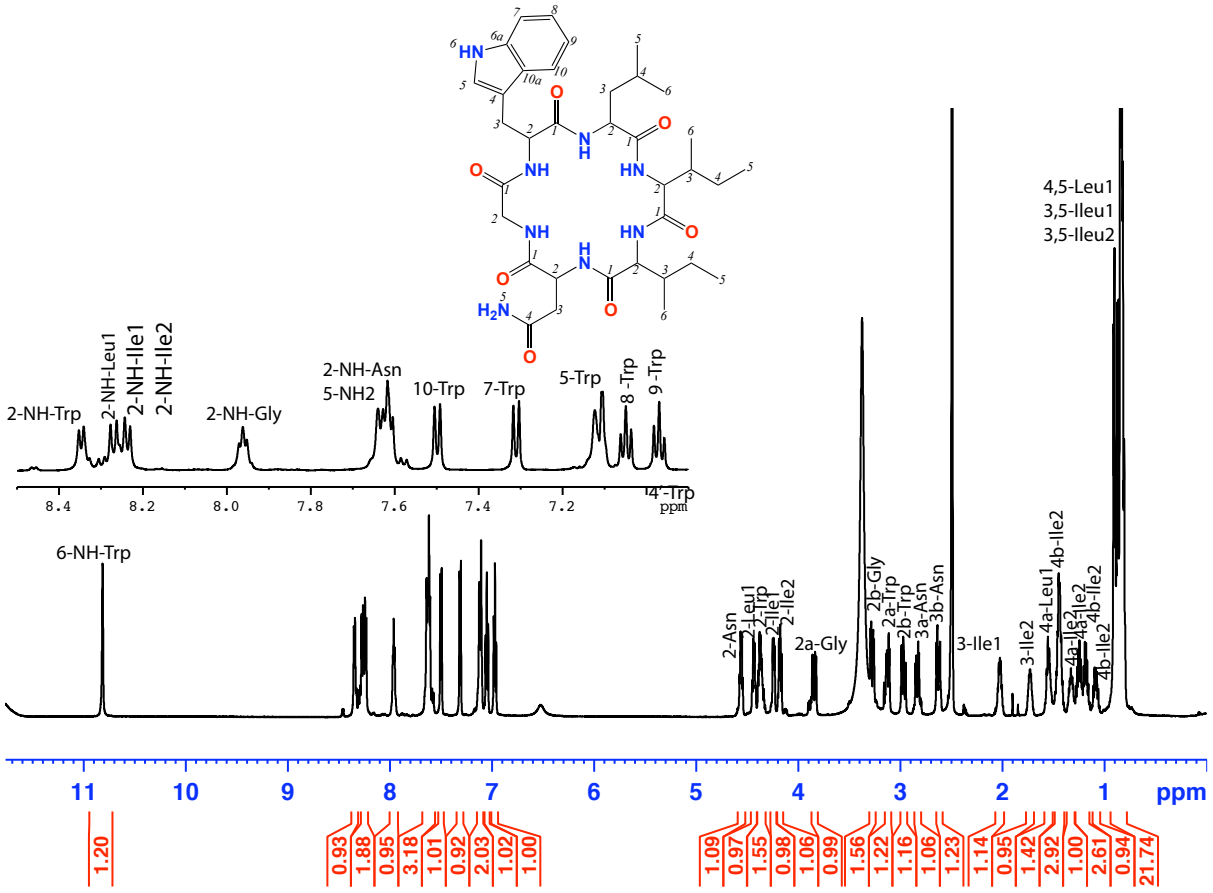

Figure 6.16. ^{1}H NMR (600 MHz, DMSO-d_6) of desotamide B (**6.02**)

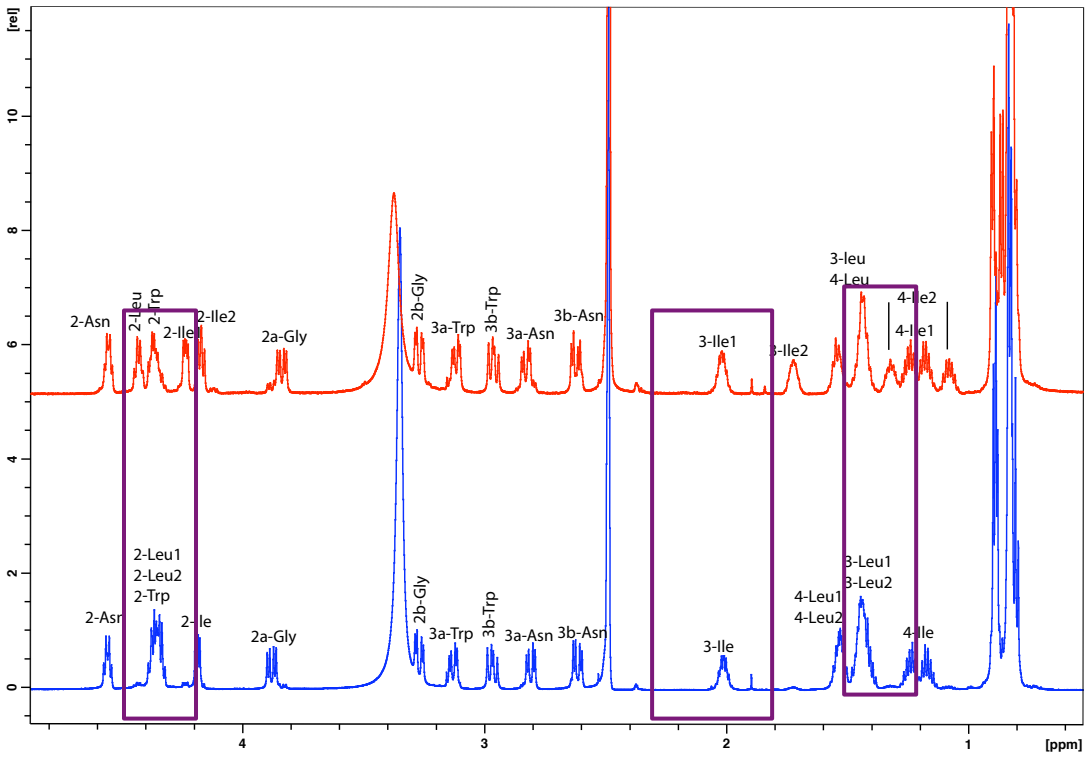

Figure 6.17. ^{1}H NMR (600 MHz, DMSO-d_6) comparison of desotamide (**6.01**) (blue) and desotamide B (**6.02**) (red)

Table 6.3. NMR (600 MHz, DMSO-d_6) data of desotamide B (**6.02**)

#	Pos.	δ_H, mult (*J* in Hz)[a]	δ_C[a]	COSY	^{1}H-^{13}C HMBC	ROESY
Trp.	1		170.6			
	2	4.36[b], m	54.9	2-NH, 3a,b		
	3	a 3.11, dd *(15.1, 10.3)*	27.2	2, 3b	1, 4, 5	
		b 2.96, dd *(15.1, 10.3)*		2, 3a	1, 4, 5	
	4		109.9			
	5	7.12, brd	123.1	6	3, 4, 6a	
	6a		135.8			6a
	7	7.31, d *(7.8)*	111.1	8	10, 10a	
	8	7.04, t *(7.8)*	120.7	7, 9	6a, 10	
	9	6.96, t *(7.8)*	118.2	8, 10	4, 10a	
	10	7.49, d *(7.8)*	117.9	9	4, 6a, 8, 10a	3a,b
	10a		126.7			
	2-NH	8.34, d *(5.9)*		2	1-Gly	2-Leu
	6-NH	10.81, s		5	4, 5, 6a, 10a	5, 7
Gly.	1		168.3			
	2	a 3.83, dd *(16.1, 5.3)*	43.0	2b, 2-NH	1, 1-Asn	
		b 3.27, dd *(16.1, 5.3)*		2a, 2-NH	1, 1-Asn	
	2-NH	7.96, t *(5.3)*		2a,b	1, 1-Asn	2-NH-Asn
Asn.	1		171.4			
	2	4.55, m	48.8	3a,b, 2-NH	1-Ile, 3	NH-Gly
	3	a 2.83, dd *(16.5, 5.4)*	36.6	2, 3b	2, 4	
		b 2.62, dd *(16.5, 5.4)*		2, 3a	2, 4	
	4		171.1			
	2-NH	7.61[b]		2	1	
	NH_2	7.60, s			4	
Ile#1	1		171.5			
	2	4.17, dd *(8.5, 6.1)*	57.7	2-NH, 3	1, 3, 5/6	2-NH-Trp
	3	1.77[b], m	34.6	2, 6-Me, 4		
	4	1.10[b], m	24.8		5/6-Me	
	5-Me	0.82[b]	11.6[c]			
	6-Me	0.87[b]	14.5[c]			
	2-NH	8.21, d *(7.8)*		2		
Ile#2	1		172.3			
	2	4.23, dd *(7.8, 4.1)*	55.9	2-NH, 3	1, 5/6	
	3	2.02, m	34.9	2, 6		
	4	a 1.08 - 1.21, m	25.4	5	5/6	
	5-Me	0.82[b]	10.8[c]			
	6-Me	0.83[b]	14.4[c]			
	2-NH	8.23[b]		2		2-NH-Ile2
Leu	1		171.8			
	2	4.43, dd *(14.0, 7.2)*	50.6	3a,b, 2-NH	1, 3	
	3	a 1.54[b], m	41.5	2, 4	5/6-Me	
		b 1.43[b], m		2, 4	1, 5/6-Me	
	4	1.43[b], m	24.1	3a,b, 4/5-Me	1, 5/6-Me	
	5-Me	0.90, d	22.1	4		
	6-Me	0.83, d	22.4	4		
	2-NH	8.26, d *(8.5)*		2		2-NH-Trp

*(a) ^{13}C assignments obtained from gHSQC and gHMBC data. (b) Overlapping resonances. (c) Interchangeable resonances

Table 6.4. NMR (600 MHz, DMSO-d_6) comparison of desotamide (**6.01**) and desotamide B (**6.02**)

Desotamide B (**6.02**)				Desotamide (**6.01**)			
#	Pos.	δ_H, mult (*J* in Hz)[a]	δ_C[a]	#	Pos.	δ_H, mult (*J* in Hz)[a]	δ_C[a]
Trp.	1		170.6	Trp.	1		170.9
	2	4.36[b], m	54.9		2	4.36, m	55.4
	3	a 3.11, dd *(14.9, 4.7)*	27.2		3	3.31, dd (*14.7, 5.0*)	27.3
		b 2.96, dd *(15.1, 10.3)*				2.96, dd (*14.7, 10.1*)	
	4		109.9		4		110.0
	5	7.12, brd	123.1		5	7.11, s	123.5
	6a		135.8		6a		136.1
	7	7.31, d *(7.8)*	111.1		7	7.30, d (*8.1*)	111.3
	8	7.04, t *(7.8)*	120.7		8	7.04, t (*7.7*)	120.9
	9	6.96, t *(7.8)*	118.2		9	6.96, t (*7.7*)	118.3
	10	7.49, d *(7.8)*	117.9		10	7.49, d (*7.7*)	118.1
	10a		126.7		10a		127.1
	2-NH	8.34, d *(5.9)*			2-NH	8.24, d (*8.3*)	
	6-NH	10.81, s			6-NH	10.76, s	
Gly.	1		168.3	Gly.	1		169.1
	2	a 3.83, dd *(16.1, 5.3)*	43.0		2	a 3.88, dd (*15.8, 6.5*)	43.3
		b 3.27, dd *(16.1, 5.3)*				b 3.26, dd (*15.8, 6.5*)	
	2-NH	7.96, t *(5.3)*			NH	7.94, t (*5.9*)	
Asn.	1		171.4	Asn.	1		171.2
	2	4.55, m	48.8		2	4.55, m	48.9
	3	a 2.83, dd *(16.5, 5.4)*	36.6		3	a 2.80, dd (*16.2, 5.5*)	36.5
		b 2.62, dd *(16.5, 5.4)*				b 2.61, dd (*16.2, 5.5*)	
	4		171.1		4		172.0
	2-NH	7.61[b]			2-NH	7.57, d *(8.6)*	
	NH_2	7.60, s			NH_2	7.62, br s	
Ile#1	1		171.5	*allo*-Ile	1		170.9
	2	4.17, dd *(8.5, 6.1)*	57.7		2	4.18, dd (*7.8, 4.3*)	56.1
	3	1.77[b], m	34.6		3	2.01, m	34.9
	4	1.10[b], m	24.8		4	1.17-1.23, m	25.3
	5-Me	0.82[b]	11.6[c]		5-Me	0.81[b]	11.1
	6-Me	0.87[b]	14.5[c]		6-Me	0.81[b]	14.3
	2-NH	8.21, d *(7.8)*			NH	8.24, d (*8.6*)	
Leu	1		171.8	Leu1	1		173.1
	2	4.43, dd *(14.0, 7.2)*	50.6		2	4.35[b], m	51.3
	3	a 1.54[b], m	41.5		3	1.53, m	39.3
		b 1.43[b], m					
	4	1.43[b], m	24.1		4	1.53[b]	23.7
	5-Me	0.90, d	22.1		5-Me	0.82[b]	22.1[c]
	6-Me	0.83, d	22.4		6-Me	0.82[b]	22.1[c]
	2-NH	8.26, d *(8.5)*			2-NH	8.29, d (*8.6*)	
Ile#2	1		172.3	Leu2	1		172.2
	2	4.23, dd *(7.8, 4.1)*	55.9		2	4.35[b], m	50.3
	3	2.02, m	34.9		3	1.43, m	41.3
	4	a 1.08 - 1.21, m	25.4		4	1.53[b], m	24.1
	5-Me	0.82[b]	10.8[c]		5-Me	0.88[b], d (*6.9*)	22.1[c]
	6-Me	0.83[b]	14.4[c]		6-Me	0.87[b], d (*6.9*)	22.1[c]
	2-NH	8.23[b]			2-NH	7.64, d (*7.6*)	

*(a) ^{13}C assignments obtained from gHSQC and gHMBC data. (b) Overlapping resonances. (c) Interchangeable resonances

6.4.3 Desotamide C (6.03)

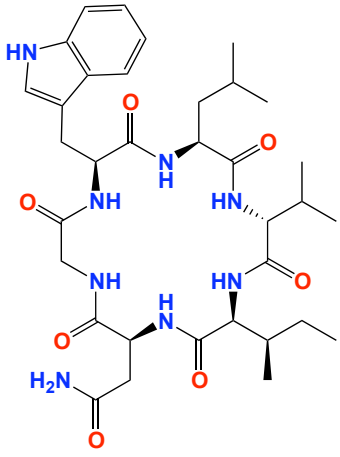

desotamide C (**6.03**)

HRESI(+)MS analysis of desotamide C (**6.03**) returned an adduct ion $[M+Na]^+$ consistent with the molecular formula ($C_{35}H_{50}N_8O_7$, Δmmu +0.9), UV-vis shows that **6.03** and **6.01** have Trp-residue. NMR (600 MHz, DMSO-d_6) comparison for both **6.01** and **6.03** suggested replacement of a Leu residue in **6.01** with a Val residue in **6.03** (Figure 6.27). A C_3 Marfey's analysis of **6.03** confirmed this hypothesis, revealing the presence of L-Trp, L-Leu, D-Val, L-*allo*-Ile, L-Asn and Gly residues (Figure 6.18 and Figure 6.19). While the NMR comparisons between **6.01** and **6.03** (Figure 6.27) suggested a very similar amino acid sequence, to be confident of this required assignment of the 1D NMR data, and careful consideration of the 2D NMR correlations. Following the strategy outlined previously for desotamide (**6.01**), it was possible to fully assign the data to the respective amino acids, as indicated in Table 6.5, and as illustrated in Figure 6.26. Of particular importance, diagnostic HMBC correlations permitted unambiguous assignment of the ^{13}C NMR resonances for all amide carbonyls. The sequence of amino acid residues is tentatively proposed as indicated, but will be addressed towards the end of this chapter.

6.4.3.1 C_3 Marfey's analysis of 6.03

Employing the C_3 Marfey's method as previously described, **6.03** was subjected to acid hydrolysis using 6 M HCl/5% thioglycolic acid, derivatized with D-FDAA, and subjected to HPLC analysis to determine the absolute stereochemistry of the amino acids. Absolute configuration of **6.03** amino acid residues was determined by comparing the retention times of derivatized standard amino acids with the derivatized hydrolysate of **6.03**. The amino acid residues of **6.03** were confirmed to be L-Trp, L-Leu, L-Leu, L-*allo*-Ile, D-Val, L-Asn and Gly (Figure 6.18 and Figure 6.19).

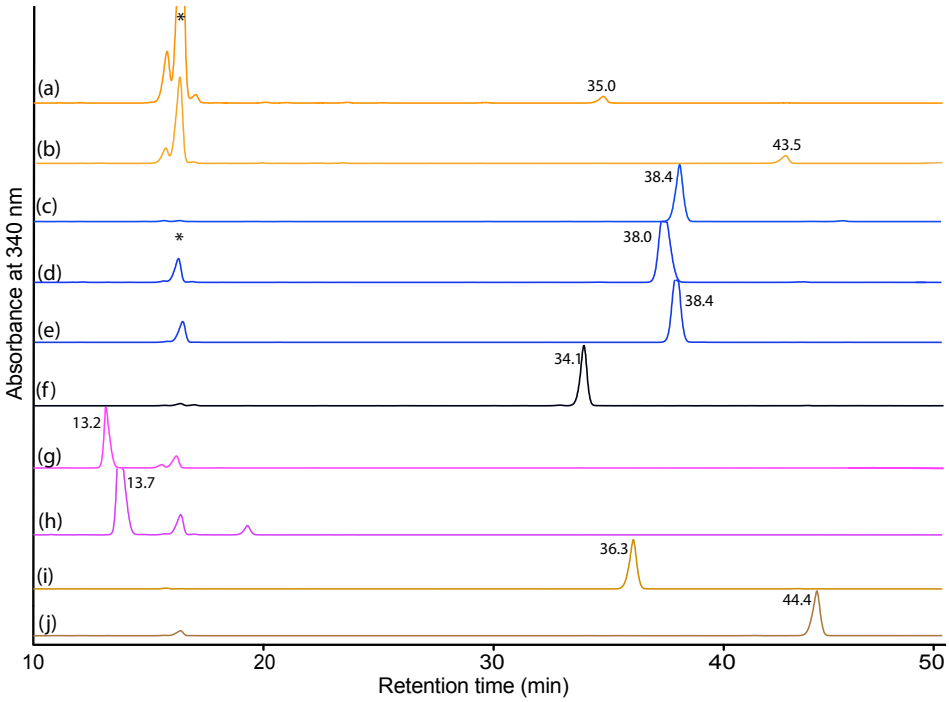

Figure 6.18. HPLC trace (340 nm) from HPLC-DAD-MS C_3 Marfey's analysis of standard amino acids reacting with D-FDAA. Identity of amino acids was confirmed by retention time and molecular weight. (a) L-*allo*-Ile + L-FDAA (t_R = 35.0 min), (b) L-*allo*-Ile + D-FDAA (t_R = 43.5 min), (c) D-Val + D-FDAA (t_R = 38.4 min), (d) L-Val + D-FDAA (t_R = 38.0 min), (e) L-Trp + L-FDAA (t_R = 34.1 min) and (f) L-Trp + D-FDAA (t_R = 38.2 min) (g) D-Asn + D-FDAA (t_R = 13.2 min), (h) L-Asn + D-FDAA (t_R = 13.7 min), (i) D-Leu + D-FDAA (t_R = 36.3 min) and (j) L-Leu + D-FDAA (t_R = 44.4 min). HPLC conditions, Zorbax, SB-C_3 column (150 × 4.6 mm, 5 μM), 1 mL/min, gradient of 15 – 60% MeOH/H_2O (isocratic 5% MeCN containing 1% formic acid) over 55 min

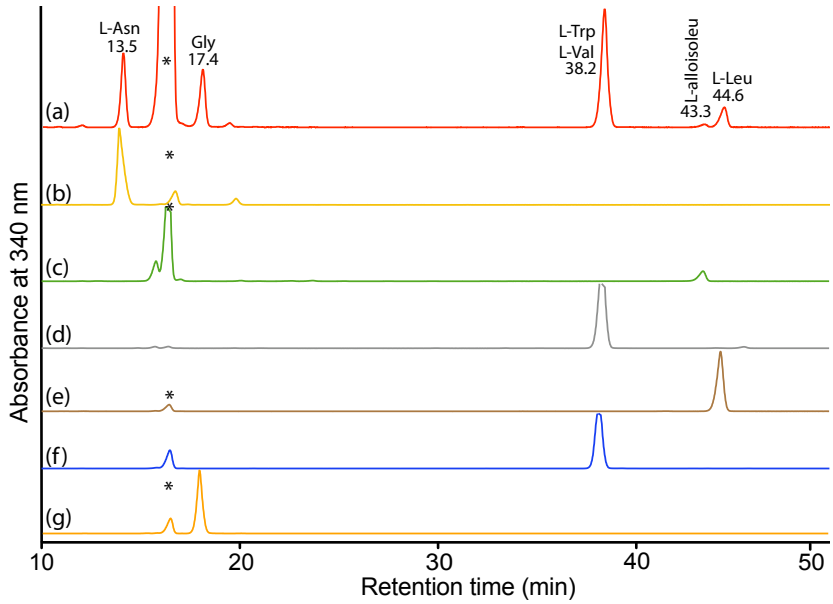

Figure 6.19. HPLC trace (340 nm) from HPLC-DAD-MS C_3 Marfey's analysis of desotamide C (**6.03**). Identity of amino acids was confirmed by retention time and molecular weight. (a) Co-injection of hydrolysate of **6.03** (200 μg) with L-Asn, Gly, D-Val, L-Leu, L-Trp, L-*allo*-Ile + D-FDAA, (b) L-Asn + D-FDAA, (c) L-*allo*-Ile + D-FDAA, (d) D-Val + D-FDAA, (e) L-Leu + D-FDAA, (f) L-Trp + D-FDAA and (g) Gly + D-FDAA. HPLC conditions, Zorbax, SB-C_3 column (150 × 4.6 mm, 5 μM), 1 mL/min, gradient of 15 – 60% MeOH/H_2O (isocratic 5% MeCN containing 1% formic acid) over 55 min.

Six amino acids fragments:

L-Tryptophan #1: Analysis of the COSY NMR (DMSO-d_6) data of **6.03** revealed diagnostic correlation sequences consistent with the structure fragment (i) H-7 to H-8 to H-9 to H-10, (ii) 2-NH to H-2 to H_2-3, and (iii) H-5 to 6-NH. Key HMBC correlation permitting assignment of the quaternary carbons included (i) 2-NH to C-1, (ii) H_2-3 to C-5 and C-4, and (iii) 6-NH and H-8 to C-6a (Figure 6.20).

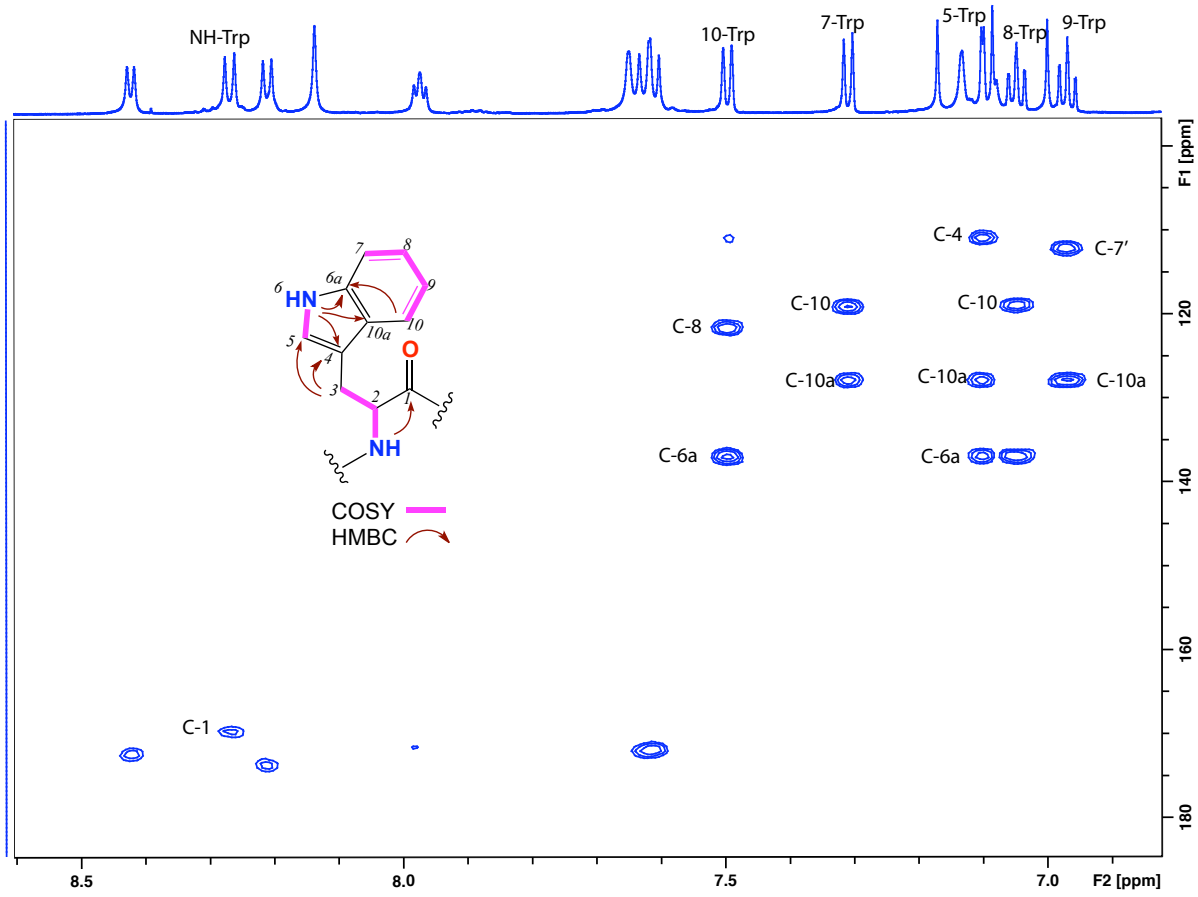

Figure 6.20. HMBC (600 MHz, DMSO d_6) spectrum with key correlations (Trp) of desotamide C (**6.03**)

L-Leucine #2: COSY NMR (DMSO-d_6) correlations readily identified the sequence 2-NH to H-2 to H_2-3 to H-4 to H_3-5/H3-6, while HMBC correlations linked H-2 and 2-NH to C-1 (Figure 6.21).

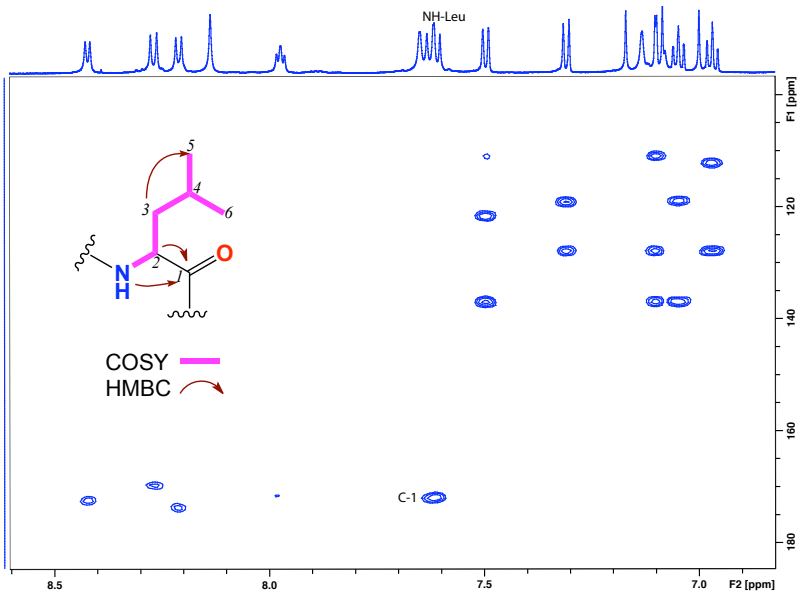

Figure 6.21. HMBC (600 MHz, DMSO d_6) spectrum with key correlations of desotamide C (**6.03**)

D-Valine #3: COSY NMR (DMSO-d_6) correlations readily identified the sequence 2-NH to H-2 to H-3 to H_3-4/H_3-5, while HMBC correlations linked 2-NH to C-1 (Figure 6.22).

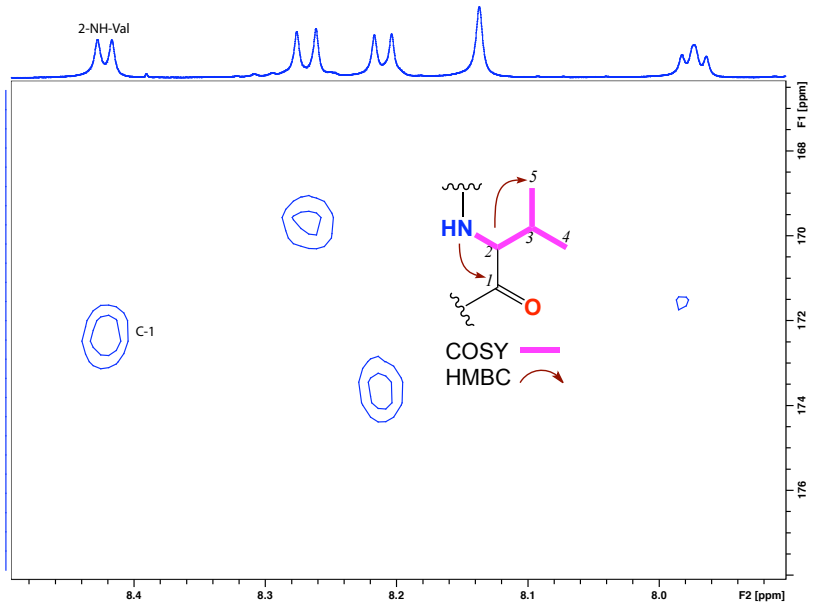

Figure 6.22. HMBC (600 MHz, DMSO-d_6) spectrum with key correlations (Val) of desotamide C (**6.03**)

L-*allo*-isoleucine #4: Analysis of the COSY NMR (DMSO-d_6) data for **6.03** identified the sequence 2-NH to H-2 to H-3/H_3-3 to H_2-4 to H_3-5, while HMBC correlations linked 2-NH to C-1 (Figure 6.23).

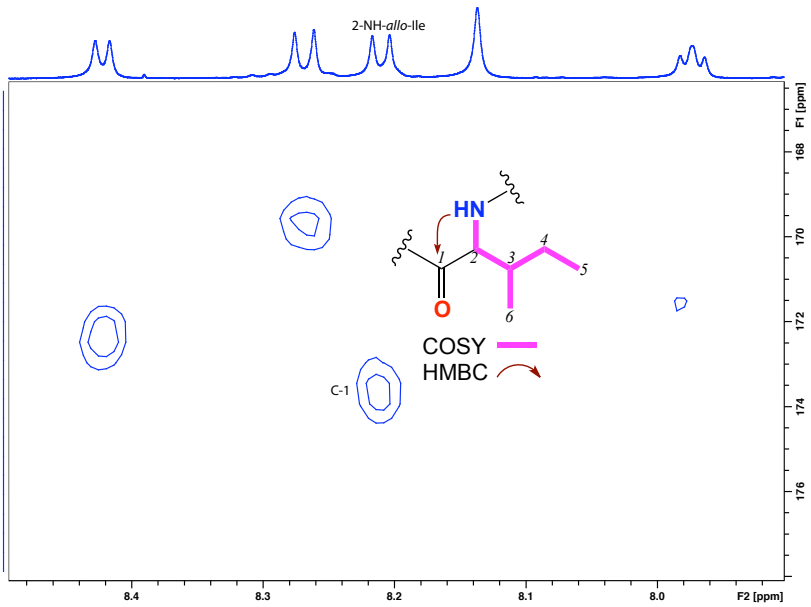

Figure 6.23. HMBC (600 MHz, DMSO d_6) spectrum with key correlations (Ile) of desotamide C (**6.03**)

L-Asn #5: COSY NMR (DMSO-d_6) correlations readily identified the sequence 2-NH to H-2 to H_2-3, while HMBC correlations linked H_2-3 to C-4 and 2-NH and H-2 to C-1 (Figure 6.24).

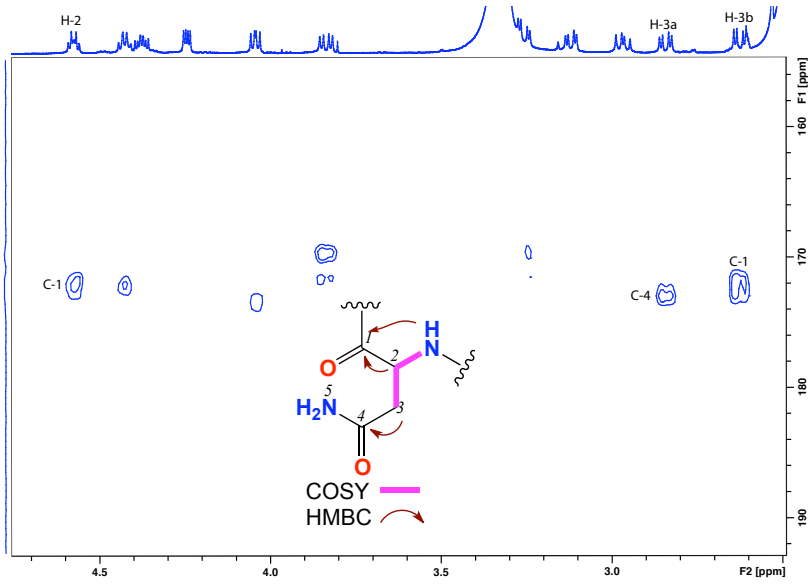

Figure 6.24. HMBC (600 MHz, DMSO-d_6) spectrum with key correlations (Asn) of desotamide C (**6.03**)

Gly #6: COSY NMR (DMSO-d_6) correlations readily identified the sequence 2-NH to H-2, while HMBC correlations linked H_2-2 to C-1 (Figure 6.25).

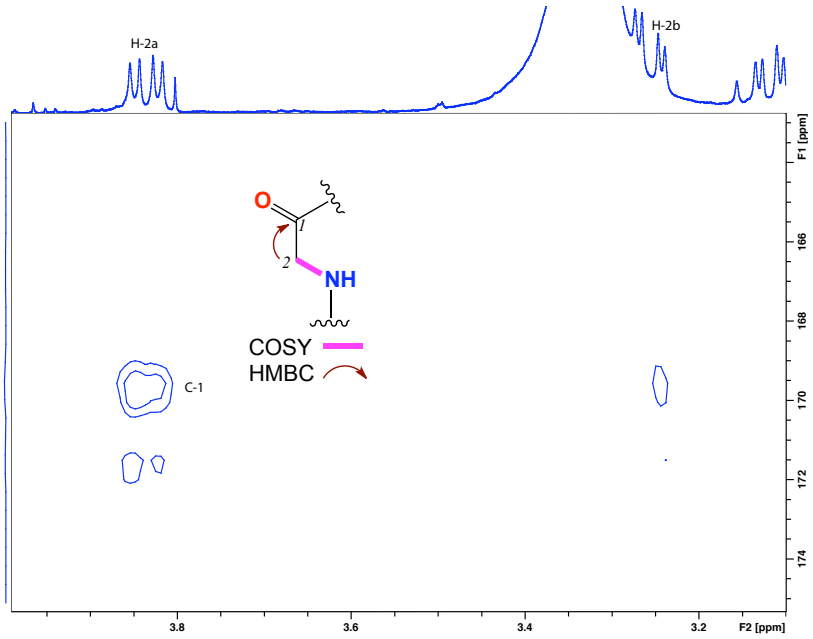

Figure 6.25. HMBC (600 MHz, DMSO-d_6) spectrum with key correlations (Gly) of desotamide C (**6.03**)

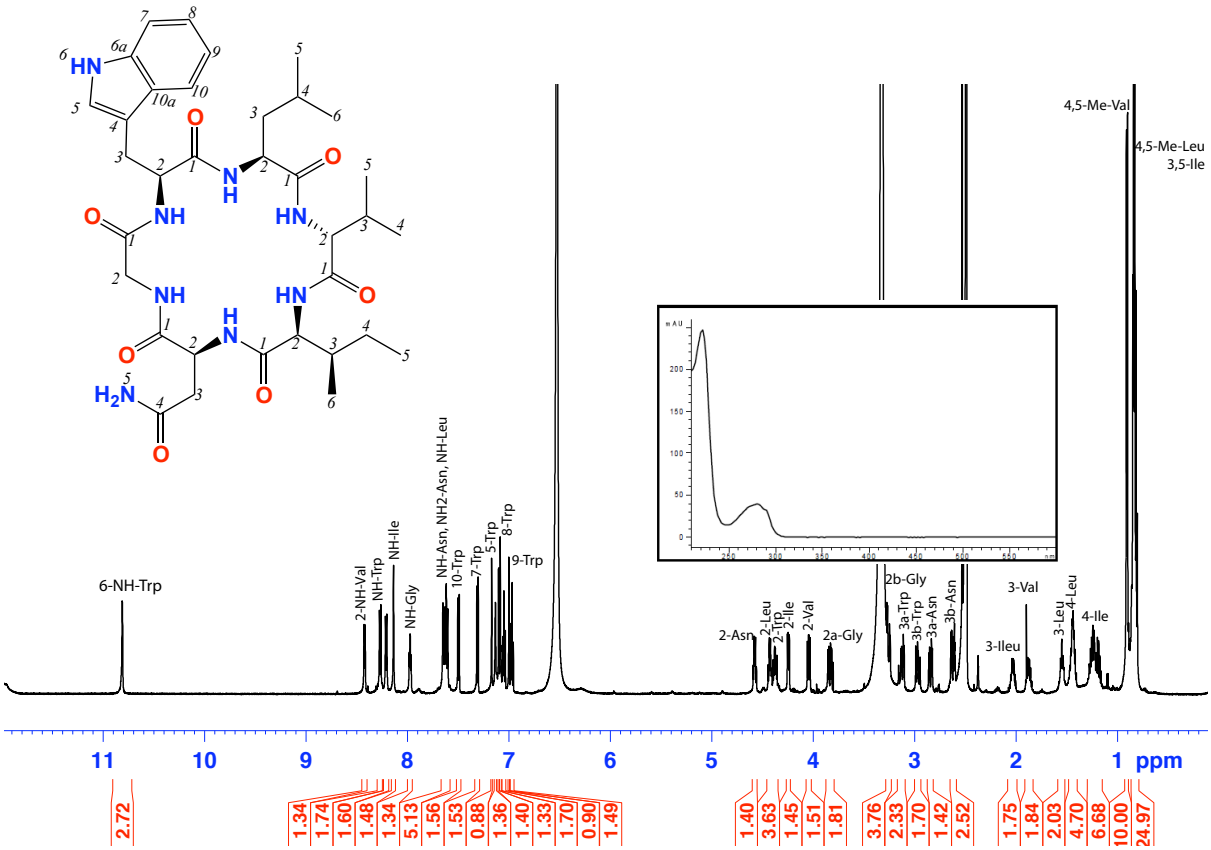

Figure 6.26. ^{1}H NMR (600 MHz, DMSO-d_6) and UV-vis (inset) spectra of desotamide C (**6.03**)

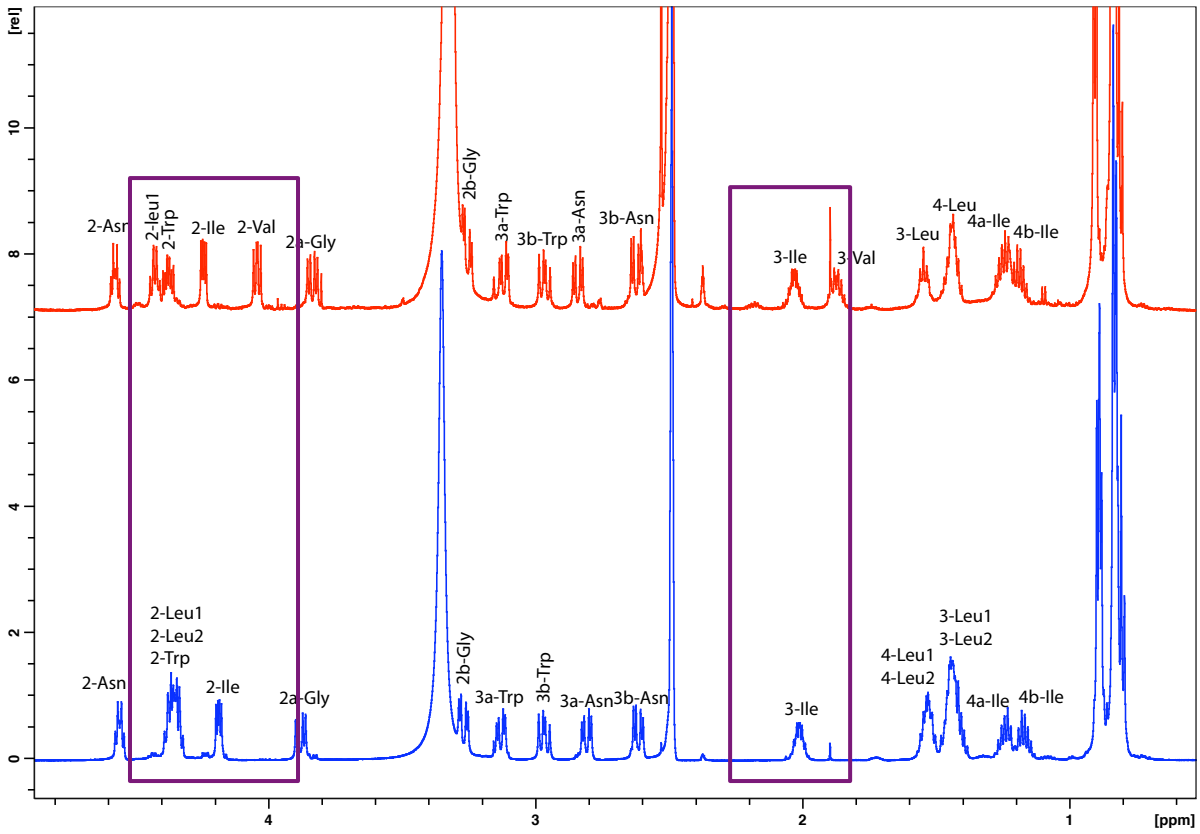

Figure 6.27. ^{1}H NMR (600 MHz, DMSO-d_6) comparison of desotamide (**6.01**) (blue) and desotamide C (**6.03**) (red)

Table 6.5. NMR (600 MHz, DMSO-d_6) data of desotamide C (**6.03**)

#	Pos.	δ_H, mult (*J* in Hz)[a]	δ_C[a]	COSY	^{1}H-^{13}C HMBC	ROESY
Trp.	1		169.9			
	2	4.38, m	55.8	2-NH, 3a/b		
	3	a 3.11, dd (*14.4, 9.0*)	28.3	2	5, 4	
		b 2.96, dd (*14.4, 9.0*)		2	2, 4	
	4		110.8			
	5	7.10, d (*1.8*)	124.3	6-NH	4, 10a, 6a	
	6a		136.6			
	7	7.30, d (*8.0*)	112.2	8	10a , 10	
	8	7.04, t (*7.7*)	121.9	9, 7	10, 6a	
	9	6.96, t (*7.7*)	119.2	10, 8	10, 10a, 6a, 7	
	10	7.49, d (*7.7*)	119.1	9	8, 6a	2-Trp
	10a		127.7			
	2-NH	8.26, d (*9.0*)		2	1	2a-Gly
	6-NH	10.81, s		5	5, 4, 10a, 6a	
Gly.	1		168.9			
	2	a 3.83, dd (*16.3, 5.3*)	44.1	2b	1	
		b 3.25, dd (*16.3, 5.3*)		2a	1	
	2-NH	7.97, t (*5.3*)		2a/b		2-Asn
Asn.	1		172.0			
	2	4.57, m	49.7	2-NH, 3a/b	1	2-NH Gly
	2-NH	7.62[b]		2	1	
	3	a 2.84, dd (*16.3, 5.5*)	37.8	2	4	
		b 2.61, dd (*16.3, 5.5*)		2	1	
	4		172.8			
	NH_2	7.60[b]				
allo-Ile	1		173.3			
	2	4.24, dd (*8.1, 3.6*)	56.8	2-NH, 3	1, 3	
	3	1.88, m	29.3	4		
	4	1.18-1.22, m	26.4	3	2	6-Me
	5-Me	0.91[b]	14.9	6-Me		
	6-Me	0.91[b]	12.9			
	2-NH	8.21, d (*8.1*)		2	1	3-Ile
Leu1	1		171.6			
	2	4.42, m	51.5	2-NH, 3a/b	1	
	3	a 1.54, m	42.5	3b, 4	5/6-Me	
		b 1.43[b], m	42.5	3a, 4	5/6-Me	
	4	1.44[b]	24.9	3a/b, 5-Me		
	5-Me	0.91[b]	22.9[c]	4		
	6-Me	0.86[b]	23.5[c]			
	2-NH	7.62[b]		2	1	
Val	1		172.3			
	2	4.04, dd (*9.0, 6.7*)	56.8	2-NH, 3	1, 3, 4/5-Me	
	3	1.87, m	29.3	2, 4/5-Me		
	4-Me	0.82[b]	19.8			
	5-Me	0.89[b]	19.8			
	2-NH	8.42, d (*6.7*)		2	1	NH-Ile

*(a) ^{13}C assignments obtained from gHSQC and gHMBC data. (b) Overlapping resonances. (c) Interchangeable resonances

Table 6.6. NMR (600 MHz, DMSO-d_6) comparison of both desotamide (**6.01**) and desotamide C (**6.03**)

Desotamide C (**6.03**)				Desotamide (**6.01**)			
#	Pos.	δ_H, mult (*J* in Hz)[a]	δ_C[a]	#	Pos.	δ_H, mult (*J* in Hz)[a]	δ_C[a]
Trp.	1		169.9	Trp.	1		170.9
	2	4.38, m	55.8		2	4.36, m	55.4
	3	a 3.11, dd (*14.4, 4.9*)	28.3		3	3.31, dd (*14.7, 10.1*)	27.3
		b 2.96, dd (*14.4, 4.9*)				2.96, dd (*14.7, 10.1*)	
	4		110.8		4		110.0
	5	7.10, d (*1.8*)	124.3		5	7.11, s	123.5
	6a		136.6		6a		136.1
	7	7.30, d (*8.0*)	112.2		7	7.30, d (*8.1*)	111.3
	8	7.04, t (*7.7*)	121.9		8	7.04, t (*7.7*)	120.9
	9	6.96, t (*7.7*)	119.2		9	6.96, t (*7.7*)	118.3
	10	7.49, d (*7.7*)	119.1		10	7.49, d (*7.7*)	118.1
	10a		127.7		10a		127.1
	2-NH	8.26, d (*9.0*)			2-NH	8.24, d (*8.3*)	
	6-NH	10.81, s			6-NH	10.76, s	
Gly.	1		168.9	Gly.	1		168.9
	2	a 3.83, dd (*16.3, 5.3*)	44.1		2	a 3.88, dd (*15.8, 6.5*)	42.9
		b 3.25, dd (*16.3, 5.3*)				b 3.26, dd (*15.8, 6.5*)	
	2-NH	7.97, t (*5.3*)			NH	7.94, t (*5.9*)	
Asn.	1		171.8	Asn.	1		171.2
	2	4.57, m	49.7		2	4.55, m	48.9
	2-NH	7.62[b]			2-NH	7.57, d (*8.6*)	
	3	a 2.84, dd (*16.3, 5.5*)	37.8		3	a 2.80, dd (*16.2, 5.5*)	36.5
		b 2.61, dd (*16.3, 5.5*)				b 2.61, dd (*16.2, 5.5*)	
	4		172.0		4		172.0
	NH_2	7.62[b]			NH_2	7.62, br s	
allo-Ile	1		173.3	*allo*-Ile	1		170.9
	2	4.24, dd (*8.1, 3.6*)	56.8		2	4.18, dd (*7.8, 4.3*)	56.1
	3	2.03, m	36.0		3	2.01, m	34.9
	4	1.18-1.22, m	26.4		4	1.17-1.23, m	25.3
	5-Me	0.81[b]	14.9[c]		5-Me	0.81[b]	11.1
	6-Me	0.82[b]	12.9[c]		6-Me	0.81[b]	14.3
	2-NH	8.21, d (*7.9*)			NH	8.24, d (*8.6*)	
Leu1	1		171.6	Leu1	1		173.1
	2	4.42, m	51.5		2	4.35[b], m	51.3
	3	a 1.54, m	42.5		3	1.53, m	39.3
		b 1.43[b], m	42.5				
	4	1.44[b]	24.9		4	1.53[b]	23.7
	5-Me	0.91[b]	22.9[c]		5-Me	0.82[b]	22.1[c]
	6-Me	0.86[b]	23.5[c]		6-Me	0.82[b]	22.1[c]
	2-NH	7.62[b]			NH	8.29, d (*8.6*)	
Val	1		173.3	Leu2	1		172.2
	2	4.04, dd (*9.0, 6.7*)	56.8		2	4.35[b], m	50.3
	3	1.83, m	29.3		3	1.43, m	41.3
	4-Me	0.82[b]	19.8[c]		4	1.53[b], m	24.1
	5-Me	0.81[b]	19.8[c]		5-Me	0.88[b], d (*6.9*)	22.1[c]
	2-NH	8.42, d (*6.7*)			6-Me	0.87[b], d (*6.9*)	22.1[c]

*(a) ^{13}C assignments obtained from gHSQC and gHMBC data. (b) Overlapping resonances. (c) Interchangeable resonances

6.4.4 Desotamide D (6.04)

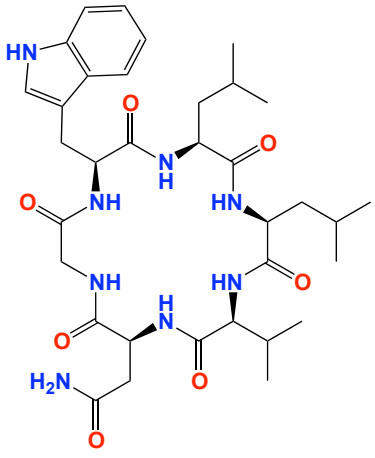

desotamide D (**6.04**)

HRESI(+)MS analysis of desotamide D (**6.04**) returned an adduct ion $[M+Na]^+$ consistent with the molecular formula ($C_{34}H_{50}N_8O_7$, Δmmu +1.2) suggestive of an analogue of desotamide (**6.01**) as both of them has similar UV. A C_3 Marfey's analysis of **6.04** confirmed this hypothesis, revealing the presence of L-Trp, L-Leu, L-Val, L-Asn and Gly residue. While the NMR comparisons between **6.01** and **6.03** to **6.04** suggested a very similar amino acid sequence. To be confident of this assignment required careful consideration of the 2D NMR correlations. Following the strategy outlined previously for desotamide (**6.01**), it was possible to fully assign the data to the respective amino acids, as indicated in Table 6.7 and as illustrated in Figure 6.30. Of particular importance, diagnostic HMBC correlations permitted unambiguous assignment of the ^{13}C NMR resonances for all amide carbonyls. The sequence of amino acid residues is tentatively proposed as indicated, but will be addressed towards the end of this chapter.

6.4.4.1 C_3 Marfey's analysis of 6.04

Employing a C_3 Marfey's analysis as previously described, **6.04** was subjected to acid hydrolysis using 6 M HCl/5% thioglycolic acid, derivatized with D-FDAA, and subjected to HPLC analysis to determine the absolute stereochemistry of the amino acids. Absolute configuration of **6.04** was determined by comparing the retention times of derivatized standard amino acids with the derivatized hydrolysate of **6.04**. The amino acids of **6.04** were confirmed to be L-Trp, L-Leu, L-Val, L-Asn and Gly as shown in Figure 6.28 and Figure 6.29.

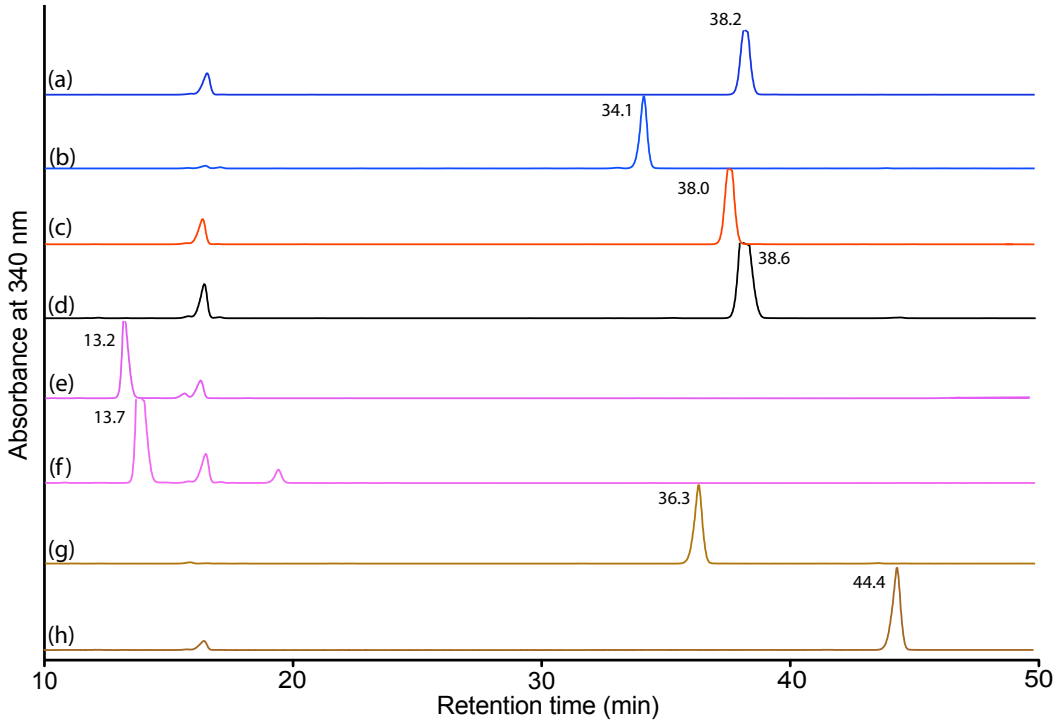

Figure 6.28. HPLC trace (340 nm) from HPLC-DAD-MS C_3 Marfey's analysis of derivatized standard amino acids reacting with D-FDAA. Identity of derivatized amino acids was confirmed by retention time and molecular weight. (a) L-Trp + D-FDAA (t_R = 38.2 min), (b) L-Trp + L-FDAA (t_R = 34.1 min), (c) L-Val + D-FDAA (t_R = 38.0 min), (d) D-Val + D-FDAA (t_R = 38.4 min), (e) D-Asn + D-FDAA (t_R = 13.2 min), (f) L-Asn + D-FDAA (t_R = 13.7 min), (g) D-Leu + D -FDAA (t_R = 36.3 min) and (h) L-Leu + D-FDAA (t_R = 44.4 min). HPLC conditions, Zorbax, SB-C_3 column (150 × 4.6 mm, 5 μM), 1 mL/min, gradient of 15 - 60% MeOH/H_2O (isocratic 5% MeCN containing 1% formic acid) over 55 min

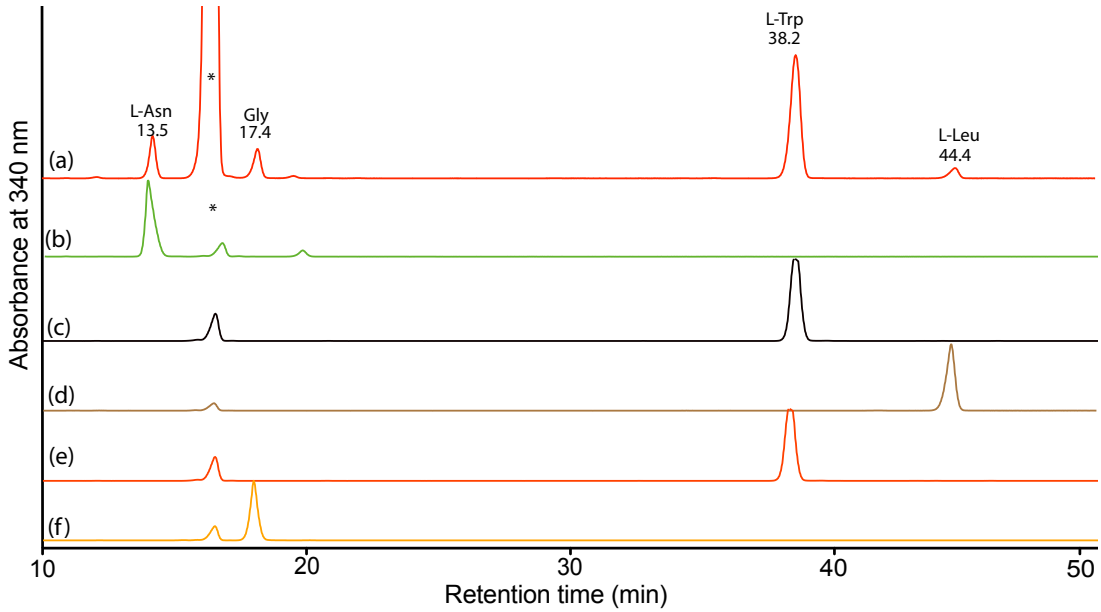

Figure 6.29. HPLC trace (340 nm) from HPLC-DAD-MS C_3 Marfey's analysis of desotamide D (**6.04**). Identity of amino acids was confirmed by retention time and molecular weight. (a) Co-injection of hydrolysate of **6.04** (300 μg) with L-Asn, Gly, L-Val, L-Leu, L-Trp, Gly + D-FDAA, (b) L-Asn + D-FDAA, (c) L-Val + D-FDAA, (d) L-Leu + D-FDAA, (e) L-Trp + D-FDAA and (f) Gly + D-FDAA. HPLC conditions, Zorbax, SB-C_3 column (150 × 4.6 mm, 5 μM), 1 mL/min, gradient of 15 – 60% MeOH/H_2O (isocratic 5% MeCN containing 1% formic acid) over 55 min.

Six amino acids fragments:

L-Trptophan #1: Analysis of the COSY NMR (DMSO-d_6) data of **6.04** revealed diagnostic correlation sequences consistent with the structure fragment (i) H-7 to H-8 to H-9 to H-10, (ii) 2-NH to H-2 to H_2-3, and (iii) 6-NH to H-5. Key HMBC correlation permitting assignment of the quaternary carbons included (i) 2-NH to C-1 and (ii) 6-NH and H-8 to C-6a (Figure 6.30).

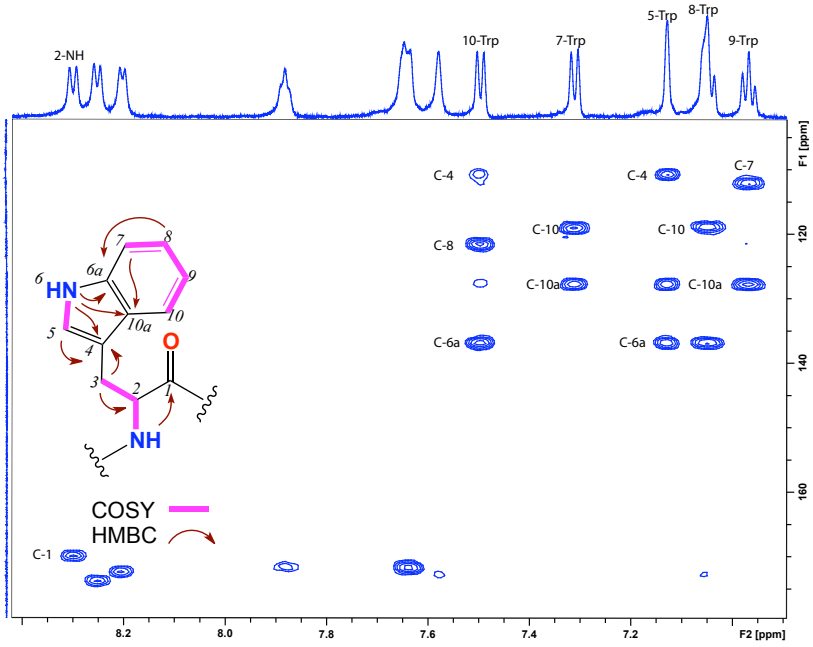

Figure 6.30. HMBC (600 MHz, DMSO-d_6) spectrum with key correlations (Trp) of desotamide D (**6.04**)

Leucine #2 and 3: From the Marfey's analysis, the presence of only L-Leu residue was proved, which contributes to both Leu #2 and #3 and can explain the overlapping of the signals due to similarity of two Leu residues as L configuration. COSY NMR (DMSO-d_6) correlations readily identified the sequence 2-NH to H-2 to H_2-3 to H-4 to H_3-5/H_3-6, while HMBC correlations linked 2-NH to C-1 (Figure 6.31).

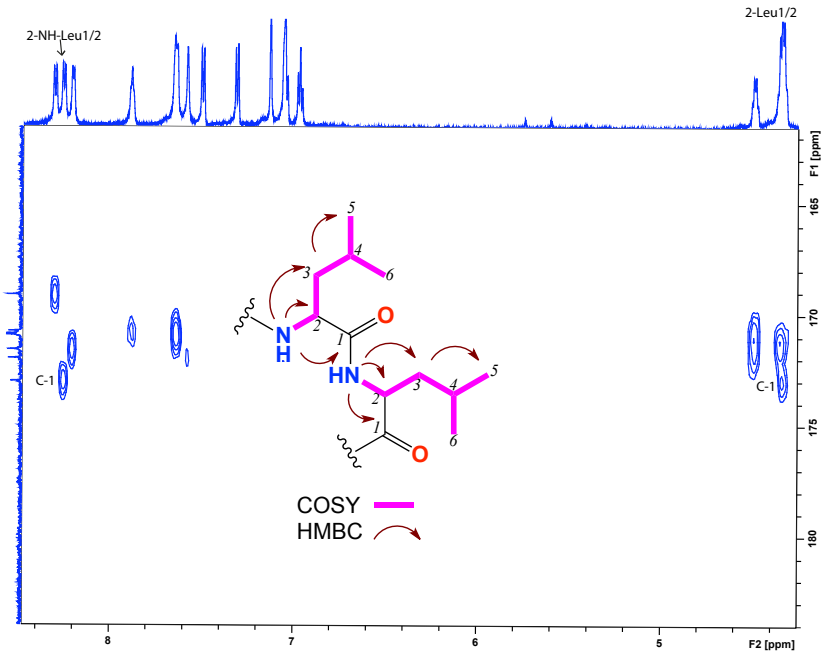

Figure 6.31. HMBC (600 MHz, DMSO-d_6) spectrum with key correlations of desotamide D (**6.04**)

L-Val #4: COSY NMR (DMSO-d_6) correlations readily identified the sequence 2-NH to H-2 to H-3 to H_3-4 and H_3-5, while HMBC correlations linked H-2 to C-1 to C-4 and C-5.

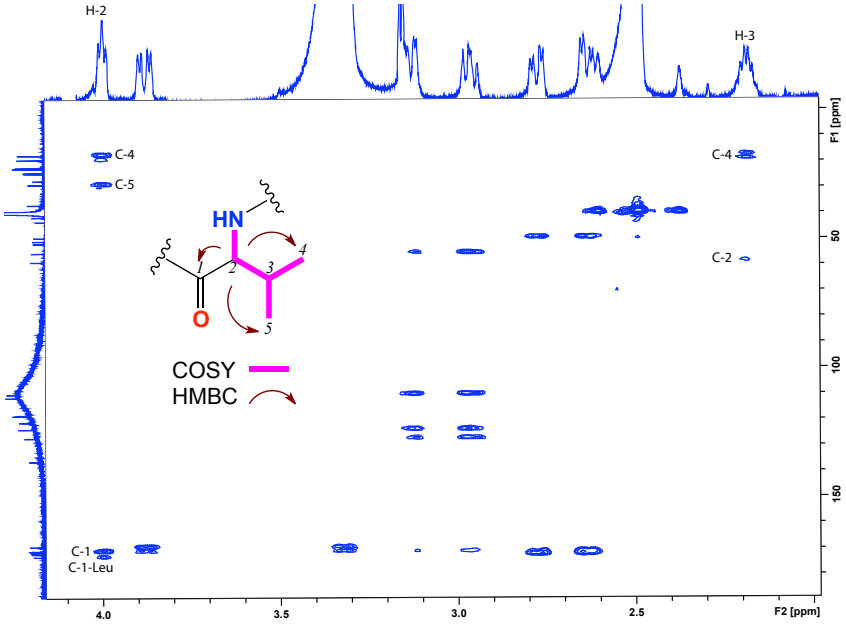

Figure 6.32. HMBC (600 MHz, DMSO-d_6) spectrum with key correlations (Val) of desotamide D (**6.04**)

L-Asn #5: COSY NMR (DMSO-d_6) correlations readily identified the sequence 2-NH to H-2 to H_2-3, while HMBC correlations linked H_2-3, NH_2 to C-4, H-2 to C-1, 2-NH.

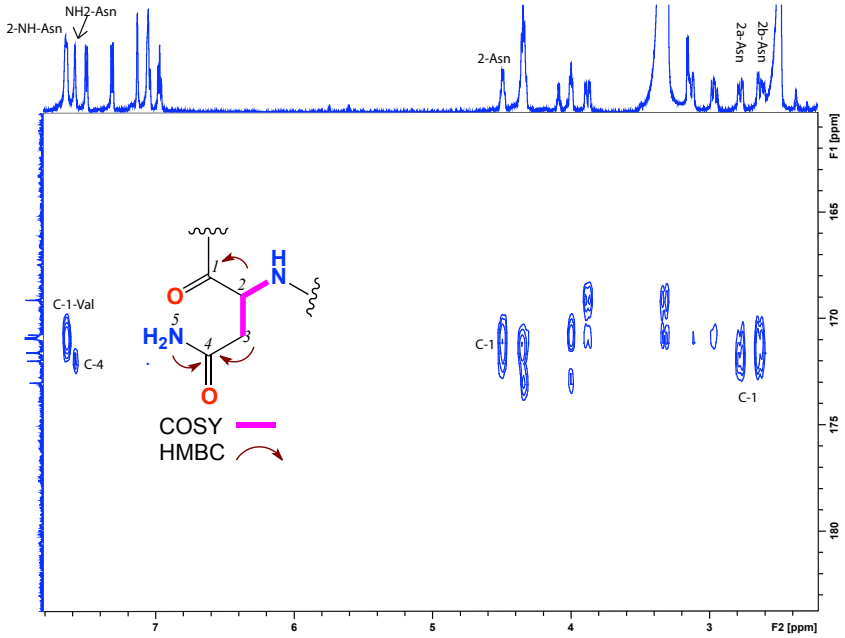

Figure 6.33. HMBC (600 MHz, DMSO-d_6) spectrum with key correlations (Asn) of desotamide D (**6.04**)

Gly #6: COSY NMR (DMSO-d_6) correlations readily identified the sequence 2-NH to H_2-2, while HMBC correlations linked H_2-2 and NH to C-1 and linking H_2-2.

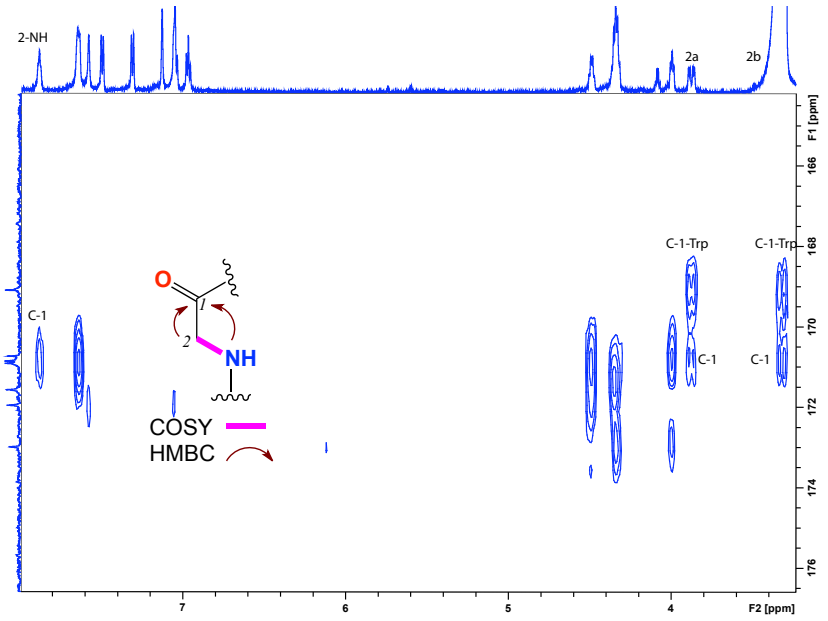

Figure 6.34. HMBC (600 MHz, DMSO-d_6) spectrum with key correlations (Gly) of desotamide D (**6.04**)

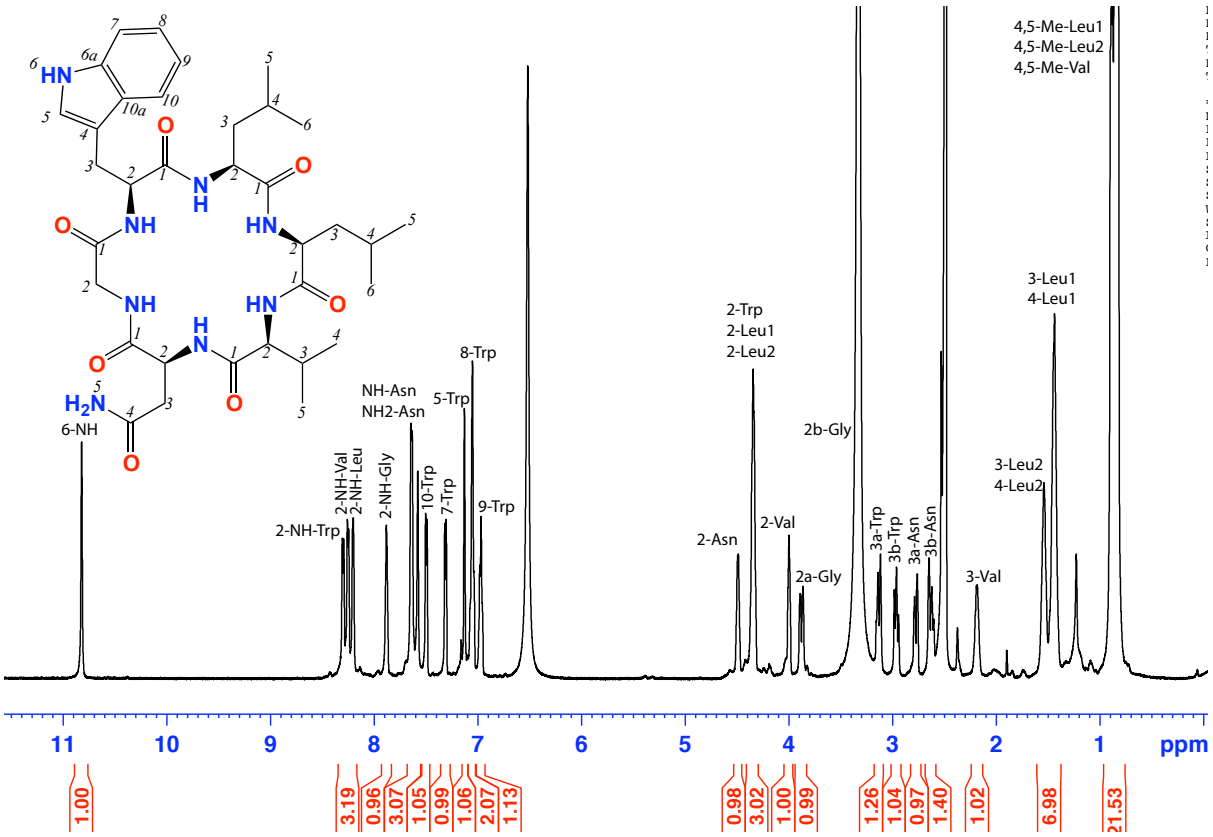

Figure 6.35. ^{1}H NMR (600 MHz, DMSO-d_6) of desotamide D (**6.04**)

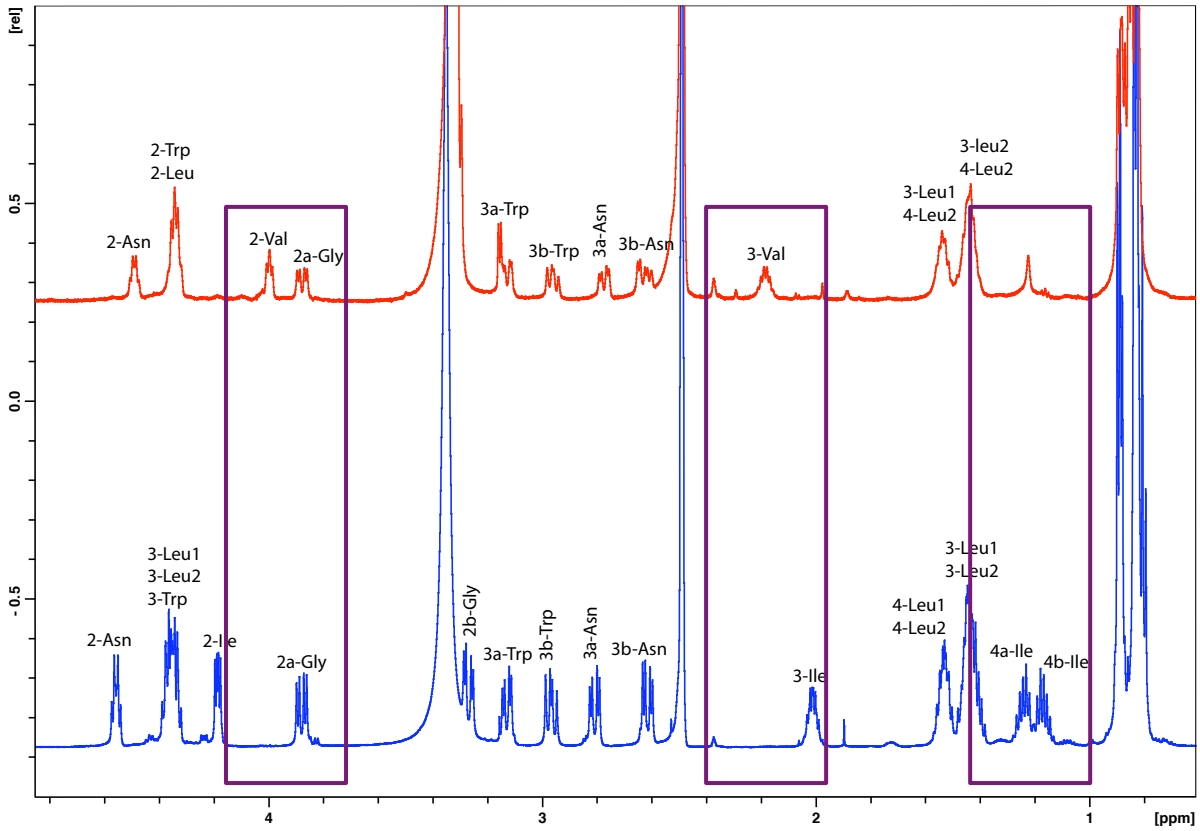

Figure 6.36. ^{1}H NMR (600 MHz, DMSO-d_6) comparison of desotamide (**6.01**) (blue) and desotamide D (**6.04**) (red)

Table 6.7. NMR (600 MHz, DMSO-d_6) data of desotamide D (**6.04**)

#	Pos.	δ_H, mult (*J* in Hz)[a]	δ_C[a]	COSY	^{1}H-^{13}C HMBC	ROESY
Trp.	1		170.9			
	2	4.34[b], m	56.1	2-NH, 3a,b		
	3	a 3.12, dd *(14.3, 5.6)*	28.1	2, 3b	4, 5, 10a	
		b 2.96, dd *(14.3, 5.6)*		2, 3a	4, 5, 10a	
	4		110.7			
	5	7.12, brd	124.1	6-NH	4, 6a, 10a	
	6a		136.5			
	7	7.31, d *(7.8)*	112.0	8	10a, 10	
	8	7.05, brd	121.6	7, 9	6a, 10	
	9	6.96, t *(7.8)*	119.1	8, 10	7, 10a	
	10	7.49, d *(7.8)*	118.8	9	4, 8, 6a	
	10a		128.2			
	2-NH	8.30, d *(8.1)*		2	1	
	6-NH	10.82, s		5	5, 4, 6a, 10a	
Gly.	1		169.9			
	2	a 3.87, d *(16.1, 5.6)*	43.8	2b	1	
		b 3.34[c]		2a	1	
	2-NH	7.88, t *(5.6)*				2-Asn
Asn.	1		171.3			
	2	4.48, brd	50.2	2-NH, 3,b	1	2-NH-Gly
	3	a 2.77, d *(15.8)*	37.3	2, 3b	4	
		b 2.63, d *(15.8)*		2, 3a		
	4		171.8			
	2-NH	7.64[b]			1-Val	2-Val
	NH_2	7.57, s			4	
Leu1	1		173.7[d]			
	2	4.34[b], m	51.9[d]	2-NH, 3a,b	5/6-Me	
	3	a 1.54[b]	42.1	2, 3b, 4	1	
		b 1.45[b]		2, 3a, 4	1	
	4	1.45[b]	24.8[d]	3a,b, 5/6-Me		
	5-Me	0.83[b]	17.8[d]	4	2	
	6-Me	0.84[b]	20.1[d]	4		
	2-NH	8.20, d *(5.8)*		2		
Leu2	1		173.7[d]			
	2	4.34[b], m	51.9[d]	2-NH, 3a,b	1, 5/6-Me	NH-Val
	3	a 1.53[b]	40.5	2, 3b, 4		
		b 1.44[b]		2, 3a, 4		
	4	1.45[b]	25.2[d]	3a,b, 5/6-Me		
	5-Me	0.83[b]	17.8[d]	4	2	
	6-Me	0.84[b]	20.1[d]	4		
	2-NH	7.64[b]		2		
Val	1		170.8			
	2	3.99, t *(7.8)*	59.6	2-NH, 3	1, 3, 4/5-Me	NH-Asn
	3	2.18, q *(6.3)*	29.4	2, 4/5-Me		
	4-Me	0.88	17.4	3		
	5-Me	0.85	22.1	3		
	2-NH	8.25, d *(7.8)*		2		2-Leu

(a) ^{13}C assignments obtained from gHSQC and gHMBC data. (b) Overlapping resonances. (c) Obscured by solvent. (d) Interchangeable resonances

Table 6.8. NMR (600 MHz, DMSO-d_6) comparison of desotamide (**6.01**) and desotamide D (**6.04**)

Desotamide D (**6.04**)				Desotamide (**6.01**)			
#	Pos.	δ_H, mult (*J* in Hz)[a]	δ_C[a]	#	Pos.	δ_H, mult (*J* in Hz)[a]	δ_C[a]
Trp.	1		170.9	Trp.	1		170.9
	2	4.34[b], m	56.1		2	4.36, m	55.4
	3	a 3.12, dd *(14.3, 5.6)*	28.1		3	3.31, dd (*14.7, 5.0*)	27.3
		b 2.96, dd *(14.3, 5.6)*				2.96, dd (*14.7, 10.1*)	
	4		110.7		4		110.0
	5	7.12, brd	124.1		5	7.11, s	123.5
	6a		136.5		6a		136.1
	7	7.31, d *(7.8)*	112.0		7	7.30, d (*8.1*)	111.3
	8	7.05, brd	121.6		8	7.04, t (*7.7*)	120.9
	9	6.96, t *(7.8)*	119.1		9	6.96, t (*7.7*)	118.3
	10	7.49, d *(7.8)*	118.8		10	7.49, d (*7.7*)	118.1
	10a		128.2		10a		127.1
	2-NH	8.30, d *(8.1)*			2-NH	8.24, d (*8.3*)	
	6-NH	10.82, s			6-NH	10.76, s	
Gly.	1		169.9	Gly.	1		168.9
	2	a 3.87, dd *(16.1, 6.1)*	43.8		2	a 3.88, dd (*15.8, 6.5*)	42.9
		b 3.34[c]				b 3.26, dd (*15.8, 6.5*)	
	2-NH	7.88, t *(6.1)*			NH	7.94, t (*6.5*)	
Asn.	1		171.3	Asn.	1		171.2
	2	4.48, brd	50.2		2	4.55, m	48.9
	3	a 2.77, d *(15.4)*	37.3		3	a 2.80, dd (*16.2, 5.5*)	36.5
		b 2.63, d *(15.4)*				b 2.61, dd (*16.2, 5.5*)	
	4		171.8		4		172.0
	2-NH	7.64[b]			2-NH	7.57, d (*5.5*)	2-NH
	NH_2	7.57, s			NH_2	7.62, br s	
Val	1		170.8	*allo*-Ile	1		170.9
	2	3.99, t *(7.8)*	59.6		2	4.18, dd (*8.6, 4.3*)	56.1
	3	2.18, q *(7.8)*	29.4		3	2.01, m	34.9
	4-Me	0.88[b]	17.4		4	1.17-1.23, m	25.3
	5-Me	0.85[b]	22.1		5-Me	0.81[b]	11.1
	2-NH	8.25, d *(7.8)*			6-Me	0.81[b]	14.3
					2-NH	8.24, d (*8.6*)	
Leu1	1		173.7[d]	Leu1	1		173.1
	2	4.34[b], m	51.9[d]		2	4.35[b], m	51.3
	3	a 1.54[b]	42.1		3	1.53, m	39.3
		b 1.45[b]					
	4	1.45[b]	24.8[d]		4	1.53[b]	23.7
	5-Me	0.83[b]	17.8[d]		5-Me	0.82[b]	22.1[d]
	6-Me	0.84[b]	20.1[d]		6-Me	0.82[b]	22.1[d]
	2-NH	8.20, d *(5.8)*			2-NH	8.29, d (*8.6*)	
Leu2	1		173.7[d]	Leu2	1		172.2
	2	4.34[b], m	51.9[d]		2	4.35[b], m	50.3
	3	a 1.53[b]	40.5		3	1.43, m	41.3
		b 1.44[b]					
	4	1.45[b]	25.2[d]		4	1.53[b], m	24.1
	5-Me	0.83[b]	17.8[d]		5-Me	0.88[b], d (*6.9*)	22.1[d]
	6-Me	0.84[b]	20.1[d]		6-Me	0.87[b], d (*6.9*)	22.1[d]
	2-NH	7.64[b]			2-NH	7.62[b]	

(a) ^{13}C assignments obtained from gHSQC and gHMBC data. (b) Overlapping resonances. (c) Obscured by solvent. (d) Interchangeable resonances

6.4.5 Desotamide E (6.05)

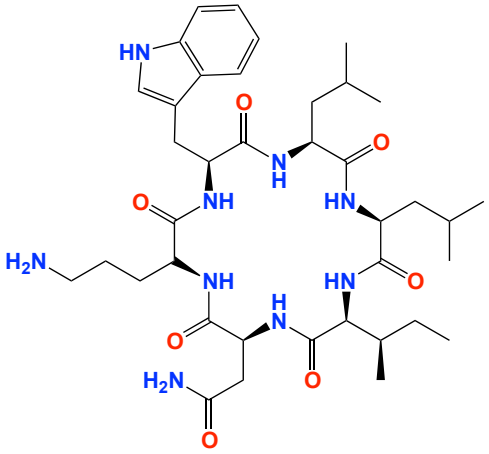

desotamide E (**6.05**)

HRESI(+)MS analysis of desotamide E (**6.05**) returned a quasi-molecular ion $[M+H]^+$ consistent with the molecular formula ($C_{38}H_{59}N_9O_7$, Δmmu +2.2) suggestive of an analogue of desotamide (**6.01**) as both of them has similar UV. A C_3 Marfey's analysis of **6.05** confirmed this hypothesis, revealing the presence of L-Trp, L-Leu, L-Leu, L-*allo*-Ile, L-Asn and L-Orn residues. While the NMR comparisons between **6.01** and **6.05** suggested a very similar amino acid sequence, to be confident of this required assignment of the 1D NMR data, and careful consideration of the 2D NMR correlations. Following the strategy outlined previously for desotamide (**6.01**), it was possible to fully assign the data to the respective amino acids, as indicated in Table 6.9, Table 6.10 and as illustrated in Figure 6.44 and Figure 6.45. Of particular importance, diagnostic HMBC correlations permitted unambiguous assignment of the ^{13}C NMR resonances for all amide carbonyls. The sequence of amino acid residues is tentatively proposed as indicated, but will be addressed towards the end of this chapter.

Ornithine is a nonessential amino acid and is manufactured by the body. The amino acid, arginine, is metabolized during urea production as it acts as a precursor of citrulline, proline and glutamic acid. Ornithine plays an important role in the urea cycle and is the precursor of the amino acids citrulline, glutamic acid, and proline. Another primary role of ornithine is being an intermediate in arginine biosynthesis, although this is due to its participation in the urea cycle (responsible for the production of urea). Ornithine is not directly incorporated into proteins and enzymes and does not have a codon in the genetic code.[211]

6.4.5.1 C_3 Marfey's analysis of 6.05

Employing the C_3 Marfey method as previously described, **6.05** was subjected to acid hydrolysis using 6 M HCl/5% thioglycolic acid, derivatized with D-FDAA, and subjected to HPLC analysis to determine the absolute stereochemistry of the derivatized amino acids. Absolute configuration of **6.05** was determined by comparing the retention times of standard amino acids with the derivatized hydrolysate of **6.05**. The amino acids of **6.05** were confirmed to be L-Trp, L-Leu, L-Orn, L-Asn, L-*allo*-Ile and Gly as shown in Figure 6.37 and **Figure 6.38**.

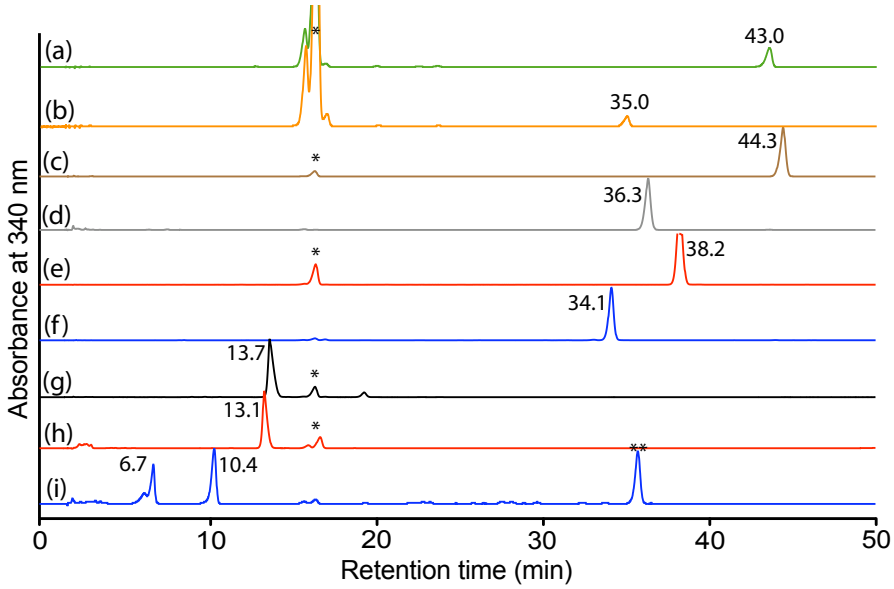

Figure 6.37. HPLC trace (340 nm) from HPLC-DAD-MS C_3 Marfey's analysis of the standard amino acids reacting with D-FDAA. Identity of amino acids was confirmed by retention time and molecular weight. (a) L-*allo*-Ile + D-FDAA (t_R = 43.0 min), (b) L-*allo*-Ile + D-FDAA (t_R = 35.0 min), (c) L-Leu + D-FDAA (t_R = 44.3 min), (d) D-Leu + D-FDAA (t_R = 36.3 min), (e) L-Trp + D-FDAA (t_R = 38.2 min), (f) L-Trp + L-FDAA (t_R = 34.1 min), (g) L-Asn + D-FDAA (t_R = 13.7 min), (h) D-Asn + D-FDAA (t_R = 13.1 min) and (i) L-Orn + D-FDAA (t_R = 36.2 min). HPLC conditions, Zorbax, SB-C_3 column (150 × 4.6 mm, 5 µm), 1 mL/min, gradient of 15 – 60% MeOH/H_2O (isocratic 5% MeCN containing 1% formic acid) over 55 min. * excess Marfey reagent. ** di-substituted derivatized L-Orn + D-FDAA (t_R = 35.7 min)

As expected Marfey reagent reacted with each γ and α amino group of L-Orn to afford two derivatized L-Orn *m/z* 385 [M+H] with retention times 6.7 and 10.4 min. Also, Marfey reagent reacted with both γ and α amino group of L-Orn to afford derivatized L-Orn *m/z* 637 [M+H] with retention time 35.7 min

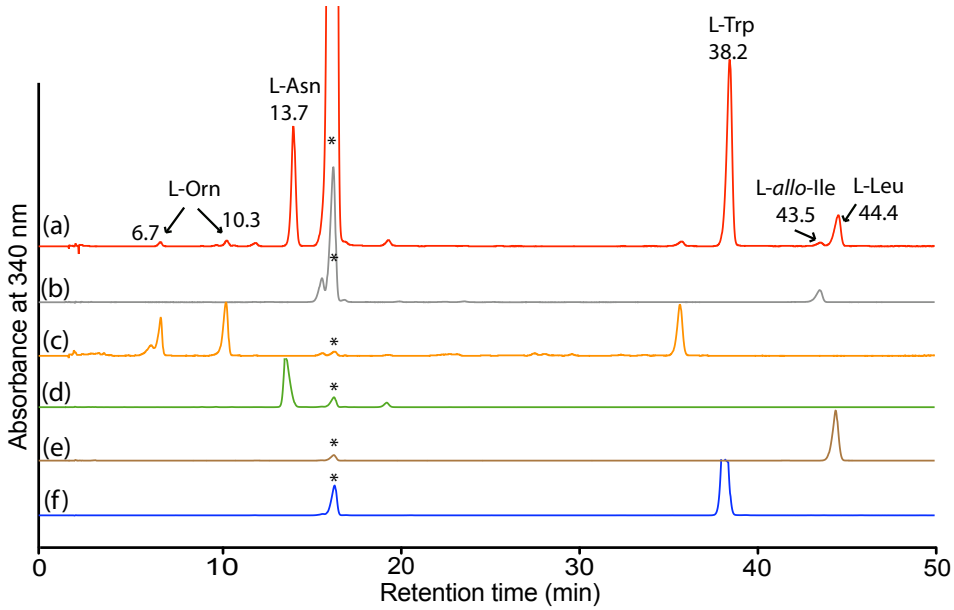

Figure 6.38. HPLC trace (340 nm) from HPLC-DAD-MS Marfey's analysis of desotamide E (**6.05**). Identity of amino acids was confirmed by retention time and molecular weight. (a) Co-injection of hydrolysate of **6.05** (300 µg) with L-Asn, L-*allo*-Ile, L-Orn, L-Leu, L-Trp + D-FDAA, (b) L-*allo*-Ile + D-FDAA, (c) L-Orn + D-FDAA, (d) L-Asn + D-FDAA, (e) L-Leu + D-FDAA and (f) L-Trp + D-FDAA and. HPLC conditions, Zorbax, SB-C_3 column (150 × 4.6 mm, 5 µm), 1 mL/min, gradient of 15 – 60% MeOH/H_2O (isocratic 5% MeCN containing 1% formic acid) over 55 min.* excess Marfey reagant

Six amino acids fragments:

L-Trptophan #1: Analysis of the COSY NMR (DMSO-d_6) data of **6.05** revealed diagnostic correlation sequences consistent with the structure fragment (i) H-4′ to H-5′ to H-6′ to H-7′, (ii) 2-NH to H-2 to H_2-3, and (iii) 5-H to 6-NH. Key HMBC correlation permitting assignment of the quaternary carbons included (i) 2-NH to C-1, (ii) H_2-3 to C-4 and C-5 and (iii) 6-NH and H-8 to C-6a (Figure 6.39).

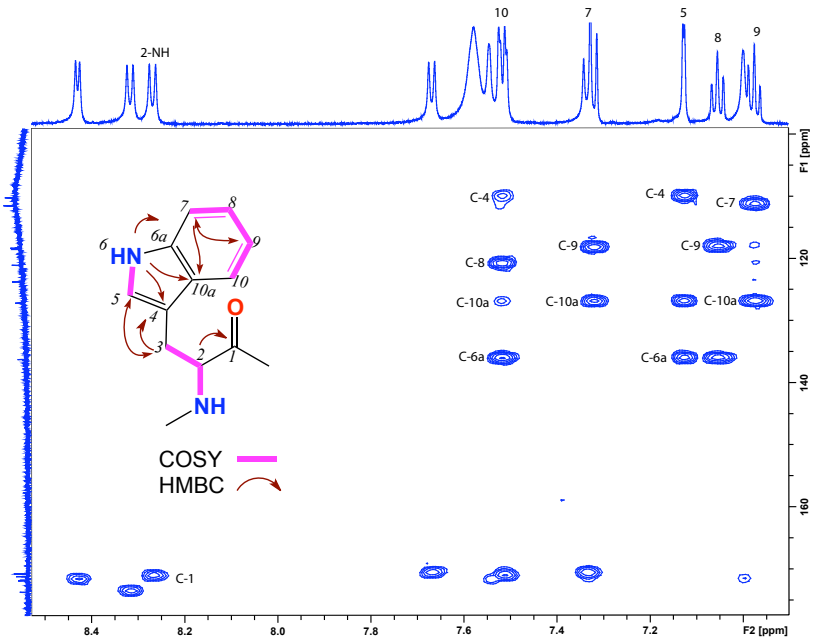

Figure 6.39. HMBC (600 MHz, DMSO-d_6) spectrum with the key correlations (Trp) of desotamide E (**6.05**)

L-Leucine #2 and 3: From the Marfey's analysis, we proved the presence of only L-Leu residue, which contributes to both Leu #2 and #3 and can explain the overlapping of the signals due to similarity of two Leu residues as L configuration. COSY NMR (DMSO-d_6) correlations readily identified the sequence 2-NH to H-2 to H_2-3 to H-4 to H_3-5/H_3-6, while HMBC correlations linked 2-NH to C-1 (Figure 6.40).

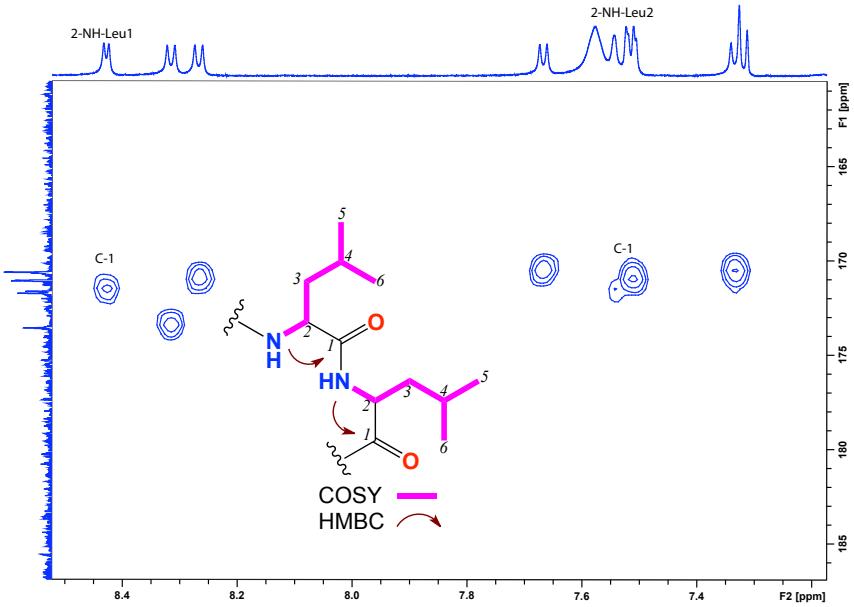

Figure 6.40. HMBC (600 MHz, DMSO-d_6) spectrum with the key correlations of desotamide E (**6.05**)

L-*allo*-Ile #4: COSY NMR (DMSO-d_6) correlations readily identified the sequence 2-NH to H-2 to H-3 to H_3-6 to H_2-4 to H_3-5, while HMBC correlations linked H-2 and 2-NH to C-1 (Figure 6.41).

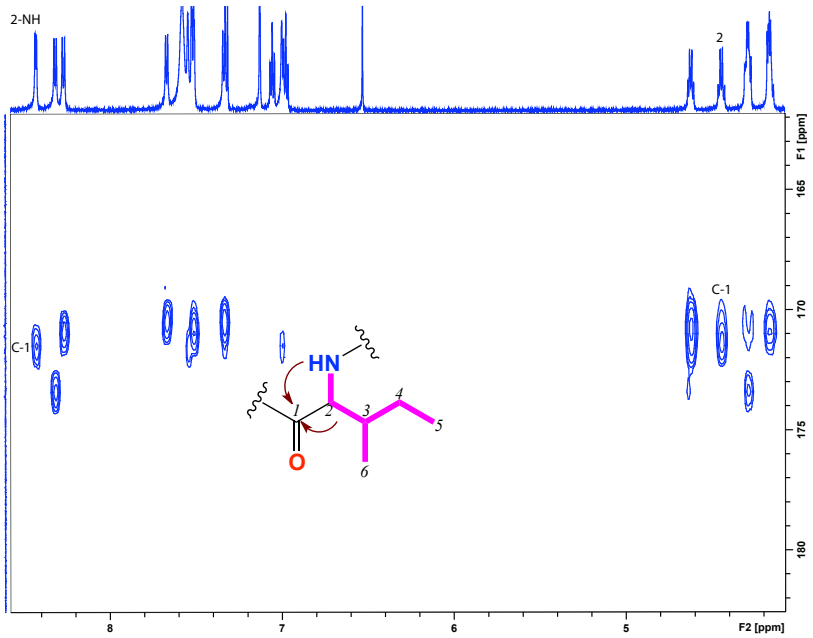

Figure 6.41. HMBC (600 MHz, DMSO-d_6) spectrum with the key correlations (*allo*-Ile) of desotamide E (**6.05**)

L-Asn #5: COSY NMR (DMSO-d_6) correlations readily identified the sequence 2-NH to H-2 to H-3, while HMBC correlations linked H-2 to C-1, H_2-3 and NH_2 to C-4 (Figure 6.42).

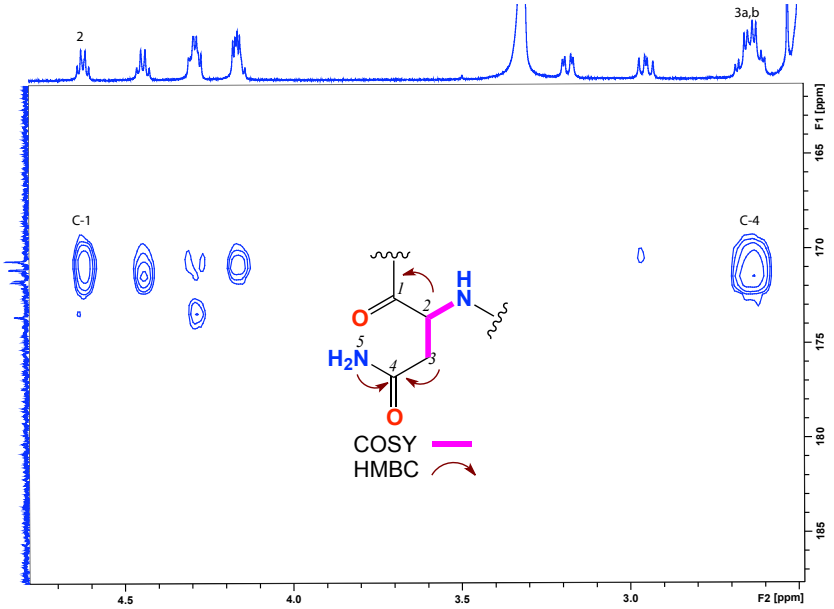

Figure 6.42. HMBC (600 MHz, DMSO-d_6) spectrum with the key correlations (Asn) of desotamide E (**6.05**)

L-Orn #6: COSY NMR (DMSO-d_6) correlations readily identified the sequence 2-NH to H-2 to H_2-3 to H_2-4 to H_2-5, while HMBC correlations linked 2-NH to C-1 (Figure 6.43).

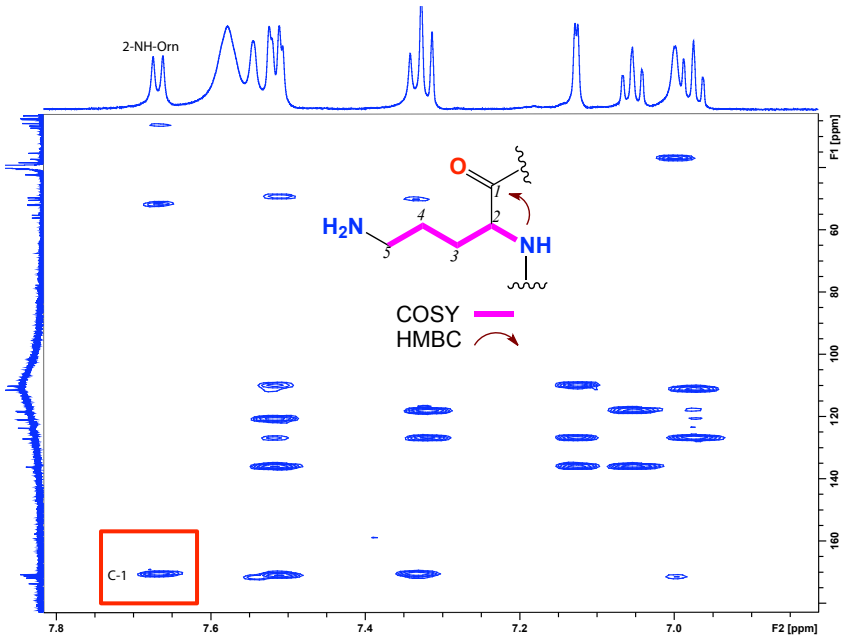

Figure 6.43. HMBC (600 MHz, DMSO-d_6) spectrum with the key correlations (Orn) of desotamide E (**6.05**)

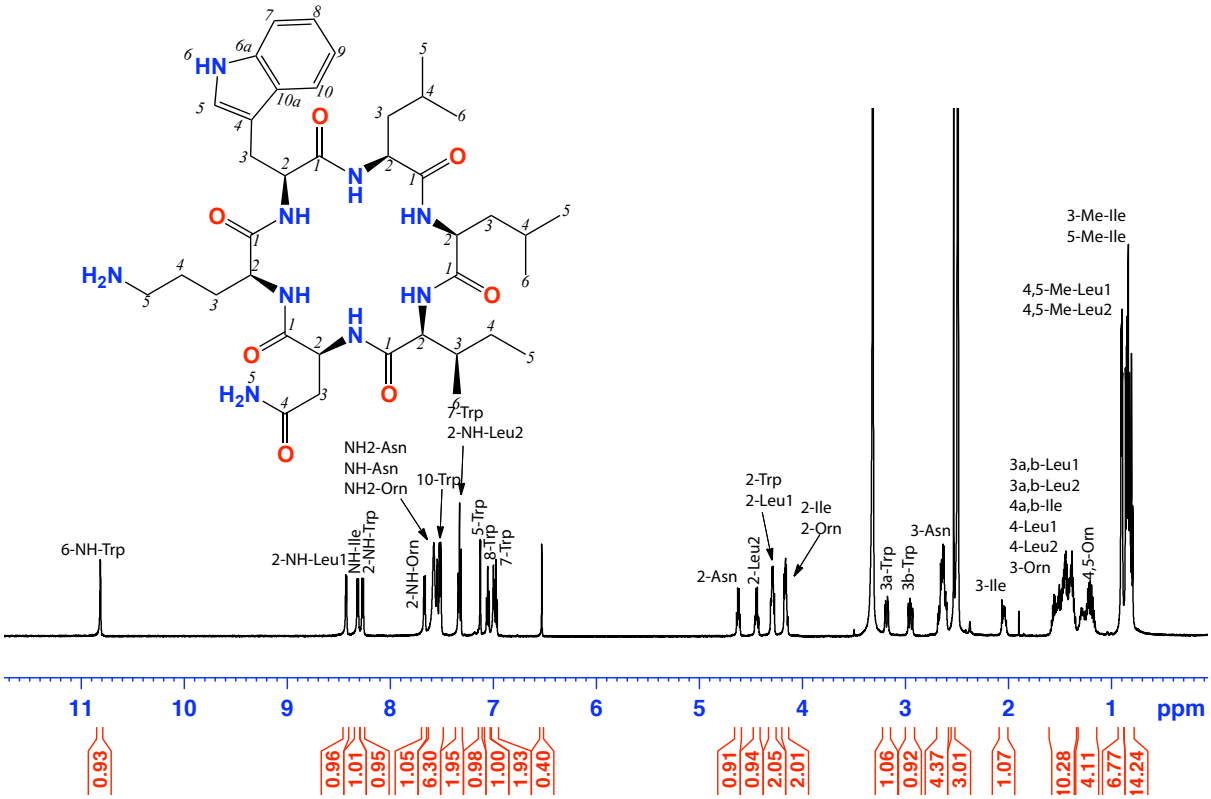

Figure 6.44. ^{1}H NMR (600 MHz, DMSO-d_6) of desotamide E (**6.05**)

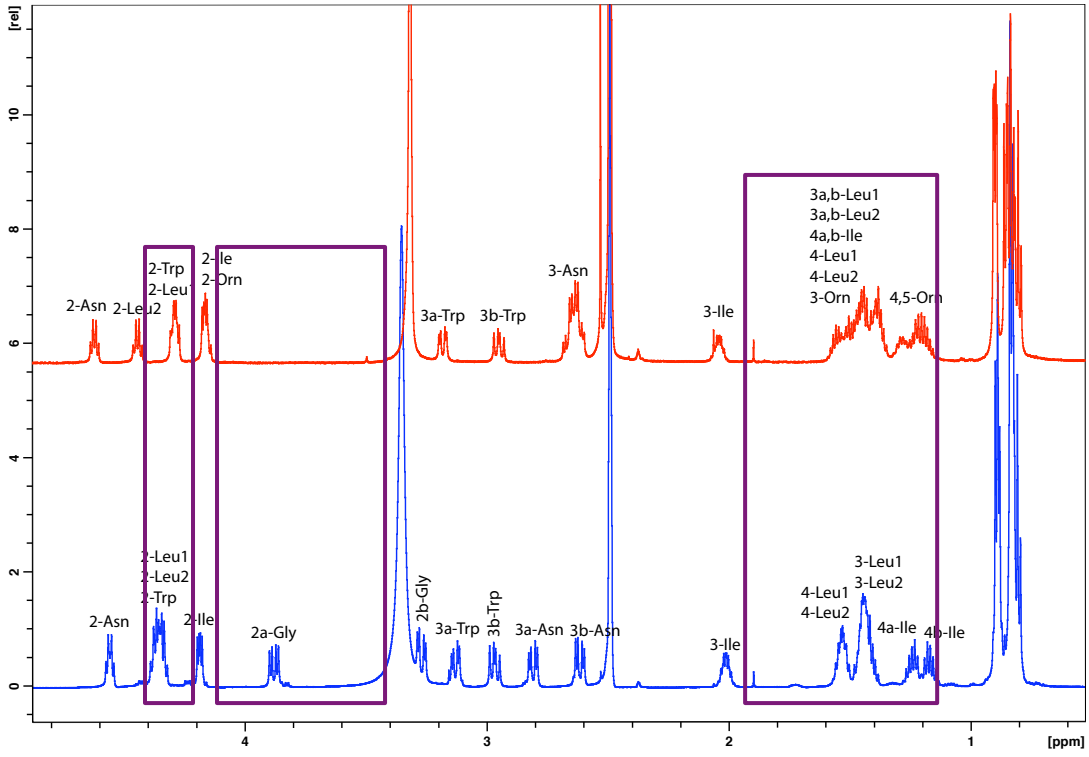

Figure 6.45. ^{1}H NMR (600 MHz, DMSO-d_6) spectra comparison of desotamide E (**6.05**) (red) and deostamide (**6.01**) (blue)

Table 6.9. NMR (600 MHz, DMSO-d_6) data of desotamide E (**6.05**)

#	Pos.	δ_H, mult (*J* in Hz)[a]	δ_C[a]	COSY	^{1}H-^{13}C HMBC	ROESY
Trp.	1		171.0			
	2	4.28[b], m	55.8	2-NH, 3a,b	1	
	3	a 3.18, dd *(14.8, 5.1)*	27.9	2, 3b	5	
		b 2.95, dd *(14.8, 10.1)*	27.9	2, 3a	5	
	4		110.4			
	5	7.12, d *(2.0)*	124.3	6-NH	3, 4, 6a, 10a	
	6a		136.5			
	7	7.32, d *(7.3)*	112.1	8	1-Orn, 10a	
	8	7.05, t *(7.3)*	121.7	7, 9	6a, 10	
	9	6.97, t *(7.3)*	119.2	8, 10	7, 10a	
	10	7.51[b]	118.9	9	4, 6a, 8	
	10a		127.6			
	2-NH	8.42, d *(5.1)*		2	1-Orn, 3	2-Orn
	6-NH	10.81, s		5	5, 4, 6a, 10a	
Orn	1		170.0			
	2	4.16[b], m	51.5	2-NH		2-NH-Trp
	3a	1.40[b], m	22.8			
	3b	1.28[b], m				
	4	1.20[b], m	25.4			
	5	1.20[b], m	25.4			
	2-NH	7.66, d *(7.3)*		2		2-Asn
	NH_2	[c]				
Asn.	1		170.8			
	2	4.62, dd *(14.1, 6.4)*	50.1	2-NH, 3	1, 3	2-NH-Orn
	3	a 2.64[b], m	37.8	2	4	
		b 2.63[b], m				
	4		171.2			
	2-NH	7.56, br		2		
	NH_2	7.33, s		4	3	2-Asn
Leu#1	1		171.6			
	2	4.28[b], m	52.6	2-NH, 3		
	3	a 1.48[b], m	41.9	2, 4		
		b 1.39[b], m		2, 4		
	4	1.55[b], m	24.7[c]	3		
	5-Me	0.86[b]	24.1[c]			
	6-Me	0.90[b]	23.9[c]			
	2-NH	8.42, d *(5.5)*		2	1	2-Leu#2
Leu#2	1		170.6			
	2	4.44, dd *(15.1, 7.3)*	50.9	2-NH, 3a,b	1, 3	NH-Ile
	3	a 1.45[b], m	39.2	2, 3b,		
		b 1.36[b], m		2, 3a, 4		
	4	1.47[b], m	24.9[c]	3, 5/6-Me		
	5-Me	0.85[b]	21.8[c]	4		
	6-Me	0.89[b]	22.0[c]	4		
	2-NH	7.52, brd		2		
allo-Ile	1		174.1			
	2	4.16[b], m	56.7	2-NH, 3	1	
	3	2.04, m	36.1	4		
	4	a 1.52[b], m	26.1	3		
		b 1.43[b], m		3		
	5-Me	0.80	11.1			
	6-Me	0.84	14.1			
	2-NH	8.31, d *(7.6)*		2	1	2-Leu#2

*(a) ^{13}C assignments obtained from gHSQC and gHMBC data. (b) Overlapping resonances. (c) Interchangeable resonaces. (d) Not observed

Table 6.10. NMR (600 MHz, DMSO-d_6) comparison of both desotamide E (**6.05**) and desotamide (**6.01**)

Desotamide E (**6.05**)				Desotamide (**6.01**)			
#	Pos.	δ_H, mult (*J* in Hz)[a]	δ_C[a]	#	Pos.	δ_H, mult (*J* in Hz)[a]	δ_C[a]
Trp.	1		171.0	Trp.	1		170.9
	2	4.28[b], m	55.8		2	4.36, m	55.4
	3	a 3.18, dd *(14.8, 10.1)*	27.9		3	3.31, dd (*14.7, 10.1*)	27.3
		b 2.95, dd *(14.8, 10.1)*	27.9			2.96, dd (*14.7, 10.1*)	
	4		110.4		4		110.0
	5	7.12, d *(2.0)*	124.3		5	7.11, s	123.5
	6a		136.5		6a		136.1
	7	7.32, d *(7.3)*	112.1		7	7.30, d (*8.1*)	111.3
	8	7.05, t *(7.3)*	121.7		8	7.04, t (*7.7*)	120.9
	9	6.97, t *(7.3)*	119.2		9	6.96, t (*7.7*)	118.3
	10	7.51[b]	118.9		10	7.49, d (*7.7*)	118.1
	10a		127.6		10a		127.1
	2-NH	8.42, d *(5.1)*			2-NH	8.24, d (*8.3*)	
	6-NH	10.81, s			6-NH	10.76, s	
Orn	1		170.0	Gly.	1		168.9
	2	4.16[b], m	51.5		2	a 3.88, dd (*15.8, 6.5*)	42.9
	3	a 1.40[b], m	22.8			b 3.26, dd (*15.8, 6.5*)	
		b 1.28[b], m			NH	7.94, t (*5.9*)	
	4	1.20[b], m	25.4				
	5	1.20[b], m	25.4				
	2-NH	7.66, d *(7.3)*					
	NH_2	[d]					
Asn.	1		170.8	Asn.	1		171.2
	2	4.62, dd *(14.1, 6.4)*	50.1		2	4.55, m	48.9
	3	a 2.64[b], m	37.8		3	a 2.80, dd (*16.2, 5.5*)	36.5
		b 2.63[b], m				b 2.61, dd (*16.2, 5.5*)	
	4		171.2		4		172.0
	2-NH	7.56, br			2-NH	7.57, d *(8.6)*	
	NH_2	7.33, s			NH_2	7.62, br s	
allo-Ile	1		174.1	*allo*-Ile	1		170.9
	2	4.16[b], m	56.7		2	4.18, dd (*7.8, 4.3*)	56.1
	3	2.04, m	36.1		3	2.01, m	34.9
	4	1.43-1.52, m	26.1		4	1.17-1.23, m	25.3
	5-Me	0.80	11.1		5-Me	0.81[b]	11.1
	6-Me	0.84	14.1		6-Me	0.81[b]	14.3
	2-NH	8.31, d *(7.6)*			NH	8.24, d (*8.6*)	
Leu#1	1		171.6	Leu#1	1		173.1
	2	4.28[b], m	52.6		2	4.35[b], m	51.3
	3	a 1.48[b], m	41.9		3	1.53, m	39.3
		b 1.39[b], m					
	4	1.55[b], m	24.7[c]		4	1.53[b]	23.7
	5-Me	0.86[b]	24.1[c]		5-Me	0.82[b]	22.1[c]
	6-Me	0.90[b]	23.9[c]		6-Me	0.82[b]	22.1[c]
	2-NH	8.42, d *(5.5)*			2-NH	8.29, d (*8.6*)	
Leu#2	1		170.6	Leu#2	1		172.2
	2	4.44, dd *(15.1, 7.3)*	50.9		2	4.35[b], m	50.3
	3	1.35-1.45[b], m	39.2		3	1.43, m	41.3
	4	1.47[b], m	24.9[c]		4	1.53[b], m	24.1
	5-Me	0.85[b]	21.8[c]		5-Me	0.88[b], d (*6.9*)	22.1[c]
	6-Me	0.89[b]	22.0[c]		6-Me	0.87[b], d (*6.9*)	22.1[c]
	2-NH	7.52, brd			2-NH	7.64, d (*7.6*)	

*(a) ^{13}C assignments obtained from gHSQC and gHMBC data. (b) Overlapping resonances. (c) Interchangeable resonaces. (d) Not observed

6.4.6 Desoatmide F (6.06)

HRESI(+)MS analysis of desotamide F (**6.06**) returned a quasi-molecular ion $[M+H]^+$ corresponding to a molecular formula ($C_{39}H_{59}N_6O_8$, Δmmu –1.9). Analysis of the NMR data suggested that the *allo*-Ile in **6.05** had been replaced by a Val in **6.06**. The structure elucidation was performed using 2D NMR spectra including HSQC, COSY and HMBC correlation outline in Figure 6.46, Figure 6.47 and Table 6.11. From the NMR analysis, we predict the presence of Trp, Leu (× 2), Val, Asn and Orn residues, however, these assignments will be confirmed by C_3 Marfey's analysis which still under investigation. The sequence of amino acid residues is tentatively proposed as indicated, but will be addressed towards the end of this chapter.

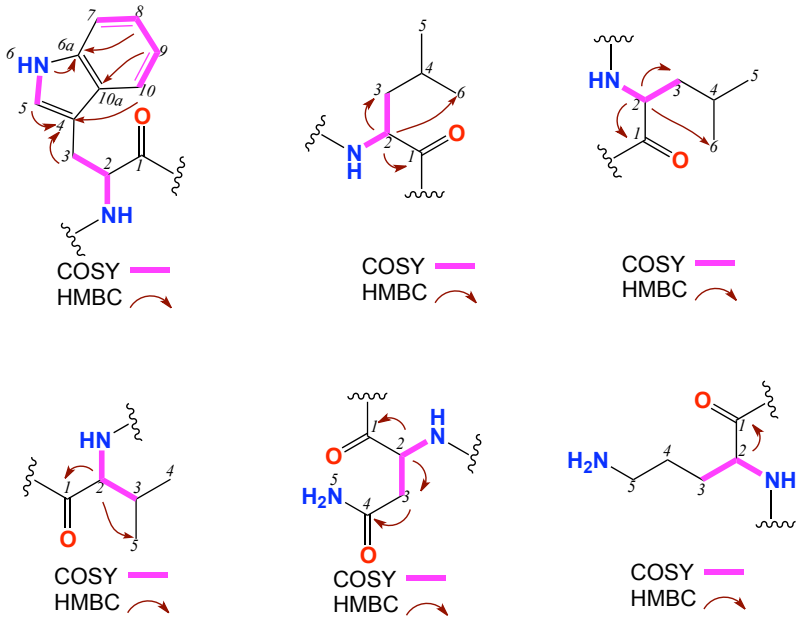

Figure 6.46. Key 2D NMR correlations of desotamide F (**6.06**)

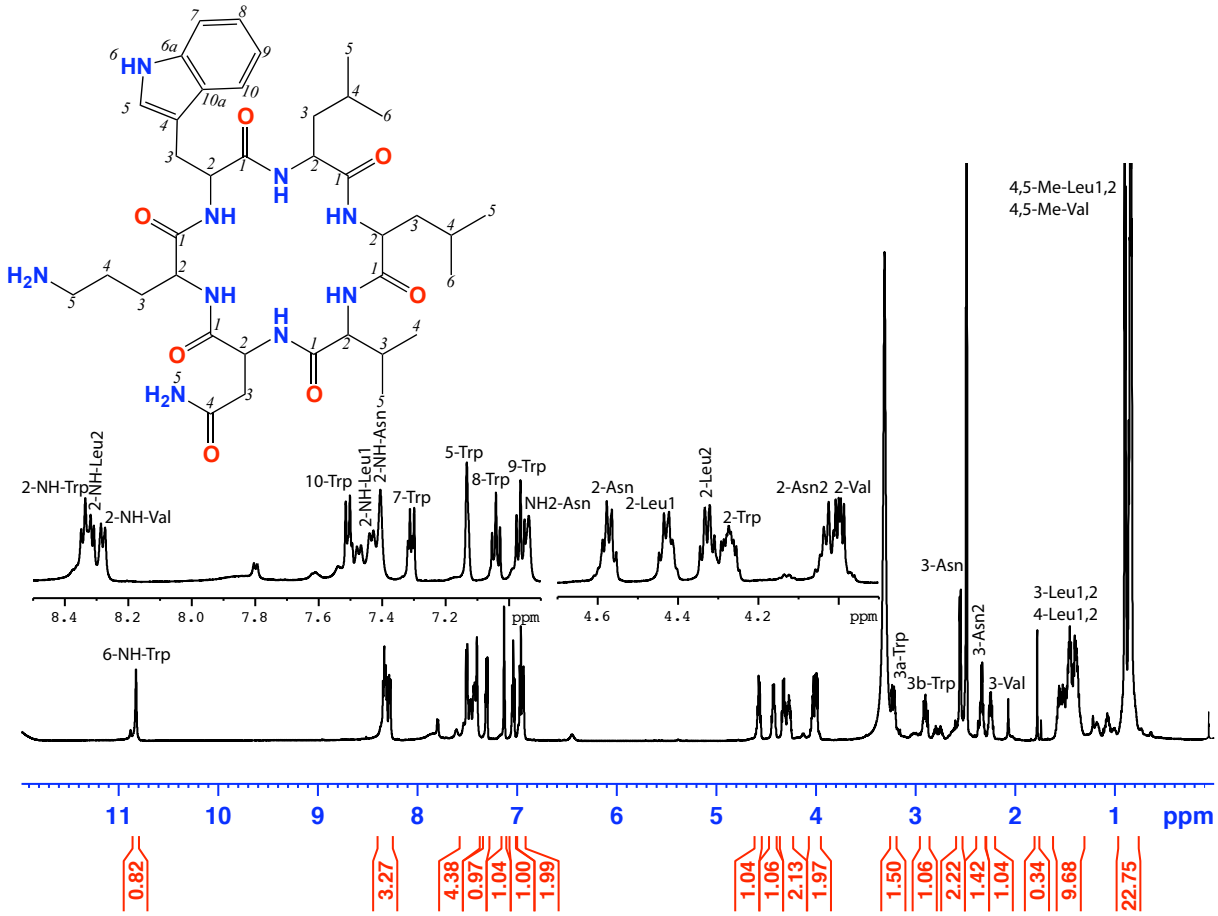

Figure 6.47. ^{1}H NMR (600 MHz, DMSO-d_6) spectrum of desotamide F (**6.06**)

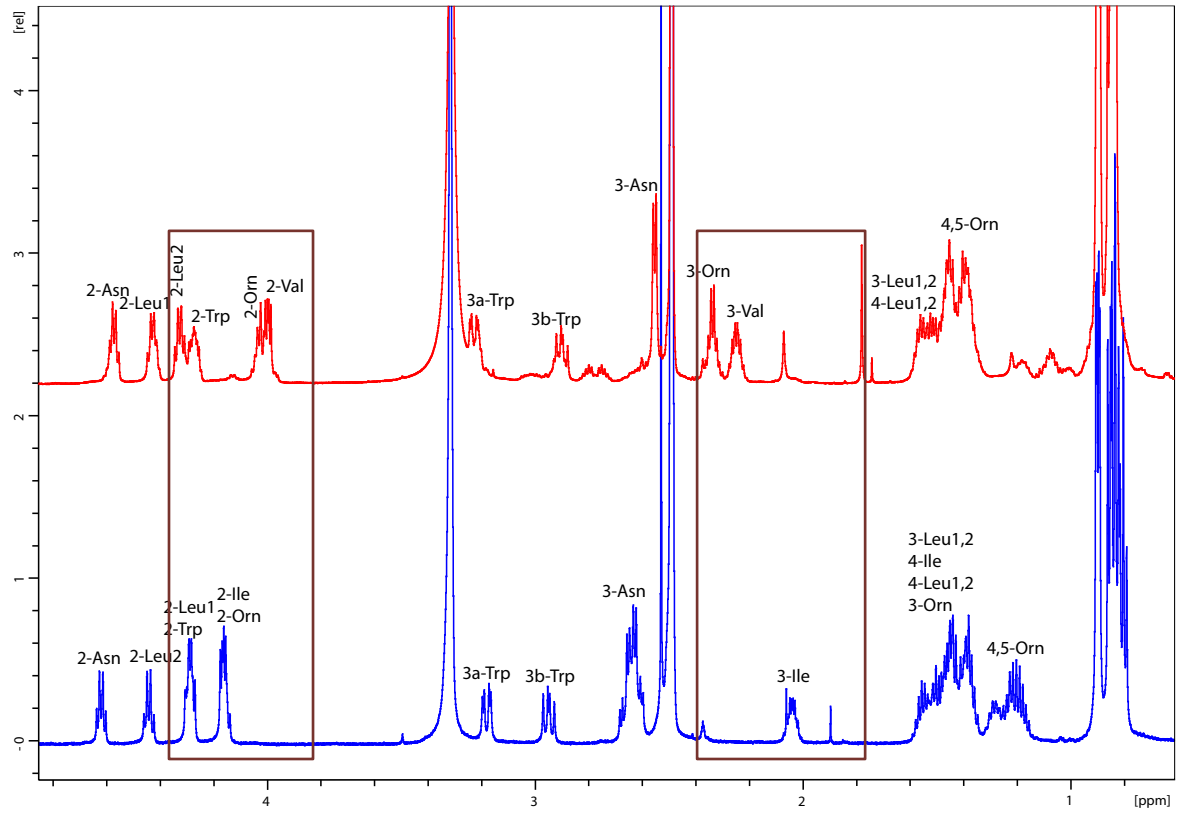

Figure 6.48. ^{1}H NMR (600 MHz, DMSO-d_6) spectra comparison of **6.05** (blue) and **6.06** (red)

Table 6.11. NMR (600 MHz, DMSO-d_6) data of desotamide F (**6.06**)

#	Pos.	δ_H, mult (*J* in Hz)[a]	δ_C[a]	COSY	^{1}H-^{13}C HMBC	ROESY
Trp.	1		170.7			
	2	4.27, m	54.5	2-NH, 3a,b	3, 4, 6a, 10a	
	3	a 3.22, dd *(14.4, 10.6)*	26.8	2, 3b	2, 4, 5	
		b 2.90, dd *(14.4, 10.6)*	26.8	2, 3a	2, 4, 5	
	4		109.7			
	5	7.31, br	123.2	6-NH	3, 4, 6a, 10a	
	6a		135.6			
	7	7.31, d *(7.4)*	111.1	8	10, 10a	
	8	7.04, t *(7.4)*	120.6	7, 9	6a, 10	
	9	6.96, t *(7.4)*	118.1	8, 10	7, 10a	
	10	7.50, d *(7.4)*	117.8	9	4, 8, 6a	
	10a		126.5			
	2-NH	8.33[b]		2		NH-Leu, 2-Orn
	6-NH	10.81, s		5	5, 4, 6a, 10a	
Asn	1		170.2			
	2	4.57, dd *(13.6, 6.2)*	49.1	1, 3		
	3	2.55, d *(6.2)*	37.0	2, 4		
	4		170.3			
	2-NH	7.39, br				2-Asn, NH-Val
	NH_2	6.95, s			3	
Orn	1		170.3			
	2	4.02, t *(7.2)*		2-NH, 3	1	NH-Trp
	3	2.55, d *(6.7)*	40.8	2	2, 4	
	4	1.38[b]	26.9			
	5	1.38[b]	26.9			
	2-NH	7.40, br		2		3, 2-Asn
	NH_2	[d]				
Leu#1	1		170.5			
	2	4.43, dd *(14.8, 7.4)*	50.4	2-NH, 3	1, 3, 5/6	
	3	a 1.51[b], m	41.6			
		b 1.44[b], m				
	4	1.56[b], m	23.6			
	5-Me	0.89[b], m	22.2[c]			
	6-Me	0.84[b], m	22.1[c]			
	2-NH	7.47[b]		2		NH-Leu#2
Leu#2	1		172.7			
	2	4.32, dd *(14.3, 6.6)*	51.3	2-NH, 3	1	
	3	a 1.40[b]	39.3	2	3	
		b 1.46[b]				
	4	1.46[b], m	24.1			
	4-Me	0.86[b], m	22.4[c]			
	5-Me	0.85[b], m	22.0[c]			
	2-NH	8.29[b]		2	2, 3	NH-Leu#1
Val	1		171.4			
	2	3.99, dd *(7.8, 4.5)*	58.2	2-NH, 3	1, 4/5-Me	
	3	2.24, m	28.5	2		
	4-Me	0.86[b], m	16.7	3		
	5-Me	0.89[b], m	18.9	3		
	2-NH	8.33[b]		2		NH-Asn, NH-Leu#2

*(a) ^{13}C assignments obtained from gHSQC and gHMBC data. (b) Overlapping resonances. (c) Interchangeable resonances. (d) not observed

Table 6.12. ^{1}H NMR (600 MHz, DMSO-d_6) comparison of desotamide E (**6.05**) and desotamide F (**6.06**)

Desotamide E (**6.05**)				Desotamide F (**6.06**)			
#	Pos.	δ_H, mult (*J* in Hz)[a]	δ_C[a]	#	Pos.	δ_H, mult (*J* in Hz)[a]	δ_C[a]
Trp.	1		171.0	Trp.	1		170.7
	2	4.28[b], m	55.8		2	4.27, m	54.5
	3	a 3.18, dd *(14.6, 10.1)*	27.9		3	a 3.22, dd *(14.4, 10.6)*	26.8
		b 2.95, dd *(14.6, 10.1)*	27.9			b 2.90, dd *(14.4, 10.6)*	26.8
	4		110.4		4		109.7
	5	7.12, d *(2.0)*	124.3		5	7.31, brd	123.2
	6a		136.5		6a		135.6
	7	7.32, d *(7.3)*	112.1		7	7.31, d *(7.4)*	111.1
	8	7.05, t *(7.3)*	121.7		8	7.04, t *(7.4)*	120.6
	9	6.97, t *(7.3)*	119.2		9	6.96, t *(7.4)*	118.1
	10	7.51[b]	118.9		10	7.50, d *(7.4)*	117.8
	10a		127.6		10a		126.5
	2-NH	8.42, d *(5.1)*			2-NH	8.33[b]	
	6-NH	10.81, s			6-NH	10.81, s	
Orn	1		170.0	Orn	1		170.3
	2	4.16[b], m	51.5		2	4.02, t *(6.7)*	
	3	1.28-1.40[b], m	22.8		3	2.55, d *(6.7)*	40.8
	4	1.20[b], m	25.4		4	1.38[b]	26.9
	5	1.20[b], m	25.4		5	1.38[b]	26.9
	2-NH	7.66, d *(7.3)*			2-NH	7.40, brd	
	NH_2	[d]			NH_2	[d]	
Asn.	1		170.8	Asn	1		170.2
	2	4.62, dd *(14.1, 6.4)*	50.1		2	4.57, dd *(13.6, 6.2)*	49.1
	3	2.63-2.64[b], m	37.8		3	2.55, d *(6.2)*	37.0
	4		171.2		4		170.3
	2-NH	7.56, br			2-NH	7.39, brd	
	NH_2	7.33, s			NH_2	6.95, s	
allo-Ile	1		174.1	Val	1		171.4
	2	4.16[b], m	56.7		2	3.99, dd *(7.8, 4.5)*	58.2
	3	2.04, m	36.1		3	2.24, m	28.5
	4	1.43-1.52, m	26.1		4-Me	0.86[b], m	16.7
	5-Me	0.80	11.1		5-Me	0.89[b], m	18.9
	6-Me	0.84	14.1		2-NH	8.33[b]	
	2-NH	8.31, d *(7.6)*					
Leu#1	1		171.6	Leu#1	1		170.5
	2	4.28[b], m	52.6		2	4.43, dd *(14.8, 7.4)*	50.4
	3	a 1.48[b], m	41.9		3	a 1.51[b], m	41.6
		b 1.39[b], m				b 1.44[b], m	
	4	1.55[b], m	24.7[c]		4	1.56[b], m	23.6
	5-Me	0.86[b]	24.1[c]		5-Me	0.89[b], m	22.2[c]
	6-Me	0.90[b]	23.9[c]		6-Me	0.84[b], m	22.1[c]
	2-NH	8.42, d *(5.5)*			2-NH	7.47[b]	
Leu#2	1		170.6	Leu#2	1		172.7
	2	4.44, dd *(15.1, 7.3)*	50.9		2	4.32, dd *(14.3, 6.6)*	51.3
	3	1.35-1.45[b], m	39.2		3	a 1.40[b]	39.3
	4	1.47[b], m	24.9[c]		4	b 1.46[b]	
	5-Me	0.85[b]	21.8[c]		5-Me	1.46[b], m	24.1
	6-Me	0.89[b]	22.0[c]		6-Me	0.86[b], m	22.4[c]
	2-NH	7.52, br			2-NH	0.85[b], m	22.0[c]

*(a) ^{13}C assignments obtained from gHSQC and gHMBC data. (b) Overlapping resonances. (c) Interchangeable resonances. (d) not observed

6.4.7 Amino acid residues correlations for deostamides (6.01 – 6.06)

Based on the data listed above including HMBC (Figure 6.49) and ROSEY (Figure 6.50) correlations and NMR comparison with known desotamide (**6.01**), we could acknowledge that 2D NMR data does not permit unambiguous sequence assigned for some correlations. Based on the biosynthetic grounds for the desotamides, it is obvious that all of them share Trp, Leu and Asn residues, and that they only differ in three amino acid residues A, B and C (Figure 6.51) in which it ranges from Ile, Leu, Val, Gly and Orn (arginine through arginase produces ornithine). In most cases, the amino acids codes for these amino acids can undergo slight variation in one code to give a rise to another amino acid, for example, Ile (ATT, ATC, ATA), while Leu (CTT, CTC, CTA).

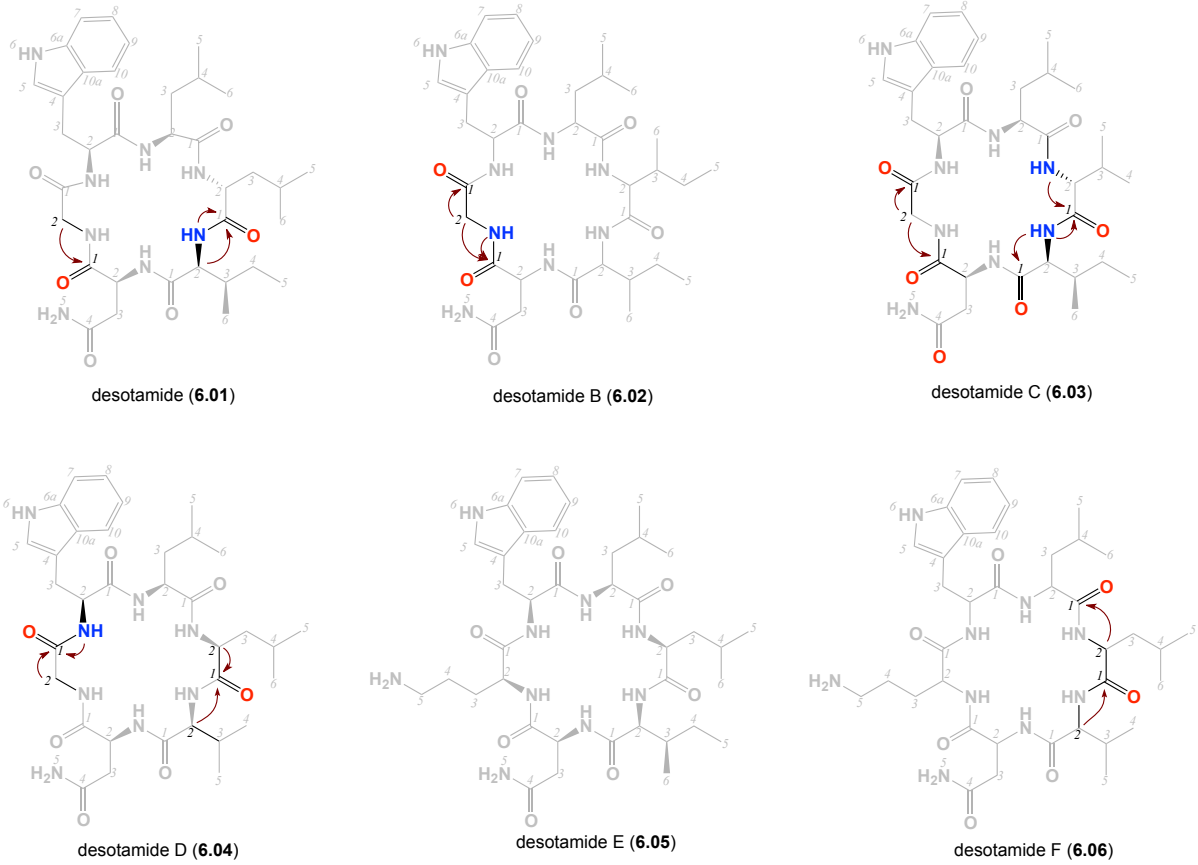

Figure 6.49. HMBC (600 MHz, DMSO-d_6) correlations for amide/carbonyl of the amino acid residues of six desotamides (**6.01 – 6.06**)

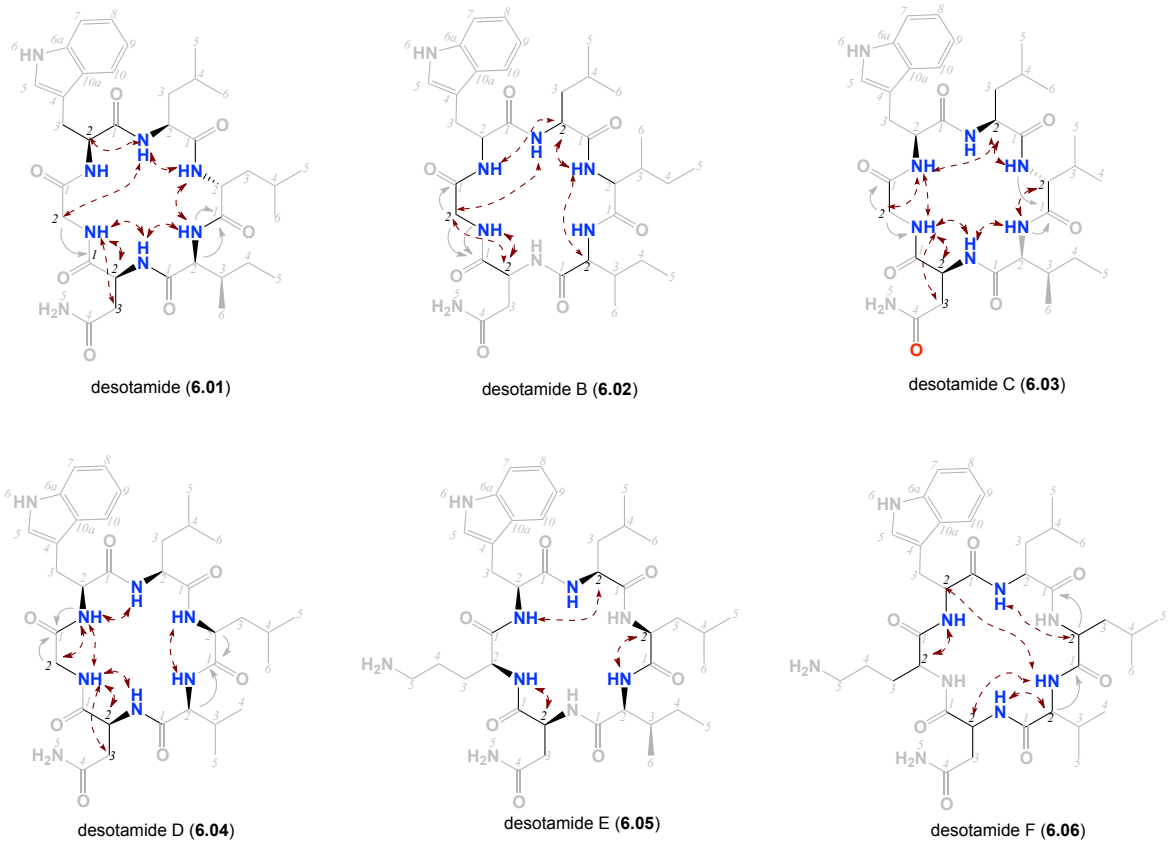

Figure 6.50. ROESY (600 MHz, DMSO-d_6) correlations of amino acid residues of desotmaides (**6.01 – 6.06**)

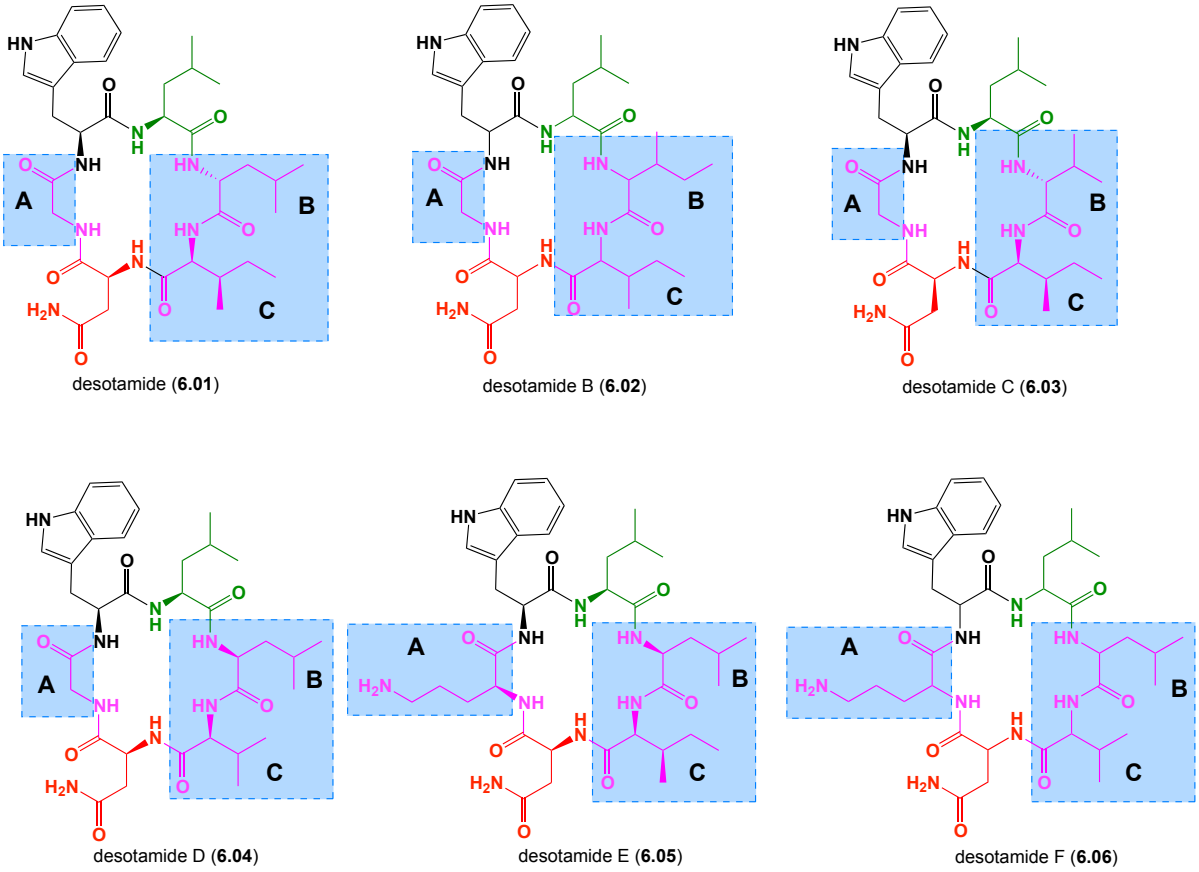

Figure 6.51. Proposed sequence homology based on biosynthetic grounds

6.4.8 Biological screening

6.4.8.1 Antimicrobial and cytotoxicity assay

The desotamides (**6.01** - **6.06**) have been screened against the in-house biological assays, antibacterial, antifungal (Figure 6.52 and Table 6.13) and cytotoxic assay (Figure 6.53). The desotamides (**6.01** – **6.06**), displayed no antibiotic activity against the Gram negative bacteria *Escherichia coli* (ATCC 11775) and *Pseudomonas aeruginosa* (ATCC 10145), but moderate antibacterial activity against the Gram positive bacteria Bacillus *subtilis* (ATCC 6633 and ATCC 6051), while desotamide B (**6.02**) and F (**6.06**) exhibit antibacterial activity against *Staphylococcus aureus* (ATCC 9144 and ATCC 25923) (Table 6.13 and Figure 6.52). Likewise, these same compounds failed to exhibit cytotoxicity (IC_{50} >30 μM) against the human colon cancer cell line SW620, lung cancer cell line NCIH460 (Figure 6.53).

Table 6.13. Antibacterial and antifungal screening results

	Staphylococcus aureus ATCC 25923		*Staphylococcus aureus* ATCC 9144		*Bacillus subtilis* ATCC 6051		*Bacillus subtilis* ATCC 6633	
Compounds	**MIC (μM)**	**IC_{50} (μM)**	**MIC (μM)**	**IC_{50} (μM)**	**MIC (μM)**	**IC_{50} (μM)**	**MIC (μM)**	**IC_{50} (μM)**
desotamide (**6.01**)	--	--	--	--	15	7.5	15	7.5
desotamide B (**6.02**)	15	7.5	15	9	3.7	1.5	3.7	1.8
desotamide C (**6.03**)	--	--	--	--	15	7.5	15	7.5
desotamide D (**6.04**)	--	--	--	--	15	7.5	15	7.5
desotamide E (**6.05**)	--	--	--	--	7.5	3.5	7.5	3.5
desoatmide F (**6.06**)	3.7	0.9	3.7	0.8	15	9.2	15	12.0

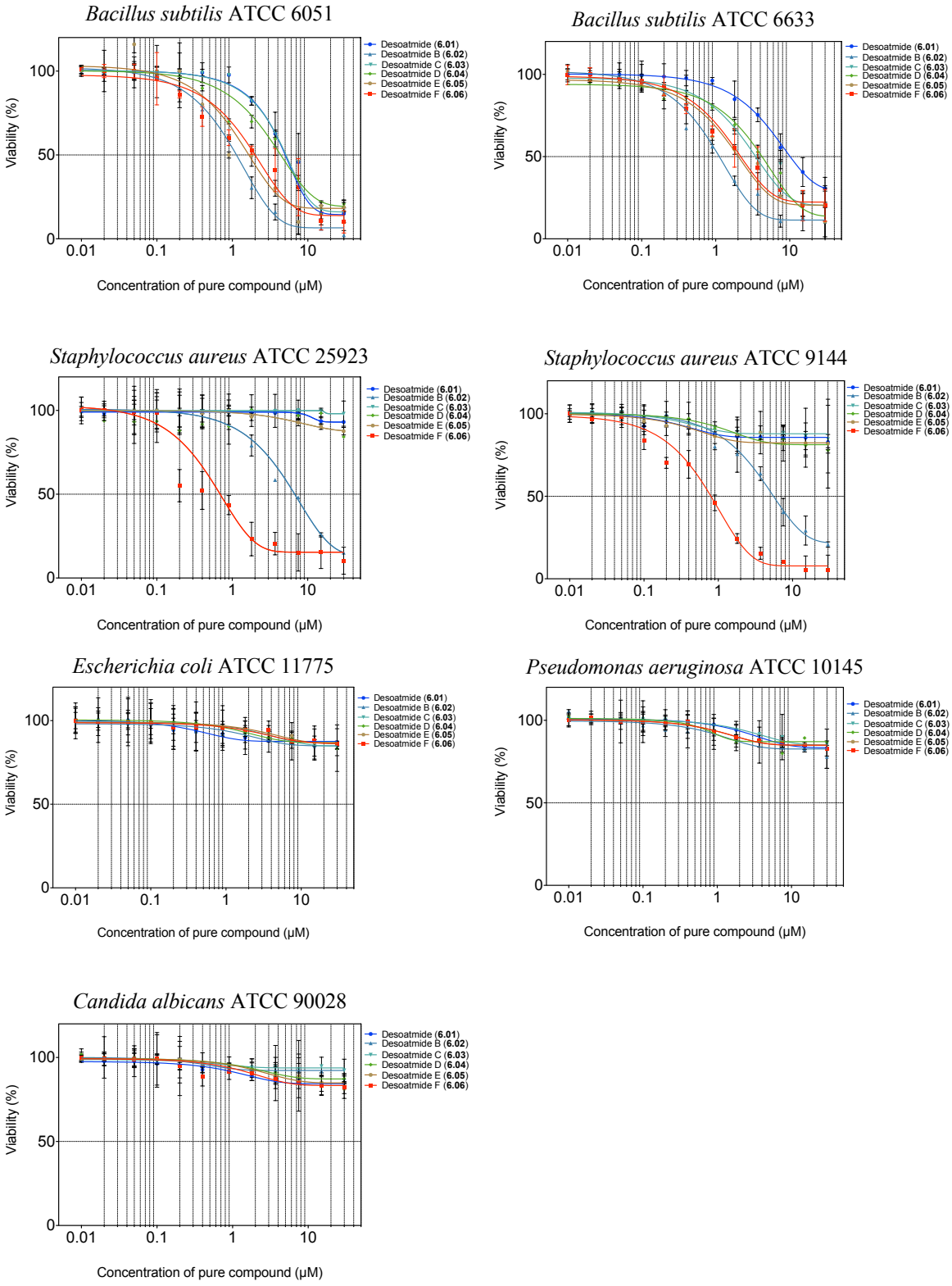

Figure 6.52. Antimicrobial assay screening graphs of desotamides (**6.01** - **6.06**)

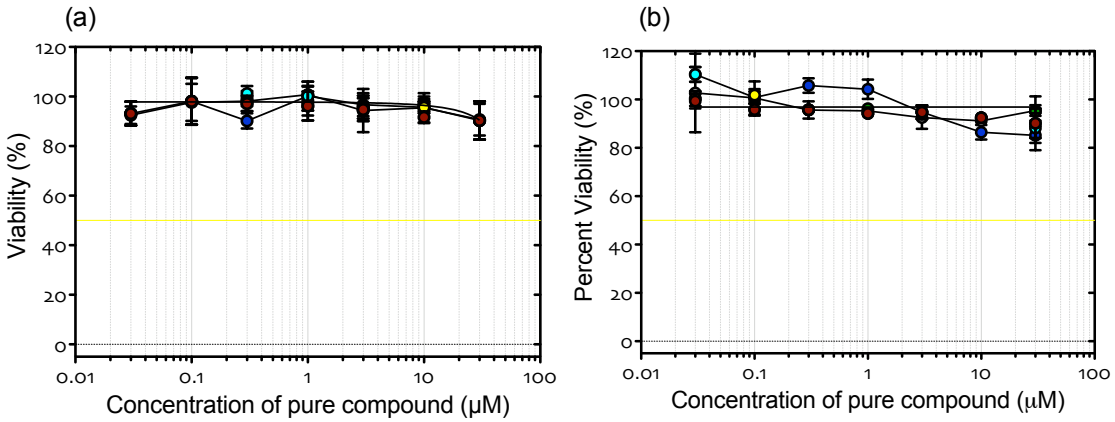

Figure 6.53. Cytotoxicity assay of the desotamides (**6.01 – 6.06**) against (a) SW620 (human colon cancer cell line), (b) NCIH460 (lung cancer cell line)

6.4.8.2 Activity against *Mycobacterium bovis* (BCG)

The early bactericidal activity of the desotamides (**6.01** – **6.06**) prompted us to further test their activity against *Mycobacterium bovis*. In collaboration with Dr Antje Blumenthal (Diamantina Institute, The University of Queensland) we conducted preliminary studies using the vaccine strain *Mycobacterium bovis*, Bacille Calmette Guerin and observed that desotamide E (**6.05**) and F (**6.06**) inhibited mycobacterial growth and showed bactericidal activity *in vitro* with IC_{50} 2.79 and 3.09 μM respectively.

Mycobacterium bovis, Bacille Calmette Guerin (BCG) (strain Pasteur, ATCC) was grown until early-mid log phase in 7H9 liquid medium (Difco) containing 0.2% glycerol, 0.05% Tween80, 0.5% BSA, 0.2% dextrose, and 0.085% sodium chloride. Single cell suspensions of independent cultures were prepared by centrifuging the bacterial cultures for 10 min, at room temperature, 130 x g and then diluted to an optical density (OD; 600 nm) of 0.02. Bacterial growth in the presence of desotamides (**6.01** – **6.06**) (200 μl aliquots) was monitored in 96 well plates by OD measurements. To analyse bacterial survival, serial dilutions of culture material were plated on Middlebrook 7H10 plates supplemented with 10% oleic acid/albumin/dextrose catalase (OADC; Middlebrook) and 0.5% glycerol. Plates were incubated at 37 °C for 3 weeks and colonies enumerated to calculate colony forming units (CFU). Isoniazid (INH) was used as a positive control (20 μg/mL in 10% DMSO) (Figure 6.54 and Figure 6.55).

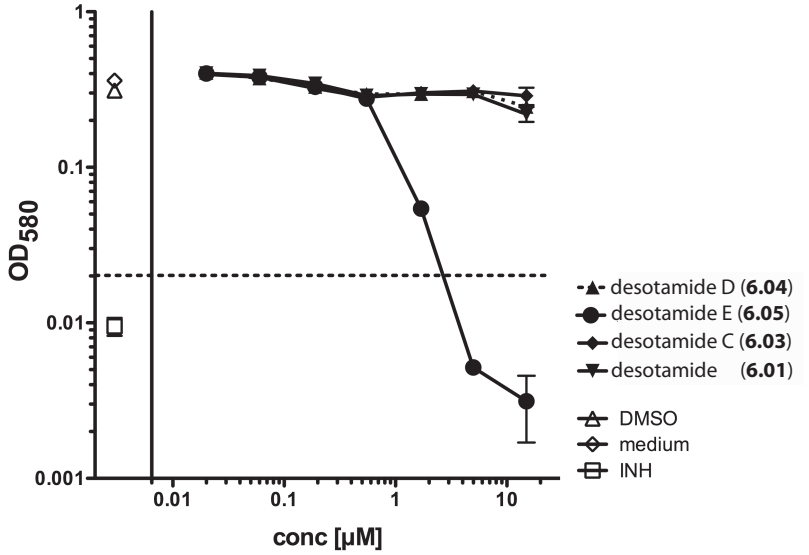

Figure 6.54. Inhibition of *M. bovis*, BCG growth by desotamides **6.05** and **6.06** *in vitro*.

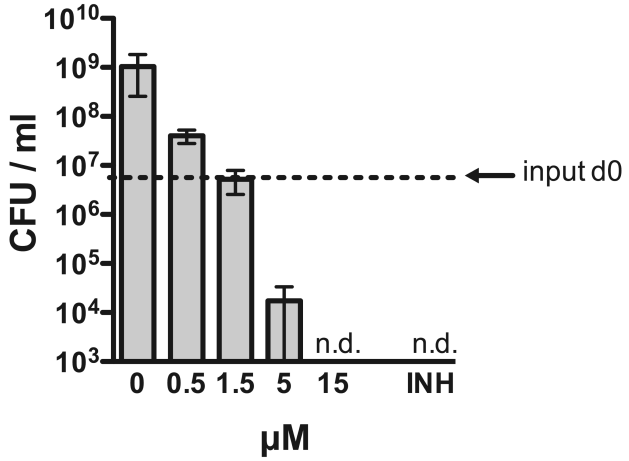

Figure 6.55. Desotamide E (**6.05**) has bactericidal activity against *M. bovis*, BCG in vitro. CFU determined on d7 post exposure to desotamide. *n.d. = not detectable, dotted line = indicates the bacterial number present in the culture at the beginning of the experiment on d0

6.4.9 Conclusion for the desotamides

The desotamides compounds were provided from Microbial Screening Technology (MST) in Sydney for structure elucidation and biological analysis. This chapter reports the identification of one known desotamide (**6.01**) and five new desotamides B – F (**6.02** – **6.06**). The desotamides exhibited moderate antibacterial activity *S. aureus* (ATCC 25923 and 9144) and *B. subtilis* (ATCC 6051 and 6633) with MIC ranging from 7.5 to 15 µM and IC_{50} ranging from 3.5 to 7.5 µM and were tested for their activity against *Mycobacterium bovis*. Desotamide E and F (**6.05** and **6.06**) exhibited good anti-BCG activity. Likewise, these same compounds failed to exhibit cytotoxicity (IC_{50} >30 µM) against the human colon cancer cell line SW620 and lung cancer cell line (NCIH460). These results suggest that **6.05** and **6.06** may be potent inhibitors of *Mycobacterium*

tuberculosis pharmacophore with minimal (low) mammalian cytotoxicity. The SAR by co-metabolites study further demonstrates the critical importance of the L-Orn residue for anti-TB activity, and suggests that all L-cyclohexapeptides is preferred.

6.4.10 Future work for the desotamides

C_3 Marfey's analysis for both desotamide B (**6.02**) and desotamide F (**6.06**) to assign the absolute stereochemistry of the amino acids residues, C_3 Marfey analysis for D-Orn to confirm the presence of L-Orn as well as finishing the antibacterial screening assay against *Mycobacterium bovis* and macrophage screening assay. Further studies will also be directed at the synthesis of analogues with L-Orn is replaced by L-Lys, or L-Arg to further probe optimize and document the antibacterial desotamide pharmacophore.

6.5 Experimental section

Desotamide (6.01): white powder; $[\alpha]^{22}_{D}$ –29.3 (*c* 0.05, MeOH); ^{1}H NMR (600 MHz, DMSO-d_6) see **Figure 6.5** and Table 6.1; HRESI(+)MS *m*/*z* 719.3857 (calcd for $C_{35}H_{52}N_8O_7Na$, 719.3851).

Desotamide B (6.02): white powder; $[\alpha]^{22}_{D}$ +20.2 (*c* 0.01, MeOH); ^{1}H NMR (600 MHz, DMSO-d_6) see Figure 6.16 and Table 6.3; HRESI(+)MS *m*/*z* 719.3835 (calcd for $C_{35}H_{52}N_8O_7Na$, 719.3851).

Desotamide C (6.03): white powder; $[\alpha]^{22}_{D}$ +80.2 (*c* 0.05, MeOH); ^{1}H NMR (600 MHz, DMSO-d_6) see Figure 6.26 and Table 6.5. HRESI(+)MS *m*/*z* 705.3686 (calcd for $C_{34}H_{50}N_8O_7Na$, 705.3695).

Desotamide D (6.04): white powder; $[\alpha]^{22}_{D}$ +95.7 (*c* 0.05, MeOH); ^{1}H NMR (600 MHz, DMSO-d_6) see Figure 6.35 and Table 6.7; HRESI(+)MS *m*/*z* 705.3683 (calcd for $C_{34}H_{50}N_8O_7Na$, 705.3695).

Desotamide E (6.05): white powder; $[\alpha]^{22}_{D}$ + 78.8 (*c* 0.05, MeOH); ^{1}H NMR (600 MHz, DMSO-d_6) see Figure 6.44 and Table 6.9; HRESI(+)MS *m*/*z* 705.3673 (calcd for $C_{34}H_{50}N_8O_7Na$, 705.3695).

Desotamide F (6.06): white powder; $[\alpha]^{22}_{D}$ + 20.2 (*c* 0.01, MeOH); NMR (600 MHz, DMSO-d_6) see Figure 6.47 and Table 6.11; HRESI(+)MS *m*/*z* 740.4473 (calcd for $C_{37}H_{58}N_9O_7$, 740.4454).

6.5.1 Marfey analysis for desotamides

Marfey's analysis were prepared according to the method described[210]. About 200 μg of desotamide (**6.01** - **6.02**) mixed with 100 μL of 5% thioglycolic acid/6 M HCl. The mixture was degassed with N_2 and heated at 110 °C overnight in tightly capped vial. The vial was left to cool, and then the solvent was removed under N_2. The remaining residue was mixed with 50 μL D-FDAA solution (10 mg/mL in acetone) and 100 μL 1 M $NaHCO_3$ solution. The mixture was heated at 60 °C for 5 min in a tightly capped vial. After cooling, 50 μL of 2 M HCl and 500 μL of 1:1 MeCN/H_2O were added. The mixture was analysed using HPLC conditions, Zorbax, SB-C_3 column (150 × 4.6 mm, 5 μM), 1 mL/min, gradient of 15 – 60% MeOH/H_2O (isocratic 5% MeCN containing 1% formic acid) over 55 min.[45]

7 Chapter 7. Aranciamycins: New Anthraquinones antibiotics

7.1 Introduction

During our screening for microbial metabolites with antibacterial activity, we tested a crude extract from CMB-M448 and detected antibacterial activity against Gram-positive bacteria *Bacillus subtilis* (ATCC 6051 and 6633). Large-scale cultivation yielded two known metabolites aranciamycin A (**7.01**) and aranciamycin (**7.02**) as well as two new metabolites aranciamycin I (**7.03**) and aranciamycin J (**7.04**). This chapter provides a brief account of the isolation, structure elucidation and antimicrobial assessment of these metabolites.

7.2 Results and discussion

7.2.1 Analytical cultivation and chemical analysis

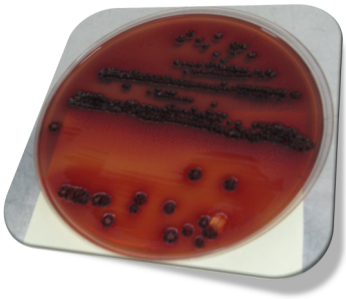

Figure 7.1. Solid phase culture of *Streptomyces* sp. (CMB-M448)

Streptomyces sp. (CMB-M448) was obtained from our in house marine microbial library. The crude extracts revealed interesting metabolites and antibacterial activity. A single colony of CMB-M448 was sub-sampled into seawater medium (100 mL of Ocean Nature seawater, 1% starch, 0.4% yeast extract and 0.2% peptone) and incubated at 27 °C for 10 d at 190 rpm. The culture was extracted with EtOAc (100 mL), and the organic phase concentrated *in vacuo* to yield an extract (12.7 mg) that was subsequently analysed by HPLC-DAD-MS with conditions set as follows (Zorbax C_8 column, 150 × 4.6 mm, 5 μm, 1 mL/min, gradient from 90 – 10 % H_2O/MeCN, with an isocratic 0.05% formic acid modifier, over 15 min, with a hold at 100% MeCN for 5 min). Peaks with the following retention times t_R = 8.1, 8.4, 6.8 and 6.9 min exhibited the following *m*/*z* $[M–H]^-$ 499 (**7.01**), 543 (**7.02**), 485 (**7.03**) and 513 (**7.04**) as shown in Figure 7.2.

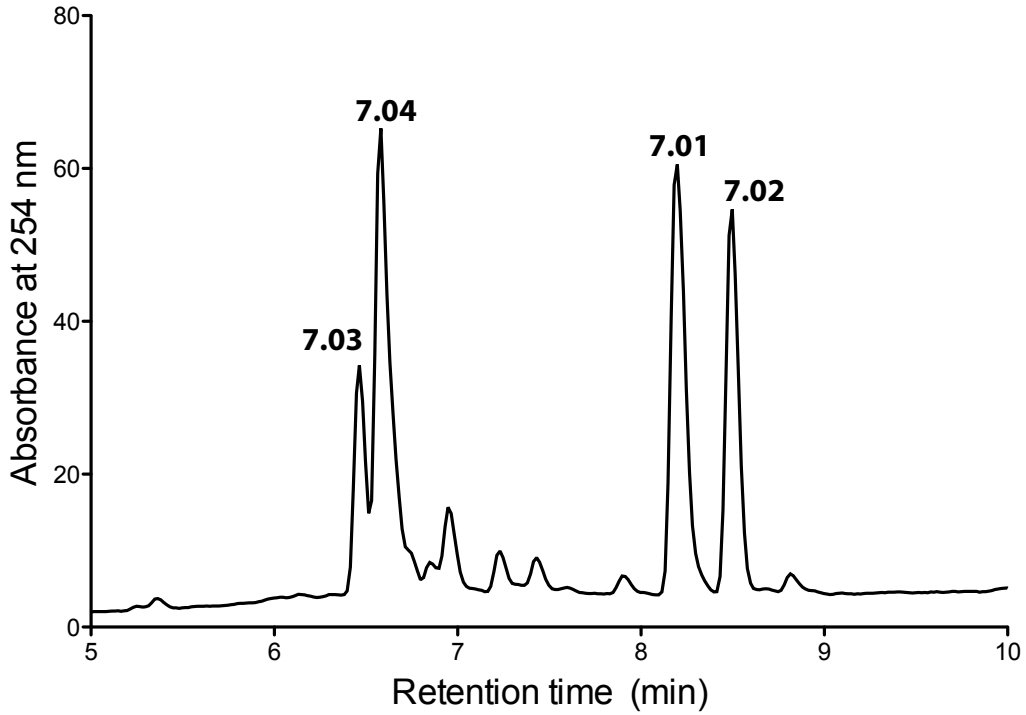

Figure 7.2. HPLC-DAD chromatogram from analytical gradient H_2O/MeCN with 0.05% HCO_2H using Zorbax C_8 at 254 nm of the crude extract from *Streptomyces* sp. (CMB-M448)

7.2.2 Preparative cultivation

A seed culture was prepared by inoculating *Streptomyces* sp. (CMB-M448) in liquid M1 media (50 mL) containing 1% starch, 0.4% yeast extract, 0.2% peptone and Ocean Nature seasalt (3.3%). Aliquots of the seed culture (5 mL) were transferred to six 3 L Fernbach flasks, each containing the same M1 liquid media (500 mL), and the flasks were shaken at 190 rpm for 10 d at 27 °C. The resulting cultures were extracted with EtOAc (400 mL) and the combined organic phase concentrated *in vacuo* to yield an extract (80.5 mg). The extract was sequentially triturated with hexane (8 mL), DCM (8 mL) and MeOH (8 mL) to afford, after concentration *in vacuo*, hexane (3 mg), CH_2Cl2 (4.2 mg) and MeOH (45 mg) soluble fractions. The MeOH fraction, rich in the target metabolites **7.01 – 7.04**, was subjected to semi-preparative reversed-phase HPLC (Zorbax C_8 column, 250 × 9.4 mm, 5 μm, 3 mL/min gradient elution 90 – 10% H_2O/MeCN over 30 min) to yield aranciamycin I (**7.03**) (t_R = 11.8 min, 0.8 mg, 0.8%), aranciamycin J (**7.04**) (t_R = 12.2 min, 1.8 mg, 0.8%), aranciamycin A (**7.02**) (t_R = 16.1 min, 1.1 mg, 0.7%) and aranciamycin (**7.01**) (t_R = 15.5 min, 1.0 mg, 1%) (Scheme 7.1). A UV-Vis λ_{max} 440 nm common to all of **7.01 – 7.04** (Figure 7.3) was suggestive of a quinone chromophore.

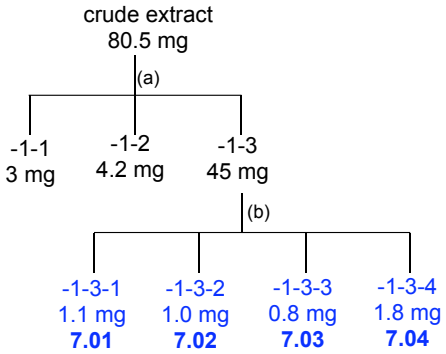

Scheme 7.1. Isolation scheme of the microbial metabolites, **7.01 - 7.04**. (a) Trituration [hexane (-1-1), CH_2Cl_2 (-1-2) and MeOH (-1-3)], (b) Semi-preparative HPLC: Zorbax C_8, 90 – 10% H_2O/MeCN, 3 mL/min, 30 min

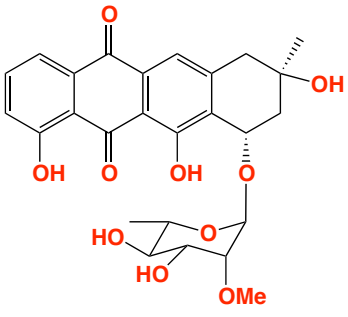

aranciamycin A (**7.01**)

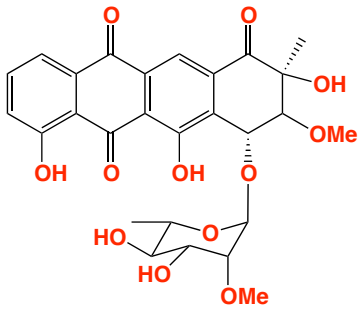

aranciamycin (**7.02**)

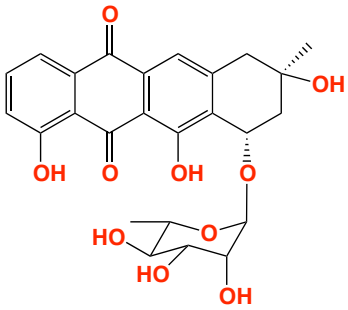

aranciamycin I (**7.03**)

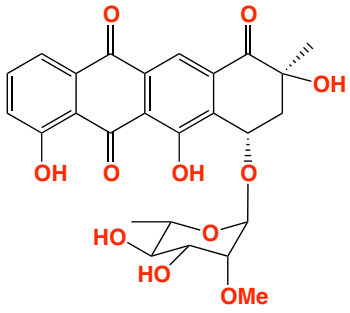

aranciamycin J (**7.04**)

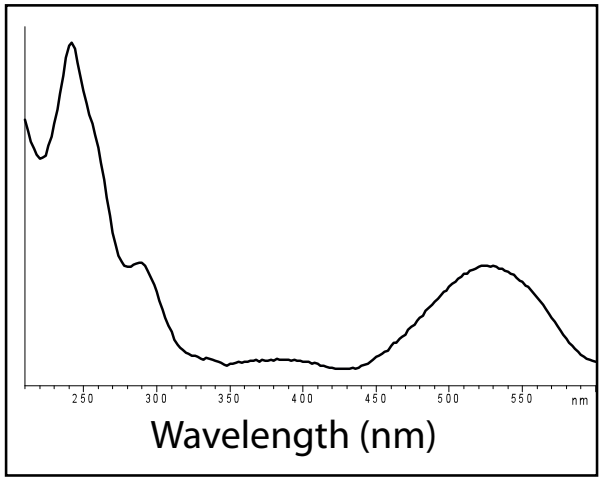

Figure 7.3. UV-vis (DAD) at 254 nm of aranciamycin A (**7.01**)

7.2.2.1 Aranciamycin A (7.01)

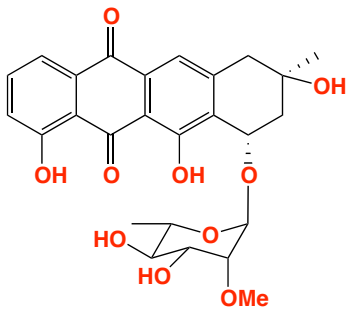

aranciamycin A (**7.01**)

HRESI(+)MS data of **7.01** revealed an adduct ion $(M+Na)^+$ indicative of a molecular formula $C_{26}H_{28}O_{10}$ (Δmmu −0.5). The ^1H NMR (DMSO d_6) data of **7.01** (Figure 7.5 and Table 7.1) revealed resonances attributed to an anthraquinone fragment, with analysis of 2D NMR data (HSQC, COSY and HMBC) as outlined in Figure 7.4. A literature search suggested that **7.01** was the known microbial anthraquinone aranciamycin A,[212] first isolated in 2007 from *S. diastatochromogenes* TE6028 through cloning and expression of aranciamycin gene cluster. To our knowledge, aranciamycin A was identified through spectroscopic analysis and although no optical properties (i.e $[\alpha]_D$) have been reported of **7.01,** our reisolated sample exhibited an $[\alpha]_D$ +119 (*c* 0.10, MeOH)

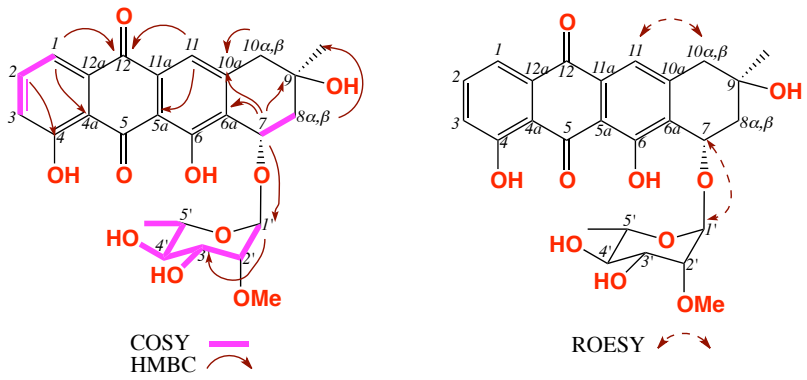

Figure 7.4. Key 2D NMR (600 MHz, DMSO-d_6) correlations of aranciamycin A (**7.01**)

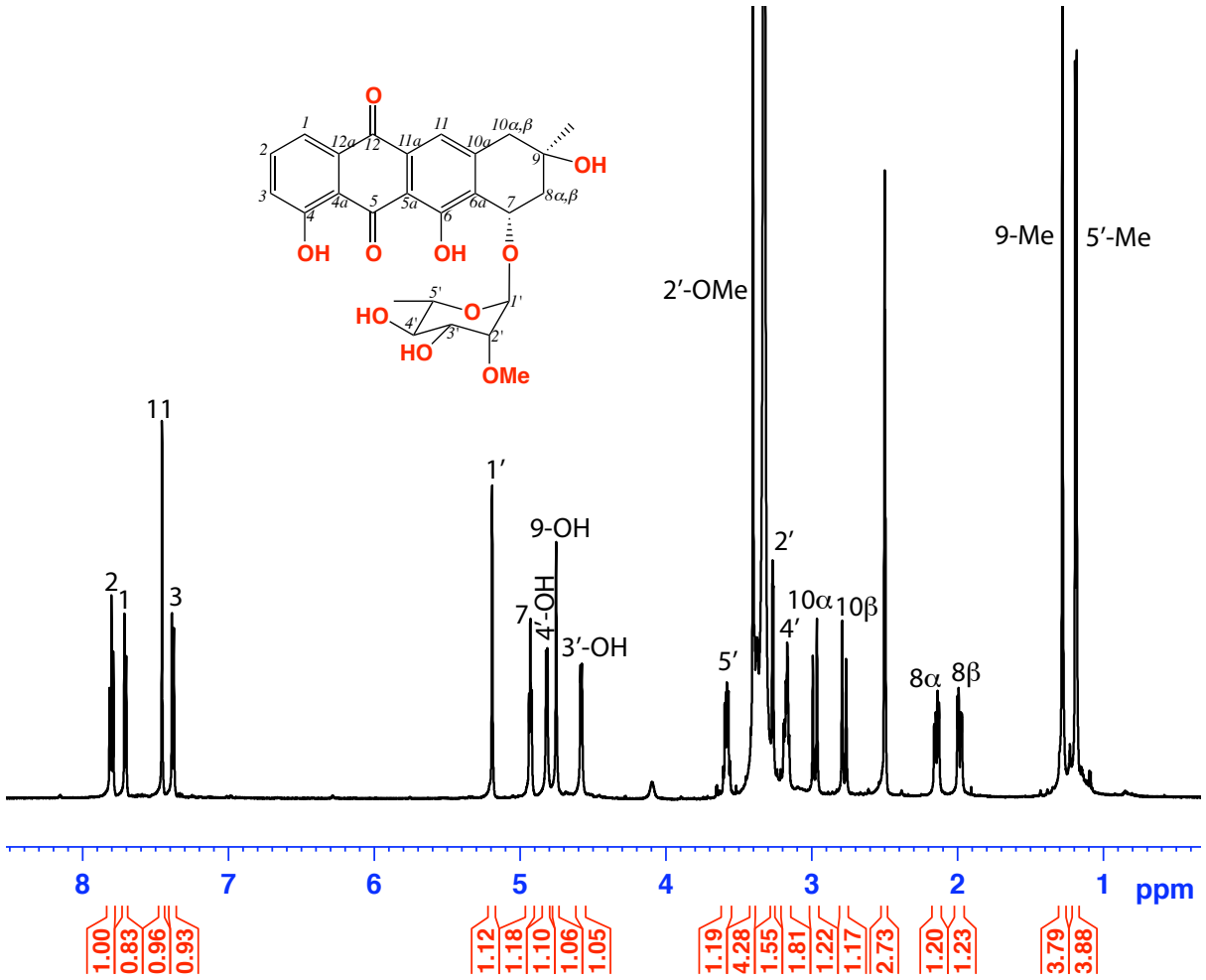

Figure 7.5. ^{1}H NMR (600 MHz, DMSO-d_6) of aranciamycin A (**7.01**)

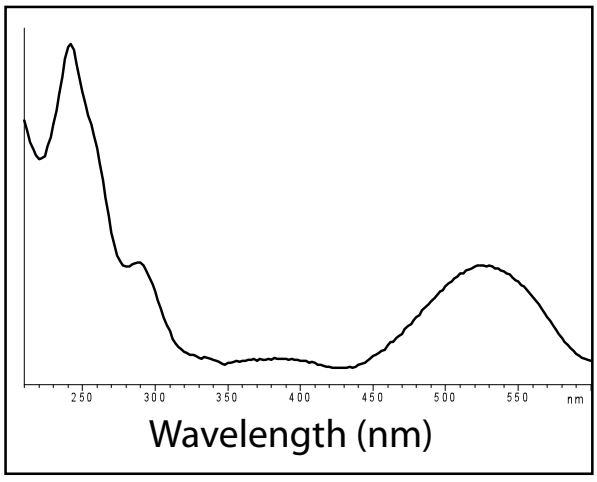

Figure 7.6. UV-vis (DAD) at 254 nm of aranciamycin A (**7.01**)

Table 7.1. NMR (600 MHz, DMSO-d_6) data of aranciamycin A (**7.01**)

Pos	δ_H, mult, (*J* in Hz)	δ_C[a]	COSY	$^1H - ^{13}C$ HMBC	ROESY
1	7.71, d, (*7.8*)	119.1	2	3, 4a, 12	
2	7.80, dd, (*8.0, 8.0*)	136.8	1, 3	4, 12a	
3	7.38, d, (*8.0*)	123.8	2	1, 4a	
4		160.8			
4a		115.7			
5		[b]			
5a		113.4			
6		161.0			
6a		130.9			
7	4.93, dd, (*7.8, 5.5*)	72.2	8α/β	1′, 6, 6a, 9, 10a	1′, 8α/β
8	α 2.14, dd, (*13.8*, *7.8*)	42.7	7, 8β	6, 6a, 9, 9-Me, 10	5′, 7
	β 1.98, dd, (*13.8*, *7.8*)		7, 8α	6a, 7, 9, 10	5′, 7
9		67.0			
10	α 2.98, d, (*16.9*)	44.4	10β	6a, 8, 9, 9-Me, 10a, 11	11
	β 2.78, d, (*16.9*)		10α	6a, 8, 9, 9-Me, 10a, 11	11
10a		146.8			
11	7.45, s	119.6	13	5a, 6a, 10, 12	10α/β
11a		[b]	12		
12		180.9			
12a		132.9			
1′	5.19, s	100.1	2′	2′, 3′, 5′	2′, 7
2′	3.26, m	80.9	1′, 3′	2′-OMe, 3′, 4′	1′
3′	3.38, m	70.2	2′, 3′-OH, 4′		
4′	3.17, m	71.6	3′, 4′-OH, 5′		5′-Me
5′	3.58, m	69.1	4′, 5′-Me	4′	5′-Me 4′-OH, 9-Me
5′-Me	1.18, d, (*6.1*)	17.7	5′	4′, 5′	4′, 5′
9-Me	1.28, s	28.3		8, 9, 10	5′
2′-OMe	3.40, s	57.9		2′	
3′-OH	4.58, d, (*5.6*)		3′	3′, 4′	
4′-OH	4.81, d, (*5.2*)		4′	4′, 5′	5′
9-OH	4.75, s			8, 9, 9-Me, 10	

*(a) assignments supported by HSQC. (b) signals not observed

Table 7.2. NMR and ^{13}C (600 MHz, DMSO-d_6) comparison of experimental and literature[212] data of aranciamycin A (**6.08**)

Pos	δ_H, mult, (*J* in Hz) (experimental)	δ_C[a]	δ_H, mult, (*J* in Hz) (literature)	δ_C[a]
1	7.71, d, (*7.8*)	119.1	7.66, d *(7.7)*	118.9
2	7.80, dd, (*8.0, 7.8*)	136.8	7.75, dd *(8.2, 7.7)*	137.0
3	7.38, d, (*8.0*)	123.8	7.33, d *(8.2)*	124.6
4		160.8		161.6
4a		115.7		116.1
5		[b]		191.4
5a		113.4		113.6
6		161.0		162.0
6a		130.9		131.4
7	4.93, dd, (*6.0, 5.5*)	72.2	4.92, dd *(5.6, 5.1)*	72.5
8	α 2.14, dd, (*13.8*, *7.8*)	42.7	α 2.11, dd *(13.8, 6.1)*	43.1
	β 1.98, dd, (*13.8*, *7.8*)		β 1.97, dd *(13.8, 5.1)*	
9		67.0		67.3
10	α 2.98, d, (*16.9*)	44.4	α 2.94, d *(16.4)*	44.4
	β 2.78, d, (*16.9*)		β 2.75, d *(16.4)*	
10a		146.8		146.7
11	7.45, s	119.6	7.39, s	119.6
11a		[b]		131.8
12		180.9		181.4
12a		132.9		133.4
1′	5.19, s	100.1	5.20, s	100.1
2′	3.26, m	80.9	3.25[a]	80.8
3′	3.38, m	70.2	3.37, m	70.4
4′	3.17, m	71.6	3.17, m	72.0
5′	3.58, m	69.1	3.57, dq *(9.2, 6.1)*	69.3
5′-Me	1.18, d, (*6.1*)	17.7	1.17, d *(6.1)*	17.8
9-Me	1.28, s	28.3	1.27, s	28.4
2′-OMe	3.40, s	57.9	3.39, s	58.4
3′-OH	4.58, d, (*5.6*)		4.51, br d *(5.1)*	
4′-OH	4.81, d, (*5.2*)		4.76, br d *(5.1)*	
9-OH	4.75, s		4.69, br s	

*(a) assignments supported by HSQC. (b) signals not observed

7.2.2.2 Aranciamycin (7.02)

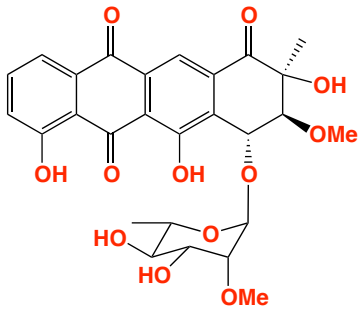

aranciamycin (**7.02**)

HRESI(+)MS data of **7.02** revealed a quasi-molecular ion $(M+H)^+$ indicative of a molecular formula $C_{27}H_{26}O_{12}$ (Δmmu –0.3). The ^1H NMR ($CDCl_3$) data of **7.02** (Figure 7.8 and Table 7.3) were very similar to **7.01** with the exception that **7.02** featured an oxidized C-8 bearing an 8-OMe (δ_H 3.55, δ_C 60.2). The structure elucidation of **7.02** was further supported by 2D NMR data (HSQC, COSY and HMBC) as outlined in Figure 7.7. A literature search suggested that **7.02** was the known microbial metabolite anthraquinone aranciamycin[213,214] first reported in 1970 from *Streptomyces echinatus* [215] then in 1993, Schmidt *et al*., were able to crystalize aranciamycin [216]to confirm the absolute stereochemistry that was reported in 1970. Aranciamycin (**7.02**) was re-isolated again from *Streptomyces* sp. associated with a marine sponge, *Haliclona* sp. This assignment was further confirmed by a measuring the $[\alpha]_D$ +161 (*c* 0.10, MeOH) of **7.02** compared to $[\alpha]^{23}_D$ +140 (*c* 0.1, MeOH) for the reported aranciamycin.[213]

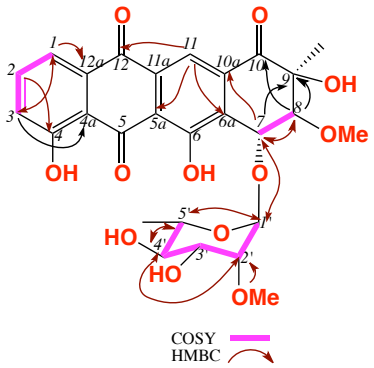

Figure 7.7. Key 2D NMR (600 MHz, DMSO-d_6) correlations of aranciamycin (**7.02**)

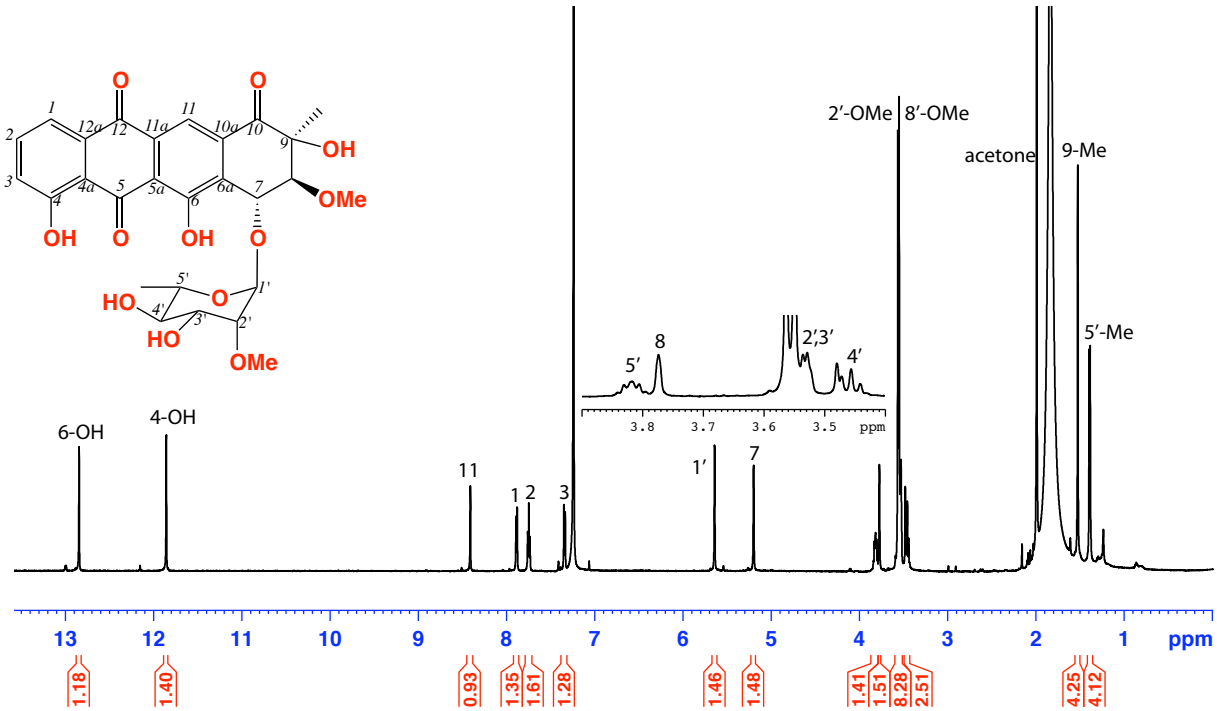

Figure 7.8. ^{1}H NMR (600 MHz, $CDCl_3$) spectrum of aranciamycin (**7.02**)

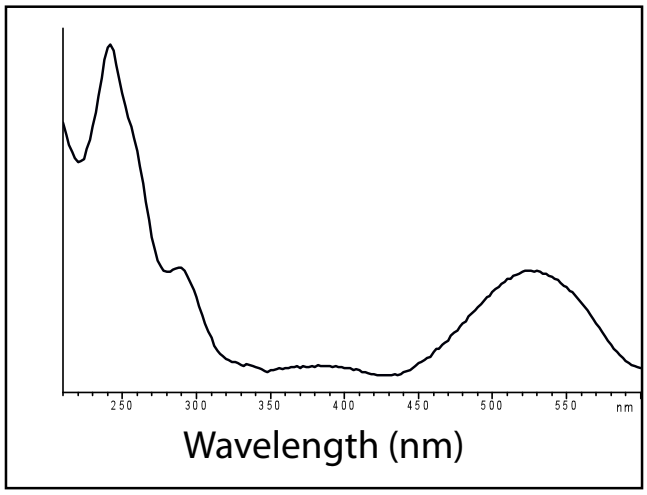

Figure 7.9. UV-vis (DAD) at 254 nm of aranciamycin (**7.02**)

Table 7.3. NMR (600 MHz, $CDCl_3$) data of aranciamycin (**7.02**)

Pos	δ_H, mult, (*J* in Hz)	δ_C[a]	COSY	$^1H - ^{13}C$ HMBC
1	7.88, d *(7.9)*	120.8	2	3, 4a, 12
2	7.74, dd *(8.2, 7.9)*	138.3	1, 3	4, 12a
3	7.34, d *(8.2)*	125.2	2	4a
4		163.1		
4a		115.2		
5		193.1		
5a		118.5		
6		162.6		
6a		133.1		
7	5.20, br s	72.1	8	1′, 6, 6a, 8, 9, 10a
8	3.77, br s	85.6	7	7, 6a, 9, 8-OMe, 10
9		76.6		
10		198.5		
10a		135.9		
11	8.41, s	117.7		5a, 6a, 12
11a		133.4		
12		180.4		
12a		133.5		
1′	5.64, s	100.6		3′, 5′
2′	3.52[b], m	80.1	3′	2′-OMe
3′	3.54[b], m	71.5	2′, 4′	
4′	3.45, dd *(9.7, 6.2)*	73.4	3′, 5′	
5′	3.82, dq *(9.7, 6.2)*	69.5	4′, 5′-Me	
5′-Me	1.39, d *(6.2)*	17.6	5′	
9-Me	1.52, s	22.9		9
2′-OMe	3.56, s	58.9		2′
8-OMe	3.55, s	60.2		8
3′-OH	[c]			
4′-OH	[c]			
4-OH	11.85, s			5a, 6a, 6
6-OH	12.85, s			3, 4a, 4

*(a) assignments supported by HSQC, (b) signals are overlapping, (c) not observed

Table 7.4. NMR (600 MHz, DMSO-d_6) data of aranciamycin (**7.02**)

Pos	δ_H, mult, (*J* in Hz)	δ_C[a]	COSY	$^1H - ^{13}C$ HMBC
1	7.73, d, (*7.3*)	119.2	2	3, 4a, 12
2	7.82, dd, (*8.3*, *7.3*)	137.3	1, 3	4, 12a
3	7.40, d, (*8.3*)	124.4	2	1, 4, 4a
4		161.5		
4a		116.1		
5		[b]		
5a		118.7		
6		161.4		
6a		133.0		
7	5.09, d, (*2.3*)	71.4	8	1′, 6, 6a, 8, 9, 10a
8	3.62, d, (*2.3*)	85.8	7	6a, 7, 8-OMe, 9, 9-Me, 10
9		76.1		
10		198.7	10β	
10a		135.3		
11	8.03, s	114.5	13	5a, 6a, 10, 12
11a		[b]		
12		180.5		
12a		133.0		
1′	5.46, s	100.5	2′	2′, 3′, 5′
2′	3.33, dd, (*3.2*, *1.6*)	80.4	1′, 3′	2′-OMe, 3′, 4′
3′	3.41, m	70.2	2′, 4′	
4′	3.24, ddd, (*9.1*, *9.0*, *6.2*)	71.8	3′, 5′	3′, 5′-Me
5′	3.66, dq, (*9.1*, *6.2*)	70.0	4′, 5′-Me	4′
5′-Me	1.26, d, (*6.2*)	17.6	5′	4′, 5′
9-Me	1.40, s	23.1		8, 9, 10
2′-OMe	3.44, s[a]	58.3		2′
3′-OH	4.71, s		3′	
4′-OH	4.94, d, (*5.6*)		4′	
8-OMe	3.45, s	59.5		8
9-OH	5.68, s		9-Me	8, 9, 9-Me, 10

*(a) assignments supported by HSQC. (b) signals not observed

Table 7.5. NMR (600 MHz, $CDCl_3$) comparison of experimental and literature[213] data of aranciamycin (**7.02**)

Pos.	δ_H, mult, (*J* in Hz) (experimental)	δ_C [a]	δ_H, mult, (*J* in Hz) (literature)	δ_C
1	7.88, d *(7.9)*	120.8	7.90, dd *(8.2, 1.1)*	121.1
2	7.74, dd *(8.2, 7.9)*	138.3	7.76, t *(8.2)*	138.5
3	7.34, d *(8.2)*	125.2	7.36, dd *(8.2, 1.1)*	125.3
4		163.1		163.2
4a		115.2		115.9
5		193.1		193.2
5a		118.5		118.9
6		162.6		162.6
6a		133.1		133.6
7	5.20, br s	72.1	5.23, d *(2.3)*	72.2
8	3.77, br s	85.6	3.79, d *(2.3)*	85.8
9		76.6		77.0
10		198.5		199.1
10a		135.9		136.3
11	8.41, s	117.7	8.42, s	118.0
11a		133.4		133.6
12		180.4		180.7
12a		133.5		133.9
1′	5.64, s	100.6	5.66, d *(1.3)*	100.7
2′	3.52[b], m	80.1	3.53, dd *(3.6, 1.3)*	80.2
3′	3.54[b], m	71.5	3.54, m	71.7
4′	3.45, dd *(9.7, 5.6)*	73.4	3.45, t *(9.6)*	73.6
5′	3.82, dq *(9.7, 6.2)*	69.5	3.83, dq *(9.6, 6.1)*	69.7
5′-Me	1.39, d *(6.2)*	17.6	1.40, d *(6.1)*	178.6
9-Me	1.52, s	22.9	1.53, s	23.1
2′-OMe	3.56, s	58.9	3.56, s	59.1
8-OMe	3.55, s	60.2	3.57, s	60.3
3′-OH	[c]		[c]	
4′-OH	[c]		[c]	
4-OH	11.85, s		11.86, s	
6-OH	12.85, s		12.85, s	

*(a) assignments supported by HSQC. (b) Overlapping resonaces. (c) signals not observed

7.2.2.3 Aranciamycin I (7.03)

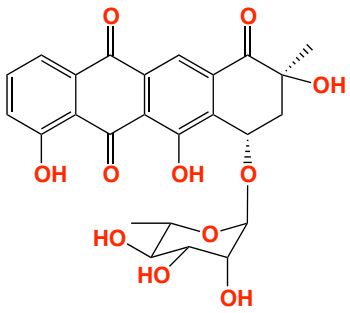

aranciamycin I (**7.03**)

HRESI(+)MS analysis of **7.03** revealed a quasi-molecular ion $(M+H)^+$ indicative of a molecular formula $C_{25}H_{26}O_{10}$ (Δmmu –0.2). The NMR (DMSO-d_6) data (Figure 7.11 and Table 7.6) for **7.03** was very similar to **7.01** and **7.02** (Figure 7.13 and Table 7.7). A comprehensive analysis of the 1D and 2D NMR (DMSO d_6) was supportive of **7.03** being a new member of the aranciamycin structure class, attributed the structure and trivial name aranciamycin I (**7.03**). The absolute configuration of aranciamycin I (**7.03**) was proposed on the basis it is being a co-metabolite with aranciamycin (**7.02**), both of which exhibit similar specific rotations; **7.02**, $[\alpha]_D$ +145 (*c* 0.1, MeOH); **7.03**, $[\alpha]_D$ +139 (*c* 0.1, MeOH). The configuration of the anomeric proton was determined by its small vicinal coupling constant with H-2′ ($J_{1'2'}$ = 1.1 Hz), which is only reasonable for an equatorial position. The orientation of H-4′ (δ_H 3.23) was proven by its large antiperiplanar coupling to H-5′ (δ_H 3.60, m) ($J_{4'5'}$ = 9.3 Hz).

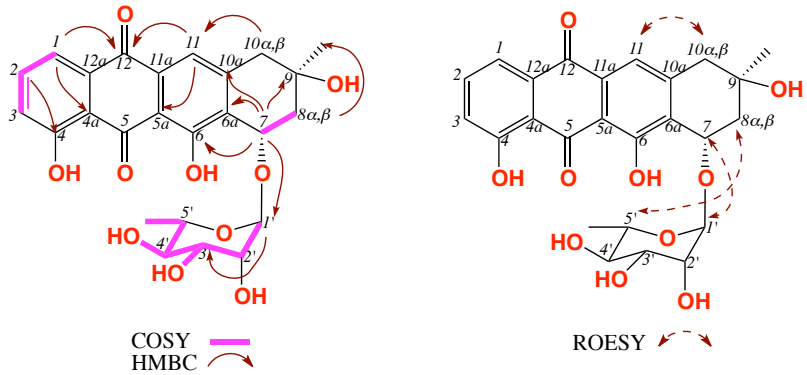

Figure 7.10. Key 2D NMR (600 MHz, DMSO-d_6) correlations of aranciamycin I (**7.03**)

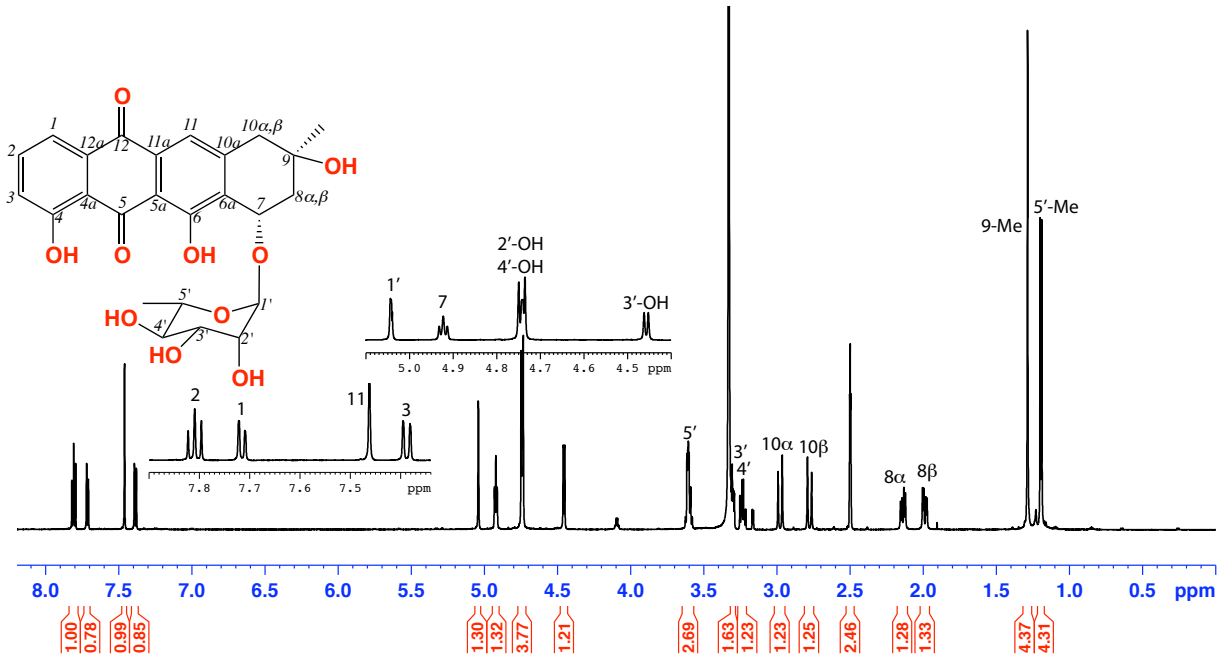

Figure 7.11. ^{1}H NMR (600 MHz, DMSO-d_6) of aranciamycin I **(7.03)**

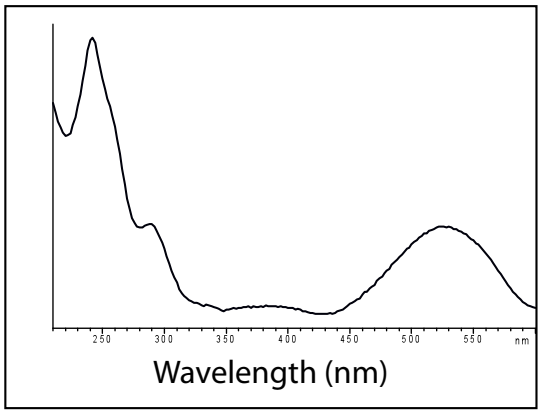

Figure 7.12. UV-vis (DAD) at 254 nm of aranciamycin I **(7.03)**

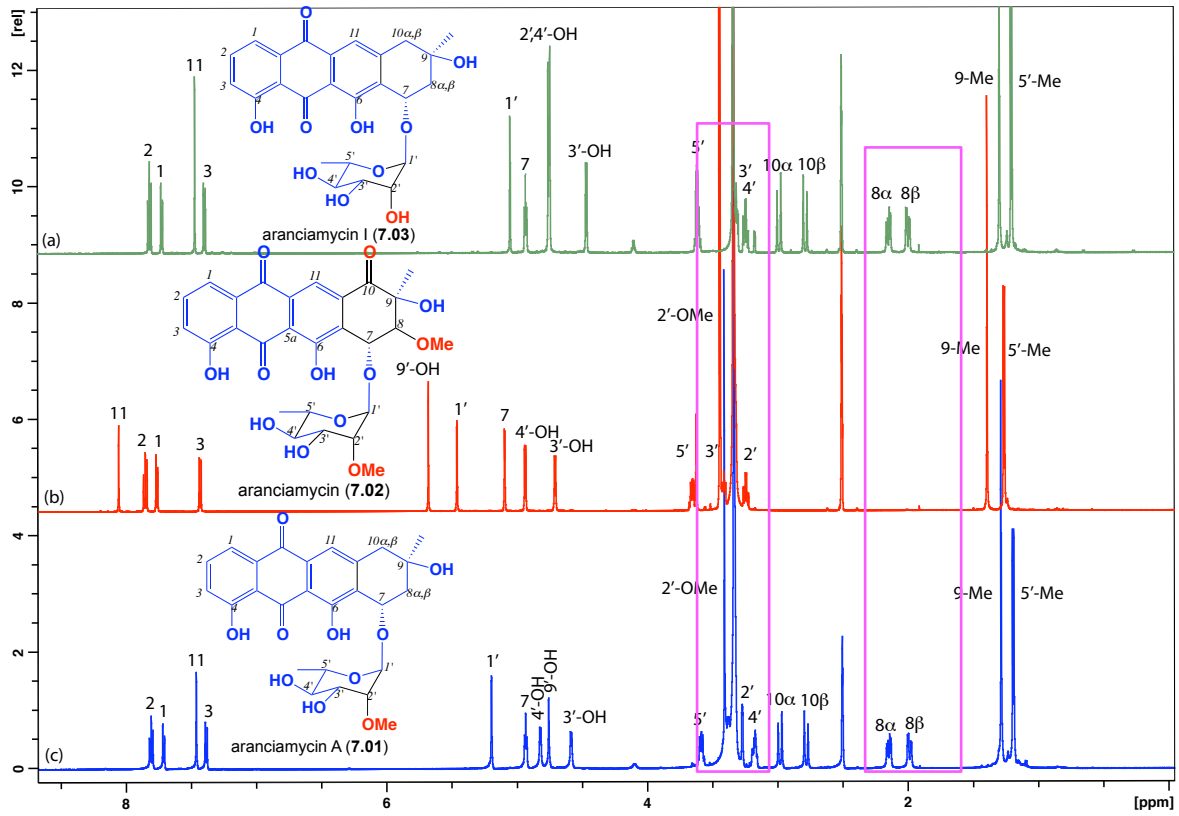

Figure 7.13. ^{1}H NMR (600 MHz, DMSO-d_6) spectra showing the comparisons between (a) **7.03**, (b) aranciamycin (**7.02**) and (c) aranciamycin A (**7.01**)

Table 7.6. NMR (600 MHz, DMSO-d_6) data of aranciamycin I (**7.03**)

Pos	δ_H, mult, (*J* in Hz)	δ_C[a]	COSY	^{1}H – ^{13}C HMBC	ROESY
1	7.71, d, (*7.4*)	119.0	2	3, 4a, 12	
2	7.80, t, (*7.4*)	137.2	1, 3	4, 12a	
3	7.38, d, (*8.6*)	124.1	2	1, 4a	
4		160.9			
4a		115.6			
5		[c]			
5a		113.4			
6		161.0			
6a		130.9			
7	4.92, t *(6.4)*	71.8	8α/β	1′, 6, 6a, 9, 10a	
8	α 2.13, dd, (*13.5*, *6.4*)	42.8	7, 8β	6a, 7, 9-Me, 10a	
	β 1.99, dd, (*13.5*, *6.4*)		7, 8α	6a, 7, 9, 10	5′
9		67.0			
10	α 2.98, d, (*17.4*)	44.1	10β	6a, 8, 9, 9-Me, 10a, 11	11
	β 2.77, d, (*17.4*)	44.1	10α	6a, 8, 9, 9-Me, 10a, 11	11
10a		146.9			
11	7.46, s	119.8	13	5a, 6a, 10, 12	10α/β
11a		[c]			
12		180.9			
12a		132.9			
1′	5.04, d *(1.1)*	103.2	2′	3′, 4′, 5′	
2′	3.61[b], m	70.4	1′, 2′-OH, 3′		
3′	3.30, dd (*9.3*, *5.4*)	70.3	2′, 3′-OH, 4′	4′	
4′	3.23, ddd (*9.3*, *9.3*, *5.4*)	71.5	3′, 4′-OH, 5′	3′, 5′, 5′-Me	
5′	3.60, d *(9.3)*	69.0	4′, 5′-Me		8β
5′-Me	1.19, d (*9.3*)	17.5	5′	4′, 5′	
9-Me	1.28, s	28.4		8, 9, 10	
2′-OH	4.74[b], d (*4.8*)		2′		
3′-OH	4.45, d (*5.8*)		3′	3′	
4′-OH	4.75[b], d (*5.4*)		4′		
9-OH	4.73, s			8, 9, 9-Me, 10	

*(a) assignments supported by HSQC. (b) Overlapping resonances. (c) signals not observed

Table 7.7. NMR (600 MHz, DMSO-d_6) data comparison of aranciamycin I (**7.03**), aranciamycin (**7.02**) and aranciamycin A (**7.01**)

Pos	δ_H, mult, (*J* in Hz) (**7.03**)	δ_C[a]	δ_H, mult, (*J* in Hz) (**7.02**)	δ_C[a]	δ_H, mult, (*J* in Hz) (**7.01**)	δ_C[a]
1	7.71, d, (*7.4*)	119.0	7.73, d, (*7.3*)	119.2	7.71, d, (*7.8*)	119.1
2	7.80, t, (*7.4*)	137.2	7.82, dd, (*8.3*, *7.3*)	137.3	7.80, dd, (*8.0, 8.0*)	136.8
3	7.38, d, (*8.6*)	124.1	7.40, d, (*8.3*)	124.4	7.38, d, (*8.0*)	123.8
4		160.9		161.5		160.8
4a		115.6		116.1		115.7
5		[c]		[c]		[c]
5a		113.4		118.7		113.4
6		161.0		161.4		161.0
6a		130.9		133.0		130.9
7	4.92, t *(6.4)*	71.8	5.09, d, (*2.3*)	71.4	4.93, dd, (*6.0, 5.5*)	72.2
8	α 2.13, dd, (*13.5*, *6.4*)	42.8	3.62, d, (*2.3*)	85.8	2.14, dd, (*13.8*, *6.0*)	42.7
	β 1.99, dd, (*13.5*, *6.4*)				1.98, dd, (*13.8*, *6.0*)	42.7
9		67.0		76.1		67.0
10	α 2.98, d, (*17.4*)	44.1		198.7	2.98, d, (*16.9*)	44.4
	β 2.77, d, (*17.4*)	44.1			2.78, d, (*16.9*)	44.4
10a		146.9		135.3		146.8
11	7.46, s	119.8	8.03, s	114.5	7.45, s	119.6
11a		[c]		[b]		[b]
12		180.9		180.5		180.9
12a		132.9		133.0		132.9
1′	5.04, d *(1.1)*	103.2	5.46, s	100.5	5.19, s	100.1
2′	3.61[b], m	70.4	3.33, dd, (*3.2*, *1.6*)	80.4	3.26, m	80.9
3′	3.30, dd (*9.3*, *5.4*)	70.3	3.41, m	70.2	3.38, m	70.2
4′	3.23, ddd (*9.3*, *9.3*, *5.4*)	71.5	3.24, ddd, (*9.1*, *9.0*, *5.6*)	71.8	3.17, m	71.6
5′	3.60, d *(9.3)*	69.0	3.66, dq, (*9.1*, *6.2*)	70.0	3.58, m	69.1
5′-Me	1.19, d (*9.3*)	17.5	1.26, d, (*6.2*)	17.6	1.18, d, (*6.1*)	17.7
9-Me	1.28, s	28.4	1.40, s	23.1	1.28, s	28.3
2′-OH	4.74[b], d (*4.8*)		3.44, s[a]	58.3	3.40, s	57.9
3′-OH	4.45, d (*5.8*)		4.71, s		4.58, d, (*5.6*)	
4′-OH	4.75[b], d (*5.4*)		4.94, d, (*5.6*)		4.81, d, (*5.2*)	
8-OMe	4.73, s		3.45, s	59.5		
9-OH	7.71, d, (*7.4*)		5.68, s		4.75, s	

*(a) assignments supported by HSQC. (b) Overlapping resonances. (c) signals not observed

7.2.2.4 Arancimaycin J (7.04)

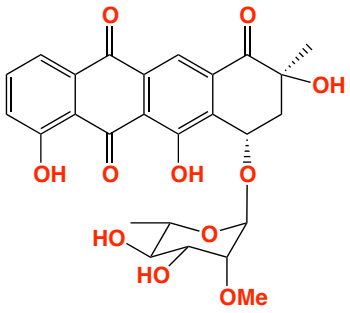

aranciamycin J (**7.04**)

HRESI(+)MS analysis of **7.04** revealed a quasi-molecular ion $(M+H)^+$ indicative of a molecular formula $C_{26}H_{26}O_{11}$(Δmmu −0.3). The ^{1}H NMR (DMSO-d_6) data of **7.04** were very similar that recorded for aranciamycin (**7.02**), with the only significant difference being the absence of 8-OMe moiety and the appearance of an H_2-8 methylene. A comprehensive analysis of the 1D and 2D NMR (DMSO d_6) was supportive of **7.04** being a new member of the aranciamycin structure class, attributed the structure and trivial name aranciamycin J (**7.04**) The absolute configuration of aranciamycin J (**7.04**) was proposed on the basis it is being a co-metabolite with aranciamycin (**7.02**), both of which exhibit similar specific rotations; **7.02**, $[\alpha]_D$ +145 (*c* 0.1, MeOH); **7.04**, $[\alpha]_D$ +136 (*c* 0.1, MeOH), establishing the 7*R*, 8*S*, 9*S* configuration in addition to the sugar component 2-*O*-methyl-α-L-rhamnose.[216]

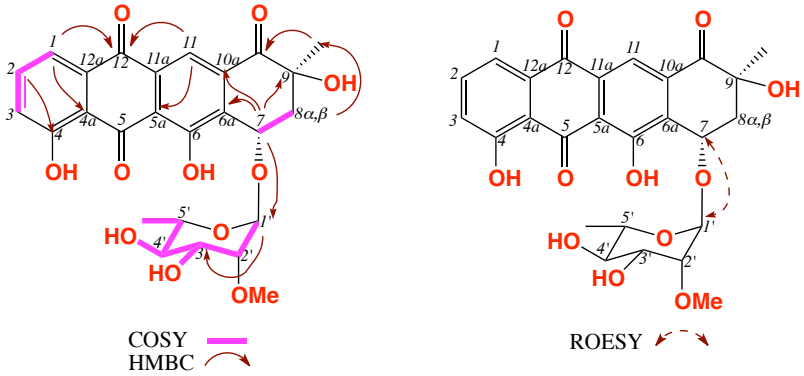

Figure 7.14. Key 2D NMR (600 MHz, DMSO-d_6) correlations of aranciamycin J (**7.04**)

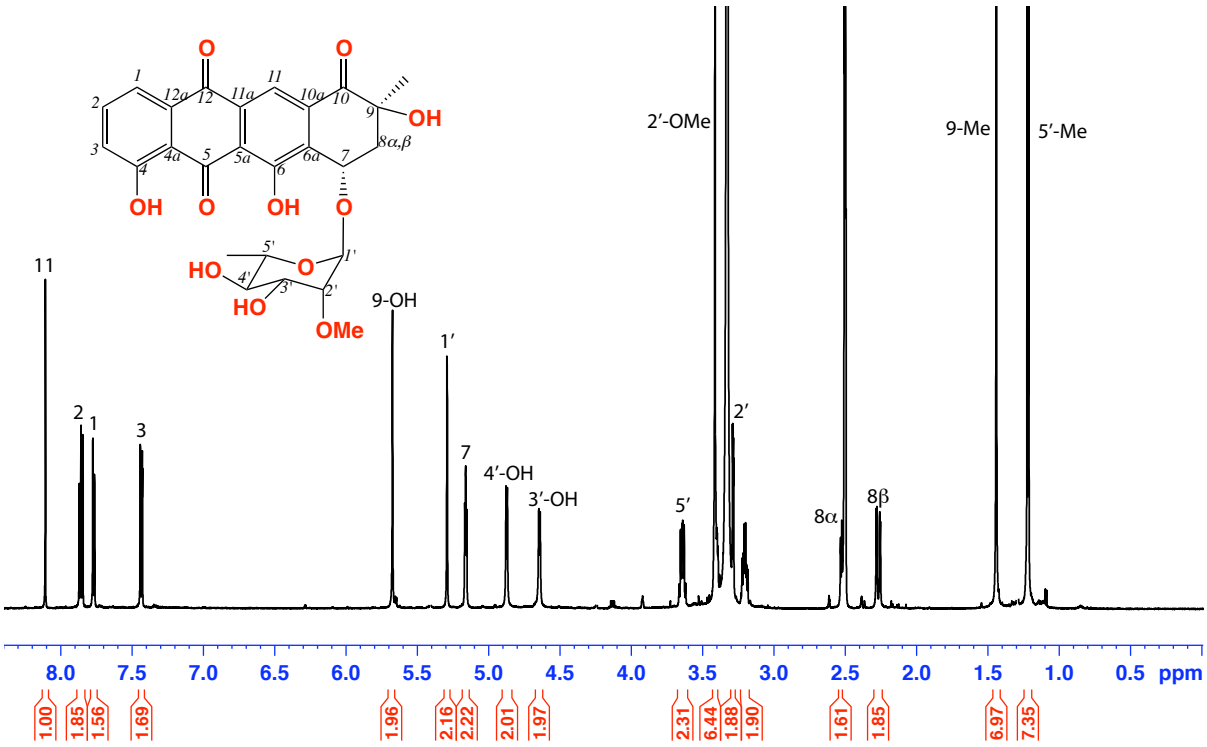

Figure 7.15. ^{1}H NMR (600 MHz, DMSO-d_6) of aranciamycin J (**7.04**)

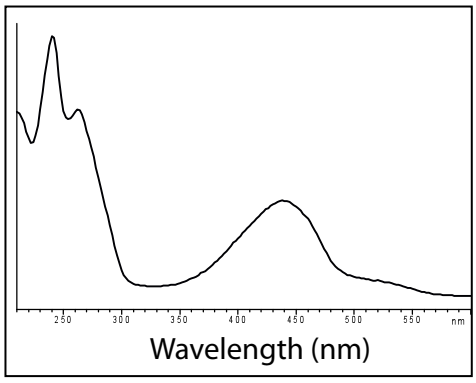

Figure 7.16. UV-vis (DAD) at 254 nm of aranciamycin J **(7.04)**

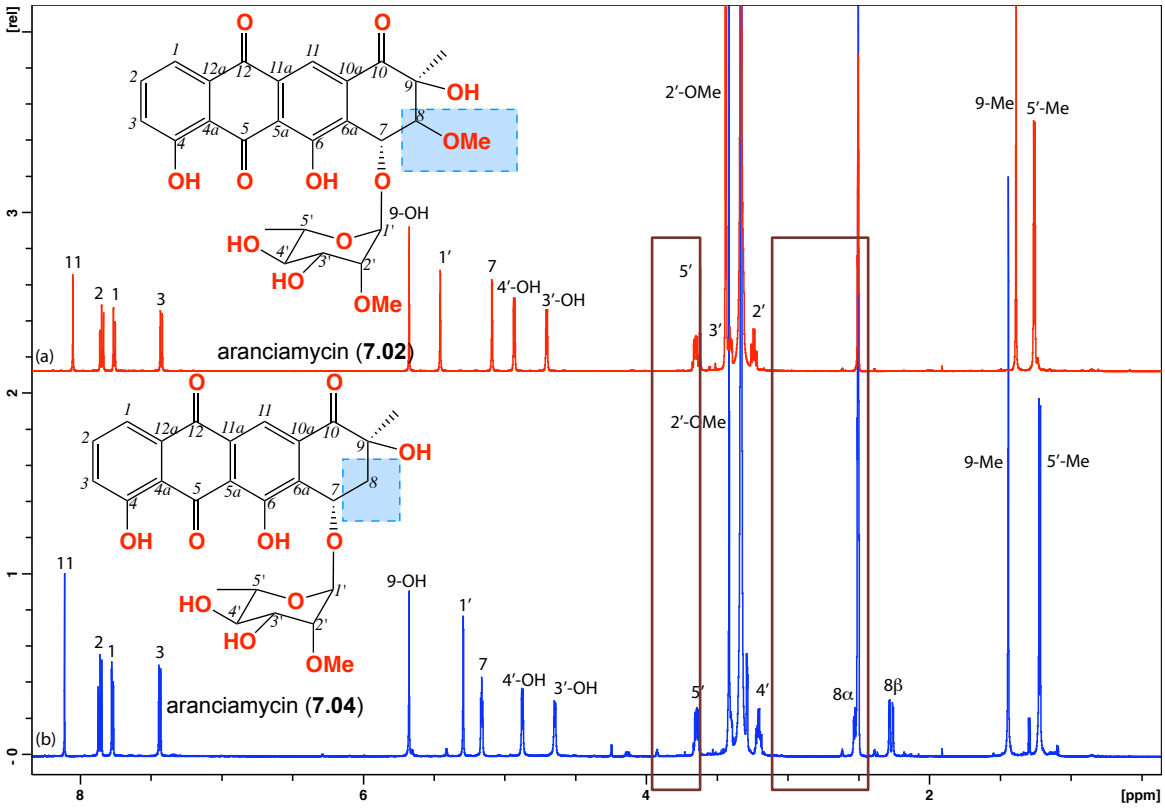

Figure 7.17. ^{1}H NMR (600 MHz, DMSO-d_6) comparison of aranciamycian J (**7.04**) in blue and aranciamycin (**7.02**) in red. The spectra highlights the replacement of OMe with H-8 methylene

Table 7.8. NMR (600 MHz, DMSO-d_6) data of aranciamycin J (**7.04**)

Pos	δ_H, mult, (*J* in Hz)	δ_C[a]	COSY	^{1}H – ^{13}C HMBC	ROESY
1	7.76, dd (*7.5*, *1.1*)	120.0	2	3, 4a, 12	
2	7.85, dd (*8.3*, *7.5*)	138.2	1, 3	4, 12a	
3	7.43, dd (*8.3*, *1.1*)	125.1	2	1, 4, 4a	
4		161.8			
4a		116.8			
5		[c]			
5a		118.9			
6		[c]			
6a		136.4			
7	5.16, dd (*5.3*, *3.5*)	70.2	8α/β	1′, 9	8α/β
8	α 2.52, d *(5.3)*	41.8	7, 8β	9, 9-Me, 10	7
	β 2.26, dd (*14.6*, *5.3*)		7, 8α	6a, 9, 10	5′, 7
9		72.5			
10		199.7			11
10a		[c]			
11	8.10, s	116.2	13	5a, 6a, 10, 12	9-Me
11a		[c]			
12		181.2			
12a		133.9			
1′	5.29, d, (*1.4*)	100.7	2′	2′, 5′	
2′	3.28, dd, (*3.2*, *1.4*)	81.2	1′, 3′	2′-OMe, 3′, 4′	
3′	3.40, m[b]	70.9	2′, 3′-OH, 4′		
4′	3.20, ddd, (*9.6*, *9.4*, *6.2*)	72.4	3′, 4′-OH, 5′		
5′	3.64, dq, (*9.6*, *6.2*)	70.1	4′, 5′-Me	4′	8β
5′-Me	1.21, d, (*6.2*)	18.3	5′	4′, 5′	
9-Me	1.43, s	26.0		8, 9, 10	
2′-OMe	3.41, s	58.9		2′	
3′-OH	4.64, d, (*5.8*)		3′		9-OH
4′-OH	4.87, d, (*5.8*)		4′		9-OH
9-OH	5.67, s			8, 9, 9-Me	3′-OH, 4′-OH

*(a) assignments supported by HSQC. (b) Overlapping resoances. (c) signals not observed

Table 7.9. NMR (600 MHz, DMSO-d_6) data comparison of aranciamycin J (**7.04**) and aranciamycin (**7.02**)

Pos	δ_H, mult, (*J* in Hz) (**7.04**)	δ_C[a]	δ_H, mult, (*J* in Hz) (**7.02**)	δ_C[a]
1	7.76, dd (*7.5*, *1.1*)	120.0	7.73, d, (*7.3*)	119.2
2	7.85, dd (*8.3*, *7.5*)	138.2	7.82, dd, (*8.3*, *7.3*)	137.3
3	7.43, dd (*8.3*, *1.1*)	125.1	7.40, d, (*8.3*)	124.4
4		161.8		161.5
4a		116.8		116.1
5		[c]		[c]
5a		118.9		118.7
6		[c]		161.4
6a		136.4		133.0
7	5.16, dd (*5.3*, *3.5*)	70.2	5.09, d, (*2.3*)	71.4
8	α 2.52, d *(5.3)*	41.8	3.62, d, (*2.3*)	85.8
	β 2.26, dd (*14.6*, *5.3*)			
9		72.5		76.1
10		199.7		198.7
10a		[c]		135.3
11	8.10, s	116.2	8.03, s	114.5
11a		[c]		[b]
12		181.2		180.5
12a		133.9		133.0
1′	5.29, d, (*1.4*)	100.7	5.46, s	100.5
2′	3.28, dd, (*3.2*, *1.4*)	81.2	3.33, dd, (*3.2*, *1.6*)	80.4
3′	3.40[b], m	70.9	3.41, m	70.2
4′	3.20, ddd, (*9.4*, *9.4*, *6.2*)	72.4	3.24, ddd, (*9.1*, *9.0*, *6.2*)	71.8
5′	3.64, dq, (*9.4*, *6.2*)	70.1	3.66, dq, (*9.1*, *6.2*)	70.0
5′-Me	1.21, d, (*6.2*)	18.3	1.26, d, (*6.2*)	17.6
9-Me	1.43, s	26.0	1.40, s	23.1
2′-OMe	3.41, s	58.9	3.44, s	58.3
3′-OH	4.64, d, (*5.8*)		4.71, s	
4′-OH	4.87, d, (*5.8*)		4.94, d, (*5.6*)	
8-OMe			3.45, s	59.5
9-OH	5.67, s		5.68, s	

*(a) assignments supported by HSQC. (b) Overlapping resonances. (c) signals not observed

7.2.3 Antimicrobial assay

Arancimycins (**7.01** – **7.04**) were screened against different Gram-negative and Gram-positive bacteria (see General experimental part) and they showed inhibitory effect against *B. subtilis* (ATCC 6051 and 6633) (Figure 7.18 and Table 7.10).

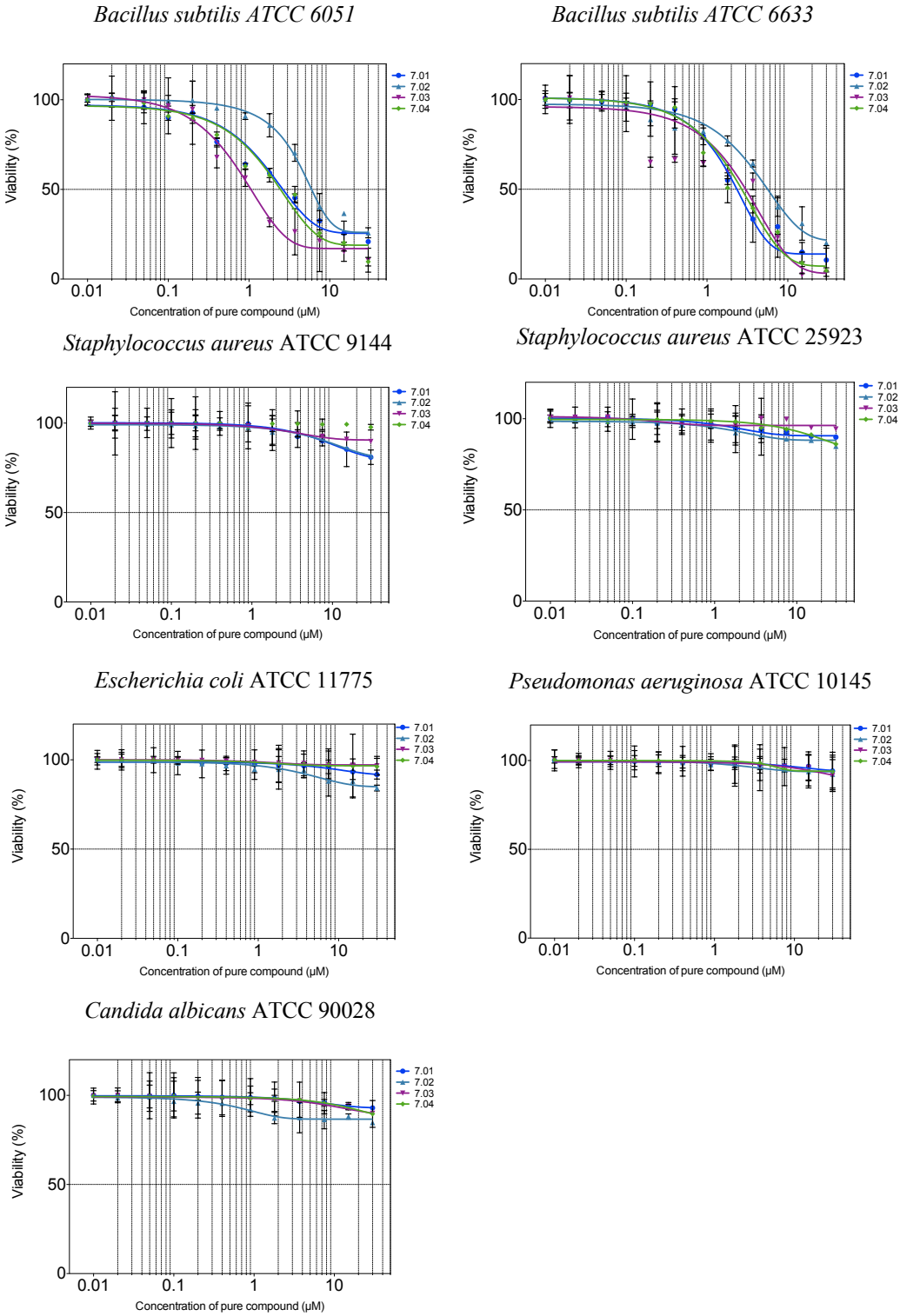

Figure 7.18. Antimicrobial assay of aranciamycins (**7.01** – **7.04**)

Table 7.10. Antibacterial and antifungal screening results of aranciamycins (**7.01** – **7.04**)

	***Escherichia coli* ATCC 11775**		***Pseudomonas aeruginosa* ATCC 10145**		***Bacillus subtilis* ATCC 6051**		***Bacillus subtilis* ATCC 6633**	
Compounds	**MIC (μM)**	**IC_{50} (μM)**	**MIC (μM)**	**IC_{50} (μM)**	**MIC (μM)**	**IC_{50} (μM)**	**MIC (μM)**	**IC_{50} (μM)**
Aranciamycin A (**7.01**)	--	--	--	--	7.1	2.3	7.0	2.0
Aranciamycin (**7.02**)	--	--	--	--	7.0	2.2	6.5	2.0
Aranciamycin I (**7.03**)	--	--	--	--	3.5	1.5	7.5	3.1
Aranciamycin J (**7.04**)	--	--	--	--	7.0	2.0	3.7	2.5

7.3 Conclusion for the aranciamycins

Aranciamycins belong to the anthracycline group of microbial natural products. Anthracyclines have contributed as effective antitumor drugs such as doxorubicin and danunorubicin, as well as antibiotics such as tetracycline and tigecycline. The known auranciamycins illustrated in Figure 7.19 are uniquely isolated from *Streptomyces* sp.[216 217] showed a potent antibacterial activity.
Most there great antitumor activity, many side effects are observed during the treatment. In order to overcome this problem, combinatorial biosynthesis where found to be the most promising tool to overcome the toxicity and increase the effectivety. Therefore, new arancimycin analogs have been generated by combinatorial biosynthesis to give the next generation of different aranciamycins analogues (**7.05** – **7.13**) through the expression of the aranciamycin biosynthetic gene cluster in *Streptomyces diastatochromogenes* Tü6028.[217] Also, it was found that aranciamycin analogues (**7.08** – **7.13**) inhibits collagenase, the metalloprotease that cleaves collagen, and plays an important role in the organism by connecting its connective tissue.[214] Then synthetic studies were directed at the synthesis of aranciamycinone and its analogues (**7.05** – **7.07**)[218](Figure 7.19).

In our study, aranciamyins **7.01** – **7.04** were isolated from marine derived Streptomyces sp. (CMB-M0448) including two new aranciamycins (**7.03** and **7.04**) providing an excellent opportunity for antibiotic SAR analysis. In the event, this analysis revealed significant antibacterial SAR tolerance for C-10 methyelene; C-8 methoxy versus methyelen, and C-2′ hydroxyl versus methoxy. By screening these metabolites in our in house antibacterial activity and they showed antibacterial effect against *B. subtilis* (ATCC 6051 and 6633) (IC_{50} = 3.5 μM)

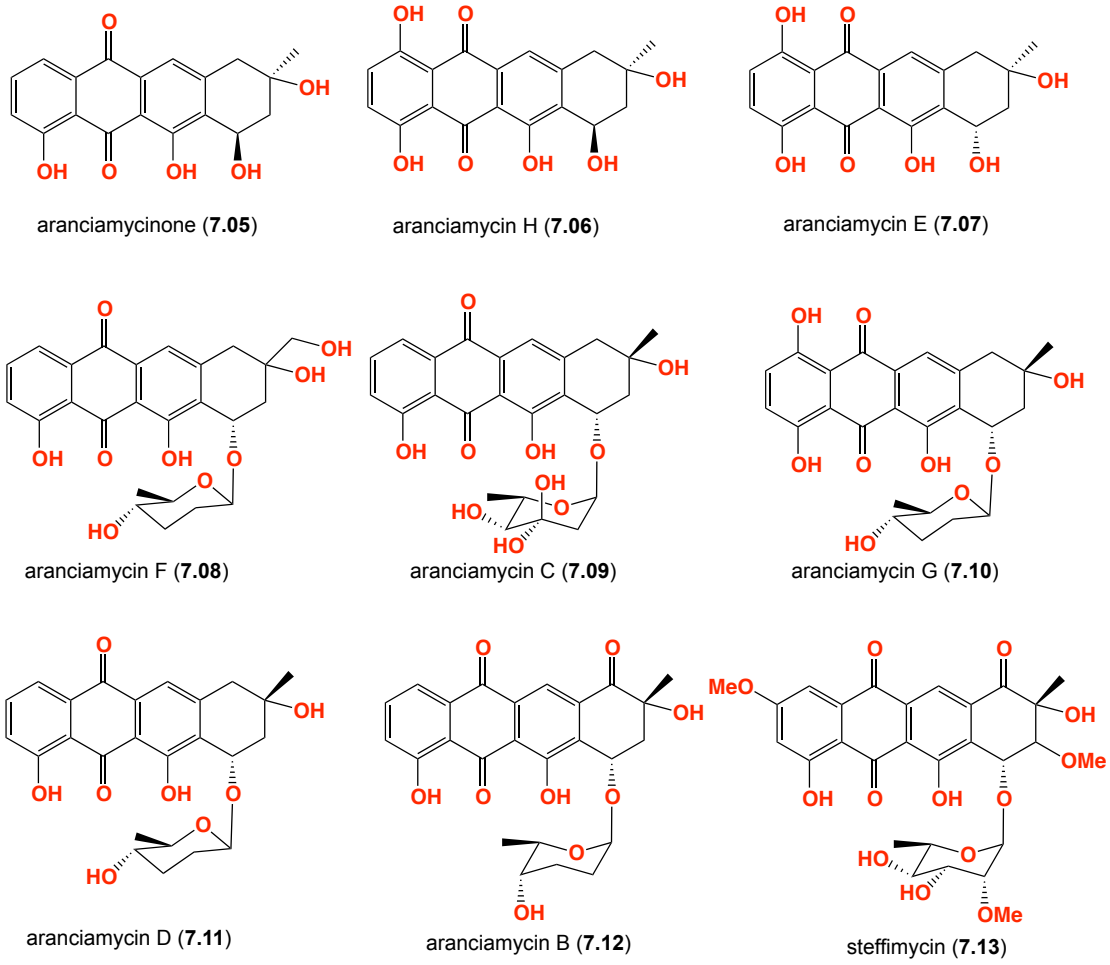

Figure 7.19. Aranciamycins structures

7.4 Experimental section

7.4.1 Analytical cultivation and chemical analysis

A single colony of CMB-M448 was sub-sampled into seawater medium of Ocean Nature seawater (80 mL, 3.3%), starch (1%), yeast extract (0.4%) and peptone (0.2%) and incubated at 27 °C for 10 d at 190 rpm. The culture was extracted with EtOAc (100 mL), and the organic phase concentrated *in vacuo* to yield an extract (12.7 mg) that was subsequently analysed by HPLC-DAD-MS with conditions set as follows (Zorbax C_8 column, 150 × 4.6 mm, 5 μm, 1 mL/min, gradient from 90 – 10 % H_2O/MeCN, with an isocratic 0.05% formic acid modifier, over 15 min, with a hold at 100% MeCN for 5 min). Peaks with the following retention times t_R = 8.1, 8.4, 6.8 and 6.9 min exhibited the following *m*/*z* $[M–H]^-$ 499 (**7.01**), 543 (**7.02**), 485 (**7.03**) and 513 (**7.04**)

7.4.2 Preparative cultivation

A seed culture was prepared by inoculating *Streptomyces* sp. (CMB-M448) in liquid M1 media (50 mL) containing 1% starch, 0.4% yeast extract, 0.2% peptone and Ocean Nature seasalt (3.3%). Aliquots of the seed culture (5 mL) were transferred to six 3 L Fernbach flasks, each containing the same M1 liquid media (500 mL), and the flasks were shaken at 190 rpm for 10 d at 27 °C. The resulting cultures were extracted with EtOAc (400 mL) and the combined organic phase concentrated *in vacuo* to yield an extract (80.5 mg). The extract was sequentially triturated with hexane (8 mL), CH_2Cl_2 (8 mL) and MeOH (8 mL) to afford, after concentration *in vacuo*, 3, 4.2 and 45 mgs respectively. The MeOH fraction, rich in the target metabolites **7.01 – 7.04**, was subjected to semi-preparative reversed-phase HPLC (Zorbax C_8 column, 250 × 9.4 mm, 5 μm, 3 mL/min gradient elution 90 – 10% H_2O/MeCN over 30 min) to yield aranciamycin I (**7.03**) (t_R = 11.8 min, 0.8 mg, 0.8%), aranciamycin J (**7.04**) (t_R = 12.2 min, 1.8 mg, 0.8%), aranciamycin A (**7.02**) (t_R = 16.1 min, 1.1 mg, 0.7%) and aranciamycin (**7.01**) (t_R = 15.5 min, 1.0 mg, 1%).

Aranciamycin A (**7.01**); Orange solid; $[\alpha]_D$ +119 (*c* 0.10, MeOH); UV (MeOH) λ_{max} (log ε) 228 (4.28), 258 (4.10), 289 (3.70), 432 (3.78); NMR (600 MHz, DMSO-d_6) see Table 7.1; HRESI(+)MS *m*/*z* 523.1580 (calcd for $C_{26}H_{28}O_{10}Na$, 523.1575).

Aranciamycin (**7.02**): Orange solid; $[\alpha]_D$ +161 (*c* 0.13, MeOH); UV (MeOH) λ_{max} (log ε) 237 (4.39), 260 (4.21), 435 (3.84); NMR (600 MHz, $CDCl_3$) see Table 7.3; HRESI(+)MS *m*/*z* 567.1476 (calcd for $C_{27}H_{28}O_{12}Na$, 567.1473).

Aranciamycin I (**7.03**): Orange solid; $[\alpha]_D$ +139 (*c* 0.10, MeOH); UV (MeOH) λ_{max} (log ε) 228 (4.37), 258 (4.18), 432 (3.86); NMR (600 MHz, DMSO-d_6) see Table 7.6; HRESI(+)MS *m*/*z* 509.1421 (calcd for $C_{25}H_{26}O_{10}Na$, 509.1418)

Aranciamycin J (**7.04**): Orange solid; $[\alpha]_D$ +150 (*c* 0.10, MeOH); UV (MeOH) λ_{max} (log ε) 240 (4.32), 261 (4.15), 435 (3.87); NMR (600 MHz, DMSO-d_6) see Table 7.8; HRESI(+)MS *m*/*z* 537.1368 (calcd for $C_{26}H_{26}O_{11}Na$, 537.1367).

8 Chapter 8. Citrinaline X and the importance of physicochemical characterization

8.1 Introduction

Natural products containing nitro groups have been isolated from different plants, fungi, bacteria and mammals. These compounds exhibit structural diversity and a wide range of biological activities, including antibiotic, antitumor as well as cell signalling properties.[219] There are different biosynthetic pathways leading to the incorporation of nitro groups such as, direct nitration, as demonstrated for the nitroaromatics pyrrolnitrin and aureothin, the sugar D-rubranitrose, and the antibiotic pyrrolomycins antibiotics (**8.01** – **8.09**) produced by *Pseudomonas* sp. and *Myxococcus fulvus*[220,221] as shown in Figure 8.1 and the gene cluster *prnD* responsible for utilizing molecular oxygen as a co-substrate, leading to oxidation of the aryl amino group to a nitro through an aryl hydroxylamine and aryl nitroso species.[222] Aureothin and its analogues (**8.10** – **8.14**) (Figure 8.2) isolated from *Streptomyces luteoreticuli* and *Streptomyces griseus* were assembled by polyketide synthase (PKS) in which the gene cluster *aurF* encodes for a monooxygenase that utilizes molecular oxygen to catalyse the oxidation of 4-aminobenzoic acid to 4-nitrobenzoic acid, as a polyketide starter unit.[223]

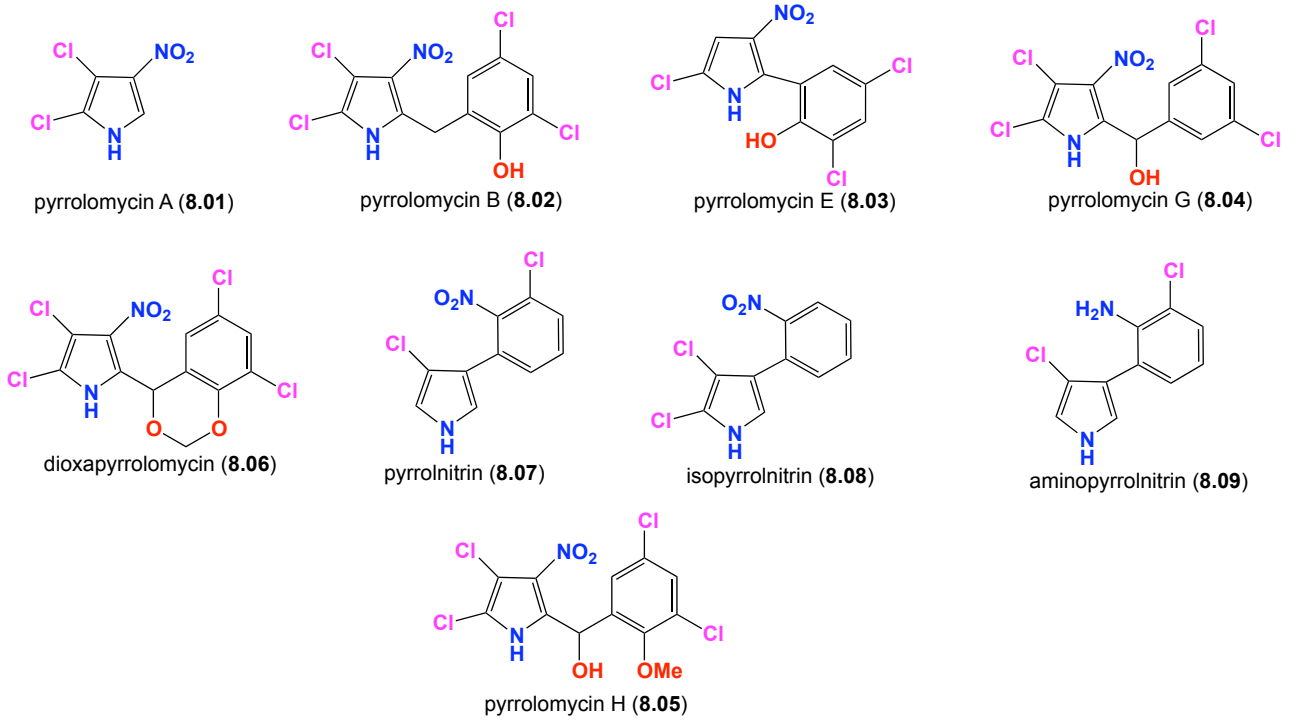

Figure 8.1. Structures of pyrrolomycin analogues

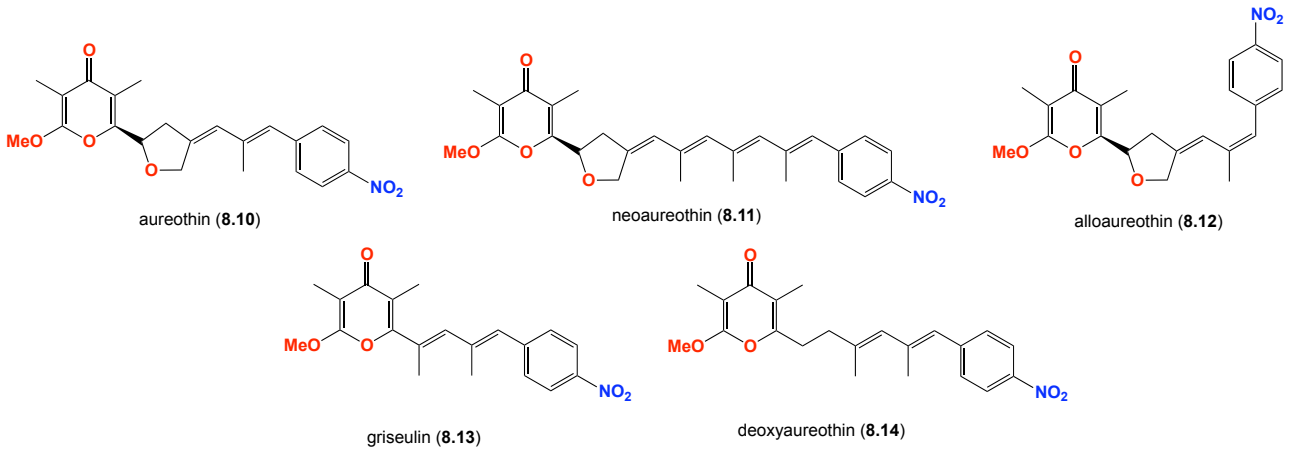

Figure 8.2. Structures of aureothin derivatives

Fungi have proved to be an important source of bioactive and structurally diverse natural products. The first known paraherquamides A (**8.15**) was isolated in 1980 from *Penicillium paraherquei*, [224] since then several analogues of the paraherquamides family characteristic with oxindole moiety as potent anthelmintics have been isolated from other *Penicillium* sp. For example, in 1981 Yamazaki *et al.,* isolated paraherquamides B-G (**8.16** – **8.22**) with a characteristic oxindole moiety as potent anthelmintics (Figure 8.3).[225] In 1990, Ostlind *et al.* expanded on the anthelmintic properties of paraherquamide against *Trichostrongylus cloubriformis*.[226] Most recently a semi-synthetic paraherquamide, 2-deoxy-paraherquamide (derquantel) (**8.23**), was marketed by Pfizer Animal Health as a new generation animal health anthelmintic which induces paralysis by acting as selective and competitive cholinergic antagonists.[227]

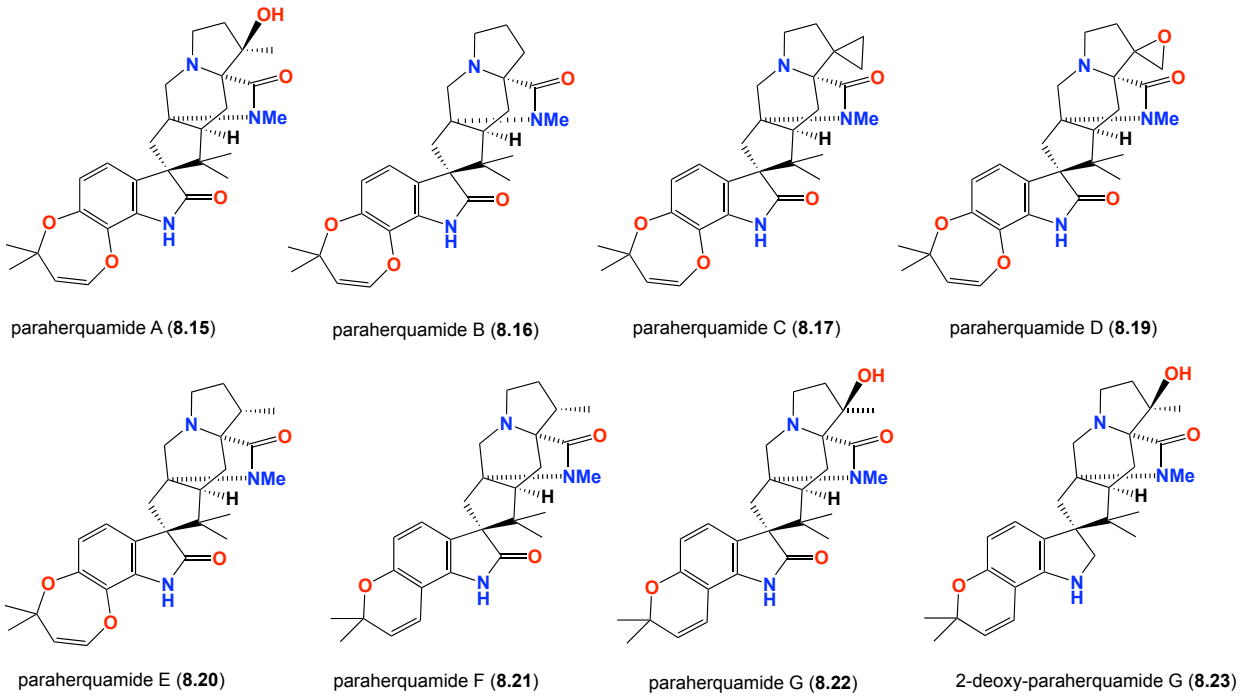

Figure 8.3. Structures of the paraherquamides derivatives

The paraherquamides are closely related to the marcfortines (**8.24**)[228] and brevianamides (**8.25**) from various *Penicillium* sp. In 2002, Qian *et al*., isolated closely related antitumor agents, stephacidin A (**8.26**), and avrainvillamide (**8.27**)[229] from *Aspergillus* sp. (Figure 8.4).

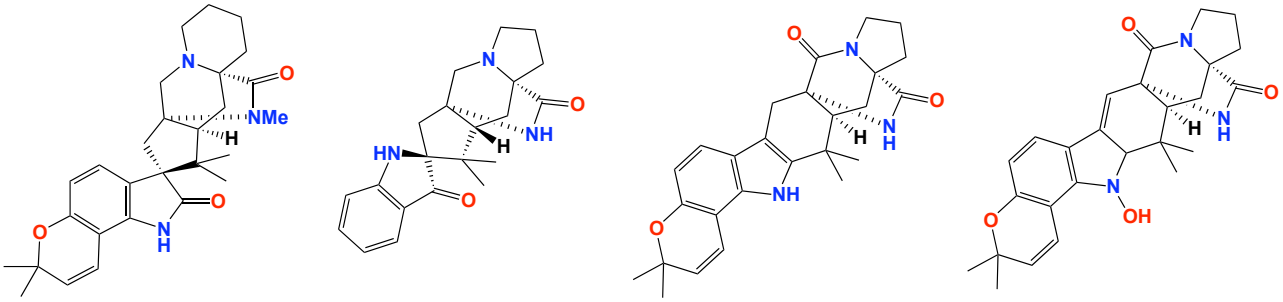

Figure 8.4. Structures of marcfortine A, brevianamide B, stephacidin A and avrainvillamide

Recently, Pimenta *et al*.[230] using an innovative procedure to optimize cultivation conditions that enhanced secondary metabolite production, isolated the new nitro diketopiperazines analogue citrinalines A (**8.28**) and B (**8.29**) from *Penicillium citrinum*.

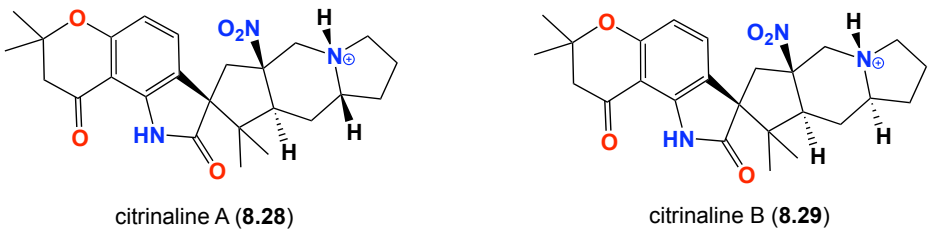

This chapter describes our further contribution to the citrinalines structure class, including citrinaline X. In the course of investigating the citrinalines we had cause to examine their likely biosynthesis and explore stereochemical intricacies, leading to a rearrangement of the structure for citrinaline B (**8.29**).

8.2 Results and discussion

8.2.1 Isolation and taxonomy

Penicillium sp. (CMB-TF438) was isolated from a terrestrial soil sample collected from North Stradbroke Island. The soil sample was added to sterile buffer solution (10 mL), shaken vigorously and heat shocked at 55 ˚C for 8 min. An aliquot of the supernatant (50 μL) was dispersed across a solid phase agar isolation plate (ISP-2 media) and incubated at 27 ˚C for 2 – 6 weeks. The plate was monitored on a regular basis for microbial growth. A pure culture was obtained for strain CMB-TF438 by repeated, single colony transfer on solid media. The 16S rRNA gene sequence (Appendix) showed 96% homology with other members of the genus *Penicillium* by the use of the BLAST database.

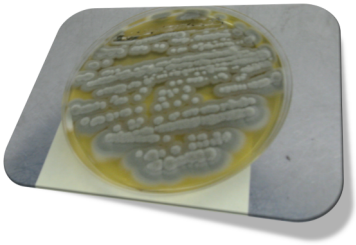

Figure 8.5. *Pencillium* sp. (CMB-TF438)

8.2.2 Analytical cultivation and chemical analysis

A single colony of *Penicillium* sp. (CMB-TF438) was used to inoculate a seed culture on ISP-2 agar media, which was cultivated for a period of 10 days at 26 °C. After incubation the agar was sliced and soaked in 75% EtOAc:MeOH (50 mL) for 1 h. and the decanted organic crude extract dried *in vacuo* to yield a crude extract (10.2 mg) which was resuspended in MeOH (1 mg/mL) and analysed by HPLC-DAD-MS. The analysis revealed peaks attributed to the new metabolite (t_R = 7.8 min, *m/z* 453 $(M-H)^-$, **8.30**) and the very well known citrinin (t_R = 9.1 min, *m/z* 254 (M+H), **8.31**) (Figure 8.6). *Noting the presence of other isomers of citrinaline X (**8.30**).

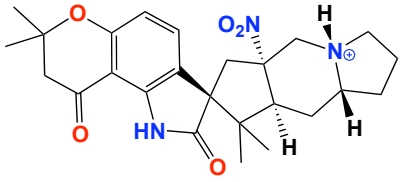

citrinaline X (**8.30**)

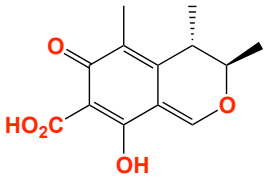

citrinin (**8.31**)

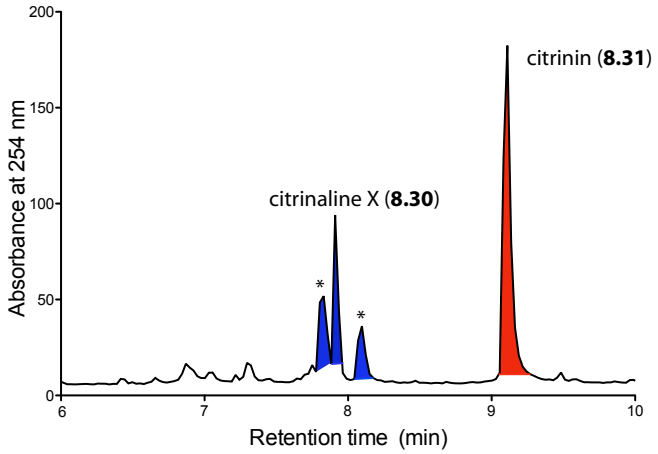

Figure 8.6. HPLC (254 nm) chromatogram from analytical gradient H_2O/MeCN plus 0.05% HCO_2H using Zorbax C_8, of the crude extract from *Penicillium* sp. cultivated on ISP-2 agar medium. *citrinaline X isomers

8.2.3 Preparative cultivation and isolation

Fifty petri dishes containing ISP-2 agar were inoculated with *Penicillium* sp. (CMB-TF0438) and incubated at 26 °C for 10 d. The agar was extracted with EtOAc (250 mL/10 plates), and the combined organic layer concentrated *in vacuo* to yield an EtOAc extract (95 mg). The EtOAc extract was sequentially triturated with hexane (8 mL), CH_2Cl_2 (8 mL) and MeOH (8 mL), which were concentrated under N_2 to yield 10, 19.5, and 60 mgs respectively. The MeOH soluble material was further fractionated by semi-preparative reversed phase HPLC (Zorbax 5 μm C_{18}, 250 × 9.4 mm column, 3 mL/min gradient elution from 90 – 40% H_2O/MeCN over 30 min, with isocratic 0.01% TFA modifier) to afford citrinaline X (**8.30**) (t_R= 19 min, 3 mg, 3.1%) and citrinin (**8.31**) (t_R= 25 min, 5 mg, 5.2%). [Note - % yields are determined on a mass-to-mass basis against the weight of EtOAc crude extract] (Scheme 8.1)* The minor metabolites were not isolated at this time, but will be discussed at the end of the chapter.

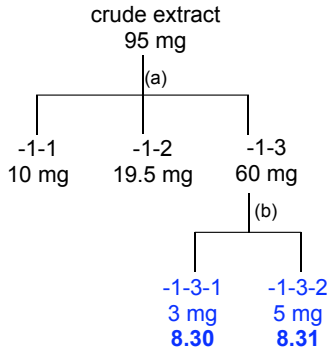

Scheme 8.1. Isolation scheme of crude extract *Penicillium* sp. (CMB-TF438). (a) Trituration [hexane (-1-1), CH_2Cl_2 (-1-2) and MeOH (-1-3)], (b) Semi-preparative HPLC: Zorbax C_8, 90 – 40% H_2O/MeOH plus 0.01% TFA, 3 mL/min, 30 min

8.2.3.1 Structural elucidation of citrinaline X (8.30)

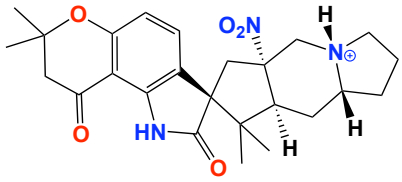

8.30

HRESI(–)MS analysis of **8.30** revealed a quasi molecular ion $[M-H]^-$ indicative of a molecular formula ($C_{25}H_{32}N_3O_5$, Δmmu +0.5). The 1D and 2D NMR (MeOH, d_4) data for **8.30** revealed a number of diagnostic resonances and correlations that could be assembled into significant structure fragments (Figure 8.7 and Table 8.1). These included COSY correlations (i) a sequence from H-9 to H-10, HMBC correlations from H-10 to C-12, C-8, C-7, C-11 and C-1), (ii) HMBC correlations from H-9 to C-6, C-7, C-8 and C-11, (iii) HMBC correlations from H_3-24, H_3-25 and H_2-5 to C-4 (δ_c 80.4), all of which were suggestive of fragment A (Figure 8.7). Likewise, (iv) a COSY correlation sequence from H-14 to H_2-15 to H-16 to H_2-19 (inclusive of H_2-17 and H_2-18 due to overlapping), (v) HMBC correlations from H_2-23 to C-2 (δ_c 185.4), C-11 (δ_c 121.8), to C-1 (δ_c 59.4), to C-13 (δ_c 47.7) and C-22 (δ_c 93.9), together with (vi) HMBC correlations from H-14, H_3-26 and H_3-27 to C-13, and H_2-15 to C-17/18, were suggestive of planar fragment B (Figure 8.7 and Figure 8.8). ROESY correlations from H-14 to H-15b; and H-16 to H-15a, support the proposition that H-14 and H-16 were *trans* to each other (Figure 8.9 and Figure 8.10).

To establish the relative configuration for citrinaline X (**8.30**) required consideration of the ROESY NMR data (Figure 8.9 and Figure 8.10). Correlations from H_3-27 to both H-14 and H-15b, and from H-14 to H-15b (not H-15a), established that all were positioned on a common (α) face, while correlation from H-16 to H-15a (but not H-15b) suggested that these protons occupied the opposite (β) face of the molecule (Figure 8.11a). Likewise, correlations from H-10 to H_3-26 and H-23a confirmed that these moieties occupied the same (β) face as H-16 and H-15a (Figure 8.11b). Finally, a correlation from H-23b to H-21b required that they occupied the same (α) face, while correlation from H-21a to H-19a was consistent with placement on the opposite (β) face (Figure 8.11b). These ROESY observations established the relative configuration about C-1, C-14, C-16 and N-20 to be the same as that reported (and confirmed by X-ray analysis) for citrinaline A (**8.28**). Citrinaline X (**8.30**) did not possess NMR (600 MHz, MeOH-d_4) data in common with citrinaline A (**8.28**) (**Table 8.2**), nor did it co-elute on HPLC (Figure 8.12) this necessitated the configuration about C-22 in **8.30** was opposite to that in **8.28** (with a α disposed NO_2 moiety). Supportive of this hypothesis, careful comparison of the 1D NMR (600 MHz, MeOH-d_4) data for **8.30** and **8.28**

established that differences were localized about C-9 and C-10 (Figure 8.15 and Figure 8.17), and C-23 and C-26 (Figure 8.16), fully consistent with inversion of the configuration about C-22.

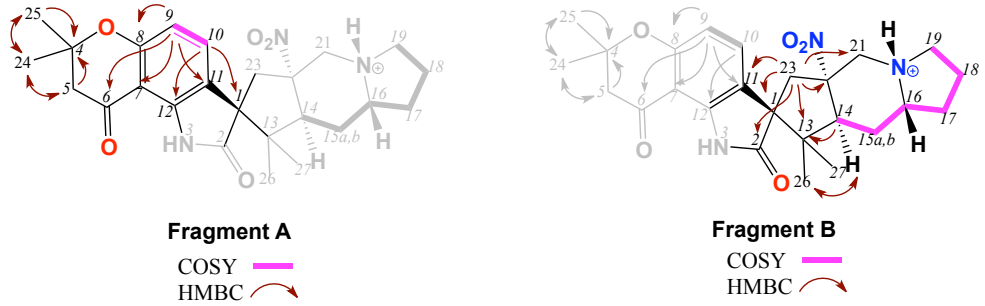

Figure 8.7. Key correlations of citrinaline X (**8.30**) showing the assigned fragments

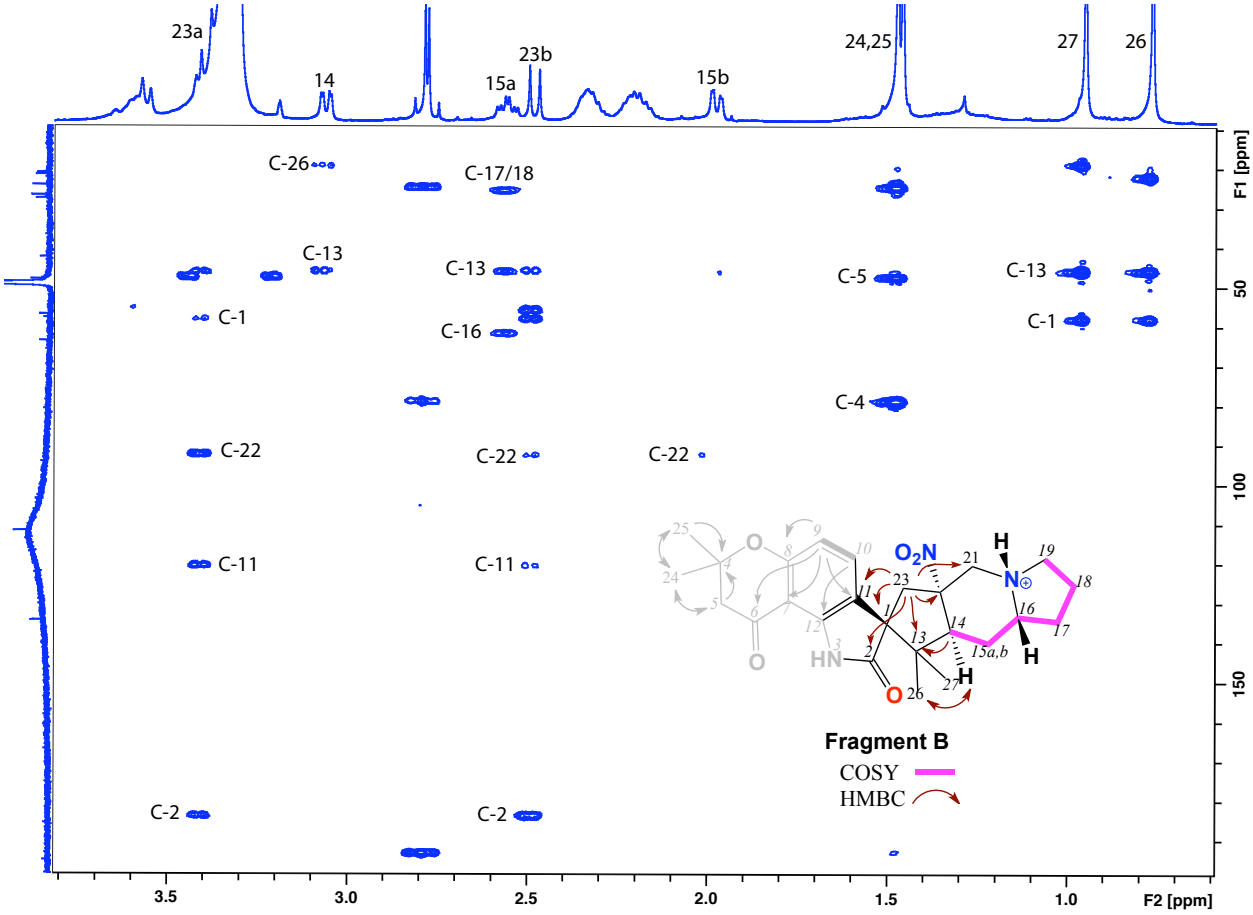

Figure 8.8. HMBC (600 MHz, MeOH-d_4) spectrum with key correlation for citrinaline X (**8.30**) - fragment B

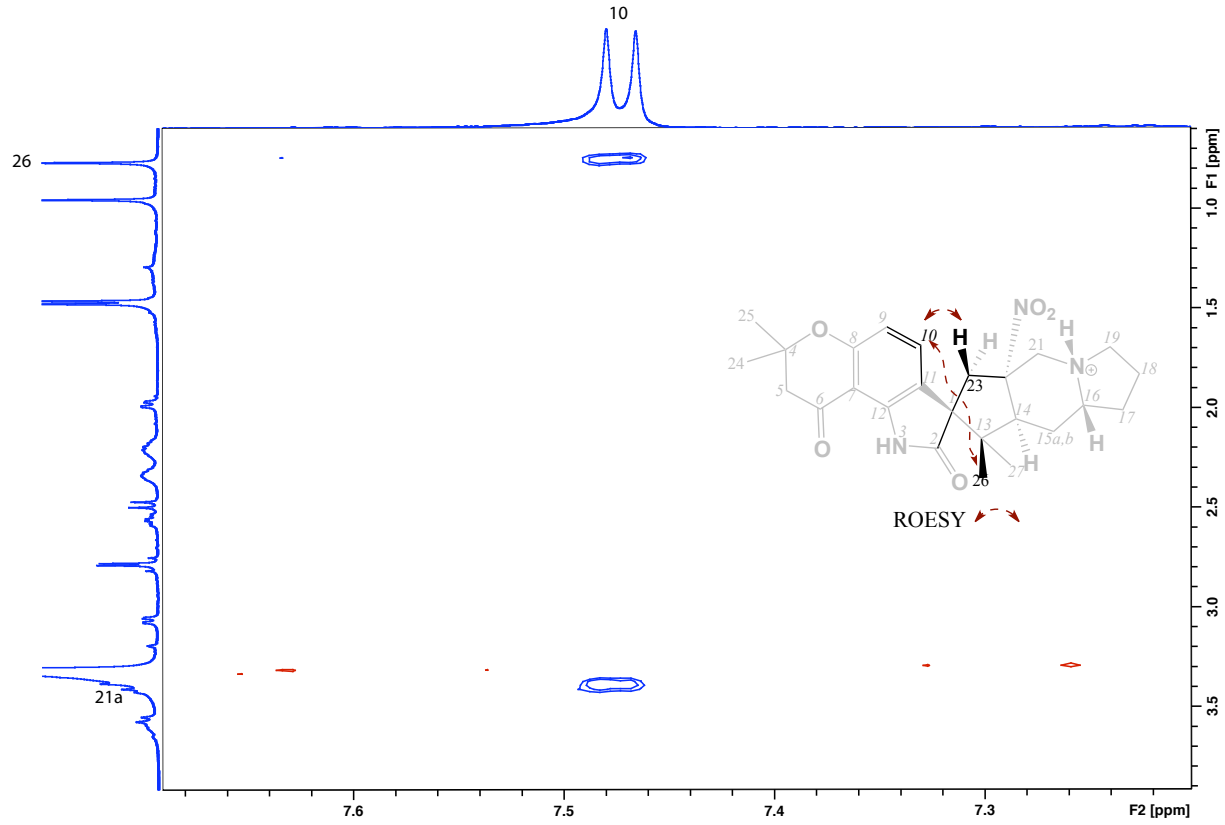

Figure 8.9. ROESY (600 MHz, MeOH-d_4) spectrum of citrinaline X showing key correlations from H-10 to H-23a to H_3-26 (**8.30**)

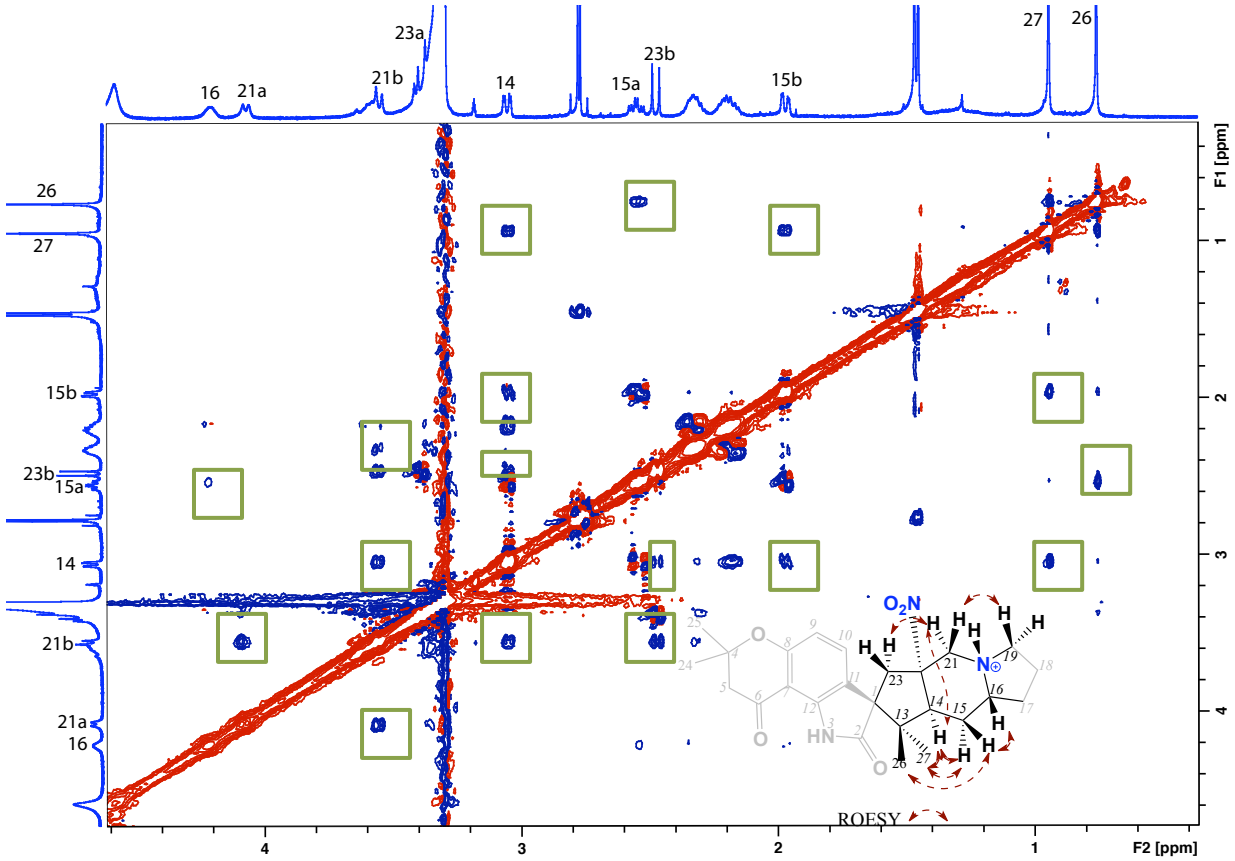

Figure 8.10. ROESY (600 MHz, MeOH-d_4) spectrum of citrinaline X (**8.28**)

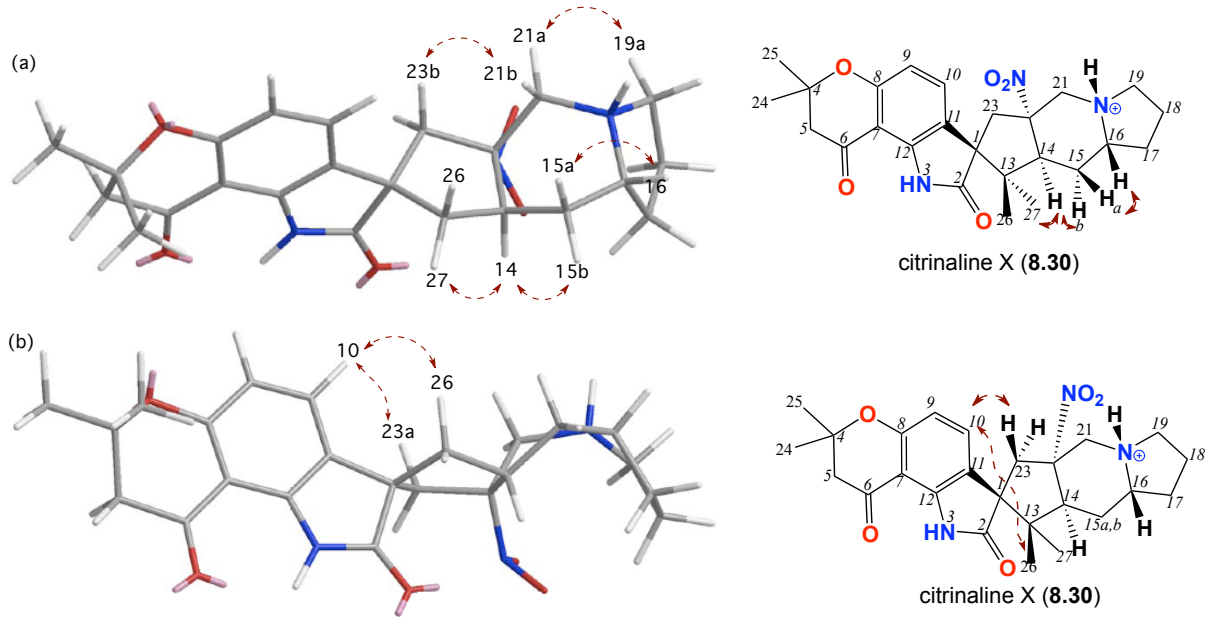

Figure 8.11. Energy minimized molecular model (Chem, 3D, MM2) structure (a) and (b) of citrinaline X (**8.30**) showing key ROESY correlations

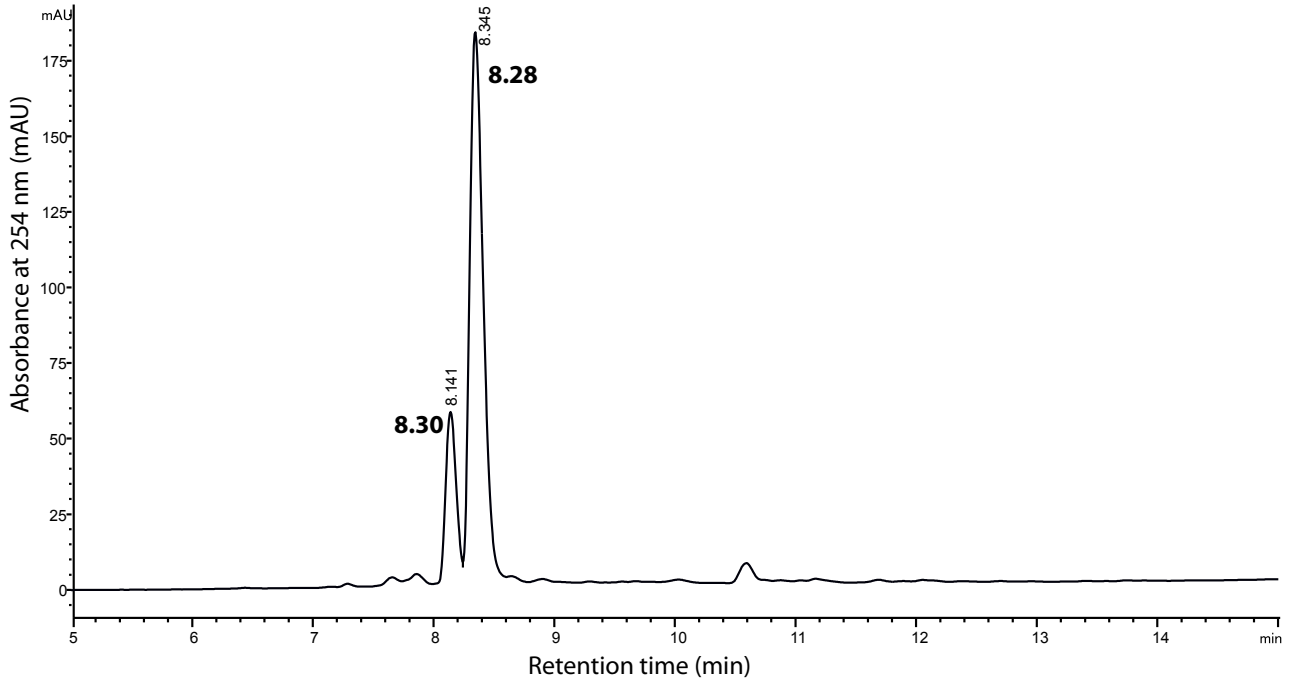

Figure 8.12. The chromatogram of citrinaline X (**8.30**) and citrinaline A (**8.28**) using HPLC-DAD-MS 90 – 0% H_2O/MeCN (0.05% HCO_2H modifier) over 15 min at 254 nm (DAD)

As citrinaline X (**8.30**) and citrinaline A (**8.28**) generate almost identical CD spectra (Figure 8.13), we infer that they both possess the same absolute configuration about C-1 – the only chiral centre positioned in proximity to the UV chromophore. Hence we propose that citrinaline X (**8.30**) in the C-22 epimer of citrinaline A (**8.28**), as shown. Having completed our structure elucidation of **8.30**, we were surprised to learn (personal correspondence) that the published structure for citrinaline B (**8.29**) was to be corrected to one identical to that proposed for citrinaline X (**8.30**).

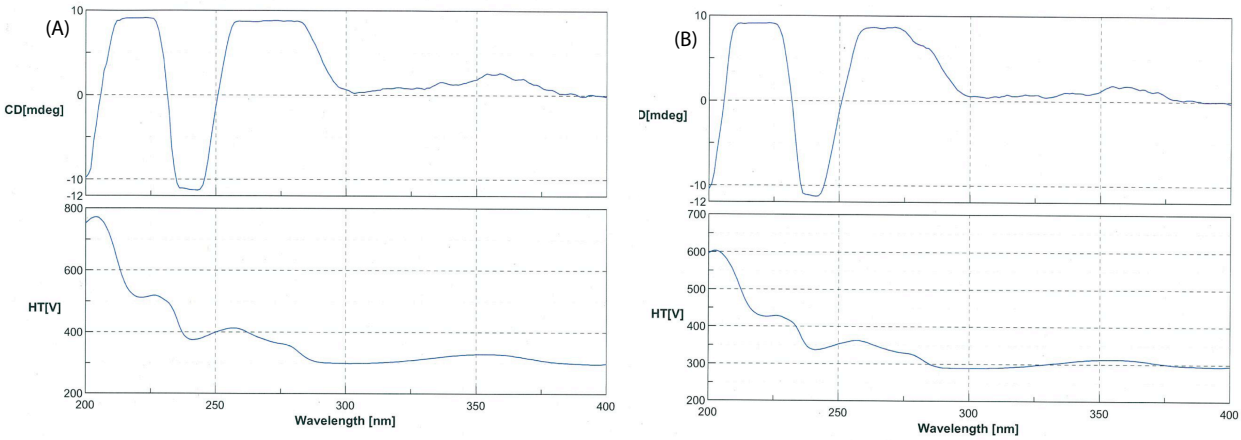

Figure 8.13. CD spectrum of citrinaline X (**8.30**) and citrinaline A (**8.28**) in MeCN at concentration 0.8 mg/mL, speed 200 nm/min, cell length 0.01 cm

In the absence of an authentic sample of citrinaline B (**8.29**), we could not make a direct comparison, but we were concerned as the $[\alpha]_D$ for **8.30** (–10) did not match that reported for **8.29** (+20). To resolve this issue, an authentic sample of citrinaline X (**8.30**) was forwarded to Dr David Williams at the University of British Columbia, for direct HPLC (co-injection) comparison with an authentic sample of citrinaline B (**8.29**).

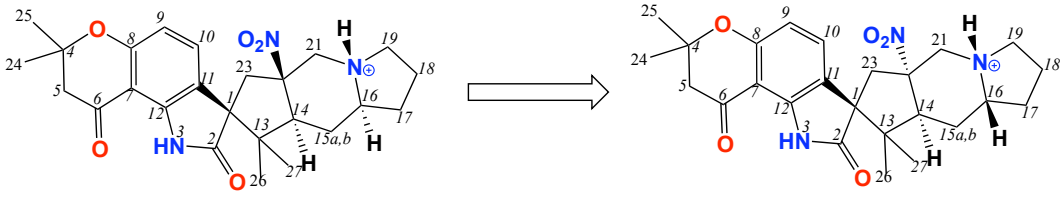

citrinaline B (**8.29**)

Revised citrinaline B (**8.30**)
citrinaline X (**8.30**)

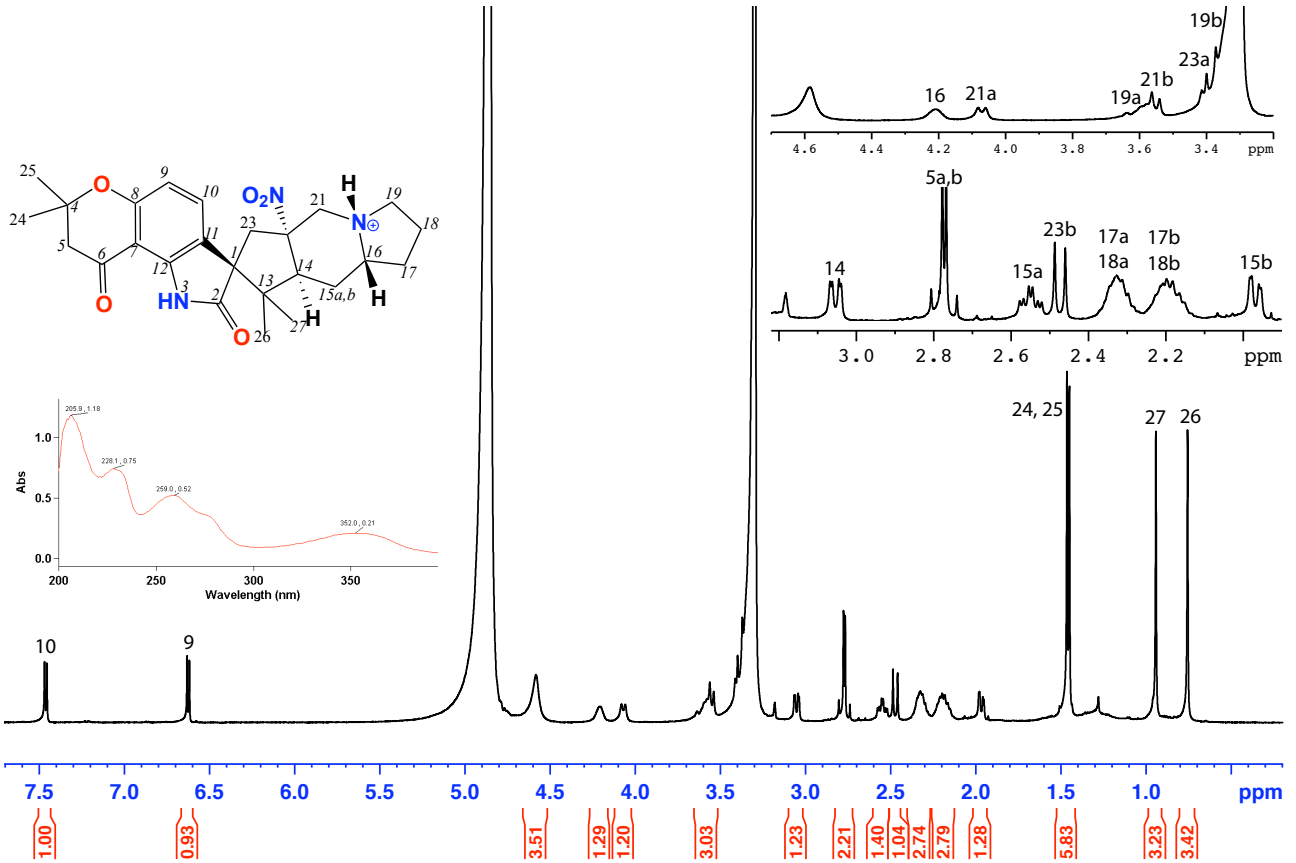

Figure 8.14. ^{1}H NMR (600 MHz, MeOH-d_4) and UV-vis (inset) spectra of citrinaline X (**8.30**)

Table 8.1. NMR data (600 MHz, MeOH-d_4) of citrinaline X (**8.30**)

Pos.	δ_H, mult (*J* in Hz)[a]	δ_C[a]	COSY	ROESY	^{1}H-^{13}C HMBC
1		59.4			
2		185.4			
3-NH					
4		80.4			
5	a 2.79, d *(16.7)*	49.3		24/25	24/25
	b 2.75, d *(16.7)*				
6		194.8			
7		106.7			
8		160.8			
9	6.63, d *(8.4)*	111.7	10		6, 8, 7, 11
10	7.46, d *(8.4)*	134.4	9	23a, 26	1, 8, 7, 11, 12
11		121.8			
12		143.7			
13		47.7			
14	3.05, dd *(14.1, 3.7)*	47.1	15a, b	17b/18b, 15b, 21b, 23b, 27	13, 26
15	a 2.55, ddd *(14.1, 13.9, 6.3)*	21.7	14, 15b, 16	16, 26	13, 16, 17
	b 1.97, dd *(14.1, 6.3)*		14, 15a	27	14, 22
16	4.21, br s	63.0	17a/18a, 17b/18b	15a	
17	a 2.34[b], m	27.7			
	b 2.18[b], m				
18	a 2.32[b], m	20.9			
	b 2.20[b], m				
19	a 3.60[b], m	57.1		21a	
	b 3.36[c]				
20					
21	a 4.07, br d *(13.3)*	57.8	19b, 21b	19a	
	b 3.55, d *(13.3)*		21a	14, 23b	
22		93.9			
23	a 3.39, d *(16.4)*	42.1	23b	10	1, 2, 11, 13, 22
	b 2.47, d *(16.4)*		23a	14, 21b	1, 2, 11, 13, 21
24-Me	1.46, s	26.9		5a/b	4, 5, 25
25-Me	1.45, s	26.9		5a/b	4, 5, 26
26-Me	0.75, s	20.6		10, 15a	4, 5, 27
27-Me	0.94, s	23.8		14, 15b	4, 5, 26

(a)^{13}C assignments obtained from gHSQC and gHMBC data. (b) Overlapping resonances. (c) Obscured by the solvent. (d) Interchangeable resonances

Table 8.2. NMR and ^{13}C (600 MHz, MeOH-d_4) comparison of citrinaline X (**8.30**) and citrinaline A (**8.28**)

	citrinaline X (**8.30**)		citrinaline A (**8.28**)	
Pos.	δ_H, mult (*J* in Hz)[a]	δ_C[a]	δ_H, mult (*J* in Hz)[a]	δ_C[a]
1		59.4		
2		185.4		
3-NH				
4		80.4		
5	a 2.79, d *(16.7)*	49.3	2.79, d *(16.7)*	49.2
	b 2.75, d *(16.7)*		2.75, d *(16.7)*	
6		194.8		
7		106.7		
8		160.8		
9	6.63, d *(8.4)*	111.7	6.58, d *(8.4)*	111.1
10	7.46, d *(8.4)*	134.4	7.33, d *(8.4)*	133.8
11		121.8		
12		143.7		
13		47.7		
14	3.05, dd *(14.1, 3.7)*	47.7	3.06, dd *(14.1, 3.4)*	47.7
15	a 2.55, ddd *(14.1, 13.9, 6.3)*	21.7		
	b 1.97, dd *(14.1, 6.3)*		1.75, dd *(14.1, 3.4)*	22.0
16	4.21, br s	63.0		
17	a 2.34[b], m	27.7	[b]	
	b 2.18[b], m			
18	a 2.32[b], m	20.9	[b]	
	b 2.20[b], m			
19	a 3.60[b], m	57.1	[c]	
	b 3.36[c]		[c]	
20				
21	a 4.07, br d *(13.3)*	57.8	[c]	
	b 3.55, d *(13.3)*		[c]	
22		93.9		[c]
23	a 3.39, d *(16.4)*	42.1	3.10[b]	43.7
	b 2.47, d *(16.4)*		2.50, d *(16.4)*	
24-Me	1.46, s	26.9	1.46, s	26.5
25-Me	1.45, s	26.9	1.44, s	26.5
26-Me	0.75, s	20.6	0.83, s	22.4
27-Me	0.94, s	23.7	0.91, s	23.6

*(a)^{13}C assignments obtained from gHSQC and gHMBC data. (b) Overlapping resonances. (c) signals not observed

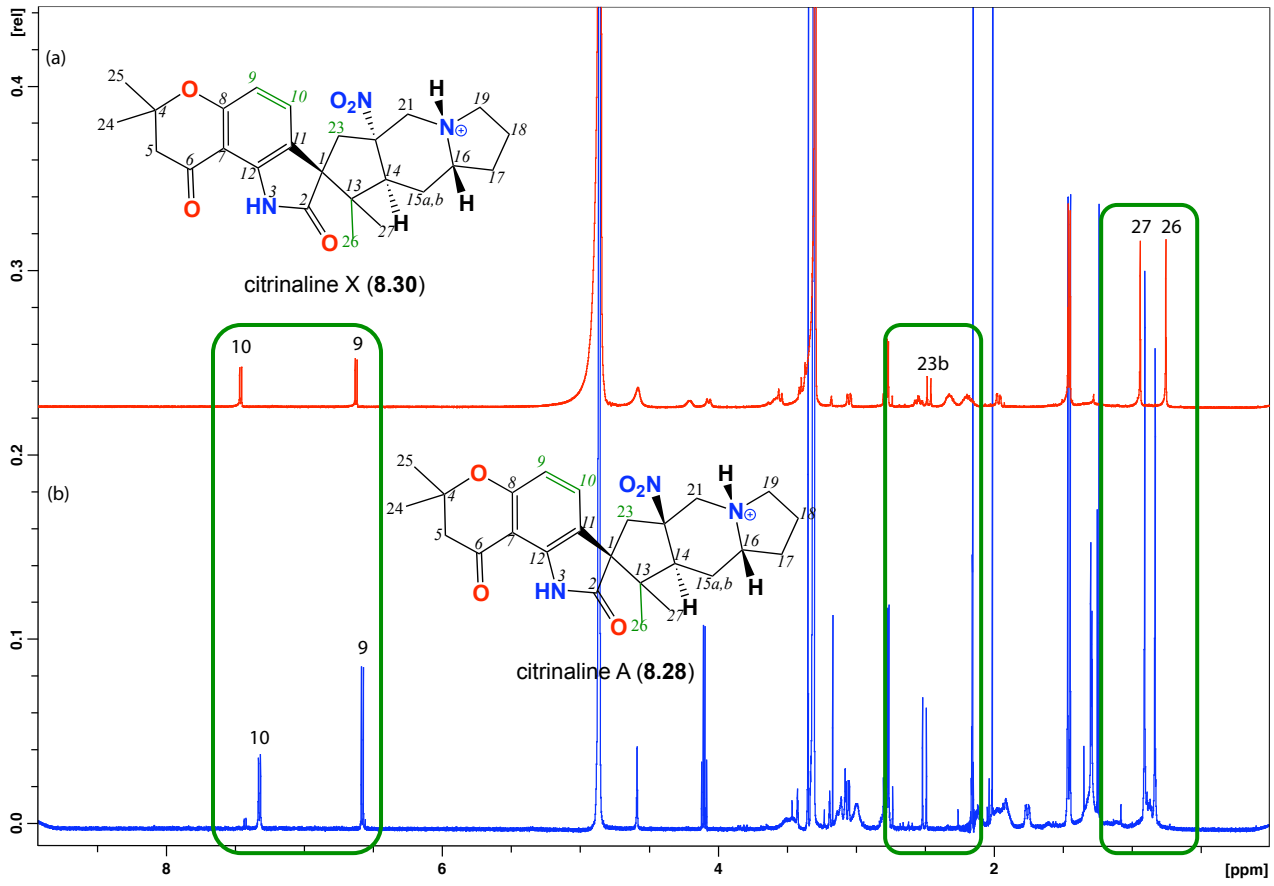

Figure 8.15. Comparison of ^{1}H NMR (600 MHz, MeOH-d_4) spectra of (A) citrinaline X (**8.28**) and (B) citrinaline A (**8.30**)

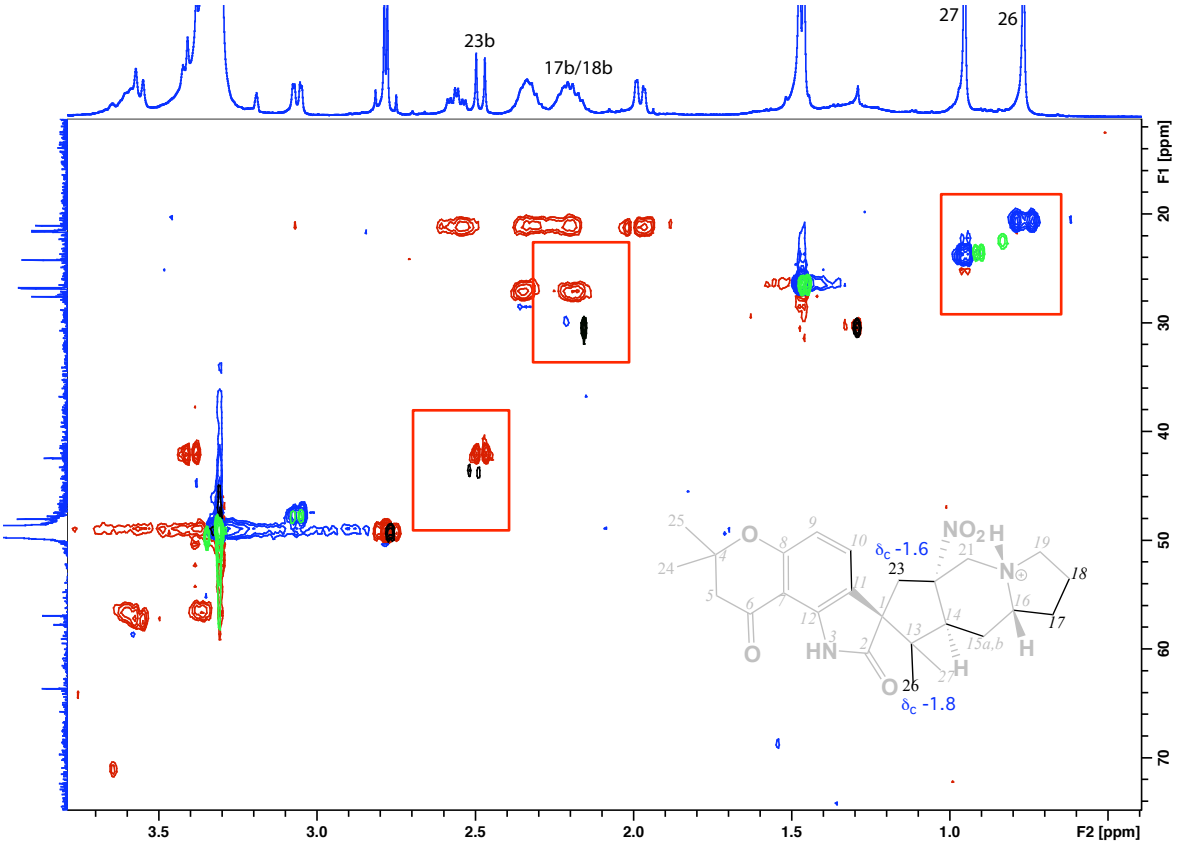

Figure 8.16. ^{1}H -^{13}C HSQC (600 MHz, MeOH-d_4) comparison of both citrinaline X (**8.28**) (red-CH_2 and blue-CH/CH_3) and citrinaline A (**8.30**) (black-CH_2 and green-CH/CH_3).*$\Delta\delta_C$ = δ_C (citrinaline X, **8.30**) - δ_C (citrinaline A, 8.28)

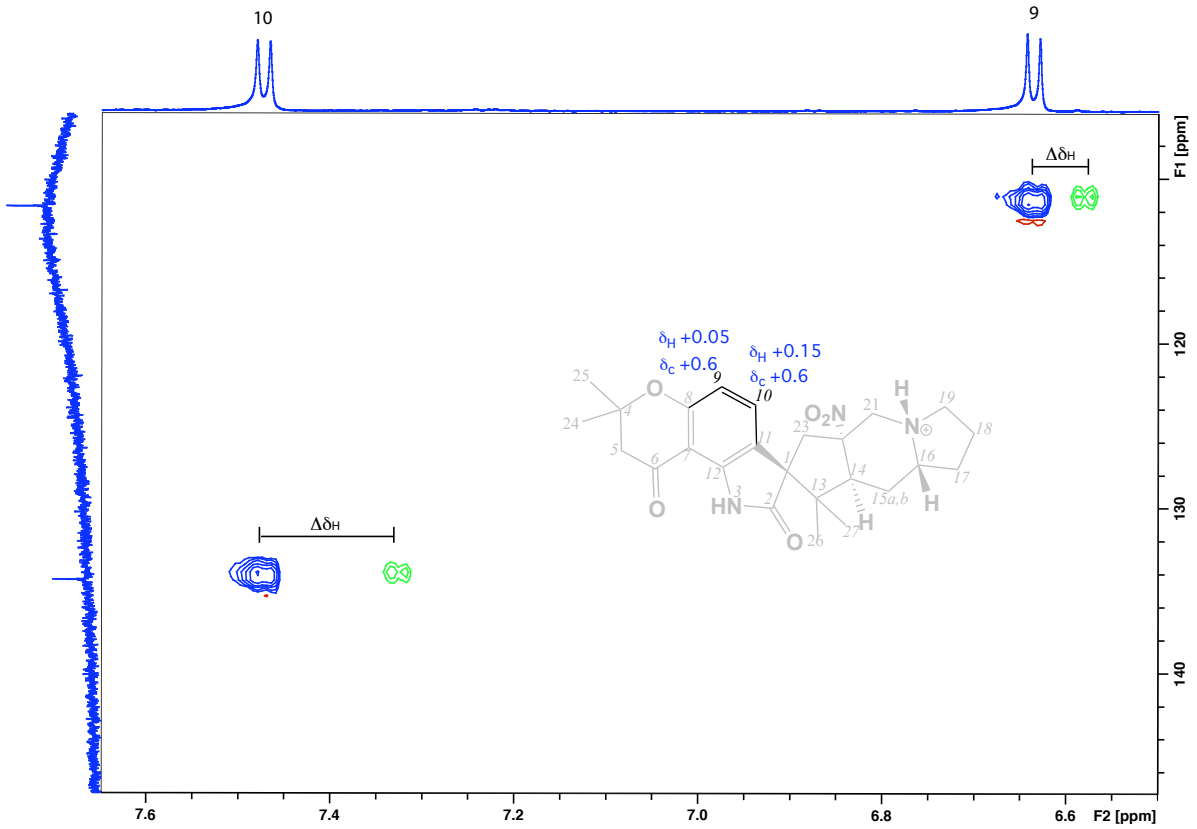

Figure 8.17. ^{1}H-^{13}C HSQC (600 MHz, MeOH-d_4) comparison of both citrinaline X (**8.28**) (blue) and citrinaline A (**8.30**). *$\Delta\delta_C = \delta_C$ (citrinaline X, **8.30**) - δ_C (citrinaline A, 8.28). *$\Delta\delta_H = \delta_H$ (citrinaline X, **8.30**) - δ_H (citrinaline A, 8.28)

8.2.4 Highlight- Plausible Biosynthesis of citrinaline X

It seems very likely that the biosynthesis of the citrinalines proceeds through an intermediate similar to that of paraherquamide F (**8.21**) with hydrolysis of the lactam heterocycle accompanied by decarboxylation and oxidation of the NH_2 to a NO_2 moiety (Figure 8.18).

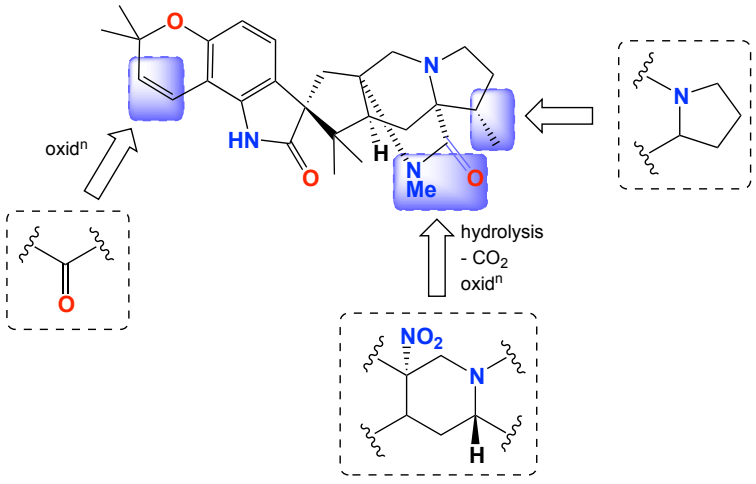

Figure 8.18 A plausible biosynthetic route to the citrinaline X (**8.30**)

8.2.5 Citrinin (8.31)

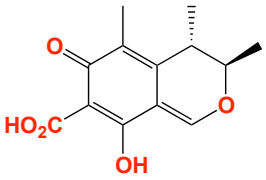

8.31

HRESI(+)MS analysis of **8.31** revealed a quasi-molecular ion $(M+H)^+$ indicative of a molecular formula $C_{13}H_{14}O_5$ (Δmmu +1.4). The UV-vis and the NMR ($CDCl_3$) spectra were very characteristic for citrinin. The structure elucidation was further supported by 2D NMR data, including HSQC, COSY and HMBC. On searching the literature, **8.31** was confirmed to be the well known fungal metabolite citrinin, previously isolated from the *Penicillium janthinellum*. This assignment was further confirmed by comparing the $[\alpha]^{22}_D$ –20.1 (*c* 0.10, $CHCl_3$) for **8.31** to the reported $[\alpha]^{21}_D$ – 17.4 (*c* 0.10, $CHCl_3$) of citrinin.[231]

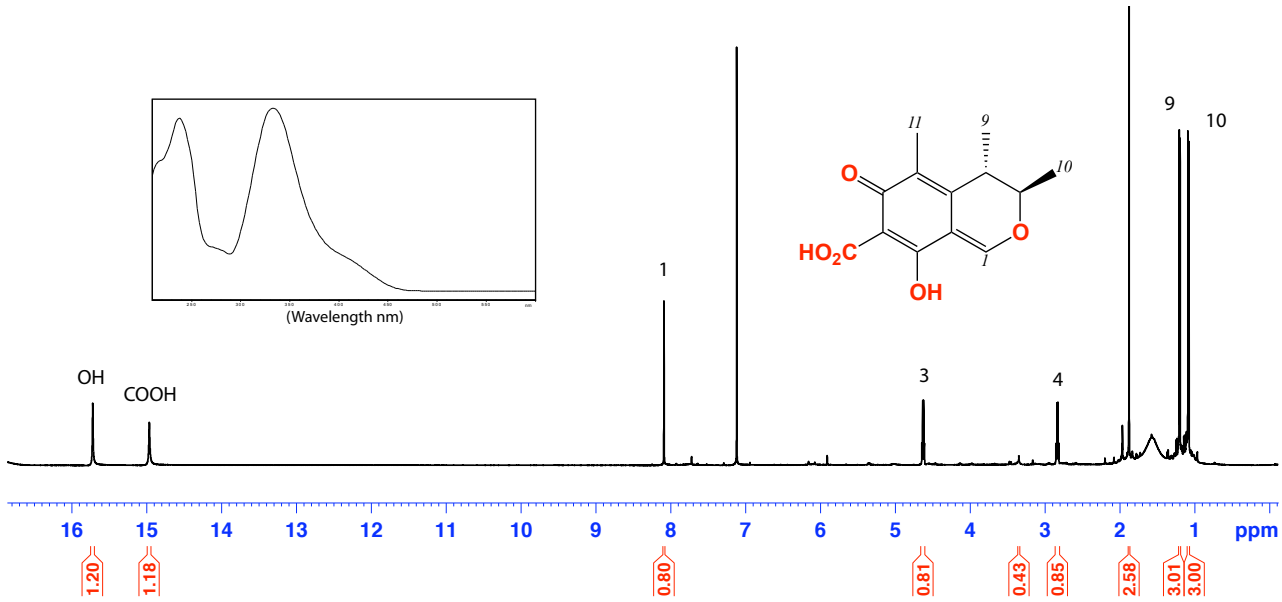

Figure 8.19. ^{1}H NMR (600 MHz, $CDCl_3$) and UV-vis (HPLC-DAD, H_2O/MeCN plus HCO_2H at 254 nm) spectra of citrinin (**8.31**)

Table 8.3. NMR data (600 MHz, $CDCl_3$) of citrinin (**8.31**)

Pos.	δ_H, mult (*J* in Hz)[a]	δ_C[a]	COSY	^1H-^{13}C HMBC
1	8.10, s	139.1	--	3, 8a
2				
3	4.67, dd *(14.4, 7.2)*	82.2	4, 9	1, 10
4	2.89, dd *(14.4, 7.2)*	34.1	3, 10	1, 5, 8a, 9
5		123.3		
6		177.2		
7		102.2		
8		184.1		
8a		107.4		
8b		163.3		
9	1.41, d *(7.2)*	18.5	3	3, 4
10	1.31, d *(6.7)*	18.2	4	1, 3, 4
11	1.81, s	9.4		1, 5
OH	15.70, s			
12-COOH	14.91, s	174.5		

*(a)^{13}C assignments obtained from gHSQC and gHMBC data.

Table 8.4. ^1H NMR ($CDCl_3$) data comparison of experimental and published data[105,232] of citrinin (**8.31**)

Pos.	δ_H, mult, (*J* in Hz)[a] (experimental)	δ_H, mult, (*J* in Hz)[b] (published)
1	8.10, s	8.25, s
3	4.67, dd *(14.4, 7.2)*	4.80, q *(6.7)*
4	2.89, dd *(14.4, 7.2)*	2.98, q *(7.1)*
9	1.41, d *(7.2)*	1.35, d *(6.7)*
10	1.31, d *(6.7)*	1.23, d *(7.1)*
11	1.81, s	2.02, s
OH	15.70, s	15.90, s
12-COOH	14.91, s	15.31, s

*measured in (a) (600 MHz, $CDCl_3$), (b) (400 MHz, $CDCl_3$)

8.3 Diketopiperazines stimulates the production of microbial metabolites

Fungal secondary metabolites are often coded by gene clusters encoded on chromosomal DNA. It has been observed that activation (transcription) of gene clusters can be influenced by unique low molecular weight compounds, transfer RNA, sigma factors and gene products formed during post-exponential development,[233] as well as nutrient and environmental factors.[234] These events can generate signals that affect regulatory pathways resulting in chemical differentiation and morphogenesis. In many secondary metabolites pathway, primary metabolites play a critical role. [235]For example, tryptophan is a substrate/precursor for dimethylallyltryptophan synthase in ergot alkaloid biosynthesis,[236] as is leucine for bacitracin[237], methionine for cephalosporin in *Cephalosporium acremonium*[238], lysine for cephamycin in *Streptomyces clavuligerus*,[239] valine for tylosin in *Streptomyces fradiae*[240] and phenylacetate for penicillin G in *Penicillium chrysogenum*. Likewise glycine, phenylalanine, tyrosine and arginine are essential for the biosynthesis of vancomycin.[233]

Diketopiperazines (DKPs) are a widely explored class of bioactive dipeptides.[241] Interest in DKPs is evident from significant bioactivities including plant-growth promotion[242], antimicrobial activity [243], quorum-sensing signaling[244,245], antitumor activity[246], antiviral activity[246], and inhibition against aflatoxin production [247]. A parallel study in my PhD (Chapter 4) described the importance of a DKP as a regulator of bNOS and heronapyrrole biosynthesis. Likewise, another aspect of my research (chapter 5) studied a novel class of fungal diketomorpholines (DKMs) as inhibitors of P-gp mediated drug efflux. During that study, we had caused to synthesize *cyclo*-(L-Trp-L-Phe) (**5.28**) (see Chapter 5). As the DKP *cyclo*-(L-Trp-L-Phe) (**5.28**) is a well known fungal metabolite with no attributed biology, we were keen to determine if this DKP has the potential to regulate fungal secondary metabolism, much as modulated in chapter 4. To test this hypothesis, **5.28** and DKPs (**4.39a – f**) listed in Chapter 4 were tested against 20 different fungal and bacterial strains. Of significance to this current chapter, **5.28** activated silent secondary metabolism in *Penicillium* sp. (CMB-TF438), while simultaneously suppressed citrinaline X and citrinin biosynthesis.

Penicillium sp. (CMB-TF438) was cultivated on two different media; ISP-2 with and without the addition of **5.28**. The presence of **5.28** (10 μM) inhibited the production of all citrinalines and citrinin, and activated the production of another two metabolites (Figure 8.20). Large-scale cultivation and isolation yielded janthinone (**8.32**) and citrinolactone B (**8.33**), which was determined to be non-cytotoxic in antibacterial and antifungal assays against *E.coli* (ATCC 11775),

S. aureus (ATCC 25923 and ATCC 9144), *B. subtilis* (ATCC 6051 and ATCC 6633) and *C. albicans* (ATCC 90028).

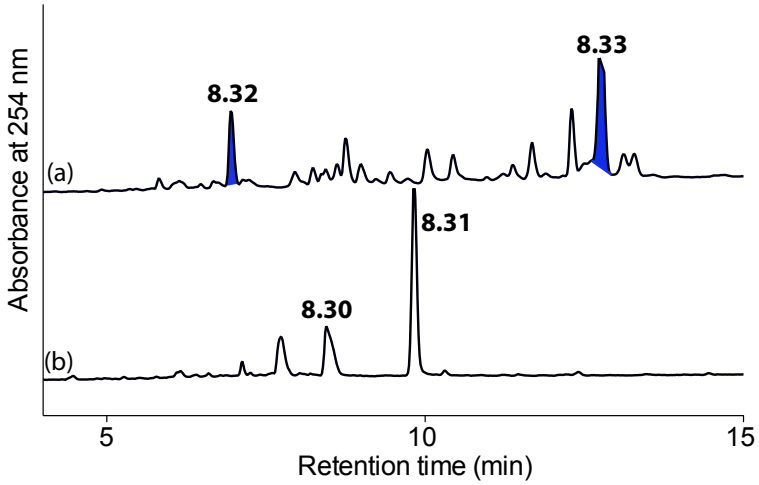

Figure 8.20. Chromatogram of *Penicillium* sp. (CMB-TF438) using HPLC-DAD-MS 90 – 0% H_2O/MeCN (0.05% HCO_2H modifier) over 15 min and detecting at 254 nm (DAD) with and without the addition of 10 μM *cyclo*-(L-Trp-L-Phe) (**5.28**) on ISP-2 agar medium.

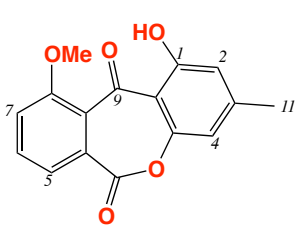

janthinona (**8.32**)

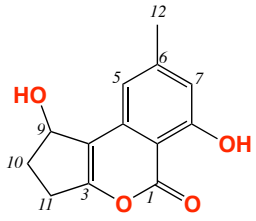

citrinolactone B (**8.33**)

8.3.1 *cyclo*-(L-Trp-L-Phe) and the secondary metabolites production of CMB-TF438

In conclusion, that *cyclo*-(L-Trp-L-Phe) (**5.28**) (Chapter 4) has such a dramatic effect on the metabolite profile of *Penicillium* sp. (CMB-TF438) is noteworthy. Future studies within our group will attempt to;

(a) Assess this effect over a range of concentrations.

(b) Apply **5.28** to other *Penicillium* sp. known to produce citrinin, to establish if the effect is strain limited, or whether it is linked to specific polyketide synthases.

(c) Monitoring the production levels of metabolites produced by *Penicillium* sp. (CMB-TF438) in the presence and absence of **5.28**, overtime (daily for 24 days), to determine if **5.28** activated silent metabolism, or alternatively accelerates the development of the culture.

8.3.1.1 Janthinona (8.32)

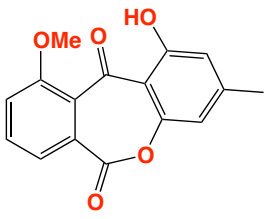

8.32

HRESI(+)MS analysis of **8.32** revealed an adduct ion $(M+Na)^+$ indicative of molecular formula $C_{16}H_{12}O_5$ (Δmmu +0.9). The NMR ($CDCl_3$) (Figure 8.21 and Table 8.5) showed the presence of five aromatic protons (δ_H 6.74, H-2; δ_H 6.62, H-4; δ_H 7.51, H-5; δ_H 7.72, H-6; and δ_H 7.28, H-7) in addition to the presence of a methoxy (δ_H 4.01) and a deshielded OH/NH (δ_H 12.13). The structure elucidation was further supported by 2D NMR data, including HSQC, COSY and HMBC (Table 8.5). On searching the literature, **8.32** was consistent with the known fungal metabolite janthinona isolated from *Penicillium janthinellum*.[232]

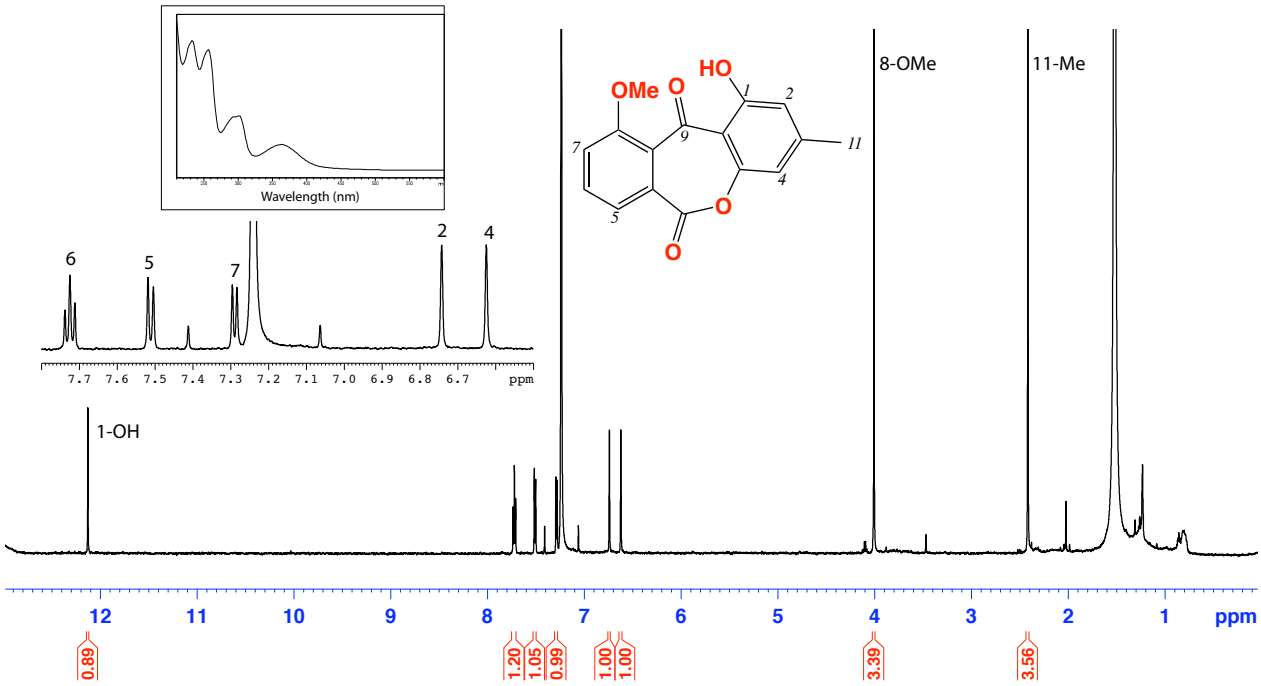

Figure 8.21. ^{1}H NMR (600 MHz, $CDCl_3$) and UV-vis (HPLC-DAD, H_2O/MeCN plus HCO_2H at 254 nm) spectra of janthinona (**8.32**)

Table 8.5. NMR (600 MHz, $CDCl_3$) data of janthinona (**8.32**)

Pos.	δ_H, mult (*J* in Hz)[a]	δ_C[a]	COSY	^1H-^{13}C HMBC
1	12.13, s			
2	6.74, s	107.4	11-Me	
3		[b]		
4	6.62, s	112.4	11-Me	2
4a		149.9		
5	7.51, d *(8.3)*	119.8	6	7
5a		133.6		
6	7.72, t *(8.3)*	135.3	5, 7	5a, 7, 8
7	7.28, d *(8.3)*	122.9	6	5
8		155.9		
8-OMe	4.01, s	53.5		9
8a		120.2		
9		170.3		
9a		[b]		
10		[b]		
11-Me	2.41, s	22.9		2, 4, 4a

(a)^{13}C assignments obtained from gHSQC and gHMBC data. (b) signals not observed

Table 8.6. NMR ($CDCl_3$) data comparison of experimental and literature[232] data of janthinona (**8.32**)

Pos	δ_H, mult, (*J* in Hz)[a] (experimental)	δ_H, mult, (*J* in Hz)[b] (published)
1	12.13, s	[c]
2	6.74, s	6.74, d *(1.8)*
4	6.62, s	6.62, d *(1.8)*
5	7.51, d *(8.3)*	7.51, dd *(8.2, 2.0)*
6	7.72, t *(8.3)*	
7	7.28, d *(8.3)*	7.30, dd *(7.3, 2.0)*
8-OMe	4.01, s	4.03, s
11-Me	2.41, s	2.43, br s

*measured (a) (600 MHz, $CDCl_3$), (b) (400 MHz, $CDCl_3$), (c) (signal not observed)

8.3.1.2 Citrinolactone B (8.33)

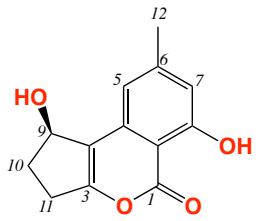

8.33

HRESI(+)MS analysis of **8.33** returned a quasi-molecular ion $(M+Na)^+$ indicative of formula $C_{13}H_{12}O_4$ (Δ mmu +0.3). The NMR and ^{13}C (DMSO-d_6) spectra (Figure 8.22 and **Table 8.7**) showed one methyl, two aliphatic methylenes, two aromatic protons, six aromatic quaternary carbons, one carbonyl and one OH group. The structure elucidation was further supported by 2D NMR data, including HSQC, COSY and HMBC. On searching the literature, **8.33** was confirmed to be citrinolactone B, first isolated from *Penicillium citrinum*.[248] This assignment was further supported by comparison of the $[\alpha]^{23}_D$ +20 (*c* 0.1, MeOH) of **8.33** with the reported $[\alpha]^{20}_D$ +86 (*c* 0.7, EtOAc) of citrinolactone B.[248]

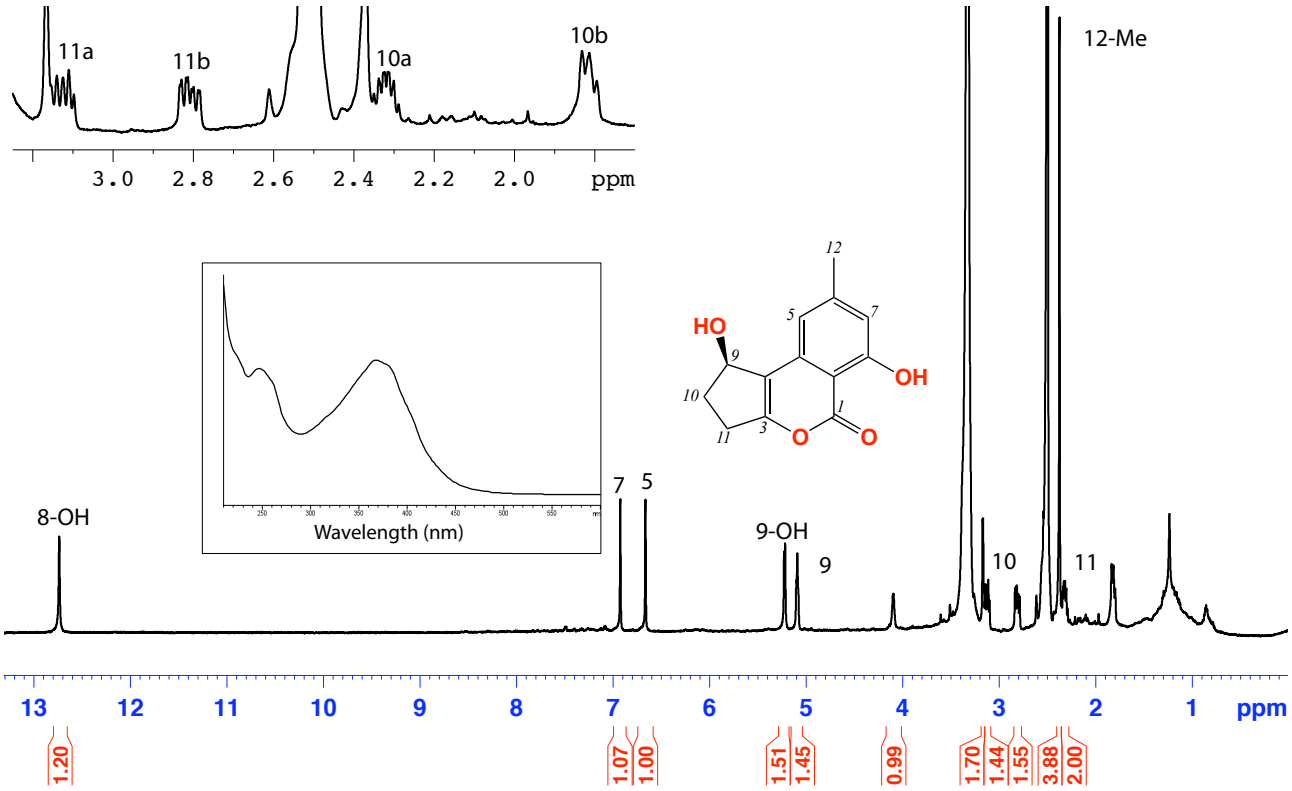

Figure 8.22. ^1H NMR (600 MHz, DMSO-d_6) and UV-vis (HPLC-DAD, H_2O/MeCN plus HCO_2H at 254 nm) spectra of citrinolactone B (**8.33**)

Table 8.7. NMR (600 MHz, DMSO-d_6) data of citrinolactone B (**8.33**)

Pos.	δ_H, mult (*J* in Hz)[a]	δ_C[a]	COSY	ROESY	^{1}H-^{13}C HMBC
1		172.8			
2		[b]			
3		[b]			
4		[b]			
4a		147.9			
5	6.67, s	112.8	12		7, 12
6		147.1			
7	6.94, s	107.8	12		5, 7, 12
8		160.4			
8-OH	12.73, s				5, 7, 8
8a		[b]			
9	5.08, d *(6.6)*	69.4	9-OH		1
9-OH	5.21, d *(6.6)*		9	10a	
10	a 3.11, m	29.9	10a, 11b	9-OH	1
	b 2.80, m		10b, 11a		1
11	a 2.32, m	31.1	10b		
	b 1.56, m		10a		
12	2.37, s	21.7			4a, 5, 7

*(a)^{13}C assignments obtained from gHSQC and gHMBC data. (b) signals not observed

Table 8.8. NMR ($CDCl_3$) data comparison of experimental and published data[248] of citrinolactone B (**8.33**)

Pos.	δ_H, mult, (*J* in Hz)[a] (experimental)	δ_H, mult, (*J* in Hz)[b] (published)
5	6.61, s	6.61, d *(0.5)*
7	6.70, s	6.69, d *(0.5)*
9	5.43, br	5.43, dd *(14.0, 3.8)*
10a	2.49, m	2.77, m
10b	2.03, m	2.03, m
11a	3.09, m	3.11, m
11b	2.82, m	2.83, m
12-Me	2.37, s	2.39, m
8-OH	[c]	12.32, s

*measured in (a) (600 MHz, $CDCl_3$), (b) (500 MHz, $CDCl_3$), (c) (signal not observed)

8.3.2 Biological assays

The natural products, janthinona (**8.32**) and citrinolactone X (**8.33**) were tested in antimicrobial and cytotoxicity assays (see General experimental part). For the antimicrobial assay, the compounds were evaluated for the growth inhibitory against *Staphylococcus aureus* (ATCC 25923 and 9144), *Bacillus subtilis* (ATCC 6051 and 6633), *Escherichia coli* (ATCC 11775), *Pseudomonas aeruginosa* (ATCC 10145) and *Candida albicans* (ATCC 10231) as shown in Figure 8.24 and for cytotoxic assay, the compounds were also tested against two different cell lines, AGS (human stomach adrenocarcinoma) and HT 29 (human colon adrenocarcinoma) as shown in Figure 8.23. The compounds were tested in two fold dilution starting from 30 μM to 0.1 μM in 1% DMSO. These compounds did not show any biological activity.

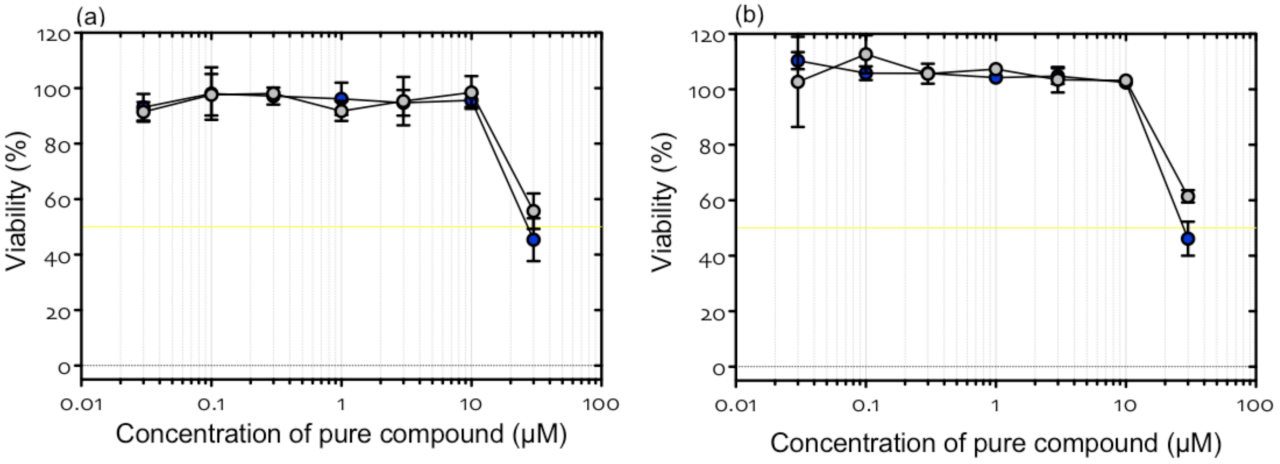

Figure 8.23. Graphs showing the cytotoxic activity of citrinaline X (**8.30**) and citrinaline A (**8.28**) against (a) human gastric cell line (AGS) and (b) colonadenocarcinoma (HT-29) cells as measured by plate reader spectrophotometer at OD_{600} with IC_{50} for citrinaline X (**8.30**) = 27.1±0.1 and 29.5±0.1 μM respectively

Bacillus subtilis ATCC 6051

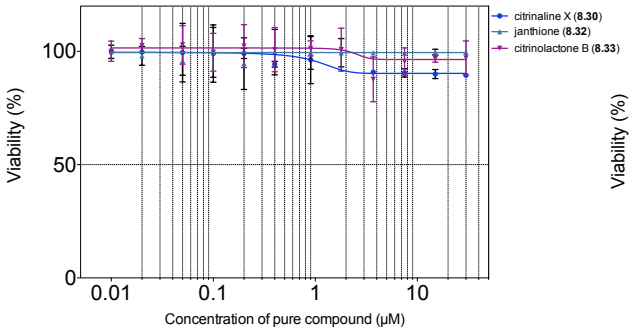

Bacillus subtilis ATCC 6633

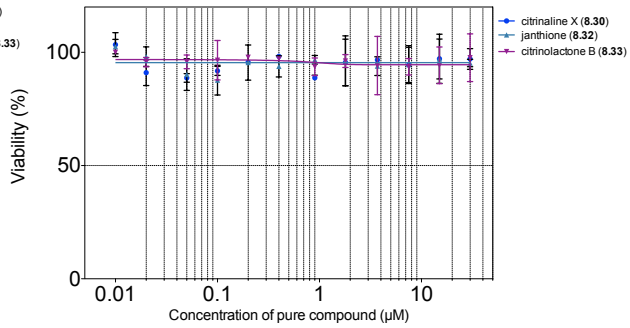

Staphylococcus aureus ATCC 25923

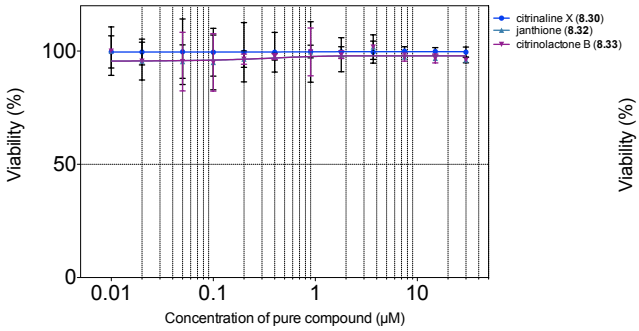

Staphylococcus aureus ATCC 9144

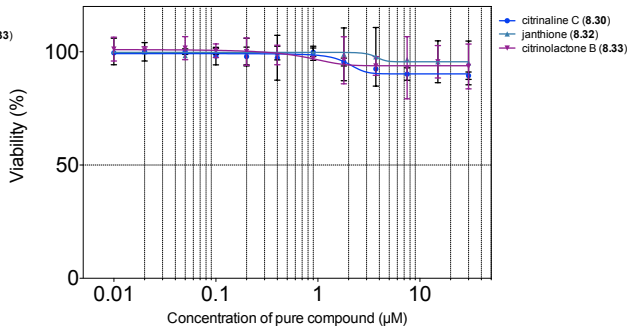

Escherichia coli ATCC 11775

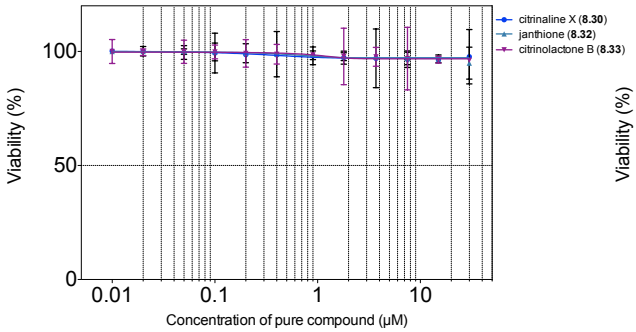

Pseudomonas aeruginosa ATCC 10145

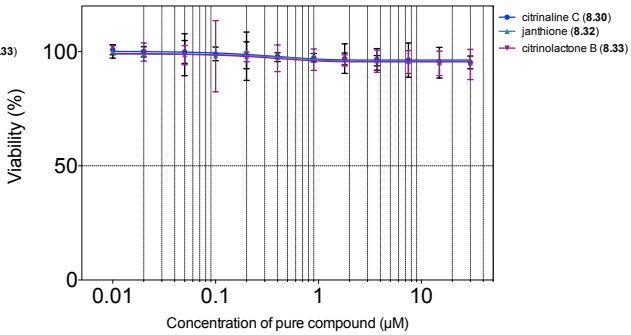

Candida albicans ATCC 90028

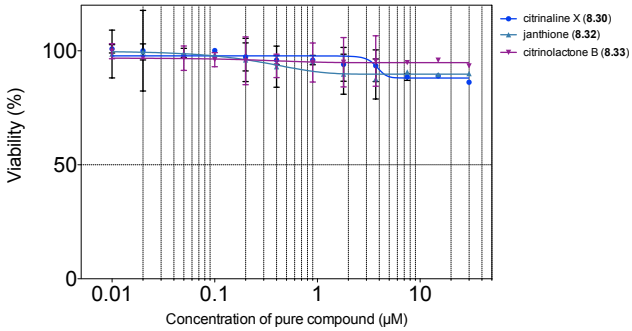

Figure 8.24. Graphs showing the antibacterial and antifungal activity of **8.30**, **8.32** and **8.33** as measured by plate reader spectrophotometer at OD_{600}

8.4 Conclusion

This chapter outlines the isolation of citrinaline X (**8.30**) as a new DKP metabolite from a terrestrial *Penicillium* sp. (CMB-TF438) together with the well-known fungal metabolite citrinin (**8.31**). The structure of citrinaline X was established by analysis of spectroscopic data using both 1D and 2D NMR data. During this study, citrinaline A and B were published by Pimenta *et al*. Further analysis of NMR data for **8.30** confirmed that it was the C-22 epimer of citrinaline A (**8.28**). A comparison between authentic sample citrinaline A (**8.28**) and citrinaline X (**8.30**) confirmed that citrinaline X (**8.30**) was not citrinaline A (**8.28**). We note from private communication that the published structure for citrinaline B (**8.29**) is to be revised, to be identical with that we now propose of **8.30**. However, we also note that these two compounds citrinaline B (**8.29**) and citrinaline X (**8.30**) possess opposite $[\alpha]_D$ measurements. To resolve this matter, the sample of **8.30** had been forward to collaborate for direct HPLC comparison with **8.29**. Although these results are pending, we strongly suspect the **8.30** and **8.29** are not the same, and that the proposed structure revision to **8.29** may required close inspection.

No biological activity has been reported for citrinaline A.[230] Also, citrinaline X was inactive in antimicrobial assay against *Staphylococcus aureus* (ATCC 25923 and 9144), *Bacillus subtilis* (ATCC 6051 and 6633), *Escherichia coli* (ATCC 11775), *Pseudomonas aeruginosa* (ATCC 10145) and *Candida albicans* (ATCC 10231) as well as against different cell line in the cytotoxic assay. In the same time, DKP *cyclo*-(L-Trp-L-Phe) was synthesized and added at different concentrations to *Penicillium* sp. (CMB-TF438) at 10 μM, it completely inhibited the production of citrinaline X and citrinin and activates the production of another metabolites, which where purified and the structures were solved to afford two known metabolites, janthinona (**8.32**) and citrinolactone B (**8.33**).

8.5 Future work

We hypothesize that *cyclo*-(L-Trp-L-Phe), which is present in many fungal metabolites, plays a role in the activation of secondary metabolites that may have in the future an important biological activity (see p.371).

8.6 Experimental section

8.6.1 Isolation and identification of strain CMB-TF0438:

The terrestrial derived fungus strain CMB-TF0438 was isolated from a terrestrial sample collected from North Stradbroke Island, Queensland. The fresh terrestrial sample was transferred to the laboratory in a sealed 50 mL Falcon tube at room temperature (24 h), where it is stored in the dark at −30 °C for one week. Approximately, 1 g of the thawed terrestrial sample was suspended in 8 mL sterile 0.9% saline solution and then subjected to heat-shock at 60 °C for 30 min after which 100 μL was serially diluted to 10^{-1}, 10^{-2} and 10^{-3} and transferred into 1000 μL sterile saline solution by means of sterile micro titre pipette. Furthermore, 50 μL from each diluted portion is dispersed across agar plates comprising (25 mL of 0.4% yeast extract, malt extract 1%, glucose 0.4%, agar 2% and 0.0005% rifampicin). The resulting agar plate was incubated at 27 °C for three weeks. Pure strains of individual colonies were obtained by standard microbiological techniques, and were grown to dense colonies on a single agar plate.

8.6.2 Chemical profiling:

A single colony of *Penicillium* sp. (CMB-TF0438) was sub-sampled into distilled water agar medium (25 mL of distilled water, 0.4% yeast extract, malt extract 1%, glucose 0.4%, agar 2%) and incubated at 27 °C for 10 d. The agar plate was soaked with EtOAc (100 mL), and shaken on the rotary shaker at 100 rpm overnight. The organic phase was concentrated *in vacuo* to yield an extract that was subsequently analysed by HPLC-DAD-ESI(±)MS and NMR.

8.6.3 Large-scale cultivation and extraction of strain CMB-TF0438:

A seed culture was prepared by inoculating a 25 mL agar plate containing (15 mL distilled water containing 0.4% yeast extract, malt extract 1%, glucose 0.4%, agar 2%) with 50 μL from the frozen culture followed by incubating the plate for 10 d at 27 °C. A loop of the seed culture was transferred to 30 agar plates with dimensions 150 × 120mm, and the plates were incubated for 10 d at 27 °C. The resulting cultures were sliced and soaked in 400 mL EtOAc and shake on the rotary shaker at 100 rpm overnight. The organic layer was concentrated *in vacuo* to yield an extract (190 mg). The extract was sequentially triturated with 25 mL each of hexane, CH_2Cl_2 and MeOH to afford 10 mg, 19.5 mg and 151.4 mg fractions, respectively. Each fraction was analysed by HPLC-DAD-MS and NMR. The MeOH fraction, which was found to be rich in the secondary metabolites, was subsequently subjected to semi-preparative reversed-phase HPLC (Zorbax C_{18} 250 × 9.4 mm, 5

μm column, 3 mL/min gradient elution from 70 – 10% H_2O/MeCN over 30 min with constant 0.01% TFA with a hold at 100% MeCN for 5 min), to yield citrinlaine X (**8.30**) (t_R = 19 min, 3 mg, 3.1%) and citrinin (**8.31**) (t_R= 25 min, 5 mg, 5.2%). [Note - % yields are determined on a mass-to-mass basis against the weight of EtOAc crude extract].

8.6.4 Large-scale cultivation and extraction of CMB-TF0438 in the presence of 8.32

A seed culture was prepared by inoculating a 80 mL ISP-2 broth containing (80 mL distilled water containing 0.4% yeast extract, malt extract 1%, glucose 0.4%) followed by incubating for 10 d at 27 °C. Seed culture (5 mL) was transferred to 400 mL ISP-2 broth containing **8.32** (10 μM) and incubated for 10 d at 27 °C. The broth was extracted with 2 × 400 mL EtOAc. The organic layer was concentrated *in vacuo* to yield an extract (190 mg). The extract was sequentially triturated with 8 mL each of hexane, CH_2Cl_2 and MeOH to afford 2 mg, 40 mg and 3 mg fractions, respectively. Each fraction was analysed by HPLC-DAD-MS and NMR. The CH_2Cl_2 fraction, which was found to be rich in the secondary metabolites, was subsequently subjected to semi-preparative reversed-phase HPLC (Zorbax C_8 250 × 9.4 mm, 5 μm column, 3 mL/min gradient elution from 90 – 10% H_2O/MeCN over 30 min with constant 0.01% TFA with a hold at 100% MeCN for 5 min), to yield janthinona (**8.33**) (t_R = 15 min, 1.5 mg, 3.1%) and citrinolactone B (**8.34**) (t_R= 22 min, 1 mg, 5.2%). [Note - % yields are determined on a mass-to-mass basis against the weight of EtOAc crude extract].

Citrinaline X (8.30): pale yellow powder $[\alpha]_D$ –8.1 (*c* 0.01, $CHCl_3$). UV (MeOH) λ_{max} ($\log_\varepsilon$): 206 (3.94), 228 (3.75, 259 (3.59), 352 (3.20) nm. IR (film) ν_{max}: 3348, 2946, 2833, 2360, 1449 cm^{-1}. NMR (600 MHz, MeOH-d_4) see Table 8.1; HRESI(+)MS *m/z* 454.2331 [M+H] (Δmmu +0.5) (calcd for $C_{25}H_{32}N_3O_5$ 454.2336)

Citrinin (8.31): yellowish brown oil; ^{1}H NMR (600 MHz, DMSO-d_6) see Table 8.3; HRESI(+)MS *m/z* 251.090 $[M+H]^+$ (calcd for $C_{13}H_{14}O_5$ 251.0914).

Janthinona (8.32): yellow oil; ^{1}H NMR (600 MHz, $CDCl_3$); see Table 8.5; HRESI(+)MS *m/z* 307.0577 $[M+Na]^+$ (calcd for $C_{22}H_{17}O_7Na$ 307.0586).

Citrinolactone B (8.33): colourless oil; $[\alpha]^{22}_D$ + 20.2 (*c* 0.01, MeOH); see **Table 8.7**; HRESI(+)MS *m/z* 255.0625 $[M+H]^+$ (calcd for $C_{22}H_{17}O_7Na$ 255.0628).

9 Chapter 9. Additional Microbial Chemical Diversity

9.1 Introduction

A diverse range of known secondary metabolites was isolated from various strains obtained from diverse locations around coastal areas of Australia. This chapter describes in brief an overview of known secondary metabolites from different strains. All analytical cultivation procedures were performed in which a single colony of the microbes was used to inoculate a seed culture composed of M1 media (100 mL in a 250 mL Schott flask). The strain was shaken at 190 rpm for 7 d at 27 °C, extracted with EtOAc (2 × 50 mL per flask), and the crude extract was redissolved in MeOH generating a concentration of 1 mg/mL and analysed by HPLC-DAD-ESI(±)MS (Zorbax C_8 column, 150 × 4.6 mm, 5 μm, 1 mL/min, gradient from 90 – 0% H_2O/MeCN (isocratic 0.05% formic acid) over 15 min, with a hold at 100% MeCN for 5 min). Large-scale cultivation was performed using two 2-L Erlenmeyer flasks containing M1 broth (400 mL) were inoculated with seed culture (5 mL) of the microbe. The flasks were incubated at 27 °C on a rotary shaker at 190 rpm for 7 d, extracted with EtOAc (2 × 300 mL per flask),

9.2 *Streptomyces* sp. (CMB-M0137)

A previous PhD student isolated *Streptomyces* sp. (CMB-M0137) from a marine sediment sample collected from Queensland, Australia. Analytical cultivation yielded peaks with the retention times t_R = 10.2 min and 11.4 min, which exhibited the following *m/z* $[M+H]^+$ 507 (**9.01**), 271 (**9.02**). Large-scale cultivation yielded a crude extract (60 mg). The crude extract was sequentially triturated with hexane and CH_2Cl_2 (10 mL aliquots), which were concentrated *in vacuo*, to yield 15.3 and 35 mg respectively (Scheme 9.1).

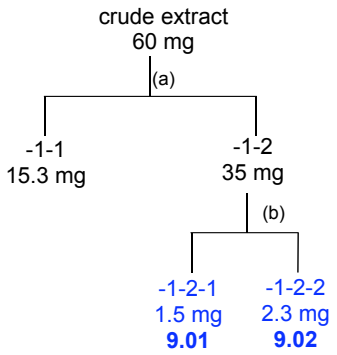

Scheme 9.1. Isolation scheme of crude extract from CMB-M0137 (a) Trituration [hexane (-1-1) and CH_2Cl_2 (-1-2)], (b) Semi-preparative HPLC: Zorbax C_8, 90 – 10% H_2O/MeOH, 3 mL/min, 30 min.

9.2.1 Streptonigrin (9.01)

HRESI(+)MS analysis of **9.01** revealed a quasi-molecular ion $[M+H]^+$ corresponding to a molecular formula ($C_{25}H_{22}N_4O_8$, Δmmu –0.6). On searching the literature, **9.01** was determined to be consistent with the known bacterial metabolite streptonigrin. Analysis of all the NMR (600 MHz, $CDCl_3$) data with comparison to literature data (Figure 9.1, Table 9.1 and Table 9.2) confirmed that **9.01** was streptonigrin. Herlt *et al*. isolated streptonigrin from *Streptomyces* sp. as a novel heterocyclic compound with antibacterial and antifungal activity.[249]

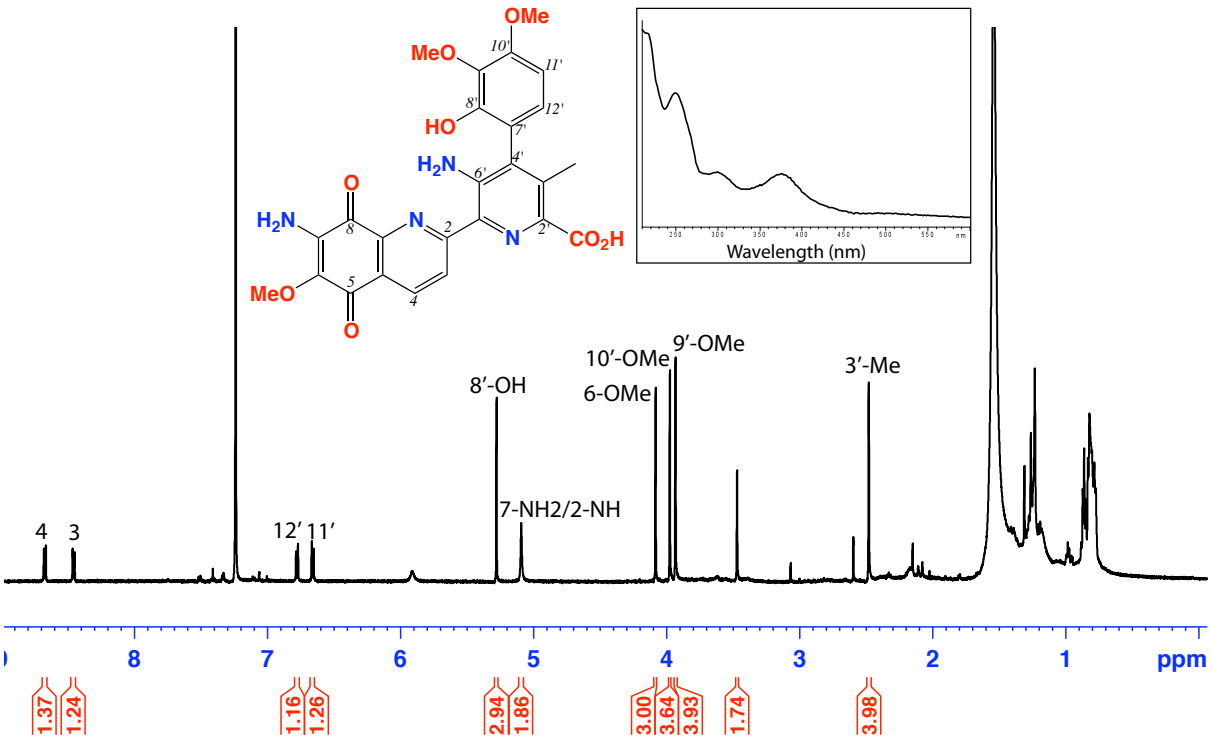

Figure 9.1. ^{1}H NMR (600 MHz, $CDCl_3$) and UV-vis (HPLC-DAD, H_2O/MeCN plus HCO_2H at 254 nm) spectra of streptonigrin (**9.01**)

Table 9.1. NMR (600 MHz, $CDCl_3$) data of streptonigrin (**9.01**)

Pos	δ_H, mult, (*J* in Hz)	δ_C[a]	COSY	$^1H - ^{13}C$ HMBC
1				
2		144.8		
3	8.50, d *(8.3)*	134.8	4	7, 8a
4	8.72, d *(8.3)*	125.8	3	2, 4a
4a		126.5		
5		179.9		
6		137.5		
7		[b]		
8		[b]		
8a		159.7		
1′		[b]		
2′		134.5		
3′		139.6		
4′		132.2		
5′		147.4		
6′		136.8		
7′		113.6		
8′		[b]		
9′		136.8		
10′		159.6		
11′	6.70, d *(8.3)*	105.6	12′	7′, 9′
12′	6.82, d *(8.3)*	125.4	11′	5′, 10′
6-OMe	4.13, s	60.9		6
7-NH_2/NH	5.75, s			5
8′-OH	5.92, s			
2′-COOH	[b]			
3′-Me	2.52, s	17.8		2′, 3′, 4′
9′-OMe	3.98, s	56.6		10′
10′-OMe	4.02, s	62.1		6′

(a) assignments supported by HSQC and HMBC, (b) signals not observed

Table 9.2. ^1H NMR (600 MHz, $CDCl_3$) comparison of experimental and literature[250] data of streptonigrin (**9.01**)
[250]

Pos	δ_H, mult, (*J* in Hz) (experimental)	δ_H, mult, (*J* in Hz) (literature)
3	8.50, d *(8.3)*	8.48, d *(8.4)*
4	8.72, d *(8.3)*	8.69, d *(8.4)*
11′	6.70, d *(8.3)*	6.68, d *(8.5)*
12′	6.82, d *(8.3)*	6.80, d *(8.5)*
6-OMe	4.13, s	4.10, s
7-NH_2/NH	5.75, s	5.12, br s
8′-OH	5.92, s	5.95, br s
2′-COOH	[b]	12.39, br s
3′-Me	2.52, s	2.50, s
9′-OMe	3.98, s	3.95, s
10′-OMe	4.02, s	3.99, s

*(a) assignments supported by HSQC, (b) signals not observed

9.2.2 1-*N*-methylalbonourisin (9.02) and lansai D (9.03)

ESI(+)MS data for **9.02** revealed a *m/z* 271[M+H]$^+$ consistent with 1-*N*-methylalbonourisin. On searching the literature, **9.02** was determined to be consistent with the known bacterial metabolite (*3Z*, *6E*)1-*N*-methylalbonourisin. Analysis of all the NMR (600 MHz, $CDCl_3$) data with comparison to literature data (Figure 9.2 and Table 9.3) confirmed that **9.02** was 1-*N*-methylalbonourisin. 1-*N*-methylalbonourisin was isolated from the culture of first isolated from *Streptomyces* sp.[251] and then was reisolated from *Micromonospora* sp.[250]. Lansai D (**9.03**) is similar 1-*N*-methylalbonourisin but with (*3E*, *6E*).[252] Our molecule was a mixture of 1-*N*-methylalbonourisin and lansai D. We hypothesize that **9.03** during handling and isolation procedures can undergo double isomerization to give the more stable analogue **9.02**. Wang *et al* isolated **9.03** using TFA, while Tuntiwachwuttikul *et al*. isolated **9.03** only with EtOAc and MeOH.

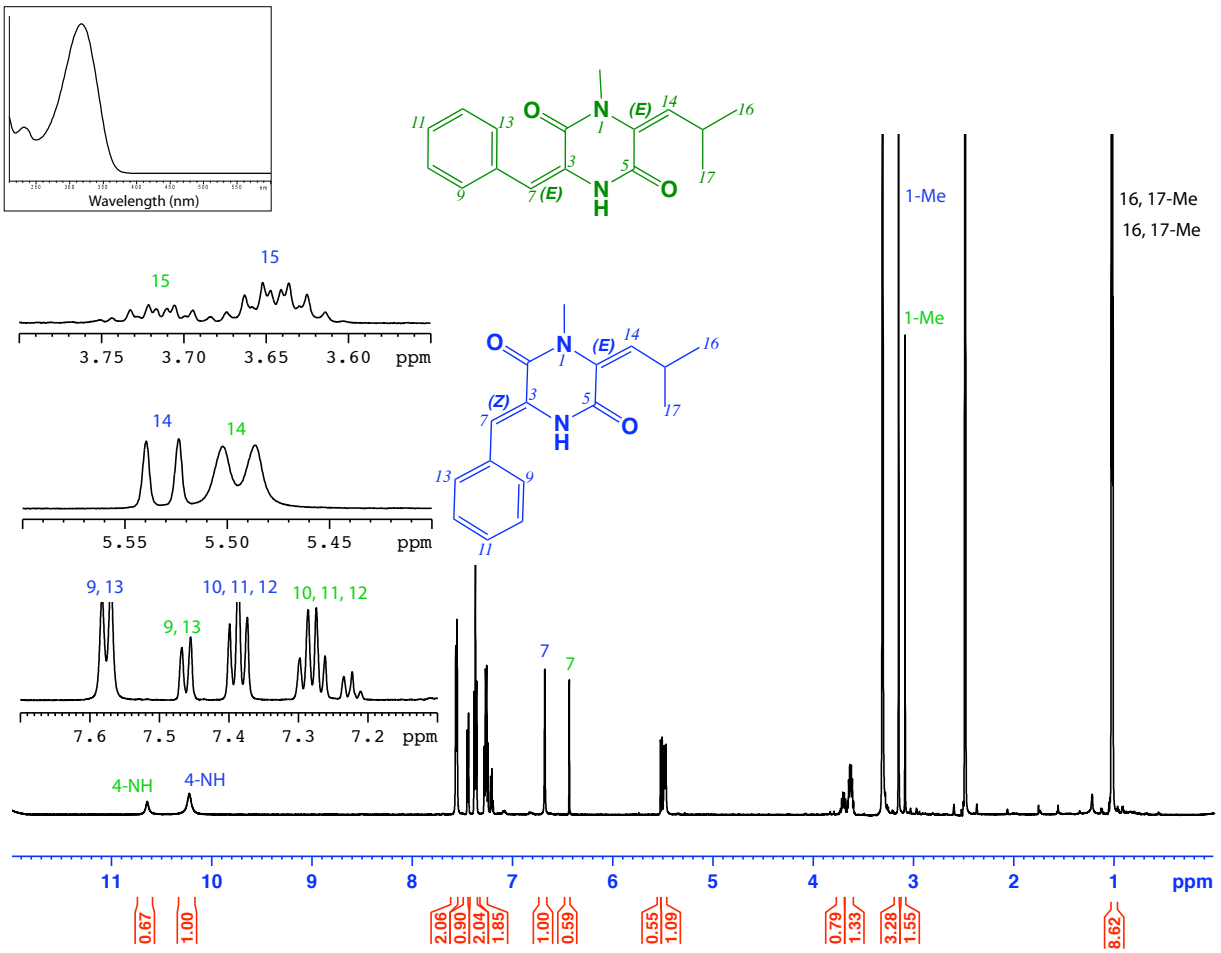

Figure 9.2. ^{1}H NMR (600 MHz, DMSO-d_6) and UV-vis (HPLC-DAD, H_2O/MeCN plus HCO_2H at 254 nm) spectra of 1-*N*-methylalbonourisin (**9.02**) (blue) and lansai D (**9.03**)

Table 9.3. NMR (600 MHz, DMSO-d_6) data of 1-*N*-methylalbonourisin (**9.02**) and lansai D (**9.03**)

Pos	δ_H, mult, (*J* in Hz) (**9.02**)	δ_C[a] (**9.02**)	δ_H, mult, (*J* in Hz) (**9.03**)	δ_C[a] (**9.03**)
1-Me	3.16, s	29.9	3.10, s	29.0
2		159.7		158.2
3		129.5		128.3
4-NH	10.23, s		10.67, s	
5		156.8		156.6
6		128.7		128.3
7	6.69, s	114.8	6.45, s	119.8
8		129.5		130.3
9, 13	7.57, d *(7.8)*	129.1		129.9
10, 11, 12	7.38, t *(7.8)*	128.5		127.6
14	5.53,d *(9.3)*	132.3	5.49, d *(9.3)*	131.6
15	3.64, m	26.1	3.71, m	29.9
16	1.03, d *(3.3)*[b]	22.9[b]	1.03, d *(3.3)*[b]	22.9[b]
17	1.02, d *(3.1)*[b]	22.9[b]	1.02, d *(3.1)*[b]	22.9[b]

*(a) assignments supported by HSQC and HMBC, (b) Overlapping resonances

9.3 *Streptomyces* sp. (CMB-TB376)

Streptomyces sp. (CMB-TB376) was isolated from a terrestrial sample collected from North Stradbroke Island, Queensland, Australia. Analytical cultivation yielded peaks with the retention times t_R = 6.2 min and 8.3 min exhibited the following *m/z* $[M+H]^+$ 394 (**9.04**), 393. Large-scale cultivation yielded a crude extract (30 mg), which was sequentially triturated with hexane, CH_2Cl_2 and MeOH (10 mL aliquots), concentrated *in vacuo*, to yield 4, 3 and 20 mg respectively (Scheme 9.2).

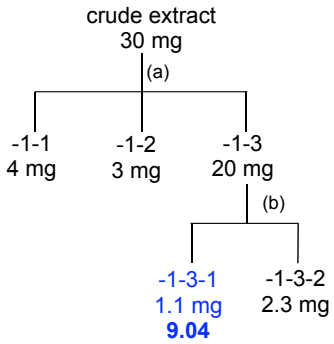

Scheme 9.2. Isolation scheme of crude extract from CMB-TB385 (a) Trituration [hexane (-1-1), CH_2Cl_2 (-1-2) and MeOH (-1-3)], (b) Semi-preparative HPLC: Zorbax-C_{18}, 60 – 10% H_2O/MeCN, isocratic 0.01% TFA, 3 mL/min, 30 min.

9.3.1 Undecyl prodigiosin (9.04)

HRESI(+)MS analysis of **9.04** revealed an adduct molecular ion $[M+Na]^+$ corresponding to a molecular formula ($C_{25}H_{35}N_3O_1$, Δ mmu –1.8). On searching the literature, **9.04** was determined to be consistent with the known bacterial metabolite undecyl prodigiosin. Analysis of all the NMR (600 MHz, DMSO-d_6) data with comparison to literature data (Figure 9.3, Table 9.4 and Table 9.5) confirmed that **9.04** was undecyl prodigiosin. Wasserman *et al*. isolated undecyl prodigiosin from *Streptomyces longisporus ruber* sp.[253,254]

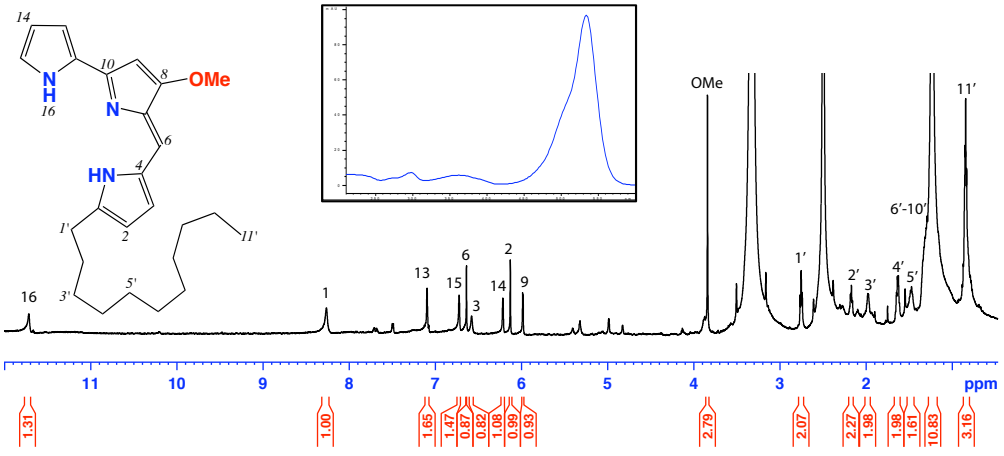

Figure 9.3. ^{1}H NMR (600 MHz, DMSO-d_6) and UV-vis (HPLC-DAD, H_2O/MeCN plus HCO_2H at 254 nm) spectra of undecyl prodigiosin **(9.04)**

Table 9.4. NMR (600 MHz, DMSO-d_6) data of undecyl prodigiosin (**9.04**)

Pos	δ_H, mult, (*J* in Hz)	δ_C[a]	COSY	$^1H - ^{13}C$ HMBC
1		149.2		
2	6.13, br	110.1	3	
3	6.58, br	118.3	2	
4		[c]		
5				
6	6.63, s	114.0		8
7		[c]		
8		160.2		
9	5.98, br	95.8		
10		[c]		
11				
12		123.4		
13	7.09, br	121.9		
14	6.21, br	109.5		12
15	6.72, br	111.8	16	
16-NH	11.71, br		15	
8-OMe	3.84, s	57.9		6
1′	2.75, t *(7.8)*	27.5	2′	1
2′	2.17, m	26.9	1′, 3′	
3′	1.97, m	26.1	2′, 4′	
4′	1.63, m	25.2	3′, 5′	
5′	1.47, m	24.2	4′	
6′-10′	1.30[b]	21.6		
11′-Me	0.84, t *(6.1)*	13.5		

*(a)assignments supported by HSQC and HMBC, (b) Overlapped resonances, (c) signals not observed

Table 9.5. ^1H NMR comparison ($CDCl_3$) of experimental and literature[122] data of undecyl prodigiosin (**9.04**)

Pos	δ_H, mult, (*J* in Hz) (experimental)	δ_H, mult, (*J* in Hz) (literature)
2	6.10, d *(3.4)*	6.18, d *(3.7)*
3	6.79, d *(3.4)*	6.81, d *(3.7)*
6	6.99, s	6.98, s
9	6.02, s	6.08, s
13	7.31, br	7.32, brs
14	6.38, dd *(3.1, 2.0)*	6.37, dd *(3.5, 2.5)*
15	6.99, dd *(3.1, 2.0)*	6.97, dd *(3.7, 1.1)*
8-OMe	4.03, s	4.01, s
1′	2.88, m	2.79, m
2′-10′	1.21 – 1.39, m	1.25 – 1.35, m
11′-Me	0.88, t *(6.2)*	0.87, t *(6.6)*

9.4 *Streptomyces* sp. (CMB0-TB385)

Streptomyces sp. (CMB-TB385) was isolated from a terrestrial sample collected from New South Wales, Australia. Analytical cultivation yielded peaks with the following retention times t_R = 9.1 min and 15.6 min exhibited the following *m/z* $[M+H]^+$ 193 (**9.05**), 364 (**9.06**). Large-scale cultivation yielded a crude extract (30 mg), which was sequentially triturated with hexane, CH_2Cl_2 and MeOH (10 mL aliquots), concentrated *in vacuo*, to yield 1, 10 and 32.3 mg respectively (Scheme 9.3).

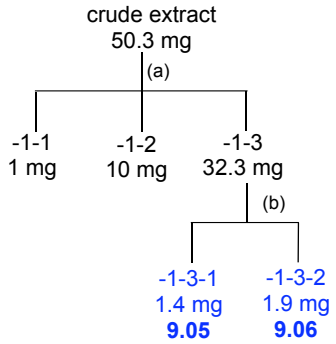

Scheme 9.3. Isolation scheme of crude extract from CMB-TB385 (a) Trituration [hexane (-1-1), CH_2Cl_2 (-1-2) and MeOH (-1-3)], (b) Semi-preparative HPLC: Zorbax C_8, 90 – 10% H_2O/MeOH, 3 mL/min, 30 min.

9.4.1 6,8-dihydroxy-3-methylisocoumarin (9.05)

HRESI(+)MS analysis of **9.05** revealed an adduct molecular ion $[M+H]^+$ corresponding to a molecular formula ($C_{10}H_8O_4$, Δmmu –0.1). On searching the literature, **9.05** was determined to be consistent with the known bacterial metabolite 6,8-dihydroxy-3-methylisocoumarin. Analysis of all the NMR (600 MHz, DMSO-d_6) data with comparison to literature data (Figure 9.4, Table 9.6 and Table 9.7) confirmed that **9.05** was 6,8-dihydroxy-3-methylisocoumarin. Mehdi *et al*., isolated 6,8-dihydroxy-3-methylisocoumarin from *Streptomyces* sp.[255]

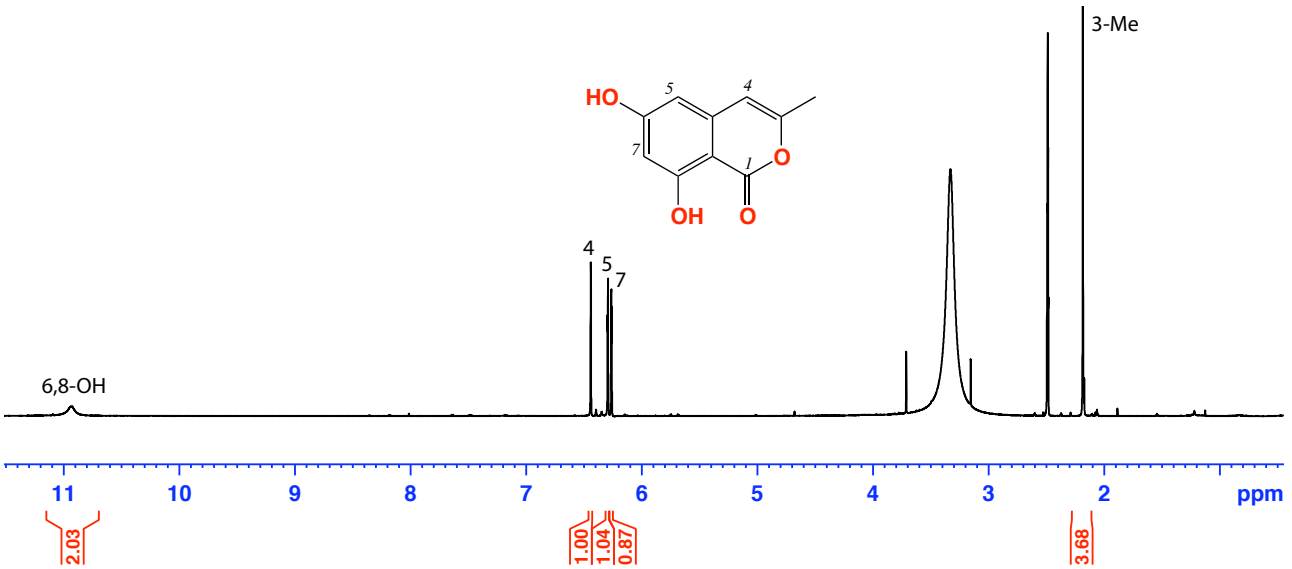

Figure 9.4. ^{1}H NMR (600 MHz, DMSO-d_6) of 6,8-dihydroxy-3-methylisocoumarin (**9.05**)

Table 9.6. NMR (600 MHz, DMSO-d_6) data of 6,8-dihydroxy-3-methylisocoumarin **9.05**

Pos	δ_H, mult, (J in Hz)	δ_C[a]	^{1}H – ^{13}C HMBC
1		166.2	
2			
3		155.6	
4	6.44, s	102.6	4a
4a		141.2	
5	6.29, s	100.9	
6		166.2	
7	6.26, s	103.7	6
8		[b]	
7,8-OH	10.91, brs		
9-Me	2.18, s	18.4	1, 3

(a)assignments supported by HSQC, (b) Overlapped resonances

Table 9.7. ^{1}H NMR (DMSO-d_6) comparison of experimental and literature[255] data of **9.05**

Pos	δ_H, mult, (J in Hz) (experimental)[a]	δ_H, mult, (J in Hz) (literature)[b]
4	6.44, s	6.47, s
5	6.29, s	6.33, s
7	6.30, s	6.30, s
7,8-OH	10.91, br s	[c]
9-Me	2.18, s	2.22, s

(a) measured 600 MHz, (b) 300 MHz, (c) not observed

9.4.2 Trindoline (9.06)

HRESI(+)MS analysis of **9.06** revealed an adduct molecular ion $[M+Na]^+$ corresponding to a molecular formula ($C_{24}H_{17}N_3O_1$, Δmmu –0.1). On searching the literature, **9.06** was determined to be consistent with the known bacterial metabolite trindoline. Analysis of all the NMR (600 MHz, DMSO-d_6) data with comparison to literature data (Figure 9.5, Table 9.8 and Table 9.9) confirmed that **9.06** was trindoline. Kobayashi *et al*., isolated trindoline from *Vibrio* sp. as new antibiotic indole dimer.[256]

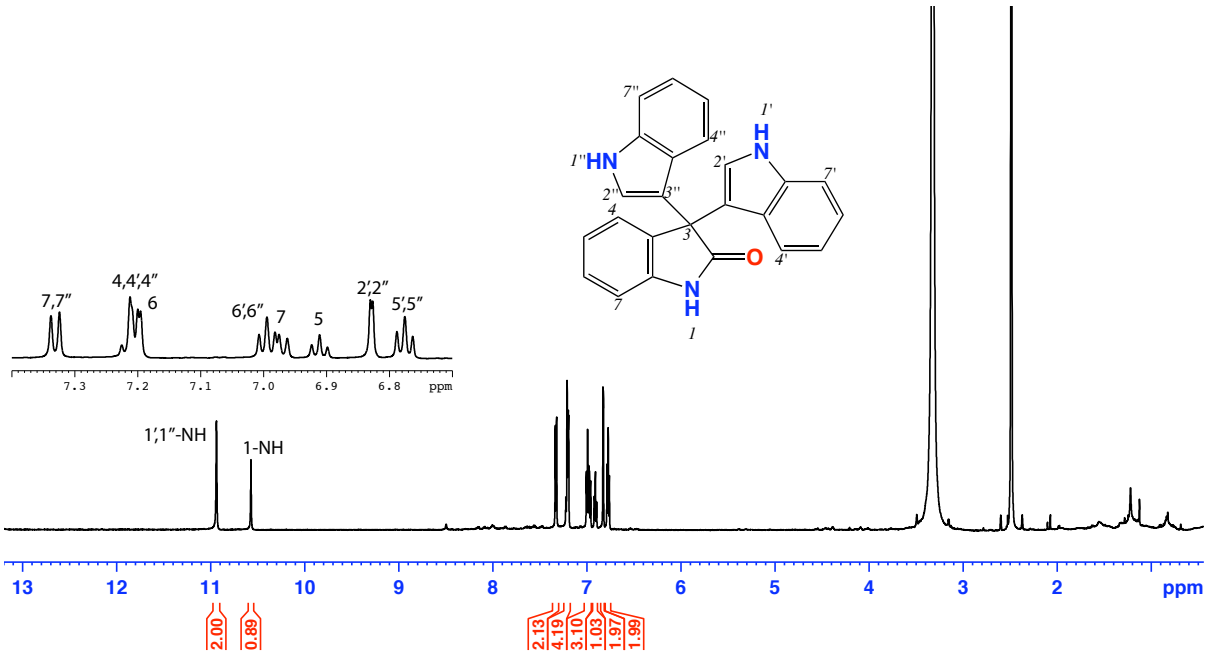

Figure 9.5. ^{1}H NMR (600 MHz, DMSO-d_6) of trindoline (**9.06**)

Table 9.8. NMR (600 MHz, DMSO-d_6) data of trindoline (**9.06**)

Pos	δ_H, mult, (*J* in Hz)	δ_C[a]	COSY	^{1}H – ^{13}C HMBC
1	10.57, s			3
2		[c]		
3		56.2		
3a		136.2		
4	7.23[b], m	128.2	5	7a
5	6.91, t *(7.3)*	122.0	4, 6	
6	7.19, d *(2.6)*	121.3	5, 7	
7	6.99, d *(7.8)*	121.5	6	3a
7a		142.1		
1′, 1″	10.94, s		2′/2″	
2′, 2″	6.82, d *(2.4)*	124.8	1′/1″	3′a/3″b, 4′/4″
3′, 3″		117.3		
3′a, 3″b		126.2		
4′, 4″	7.22[b], m	125.5	5′/5″	
5′, 5″	6.79, t *(8.1)*	118.8	4′/4″, 6′/6″	
6′, 6″	6.96, t *(7.8)*	110.2	5′/5″, 7′/7″	
7′, 7″	7.33, d *(8.1)*	112.1	6′/6″	7′a/7″a
7′a, 7″a		140.1		

*(a) assignments supported by HSQC and HMBC, (b) Overlapping resonances, (c) signals not observed

Table 9.9. NMR comparison (MeOH-d_4) of experimental and literature[256] data of trindoline (**9.06**)

Pos	δ_H, mult, (*J* in Hz)[a] (experimental)	δ_H, mult, (*J* in Hz)[b] (literature)
4	7.25, d *(7.6)*	7.27, d *(7.5)*
5	6.98, dd *(7.6, 6.8)*	6.97, ddd *(7.5, 7.5, 1.0)*
6	7.27, dd *(7.6, 7.5)*	7.25, ddd *(7.5, 7.5, 1.0)*
7	7.01, d *(7.5)*	7.05, d *(7.5)*
2′, 2″	6.91, s	6.90, s
4′, 4″	7.27, d *(7.6)*	7.27, d *(7.5)*
5′, 5″	6.80, ddd *(7.6, 7.2, 1.1)*	6.81, ddd *(7.5, 7.5, 1.0)*
6′, 6″	7.01, ddd *(7.6, 7.5, 1.2)*	7.03, ddd *(7.5, 7.5, 1.0)*
7′, 7″	7.29, d *(7.6)*	7.32, d *(7.5)*

*(a) measured at 600 MHz, (b) measured at 500 MHz

9.5 *Streptomyces* sp. (CMB-TB350)

Streptomyces sp. (CMB-TB350) was isolated from a terrestrial sample collected from North Stradbroke Island, Queensland, Australia. A single colony of strain CMB-TB350 was used to inoculate a seed culture composed of ISP-2 media. Analytical cultivation yielded peaks with retention times t_R = 11.1 min and 13.2 min exhibited the following *m/z* $[M+2H]^{2+}$ 649 (**9.07**). Large-scale cultivation, yield a crude extract (45 mg), which was sequentially triturated with hexane and CH_2Cl_2 (10 mL aliquots), concentrated *in vacuo*, to yield 12, and 25.4 mg respectively (Scheme 9.4).

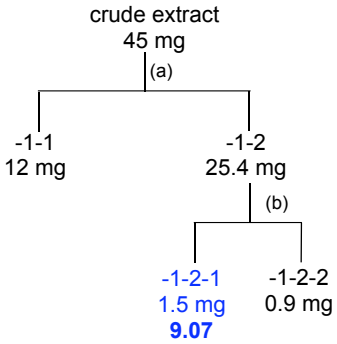

Scheme 9.4. Isolation scheme of crude extract from CMB-TB350 (a) Trituration [hexane (-1-1) and CH_2Cl_2 (-1-2)], (b) Semi-preparative HPLC: Zorbax-C_8, 90 – 10% H_2O/MeCN (isocratic 0.01% TFA), 3 mL/min, 30 min.

9.5.1 Actinomycin Z (9.07)

ESI(+)MS analysis of **9.07** revealed a molecular ion *m/z* 649 $[2M+2H]^+$. On searching the literature, **9.07** was determined to be consistent with the known bacterial metabolite actinomycin Z_1. Analysis of all the NMR (600 MHz, $CDCl_3$) data with comparison to literature data (Figure 9.6, Table 9.10 and Table 9.11) confirmed that **9.07** was actinomycin Z_1. Lackner *et al*., isolated actinomycin Z_1 from *Streptomyces fradiae* sp. as new antibiotic.[257]

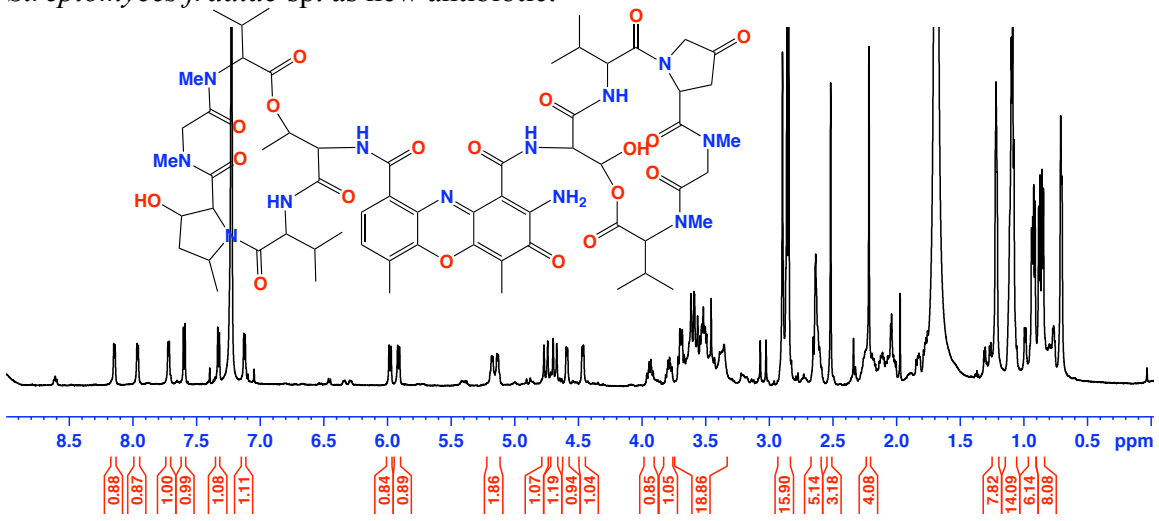

Figure 9.6. ^1H NMR (600 MHz, $CDCl_3$) of actinomycin Z_1 (**9.07**)

Table 9.10. NMR (600 MHz, $CDCl_3$) data of actinomycin Z_1 (**9.07**)

#	Pos.	δ_H, mult (*J* in Hz)[a] α-ring	β-ring	δ_C[a]	COSY	HMBC
Thr	1			168.3/170.1		
	2	4.65, d *(9.0)*	5.01, m	55.2	3	1, 4
	3	5.24, dd *(9.0, 3.1)*	5.10, m	77.6	4	
	4	1012, d *(6.0)*	3.66[b], m	17.2	3	2
	NH	7.14, d *(6.0)*	[c]			
	OH	[c]	[c]			
Val	1			172.3/173.4		
	2	3.42[b], m	3.82[b], m	57.6/57.8	3	1
	3	2.11, m	2.18, m	32.9	2	
	3-Me	0.90, m	0.91, d *(6.1)*	18.9	3	
		1.12, d *(6.5)*	1.12, d *(6.1)*			
	NH	8.16, d *(6.5)*	[c]			
3-OH-5-Me-Pro	1			171.3/169.2		
	2	5.91, d *(9.1)*	6.14, d *(6.5)*	66.3	3	
	3	3.95[b], m	2.32[c], m	77.2	2	1
			3.92[c], m			
	4	a 2.11[b], m		40.2		
		b 2.17[b], m				
	5	4.70, d *(4.5)*	4.52, dd *(7.2, 2.3)*	55.4	5-Me	
	5-Me	1.48, br d	1.58[d]	17.8	5	
	OH	[c]	[c]			
Sar	1			167.8		
	2	a 3.59[c], m	3.62[c], m	71.7		1
		b 4.62, d *(6.1)*	4.52, d *(16.5)*			
	N-Me	2.87, s	2.86, s	22.1		
Me Val	1			166.8		
	2	2.68[c], m	3.21[c]	52.3	3	3
	3	2.67[c], m	1.31, d *(6.1)*		2	1
	3-Me	0.72, d *(6.1)*		36.1	3	
		0.93, d *(6.1)*				
	N-Me	2.84, s	2.87, s	29.2		
Chrom.	4-Me	2.12, s		33.1		
	6-Me	2.51, s		36.1		8
	7	7.35, d (7.6)		122.6	8	
	8	7.51, d (7.6)		125.9	7	
	NH_2	[c]				

*(a) assignments supported by HSQC and HMBC, (b) Overlapped resonances, (c) signals not observed

Table 9.11. ^{1}H NMR ($CDCl_3$) comparison of experimental and literature[257] data of actinomycin Z_1 (**9.07**)

#	Pos.	δ_H, mult (*J* in Hz)[a] experimental		δ_H, mult (*J* in Hz)[a] literature	
		α-ring	β-ring	α-ring	β-ring
Thr	1				
	2	4.65, d *(9.0)*	5.01, m	4.62, dd, br	2.01, dd br
	3	5.24, dd *(9.0, 3.1)*	5.10, m	52.4, dq *(10.1, 3.2)*	5.10, m
	4	1012, d *(6.0)*	3.66[b], m	1.12, d *(6.4)*	3.69, m
	NH	7.14, d *(6.0)*	[c]	7.18, brs	8.13, d *(6.2)*
	OH	[c]	[c]		3.22, s
Val	1				3.83, dd *(9.9, 6.2)*
	2	3.42[b], m	3.82[b], m	3.44, dd *(9.9, 6.9)*	2.18, m
	3	2.11, m	2.18, m	2.11, m	0.92, d *(6.2)*
	3-Me	0.90, m	0.91, d *(6.1)*	0.90, d *(6.2)*	1.15, d *(6.6)*
		1.12, d *(6.5)*	1.12, d *(6.1)*	1.12, d *(6.3)*	
	NH	8.16, d *(6.5)*	[c]	8.15, d *(6.9)*	8.30, brs
3-OH-5-Me-Pro	1				
	2	5.91, d *(9.1)*	6.14, d *(6.5)*	5.86, s	6.42, dd *(11.0, 2.0)*
	3	3.95[b], m	2.32[c], m	4.16, dd *(11.3, 5.2)*	2.32, d *(17.6)*
			3.92[c], m		3.93, dd *(17.6, 11.0)*
	4	a 2.11[b], m		2.11, m	
		b 2.17[b], m		2.18, m	
	5	4.70, d *(4.5)*	4.52, dd *(7.2, 2.3)*	4.71, m	4.55,q *(7.1)*
	5-Me	1.48, br d	1.58[d]	1.49, d *(5.8)*	1.59, d *(7.1)*
	OH	[c]	[c]	4.46, m	
Sar	1				
	2	a 3.59[c], m	3.62[c], m	3.61, d *(17.5)*	3.65, d *(17.5)*
		b 4.62, d *(6.1)*	4.52, d *(16.5)*	4.73, d (17.5)	4.56, d *(17.5)*
	N-Me	2.87, s	2.86, s	2.88, s	2.85, s
Me Val	1				
	2	2.68[c], m	3.21[c]	2.69, d *(9.3)*	3.22, q *(6.9)*
	3	2.67[c], m	1.31, d *(6.1)*	2.64, m	1.32, d *(6.9)*
	3-Me	0.72, d *(6.1)*		0.73, d *(6.7)*	
		0.93, d *(6.1)*		0.94, d *(6.4)*	
	N-Me	2.84, s	2.87, s	2.88, s	2.89, s
Chrom.	4-Me	2.12, s		1.93, s	
	6-Me	2.51, s		2.51, s	
	7	7.35, d (7.6)		7.34, d *(7.6)*	
	8	7.51, d (7.6)		7.48, d *(7.6)*	
	NH_2	[c]		7.20 + 8.10 br	

*(a) assignments supported by HSQC and HMBC, (b) Overlapping resonances, (c) signals not observed

10 Chapter 10. Microbial Community isolation and analysis

10.1 Introduction

Soil microbes play an important role in various aspects of terrestrial ecosystems. In order to access these microbial communities, terrestrial soil/sediment samples collected from different regions in Australia were used to inoculate solid phase culture media, and facilitate the recovery of pure isolates using standard microbiological techniques.

10.2 Sampling

A total of 120 (~ 5 g) sediment samples were collected during the period from January 2009 to December 2009, from different environments in Australia, to maximize access to a diversity of soil microorganisms. Samples were collected in sterile 50 mL falcon tubes, and debris/plant residues removed by manual inspection.

10.3 Transportation and storage conditions

Environmental factors such as freezing, thawing and moisture can have a great impact on microbial cell wall and may cause cell lysis for microbes with fragile cell structures. Hence, the transportation and storage conditions can impact on microbial community diversity. We employed transportation and storage methods designed to minimize the loss of microbial diversity. Samples were rapidly transferred to the laboratory in sealed containers and processed immediately after arrival (or stored at −32 °C freezer).

10.4 Isolation of microbes

The samples were processed by two different methods; (1) stamping and (2) dilution and heat-shock; and were inoculated into different isolation media (M1, LB, YPD, M7, ISP-2, MH, mannitol and TSA) (Table 10.1).

10.4.1 Stamping

In the stamping method a sediment sample (1 g) was placed aseptically in a sterile petri dish, dried (approx. 24 h) in a laminar flow hood, and then inoculated onto agar media by stamping 8 to 9 times in a circular way to give a serial dilution effect.[258,259]

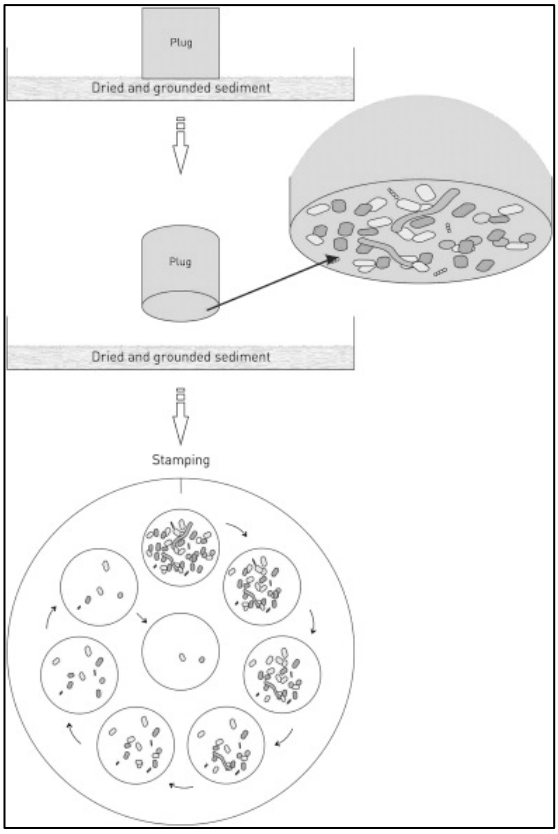

Figure 10.1. Schematic demonstration of stamping technique. Figure from Tresner *et al*. [259]

10.4.2 Dilution and heat-shock

In the dilution and heat-shock, sterile brine (9 mL) was added to a soil sample (1 g), which was shaken well. The resulting suspension was heated at 55 °C for 30 min with vigorous shaking on a water bath. The supernatant from this heat-shock processing was diluted serially (10^{-1} to 10^{-6}) by transferring 1 mL into 9 mL sterile brine solution. Furthermore, 50 μL from each diluted portion was dispersed across a culture plate (Petri dish) containing one of several defined media by means of disposable sterile rods (Scheme 10.1).

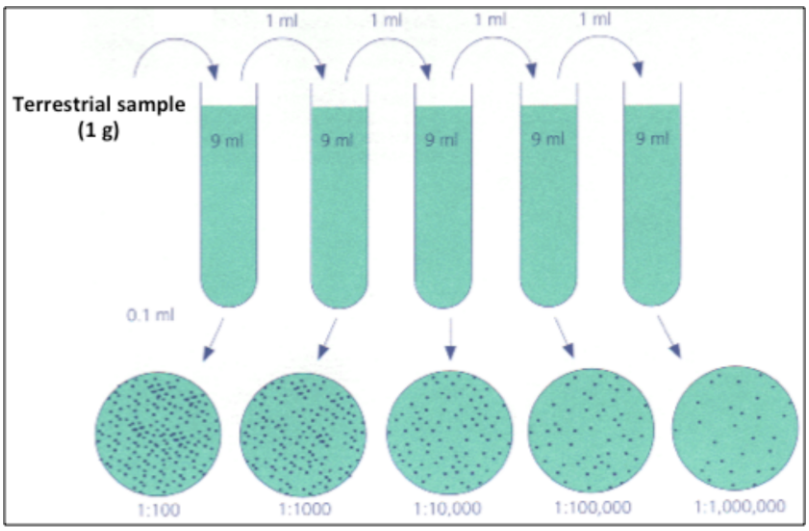

Scheme 10.1. Schematic demonstration of heat shock and dilution technique.

For both methods, culture plates were grown for 1 – 5 weeks in an incubator set at 26.5 – 30° C, with periodic inspection to note for significant growth. Standard microbiological technique of sampling and replating was used to acquire pure isolates of individual colonies. Actinomycetes usually appeared between one and six weeks of incubation. The pure actinomycetes colony was considered the colony with tough leathery texture, dry or folded appearance, and branching filaments with or without aerial mycelia (Scheme 10.2).

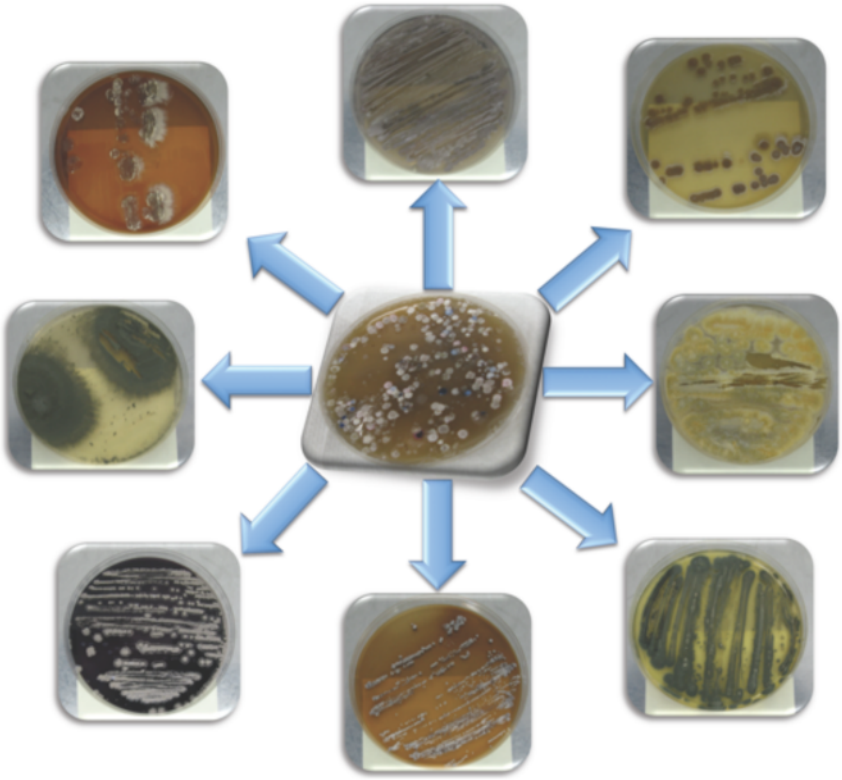

Scheme 10.2. Schematic demonstration for the microbial isolation from sediment samples

Table 10.1. Summary for the description of the different isolation media

#	Description
Media 1 (LB)	LB agar: comprising H_2O (1 L), casein peptone (10 g), yeast extract (5 g), NaCl (5 g) and agar (15 g).
Media 2 (Manniol agar)	Mannitol agar: comprising H_2O (1 L), peptone (3 g), yeast extract* (5 g), D-mannitol (25 g) and agar* (15 g).
Media 3 (YPD)	YPD agar: comprising H_2O (1 L), yeast extract* (10 g), peptone* (20 g), D-glucose* (20 g) and agar (20 g).
Media 4 (M1)	M1 agar: comprising H_2O (1 L), yeast extract (4 g), peptone (2 g) and agar (18 g).
Media 5 (M7)	M7 agar: comprising H_2O (1 L), D-mannitol (0.5 g), tryptone (0.1 g) and agar (8 g).
Media 6 (ISP-2)	ISP-2: comprising H_2O (1 L), yeast extract (4 g), malt extract (10 g), D-glucose (4 g) and agar (20 g).
Media 7 (Muller Hinton)	Muller Hinton agar: comprising H_2O (1 L), beef extract powder (2 g), acid digest casein (17.5 g), starch (1.5 g) and agar (17 g).
Media 8 (Tryptic soy)	Tryptic soy agar: comprising pancreatic digest of casein (15 g), papaic digest of soybean (5 g), NaCl (5 g) and agar (15 g).

All the isolation media were supplemented with either the antifungal cycloheximide (100 μg/mL) (**10.01**) for actinomycetes selection, and either of the antibacterials rifampin (5 μg/mL) (**10.02**) or novobiocin sodium salt (25 μg/mL) (**10.03**) for fungal selection.

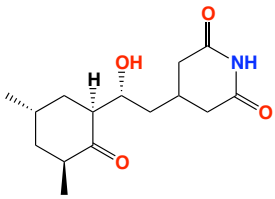

cycloheximide (**10.01**)

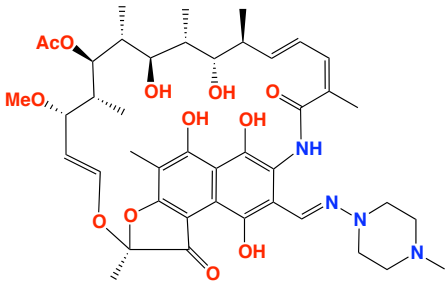

rifampicin (**10.02**)

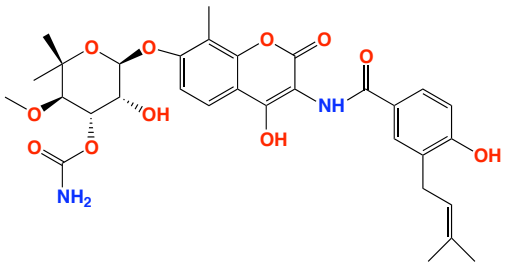

novobiocin (**10.03**)

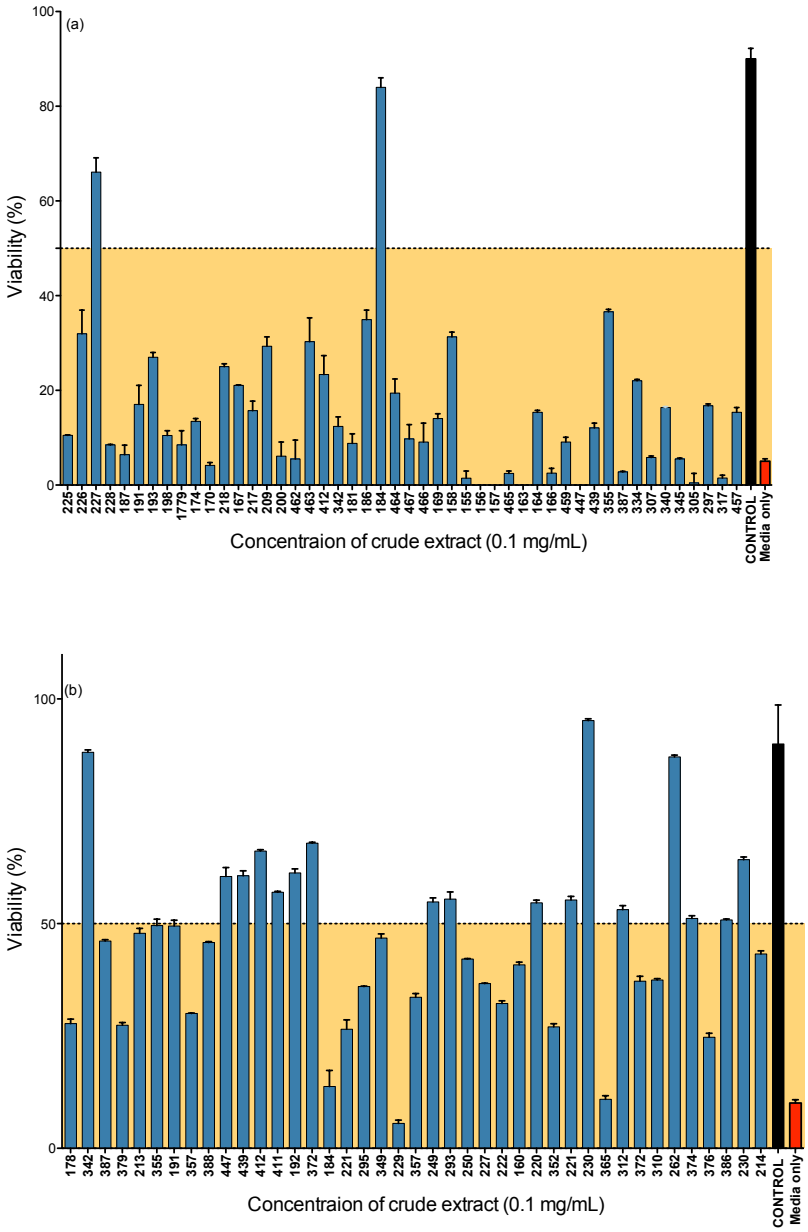

Figure 10.2. Example for antimicrobial screening for the microbial crude extracts against (a) *Bacillus subtilis* (ATCC 6051) and (b) *Candida albicans* (ATCC 10231). Control is either *Bacillus subtilis* (ATCC 6051) or *Candida albicans* (ATCC 10231) in the presence of 1% DMSO, negative control is media only.

10.5 Primary cultivation and preservation of pure microbial isolates

All pure isolates were cultured in 100 mL shaken flasks at 150 rpm for 7 – 10 d, or in a micro-bioreactor (1.5 mL). After cultivation, sample of each isolates were preserved in 20% aqueous glycerol and stored at −80 °C, while the remaining cultures were extracted with equal volumes of EtOAc and the organic layer were concentrated to dryness by rotary evaporation, and the resulting crude extracts weighed and redissolved at 1 mg/mL in MeOH prior to HPLC-DAD-MS analysis. Crude extracts were stored at −30 °C for future bioassay.

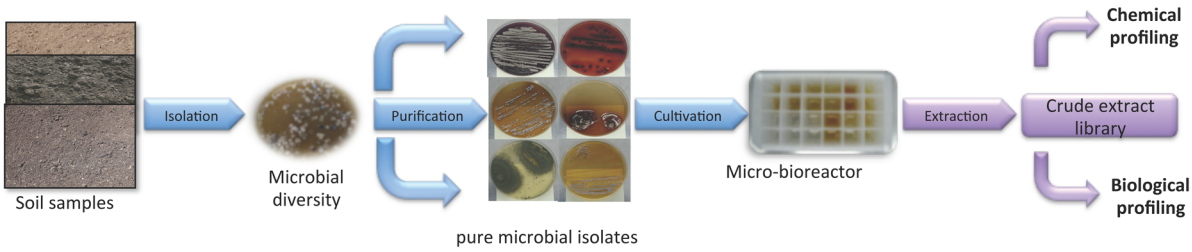

Scheme 10.3. Scheme for the purification, chemical and biological profiling of microbes

10.6 Cultivation of isolates for chemical profiling

10.6.1 Actinomycetes

Actinomycetes isolates were prioritized for detailed chemical investigation depending on their chemical (secondary metabolite) profile, morphological appearance and biological activity. A primary culture of each isolate was started using the total volume of a cryo-preserved stock vial as a seed culture in a 100 mL shake flask. Isolates were then cultured at 150 rpm for 7 – 10 d, after which the culture was extracted with EtOAc (100 mL). The EtOAc fraction was dried using the rotary evaporation, and analysed by HPLC-DAD-MS (Zorbax C_8 analytical column, 150 × 4.6 mm, 5 μm, 15 min eluting gradient with 1.0 mL/min 90% H_2O/MeCN to MeCN with a constant 0.05% HCO_2H/MeCN modifier), followed by 5 min hold, monitoring at 210 and 254 nm. The crude extracts were stored at –32 °C in 96-well microtiter plate for further investigation

10.6.2 Fungi

The fungal colony was inoculated from the cryo-preserved stock into agar-based media. After 5 – 10 d, the agar plates were cut from the culture plates into 1.5 cm cubes. These cubes were used to inoculate the broth media. Cultivation conditions and media used were identical to those used for actinomycetes. The crude extracts were stored at –32 °C in 96-well microtiter plate for further investigation.

10.7 Biological assays

The crude extract from either actinomycetes or fungi were screened for their antibacterial activity against the Gram negative *Escherichia coli* (ATCC 11775) and *Pseudomonas aeruginosa* (ATCC 10145), and the Gram positive bacteria *Staphylococcus aureus* (ATCC 25923 and ATCC 9144) and *Bacillus subtilis* (ATCC 6051 and ATCC 6633) and the fungi *Candida albicans* (ATCC 10231),

Candida parapsilosis (ATCC 22019) and *Candida krusei* (ATCC 6258); Cytotoxicity was measured against different cancer cell lines including human gastric cancer cell line (AGS), human colon cancer cell line (HT29), Hela cancer cell line and human neuroblastoma cancer cell line (SH-SY5Y). The microbial crude extracts were prioritized depending on their biological activity.

10.8 Isolation of secondary metabolites

Isolates were prioritized based on chemical profiling and the biological activity. High priority isolates were cultivated on a large scale (400 mL × 6) to facilitate isolation and structural elucidation of secondary metabolites.

10.8.1 Cultivation of actinomycetes on large scale-broth based media

An aliquot (5 mL) from a seed culture was used to inoculate six 2 L Erlenmeyer flasks containing 350 – 400 mL of water – based media, and the resulting culture was shaken at 190 rpm for 7 – 10 d. After the cultivation period, the culture was extracted with EtOAc (400 mL × 3) and the EtOAc fraction dried using rotary evaporation. The resulting EtOAc soluble residue was sequentially triturated into hexane, CH_2Cl_2 and MeOH fractions (8 mL each), and prioritized for futher chemical fractionation on the basis of HPLC-DAD-MS and NMR data.

10.8.2 Cultivation of actinomycetes on large scale-agar based media

As some of the actinomycetes do not produce secondary metabolites when grown in liquid media, they were cultured on agar–based media in large petri dishes (145 × 20 mm) for 7 – 10 d at 26.5 °C. After the cultivation period, the agar media was sliced into 1.5 cm^3 cubes, extracted with EtOAc (400 mL × 2), dried by rotary evaporation. The resulting crude extracts from EtOAc fraction were dried using the rotary evaporation and sequentially triturated into hexane, CH_2Cl_2 and MeOH fractions (8 mL each). Fractions were prioritized for further chemical fractionation based on HPLC-DAD-MS and NMR analysis.

11 Chapter 11. List of Publications during Candidature

During my PhD studies and as a member of microbial biodiscovery team, I screened pure compounds and crude extracts (marine or microbial) from Capon group members against different G-ve and G+ve bacteria and fungi as a drug discovery paradigm. The outcomes of these screening assays are outlined in the publications listed in the preliminary pages.

12 General Experimental Details

12.1 Chiroptical measurements

Chiroptical measurements ($[\alpha]_D$) were obtained on a JASCO P-1010 intelligent remote module type polarimeter, in a 100 × 2 mm cell, at 22 °C, unless otherwise specified. Optical rotations were recorded at the sodium D line (589 nm) with values reported in degL/gdm, and concentrations in g/100 mL.

12.2 High Performance Liquid Chromatography (HPLC)

HPLC was performed using an Agilent 1100 Series separations module equipped with Agilent 1100 Series diode array and/or multiple wavelength detectors and Agilent 1100 Series fraction collector, controlled using ChemStation Rev.9.03A and Purify version A.1.2 software.

12.3 Ultraviolet-visble

Ultraviolet-visble (UV-vis) absorption spectra were obtained using a Varian CARY 50 UV-visible spectrophotometer with 1 cm quartz cells.

12.4 NMR

1D and 2D NMR spectra were acquired on the following systems: Bruker Avance DRX600 spectrometer with SEI $^{1}H/^{13}C$/Z-GRD 5 mm probe and 900 MHz Bruker Avance III with a TCI $^{1}H/^{13}C/^{15}N$/Z-GRD cryoprobe, in the solvents indicated and referenced to residual signals in deuterated solvents.

12.5 Electrospray ionization mass spectra

Electrospray ionization mass spectra (ESIMS) were acquired using Agilent 1100 Series separations module equipped with an Agilent 1100 Series LC/MS single quadrupole mass detector in both positive and negative ion modes under the following conditions (Zorbax C_8 column, 150 × 406 mm, eluting with 1.0 mL/min 90% H_2O/MeCN to MeCN (with isocartic 0.05% HCO_2H modifier) over 15 min, then held for 5 min with detection at 210 and 254 nm).

12.6 High-resolution mass spectra

High-resolution ESIMS measurements were obtained on a Bruker micrOTOF mass spectrometer by direct infusion in MeCN at 3 μL/min using sodium formate clusters as an internal calibrant.

12.7 Antibacterial assay:

The bacterium to be tested was streaked onto a tryptic soy agar plate and was incubated at 37 °C for 24 h. One colony was then transferred to fresh tryptic soy broth (15 mL) and the cell density was adjusted to $10^4 – 10^5$ cfu/mL. The compounds to be tested were dissolved in DMSO and diluted with H_2O to give 300 μM stock solutions (10% DMSO). The stock solutions were then serially diluted with 10% DMSO to give final concentrations of 30 μM to 0.01 μM in 1% DMSO. An aliquot (20 μL) of each dilution was transferred to a 96-well microtiter plate and freshly prepared microbial broth (180 μL) was added to each well. The plates were incubated at 37 °C for 24 h and the optical density of each well was measured spectrophotometrically at 600 nm using POLARstar Omega plate (BMG LABTECH, Offenburg, Germany). Each test compound was screened against the Gram-negative bacteria *Escherichia coli* (ATCC 11775) and *Pseudomonas aeruginosa* (ATCC 10145) and the Gram-positive bacteria *Staphylococcus aureus* (ATCC 9144 and ATCC 25923) and *Bacillus subtilis* (ATCC 6633 and ATCC 6051). The IC_{50} value was calculated as the concentration of the compound or anticancer drug required for 50% inhibition of the cancer cells using Prism 5.0 from GraphPad Software Inc. (La Jolla, CA).

12.8 Antifungal assay

The fungus to be tested was streaked onto a Sabouraud agar plate and was incubated at 26.5 °C for 48 h. One colony was then transferred to fresh Sabouraud broth (15 mL) and the cell density was adjusted to 10^4-10^5 cfu/mL. Test compounds were dissolved in DMSO and diluted with H_2O to give a 300 μM stock solution (10% DMSO). The stock solution was then serially diluted with 10% DMSO to give final concentrations of 30 μM to 0.01 μM in 1% DMSO. An aliquot (20 μL) of each dilution was transferred to a 96-well microtiter plate and freshly prepared microbial broth (180 μL) was added to each well. The plates were incubated at 26.5 °C for 48 h and the optical density of each well was measured spectrophotometrically at 600 nm using POLARstar Omega plate (BMG LABTECH, Offenburg, Germany). Each test compound was screened against the fungus *Candida albicans* (ATCC 90028). The IC_{50} value was calculated as the concentration of the compound or anticancer drug required for 50% inhibition of the cancer cells using Prism 5.0 from GraphPad Software Inc. (La Jolla, CA).

12.9 Cytotoxicity assay

The cytotoxicity MTT assay was used to evaluate the cytotoxicity of compounds against cancer cell. This assay was modified slightly from that previously described.[209] Briefly, cells (2,000/well in 180 μL of RPMI 1640 supplemented with 10% FBS for SW620 and NCIH-460 or DMEM supplemented with 10% FBS for both AGS and HT-29 cells 3,000/well in 180 μL of DMEM supplemented with 10% FBS) were seeded evenly in a 96-well micro-plate, and the plate was incubated for 18 hours (37 °C; 5% CO_2) to allow cells to attach. Compounds to be tested were dissolved in 5% DMSO (v/v) and diluted from 300 μM-100 nM. Aliquots (20 μL) of each dilution (or of 5% aqueous DMSO for control wells) were added to the plate in duplicate. After 68 hours of incubation (37 °C; 5% CO_2), a solution of 3-(4,5-dimethylthiazol-2-yl)-2,5-diphenyltetrazolium bromide (MTT; Sigma Chemical CO., St Louis, Mo, USA) in PBS was added to each well to a final concentration of 0.4 mg/mL and the plate was incubated for a further 4 hours (37 °C; 5% CO_2). After that, medium was carefully aspirated and precipitated formazan crystals were dissolved in DMSO (100 μL/well). Finally, the absorbance of each well at 570 nm was measured with a PowerWave XS Microplate Reader from Bio-Tek Instruments Inc. (Vinooski, VT). The IC_{50} value was calculated as the concentration of the compound required for 50% inhibition of the cancer cells using Prism 5.0 from GraphPad Software Inc. (La Jolla, CA).

12.10 Chemicals

Chemicals were purchased from Merck, Sigma, Aldrich or Fluka. Solvents used for purification by HPLC were HPLC grade, and were filtered through an Alltech 0.45 μm polytetrafluoroethylene (PTFE) filter before use. Water for HPLC was filtered through a Millipore filtration system. Analytical grade solvents were used for solvent extractions. Substructure, and all other literature searches were carried out using Antibase 2002 and Scifinder.

13 References

1. Newman, D. J., Cragg, G. M., Snader, K. M. Natural Products as Sources of New Drugs over the Period 1981-2002. *J. Nat. Prod.* **2003**;*66*:1022-1037.
2. Berdy, J. Bioactive microbial metabolites: A personal view. *J. Antibiot.* **2005**;*58*:1-26.
3. Pelaez, F. The historical delivery of antibiotics from microbial natural products-Can history repeat? *Biochem. Pharmacol.* **2006**;*71*:981-990.
4. Baker, D. D., Chu, M., Oza, U., Rajgarhia, V. The value of natural products to future pharmaceutical discovery. *Nat Prod Rep* **2007**;*24*:1225-1244.
5. Lazzarini, A., Cavaletti, L., Toppo, G., Marinelli, F. Rare genera of actinomycetes as potential producers of new antibiotics. *Antonie van Leeuwenhoek* **2000**;*78*:399-405.
6. Ganesan, A. The impact of natural products upon modern drug discovery. *Curr. Opin. Chem. Biol.* **2008**;*12*:306-317.
7. Arasu, M. V., Duraipandiyan, V., Ignacimuthu, S. Antibacterial and antifungal activities of polyketide metabolite from marine *Streptomyces* sp. AP-123 and its cytotoxic effect. *Chemosphere* **2013**;*90*:479-487.
8. Marinelli, F. Chapter 2. From microbial products to novel drugs that target a multitude of disease indications. *Methods Enzymol.* **2009**;*458*:29-58.
9. Clatworthy, A. E., Pierson, E., Hung, D. T. Targeting virulence: a new paradigm for antimicrobial therapy. *Nat. Chem. Biol.* **2007**;*3*:541-548.
10. Hoban, D. J., Bouchillon, S. K., Johnson, B. M., Johnson, J. L., Dowzicky, M. J. In vitro activity of tigecycline against 6792 Gram-negative and Gram-positive clinical isolates from the global Tigecycline Evaluation and Surveillance Trial (TEST Program, 2004). *Diagn. Microbiol. Infect. Dis.* **2005**;*52*:215-227.
11. Draghi, D. C., Tench, S., Dowzicky, M. J., Sahm, D. F. Baseline in vitro Activity of Tigecycline among Key Bacterial Pathogens Exhibiting Multidrug Resistance. *Chemotherapy* **2008**;*54*:91-100.
12. Wang, J., Soisson, S. M., Young, K., Shoop, W., Kodali, S., Galgoci, A., Painter, R., Parthasarathy, G., Tang, Y. S., Cummings, R., Ha, S., Dorso, K., Motyl, M., Jayasuriya, H., Ondeyka, J., Herath, K., Zhang, C., Hernandez, L., Allocco, J., Basilio, A., Tormo, J. R., Genilloud, O., Vicente, F., Pelaez, F., Colwell, L., Lee, S. H., Michael, B., Felcetto, T., Gill, C., Silver, L. L., Hermes, J. D., Bartizal, K., Barrett, J., Schmatz, D., Becker, J. W., Cully, D., Singh, S. B. Platensimycin is a selective FabF inhibitor with potent antibiotic properties. *Nature* **2006**;*441*:358-361.
13. Jayasuriya, H., Herath, K. B., Zhang, C., Zink, D. L., Basilio, A., Genilloud, O., Diez, M. T., Vicente, F., Gonzalez, I., Salazar, O., Pelaez, F., Cummings, R., Ha, S., Wang, J., Singh, S. B. Isolation and structure of Platencin: a FabH and FabF dual inhibitor with potent broad-spectrum antibiotic activity. *Angew. Chem. Int. Ed.* **2007**;*46*:4684-4688.
14. Singh, S. B., Jayasuriya, H., Ondeyka, J. G., Herath, K. B., Zhang, C., Zink, D. L., Tsou, N. N., Ball, R. G., Basilio, A., Genilloud, O., Diez, M. T., Vicente, F., Pelaez, F., Young, K., Wang, J. Isolation, structure, and absolute stereochemistry of platensimycin, a broad spectrum antibiotic discovered using an antisense differential sensitivity strategy. *J. Am. Chem. Soc.* **2006**;*128*:11916-11920.
15. Wang, J., Kodali, S., Lee, S. H., Galgoci, A., Painter, R., Dorso, K., Racine, F., Motyl, M., Hernandez, L., Tinney, E., Colletti, S. L., Herath, K., Cummings, R., Salazar, O., Gonzalez, I., Basilio, A., Vicente, F., Genilloud, O., Pelaez, F., Jayasuriya, H., Young, K., Cully, D. F., Singh, S. B. Discovery of platencin, a dual FabF and FabH inhibitor with in vivo antibiotic properties. *Proc. Natl. Acad. Sci.* **2007**;*104*:7612-7616.
16. Zhang, C., Ondeyka, J., Zink, D. L., Burgess, B., Wang, J., Singh, S. B. Isolation, structure and fatty acid synthesis inhibitory activities of platensimycin B1-B3 from Streptomyces platensis. *Chem. Commun.* **2008**:5034-5036.

17. Zhang, C., Ondeyka, J., Guan, Z., Dietrich, L., Burgess, B., Wang, J., Singh, S. B. Isolation, structure and biological activities of platensimycin B4 from Streptomyces platensis. *J. Antibiot.* **2009**;*62*:699-702.
18. Jacob, M. R., Walker, L. A. Natural products and antifungal drug discovery. *Methods Mol. Med.* **2005**;*118*:83-109.
19. Deresinski, S. C., Stevens, D. A. Caspofungin. *Clin. Infect. Dis.* **2003**;*36*:1445-1457.
20. Westby, M., van, d. R. E. CCR5 antagonists: Host-targeted antivirals for the treatment of HIV infection. *Antiviral Chem. Chemother.* **2005**;*16*:339-354.
21. Ziolkowska, N. E., Wlodawer, A. Structural studies of algal lectins with anti-HIV activity. *Acta. Biochim. Pol.* **2006**;*53*:617-626.
22. Halfon, P., inventor Panmed Ltd., Belg. . assignee. Treatment of hepatitis C virus related diseases using hydroxychloroquine or a combination of hydroxychloroquine and an anti-viral agent patent WO2011161644A1. **2011**.
23. Yu, D., Morris-Natschke, S. L., Lee, K.-H. New developments in natural products-based anti-AIDS research. *Med. Res. Rev.* **2007**;*27*:108-132.
24. Taubes, G. The Bacteria Fight Back. *Science* **2008**;*321*:356-361.
25. Chait, R., Vetsigian, K., Kishony, R. What counters antibiotic resistance in nature? *Nat. Chem. Biol.* **2012**;*8*:2-5.
26. D'Costa, V. M., King, C. E., Kalan, L., Morar, M., Sung, W. W. L., Schwarz, C., Froese, D., Zazula, G., Calmels, F., Debruyne, R., Golding, G. B., Poinar, H. N., Wright, G. D. Antibiotic resistance is ancient. *Nature* **2011**;*477*:457-461.
27. Allen, H. K., Donato, J., Wang, H. H., Cloud-Hansen, K. A., Davies, J., Handelsman, J. Call of the wild: antibiotic resistance genes in natural environments. *Nat. Rev. Microbiol* **2010**;*8*:251-259.
28. Wright, G. D. Antibiotic resistance in the environment: a link to the clinic? *Curr. Opin. Microbiol.* **2010**;*13*:589-594.
29. Gottesman, M. M., Fojo, T., Bates, S. E. Multidrug resistance in cancer: role of ATP-dependent transporters. *Nat. Rev. Cancer* **2002**;*2*:48-58.
30. Bok, J. W., Chiang, Y.-M., Szewczyk, E., Reyes-Domingez, Y., Davidson, A. D., Sanchez, J. F., Lo, H.-C., Watanabe, K., Strauss, J., Oakley, B. R., Wang, C. C. C., Keller, N. P. Chromatin-level regulation of biosynthetic gene clusters. *Nat. Chem. Biol.* **2009**;*5*:462-464.
31. Scherlach, K., Hertweck, C. Triggering cryptic natural product biosynthesis in microorganisms. *Org. Biomol. Chem.* **2009**;*7*:1753-1760.
32. Omura, S., Ikeda, H., Ishikawa, J., Hanamoto, A., Takahashi, C., Shinose, M., Takahashi, Y., Horikawa, H., Nakazawa, H., Osonoe, T., Kikuchi, H., Shiba, T., Sakaki, Y., Hattori, M. Genome sequence of an industrial microorganism *Streptomyces avermitilis*: deducing the ability of producing secondary metabolites. *Proc. Natl. Acad. Sci.* **2001**;*98*:12215-12220.
33. Bentley, S. D., Chater, K. F., Cerdeno-Tarraga, A. M., Challis, G. L., Thomson, N. R., James, K. D., Harris, D. E., Quail, M. A., Kieser, H., Harper, D., Bateman, A., Brown, S., Chandra, G., Chen, C. W., Collins, M., Cronin, A., Fraser, A., Goble, A., Hidalgo, J., Hornsby, T., Howarth, S., Huang, C. H., Kieser, T., Larke, L., Murphy, L., Oliver, K., O'Neil, S., Rabbinowitsch, E., Rajandream, M. A., Rutherford, K., Rutter, S., Seeger, K., Saunders, D., Sharp, S., Squares, R., Squares, S., Taylor, K., Warren, T., Wietzorrek, A., Woodward, J., Barrell, B. G., Parkhill, J., Hopwood, D. A. Complete genome sequence of the model actinomycete *Streptomyces coelicolor* A3(2). *Nature* **2002**;*417*:141-147.
34. McAlpine, J. B., Bachmann, B. O., Piraee, M., Tremblay, S., Alarco, A.-M., Zazopoulos, E., Farnet, C. M. Microbial Genomics as a Guide to Drug Discovery and Structural Elucidation: ECO-02301, a Novel Antifungal Agent, as an Example. *J. Nat. Prod.* **2005**;*68*:493-496.
35. Udwary, D. W., Zeigler, L., Asolkar, R. N., Singan, V., Lapidus, A., Fenical, W., Jensen, P. R., Moore, B. S. Genome sequencing reveals complex secondary metabolome in the marine actinomycete *Salinispora tropica*. *Proc. Natl. Acad. Sci.* **2007**;*104*:10376-10381.

36. Elander, R. P. Industrial production of β-lactam antibiotics. *Appl. Microbiol. Biotechnol.* **2003**;*61*:385-392.
37. Paranagama, P. A., Wijeratne, E. M. K., Gunatilaka, A. A. L. Uncovering Biosynthetic Potential of Plant-Associated Fungi: Effect of Culture Conditions on Metabolite Production by *Paraphaeosphaeria quadriseptata* and *Chaetomium chiversii*. *J. Nat. Prod.* **2007**;*70*:1939-1945.
38. Ayer, S. W., McInnes, A. G., Thibault, P., Walter, J. A., Doull, J. L., Parnell, T., Vining, L. C. Jadomycin, a novel 8H-benz[b]oxazolo[3,2-f]phenanthridine antibiotic from *Streptomyces venezuelae* ISP5230. *Tetrahedron Lett.* **1991**;*32*:6301-6304.
39. Doull, J. L., Singh, A. K., Hoare, M., Ayer, S. W. Conditions for the production of jadomycin B by *Streptomyces venezuelae* ISP5230: effects of heat shock, ethanol treatment and phage infection. *J. Ind. Microbiol.* **1994**;*13*:120-125.
40. Overy, D. P., Smedsgaard, J., Frisvad, J. C., Phipps, R. K., Thrane, U. Host-derived media used as a predictor for low abundant, in planta metabolite production from necrotrophic fungi. *J. Appl. Microbiol.* **2006**;*101*:1292-1300.
41. Cueto, M., Jensen, P. R., Kauffman, C., Fenical, W., Lobkovsky, E., Clardy, J. Pestalone, a new antibiotic produced by a marine fungus in response to bacterial challenge. *J. Nat. Prod.* **2001**;*64*:1444-1446.
42. Chiang, Y.-M., Szewczyk, E., Nayak, T., Davidson, A. D., Sanchez, J. F., Lo, H.-C., Ho, W.-Y., Simityan, H., Kuo, E., Praseuth, A., Watanabe, K., Oakley, B. R., Wang, C. C. C. Molecular Genetic Mining of the *Aspergillus* Secondary Metabolome: Discovery of the Emericellamide Biosynthetic Pathway. *Chem. Biol.* **2008**;*15*:527-532.
43. Latifi, A., Winson, M. K., Foglino, M., Bycroft, B. W., Stewart, G. S. A. B., Lazdunski, A., Williams, P. Multiple homologs of LuxR and LuxI control expression of virulence determinants and secondary metabolites through quorum sensing in *Pseudomonas aeruginosa* PAO1. *Mol. Microbiol.* **1995**;*17*:333-343.
44. Bode, H. B. No Need To Be Pure: Mix the Cultures! *Chem Biol* **2006**;*13*:1245-1246.
45. Ratnayake, R., Fremlin, L. J., Lacey, E., Gill, J. H., Capon, R. J. Acremolides A-D, lipodepsipeptides from an Australian marine-derived fungus, *Acremonium* sp. *J. Nat. Prod.* **2008**;*71*:403-408.
46. Horinouchi, S., Beppu, T. Autoregulatory factors and communication in actinomycetes. *Annu. Rev. Microbiol.* **1992**;*46*:377-398.
47. Kleiner, E. M., Pliner, S. A., Soifer, V. S., Onoprienko, V. V., Balashova, T. A., Rozynov, B. V., Khokhlov, A. S. Structure of the A factor, a bioregulator from *Streptomyces griseus*. *Bioorg. Khim.* **1976**;*2*:1142-1147.
48. Hashimoto, M., Kondo, T., Kozone, I., Kawaide, H., Abe, H., Natsume, M. Relationship between response to and production of the aerial mycelium-inducing substances pamamycin-607 and A-factor. *Biosci, Biotechnol, Biochem* **2003**;*67*:803-808.
49. Recio, E., Colinas, A., Rumbero, A., Aparicio, J. F., Martin, J. F. PI factor, a novel type quorum-sensing inducer elicits pimaricin production in *Streptomyces natalensis*. *J. Biol. Chem.* **2004**;*279*:41586-41593.
50. Onaka, H., Tabata, H., Igarashi, Y., Sato, Y., Furumai, T. Goadsporin, a chemical substance which promotes secondary metabolism and morphogenesis in *streptomycetes*. I. Purification and characterization. *J. Antibiot.* **2001**;*54*:1036-1044.
51. Asad, S., Opal, S. M. Bench-to-bedside review: Quorum sensing and the role of cell-to-cell communication during invasive bacterial infection. *Crit. Care* **2008**;*12*:236.
52. Hwang, I., Cook, D. M., Farrand, S. K. A new regulatory element modulates homoserine lactone-mediated autoinduction of Ti plasmid conjugal transfer. *J. Bacteriol.* **1995**;*177*:449-458.
53. Jones, B., Yu, B., Bainton, N. J., Birdsall, M., Bycroft, B. W., Chhabra, S. R., Cox, A. J. R., Golby, P., Reeves, P. J., et, a. The lux autoinducer regulates the production of exoenzyme

virulence determinants in *Erwinia carotovora* and *Pseudomonas aeruginosa*. *EMBO J.* **1993**;*12*:2477-2482.

54. Zazopoulos, E., Huang, K., Staffa, A., Liu, W., Bachmann, B. O., Nonaka, K., Ahlert, J., Thorson, J. S., Shen, B., Farnet, C. M. A genomics-guided approach for discovering and expressing cryptic metabolic pathways. *Nat. Biotechnol.* **2003**;*21*:187-190.
55. Scherlach, K., Hertweck, C. Discovery of aspoquinolones A-D, prenylated quinoline-2-one alkaloids from *Aspergillus nidulans*, motivated by genome mining. *Org. Biomol. Chem.* **2006**;*4*:3517-3520.
56. Perrin, R. M., Fedorova, N. D., Bok, J. W., Cramer, R. A., Jr., Wortman, J. R., Kim, H. S., Nierman, W. C., Keller, N. P. Transcriptional regulation of chemical diversity in *Aspergillus fumigatus* by LaeA. *PLoS Pathog.* **2007**;*3*:508-517.
57. Bok, J. W., Hoffmeister, D., Maggio-Hall, L. A., Murillo, R., Glasner, J. D., Keller, N. P. Genomic Mining for *Aspergillus* Natural Products. *Chem. Biol.* **2006**;*13*:31-37.
58. Shwab, E. K., Keller, N. P. Regulation of secondary metabolite production in filamentous ascomycetes. *Mycol. Res.* **2008**;*112*:225-230.
59. Williams, R. B., Henrikson, J. C., Hoover, A. R., Lee, A. E., Cichewicz, R. H. Epigenetic remodeling of the fungal secondary metabolome. *Org. Biomol. Chem.* **2008**;*6*:1895-1897.
60. Girard, P., Jordan, M., Tsao, M., Wurm, F. M. Small-scale bioreactor system for process development and optimization. *Biochem. Eng. J.* **2001**;*7*:117-119.
61. Betts, J. I., Baganz, F. Miniature bioreactors: current practices and future opportunities. *Microb. Cell Fact.* **2006**;*5*:21-35.
62. Gupta, A., Rao, G. A study of oxygen transfer in shake flasks using a non-invasive oxygen sensor. *Biotechnol. Bioeng.* **2003**;*84*:351-358.
63. Mere, L., Bennett, T., Coassin, P., England, P., Hamman, B., Rink, T., Zimmerman, S., Negulescu, P. Miniaturized FRET assays and microfluidics: key components for ultra-high-throughput screening. *Drug Discov. Today.* **1999**;*4*:363-369.
64. Minas, W., Bailey, J. E., Duetz, W. *Streptomycetes* in micro-cultures: Growth, production of secondary metabolites, and storage and retrieval in the 96-well format. *Antonie van Leeuwenhoek* **2000**;*78*:297-305.
65. Isett, K., George, H., Herber, W., Amanullah, A. Twenty-four-well plate miniature bioreactor high-throughput system: assessment for microbial cultivations. *Biotechnol. Bioeng.* **2007**;*98*:1017-1028.
66. Harms, P., Kostov, Y., French, J. A., Soliman, M., Anjanappa, M., Ram, A., Rao, G. Design and performance of a 24-station high throughput microbioreactor. *Biotechnol. Bioeng.* **2005**;*93*:6-13.
67. Kensy, F., John, G. T., Hofmann, B., Buechs, J. Characterisation of operation conditions and online monitoring of physiological culture parameters in shaken 24-well microtiter plates. *Bioprocess Biosyst. Eng.* **2005**;*28*:75-81.
68. Raetz, C. R. H., Whitfield, C. Lipopolysaccharide endotoxins. *Annu. Rev. Biochem.* **2002**;*71*:635-700.
69. Giuliani, A., Pirri, G., Rinaldi, A. C. Antimicrobial peptides: the LPS connection. *Methods Mol. Biol.* **2010**;*618*:137-154.
70. Rosenfeld, Y., Shai, Y. Lipopolysaccharide (Endotoxin)-host defense antibacterial peptides interactions: Role in bacterial resistance and prevention of sepsis. *Biochim. Biophys. Acta. Biomembr.* **2006**;*1758*:1513-1522.
71. Blaser, M. J., Berg, D. E. *Helicobacter pylori* genetic diversity and risk of human disease. *J. Clin. Invest.* **2001**;*107*:767-773.
72. Basso, D., Plebani, M., Kusters, J. G. Pathogenesis of *Helicobacter pylori* infection. *Helicobacter* **2010**;*15*:14-20.
73. Kawai, T., Akira, S. Pathogen recognition with Toll-like receptors. *Curr. Opin. Immunol.* **2005**;*17*:338-344.

74. Khamri, W., Moran, A. P., Worku, M. L., Karim, Q. N., Walker, M. M., Annuk, H., Ferris, J. A., Appelmelk, B. J., Eggleton, P., Reid, K. B. M., Thursz, M. R. Variations in *Helicobacter pylori* lipopolysaccharide to evade the innate immune component surfactant protein D. *Infect. Immun.* **2005**;*73*:7677-7686.
75. Moran, A. P., Aspinall, G. O. Unique structural and biological features of *Helicobacter pylori* lipopolysaccharides. *Prog. Clin. Biol. Res.* **1998**;*397*:37-49.
76. Muotiala, A., Helander, I. M., Pyhala, L., Kosunen, T. U., Moran, A. P. Low biological activity of *Helicobacter pylori* lipopolysaccharide. *Infect Immun* **1992**;*60*:1714-1716.
77. Aspinall, G. O., Monteiro, M. A. Lipopolysaccharides of Helicobacter pylori strains P466 and MO19: structures of the O antigen and core oligosaccharide regions. *Biochemistry* **1996**;*35*:2498-2504.
78. Grebowska, A., Moran, A. P., Matusiak, A., Bak-Romaniszyn, L., Czkwianianc, E., Rechcinski, T., Walencka, M., Planeta-Malecka, I., Rudnicka, W., Chmiela, M. Anti-phagocytic activity of *Helicobacter pylori* lipopolysaccharide (LPS)--possible modulation of the innate immune response to these bacteria. *Pol. J. Microbiol.* **2008**;*57*:185-192.
79. Xu, H., Liew, L. N., Kuo, I. C., Huang, C. H., Goh, D. L.-M., Chua, K. Y. The modulatory effects of lipopolysaccharide-stimulated B cells on differential T-cell polarization. *Immunology* **2008**;*125*:218-228.
80. Texier, A.-C., Andres, Y., Illemassene, M., Cloirec, P. L. E. Characterization of Lanthanide Ions Binding Sites in the Cell Wall of *Pseudomonas aeruginosa*. *Environ. Sci. Technol.* **2000**;*34*:610-615.
81. Texier, A.-C., Andres, Y., Le, C. P. Selective Biosorption of Lanthanide (La, Eu, Yb) Ions by *Pseudomonas aeruginosa*. *Environ. Sci. Technol.* **1999**;*33*:489-495.
82. Lins, R. D., Vorpagel, E. R., Guglielmi, M., Straatsma, T. P. Computer Simulation of Uranyl Uptake by the Rough Lipopolysaccharide Membrane of *Pseudomonas aeruginosa*. *Biomacromolecules* **2008**;*9*:29-35.
83. Alexander, C., Rietschel, E. T. Bacterial lipopolysaccharides and innate immunity. *J Endotoxin Res.* **2001**;*7*:167-202.
84. Newman, M.-A., Dow, J. M., Molinaro, A., Parrilli, M. Priming, induction and modulation of plant defence responses by bacterial lipopolysaccharides. *J. Endotoxin Res.* **2007**;*13*:69-84.
85. Silipo, A., Molinaro, A., Sturiale, L., Dow, J. M., Erbs, G., Lanzetta, R., Newman, M.-A., Parrilli, M. The elicitation of plant innate immunity by lipooligosaccharide of *Xanthomonas campestris*. *J. Biol. Chem.* **2005**;*280*:33660-33668.
86. Albus, U., Baier, R., Holst, O., Puhler, A., Niehaus, K. Suppression of an elicitor-induced oxidative burst reaction in Medicago sativa cell cultures by Sinorhizobium meliloti lipopolysaccharides. *New Phytol.* **2001**;*151*:597-606.
87. Braun, S. G., Meyer, A., Holst, O., Puehler, A., Niehaus, K. Characterization of the *Xanthomonas campestris* pv. campestris lipopolysaccharide substructures essential for elicitation of an oxidative burst in tobacco cells. *Mol. Plant-Microbe Interact.* **2005**;*18*:674-681.
88. Desaki, Y., Miya, A., Venkatesh, B., Tsuyumu, S., Yamane, H., Kaku, H., Minami, E., Shibuya, N. Bacterial lipopolysaccharides induce defense responses associated with programmed cell death in rice cells. *Plant Cell Physiol.* **2006**;*47*:1530-1540.
89. Gerber, I. B., Zeidler, D., Durner, J., Dubery, I. A. Early perception responses of Nicotiana tabacum cells in response to lipopolysaccharides from *Burkholderia cepacia*. *Planta* **2004**;*218*:647-657.
90. Meyer, A., Puhler, A., Niehaus, K. The lipopolysaccharides of the phytopathogen Xanthomonas campestris pv. campestris induce an oxidative burst reaction in cell cultures of *Nicotiana tabacum*. *Planta* **2001**;*213*:214-222.
91. Zeidler, D., Zaehringer, U., Gerber, I., Dubery, I., Hartung, T., Bors, W., Hutzler, P., Durner, J. Innate immunity in *Arabidopsis thaliana*: Lipopolysaccharides activate nitric

oxide synthase (NOS) and induce defense genes. *Proc. Natl. Acad. Sci.* **2004**;*101*:15811-15816.

92. Beishuizen, A., Thijs, L. G. Endotoxin and the hypothalamo-pituitary-adrenal (HPA) axis. *J Endotoxin Res.* **2003**;*9*:3-24.
93. Elenkov, I. J., Kovacs, K., Kiss, J., Bertok, L., Vizi, E. S. Lipopolysaccharide is able to bypass corticotropin-releasing factor in affecting plasma ACTH and corticosterone levels: evidence from rats with lesions of the paraventricular nucleus. *J. Endocrinol.* **1992**;*133*:231-236.
94. Schotanus, K., Makara, G. B., Tilders, F. J. H., Berkenbosch, F. ACTH response to a low dose but not a high dose of bacterial endotoxin in rats is completely mediated by corticotropin-releasing hormone. *Ann. NY. Acad. Sci.* **1994**;*1*:300-307.
95. Suzuki, S., Oh, C., Nakano, K. Pituitary-dependent and -independent secretion of CS caused by bacterial endotoxin in rats. *Am. J. Physiol.* **1986**;*250*:E470-E474.
96. Enriquez, d. S. A., Garcia, R. Rat glomerulosa cells in primary culture and *E. coli* lipopolysaccharide action. *J. Steroid Biochem. Mol. Biol.* **2003**;*85*:81-88.
97. Vakharia, K., Renshaw, D., Hinson, J. P. Bacterial lipopolysaccharide directly stimulates cortisol secretion in human adrenal cells. *Endocr. Res.* **2002**;*28*:357-361.
98. Toney, J. H., Hammond, G. G., Fitzgerald, P. M. D., Sharma, N., Balkovec, J. M., Rouen, G. P., Olson, S. H., Hammond, M. L., Greenlee, M. L., Gao, Y.-D. Succinic acids as potent inhibitors of plasmid-borne IMP-1 metallo-β-lactamase. *J. Biol. Chem.* **2001**;*276*:31913-31918.
99. Eckardt, K., Bradler, G., Fritzsche, H., Tresselt, D. Resistoflavine, a new antibiotic from an actinomyete. *Z. Chem.* **1970**;*10*:221.
100. Kock, I., Maskey, R. P., Biabani, M. A. F., Helmke, E., Laatsch, H. Marine bacteria. XXIX. 1-Hydroxy-1-norresistomycin and resistoflavin methyl ether: New antibiotics from marine-derived *Streptomycetes*. *J. Antibiot.* **2005**;*58*:530-534.
101. Hoefle, G., Wolf, H. Isolation, carbon-13 NMR spectra, and biosynthesis of resistomycin and resistoflavin from *Streptomyces griseoflavus* B 71 (Actinomycetales). *Liebigs. Ann. Chem.* **1983**:835-843.
102. Gorajana, A., Kurada, B. V. V. S. N., Peela, S., Jangam, P., Vinjamuri, S., Poluri, E., Zeeck, A. 1-Hydroxy-1-norresistomycin, a new cytotoxic compound from a marine actinomycete, *Streptomyces chibaensis* AUBN1/7. *J. Antibiot.* **2005**;*58*:526-529.
103. Gorajana, A., Venkatesan, M., Vinjamuri, S., Kurada, B. V. V. S. N., Peela, S., Jangam, P., Poluri, E., Zeeck, A. Resistoflavine, cytotoxic compound from a marine actinomycete, *Streptomyces chibaensis* AUBN1/7. *Microbiol. Res.* **2007**;*162*:322-327.
104. Arora, S. K. Molecular structure of heliomycin, an inhibitor of RNA synthesis. *J. Antibiot.* **1985**;*38*:113-115.
105. Kock, I., Maskey Rajendra, P., Biabani, M. A. F., Helmke, E., Laatsch, H. 1-Hydroxy-1-norresistomycin and resistoflavin methyl ether: new antibiotics from marine-derived streptomycetes. *J. Antibiot.* **2005**;*58*:530-534.
106. Ishida, K., Maksimenka, K., Fritzsche, K., Scherlach, K., Bringmann, G., Hertweck, C. The Boat-Shaped Polyketide Resistoflavin Results from Re-Facial Central Hydroxylation of the Discoid Metabolite Resistomycin. *J. Am. Chem. Soc.* **2006**;*128*:14619-14624.
107. Toma, F., Bouhet, J. C., Pham, V. C. P., Fromageot, P., Haar, W., Rueterjans, H., Maurer, W. Carbon-13 NMR spectroscopy of the biological pigments luteoskyrin and rugulosin and polyhydroxyanthraquinone analogs. *Org. Magn. Reson.* **1975**;*7*:496-503.
108. Watts, P., Kittakoop, P., Veeranondha, S., Wanasith, S., Thongwichian, R., Saisaha, P., Intamas, S., Hywel-Jones, N. L. Cytotoxicity against insect cells of entomopathogenic fungi of the genera *Hypocrella (anamorph Aschersonia)*: possible agents for biological control. *Mycol. Res.* **2003**;*107*:581-586.

109. Tatsuno, T., Kobayashi, N., Okubo, K., Tsunoda, H. Toxicological research of the toxic substances of *Penicillium tardum*. I. Isolation and identification of cytotoxic substances. *Chem. Pharm. Bull.* **1975**;*23*:351-354.
110. Krivobok, S., Seigle-Murandi, F., Steiman, R., Marzin, D. R., Betina, V. Mutagenicity of substituted anthraquinones in the Ames/*Salmonella* microsome system. *Mutat Res, Genet Toxicol. Test* **1992**;*279*:1-8.
111. Dobias, J., Betina, V., Nemec, P. Insecticidal activity of ramihyfin A, citrinin, and rugulosin. *Biologia* **1980**;*35*:431-434.
112. Takeda, N., Seo, S., Ogihara, Y., Sankawa, U., Iitaka, I., Kitagawa, I., Shibata, S. Fungal metabolites. XXXI. Anthraquinonoid coloring matters of *Penicillium islandicum* and other fungi. (-)-Luteoskyrin, (-)-rubroskyrin, (+)-rugulosin and their related compounds. *Tetrahedron* **1973**;*29*:3703-3719.
113. West, R. R., Labroo, V., Piggott, J. R., Smith, R. A., McKernan, P. A., inventors; Zymogenetics, Inc., USA . assignee. Use of skyrin and analogs for the treatment of diabetes mellitus and process for their preparation patent WO9414427A2. **1994**.
114. Gill, M., Gimenez, A., McKenzie, R. W. Pigments of fungi, part 8. Bianthraquinones from *Dermocybe austroveneta*. *J. Nat. Prod.* **1988**;*51*:1251-1256.
115. Alvi, K. A., Pu, H., Luche, M., Rice, A., App, H., McMahon, G., Dare, H., Margolis, B. Asterriquinones produced by Aspergillus candidus inhibit binding of the Grb-2 adapter to phosphorylated EGF receptor tyrosine kinase. *J. Antibiot.* **1999**;*52*:215-223.
116. Joseph-Nathan, P., Gonzalez, M. P., Johnson, L. R. F., Shoolery, J. N. Natural abundance carbon-13 NMR studies of perezone and derivatives. *Org Magn Resonance* **1971**;*3*:23-29.
117. Kaji, A., Iwata, T., Kiriyama, N., Wakusawa, S., Miyamoto, K.-i. Four new metabolites of *Aspergillus terreus*. *Chem. Pharm. Bull.* **1994**;*42*:1682-1684.
118. Shaaban, K. A., Shaaban, M., Gruen-Wollny, I., Maier, A., Fiebig, H. H., Laatsch, H. Julichrome Q6 glucuronide, a monomeric subunit of the julimycin B-I complex from a terrestrial *Streptomyces* sp. *J. Nat. Prod.* **2007**;*70*:1545-1550.
119. Raju, R., Piggott, A. M., Barrientos, D. L. X., Khalil, Z., Capon, R. J. Heronapyrroles A-C: Farnesylated 2-Nitropyrroles from an Australian Marine-Derived *Streptomyces* sp. *Org. Lett.* **2010**;*12*:5158-5161.
120. Ezaki, N., Shomura, T., Koyama, M., Niwa, T., Kojima, M., Inouye, S., Ito, T., Niida, T. New chlorinated nitropyrrole antibiotics, pyrrolomycin A and B (SF-2080 A and B). *J Antibiot* **1981**;*34*:1363-1365.
121. Kato, S., Shindo, K., Kawai, H., Odagawa, A., Matsuoka, M., Mochizuki, J. Pyrrolostatin, a novel lipid peroxidation inhibitor from *Streptomyces chrestomyceticus*: taxonomy, fermentation, isolation, structure elucidation and biological properties. *J. Antibiot.* **1993**;*46*:892-899.
122. Macherla, V. R., Liu, J., Bellows, C., Teisan, S., Nicholson, B., Lam, K. S., Potts, B. C. M. Glaciapyrroles A, B, and C, pyrrolosesquiterpenes from a *Streptomyces* sp. isolated from an Alaskan marine sediment. *J. Nat. Prod.* **2005**;*68*:780-783.
123. Kwon, H. C., Espindola, A. P. D. M., Park, J.-S., Prieto-Davo, A., Rose, M., Jensen, P. R., Fenical, W. Nitropyrrolins A-E, cytotoxic farnesyl-α-nitropyrroles from a marine-derived bacterium within the actinomycete family *Streptomycetaceae*. *J. Nat. Prod.* **2010**;*73*:2047-2052.
124. Schmidt, J., Stark, C. B. W. Biomimetic Synthesis and Proposal of Relative and Absolute Stereochemistry of Heronapyrrole C. *Org Lett* **2012**;*14*:4042-4045.
125. Kers, J. A., Wach, M. J., Krasnoff, S. B., Widom, J., Cameron, K. D., Bukhalid, R. A., Gibson, D. M., Crane, B. R., Loria, R. Nitration of a peptide phytotoxin by bacterial nitric oxide synthase. *Nature* **2004**;*429*:79-82.
126. Barbaree, J. M., Payne, W. J. Products of denitrification by a marine bacterium as revealed by gas chromatography. *Mar. Biol. (Berlin)* **1967**;*1*:136-139.
127. Payne, W. J. Bacterial denitrification: asset or defect? *BioScience* **1983**;*33*:319-325.

128. Feldman, P. L., Griffith, O. W., Stuehr, D. J. The surprising life of nitric oxide. *Chem. Eng. News* **1993**;*71*:26-38.
129. Nott, A., Riccio, A. Nitric oxide-mediated epigenetic mechanisms in developing neurons. *Cell Cycle* **2009**;*8*:725-730.
130. Alderton, W. K., Cooper, C. E., Knowles, R. G. Nitric oxide synthases: structure, function and inhibition. *Biochem. J.* **2001**;*357*:593-615.
131. O'Dell, T. J., Hawkins, R. D., Kandel, E. R., Arancio, O. Tests of the roles of two diffusible substances in long-term potentiation: evidence for nitric oxide as a possible early retrograde messenger. *Proc. Natl. Acad. Sci.* **1991**;*88*:11285-11289.
132. Schuman, E. M., Madison, D. V. A requirement for the intercellular messenger nitric oxide in long-term potentiation. *Science* **1991**;*254*:1503-1506.
133. Rapoport, R. M., Draznin, M. B., Murad, F. Endothelium-dependent relaxation in rat aorta may be mediated through cyclic GMP-dependent protein phosphorylation. *Nature* **1983**;*306*:174-176.
134. Foerstermann, U., Muelsch, A., Boehme, E., Busse, R. Stimulation of soluble guanylate cyclase by an acetylcholine-induced endothelium-derived factor from rabbit and canine arteries. *Circ. Res.* **1986**;*58*:531-538.
135. Khan, B. V., Harrison, D. G., Olbrych, M. T., Alexander, R. W., Medford, R. M. Nitric oxide regulates vascular cell adhesion molecule 1 gene expression and redox-sensitive transcriptional events in human vascular endothelial cells. *Proc. Natl. Acad. Sci.* **1996**;*93*:9114-9119.
136. Pantopoulos, K., Hentze, M. W. Nitric oxide signaling to iron-regulatory protein: direct control of ferritin mRNA translation and transferrin receptor mRNA stability in transfected fibroblasts. *Proc. Natl. Acad. Sci.* **1995**;*92*:1267-1271.
137. Pfeiffer, S., Mayer, B., Hemmens, B. Nitric oxide: chemical puzzles posed by a biological messenger. *Angew. Chem. Int. Ed.* **1999**;*38*:1715-1731.
138. Lipton, S. A. Physiology: Nitric oxide and respiration. *Nature* **2001**;*413*:118-119, 121.
139. Foerstermann, U., Sessa, W. C. Nitric oxide synthases: regulation and function. *Eur. Heart. J.* **2012**;*33*:829-837.
140. Griffith, O. W., Stuehr, D. J. Nitric oxide synthases: properties and catalytic mechanism. *Annu. Rev. Physiol.* **1995**;*57*:707-736.
141. Zhou, L., Zhu, D.-Y. Neuronal nitric oxide synthase: Structure, subcellular localization, regulation, and clinical implications. *Nitric Oxide* **2009**;*20*:223-230.
142. Forstermann, U., Closs, E. I., Pollock, J. S., Nakane, M., Schwarz, P., Gath, I., Kleinert, H. Nitric oxide synthase isozymes. Characterization, purification, molecular cloning, and functions. *Hypertension* **1994**;*23*:1121-1131.
143. Nathan, C. F., Hibbs, J. B., Jr. Role of nitric oxide synthesis in macrophage antimicrobial activity. *Curr. Opin. Immunol.* **1991**;*3*:65-70.
144. Ignarro, L. J., Harbison, R. G., Wood, K. S., Kadowitz, P. J. Activation of purified soluble guanylate cyclase by endothelium-derived relaxing factor from intrapulmonary artery and vein: stimulation by acetylcholine, bradykinin and arachidonic acid. *J. Pharmacol. Exp. Ther.* **1986**;*237*:893-900.
145. Buddha, M. R., Tao, T., Parry, R. J., Crane, B. R. Regioselective Nitration of Tryptophan by a Complex between Bacterial Nitric-oxide Synthase and Tryptophanyl-tRNA Synthetase. *J. Biol. Chem.* **2004**;*279*:49567-49570.
146. Gusarov, I., Nudler, E. NO-mediated cytoprotection: Instant adaptation to oxidative stress in bacteria. *Proc. Natl. Acad. Sci.* **2005**;*102*:13855-13860.
147. Cohen, M. F., Yamasaki, H. Involvement of nitric oxide synthase in sucrose-enhanced hydrogen peroxide tolerance of *Rhodococcus* sp. strain APG1, a plant-colonizing bacterium. *Nitric Oxide* **2003**;*9*:1-9.

148. Johnson, E. G., Sparks, J. P., Dzikovski, B., Crane, B. R., Gibson, D. M., Loria, R. Plant-pathogenic *Streptomyces* species produce nitric oxide synthase-derived nitric oxide in response to host signals. *Chem. Biol.* **2008**;*15*:43-50.
149. Chen, Y., Rosazza, J. P. N. A bacterial nitric oxide synthase from a *Nocardia* species. *Biochem Biophys Res Commun* **1994**;*203*:1251-1258.
150. Fry, B. A., Loria, R. Thaxtomin A: Evidence for a plant cell wall target. *Physiol. Mol. Plant Pathol.* **2002**;*60*:1-8.
151. Rafferty, S. Nitric oxide synthases of bacteria - and other unicellular organisms. *Open Nitric Oxide J* **2011**;*3*:25-32.
152. Crane, B. R., Sudhamsu, J., Patel, B. A. Bacterial nitric oxide synthases. *Annu. Rev. Biochem.* **2010**;*79*:445-470.
153. Filippovich, S. Y. Bacterial NO synthases. *Biochemistry* **2010**;*75*:1217-1224.
154. Moncada, S., Palmer, R. M. J., Higgs, E. A. Nitric oxide: physiology, pathophysiology, and pharmacology. *Pharmacol Rev.* **1991**;*43*:109-142.
155. Joubert, J., Malan, S. F. Novel nitric oxide synthase inhibitors: a patent review. *Expert Opin. Ther. Pat.* **2011**;*21*:537-560.
156. Wach, M. J., Kers, J. A., Krasnoff, S. B., Loria, R., Gibson, D. M. Nitric oxide synthase inhibitors and nitric oxide donors modulate the biosynthesis of thaxtomin A, a nitrated phytotoxin produced by *Streptomyces* spp. *Nitric Oxide* **2005**;*12*:46-53.
157. Thomas, C., Mackey, M. M., Diaz, A. A., Cox, D. P. Hydroxyl radical is produced via the Fenton reaction in submitochondrial particles under oxidative stress: implications for diseases associated with iron accumulation. *Redox Rep.* **2009**;*14*:102-108.
158. Woodmansee, A. N., Imlay, J. A. Reduced Flavins Promote Oxidative DNA Damage in Non-respiring Escherichia coli by Delivering Electrons to Intracellular Free Iron. *J. Biol. Chem.* **2002**;*277*:34055-34066.
159. Anon. Endogenous nitric oxide protects bacteria against a wide spectrum of antibiotics. *Nat. Rev. Drug Discovery* **2009**;*8*:848.
160. Henares, B. M., Higgins, K. E., Boon, E. M. Discovery of a nitric oxide responsive quorum sensing circuit in *Vibrio harveyi*. *ACS Chem. Biol.* **2012**;*7*:1331-1336.
161. Ishikawa, M., Ninomiya, T., Akabane, H., Kushida, N., Tsujiuchi, G., Ohyama, M., Gomi, S., Shito, K., Murata, T. Pseurotin A and its analogues as inhibitors of immunoglobulin E production. *Bioorg. Med. Chem. Lett.* **2009**;*19*:1457-1460.
162. Wang, F.-Z., Li, D.-H., Zhu, T.-J., Zhang, M., Gu, Q.-Q. Pseurotin A1 and A2, two new 1-oxa-7-azaspiro[4.4]non-2-ene-4,6-diones from the holothurian-derived fungus *Aspergillus fumigatus* WFZ-25. *Can. J. Chem.* **2011**;*89*:72-76.
163. Wenke, J., Anke, H., Sterner, O. Pseurotin A and 8-O-demethylpseurotin A from *Aspergillus fumigatus* and their inhibitory activities on chitin synthase. *Biosci. Biotechnol. Biochem.* **1993**;*57*:961-964.
164. Sun, Y., Takada, K., Takemoto, Y., Yoshida, M., Nogi, Y., Okada, S., Matsunaga, S. Gliotoxin analogs from a marine-derived fungus, *Penicillium* sp., and their cytotoxic and histone methyltransferase inhibitory activities. *J. Nat. Prod.* **2012**;*75*:111-114.
165. Li, X., Kim, S.-K., Nam, K. W., Kang, J. S., Choi, H. D., Son, B. W. A new antibacterial dioxopiperazine alkaloid related to gliotoxin from a marine isolate of the fungus *Pseudallescheria*. *J. Antibiot.* **2006**;*59*:248-250.
166. Haraguchi, H., Hamatani, Y., Shibata, K., Hashimoto, K. An inhibitor of acetolactate synthase from a microbe. *Biosci. Biotechnol. Biochem.* **1992**;*56*:2085-2086.
167. Afiyatullov, S. S., Kalinovskii, A. I., Pivkin, M. V., Dmitrenok, P. S., Kuznetsova, T. A. Alkaloids from a marine isolate of the fungus *Aspergillus fumigatus*. *Chem. Nat. Compd.* **2005**;*41*:236-238.
168. Cui, C.-B., Kakeya, H., Osada, H. Novel mammalian cell cycle inhibitors, tryprostatins A, B and other diketopiperazines produced by *Aspergillus fumigatus*. II. Physico-chemical properties and structures. *J. Antibiot.* **1996**;*49*:534-540.

169. Feng, C., Ma, Y. Isolation and anti-phytopathogenic activity of secondary metabolites from Alternaria sp. FL25, an endophytic fungus in *Ficus carica*. *Yingyong Yu Huanjing Shengwu Xuebao* **2010**;*16*:76-78.
170. Hino, T., Kawate, T., Nakagawa, M. A synthesis of so-called fumitremorgin C. *Tetrahedron* **1989**;*45*:1941-1944.
171. Furtado, N. A. J. C., Pupo, M. T., Carvalho, I., Campo, V. L., Duarte, M. C. T., Bastos, J. K. Diketopiperazines produced by an *Aspergillus* fumigatus Brazilian strain. *J. Braz. Chem. Soc.* **2005**;*16*:1448-1453.
172. Figuly, G. D., Loop, C. K., Martin, J. C. Directed ortho-lithiation of lithium thiophenolate. New methodology for the preparation of ortho-substituted thiophenols and related compounds. *J. Am. Chem. Soc.* **1989**;*111*:654-658.
173. Marfey, P. Determination of D-amino acids. II. Use of a bifunctional reagent, 1,5-difluoro-2,4-dinitrobenzene. *Carlsberg Res. Commun.* **1984**;*49*:591-596.
174. Bhushan, R., Brueckner, H. Use of Marfey's reagent and analogs for chiral amino acid analysis: Assessment and applications to natural products and biological systems. *J. Chromatogr. B. Anal. Technol. Biomed. Life Sci.* **2011**;*879*:3148-3161.
175. Ameur, R. M.-B., Mellouli, L., Chabchoub, F., Fotso, S., Bejar, S. Purification and structure elucidation of two biologically active molecules from a new isolated *Streptomyces* sp. US 24 strain. *Chem. Nat. Compd.* **2004**;*40*:510-513.
176. Graham, G. C., Mayers, P., Henry, R. J. A simplified method for the preparation of fungal genomic DNA for PCR and RAPD analysis. *BioTechniques* **1994**;*16*:48-50.
177. Eguchi, C., Kakuta, A. Cyclic dipeptides. II. Isomerization among cyclo(4-hydroxyprolyl-4-hydroxyprolyl)s and a novel conversion of D-allo-hydroxyproline to L-hydroxyproline. *Bull. Chem. Soc. Jpn.* **1974**;*49*:2277-2282.
178. Kuroda, H., Kubo, S., Chino, N., Kimura, T., Sakakibara, S. Unexpected racemization of proline or hydroxy-proline phenacyl ester during coupling reactions with Boc-amino acids. *Int. J. Pept. Protein Res.* **1992**;*40*:114-118.
179. Iranpoor, N., Firouzabadi, H., Nowrouzi, N., Firouzabadi, D. Highly chemoselective nitration of aromatic amines using the Ph3P/Br2/AgNO3 system. *Tetrahedron Lett.* **2006**;*47*:6879-6881.
180. Morgan, K. J., Morrey, D. P. Nitropyrroles. I. Preparation and properties of 2- and 3-nitropyrrole. *Tetrahedron* **1966**;*22*:57-62.
181. Kalaitzis, J. A., Hamano, Y., Nilsen, G., Moore, B. S. Biosynthesis and structural revision of neomarinone. *Org. Lett.* **2003**;*5*:4449-4452.
182. Shinya, K., Furihata, K., Hayakawa, Y., Seto, H. Biosynthetic studies of naphterpin, a terpenoid metabolite of *Streptomyces*. *Tetrahedron Lett.* **1990**;*31*:6025-6026.
183. Ishibashi, M., Funayama, S., Anraku, Y., Komiyama, K., Omura, S. Novel antibiotics, furaquinocins C, D, E, F, G and H. *J. Antibiot.* **1991**;*44*:390-395.
184. Pathirana, C., Jensen, P. R., Fenical, W. Marinone and debromomarinone: antibiotic sesquiterpenoid naphthoquinones of a new structure class from a marine bacterium. *Tetrahedron Lett.* **1992**;*33*:7663-7666.
185. Hardt, I. H., Jensen, P. R., Fenical, W. Neomarinone, and new cytotoxic marinone derivatives, produced by a marine filamentous bacterium (Actinomycetales). *Tetrahedron Lett.* **2000**;*41*:2073-2076.
186. Mootz, H. D., Marahiel, M. A. Biosynthetic systems for nonribosomal peptide antibiotic assembly. *Curr. Opin. Chem. Biol.* **1997**;*1*:543-551.
187. Belin, P., Moutiez, M., Lautru, S., Seguin, J., Pernodet, J.-L., Gondry, M. The nonribosomal synthesis of diketopiperazines in tRNA-dependent cyclodipeptide synthase pathways. *Nat. Prod. Rep.* **2012**;*29*:961-979.
188. Guimaraes, D. O., Borges, W. S., Vieira, N. J., de Oliveira, L. F., da Silva, C. H. T. P., Lopes, N. P., Dias, L. G., Duran-Patron, R., Collado, I. G., Pupo, M. T. Diketopiperazines

produced by endophytic fungi found in association with two *Asteraceae* species. *Phytochemistry* **2010**;*71*:1423-1429.

189. Abe, M., Yamano, T., Yamatodani, S., Kozu, Y., Kusumoto, M., Komatsu, H., Yamada, S. On the new peptide-type ergot alkaloids, ergosecaline and ergosecalinine. *Bull. Arg. Chem. Soc.* **1959**;*23*:246-248.
190. Hasumi, K., Shinohara, C., Iwanaga, T., Endo, A. Lateritin, a new inhibitor of acyl-CoA: cholesterol acyltransferase produced by *Gibberella lateritium* IFO 7188. *J. Antibiot.* **1993**;*46*:1782-1787.
191. Pettit, R. K., Pettit, G. R., Xu, J.-P., Weber, C. A., Richert, L. A. Isolation of human cancer cell growth inhibitory, antimicrobial lateritin from a mixed fungal culture. *Planta Med.* **2010**;*76*:500-501.
192. Kagamizono, T., Nishino, E., Matsumoto, K., Kawashima, A., Kishimoto, M., Sakai, N., He, B.-M., Chen, Z.-X., Adachi, T., et al. Bassiatin, a new platelet aggregation inhibitor produced by *Beauveria bassiana* K-717. *J. Antibiot.* **1995**;*48*:1407-1412.
193. Wang, H.-j., Gloer, J. B., Wicklow, D. T., Dowd, P. F. Mollenines A and B: New dioxomorpholines from the ascostromata of *Eupenicillium molle*. *J. Nat. Prod.* **1998**;*61*:804-807.
194. Kushida, N., Yaguchi, T., Miike, N., inventors; (Meiji Seika Kaisha, Ltd., Japan). assignee. Voltage-dependent sodium channel blockers manufacture with *Aspergillus niveus*. Application: JP patent 2001-288005, 2003096080. **2003** 20010921.
195. Suntornchashwej, S., Chaichit, N., Isobe, M., Suwanborirux, K. Hectochlorin and Morpholine Derivatives from the Thai Sea Hare, *Bursatella leachii*. *J. Nat. Prod.* **2005**;*68*:951-955.
196. Nakadate, S., Nozawa, K., Horie, H., Fujii, Y., Nagai, M., Komai, S.-i., Hosoe, T., Kawai, K.-i., Yaguchi, T., Fukushima, K. New dioxomorpholine derivatives, javanicunine A and B, from *Eupenicillium javanicum*. *Heterocycles* **2006**;*68*:1969-1972.
197. Arai, K., Kimura, K., Mushiroda, T., Yamamoto, Y. Structures of fructigenines A and B, new alkaloids isolated from *Penicillium fructigenum* Takeuchi. *Chem. Pharm. Bull.* **1989**;*37*:2937-2939.
198. Smelcerovic, A., Yancheva, D., Cherneva, E., Petronijevic, Z., Lamshoeft, M., Herebian, D. Identification and synthesis of three cyclodidepsipeptides as potential precursors of enniatin B in *Fusarium sporotrichioides*. *J. Mol. Struct.* **2011**;*985*:397-402.
199. Hoye, T. R., Jeffrey, C. S., Shao, F. Mosher ester analysis for the determination of absolute configuration of stereogenic (chiral) carbinol carbons. *Nat. Protoc.* **2007**;*2*:2451-2458.
200. Hochlowski, J. E., Mullally, M. M., Spanton, S. G., Whittern, D. N., Hill, P., McAlpine, J. B. 5-N-Acetylardeemin, a novel heterocyclic compound which reverses multiple drug resistance in tumor cells. II. Isolation and elucidation of the structure of 5-N-acetylardeemin and two congeners. *J. Antibiot.* **1993**;*46*:380-386.
201. Karwowski, J. P., Jackson, M., Rasmussen, R. R., Humphrey, P. E., Poddig, J. B., Kohl, W. L., Scherr, M. H., Kadam, S., McAlpine, J. B. 5-N-Acetylardeemin, a novel heterocyclic compound which reverses multiple drug resistance in tumor cells. I. Taxonomy and fermentation of the producing organism and biological activity. *J Antibiot* **1993**;*46*:374-379.
202. Juliano, R. L., Ling, V. A surface glycoprotein modulating drug permeability in Chinese hamster ovary cell mutants. *Biochim. Biophys. Acta. Biomembr.* **1976**;*455*:152-162.
203. Huls, M., Russel, F. G. M., Masereeuw, R. The role of ATP binding cassette transporters in tissue defense and organ regeneration. *J. Pharmacol. Exp. Ther.* **2009**;*328*:3-9.
204. Zacherl, J., Hamilton, G., Thalhammer, T., Riegler, M., Cosentini, E. P., Ellinger, A., Bischof, G., Schweitzer, M., Teleky, B., et, a. Inhibition of P-glycoprotein-mediated vinblastine transport across HCT-8 intestinal carcinoma monolayers by verapamil, cyclosporine A and SDZ PSC 833 in dependence on extracellular pH. *Cancer Chemother. Pharmacol.* **1994**;*34*:125-132.

205. Glavinas, H., Krajcsi, P., Cserepes, J., Sarkadi, B. The role of ABC transporters in drug resistance, metabolism, and toxicity. *Curr. Drug Delivery.* **2004**;*1*:27-42.
206. Aouali, N., Eddabra, L., Macadre, J., Morjani, H. Immunosuppressors and reversion of multidrug-resistance. *Crit. Rev. Oncol. Hematol.* **2005**;*56*:61-70.
207. Golstein, P. E., Boom, A., van, G. J., Jacobs, P., Masereel, B., Beauwens, R. P-glycoprotein inhibition by glibenclamide and related compounds. *Pfluegers Arch.* **1999**;*437*:652-660.
208. Tullberg, M., Grotli, M., Luthman, K. Efficient synthesis of 2,5-diketopiperazines using microwave assisted heating. *Tetrahedron* **2006**;*62*:7484-7491.
209. Henrich, C. J., Bokesch, H. R., Dean, M., Bates, S. E., Robey, R. W., Goncharova, E. I., Wilson, J. A., McMahon, J. B. A high-throughput cell-based assay for inhibitors of ABCG2 activity. *J. Biomol. Screening* **2006**;*11*:176-183.
210. Miao, S., Anstee, M. R., LaMarco, K., Matthew, J., Huang, L. H. T., Brasseur, M. M. Inhibition of bacterial RNA polymerases. Peptide metabolites from the cultures of *Streptomyces sp. J. Nat. Prod.* **1997**;*60*:858-861.
211. Driessen, A. J. M., Verhoogt, H. C., Konings, W. N. Novel mechanism of guanidino compound transport in bacteria: arginine:ornithine exchange. *Guanidino Compd. Biol. Med.* **1992**:3-12.
212. Luzhetskyy, A., Mayer, A., Hoffmann, J., Pelzer, S., Holzenkaemper, M., Schmitt, B., Wohlert, S.-E., Vente, A., Bechthold, A. Cloning and heterologous expression of the aranciamycin biosynthetic gene cluster revealed a new flexible glycosyltransferase. *ChemBioChem.* **2007**;*8*:599-602.
213. Motohashi, K., Takagi, M., Shin-ya, K. Tetracenoquinocin and 5-iminoaranciamycin from a sponge-derived *Streptomyces* sp. Sp080513GE-26. *J. Nat. Prod.* **2010**;*73*:755-758.
214. Bols, M., Binderup, L., Hansen, J., Rasmussen, P. Inhibition of collagenase by aranciamycin and aranciamycin derivatives. *J. Med. Chem.* **1992**;*35*:2768-2771.
215. Keller-Schierlein, W., Sauerbier, J., Vogler, U., Zaehner, H. Metabolic products of microorganisms. 80. Aranciamycin. *Helv. Chim. Acta.* **1970**;*53*:779-789.
216. Schmidt-Baese, K., Noltemeyer, M., Egert, E., Eigelt, E., Zeeck, A. Structure of the anthracycline antibiotic aranciamycin. *Acta Crystallogr. Sect. C. Cryst. Struct. Commun.* **1993**;*C49*:250-253.
217. Luzhetskyy, A., Hoffmann, J., Pelzer, S., Wohlert, S.-E., Vente, A., Bechthold, A. Aranciamycin analogs generated by combinatorial biosynthesis show improved antitumor activity. *Appl. Microbiol. Biotechnol.* **2008**;*80*:15-19.
218. Kende, A. S., Johnson, S. Anthracyclinones by oxidative dearomatization: total synthesis of SM-173B and aranciamycinone. *J. Org. Chem.* **1985**;*50*:727-729.
219. Winkler, R., Hertweck, C. Biosynthesis of nitro compounds. *ChemBioChem.* **2007**;*8*:973-977.
220. Hashimoto, M., Hattori, K. Oxypyrrolenitrin: a metabolite of *Pseudomonas*. *Chem. Pharm. Bull.* **1966**;*14*:1314-1316.
221. El-Banna, N., Winkelmann, G. Pyrrolnitrin from *Burkholderia cepacia*: antibiotic activity against fungi and novel activities against streptomycetes. *J. Appl. Microbiol.* **1998**;*85*:69-78.
222. Lee, J., Zhao, H. Mechanistic studies on the conversion of arylamines into arylnitro compounds by aminopyrrolnitrin oxygenase: identification of intermediates and kinetic studies. *Angew. Chem. Int. Ed.* **2006**;*45*:622-625.
223. Simurdiak, M., Lee, J., Zhao, H. A new class of arylamine oxygenases: evidence that p-aminobenzoate N-oxygenase (AurF) is a di-iron enzyme and further mechanistic studies. *ChemBioChem.* **2006**;*7*:1169-1172.
224. Yamazaki, M., Okuyama, E., Kobayashi, M., Inoue, H. The structure of paraherquamide, a toxic metabolite from *Penicillium paraherquei*. *Tetrahedron Lett* **1981**;*22*:135-136.
225. Liesch, J. M., Wichmann, C. F. Novel antinematodal and antiparasitic agents from *Penicillium charlesii*. II. Structure determination of paraherquamides B, C, D, E, F, and G. *J. Antibiot.* **1990**;*43*:1380-1386.

226. Ostlind, D. A., Mickle, W. G., Ewanciw, D. V., Andriuli, F. J., Campbell, W. C., Hernandez, S., Mochales, S., Munguira, E. Efficacy of paraherquamide against immature *Trichostrongylus colubriformis* in the gerbil (Meriones unguiculatus). *Res. Vet. Sci.* **1990**;*48*:260-261.
227. Robertson, A. P., Clark, C. L., Burns, T. A., Thompson, D. P., Geary, T. G., Trailovic, S. M., Martin, R. J. Paraherquamide and 2-deoxy-paraherquamide distinguish cholinergic receptor subtypes in ascaris muscle. *J. Pharmacol. Exp. Ther.* **2002**;*303*:888.
228. Lee, B. H., Clothier, M. F., Dutton, F. E., Nelson, S. J., Johnson, S. S., Thompson, D. P., Geary, T. G., Whaley, H. D., Haber, C. L., Marshall, V. P., Kornis, G. I., McNally, P. L., Ciadella, J. I., Martin, D. G., Bowman, J. W., Baker, C. A., Coscarelli, E. M., Alexander-Bowman, S. J., Davis, J. P., Zinser, E. W., Wiley, V., Lipton, M. F., Mauragis, M. A. Marcfortine and paraherquamide class of anthelmintics: Discovery of PNU-141962. *Curr. Top Med. Chem.* **2002**;*2*:779-793.
229. Qian-Cutrone, J., Huang, S., Shu, Y.-Z., Vyas, D., Fairchild, C., Menendez, A., Krampitz, K., Dalterio, R., Klohr, S. E., Gao, Q. Stephacidin A and B: two structurally novel, selective inhibitors of the testosterone-dependent prostate LNCaP cells. *J. Am. Chem. Soc.* **2002**;*124*:14556-14557.
230. Pimenta, E. F., Vita-Marques, A. M., Tininis, A., Seleghim, M. H. R., Sette, L. D., Veloso, K., Ferreira, A. G., Williams, D. E., Patrick, B. O., Dalisay, D. S., Andersen, R. J., Berlinck, R. G. S. Use of Experimental Design for the Optimization of the Production of New Secondary Metabolites by Two *Penicillium* Species. *J. Nat. Prod.* **2010**;*73*:1821-1832.
231. Physicochemical data for some selected mycotoxins. *Pure Appl. Chem.* **1982**;*54*:2219-2284.
232. do, R. M. A. M., Rodrigues-Filho, E., Moitinho, M. d. L. R., Santos, L. S. Biologically active polyketides produced by *Penicillium janthinellum* isolated as an endophytic fungus from Fruits of Melia azedarach. *J. Braz. Chem. Soc.* **2005**;*16*:280-283.
233. Demain, A. L. Induction of microbial secondary metabolism. *Int Microbiol* **1998**;*1*:259-264.
234. Teichmann, B., Liu, L., Schink, K. O., Bolker, M. Activation of the ustilagic acid biosynthesis gene cluster in Ustilago maydis by the C2H2 zinc finger transcription factor Rua1. *Appl. Environ. Microbiol.* **2010**;*76*:2633-2640.
235. Huang, R., Zhou, X., Xu, T., Yang, X., Liu, Y. Diketopiperazines from Marine Organisms. *Chem. Biodiversity* **2010**;*7*:2809-2829.
236. Metzger, U., Schall, C., Zocher, G., Unsoeld, I., Stec, E., Li, S.-M., Heide, L., Stehle, T. The structure of dimethylallyl tryptophan synthase reveals a common architecture of aromatic prenyltransferases in fungi and bacteria. *Proc. Natl. Acad. Sci.* **2009**;*106*:14309-14314, S14309/14301-S14309/14309.
237. Supek, V., Gamulin, S., Delic, V. Enhancement of bacitracin biosynthesis by branched-chain amino acids in a regulatory mutant of *Bacillus licheniformis*. *Folia Microbiol.* **1985**;*30*:342-248.
238. Gutierrez, S., Velasco, J., Fernandez, F. J., Martin, J. F. The cefG gene of *Cephalosporium acremonium* is linked to the cefEF gene and encodes a deacetylcephalosporin C acetyltransferase closely related to homoserine O-acetyltransferase. *J. Bacteriol.* **1992**;*174*:3056-3064.
239. Khetan, A., Hu, W.-S., Sherman, D. H. Heterogeneous distribution of lysine 6-aminotransferase during cephamycin C biosynthesis in *Streptomyces clavuligerus* demonstrated using green fluorescent protein as a reporter. *Microbiology* **2000**;*146*:1869-1880.
240. Nguyen, L. T., Nguyen, K. T., Spizek, J., Behal, V. The tylosin producer, *Streptomyces fradiae*, contains a second valine dehydrogenase. *Microbiology* **1995**;*141*:1139-1145.
241. De Rosa, S., Mitova, M., Tommonaro, G. Marine bacteria associated with sponge as source of cyclic peptides. *Biomol. Eng.* **2003**;*20*:311-316.

242. Cronan, J. M., Jr., Davidson, T. R., Singleton, F. L., Colwell, R. R., Cardellina, J. H., II. Plant growth promoters isolated from a marine bacterium associated with *Palythoa* sp. *Nat. Prod. Lett.* **1998**;*11*:271-278.
243. Graz, M., Hunt, A., Jamie, H., Grant, G., Milne, P. Antimicrobial activity of selected cyclic dipeptides. *Pharmazie* **1999**;*54*:772-775.
244. De Kievit, T. R., Iglewski, B. H. Bacterial quorum sensing in pathogenic relationships. *Infect. Immun.* **2000**;*68*:4839-4849.
245. Degrassi, G., Aguilar, C., Bosco, M., Zahariev, S., Pongor, S., Venturi, V. Plant growth-promoting *Pseudomonas putida* WCS358 produces and secretes four cyclic dipeptides: cross-talk with quorum sensing bacterial sensors. *Curr. Microbiol.* **2002**;*45*:250-254.
246. Chu, M., Truumees, I., Rothofsky, M. L., Patel, M. G., Gentile, F., Das, P. R., Puar, M. S., Lin, S. L. Inhibition of c-fos proto-oncogene induction by Sch 52900 and Sch 52901, novel diketopiperazines produced by *Gliocladium* sp. *J. Antibiot.* **1995**;*48*:1440-1445.
247. Yan, P.-S., Song, Y., Sakuno, E., Nakajima, H., Nakagawa, H., Yabe, K. Cyclo(L-leucyl-L-prolyl) produced by Achromobacter xylosoxidans inhibits aflatoxin production by *Aspergillus parasiticus*. *Appl. Environ. Microbiol.* **2004**;*70*:7466-7473.
248. Kuramata, M., Fujioka, S., Shimada, A., Kawano, T., Kimura, Y. Citrinolactones A, B and C, and sclerotinin C, plant growth regulators from *Penicillium citrinum*. *Biosci. Biotechnol. Biochem.* **2007**;*71*:499-503.
249. Herlt, A. J., Rickards, R. W., Wu, J. P. The structure of streptonigrone, and a comment on the biosynthesis of the streptonigrin antibiotics. *J. Antibiot.* **1985**;*38*:516-518.
250. Wang, H., Yeo, S. L., Xu, J., Xu, X., He, H., Ronca, F., Ting, A. E., Wang, Y., Yu, V. C., Sim, M. M. Isolation of streptonigrin and its novel derivative from *Micromonospora* as inducing agents of p53-dependent cell apoptosis. *J. Nat. Prod.* **2002**;*65*:721-724.
251. Gurney, K. A., Mantle, P. G. Biosynthesis of 1-N-methylalbonoursin by an endophytic *Streptomyces* sp. isolated from perennial ryegrass. *J Nat Prod* **1993**;*56*:1194-1198.
252. Tuntiwachwuttikul, P., Taechowisan, T., Wanbanjob, A., Thadaniti, S., Taylor, W. C. Lansai A-D, secondary metabolites from *Streptomyces* sp. SUC1. *Tetrahedron* **2008**;*64*:7583-7586.
253. Wasserman, H. H., Rodgers, G. C., Keith, D. D. Metacycloprodigiosin, a tripyrrole pigment from *Streptomyces longisporus ruber*. *J. Amer. Chem. Soc.* **1969**;*91*:1263-1364.
254. Wasserman, H. H., Keith, D. D., Rodgers, G. C. The structure of metacycloprodigiosin. *Tetrahedron* **1976**;*32*:1855-1861.
255. Ben Ameur Mehdi, R., Sioud, S., Fourati Ben Fguira, L., Bejar, S., Mellouli, L. Purification and structure determination of four bioactive molecules from a newly isolated *Streptomyces* sp. TN97 strain. *Process Biochem.* **2006**;*41*:1506-1513.
256. Kobayashi, M., Aoki, S., Gato, K., Matsunami, K., Kurosu, M., Kitagawa, I. Marine natural products. XXXIV. Trisindoline, a new antibiotic indole trimer, produced by a bacterium of *Vibrio* sp. separated from the marine sponge *Hyrtios altum*. *Chem. Pharm. Bull.* **1994**;*42*:2449-2451.
257. Lackner, H., Bahner, I., Shigematsu, N., Pannell, L. K., Mauger, A. B. Structures of five components of the actinomycin Z complex from *Streptomyces fradiae*, two of which contain 4-chlorothreonine. *J. Nat. Prod.* **2000**;*63*:352-356.
258. Tresner, H. D., Hayes, J. A. Improved methodology for isolating soil microorganisms. *Appl. Microbiol.* **1970**;*19*:186-187.
259. Hames-Kocabas, E. E., Uzel, A. Isolation strategies of marine-derived actinomycetes from sponge and sediment samples. *J. Microbiol. Meth.* **2012**;*88*:342-347.
260. Graham, G. C., Mayers, P., Henry, R. J. A simplified method for the preparation of fungal genomic DNA for PCR and RAPD analysis. *BioTechniques* **1994**;*16*:48,50.
261. Hsiao, C. R., Huang, L., Bouchara, J.-P., Barton, R., Li, H. C., Chang, T. C. Identification of medically important molds by an oligonucleotide array. *J. Clin. Microbiol.* **2005**;*43*:3760-3768.

14 Appendix

Taxonomic identifucation of *Aspergillus* sp. (CMB-M0423)

DNA extraction was performed using cetyltrimethylammonium bromide (CTAB) protocol.[260] Mycelia of the fungus cultivated on M1 broth (approximately 200 – 500 mg) were frozen with liquid N_2 and ground to a fine paste in a morter and pestle in 500 µL CTAB buffer. The CTAB/mycelia mixture was incubated for 15 min at 55 °C in a recirculating water bath. The mixture was centrifuged for 5 min at 12000 g and the supernatant was transferred to a clean microcentrifuge tube. An aliquot (1 mL) of phenol:chloroform:isoamyl alcohol (25:24:1) was added, the tube was centrifuged at 12000 g for 1 min and the upper aqueous layer was transferred to clean microcentrifuge tube. To the tube, ammonium acetate (7.5 M, 150 µL) was added followed by ice cold absolute ethanol (1 mL) and the tube was incubated at –20 °C for 1 h. The tube was centrifuged at 13000 g for 30 min, the supernatant was removed and the DNA pellet was washed twice with ice cold 70% ethanol. Finally, the DNA was resuspended in distilled water (70 µL).

Amplification and sequencing of fungal DNA:

The 18S RNA genes were amplified from genomic DNA by PCR using primers ITS 1 (5′-TCCGTAGGTGAACCTGCGG-3′) and ITS 4 (5′-TCCTCCGCTTATTGATATGC-3′) purchased from Sigma-aldrich.[261]

PCR was performed on 1 µL (1 to 5 ng) of template DNA in a total reaction volume of 50 µL consisting of 10 mM Tris-HCl (pH 8.3) (5 µL), 50 mM $MgCl_2$ (1.5 µL), 10 µM deoxyribonucleoside triphosphates (2 µL), 10 µM ITS 1 primer (1.6 µL), 10 µM ITS 4 primer (1.6 µL) Taq DNA polymerase (1.25 U) (0.5 µL) and water (36.8 µL). PCR was carried out under the following conditions: initial denaturation, 95 °C, 3 min; 35 cycles of denaturation (94 °C, 30 s), annealing (55.9 °C, 30 s), and extension (72 °C, 30 s); and final extension, 72.5 °C, 5 min. A negative control was performed with each test run by replacing the template DNA with sterilized water in the PCR mixture. PCR products were purified with PCR purification kit (Qiagen, Victoria, Australia). Amplification products were examined by agarose gel electrophoresis. The 18S rRNA gene sequence showed 98% homology with other members of the genus *Aspergillus* by the BLAST database.

ITS4 sequence

CGGGCTTCCTACCTGATCCGAGGTCACCTGGAAAAACAAGTTGCAAAAAAATTGCGTCGGCAGGCG
CCGGCCGGGCCTACGGAGCGGAAGACGAAGCCCCATACGCTCGAGGACCGGACGCGGTGCCGCCGC
TGCCTTTCGGGCCCGTCCCCCGGGAGCCGGGGGACGAGGGCCCAACACACAAGCCGGGCTTGAGGG
CAGCAATGACGCTCGGACAGGCATGCCCCCCGGAATACCAGGGGGCGCAATGTGCGTTCAAAGACT

CGATGATTCACTGAATTCTGCAATTCACATTAGTTATCGCATTTCGCTGCGTTCTTCATCGATGCC

GGAACCAAGAGATCCATTGTTGAAAGTTTTAACTGATTGCAAAGAATCACACTCAGACTGCAAGCT

TTCAGAACAGGGTTCATGTTGGGGTCTCCGGCGGGCACGGGCCCGGGGGGCGAGTCGCCCCCCGGCG

GCCAGCAACGCTGGCGGGCCCGCCGAAGCAACAAGGTACAATAGTCACGGGTGGGAGGTTGGGCCA

TAAAGACCCGCACTCGGTAATGATCCTTCCGCAGGTTCACCCTACGGAAG

ITS1 sequence

GGGGTTTGAATGGGGGTCTTTATGGCCACCTCCCCCCGTGACTATTGTACCTTGTTGCTTCGGCGG

GCCCGCCACCCTAGCTAGGCGCCGGGGGGCGACTCGCCCCCGGGGCCGTGCCCGCTGGAAACAAAA

CATGAACCTAGATCTGAATGCTTGCAAACTGAAAAGATTCTTTACAATCAGTTAAAACTTTCT

```
>gb|AAJN01000138.1|  Aspergillus terreus NIH2624 cont1.138, whole genome shotgun sequence
Length=7406

 Score =  989 bits (535),  Expect = 0.0
 Identities = 565/574 (98%), Gaps = 6/574 (1%)
 Strand=Plus/Minus

Query  8     CCTACCTGATCCGAGGTC-ACCTGG--AAAAACAAGTTGCaaaaaaaTTGCGTCGGCAGG  64
             |||||||||||||||||| ||||||  ||||||||||||| ||| || |||||||||| ||
Sbjct  3342  CCTACCTGATCCGAGGTCAACCTGGAAAAAAACAAGTTGC-AAATAAATGCGTCGGCGGG  3284

Query  65    CGCCGGCCGGGCCTACGGAGCGGAAGACGAAGCCCCATACGCTCGAGGACCGGACGCGGT  124
             ||||||||||||||||||||||||||||||||||||||||||||||||||||||||||||
Sbjct  3283  CGCCGGCCGGGCCTACGGAGCGGAAGACGAAGCCCCATACGCTCGAGGACCGGACGCGGT  3224

Query  125   G-CCGCCGCTGCCTTTCGGGCCCGTCCCCCGGGAGCCGGGGGACGAGGGCCCAACACACA  183
             | ||||||||||||||||||||||||||||||||||||||||||||||||||||||||||
Sbjct  3223  GCCCGCCGCTGCCTTTCGGGCCCGTCCCCCGGGAGCCGGGGGACGAGGGCCCAACACACA  3164

Query  184   AGCCGGGCTTGAGGGCAGCAATGACGCTCGGACAGGCATGCCCCCCCGGAATACCAGGGGG  243
             ||||||||||||||||||||||||||||||||||||||||||||||||||||||||||||
Sbjct  3163  AGCCGGGCTTGAGGGCAGCAATGACGCTCGGACAGGCATGCCCCCCCGGAATACCAGGGGG  3104

Query  244   CGCAATGTGCGTTCAAAGACTCGATGATTCACTGAATTCTGCAATTCACATTAGTTATCG  303
             ||||||||||||||||||||||||||||||||||||||||||||||||||||||||||||
Sbjct  3103  CGCAATGTGCGTTCAAAGACTCGATGATTCACTGAATTCTGCAATTCACATTAGTTATCG  3044

Query  304   CATTTCGCTGCGTTCTTCATCGATGCCGGAACCAAGAGATCCATTGTTGAAAGTTTTAAC  363
             ||||||||||||||||||||||||||||||||||||||||||||||||||||||||||||
Sbjct  3043  CATTTCGCTGCGTTCTTCATCGATGCCGGAACCAAGAGATCCATTGTTGAAAGTTTTAAC  2984

Query  364   TGATTGCAAAGAATCACACTCAGACTGCAAGCTTTCAGAACAGGGTTCATGTTGGGGTCT  423
             ||||||||||||||||||||||||||||||||||||||||||||||||||||||||||||
Sbjct  2983  TGATTGCAAAGAATCACACTCAGACTGCAAGCTTTCAGAACAGGGTTCATGTTGGGGTCT  2924

Query  424   CCGGCGGGCACGGGCCCGGGGGCGAGTCGCCCCCCGGCGGCCAGCAACGCTGGCGGGCCC  483
             ||||||||||||||||||||||||||||||||||||||||||||||||||||||||||||
Sbjct  2923  CCGGCGGGCACGGGCCCGGGGGCGAGTCGCCCCCCGGCGGCCAGCAACGCTGGCGGGCCC  2864

Query  484   GCCGAAGCAACAAGGTACAATAGTCACGGGTGGGAGGTTGGGCCATAAAGACCCGCACTC  543
             ||||||||||||||||||||||||||||||||||||||||||||||||||||||||||||
Sbjct  2863  GCCGAAGCAACAAGGTACAATAGTCACGGGTGGGAGGTTGGGCCATAAAGACCCGCACTC  2804

Query  544   GGTAATGATCCTTCCGCAGGTTCACCCTACGGAA  577
             |||||||||||||||||||||||| |||||||
Sbjct  2803  GGTAATGATCCTTCCGCAGGTTCACC-TACGGAA  2771
```

Taxonomic fungal DNA of CMB-M81F

18S rRNA Gene Sequence

TGGCTTCCTTGCGATTCTCGCCGATCTTCCTTCCTTGCGTTACTAAGATCTACCGACTTAATTCAT
CCAGGCGACCGGCTAAATGTTGTGGGACGAAGAGGGTAAGTTGTTTTTGTTGCCCTAATTTTTACT
ATGATATGACACTTATTTCGCGATTCATGTTCTTTTTTCTCCTGTATAAACTTGTGATTGTCGGTT
GCATGTGGACTTTTCCATTGAGGGGACTTGTGGTCTTCCTCCCCCGGTGAATGGCGTGAGTAGCTT
GCGTTCTCATATTCCCCTTCTTCATCGTCAACTCCTGCCCCCTCAACCCCAATTTCTCCACTCCCA
GAGCCTTATTGACATGATTTTACGTTTAATTCGCCCGTTTGTTGAACAACGTAACAAAAAAAACGA
TGTTCTATTGCAGGAGATTTGTAAGCGCTACTGTTTTCGCATTATTCCCGAGAAATTTTCCGAAAT
ACAGGAGAATGACATCGGATTTTACTAAGTGGGTTCGTAAATGAAGGAGTTTAAGGAATATCCTCC
GCCATAGATCGTTAAGCCTG

Blast Search

```
gi|327296508|ref|XM_003232981.1| Trichophyton rubrum CBS 118892 serine/threonine protein kinase (TERG_06939) mRNA, complete cds

Length = 906
Score = 41.0 bits (44), Expect = 9.7
Identities = 30/34 (88%), Positives = 30/34 (88%), Gaps = 1/34 (2%)

  Query:      393 ACGATGTTCTATTGCAGGAGATTTGTAAGCGCTA
                  ||||  ||||| |||||||||||| |||||||||
Subject:      827 ACGACTTTCTAATGCAGGAGATTT-TAAGCGCTA
```

Taxonomic fungal DNA of CMB-TF438

18S rRNA Gene Sequence

GAAATCGGTTCGTCAGTCCGACTTTACATCATTTGAGAAGCGGTGAGATCGGAAGTTCTATCTTCT
ATAGGGGGGAGGTAGAGGGCGAGGATGCCGGAAGTCAACAAGGTTCACCCATCGAATTGGAATTTC
GGGATAAGACTCATACTGAAACTTCATGATCCTTTTATGTGGGCCCCTAGCGAACGCGGGGCCCGC
GTGTGTATATACCGTCGGGCAACACGGGTGGGAGGTTGGGCCCCGAGGGGCCCGCACTCGGTAATG
ATCCTTCCGCACGTTCACCTATGGAAGTTCTCGAAAGAGAGGGGGCCCCTCGGGGCCTCTCCATCA
ACATGTGCTCTTGAATTACGTTTATCGACCTAATACCTTCTGTTCACTCTTATTAAAGCTCGCACT
TTACACTTTGTCATAGGCCCTTTCCTCTTTCCTCCCATGGTACTCAAAATCTTCAAAGATTCTATT
TTTGATTTTCTTTTTTTTTTATATGTTAAGCTATAATGCATTTATAAATTTTCTCCTACTTCAATT
TTAGTCCAATCA

Blast Search

```
>gb|ABAR01000140.1|  Penicillium marneffei ATCC 18224 gcontig_1105668340088, whole
genome shotgun sequence
Length=2287

 Score =  102 bits (55),  Expect = 4e-19
 Identities = 66/71 (93%), Gaps = 1/71 (1%)
 Strand=Plus/Plus

Query  220   ACACGGGTGGGAGGTTGGGCCCCGAGGGGCCCGCACTCGGTAATGATCCTTCCGCACGTT  279
             ||| |||||||||||||||| ||| |||||||||||||||||||||||||||||| |||
Sbjct  1061  ACAAGGGTGGGAGGTTGGGCCGCGA-GGGCCCGCACTCGGTAATGATCCTTCCGCAGGTT  1119

Query  280   CACCTATGGAA  290
             |||||| ||||
Sbjct  1120  CACCTACGGAA  1130
```